AD-A241 312

WL-TR-91-3078
Volume II

OCT 0 2 1991
D

2

WRIGHT LABORATORY

Proceedings of Damping '91

13-15 February 1991
San Diego, California

(EAA-1 through GBC-16)

August 1991

Final Report for Period February 1989 to February 1991

91-12020

Approved for public release; distribution is unlimited

Sponsored by:

Wright Laboratory

Flight Dynamics Directorate

AIR FORCE SYSTEMS COMMAND
WRIGHT-PATTERSON AIR FORCE BASE, OHIO 45433-6553

DISCLAIMER NOTICE

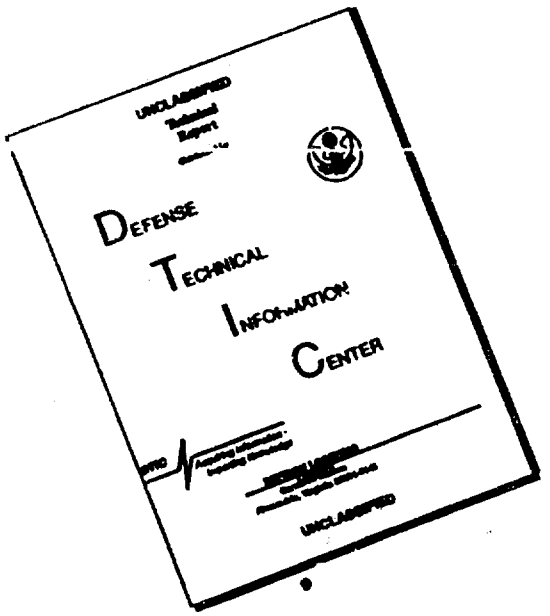

THIS DOCUMENT IS BEST QUALITY AVAILABLE. THE COPY FURNISHED TO DTIC CONTAINED A SIGNIFICANT NUMBER OF PAGES WHICH DO NOT REPRODUCE LEGIBLY.

NOTICE

When Government drawings, specifications, or other data are used for any purpose other than in connection with a definitely Government-related procurement, the United States Government incurs no responsibility or any obligation whatsoever. The fact that the government may have formulated or in any way supplied the said drawings, specifications, or other data, is not to be regarded by implication, or otherwise in any manner construed, as licensing the holder, or any other person or corporation; or as conveying any rights or permission to manufacture, use, or sell any patented invention that may in any way be related thereto.

This report is releasable to the National Technical Information Service (NTIS). At NTIS, it will be available to the general public, including foreign nations.

This technical report has been reviewed and is approved for publication.

JEROME PEARSON, Chief
Structural Dynamics Branch

LYNN ROGERS, PhD
Principal Engineer
Structural Dynamics Branch

If your address has changed, if you wish to be removed from our mailing list, or if the addressee is no longer employed by your organization please notify WL/FIBG , WPAFB, OH 45433-6553 to help us maintain a current mailing list.

Copies of this report should not be returned unless return is required by security considerations, contractual obligations, or notice on a specific document.

UNCLASSIFIED

SECURITY CLASSIFICATION OF THIS PAGE

REPORT DOCUMENTATION PAGE

Form Approved
OMB No. 0704-0188

1a. REPORT SECURITY CLASSIFICATION Unclassified	1b. RESTRICTIVE MARKINGS
2a. SECURITY CLASSIFICATION AUTHORITY	3. DISTRIBUTION/AVAILABILITY OF REPORT Approved for public release; distribution unlimited
2b. DECLASSIFICATION/DOWNGRADING SCHEDULE	
4. PERFORMING ORGANIZATION REPORT NUMBER(S) WL-TR-91-3078, Volume II	5. MONITORING ORGANIZATION REPORT NUMBER(S)
6a. NAME OF PERFORMING ORGANIZATION Flight Dynamics Directorate Wright Laboratory 6b. OFFICE SYMBOL (If applicable) WL/FIBG	7a. NAME OF MONITORING ORGANIZATION
6c. ADDRESS (City, State, and ZIP Code) Wright-Patterson AFB, OH 45433-6553	7b. ADDRESS (City, State, and ZIP Code)
8a. NAME OF FUNDING/SPONSORING ORGANIZATION 8b. OFFICE SYMBOL (If applicable)	9. PROCUREMENT INSTRUMENT IDENTIFICATION NUMBER
8c. ADDRESS (City, State, and ZIP Code)	10. SOURCE OF FUNDING NUMBERS PROGRAM ELEMENT NO: 62201F PROJECT NO: 2401 TASK NO: 04 WORK UNIT ACCESSION NO: 23

11. TITLE (Include Security Classification)

Proceedings of Damping '91

12. PERSONAL AUTHOR(S)

13a. TYPE OF REPORT	13b. TIME COVERED	14. DATE OF REPORT (Year, Month, Day)	15. PAGE COUNT
Final	FROM FEB 89 TO FEB 91	August 1991	566

16. SUPPLEMENTARY NOTATION

Pages EAA-1 through GBC-16

17. COSATI CODES			18. SUBJECT TERMS (Continue on reverse if necessary and identify by block number)
FIELD	GROUP	SUB-GROUP	
			Vibration Damping, controls/structure interaction.

19. ABSTRACT (Continue on reverse if necessary and identify by block number)

Individual papers of Damping '91 held 13-15 February 1991 in San Diego CA are presented. The subjects included: Viscoelastic Material Testing and Characterization, Passive Damping Concepts, Passive Damping Analysis and Design Techniques, Optimization, Damped Control/Structure Interaction, Viscous Dampers, Friction Damping, Other Vibration Suppression Techniques, Damping Identification and Dynamic Testing, Applications to Aircraft, Space Structures, Marine Structures, Commercial Products, Defense Applications, and Payoffs of Vibration Suppression.

20. DISTRIBUTION/AVAILABILITY OF ABSTRACT	21. ABSTRACT SECURITY CLASSIFICATION
☒ UNCLASSIFIED/UNLIMITED ☐ SAME AS RPT ☐ DTIC USERS	Unclassified
22a. NAME OF RESPONSIBLE INDIVIDUAL Dr. Lynn Rogers	22b. TELEPHONE (Include Area Code) (513) 255-6022
	22c. OFFICE SYMBOL WL/FIBG

DD Form 1473, JUN 86 Previous editions are obsolete SECURITY CLASSIFICATION OF THIS PAGE

UNCLASSIFIED

Workshop Administration

Director
Dr. Lynn C. Rogers
Wright Laboratory
Flight Dynamics Directorate

Technical Chairman
Dr. Conor D. Johnson
CSA Engineering, Inc.

Administrative Chairman
Mrs. Beryl D. Deremigio
CSA Engineering, Inc.

Assistant Administrative Chairman
Ms. Bonnie L. Portis
CSA Engineering, Inc.

Session Chairmen

Mr. Bradley Allen, *CSA Engineering, Inc.*
Capt. Walter Andress, *Space Systems Division*
Dr. Mohan Aswani, *Aerospace Corporation*
Capt. Mark Arnold, *Wright Laboratory, Flight Dynamics Directorate*
Mr. Eric Austin, *CSA Engineering, Inc.*
Lt. Col. Ronald L. Bagley, *Air Force Institute of Technology*
Dr. Andrew S. Bicos, *McDonnell Douglas Space Systems Company*
Mr. Daniel Cyphers, *W. J. Schafer Associates, Inc.*
Mr. Eric Dalton, *Teledyne Brown*
Mr. Ralph Dornsife, *US Army / CERL*
Mr. William Driscoll, *3M / Industrial Specialties Division*
Mr. Robert Dunning, *TRW*
Mr. Rod Eddleman, *US Army Strategic Defense*
Mr. Richard Ely, *LTV Aircraft Group*
Dr. James Fanson, *Jet Propulsion Laboratory*
Mr. Bryce Fowler, *CSA Engineering, Inc.*
Dr. Joseph Garibotti, *Ketema, Inc.*
Mr. Russell Gehling, *Martin Marietta Astronautics Group*
Dr. Steven Ginter, *Honeywell Satellite Systems*
Dr. John Gubser, *McDonnel Douglas Missile System Company*
Dr. John Henderson, *Consultant*
Mr. Dennis Hill, *GE Astro Space Division*

Dr. Philip Hipol, *The Aerospace Corporation*
Dr. Robert Holman, *Hughes Aircraft Company*
Mr. J. Warren Hoskins, *Lockheed Missiles and Space Company*
Dr. Roy Ikegami, *Boeing Aerospace*
Dr. Conor Johnson, *CSA Engineering, Inc.*
Mr. Derrick Johnson, *Boeing Aerospace*
Dr. David I. G. Jones, *Wright Laboratory, Flight Dynamics Directorate*
Dr. Edward Kerwin, *Bolt, Beranek and Newman, Inc.*
Mr. John Lassiter, *Warner - Robins ALC*
Mr. Paul Lindquist, *Wright Laboratory, Flight Dynamics Directorate*
Lt. John Mackaman, *Wright Laboratory, Flight Dynamics Directorate*
Dr. Ray Manning, *TRW, Space and Technology Group*
Mr. Daniel Morgenthaler, *Martin Marietta Space Systems*
Mr. Ahid Nashif, *Anatrol Corporation*
Mr. Rory Ninneman, *Phillips Laboratory*
Mr. Earl Pinson, *Lockheed Missiles and Space Company*
Mr. Ken Qassim, *Phillips Laboratory*
Mr. Keith Quinn, *Nichols Research Corporation*
Dr. Dantam Rao, *Mechanical Technology, Inc.*
Dr. Wayne Reader, *Vector Research Company, Inc.*
Dr. Kenneth Richards, *Martin Marietta*
Mr. Stanley Sattinger, *Westinghouse Science and Technology Center*
Dr. Daniel Segalman, *Sandia National Laboratories*
Mr. Leonard Shaw, *Wright Laboratory, Flight Dynamics Directorate*
Professor Young Shin, *Naval Postgraduate School*
Dr. Stepan Simonian, *TRW, Space and Technology Group*
Mr. Kevin Slimak, *Phillips Laboratory, Astronautics Directorate*
Dr. Jaak Soovere, *Lockheed Missiles and Space Company*
Mr. Clyde Stahle, *GE Astro Space*
Mr. Ralph Tate, *LTV Aircraft Products Group*
Mr. Roger Thaller, *Aeronautical Systems Division*
Capt. Steven G. Webb, *US Air Force Academy*
Mr. Kenneth R. Wentz, *Wright Laboratory, Flight Dynamics Directorate*
Maj. Stephen Whitehouse, *Wright Laboratory, Flight Dynamics Directorate*
Dr. William Witt, *The CORE Group*
Dr. Y. C. Yiu, *Lockheed Missiles and Space Company*
Mr. Wayne Yuen, *Wright Laboratory, Flight Dynamics Directorate*
Mr. Michael L. Zeigler, *Wright Laboratory, Flight Dynamics Directorate*

FOREWORD

This publication includes individual papers of **Damping '91** held February 13-15, 1991, San Diego, California. The Conference was sponsored by the Wright Laboratory Flight Dynamics Directorate, Wright-Patterson Air Force Base, Ohio.

It is desired to transfer vibration damping technology in a timely manner within the aerospace community thereby, stimulating research, development and applications.

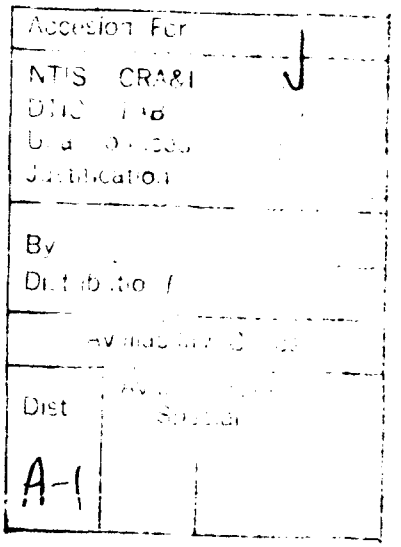

TABLE OF CONTENTS

	Paper No.
The F-117 Stealth Aircraft (Keynote Address) Mr. Paul Martin	**AAA***
Use of Passive Damping for Aircraft Cabin Noise Control (Invited Speaker) Dr. Leo Butzel	**AAB***
The Society of Damping Technology in Japan and its Activities (Invited Speaker) Dr. Yasuo Tokita and Hiroshi Okamura	**AAC**
SESSION BA - Aircraft Applications	
Integral Damping Treatment for Primary Aircraft Structures Sal Liguore, Marty Ferman, and Rudy Yurkovich	**BAA**
An Investigation of Add-on Damping Treatment for Life Extension of the F-15 Upper Outer Wing Skin Michael Parin, V. Levraea, Jr., Dr. Lynn Rogers, and A. Pacia	**BAB**
Damping Treatments for Aircraft Hardmounted Antennae Ralph E. Tate and Carl L. Rupert	**BAC***
SESSION BB - Plates and Beams	
Examination of Boundary Conditions for Sixth-Order Damped Beam Theory Ralph E. Tate	**BBA**
The Effect of Compliant Layering on Damped Beams David John Barrett	**BBB**
The Damping Property of Laminated Steel Sheet after Deep Drawing Hiroshi Okamura	**BBC**

*Not available for publication

TABLE OF CONTENTS (continued)

	Paper No.
SESSION BC - Analysis and Design 1	
Practical Design and Analysis of Systems with Fractional Derivative Materials and Active Controls Daniel R. Morgenthaler	BCA
An Implicit Fourier Transform Method for Nonlinear Dynamic Analysis with Frequency Dependent Damping Prof. F. Venancio Filho and A. M. Claret	BCB
On a Linear Property of Lightly Damped Systems Z. Liang, M. Tong, and G. C. Lee	BCC
SESSION CA - Control Structure	
Active Vibration Suppression via LQG/LTR: Analytic and Experimental Results for the PACOSS Dynamic Test Article Russell N. Gehling	CAA
H∞ Control for the PACOSS DTA Christopher T. Voth and R. Michael Stoughton	CAB
Active Damping of a Cantilever Beam Dr. Hung V. Vu, Stein Husher, and D. E. Zimmerman	CAC
The Investigation of Large Space Structure Passive Electrodynamic Dampers Dr. Roger Stettner and Dr. Paul Mlakar	CAD
SESSION CB - Damping Material and Measurements	
A Method for the Measurement of the Complex Compressional Modulus of Thin Layers Dr. Jonathan D. Rogers and Dr. Daniel J. Segalman	CBA*

*Not available for publication

TABLE OF CONTENTS (continued)

	Paper No.
The Evaluation of Young's Complex Modulus of Viscoelastic Materials Marc Tardif and Prof. Germain Ostiguy	CBB
Role of Morphology in Damping Efficiency Dr. L. H. Sperling, J. J. Fay, and Dr. D. A. Thomas	CBC*
The Thermorheologically Complex Material Lt. Col. Ronald L. Bagley	CBD*
SESSION CC - Analysis and Design 2	
Methods of Reduction of Wind Induced Dynamic Response in Solar Concentrators and Other Small Lightweight Structures Monte A. McGlaun	CCA
Analysis of a Five-Layer, Viscoelastic, Constrained-Layer Beam Michael A. Falugi	CCB
Dynamics of a Class of Viscously Damped Struts Dr. Y. C. Yiu and Dr. Steven Ginter	CCC
A Study of a Vibration Absorber to Control the Vibration of a Rectangular Plate Akio Sugimoto, Hideo Utsuno, and Toshimitsu Tanaka	CCD
SESSION DA - Analysis and Testing	
Impedance Matched Mass-Dampers: A New Approach for Improving Structural Damping Craig Gardner and Prof. Richard H. Lyon	DAA
Analytical and Experimental Modal Analysis of a Two-Tiered Structure Dr. Hung V. Vu, William C. Flynn, and T. K. Vuong	DAB

*Not available for publication

TABLE OF CONTENTS (continued)

	Paper No.
Development of a Magnetic Suspension System for Reliable Vibration Damping Measurement Dr. Dantam K. Rao	**DAC***
SESSION DB - Viscoelastic Material	
VEM Characterization Program Bryce L. Fowler	**DBA**
Data Base of the Dynamic Properties of Materials Ahid D. Nashif and Thomas M. Lewis	**DBB**
Establishing the Validity of the Master Curve Technique for Complex Modulus Data Reduction Dr. S. O. Oyadiji and Prof. G. R. Tomlinson	**DBC**
SESSION DC - Optimization	
Integrated Optimization of Composite Structures for Advanced Damped Dynamic Characteristics Dr. Dimitri C. Zervarakis and Christos C. Chamis	**DCA**
An Optimum Design Methodology for Passively Damped Truss Structures Dr. Ray Manning	**DCB**
On An Application of Complex Damping Coefficients Z. Liang, M. Tong and G. C. Lee	**DCC**
SESSION EA - DAMMPS 1	
Statistcal and Worst Case Evaluation of Orbital Jitter Reduction Using Passive Damping J. Molnar, Dennis Hill, and Clyde Stahle	**EAA**

*Not available for publication

TABLE OF CONTENTS (continued)

	Paper No.
I MSC DAMMPS Program Status J. Warren Hoskins and Dr. Y. C. Yiu	EAB
Damping of Precision Metal Matrix Trusses Dr. Stepan S. Simonian	EAC
Development of Low Modulus Damping Material for Precision Mounting Platforms Steven Kirshenbaum, Dennis Hill, and Clyde Stahle	EAD
Complex Stiffness Test Data for Three Viscoelastic Materials by the Direct Complex Stiffness Method Bradley R. Allen and Earl Pinson	EAE
SESSION EB - Viscoelastic Material Measurements	
Direct Measurement of the Dynamic Material Properties of *Polymers* for Low Frequencies Ahid D. Nashif, Thomas M. Lewis, and Paul J. Maciocc	EBA
Correlation of Complex Modulus Data by Direct Stiffness and Indirect Resonant Beam Test Techniques T. Lewis, Mona P. Khoury, and Dr. David I. G. Jones	EBB
Constitutive Modeling of Nonlinear Damping Materials Dr. Jerome Sackman, Prof. J. M. Kelly, and A. E. Javid	EBC
Results of a Round Robin Test Series to Evaluate Complex Moduli of a Selected Damping Material Dr. David I. G. Jones	EBD
SESSION EC- Analysis and Design 3	
A Mathematical Framework for the Study of Indirect Damping Mechanisms David L. Russell	ECA*

*Not available for publication

TABLE OF CONTENTS (continued)

	Paper No.
Techniques of Design and Using Viscoelastic Dampers Z. Liang, M. Tong, and G. C. Lee	ECB
Modeling of Constrained Layer Damping in Trusses Dr. Daniel J. Inman, Joseph C. Slater, and W. Keith Belvin	ECC
A Strong Criterion for Testing Proportionally Damped Systems Z. Liang, M. Tong, and G. C. Lee	ECD
SESSION ED - Applications	
Abbreviated Papers	
The PACOSS Dynamic Test Article Russell N. Gehling	EDA
Retrofitted Damping Treatment for a Three Stage Booster System Dr. Daniel J. Segalman and E. L. Marek	EDB*
Damping Design for a Disk Drive Head Flexure Eric M. Austin, James C. Goodding, and William A. Driscoll	EDC
Damping Jet Engine Front Frame Struts Capt. Vance Johnson, Kurt Nichol, and Dennis Murphy	EDD*
Isolation Joint for Flexural and Compressional Isolation Al Wignall and J. Aron	EDE
Characterization of Viscoelastic Damping in an Antenna Structure Dr. Ephrahim Garcia, James M. Argento, and Robert Alan Carlin	EDF
Laminar Blade Damper Michael Koleda	EDG
Experimental Study on Noise Reduction due to Damping Treatments Ken Okada and Junichi Kanazawa	EDH*

*Not available for publication

TABLE OF CONTENTS (continued)

Paper No.

SESSION FA - DAMMPS 2

Evaluation of Damping Concepts for Precision Mounting Platforms FAA
Dennis Hill, Clyde Stahle, and James Staley

Synergistic Design of Passive Damping and Metal Matrix Composites FAB
Earl D. Pinson, Eric M. Austin, and Michael L. Zeigler

A Three Element Viscoelastic Isolator FAC
Dr. Stepan S. Simonian

SESSION FB - Noise and Acoustics

Integrally Damped Honeycomb Structural Concepts to Increase Noise Transmission Loss FBA
Jefferson F. Newton, Dr. Roy Ikegami, and D. J. Carbery

Reduction of Acoustic Responses Using Viscoelastic Damping Materials FBB
Dr. David Chu, C. Stahle, J. Staley, J. Peir, and M. McMeekin

Design Method of Damping Treatment for Structure-Borne Noise Reduction FBC*
Iwao Honda, Tadao Nakamura, Yoshihiko Irie, and Kazuo Yamamoto

SESSION FC - Civil Structures

Earthquake Simulator Testing of Two Damping Systems for Multistory Structures FCA
Ian D. Aiken and James M. Kelly

Correlation of Experimental Results with Predictions of Viscoelastic Damping for a Model Structure FCB
T. T. Soong and Dr. Ming Lai

*Not available for publication

TABLE OF CONTENTS (continued)

	Paper No.
Damping Capacity of Reinforced Concrete External Beam Column Connections Dr. Alexander G. Tsonos, Ioannis A. Tegos, and Prof. Georgios G. Penelis	FCC*

SESSION FD - Analysis and Damping Mechanisms
Abbreviated Papers

Eddy Current-based Vibration Damping for Aerospace Structures James Goldie	FDA
The Absolute Value Modal Strain Energy Method Daniel R. Morgenthaler	FDB
An Analytical Model for the Vibration of Viscoelastically Damped Curved Sandwich Beams Dr. Mohan D. Rao and Shulin He	FDC
Bibliography of Environmental Data Measured In-Flight Lt. Col. Raymond F. Hain, III	FDD
General Motion of an Inclined Impact Damper with Friction C. N. Bapat	FDE
The Shock and Vibration Information Analysis Center (SAVIAC) Harold D. Kohn	FDF

SESSION GA - Electro-Rheological Fluids and Fluids

The Vibration Damping Effect of an Electrorheological Fluid Stephen A. Austin	GAB
Modelling of Nonlinear Dilatation Response of Fluids Containing Columns Plastic and Shear Relaxation Considered Dr. Bernd Wendlandt	GAC

*Not available for publication

TABLE OF CONTENTS (continued)

	Paper No.
Electro-Rheological Fluids Characterization by Dynamic Mechanical Thermal Analysis under Applied Fields Dr. R. E. Wetton and Dr. J. C. Duncan	GAD*

SESSION GB - Control Structure Interaction 2

On Piezoelectric Energy Conversion for Electronic Passive Damping Enhancement Dr. Donald L. Edberg, Dr. Andrew S. Bicos, and J. S. Fechter	GBA
The Need for Passive Damping in Feedback Controlled Flexible Structures Dr. Andreas von Flotow and D. W. Vos	GBB
Passive Control of a Flexible Planar Truss Using A Reaction Mass Actuator Capt. Steven G. Webb and Lt. David R. Lee	GBC

SESSION GC - Damping Indentification

A Identification Technique for Damped Distributed Structural Systems Using the Method of Collocation R. Chander, M. Meyyappa, and S. V. Hanagud	GCA
Correlation Techniques to Determine Model Form in Robust Nonlinear System Realization/Identification Greselda Stry and D. Joseph Mook	GCB
System Level Design and Analysis of Truss Structures Damped by Viscous Struts Dr. Y. C. Yiu	GCC
Damping Ratio Estimates from Autocorrelation Functions Prof. Luigi Balis-Crema and Prof. A. Agneni	GCD

*Not available for publication

TABLE OF CONTENTS (*continued*)

Paper No.

SESSION GD - Damping Materials

Dynamic Moduli of Fluorocarbon Compounds GDA*
Dr. Wayne T. Reader and Robert W. Megill

Passive Vibration Damping with Noncohesive Granular Materials GDB
Dr. Monen Abdel-Gawad

VEM Database Program GDC
Bryce L. Fowler

Measurement of the Mechanical Properties of Viscoelastics by the Direct Complex Stiffness Method GDD
Bradley R. Allen and Dr. David A. Kienholz

The Effect of Porosity on the Microstructural Damping Response of a 6061 Aluminum Alloy GDE
Jinmin Zhang, M. N. Gungor, and E. J. Lavernia

Damping Properties of Aliphatic Polyurethanes from 4, 4' - Dicyclohexylmethane Diisocyanate GDF
John D. Lee, Gilbert F. Lee, and Bruce Hartmann

An Apparatus for Measuring the Low Frequency Dynamic Characteristics of Materials GDG
Mona P. Khoury and Francis Olivier

SESSION HA - Composite and Metal Matrix

Controlling the Damping Behavior of Pitch-based Carbon Fibers HAA
Andrew J. Eckel and Steven P. Jones

Internal Damping of Metal Matrix Composites: A Technical Assessment HAB
Jacques E. Schoutens

Vibration Suppression of Thin-Walled Composite Tubes Using Embeded Viscoelastic Layers HAC
F. M. Belknap and Professor J. B. Kosmatka

*Not available for publication

TABLE OF CONTENTS (continued)

Paper No.

SESSION HB - Tubes and Shells

Directional Damping of the Global Vibration Modes of Tubular Structures by Constrained-Layer Treatments — HBA
Stanley S. Sattinger

Damped Response of Viscoelastic Thick Cylinders of Infinite Extent — HBB
Dr. Hamid Hamidzadeh, D. J. Nunez, and D. E. Chandler

SESSION HC - Circular Plates

Dynamic Analysis of Finite, Three Dimensional, Linear, Elastic Solids with Kelvin Viscoelastic Inclusions: Theory with Applications to Asymmetrically Damped Circular Plates — HCA
Prof. C. D. Mote, Jr. and I. Y. Shen

Modal Analysis of Kelvin Viscoelastic Solids Under Arbitrary Excitation: Circular Plates Under Moving Loads — HCB
I. Y. Shen and Prof. C. D. Mote, Jr.

Response of a Circular Plate with Patch Damping — HCC
Prof. Douglas Muster, Mahmoud Mezache, and G. H. Koopmann

SESSION IA - Viscous

Development of the PACOSS D-Strut — IAA
David Cunningham

Design, Analysis, and Testing of the PACOSS D-Strut Truss — IAB
Daniel R. Morgenthaler

An Advanced D-Strut — IAC
L. Porter Davis and Dr. Steve Ginter

*Not available for publication

TABLE OF CONTENTS (continued)

	Paper No.
Testing of a Viscous Damped Isolator Bradley R. Allen and David Cunningham	**IAD**
SESSION IB - Experimental Measurements	
The Effect of Source Impedance on Damping Measurements Using Resonance Dwell Testing Ralph E. Tate	**IBA**
The Dependency of Vibration Energy Dissipation on the Amplitude of Structural Motion Dale L. Jensen	**IBB***
Low-deflection Loss and Hysteresis Measurements on a Spacecraft Test Joint Eric M. Austin, James C. Goodding, and Timothy L. Flora	**IBC**
Damping Ratio Measurements in Kevlar Sandwich Samples Prof. Luigi Balis-Crema, Prof. A. Castellani, and Prof. A. Agneni	**IBD**
SESSION IC - Metals	
Characterization of the Damping Properties of High Damping Alloys Dr. Iain G. Ritchie and Z-L. Pan	**ICA**
Viscoelastic and Structural Damping Analysis Prof. Harry H. Hilton	**ICB**
Analysis of Strain Dependent Damping in Metals via Modeling of Material Point Hysteresis Dr. E. J. Graesser and C. R. Wong	**ICC**
Non-Obstructive Particle Damping Tests on Aluminum Beams Dr. Hagop V. Panossian	**ICD**

*Not available for publication

TABLE OF CONTENTS (continued)

Paper No.

SESSION JA - Experimental Measurements of Damping

Complex Dynamic Modulus of Nitinal-reinforced Composites JAA*
Dr. Amr M. Baz, R. Deigan, and Dr. J. Gilheany

Estimation of Nonproportional Damping from Experimental Measurements JAB*
Dr. T. K. Hasselman and Jon D. Chrostowski

Load Unit Deflection Correction for Forced Vibration Test System JAC
Kirk R. Biegler

SESSION JB - Friction

An Analytical Approach to Designing Friction Dampers in Turbomachinery Blading JBA
Joe Panovsky, D. Hendley, and R. MacKay

Micro Slip Damping Mechanism in Bolted Joints JBB*
Prof. M. Groper

SESSION JC - Analysis and Design 4

On a Theory of Complex Damping JCA
Z. Liang, M. Tong, and G. C. Lee

An Iterative Method in Dynamic Structural Analyses with Nonproportional Damping JCB
Dr. Wan T. Tsai and J.T. Leang

*Not available for publication

Statistical and Worst Case Evaluation of Orbital Jitter Reduction Using Passive Damping[1]

J. Molnar [2], D. Hill, and C. Stahle

GE Astro Space Division

The jitter responses of a damped and undamped precision mounting platform (PMP) are compared. The primary response is due to a platform mounted sensor which slews back and forth as it scans. The sensor torque profile is reduced to Fourier components, and the proximity of the platform resonances to the input frequencies is evaluated. If the resonance is close to a Fourier component, the mode is shifted to the Fourier frequency and the worst case jitter is computed. If the worst case response exceeds the jitter allowable, the limits above and below the Fourier frequency for shifting the mode that produces responses in excess of the allowable is determined. Then, assuming a Gaussian probability density function for the natural frequency, the probability of jitter exceedance is computed. Results show dramatic reductions in orbital jitter from the use of passive damping. Significant weight reduction is also achieved for the PMP analyzed with passive damping.

INTRODUCTION

The purpose of this paper is to present a method for evaluating orbital jitter and to describe the improvement in jitter that can be obtained with passive damping. Improved dynamic stability of remote sensing spacecraft payload mounting platforms (PMPs) is an evolving requirement resulting from improved sensor accuracy and increased satellite disturbances due to size and thermal effects. Jitter causes sensor distortions as a result of small angular motions occurring in a prescribed period of time often measured in seconds. It tends to be a high frequency phenomena that is beyond the control system bandwidth. Because of uncertainties in precisely predicting the orbital resonant frequencies of the spacecraft, "worst case" estimates that consider resonant excitation of critical modes are often used to estimate jitter. This paper describes an alternate statistical method of jitter predication that estimates the probability of exceeding a budgeted value when worst case estimates are excessive.

Passive damping provides a simple, reliable method of jitter reduction which is examined for a representative PMP. A USAF Wright Research and Development Center program, Damping and Metal Matrix Precision Structures (DAMMPS), is being

[1]This work has been performed under USAF-WRDC contract F33615-89-C3202.

[2]John Molnar, GE Astro Space, 234 Goddard Blvd., King of Prussia, Pa., 19406, (215) 354-6551

performed by GE Astro Space Division to develop and demonstrate PMP performance improvements that can be obtained with passive damping [1]. The PMP is selected from a current GE-ASD spacecraft program, Figure 1, so that a design that considers interdisciplinary constraints are satisfied. The platform is attached to the forward end of the spacecraft through three struts with ball end fittings and a ball fitting shear tie. This provides a kinematic arrangement that prevents PMP distortions due to spacecraft deflections. Nine sensors and instruments weighing 300 pounds and requiring precise alignment and pointing are mounted to this platform. The requirements are to provide a 15.5 Hertz resonant frequency and to limit jitter to 15 arcseconds peak. The benefits of damping are estimated by considering the structural weight required to provide equivalent jitter response to on-board disturbances. In addition, the damping required to achieve a budgeted jitter value is determined. Damped and baseline PMP configurations are used to quantify the benefits of damping.

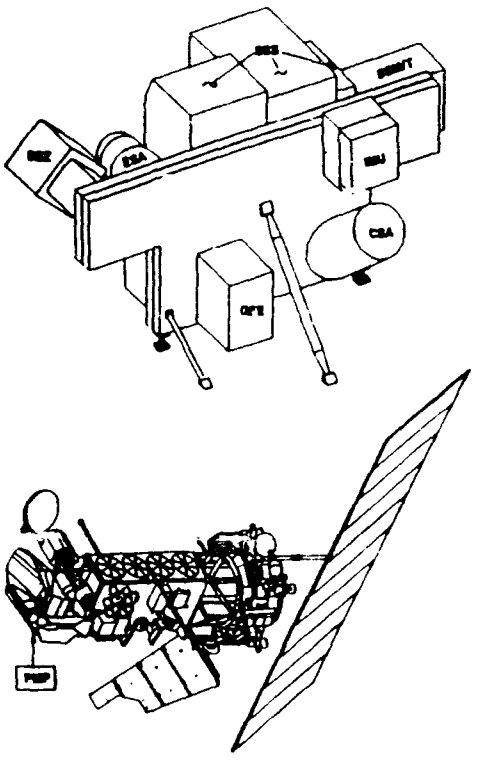

Figure 1. DAMMPS Platform

DAMPED AND UNDAMPED BASELINE PMP CONFIGURATIONS

The DAMMPS design for an advanced instrument mounting platform incorporates a viscoelastic material (VEM) layer for damping and metal matrix composite (MMC) facesheets for high specific stiffness. The configuration is a dual honeycomb sandwich composed of a viscoelastic center layer and honeycomb panels on either side. Each honeycomb panel consists of an aluminum core and MMC facesheets. The undamped baseline design is a traditional dip brazed aluminum eggcrate platform. Cross sections of both designs are shown in Figure 2.

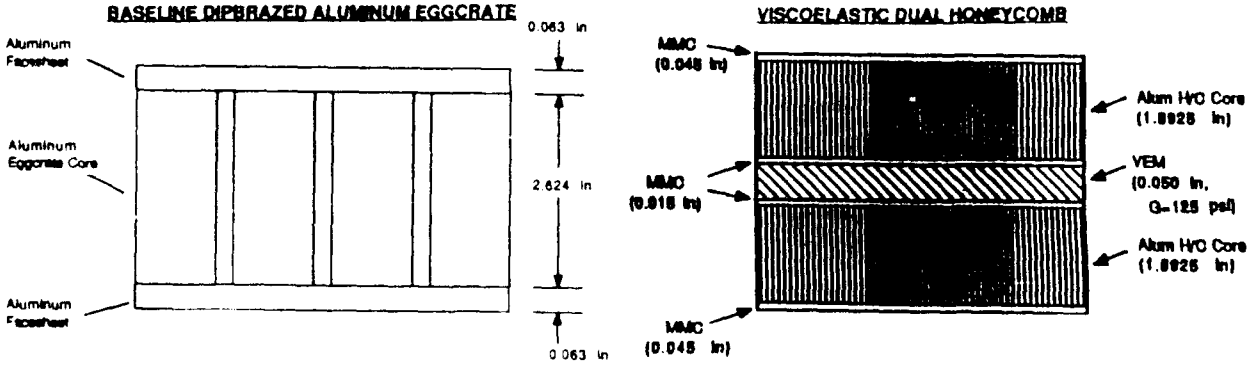

Figure 2. Cross Sectional Configuration

Finite element models were generated for both configurations. The dual honeycomb finite element model is composed of plate elements (CQUAD4) representing the honeycomb layers and solid elements (CHEXA) representing the VEM layer. Lumped masses positioned at the c.g. locations are used to simulate the instruments. The undamped eggcrate model, due to its single panel configuration, consists of only one layer of plate elements. Both models are shown in Figure 3.

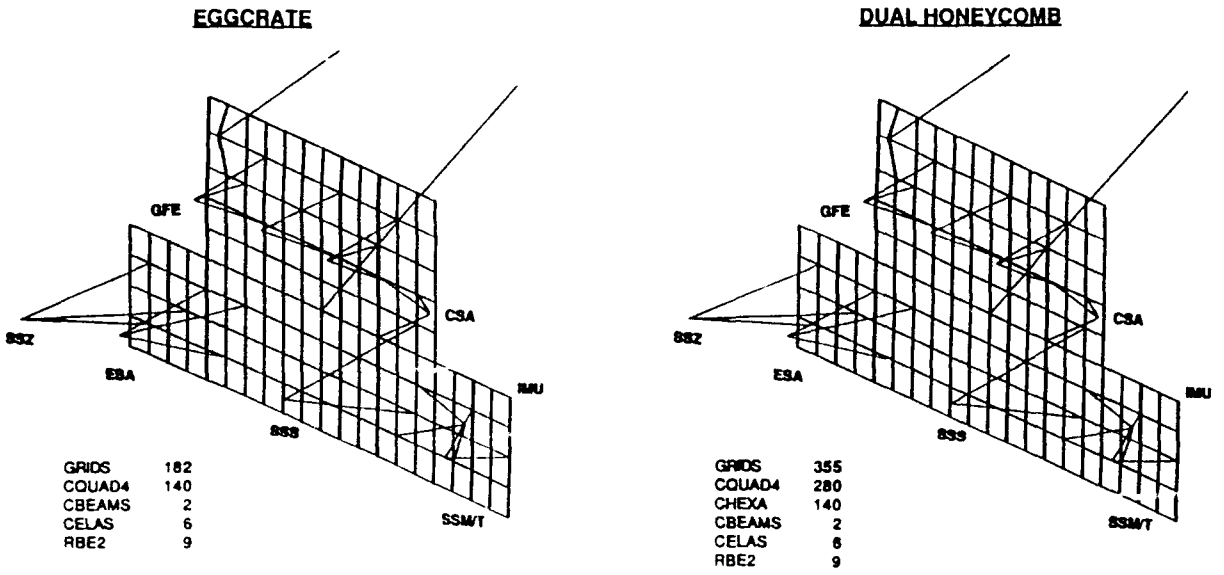

Figure 3. Finite Element Models

Modes and frequencies up to 200 Hz were generated using MSC/NASTRAN. Results, presented in Table 1, show that each design had approximately the same mass and stiffness. The primary difference between the two designs was the extent of damping. An orbital damping value of 0.002 c_c was assumed for the aluminum eggcrate platform. This damping value has been used on a variety programs incorporating precision mounting platforms where alignment tolerances are stringent. The visco-elastic dual honeycomb damping values were based on the modal strain energy method. Since development of low modulus VEM was still in progress, a material loss factor of 1.0 was assumed for the viscoelastic material. Subsequent development work of a low modulus VEM has indicated that this assumption was somewhat conservative [2]. The damping values for the most critical modes were calculated to be approximately 0.055 c_c.

Table 1. Results of FEM Analysis

MODE	EGGCRATE FREQUENCY (Hz)	EGGCRATE DAMPING (ς)	DUAL HONEYCOMB FREQUENCY (Hz)	DUAL HONEYCOMB DAMPING* (ς)
1	17.3	.002	16.8	.052
2	29.4	.002	25.2	.068
3	48.5	.002	40.0	.078
4	58.6	.002	48.3	.054
5	63.3	.002	56.0	.072
6	72.6	.002	62.9	.057
7	81.4	.002	[illegible] 5	.066
8	93.5	.002	69.1	.060
9	101.7	.002	80.3	.063
10	107.7	.002	86.3	.050
11	114.3	.002	88.0	.060
12	128.4	.002	94.8	.051
13	133.6	.002	102.0	.047
14	142.6	.002	107.2	.049
15	147.7	.002	112.4	.052
16	165.3	.002	116.0	.050
17	172.2	.002	121.6	.053
18	195.3	.002	142.2	.056
19			152.5	.053
20			183.3	.056

*DHC DAMPING VALUE BASED ON MODAL STRAIN ENERGY METHOD, $\eta_{VEM} = 1$

NOMINAL TRANSIENT JITTER ANALYSIS

A preliminary jitter study was performed using the predicted modes and frequencies for both designs. The transient jitter response of each instrument was determined for several input disturbances. The largest disturbance is the input torque to the Scanning Sensor Subsystem (SSS) which is located directly on the platform. The torque pulse, broken into its Fourier components in Figure 4, includes significant excitation as high as 102 Hz.

Results of the nominal jitter study are plotted in Figure 5. For each instrument, the undamped baseline response exceeded that of the damped design by a factor of 3.0 or more. For the SSZ instrument, which had the largest jitter response due to its c.g. offset and its relative location on the platform, the undamped eggcrate peak response exceeded that of the dual honeycomb by a factor of 6.0. Additionally, several instruments on the undamped platform had responses greater than the 15 arcsecond peak budget. The dual honeycomb design, due to its greater damping, experienced no response greater than the 15 arcsecond budget.

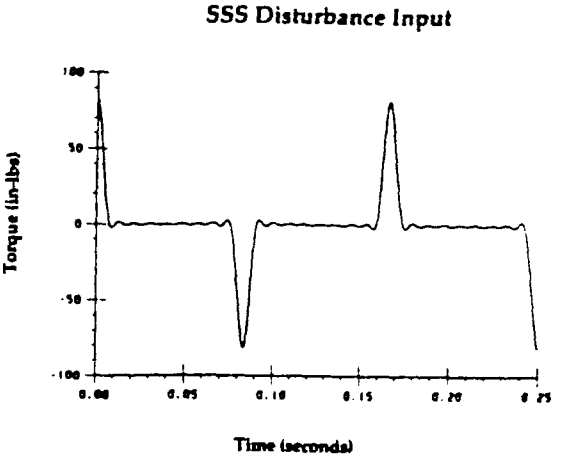

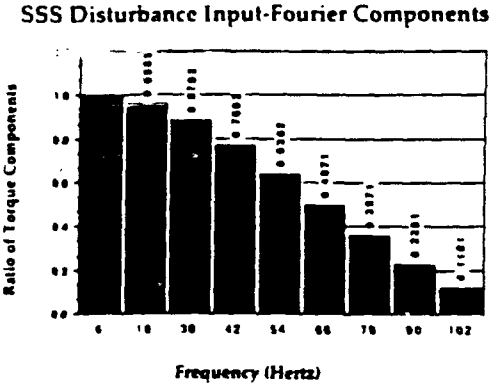

Figure 4. SSS Disturbance Input

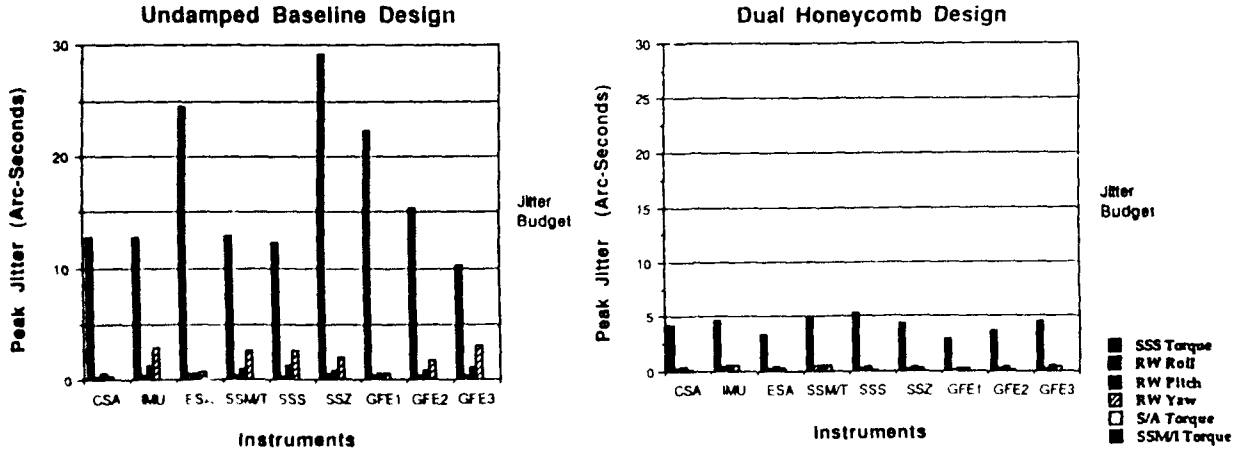

Figure 5. Nominal Jitter Response

In Figure 6, a plot of the transfer function for the DAMMPS dual honeycomb SSZ θ_x response due to a SSS torque input compares the relative location of the platform resonances and the Fourier frequencies of the SSS torque input. The magnitude of the torque pulse coupled with the proximity of the SSS Fourier frequencies to the fundamental modes of the structure account for the SSS input being the dominant disturbance. Because of this dominance, only the SSS input was considered in the worst case and statistical solutions.

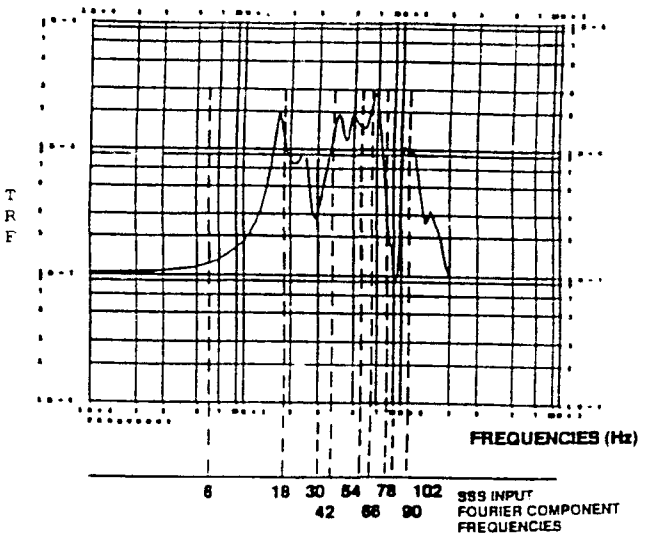

Figure 6 DHC SSZ θ_x Transfer Function to SSS Input

WORST CASE STEADY STATE JITTER ANALYSIS

Uncertainty in predicted structural natural frequencies causes an uncertainty in the estimated jitter response. If actual structural modes are closer to input disturbances than predicted, jitter responses can be significantly higher than the nominal (no shifted modes) estimates would indicate. Therefore, an approach that accounts for resonance response is required.

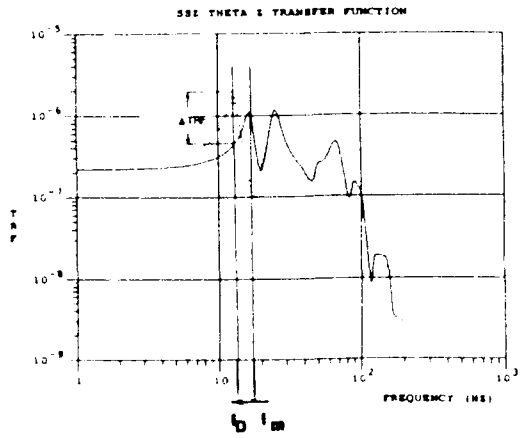

Figure 7 Mode Frequency Shift

Worst case jitter response is calculated by shifting modal frequencies to local input driving frequencies. For a mode with natural frequency f_M within 15 percent of a driving frequency f_D, f_M is shifted to f_D (see Figure 7) and the worst case jitter for a single mode shift is calculated. The mode is returned to its nominal position and another mode is shifted to its local driving frequency and peak jitter determined. The overall worst case peak jitter can be determined once each of the dominant structure modes have been shifted.

Worst case steady state results for each design are compared against their nominal values in Table 2. Note that the nominal results are steady state values and are thus slightly less than the transient values shown earlier. Only the θ_y and θ_z responses for the SSZ, ESA, and SSM/T instruments are presented. These responses were considered most critical based on results from the nominal transient analysis

The undamped baseline design, which is extremely sensitive to the location of the mode relative to the forcing function, has worst case responses that far exceed the jitter budget. The dual honeycomb design, with its higher damping values, is far less sensitive to resonant coupling. Worst case results were only slightly higher than their nominal values and none of the responses exceed the jitter budget.

Table 2. Results of Worst Case Jitter Analysis

RESPONSE	EGGCRATE		DUAL HONEYCOMB	
	NOMINAL (ARCSECS)	WORST CASE (ARCSECS)	NOMINAL (ARCSECS)	WORST CASE (ARCSECS)
SSZ θ Y	16.1	127.3	4.1	5.2
SSZ θ Z	13.9	121.9	4.5	6.7
ESA θ Y	13.3	99.6	3.2	3.3
ESA θ Z	10.2	92.3	2.9	4.6
SSM/T θ Y	6.6	105.2	4.5	6.1
SSM/T θ Z	13.3	87.1	4.1	6.0
JITTER BUDGET 15 ARCSECS				

A study was conducted to determine how much damping is required to limit the worst case response to less than the jitter budget. Assuming constant damping in each of the dual honeycomb modes, worst case jitter was calculated for several damping values. Results, shown in Figure 8, indicate that a small amount of damping can significantly reduce worst case jitter. Only 1.5 percent damping (0.015 c_c) is required in the critical modes to limit the worst case response to within the jitter budget. At higher damping values, the jitter response approaches the static solution and further damping does not significantly affect the total response.

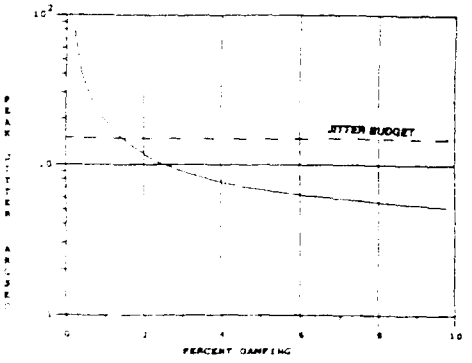

Figure 8. Worst Case Peak Jitter Versus Damping

STATISTICAL JITTER ANALYSIS

For the undamped eggcrate, nominal results indicate that the jitter response is less than the budget for most instruments. Worst case results show high jitter response. A statistical approach was implemented to ascertain the likelihood of any worst case occurrence and to quantify the design's dependability. The statistical method is based on the sensitivity of the jitter response relative to the modal frequencies.

Two assumptions were made in the statistical solution. First, it was assumed that 90 percent of the modes can be predicted to within 10 percent accuracy. This assumption, based on past correlation of modal tests and analysis, was used to generate a Gaussian distribution curve with the predicted modal frequency f_M being the mean value and the area under the curve within a 10 percent bandwidth of f_M being equal to 0.90 (see Figure 9). By assuming a Gaussian distribution, this translates into predicting 98.6 percent of the modes to within 15 percent of the

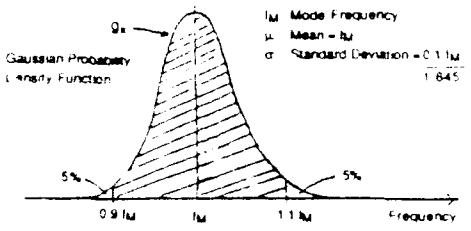

Figure 9 Gaussian Probability Density Function for Modal Frequency

measured test frequencies, 90 percent of the modes to within 10 percent, or 60 percent of the modes to within 5 percent. The second assumption states that the modal frequency predictions are statistically independent. The meaning of this assumption is that the probability of predicting one mode accurately is independent of how another is predicted, just in the same way that the probability of predicting what is thrown on a second roll of a die is independent of what was thrown on the first.

The purpose of the statistical solution is to account for the sensitivity of the jitter response relative to the modal frequencies. The assumption of statistically independent modal frequencies enables the sensitivities of several different modes to be combined to obtain a final statistical solution. If one mode dominates the response, the results of that modes sensitivity analysis will dominate the statistical solution thus making the statistically independent assumption meaningless. The DAMMPS platform response was dominated by the first two modes. Thus, the assumption, although important, was not a critical factor in the solution.

To begin the statistical solution, the selected mode's worst case solution was first determined. As described in the worst case analysis, a mode with natural frequency f_M within 15 percent of a driving frequency f_D is shifted to f_D and the worst case jitter for a single mode shift is calculated. If the worst case results exceed the jitter budget while the nominal value is less than the jitter budget, then there can be found an upper (f_U) and lower (f_L) shifted frequency value which results in jitter equal to the allowable. As an example, peak jitter as a function of the fundamental modal frequency for an instrument on the undamped platform is shown in Figure 10. The nominal response is shown to be less than the allowable. When the modal frequency is shifted to the driving frequency, the worst case response exceeds the allowable. The frequency limits for shifting the modes that produce responses in excess of the allowable are denoted by f_L and f_U. Assuming the Gaussian probability function shown in Figure 11 for the natural frequency f_M, the area under the density function bounded by f_L and f_U is the probability of jitter exceedance for that particular mode.

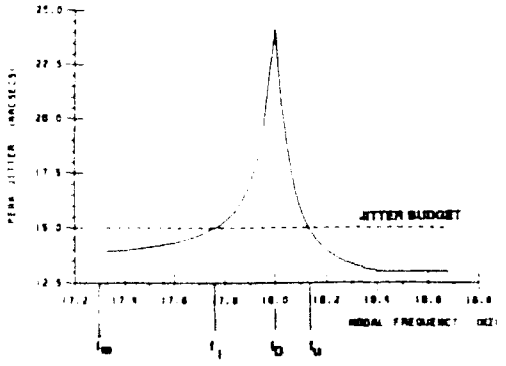

Figure 10 Peak Jitter Versus Fundamental Modal Frequency

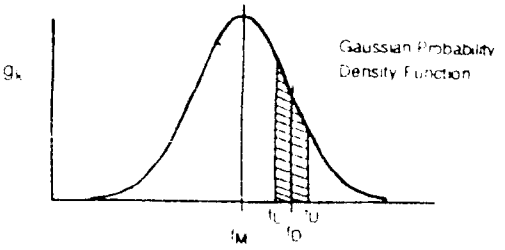

Figure 11 Probability of Jitter Exceedance Due to Single Mode Shift

Now, let $P[A_i]$ be the probability of the i^{th} event that one mode when shifted towards a specific harmonic results in jitter greater than the allowable. The complement of $P[A_i]$ is defined as

$$P[A_i]^C = 1 - P[A_i]$$

where $P[A_i]^C$ represents the probability that event A_i will not occur. Then, assuming that each A_i event is statistically independent, the probability that none of the A_i's will occur, $P[A]^C$, is given by the product of all the $P[A_i]^C$'s:

$$P[A]^C = \Pi_i P[A_i]^C$$

The probability of at least one worst case occurring, P[A], is given by the complement of $P[A]^C$:

$$P[A] = 1. - P[A]^C$$

P[A] represents the probability of exceeding the jitter budget based on all the individual mode frequency shifts. Note, that in the higher frequency ranges (above 50 Hz), the modal frequency error causes modes to be shifted to forcing frequencies both above and below its nominal value. If any single mode results in jitter values greater than the allowable in more than one harmonic, they are counted as distinct events for the statistical solution.

A plot showing jitter allowance versus the probability of exceeding the allowance is shown in Figure 12 for the undamped eggcrate and damped dual honeycomb (DHC) SSZ θ_z response. The undamped eggcrate, due to its sensitivity to resonance coupling, has a fairly wide range of possible jitter responses. The worst case response was 120 arcseconds, however the probability of this response is less than 1 percent. There is a 45 percent probability of exceeding the 15 arcsecond peak allowance, a 10 percent probability of exceeding 30 arcseconds peak, and a 5 percent probability of exceeding 60 arcseconds peak. Considering the high degree of reliability required for a spacecraft, the undamped eggcrate is not considered an adequate design. The damped dual honeycomb, which was much less sensitive to resonant coupling than the undamped eggcrate, has a small range of possible jitter responses which accounts for the nearly vertical DHC line when plotted on the same scale as the eggcrate. The worst case response was 6.7 arcseconds, significantly less than the 15 arcsecond allowance, making the dual honeycomb platform a viable concept with regard to orbital jitter.

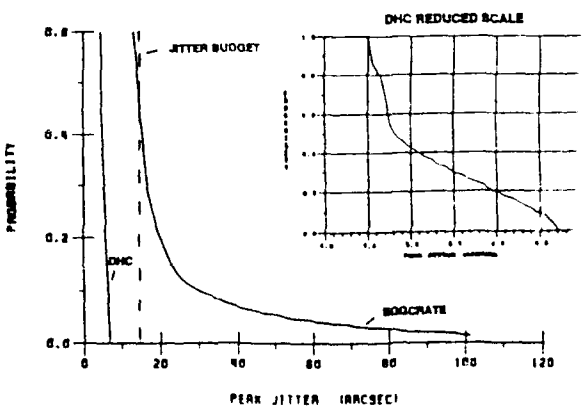

Figure 12 Probability of Exceeding Jitter Allowance

JITTER WEIGHT STUDY

The traditional method of reducing orbital jitter is to stiffen the structure. The approach taken in the DAMMPS program is to add passive damping. A weight study was conducted to determine which method, stiffening the structure or adding passive damping, is a more weight effective method for reducing orbital jitter.

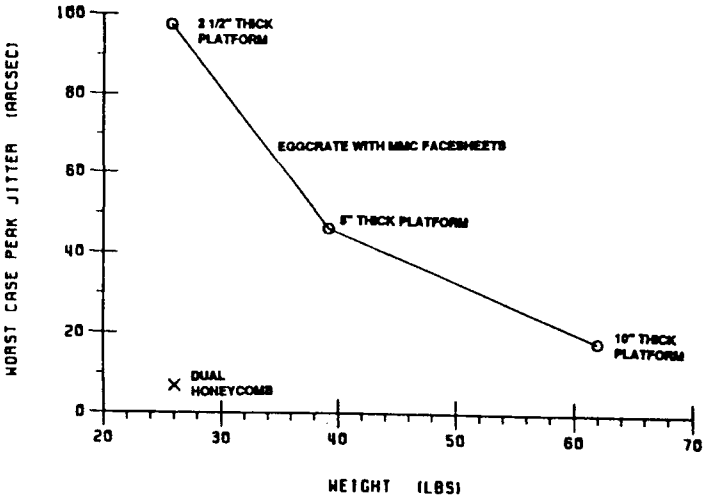

Figure 13. Worst Case Jitter Versus Platform Weight

The weight study was performed on an undamped eggcrate design with MMC facesheets. MMC facesheets were added to the eggcrate in order to remove any benefits the DAMMPS designs had due to their MMC facesheets. The eggcrate core thickness was increased stiffening the structure in the most weight effective manner. Worst case jitter was determined and plotted against the structure weight. The plot, shown in Figure 13, compares the stiffened eggcrate to the dual honeycomb design. Stiffening the eggcrate does reduce worst case orbital jitter, however, when compared to adding passive damping as done on the dual honeycomb design, there is a much greater weight penalty.

CONCLUSIONS

A worst case and statistical jitter analysis were performed on a viscoelastic dual honeycomb and an undamped baseline design. The results of the analysis clearly show the superiority of the damped design with regard to orbital jitter. The response of the instruments as a result of the input disturbances is significantly less for the damped designs. The damped structures are insensitive to resonant coupling, creating a robust design in that the structure modes do not have to be designed around the input disturbances.

A weight study conducted on the undamped eggcrate clearly demonstrated that adding passive damping is a much more weight effective method of reducing orbital jitter as compared to the traditional method of increasing stiffness. In addition, a small amount of damping (only 1.5 percent for the DAMMPS platform) may be adequate to limit even the worst case response to within an acceptable value.

Finally, using the statistical approach to describe jitter results provides additional insight for evaluating worst case responses. It allows us to assess jitter as a function of

modal frequency and its relative location near a forcing frequency. The closer a frequency is to a forcing harmonic, the more likely a worst case will occur. At the same time, the magnitude of the jitter response for a particular mode and the overlapping shifts at higher frequencies are considered.

REFERENCES

1. Hill, D., Stahle, C., and Staley, J., "Evaluation of Damping Concepts for Precision Mounting Structures", Damping '91 Conference Proceedings, Feb., 1991.

2. Kirshenbaum, Dr. S., Hill, D., and Stahle, C., "Development of Low Modulus Damping Material for Precision Mounting Platforms", Damping '91 Conference Proceedings, Feb. , 1991.

LMSC DAMMPS PROGRAM STATUS

Warren Hoskins
Y. C. Yiu

Structural Dynamics, Space Systems Division, Dept. 62-18, B/104
Lockheed Missiles & Space Company, 1111 Lockheed Way, Sunnyvale, CA 94089
Telephone : 408-742-6560

ABSTRACT

This paper summarizes the activities of the Damping and Metal Matrix for Precision Structures (DAMMPS) Program at Lockheed Missiles & Space Company. The objective of the program is to demonstrate dimensional precision for flexible aerospace structures undergoing dynamic and thermal disturbances. The approach, selection of demonstration articles, requirements are presented. The preliminary engineering activities, current achievements and future plans are also discussed.

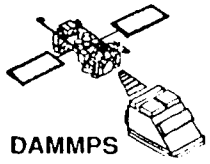

Lockheed

LMSC DAMMPS PROGRAM STATUS

Damping And Metal Matrix for Precision Structures

Warren Hoskins
Y.C. Yiu

Lockheed Missile & Space Company, Inc.
Sunnyvale, Calif.

DAMPING '91
February 13-15, 1991
San Diego, California

The design requirements of most precision mounting platforms on satellites include both vibrational and thermal environments which dictate the use of advanced materials. For satellite programs the risks are high to insert these new advanced materials which do not have a long heritage on previous satellites. In recognition of this reluctance to use advanced materials the Wright Research And Development Center - Flight Dynamics Lab has instituted a program to introduce both metal matrix composites and passive damping technology in a parallel development effort to a structure on an on-going satellite. This program will then reduce the risk of introducing this technology on a later satellite. Lockheed Missiles & Space Co. (LMSC) has been awarded one of these contracts and this paper is a report of its progress. We have selected as our Demonstrating Structural Article (DSA) a high precision mounting platform which supports a sensor suite for the attitude control system of one its communication satellite programs. The DSA is basically a small box (about 12 inches on a side) which is attached to a simulated satellite bus panel. The passive damping requirements and design was derived using the Modal Strain Energy Method developed and validated during previous work on the PACOSS and RELSAT programs.

The current status of the program is the completion of the preliminary design phase which includes several trade studies as reported in an accompanying paper. Two potential candidate viscoelastic materials (VEM) have been characterized over a broad frequency and temperature range which is also being reported in an accompanying paper. In addition the candidate isotropic continuously reinforced GrAl panel was tested to validate the manufacturing process. The results of all the testing for both the VEM and the GrAl demonstrate the design is on solid ground. In the next phase twelve additional viscoelastic materials will be characterized, joining techniques will be validated and the final design will be optimized for thermal distortion, thermal conduction and damping.

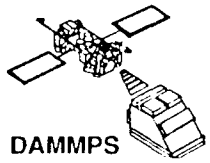

OBJECTIVE AND APPROACH

Lockheed

- DAMMPS OBJECTIVE
  - TO DEMONSTRATE DIMENSIONAL PRECISION FOR FLEXIBLE AEROSPACE STRUCTURES UNDERGOING DYNAMIC AND THERMAL DISTURBANCES.
- DAMMPS APPROACH
  - DESIGN / ANALYZE, FABRICATE, AND TEST A DEMONSTRATION STRUCTURAL ARTICLE (DSA) THAT REQUIRES PASSIVE VIBRATION DAMPING (PVD) AND METAL MATRIX COMPOSITES (MMC)
  - DESIGN, FABRICATE AND TEST AN ALUMINUM BASELINE DSA
  - ASSESSMENT OF THE BENEFITS OF PVD AND MMC FOR FUTURE SPACECRAFT
  - EXPAND THE PVD DATABASE
  - PARTICIPATE IN INFORMATION TRANSFER AT TECHNICAL CONFERENCES AND WORKSHOPS

The goal is to have available at the end of the DAMMPS program a true demonstration of what passive damping and metal matrix materials can offer a satellite program, not as an afterthought to fix a design shortcoming, but as a developed design technology that is ready to be implemented at the conceptual design phase of any program. The DAMMPS Program objectives will result in a new maturity in the technology areas of passive damping and metal matrix materials for spacecraft applications.

The approach is to construct a component from an existing satellite program as a Demonstration Structural Article (DSA) and validate the design via a test. The DAMMPS program is divided into six technical tasks. The first three tasks are associated with the development of the DSA. Task 1 is Preliminary Design, Task 2 is the Detail Design Development and Task 3 is Fabrication of the DSA and an aluminum prototype. Both material coupon characterization tests and component tests are an integral part of these tasks.

The final three tasks are associated with the verification of the DSA design via testing, assessment of the design, analysis, fabrication, and applicability to future satellites and the final task is to distribute the findings to the technical community.

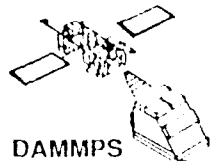

LMSC DAMMPS DSA

Lockheed

MILSTAR COMPONENT

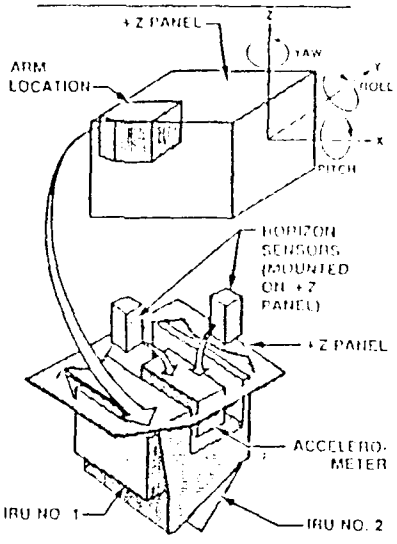

ATTITUDE REFERENCE MODULE (ARM)

- ARM IS THE CRITICAL SENSOR FOR THE ATTITUDE CONTROL SYSTEM
- STRINGENT RELATIVE ALIGNMENT REQUIREMENT BETWEEN THE MOUNTED COMPONENTS
- CRITICAL ISSUES FOR THE ARM ARE:
  - -CTE - SOLAR HEATING
  - -DAMPING - 4 RWAs
  - -HEAT CONDUCTION - IRUs GENERATE HEAT
- HIGH PAYOFF FOR THE DSA
  - -LOW CTE
  - -HIGH DAMPING
  - -HIGH HEAT CONDUCTION
- SPINOFFS
  - -BSTS
  - -SSTS

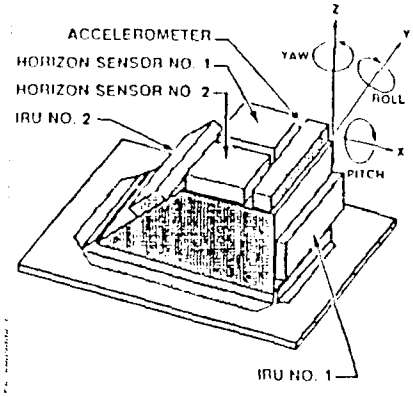

DEMONSTRATION STRUCTURAL ARTICLE (DSA)

The Altitude Reference Module (ARM) of an on-going Air Force Satellite program which is currently in the hardware phase was selected because it provides the greatest design maturity and detailed knowledge of both the thermal and vibrational environments of interest. The configuration of the ARM is somewhat complex. A modified version of the ARM was selected to be the DSA with a few simplifications which preserved its salient features. The traceability of the DSA to the ARM is presented in this viewfoil.

The ARM is an aluminum structure designed to be stiff and to conduct heat away from the boxes/sensors mounted to it. These sensors are the source of all attitude knowledge for the spacecraft:

1. two horizon sensors (HSs),
2. two inertial reference units (IRUs), and
3. one set of accelerometers.

Since they frequently operate simultaneously, it is important that the sensors do not send contradictory information to the attitude control computer - a situation which could occur if the boxes became misaligned with respect to each other. From a flow-down of system-level requirements, tolerable alignment errors between the several sensors are known. The principal purpose of the ARM is to maintain relative alignment of the sensors while conducting heat from the sensors, especially the IRUs. This means that any structure functionally similar to the ARM should be *at least* as thermally conductive as the original aluminum structure. The modified version of the ARM referred to as the DSA possesses all of these qualities, whether fabricated of aluminum or metal matrix composites.

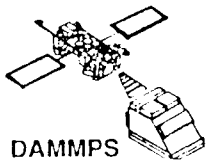

DSA DESIGN

Lockheed

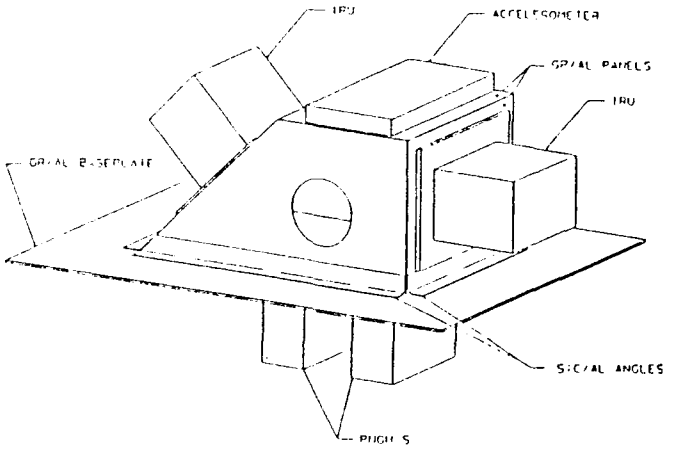

DESIGN FEATURES
BASEPLATE: Gr/Al ISOTROPIC 80 mil PANEL
BOX: Gr/Al ISOTROPIC 60 mil PANEL
ANGLES: DISCONTINUOUS SiC/Al 1x1x0.060
MASS SIMULATORS: FULL WEIGHT MATCH CG ALUMINUM FREQ. 150 Hz
JOINING: STRUCTURAL BOND PERFERRED

Graphite aluminum was selected for the primary structural material because of its high stiffness to weight ratio, relatively low CTE, no outgassing, and high thermal conductivity. Specifically, P100 fiber in an aluminum matrix using a quasi-isotropic fiber orientation was selected because it is the lowest cost fiber which meets the requirements and P100/Al has a substantial experience database in the industry. Since this graphite aluminum cannot be formed, the DSA is made of flat plates. To accomplish the joints between the plates, discontinuously reinforced silicon carbide aluminum (SiC) angles are used. At a 0.25 volume fraction of SiC particulate for reinforcement, a stiffness similar to that of titanium is achieved at about the same weight as aluminum. This material is also readily extruded and can be applied to the DSA with little or no development.

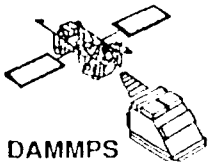

DAMPING REQUIREMENTS

Lockheed

- 19 DYNAMIC RESPONSE QUANTITIES IN 3 INPUT DIRECTIONS = 57 EVALUATIONS
- REPRESENTATIVE TRANSFER FUNCTIONS OF RELATIVE ALIGNMENT DUE TO BASE SHAKE

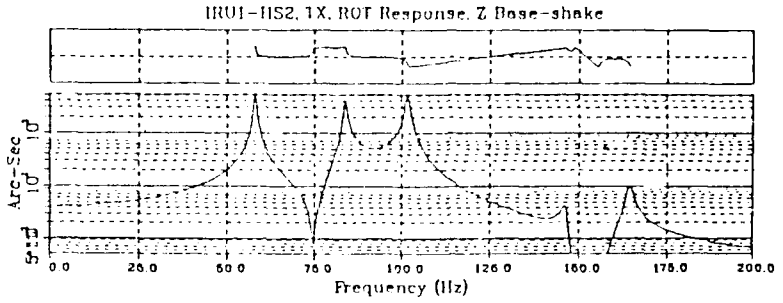

- DAMPING REQUIREMENTS

MODE NO.	1	2	3	4
DAMPING(%)	4.0	3.5	4.0	1.2

The baseline DSA was designed to capture the same dynamics as the ARM. The mass simulators and various panels were sized to place the first four modes near those of the ARM as extracted from a system level modal test of the satellite.

The DSA FEM (Finite Element Model) was subjected to an appropriate base excitation to identify the most critical modes contributing to the response. The baseline modal damping level is assumed to be 0.5% of critical for this preliminary analysis. Transfer functions were determined relating base shake inputs in the x, y, and z directions to each of the pertinent response quantities (i.e., relative alignments, component base inputs). These transfer functions represent dynamic responses to a steady-state, unit-amplitude (in g's) base shake input at any given frequency. Data thus obtained were scaled to 0.004 g to determine the responses at the actual input levels.

As expected, several different analytical modes produce dominant responses. The modal damping requirements were determined from the peak responses in each of the transfer functions when compared to the appropriate requirement. A total of 19 response quantities with 3 input directions yielded 57 plots which were examined in this manner. The lowest four modes dominated each response. Their damping values were from mode 1 to mode 4, to be 4.0%, 3.5%, 4.0%, and 1.2%, assuming that the structure is forced by steady-state input and only damping is used to bring the responses to a level consistent with the requirements.

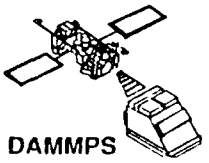

DAMMPS SCHEDULE

Lockheed

TASKS	1989	1990	1991	1992	1993	1994
MONTHS AFTER START	3	15	27	39	51	54
1. PRELIMINARY DESIGN	1		20			
2. DETAIL DESIGN			21	34		
3. FABRICATION				35	44	
4. TESTING					45	53
5. ASSESSMENT						54
6. INFORMATION TRANSFER	1					54

The DAMMPS Program schedule lists the tasks and shows the progress of each task for the four and half years program duration. The numbers appearing above the bars represent the months after the start of contract award. At the conclusion of the first year and a half the Preliminary Design task is nearing completion with material selection, sizing and coupon testing finalized. In addition the Information Transfer task is progressing on schedule with the generation of several documents, participation at two workshops and preparation of three technical papers. The contract is on schedule and with the anticipated continued funding will remain on schedule.

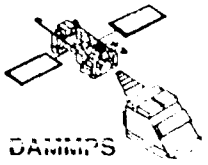

PRELIMINARY DESIGN ACTIVITIES

Lockheed

- REQUIREMENTS
  - ALUMINUM (DAMPING/CTE/HEAT CONDUCTION)
  - MMC ONLY (DAMPING)
- DESIGN / ANALYSIS
  - ALUMINUM
  - MMC ONLY
  - DAMPED MMC
- MATERIAL SELECTION
  - METAL MATRIX COMPOSITE
  - DAMPING (FREQUENCY AND TEMPERATURE)
- MATERIAL TESTING
  - METAL MATRIX COMPOSITE (2 PANELS)
  - DAMPING (2 CANDIDATE VEMs)

REQUIREMENTS: In order to derive requirements a finite element model of the aluminum baseline DSA was constructed and subjected to the vibrational environment and the thermal temperature distribution. The relative alignment between the sensors was exceeded and the damping and CTE requirements were set by linearly scaling the Q factor and CTE to meet the specified requirements.

DESIGN/ANALYSIS: With the requirements set, several metal matrix designs were examined and evaluated trying to balance the constrained layer damping placement and metal matrix manufacturing limitations on fiber lay-up thickness to achieve isotropic properties which prevent distortions during the autoclave curing cycle.

MATERIAL SELECTION: While early trades were made to select the viscoelastic and GrAl material the feasibility of using each have to be based on test data which is not readily available. The layup design of composites couple with the selected manufacturing process and require test validation. Current viscoelastic characterization material data for space applications is very sparse and also must be generated before the viscoelastic material selection can be finalized.

MATERIAL TESTING: Two viscoelastic materials were characterized over a broad frequency and temperature range validating the material selection. A panel of GrAL was inspected via C-scan and mechanically tested to ensure the properties agree with the rule of mixture values. All test data was within acceptable bounds validating the panel material selection.

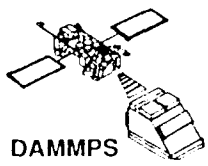

PRELIMINARY DESIGN ACCOMPLISHMENTS

Lockheed

ITEM	STATUS	DESCRIPTION
1	√	MASTER PLANNING AND CONTROL DOCUMENT
2	√	BASELINE DESIGN REQUIREMENTS
3	√	PRELIMINARY STRUCTURAL TEST PLAN
4	√	DAMPING MATERIAL TEST PROCEDURE
5	√	FIRST SEMI-ANNUAL TECHNICAL REPORT
6	√	SECOND SEMI-ANNUAL TECHNICAL REPORT
7	√	PRESENTED DAMMPS PAPER AT 61th SHOCK AND VIBRATION SYMPOSIUM

Note: √ means item is completed

All of the Preliminary Design activities have been documented and presented at Workshops and technical conferences. The above is a list of all the documents that have been generated to date. In addition there are two papers being presented at the Damping 91 Conference documenting the design trades leading to the current design and the results of the VEM characterization testing. These documents are available upon request from Mike Zeigler, FIBAA of WRDC.

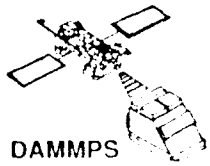

CONCLUSIONS FUTURE PLANS

Lockheed

- CONCLUSIONS
  - o CONCEPTUAL DESIGNS ARE COMPLETE
  - o MATERIAL SELECTION OPTIONS ARE UNDERSTOOD
  - o MMC AND VEM ARE A GOOD SOLUTION FOR HIGH PRECISION SENSOR PLATFORMS (WEIGHT, STIFFNESS, CTE, AND DAMPING)
  - o MATERIAL TESTING IS WELL UNDERWAY (VEM AND MMC)

- FUTURE PLANS - DETAIL DESIGN TASK
  - o INTEGRATED THERMAL/DYNAMIC MODEL FOR OPTIMIZED DESIGN
  - o FABRICATION TESTING - JOINTS AND INTEGRATED MMC/VEM
  - o COMPONENT TESTING - INTEGRATED MMC/VEM SAMPLES

Since the beginning of the contract significant progress has been made in accomplishing the goals of the Preliminary Design Task. Currently trade studies have been completed for both the aluminum and MMC DSAs. This includes material selection, damping treatment, and member sizing. Two candidate VEMs have been characterized and reported over the appropriate frequency and temperature ranges. A sample panel of the candidate graphite aluminum MMC has been tested to extract the mechanical properties validating the manufacturing process.

During the next phase our plan includes the testing of twelve additional VEM materials, integrated design optimization and component / fabrication testing. The integrated design optimization will include the simultaneous effects of MMC and VEM coupled together with the thermal and vibrational environments. The detailed finite element model accounts for the strain energy distribution and a thermal model accounts for the VEM altered thermal paths to calculate the thermal conductivity effects. These results will be presented to a formal design review prior to going into the fabrication phase.

Damping of Precision Metal Matrix Trusses

Presented at : Damping '91
February 13-15, 1991
Catamaran Hotel
San Diego, CA

S. S. Simonian
14 February 1991

AGENDA

- OBJECTIVE
- MOTIVATION
- STRUCTURE CONFIGURATION
- MATERIALS
- TECHNICAL APPROACH
- DISTURBANCES
- DESIGN CONSIDERATIONS
- ANALYSIS RESULTS

OBJECTIVE

DAMMPS Program :
Damping and metal matrix for precision structures

TO DEMONSTRATE THE DIMENSIONAL PRECISION OF DAMPED AEROSPACE STRUCTURES UNDERGOING DYNAMIC AND THERMAL EFFECTS

MOTIVATION

- **WHY design damping into structures ?**
- **Inherent damping of spacecraft: Is it sufficient ?**

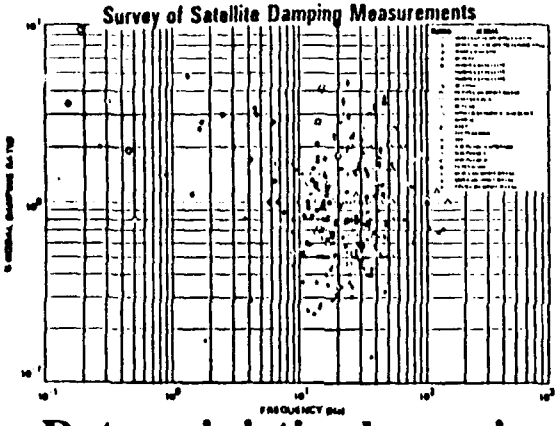

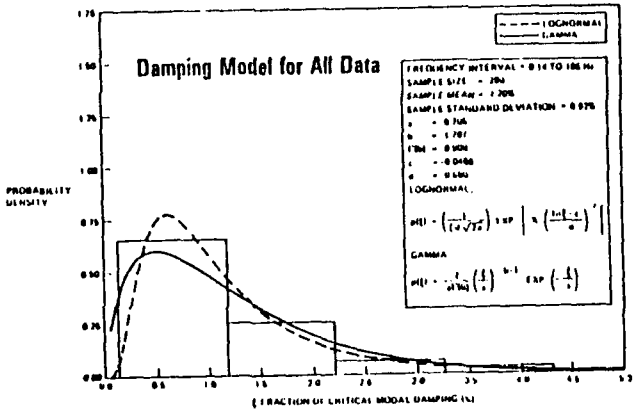

- **Deterministic dynamic performance analysis model :**

Modal damping = 0.5% (mean - 2 sigma)
= 0.2% (mean - 2.5 sigma)

- **Often damping requirements are 5-20% to meet performance measures**
- **This provides the rationale for the need for integral damping design in spacecraft**

WHY MMC & DISCRETE DAMPERS ?

- **Application: Generic Truss Structures**

- **Approaches: Discrete → Links, Joints**
  Distributed → Free layer, Constrained layer

- **Tubular truss structures**

  Requirements:
  1. **High precision & stability (hysteresis, moisture, CTE)**
  2. **High specific stiffness**
  3. **High damping**
  4. **Simple and reliable design & analysis**

  Solution:
  - **Items 1 & 2 - MMC Materials**
  - **Items 3 & 4 - DISCRETE dampers**

- **Thus for tubular precision truss structures MMC materials and discrete VEM dampers provide the best solution for above requirements**

STRUCTURE CONFIGURATION

- Precision Truss Structures

  - Widely used structural system with superior weight-stiffness characteristics

- Traceable to large number military and scientific space projects

DAMMPS

Truss Assembly

TRW

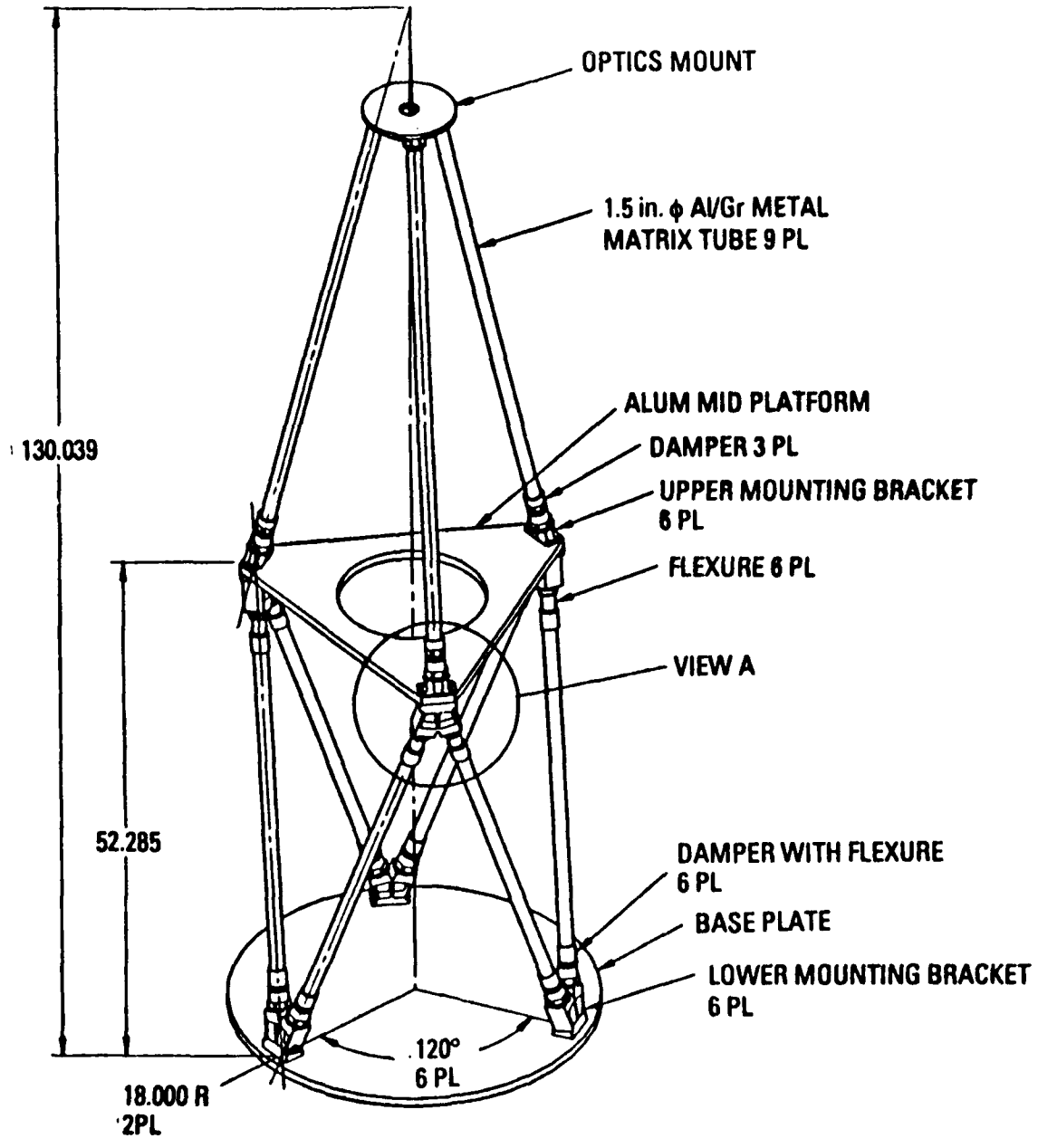

DAMMPS DEMONSTRATION STRUCTURAL ARTICLE (DSA)

DAMMPS

Mid Platform

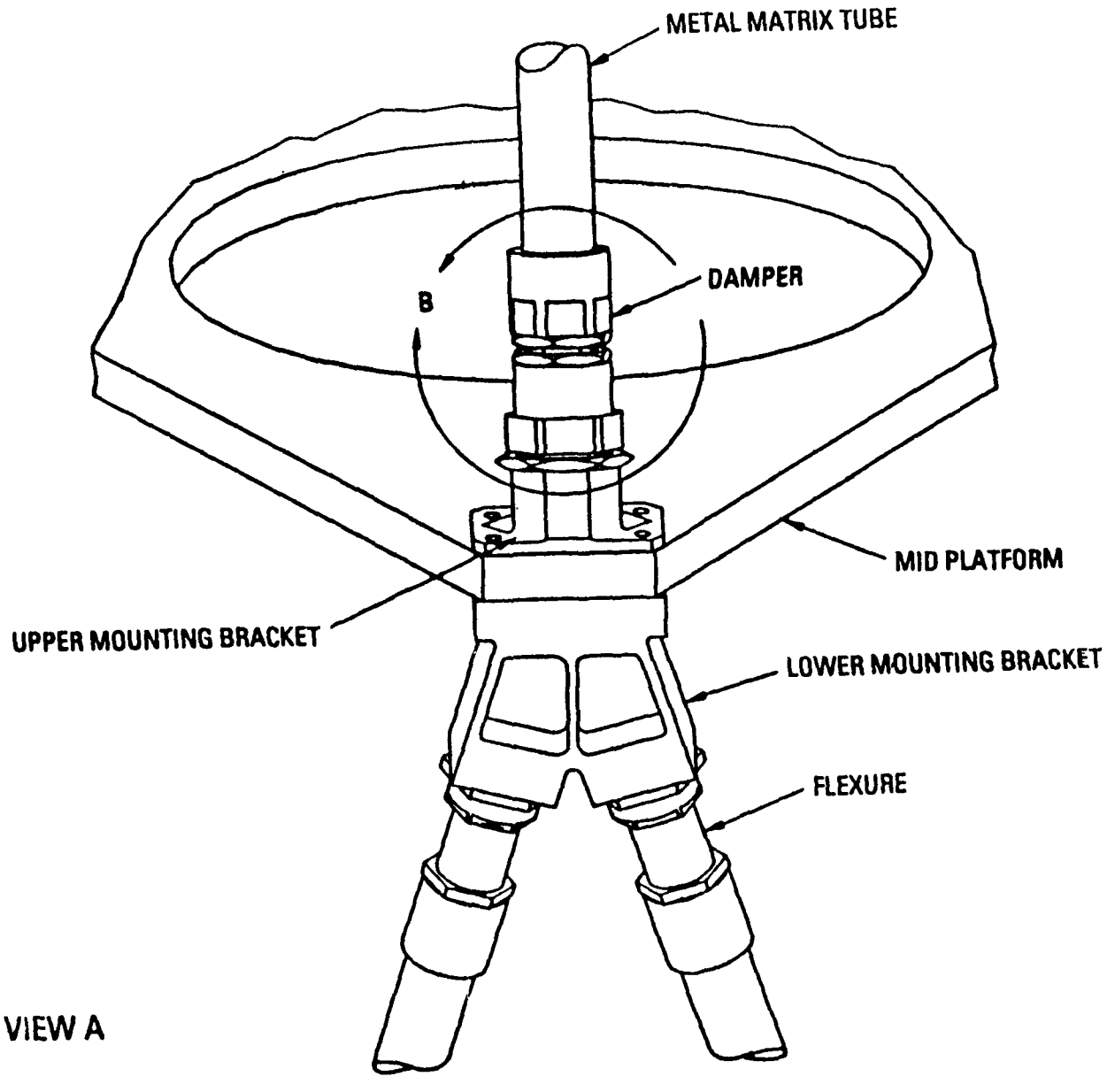

DAMMPS

Damper

TRW

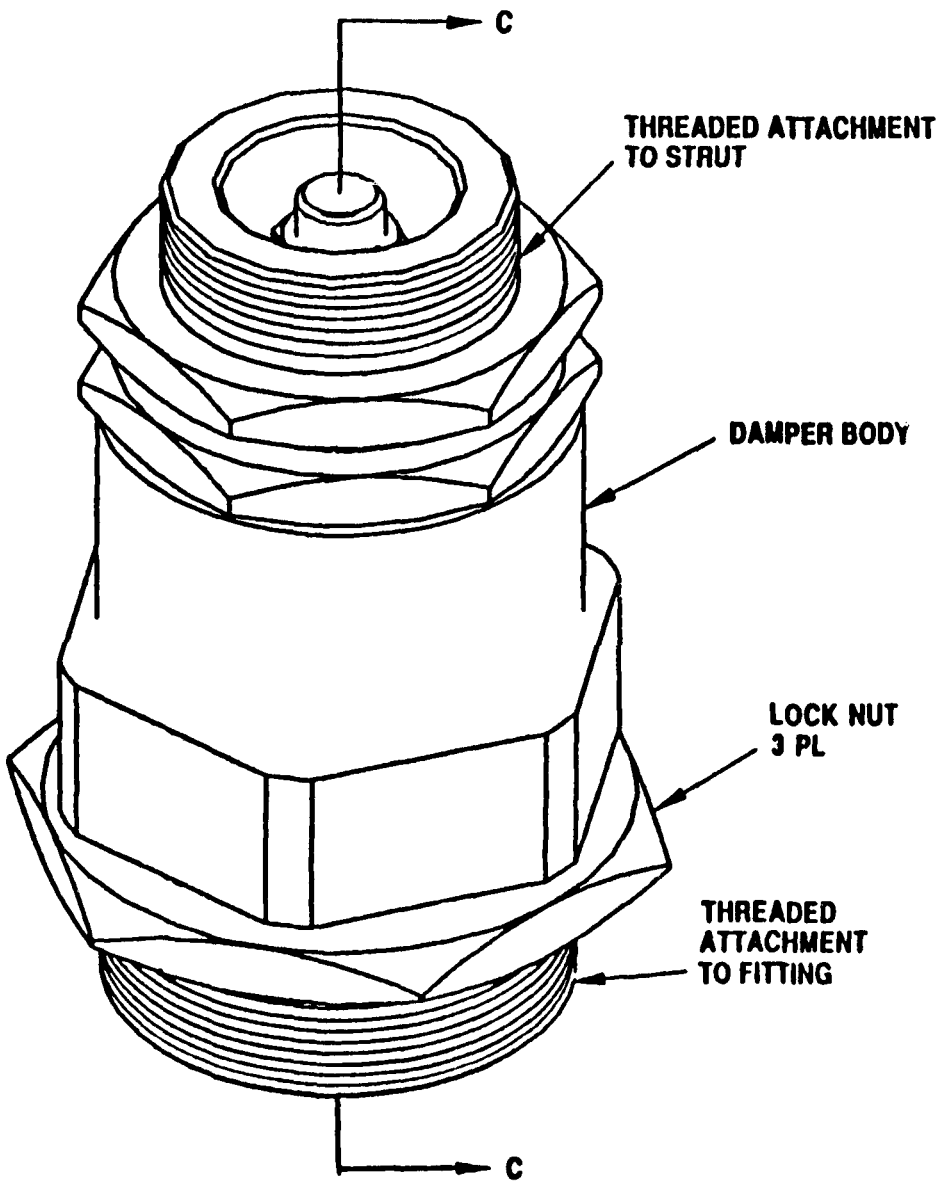

VIEW B

Damper Section View

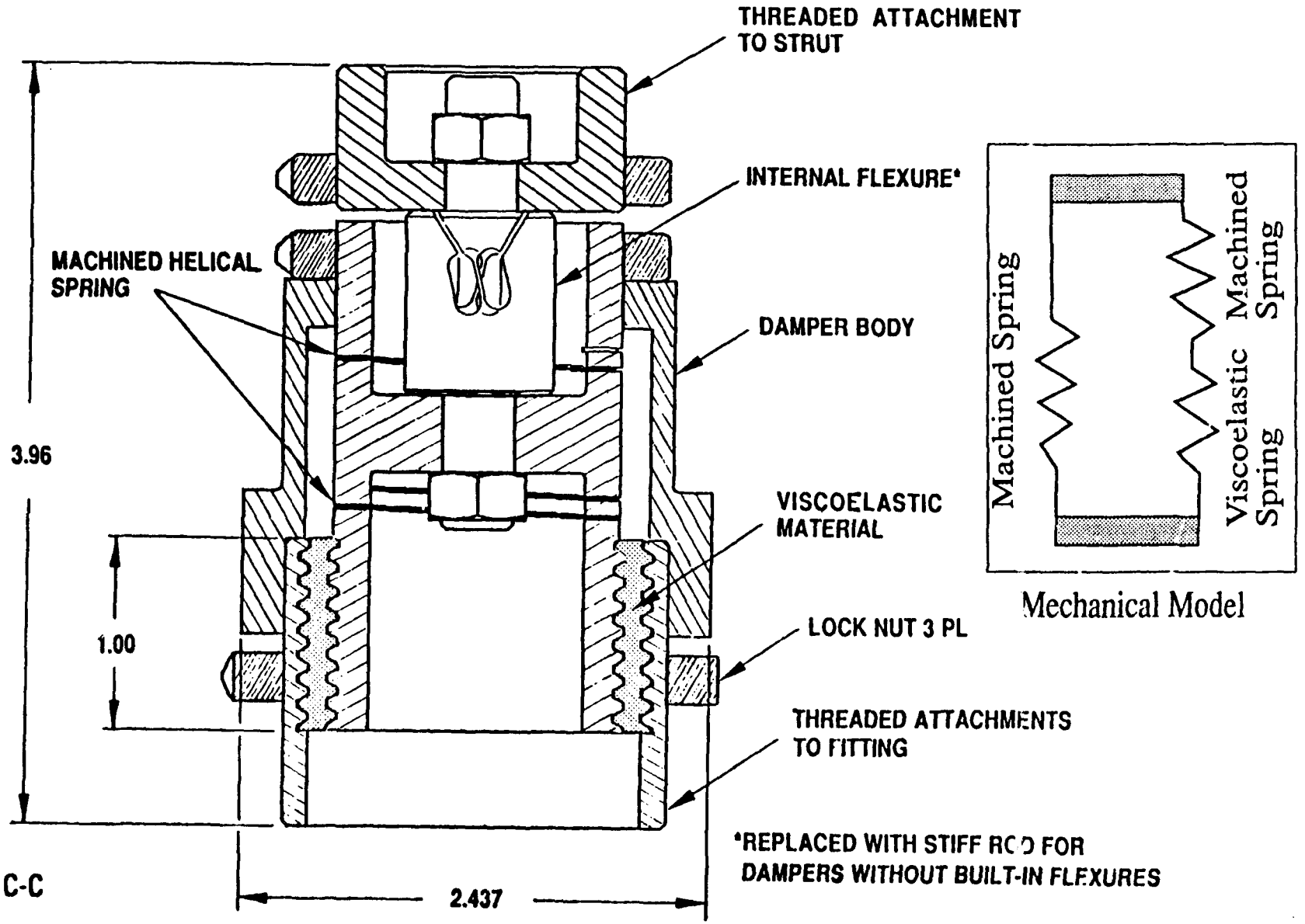

MATERIAL REQUIREMENTS

- MMC Material Considerations
  - SSS (Strength, Stiffness, Stability)

- Viscoelastic Material (VEM) Considerations
  - -High Loss Factors with broad temperature response
  - Desirable stiffness over temperature and frequency
  - Low outgassing properties

DSA Tube Requirements and MMC Material Objectives

Tubes are Part of Precision Structure -

- o High axial specific stiffness
- o Near zero axial CTE
- o Dimensionally stable

Structure Must Withstand Loads Induced During Assembly and Launch

Desired Material Features -

- o Unidirectional ultra-high modulus graphite fiber (Dupont E120), with high fiber loading and Mg matrix, for high stiffness, low density, and near zero CTE
- o Consistent fiber loading and impregnation for consistent property performance
- o Fine matrix grain structure for increased composite transverse and shear strength

Program Approach for MMC Tube Development

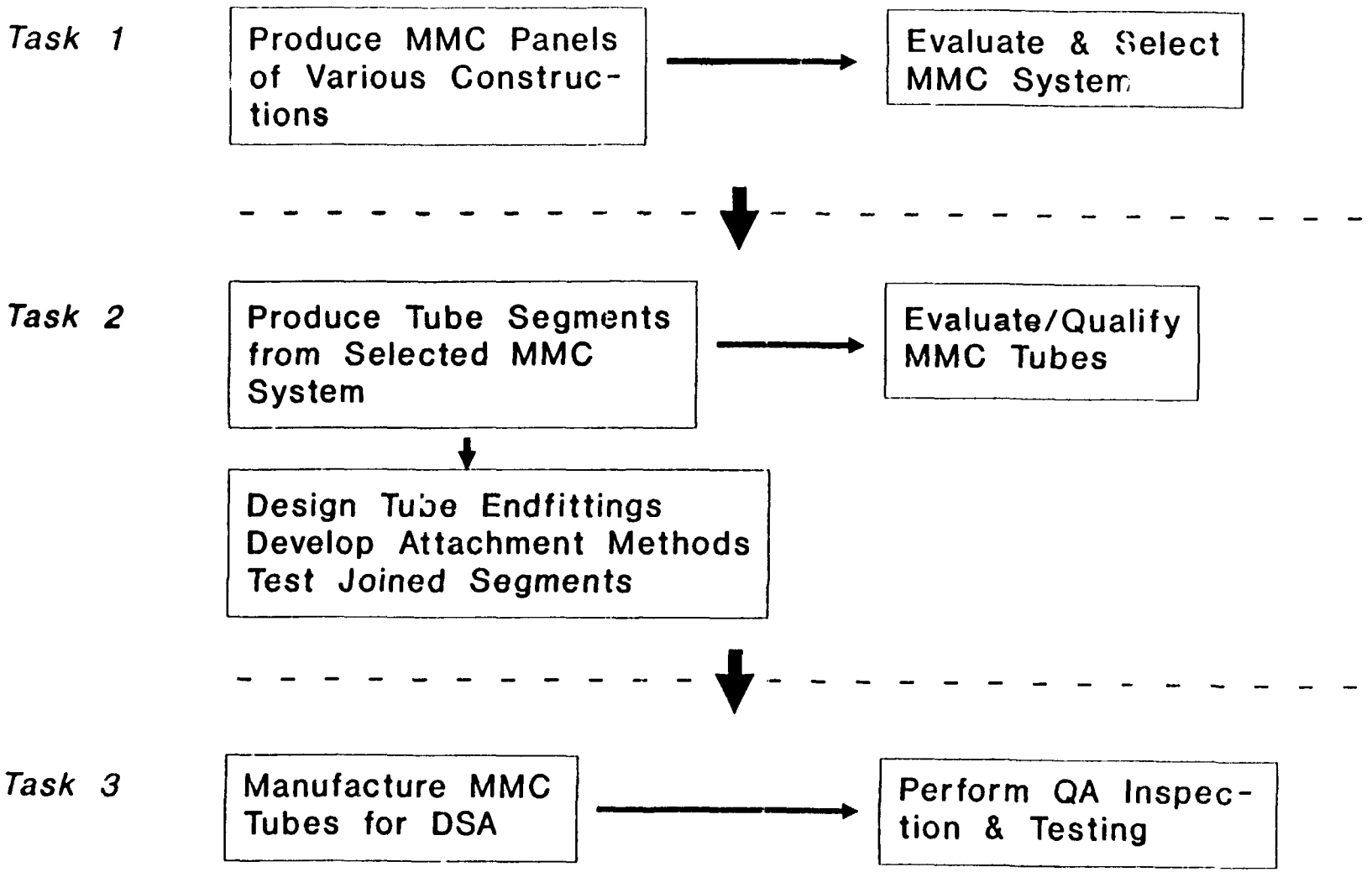

WHY VISCOELASTIC MATERIALS ?

- Unlike Metals Viscoelastic Materials (VEM) Have High Loss Factors

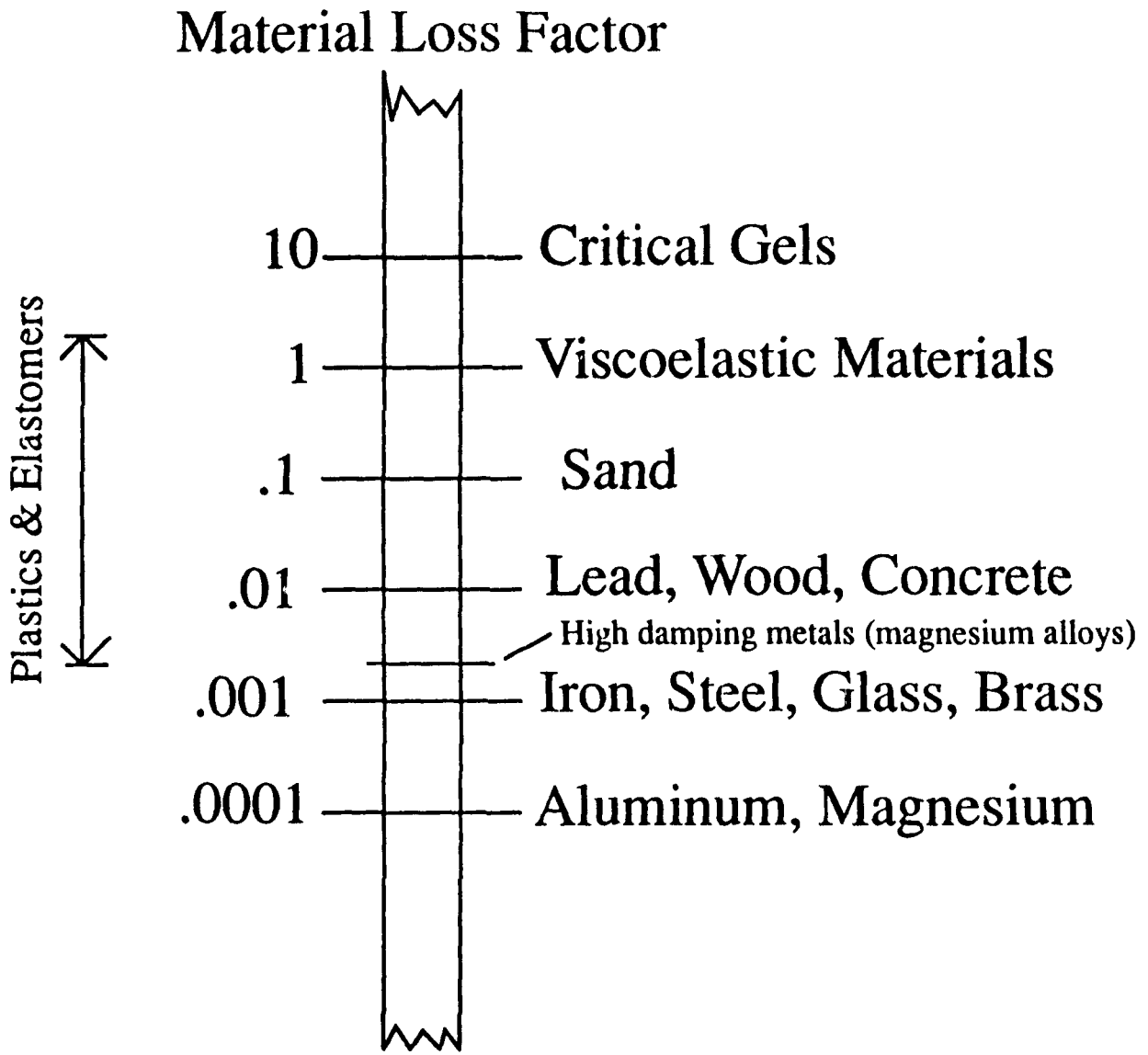

VEM DYNAMIC PROPERTIES
Scotchdamp SJ-2015X Type 110

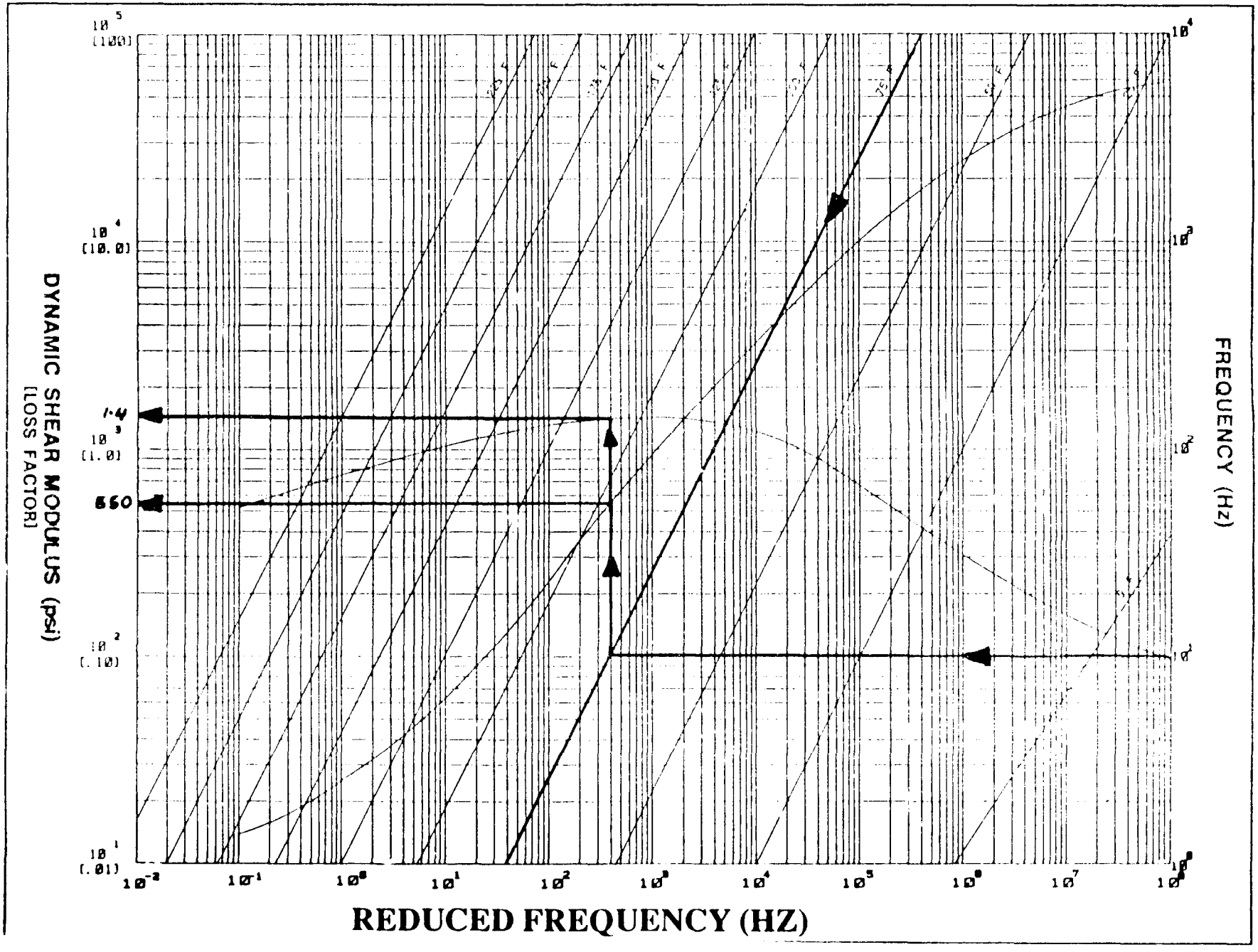

DESIGN TEMPERATURE RANGE
for VEM

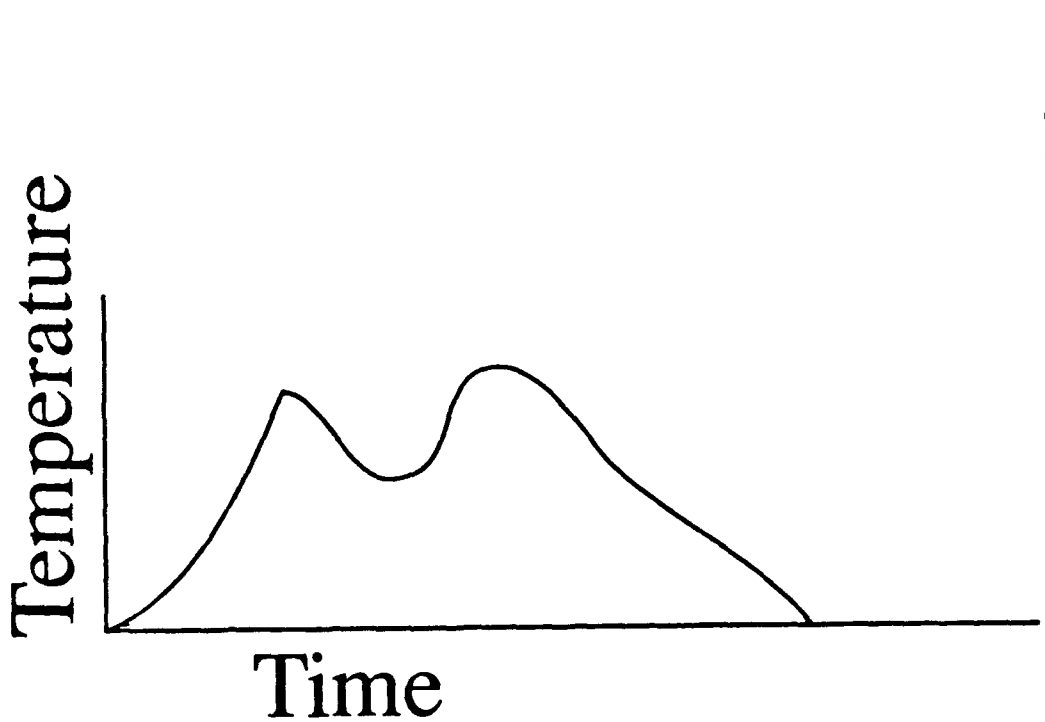

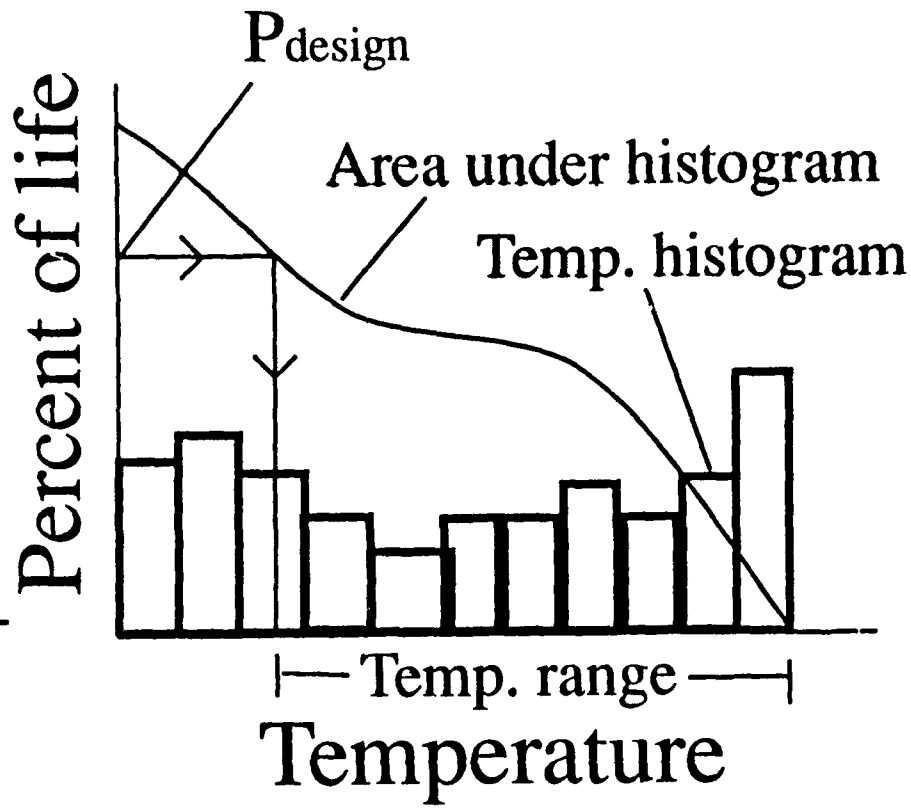

Recommended VEM Materials for DAMMPS

Material	Vendor
Isoloss HD	EAR
Isodamp C-1002	EAR
Isodamp C-1105	EAR
Isodamp C-1100	EAR
Hidamp II	Barry Controls
SPE/D	LORD
Scotchdamp Type 110	3M
DENSIL 2078 I	DENSIL
DENSIL 2078 III	DENSIL
Structural Adhesive 2216	3M
Vitron Rubber	Vitron
Kalrez 1058	DuPont

T E C H N I C A L A P P R O A C H :

ANALYSES & TESTS

- TWO UNDAMPED BASELINE STRUCTURES WILL BE STUDIED: MMC & Gr/Ep
- DETAILS OF DYNAMIC ANALYSIS AND TESTS

ITEM	BASELINE 1 (*)	BASELINE 2 (**)
MATERIAL	Gr/Ep	MMC
PERFORMANCE ANALYSES	YES	YES
• Coolent Flow Disturbance • Reaction Wheel Induced Disturbances • Settling Time - Slew Maneuver		
TESTING	NA	YES
• Component • Modal Survey • Performance		
TEST/ANALYSIS CORRELATION	NA	YES
• Updated Models and Performance Assessment		

(*) Paper Study Only
(**) Two sets of tests and analyses: with and without integrally design damping.

TECHNICAL APPROACH (CONT.)

MODULAR JOINT DESIGN

- THE MMC DSA WILL INCORPORATE MODULAR JOINT DESIGNS WHICH WILL INCORPORATE REMOVABLE VISCOELASTIC MATERIALS (VEM)
- SINCE THE VEM ELEMENTS ARE REMOVABLE, THE SAME MMC STRUCTURE WILL BE TESTED WITH AND WITHOUT DAMPING ELEMENTS
- SEVERAL JOINT DESIGNS HAVE BEEN IDENTIFIED

DISTURBANCES

- Rotating Equipment : Reaction Wheels (RWA)
- Flow Induced Disturbances
- Slew Maneuvers : Settling Time
- Thermal History

ROTOR STATIC & DYNAMIC UNBALANCE

- Force or Moment : $F = \delta M \Omega^2$

$\left\{ \begin{array}{l} F = \text{Force or Moment (lb or in-lb)} \\ M = \text{Rotor Mass (lb-sec}^2\text{/in)} \\ \Omega = \text{Wheel Speed (Rad/sec)} \\ \delta = \text{Disturbance Amplitude (in. or in.}^2 \text{ tabulated)} \end{array} \right.$

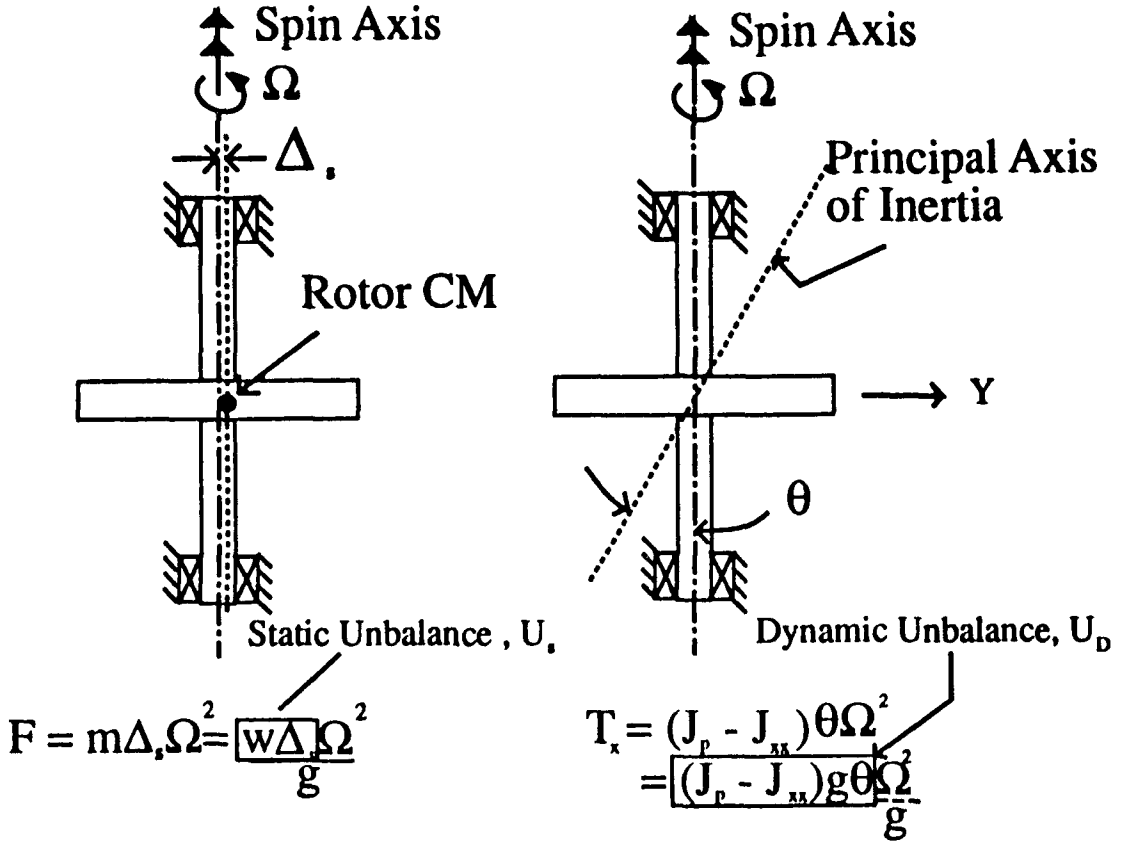

COMPARISON OF WHEEL RADIAL DISTURBANCES

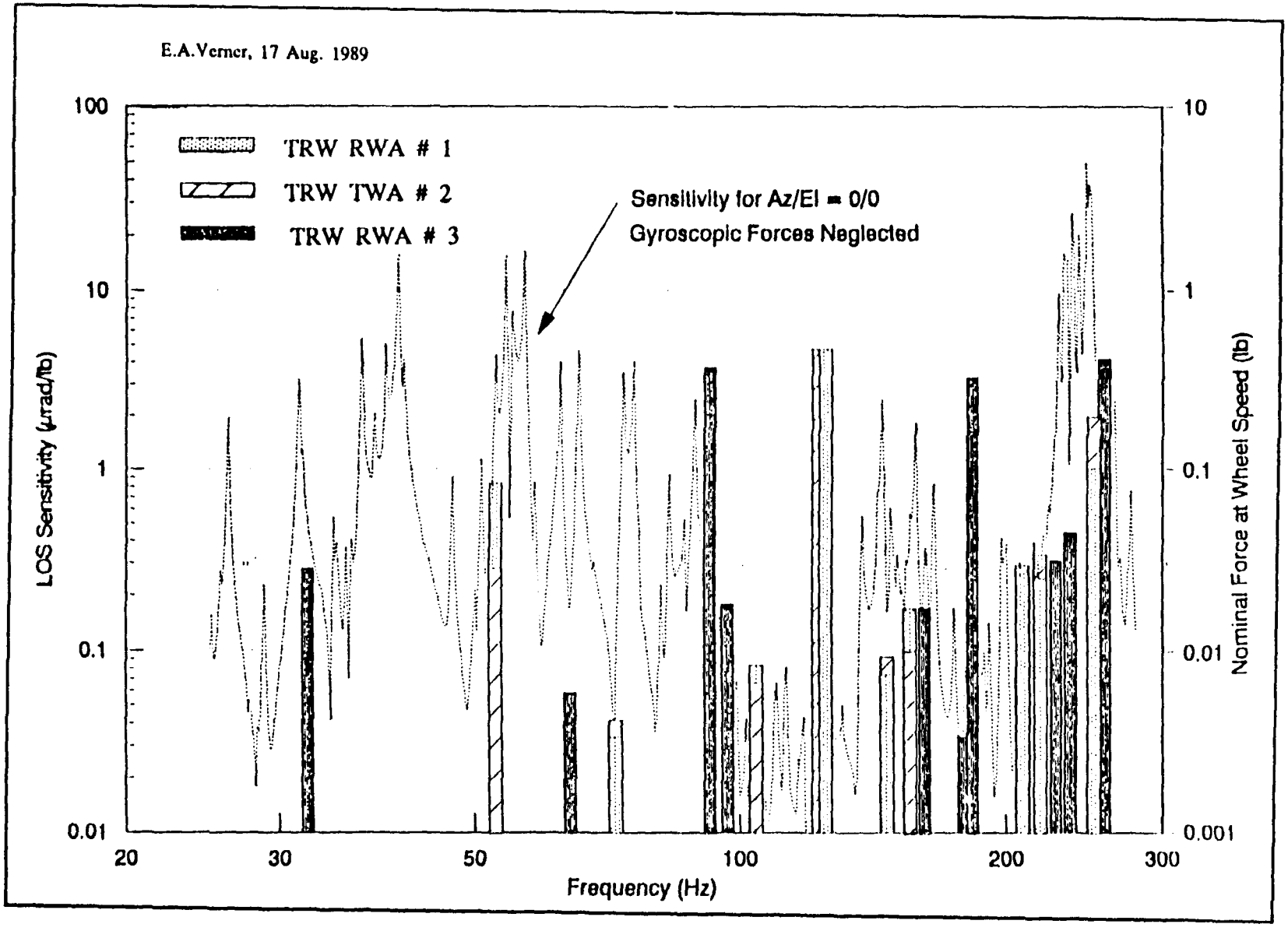

MEASURED REACTION WHEEL DISTURBANCE MODELS

- PROPORTIONALITY CONSTANTS FOR TWO TRW REACTION WHEELS

Disturbance	Harmonic	Axial Force	Lateral Force (Y)	Lateral Force (Z)	Radial Force (avg)	Lateral Moment (Y)	Lateral Moment (Z)	Radial Moment (avg)
		$(in \cdot 10^{-6})$	$(in \cdot 10^{-6})$	$(in \cdot 10^{-6})$	$(in \cdot 10^{-6})$	$(in^2 \cdot 10^{-6})$	$(in^2 \cdot 10^{-6})$	$(in^2 \cdot 10^{-6})$
Ball Group / Outer Race	1	0.061	0.150	0.200	0.175	6.0	5.0	5.5
(0.418 x Wheel Speed)	2	0.081	0.040	0.040	0.040	1.5	5.0	3.3
	3	0.098	0.040	0.080	0.060	3.0	3.0	3.0
	4	0.175	0.150	0.200	0.175	1.5	3.0	2.3
Ball Group / Inner Race	1	0.051	0.030	0.020	0.025	2.0	2.0	2.0
(0.582 x Wheel Speed)	2	0.177	0.020	0.090	0.055	2.0	4.0	3.0
	3	0.179	0.200	0.200	0.200	4.0	4.0	4.0
Inner / Outer Race	1	13.500	1.300	1.800	1.550	550.0	500.0	530.0
(1.000 x Wheel Speed)	2	1.180	0.800	1.500	1.150	20.0	20.0	20.0

Disturbance	Harmonic	Axial Force	Lateral Force (Y)	Lateral Force (Z)	Radial Force (avg)	Lateral Moment (Y)	Lateral Moment (Z)	Radial Moment (avg)
		$(in \cdot 10^{-6})$	$(in \cdot 10^{-6})$	$(in \cdot 10^{-6})$	$(in \cdot 10^{-6})$	$(in^2 \cdot 10^{-6})$	$(in^2 \cdot 10^{-6})$	$(in^2 \cdot 10^{-6})$
Ball Group / Outer Race	1	0.015	0.500	0.500	0.500	6.0	6.0	6.0
(0.418 x Wheel Speed)	2	0.010	0.030	0.070	0.050	3.0	0.7	1.9
	3	0.091	0.090	0.110	0.100	2.0	6.0	4.0
	4	0.371	0.200	0.110	0.155	2.0	1.5	1.8
Ball Group / Inner Race	1	0.026	0.020	0.020	0.020	3.0	3.0	3.0
(0.582 x Wheel Speed)	2	0.382	0.040	0.050	0.045	4.0	4.0	4.0
	3	0.383	0.200	0.100	0.150	7.0	7.0	7.0
Inner / Outer Race	1	1.230	3.000	2.500	2.750	400.0	400.0	400.0
(1.000 x Wheel Speed)	2	1.450	0.500	0.700	0.600	10.0	10.0	10.0

COOLENT FLOW INDUCED FORCE/MOMENTS

(JOSE)

SECONDARY MIRROR FORCE PSD

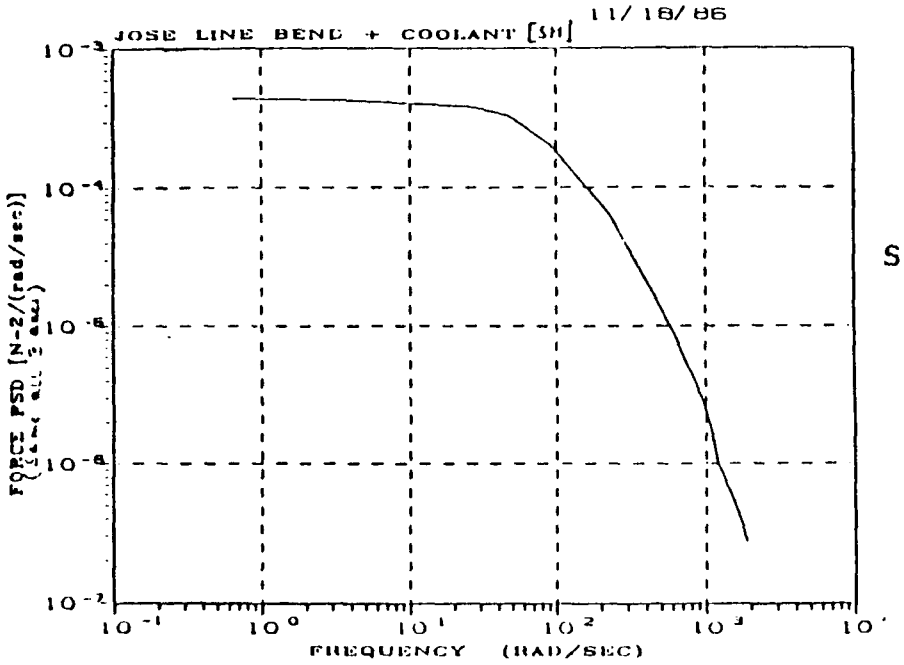

SECONDARY MIRROR X-TORQUE PSD

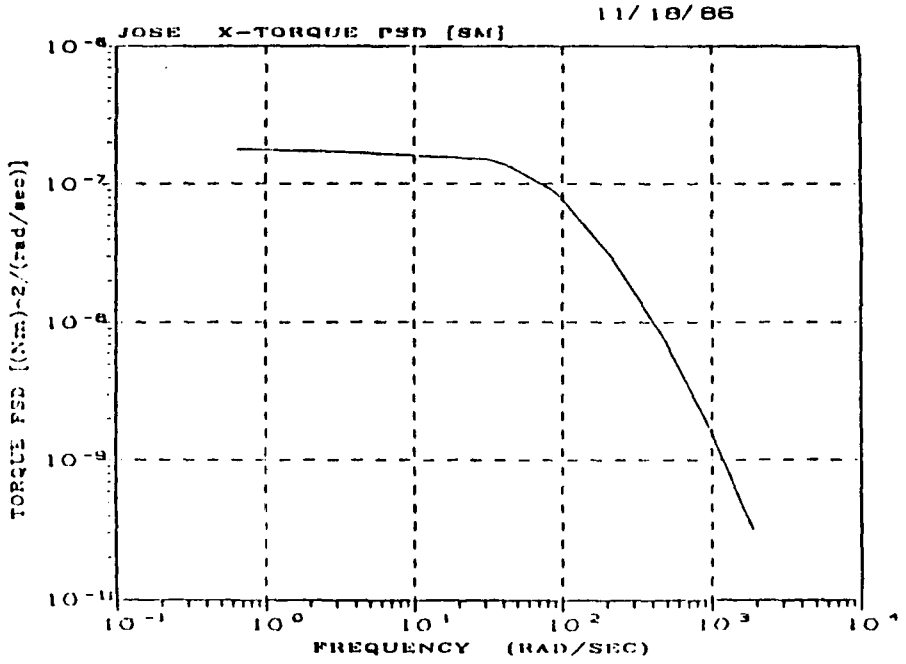

THERMAL LOAD CASES

CASE	GEO								LEO							
	Inside				Outside				Inside				Outside			
	With Heaters		Without Heaters		With Heaters		Without Heaters		With Heaters		Without Heaters		With Heaters		Without Heaters	
	L	H	L	H	L	H	L	H	L	H	L	H	L	H	L	H
1	X															
2		X														
3			X													
4				X												
5					X											
6						X										
7							X									
8								X								
9									X							
10										X						
11											X					
12												X				
13													X			
14														X		
15															X	
16																X

Definitions:

GEO : Geosynchronous orbit
LEO : Low Earth orbit
Inside : DAMMPS DSA inside spacecraft
Outside : DAMMPS DSA outside spacecraft
L : Low thermal coupling with spacecraft
H : High thermal coupling with spacecraft

DAMMPS Thermal Modeling

- TRASYS surface model was developed to provide radiation exchange factors and orbital heat fluxes for different seasons and optical properties.

- A 75 node SINDA thermal model was used to provide predicted temperatures for two sample cases:

  (1) For summer solstice with S13GLO white paint at EOL
  (2) For equinox with leafing aluminum paint at BOL

- Other assumptions:

  (a) Thermal control on the structure by using different coatings.

  (b) The structure is mounted outside a spacecraft.

  (c) Thermal conductivity of the tubes, K = 110 Btu/hr-ºF-ft.

  (d) Tube material is 50% graphite/50% magnesium alloy.

  (e) Interface conductance of 0.50 Btu/hr.-ºF between spacecraft and DAMMPS DSA.

DAMMPER (ABOVE MID-PLATFORM) TEMP IN GEO EQNOX W/ LEAF AL FOR BOL

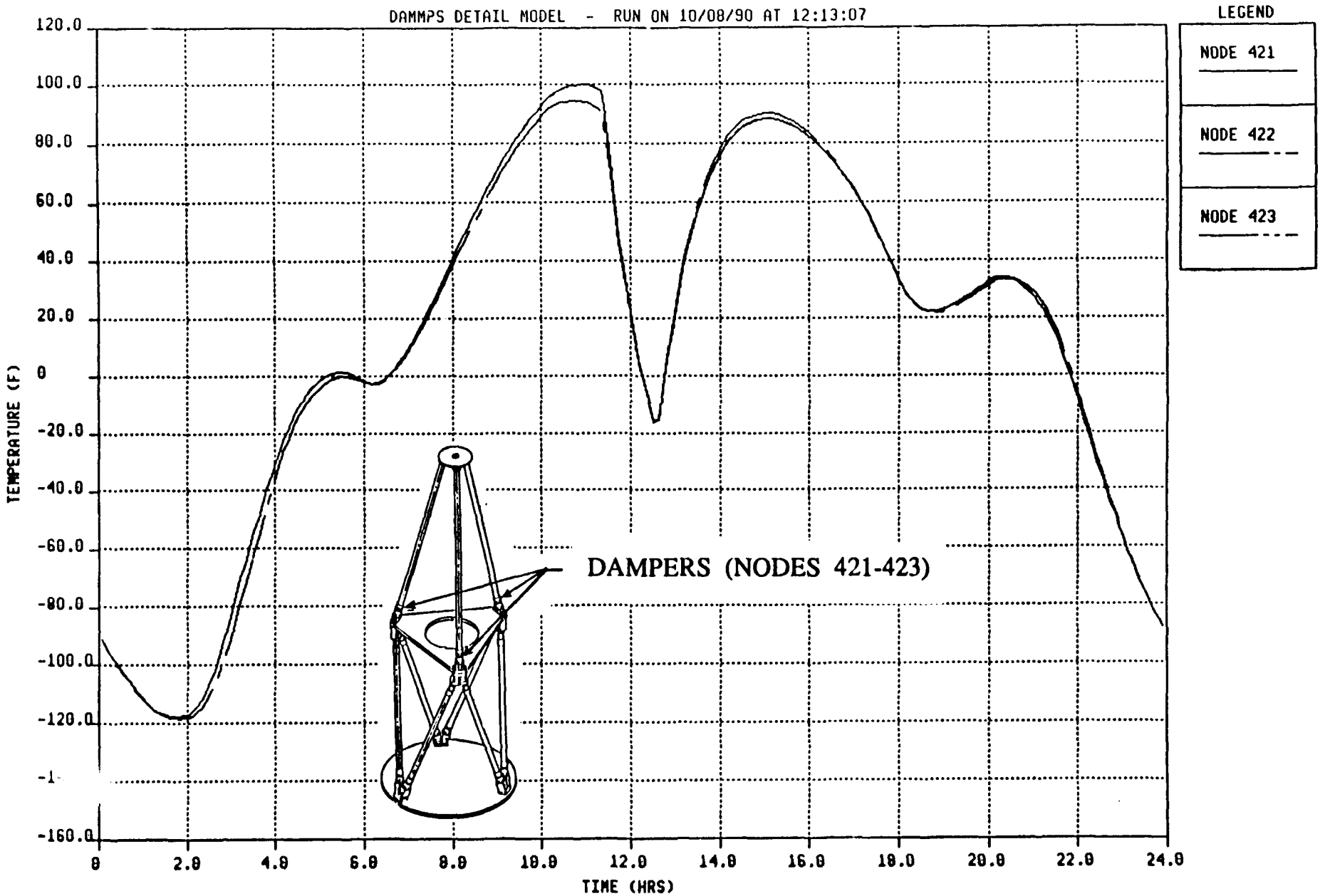

DESIGN CONSIDERATIONS

- Damper Stiffness Properties
- Design Sensitivity to Thermal History
- Thermal Data Requirements and Control

TRUSS ELEMENT STIFFNESS

- Three Element Damper : Stiffness not very sensitive to wide temperature variations

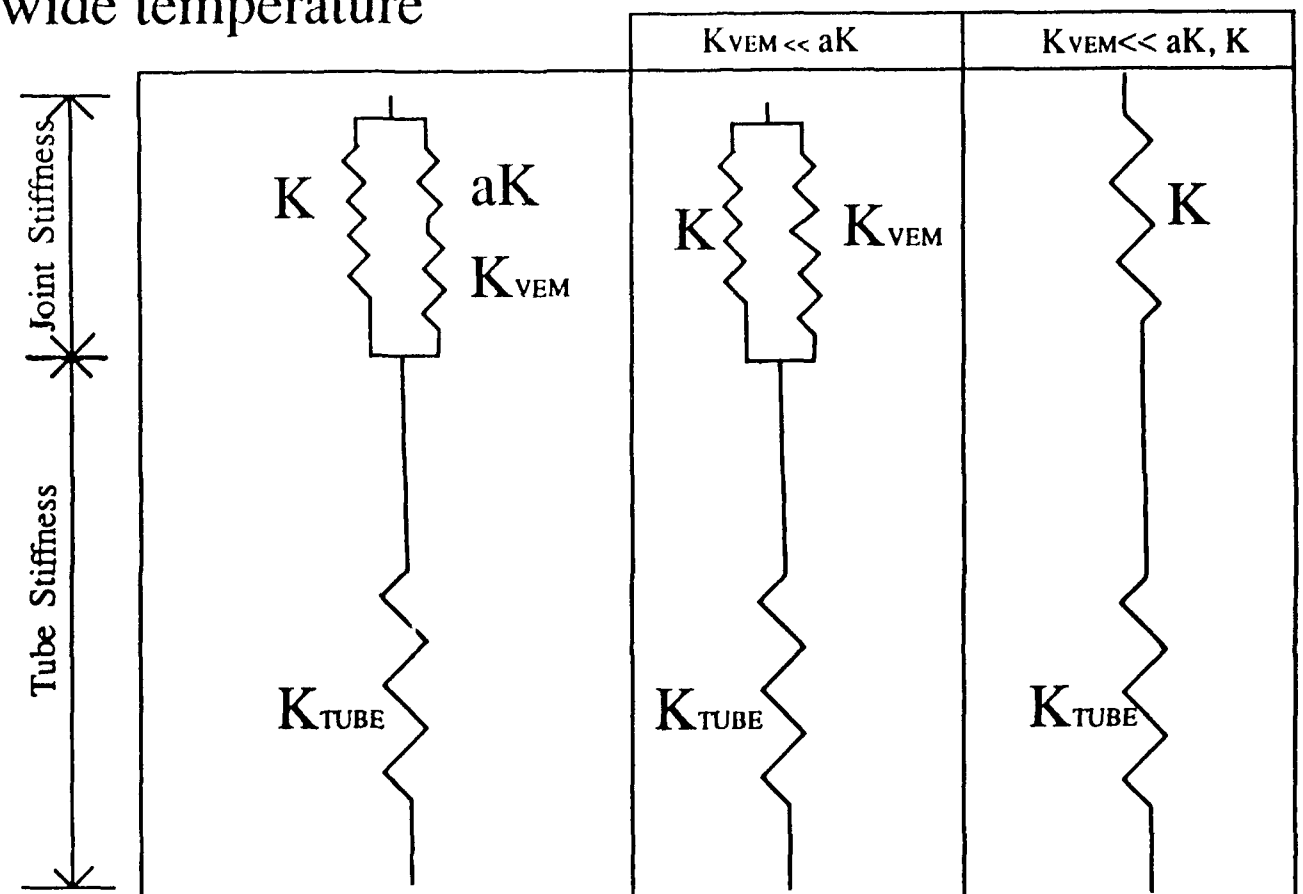

Cases	JOINT STIFFNESS : K_{JOINT}		
Nominal	$K + \frac{aK\,K_{VEM}}{aK + K_{VEM}}$	$K + K_{VEM}$	K
I : $K_{VEM} << K, aK$	K, K + aK — Design independant of K_{VEM}	K, K_{VEM} — Design dependan on K_{VEM}	K
II : $K_{VEM} >> K, aK$			K
Damping	Mod.-High	High	Low

DESIGN DAMPING LEVEL

- Damper Parameters Have Been Optimized

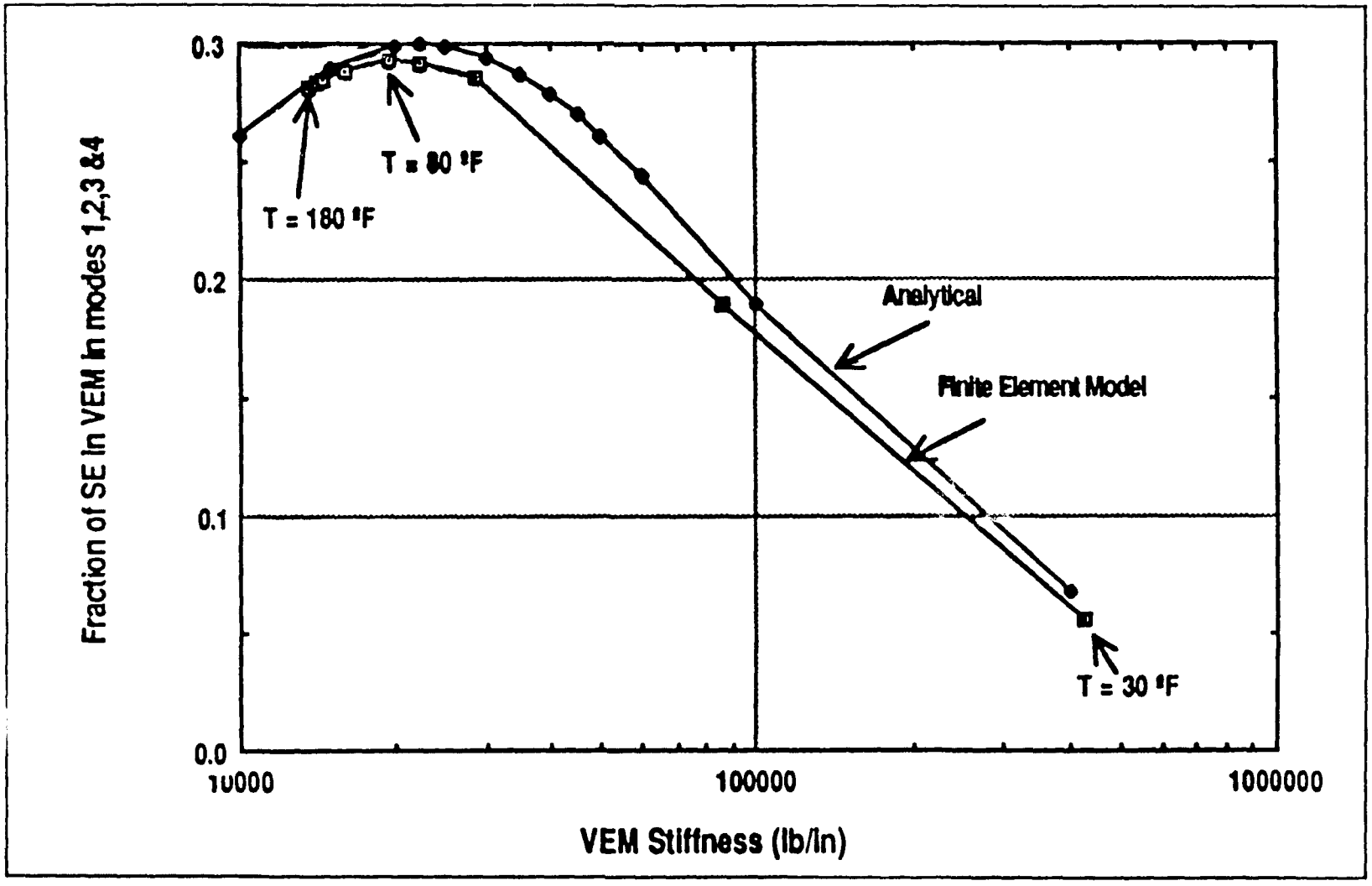

DSA DYNAMIC CHARACTERISTICS

DSA Finite Element Model : Model 220 A Orthographic View

Mode 1 : 11.4 Hz	Mode 2 : 11.4 Hz	Mode 3 : 29.4 Hz	Mode 4 : 29.4 Hz
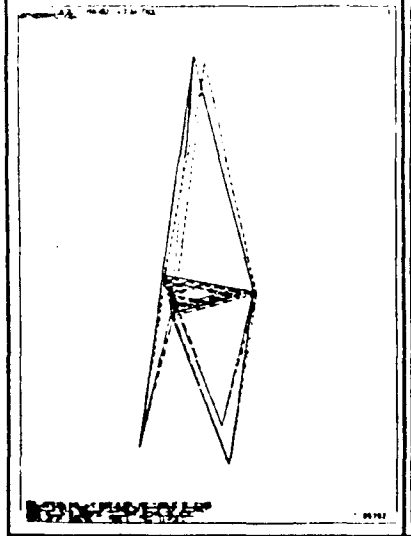	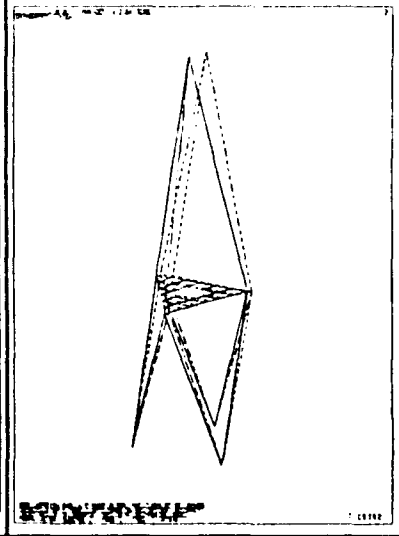	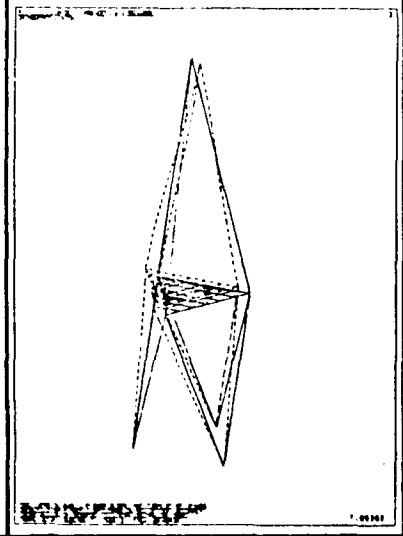	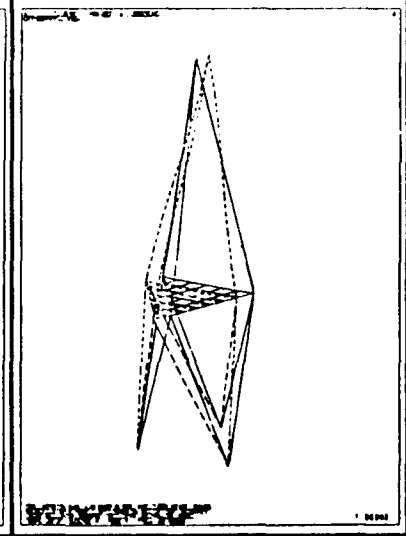
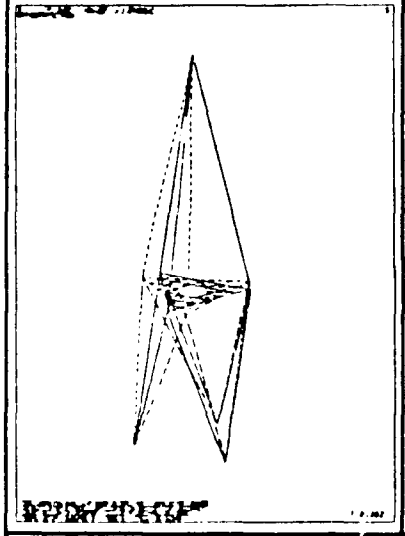	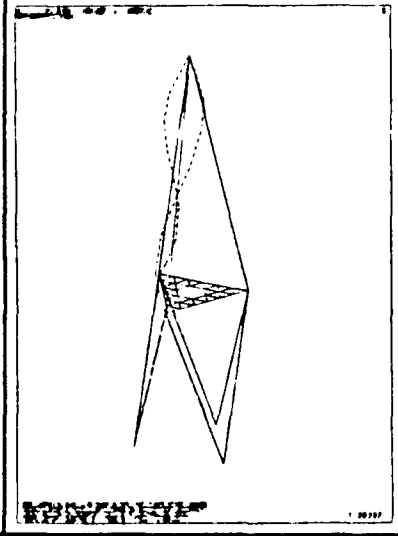	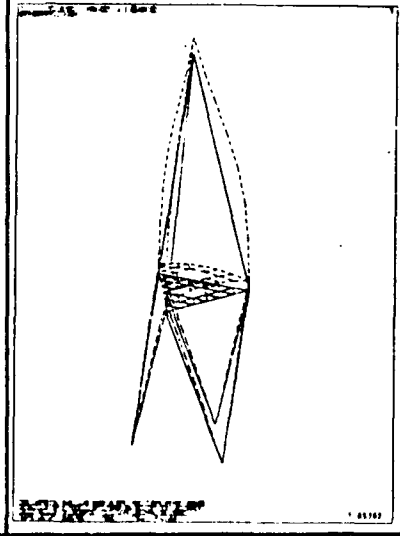	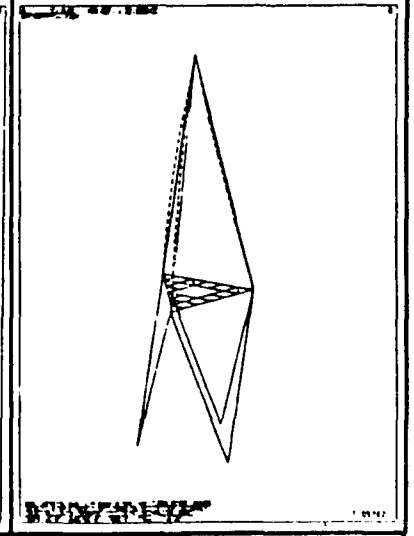
Mode 5 : 35.5 Hz	Mode 6 : 72.7 Hz	Mode 7 : 74.0 Hz	Mode 8 : 77.6 Hz

RESPONSE ANALYSES

- Response Levels Due to RWA Disturbances

  -Amplitude Reduction by a Factor of 10 to200 Hz Over Undamped Structure (Goal:Factor of 5)

- Response Levels Due to Slew Maneuvers

  - Undamped Settling Time > 10 Sec.

  -Damped Settling Time = .35 Sec.

  - Goal: Factor of Ten

RESPONSE ANALYSES

- RMS Response Levels Due to Coolant Flow Disturbance

Quantity	Undamped	Damped
Pointing X (μin)	1049	225
Pointing Y (μin)	1112	271
Pointing Z (μin)	16.34	2.116
LOS X (μrad)	6.993	2.263
LOS Y (μrad)	6.273	1.867
LOS Z (μrad)	.1828	.0649

- Response Reductions to 1000 Hz : By Factors 2.8 to 7.7

Development of Low Modulus Damping Material for Precision Mounting Platforms

S. Kirshenbaum[1], D. Hill, and C. Stahle

General Electric - Astro Space Division

ABSTRACT

A damped precision mounting platform requires a viscoelastic damping material with a shear modulus an order of magnitude lower than existing General Electric Astro Space Division SMRD™ damping material formulations. Existing SMRD™ formulations were modified to achieve low shear stiffness and high damping over a broad range of temperature and frequency. New formulations were dynamically and mechanically characterized test results are presented. Five new formulations met the low modulus, high damping objectives resulting in an efficient, highly effective damped platform design.

INTRODUCTION

The current trend toward larger and more accurate sensing instruments on precision space structures which are growing in size and flexibility has created a need for improved dynamic stability. This can be accomplished through integral use of passive damping with viscoelastic material (VEM). The damped precision mounting platform design shown in Figure 1 is a dual honeycomb sandwich with a layer of damping material in the center. The damping material is positioned in the center of the panel to recover maximum shear strain as the panel is deflected. This provides a high composite loss factor and the desired degree of improved stability. Design studies on the platform have shown that the most effective damping configuration can be achieved with a thin layer of low modulus damping material.

GE Astro Space Division produces VEM called SMRD™ which has been utilized in space applications for over 20 years. However, in past applications the damping material covered a smaller percentage of the structure requiring relatively stiff damping material for peak performance. The current precision mounting platform design with full coverage requires damping material with a shear modulus up to an order of magnitude lower than the conventional SMRD™ formulations. Past development work has shown that the properties of SMRD™ can be tailored by varying the constituents. A General Electric funded program was undertaken to develop new low modulus VEM formulations for precision platforms. The results of this successful study are presented in what follows.

[1]Dr. Steven Kirshenbaum, GE Astro Space, 234 Goddard Blvd., King of Prussia, PA, 19406, (215) 354-6551

VEM MATERIAL REQUIREMENTS

The need for a low modulus, space compatible VEM has already been discussed. Specific material property requirements for the precision mounting platform are shown in Table 1. The conventional SMRD™ formulations, 100F90 and 100F50, meet the damping and strength requirements but have shear modulli from 2000 to 4000 psi. The platform is thermally controlled, but temperatures may vary between 40 F and 75 F. Major orbital responses range in frequency from 15 to 100 Hz, and the launch acoustic loading can be significant through 2000 Hz. The VEM must maintain a high loss factor over the temperature range and frequency range of interest during launch and on orbit. The static strength requirement, 50 Psi, is low by design, although the strain to failure of the material is exceptionally high.

The outgassing requirements of less than 1 percent total mass loss (TML) and less than 0.1 percent collectible volatile condensable material (CVCM) have been established by NASA. Low outgassing is a key requirement for spacecraft materials. Material which is lost not only degrades the performance of the component, but may condense on sensors or solar array panels affecting the performance of the payload. Many commercially available damping materials meet the strength and shear modulus requirements, but have high outgassing, and are therefore unacceptable for space applications. The SMRD™ formulations have low outgassing(1) and are desirable for space applications.

DEVELOPMENT PLAN

The developmental flow plan, Figure 2, indicates the iterative nature of this study. Candidate formulations were prepared and cured in a small specimen dish for qualitative evaluation. Some formulations were rejected at this level because they separated or they never fully cured. Material formulations which looked promising on a small scale were cast into full size panels (12 inch by 12 inch by 0.25 inch) for further evaluation. In a few instances, formulations which initially looked promising were rejected at this point because of separation or incomplete curing. The remaining formulations were subjected to modified Oberst Beam tests which served as a screening test for damping characterization. Based on this data, one formulation was selected for further characterization with the Direct Complex Stiffness technique. Mechanical properties were measured with a Universal Test Machine.

MODIFICATION OF EXISTING SMRD™ FORMULATIONS

It is well known that peak damping for a VEM occurs near the glass transition temperature. In general, the glass transition can be affected by crosslink density, molecular packing, chemical constituents, cure conditions, and fillers. Because of the low outgassing requirement for space applications, modifications to the material formulation and process are limited to those which will not increase outgassing. The proprietary nature of the formulation and production process of SMRD™ precludes a detailed discussion, but it may be noted that chemical constituents and fillers were

varied in the work reported here. The properties of SMRD™ can be tailored to the needs of the application using these variables alone. Effort concentrated on reducing crosslink density to increase backbone flexibility. Plasticizers were not pursued based upon past experience which indicated the addition of these constituents caused difficulty in bonding the material to structure.

INITIAL SCREENING - MODIFIED OBERST BEAM TEST

The Modified Oberst Beam test is a relatively simple and reliable technique for measuring the damping characteristics of viscoelastic materials. Through the measurement of the natural frequencies and damping of the Oberst Beam specimen, the shear modulus and loss factor of the VEM can be determined as a function of temperature and frequency. The accuracy of the measurements, however, is limited by the beam specimen configuration, temperature control, and test technique.

A typical modified Oberst Beam configuration is shown in Figure 3. The beam is made up of an aluminum base block with a protruding arm consisting of two VEM layers bonded to an aluminum sheet. A set of 5 to 6 modified Oberst Beams were tested together inside a thermally controlled environmental test chamber. Temperature in the chamber can be maintained to 2 C. Measurements were made in 5 C increments from -5 C to 40 C. Damping and natural frequencies were determined via tap test. An instrumented hammer was used to tap the beam and the response was measured with an Endevco 2222 accelerometer attached to the tip of the beam. The input force and response acceleration were collected and reduced with a HP 5423 two channel analyzer. Each measurement consisted of 5 taps and 5 averages of the input and response.

Damping and natural frequencies of the composite beam and the density of the VEM are the raw data necessary to calculate the shear modulus and loss factor of the VEM. The data was reduced based upon equations given by Nashif(2).

Material properties of ten SMRD™ VEMs are presented in Table 2. The 100F90 and 100F50 are the original SMRD™ materials. The results indicate that seven formulations have met the material property requirements of Table 1. Five of the materials (U1015-10E, B50T2B, B50T5B, B37UF, and B37T2B) have shear modulli less than 500 Psi in the required temperature and frequency ranges, which is particularly desirable for the precision mounting platform. The peak loss factor has been increased above 1.5. As expected, the microballoon filled formulations have a lower density and higher modulus than the equivalent unfilled systems (compare 100F50 with 100F50 UF). The unfilled systems also exhibit higher loss factors.

An indication of the data quality is determined by a wicket (or inverted U) plot. If a plot of the loss factor versus storage modulus, G, forms an inverted U with small scatter, then the entire range of VEM modulus from rubbery region through the transition phase and into the glassy region is well represented. A wicket plot for the B37-T2B material is shown in Figure 4. In general, the results show some scatter, especially in

the rubbery region, which is characteristic of the Oberst Beam test. This amount of scatter, however, is acceptable for initial screening tests.

DETAILED TESTING - DIRECT COMPLEX STIFFNESS TECHNIQUE

Exceptional material properties and potential performance enhancement were demonstrated by five of the new SMRD™ formulations. Time restraints limited detailed testing to only one formulation. The B37T2B was selected; it possessed one of the lowest shear modulli, providing the lightest weight configuration, and one of the highest loss factors.

The B37T2B was further characterized at CSA Engineering with the Direct Complex Stiffness technique(3) as part of a separate program. This nonresonant technique involves application of force in the form of a sine burst across the material in shear and measurement of the resulting displacement. This burst random technique allows measurement at all frequencies simultaneously. Specimen temperature is critical to the accuracy of the results and was held to within 0.1 C by a fluid convection system.

The test results presented in the reduced temperature nomogram (Figure 5) and the subsequent wicket plot (Figure 6) show almost no scatter in the data and represent all three regions (rubbery, transition and glassy) of the B37T2B material behavior. The data points measured by the Oberst beam method are also plotted in Figure 5 for comparison. The Oberst beam data shows good agreement with the Direct Complex Stiffness test results. The confirmed peak loss factor of 1.6 is an exceptional increase from the 1.0 peak loss factor of the standard 100F90 formulation.

MECHANICAL PROPERTY TESTING

The damping material experiences the highest stress condition during launch. Design of a passively damped structure must address the two possible failure modes of the VEM, namely failure under an axial load (tension) and failure in shear. During launch the VEM is exposed to tensile stress and shear stress simultaneously. Effects of rate at which the material is strained (strain rate) and temperature have a marked influence on the material properties(4)(5) and must also be addressed. The temperatures typically experienced by a protected structure during launch conditions range from 50 F to 75 F. The strain rate depends upon the application, but typically ranges from 40 in/in/min to 150 in/in/min.

Tensile testing of VEM followed ASTM standard D638. Tests at strain rates 6.67 in/in/min or lower were performed on a 1000 lb. mechanical Instron at controlled temperatures. Tests at strain rates 33.3 in/in/min and higher were performed on a hydraulic Instron at room temperature conditions only. Strains up to 0.50 in/in were measured with an extensometer with a 1.0 inch gage length. Ultimate strains were determined by the crosshead motion. The modulus was measured as the secant of the stress-strain curve at 2 percent strain. Ultimate stress was recovered from the failure load.

TENSILE TEST RESULTS

Mechanical properties of four materials at 6.67 in/in/min strain rate and 65 F are compared in Table 3. Young's modulli measured at 2 percent strain follow the same trend as the shear modulli presented in Table 2. The modulus of the filled material (100F90) is an order of magnitude higher than the modulli of the three unfilled materials. Ultimate stress of the four materials is related to Young's modulus, although the two properties are not directly proportional. Even at this low strain rate, the ultimate stress of all four materials is higher than the 50 Psi minimum requirement. In the comparison between materials, ultimate strain appears inversely proportional to Young's modulus. All materials exhibited exceptional strain to failure enabling a great deal of flexibility in their design and use.

Mechanical property variation of the SMRD™ VEM materials with strain rate and temperature will be demonstrated with results for the B37T2B material. Young's modulus, E, as a function of strain rate, temperature held constant at 65 F is presented in Figure 7. Young's modulus ranging from 80 psi to 400 psi is observed. This wide range can be explained by examining Figure 5. At the slow strain rates, the B37T2B is in the rubbery portion of the curve. Testing at higher strain rates acts to shift the material state to the transition or glassy regions of the curve with the same effect as an increase in frequency. Young's modulus is related to a shear modulus by

$$G = E / 2(1 + \upsilon) \qquad (1)$$

where υ is Poisson's ratio. For VEM material in the transition region, the Poisson's ratio approaches 0.5. Thus, the shear modulus can be estimated as 1/3 of the Young's modulus. The shear modulus at the higher strain rates appears to correlate to the shear modulus measured dynamically with the modified Oberst beam (Table 2).

Ultimate stress as a function of strain rate (at 65 F) is presented in Figure 8. The ultimate stress of 40 psi measured at 0.07 in/in/min strain rate is doubled at the highest strain rate. Ultimate stress measured at 50 F, Figure 9, also increases with an increase in strain rate. However, at a constant strain rate, the ultimate stress measured at 50 F is double that measured at 65 F. This indicates that at 50 F the B37T2B is closer to the glassy region.

Ultimate strain as a function of strain rate and temperature is presented in Figure 10. Limitations in the hydraulic test machine crosshead displacement precluded ultimate strain measurements at the higher strain rates, but it is known that all specimens failed over 100 percent strain.

CONCLUSIONS

Development of a low modulus, space compatible VEM has been presented. Existing formulations were modified and tests were performed to screen viable candidates.

Five new material formulations have shear modulus and damping properties which meet the requirements of a precision mounting platform. One formulation was subjected to detailed characterization confirming earlier modified Oberst beam results.

Mechanical tensile test results show that Young's modulus, ultimate stress, and ultimate strain of SMRD™ VEM are dependent upon both temperature and strain rate. The existence of a relationship in the data between strain rate in mechanical testing and frequency in dynamic testing has been established. Recommendations for future work include mechanical shear tests and further investigation in the relationship between strain rate and frequency.

REFERENCES

1. Stahle, C.V., Staley, J.A., Strain, J.C., "RELSAT - Reliability for Equipment in Environmental Vibration," Final Report, AFWAL, June, 1990.

2. Nashif, A.D., "New Method for Determining Damping Properties of Viscoelastic Materials," Shock and Vibration Bulletin, No. 86.4, 1967.

3. Austin, E.M., et al, "Test Report for DAMMPS Phase I Testing of Viscoelastic Materials," CSA Report No. 90-10-01, October 1990.

4. Faupel, J.H., Engineering Design, John Wiley and Sons, New York, 1962, *Chapter* 5.

5. Landel, R.F., and Fedors, R.F., "On the Phenomenology of Rubberlike Behavior," Deformation and Fracture of High Polymers, Battelle Institute Materials Science Colloquia, Kronberg Germany, September 1972.

Table 1 VEM Material Requirements for a Precision Mounting Platform

Temperature Range (F)	40 to 75
Frequency Range (Hz)	15 to 2000
Shear Modulus Range (Psi)	50 to 1200
Loss Factor	1.0 minimum
Outgassing - TML (Percent)	1.0 maximum
Outgassing - CVCM (Percent)	0.1 maximum

Table 2 Modified Oberst Beam Test Results

	Peak Damping Data					
Material Designation	Filled (F/U)	Density (g/cm^3)	G (Psi)	Loss Factor	Temp. (F)	Freq. (Hz)
100F90 *	F	0.7	4000	1.0	65	55
100F90UF	U	1.0	1000	1.2	67	20
100F50 *	F	0.8	4200	1.0	59	90
100F50UF	U	1.0	600	1.4	50	16
U1015-5E	U	1.0	40	1.5	40	9
U1015-10E	U	1.0	80	1.6	71	57
B50T2B	U	1.0	380	1.3	61	85
B50T5B	U	1.0	370	1.1	60	84
B37UF	U	0.9	60	1.6	71	57
B37T2B	U	1.0	90	1.5	60	78

* Historical Data

Table 3 Tensile Test Results at 6.67 in/in/min strain rate and 65 F

Material Designation	Filled (F/U)	E (Psi)	Ultimate Stress (Psi)	Ultimate Strain (Psi)
100F90	F	1250	400	0.8
100F50UF	U	130	145	1.2
B50T2B	U	82	92	1.4
B37T2B	U	92	70	1.7

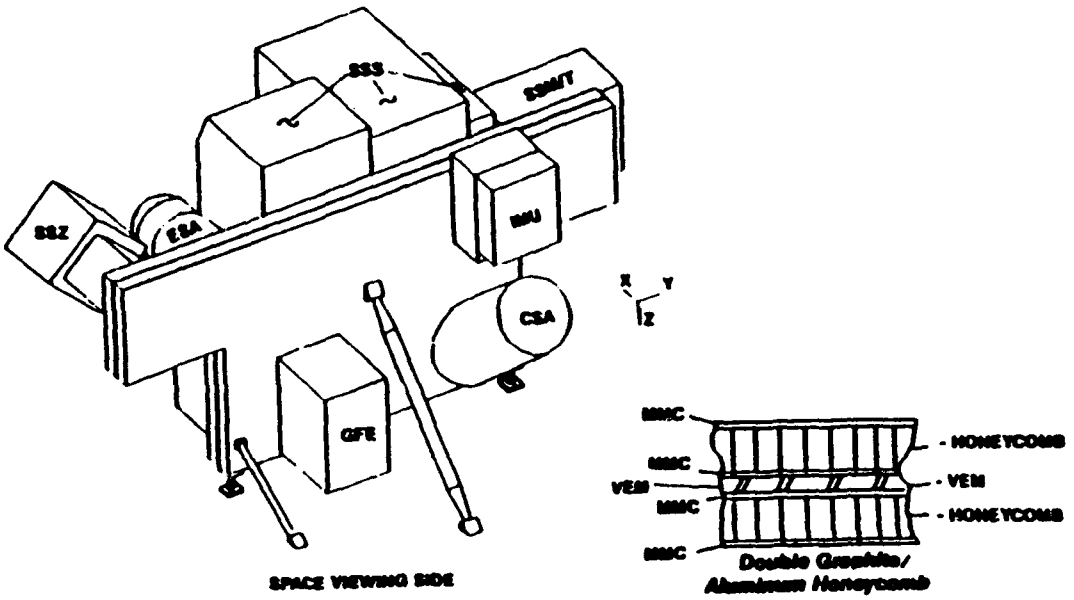

Figure 1 Damped Precision Mounting Platform Design

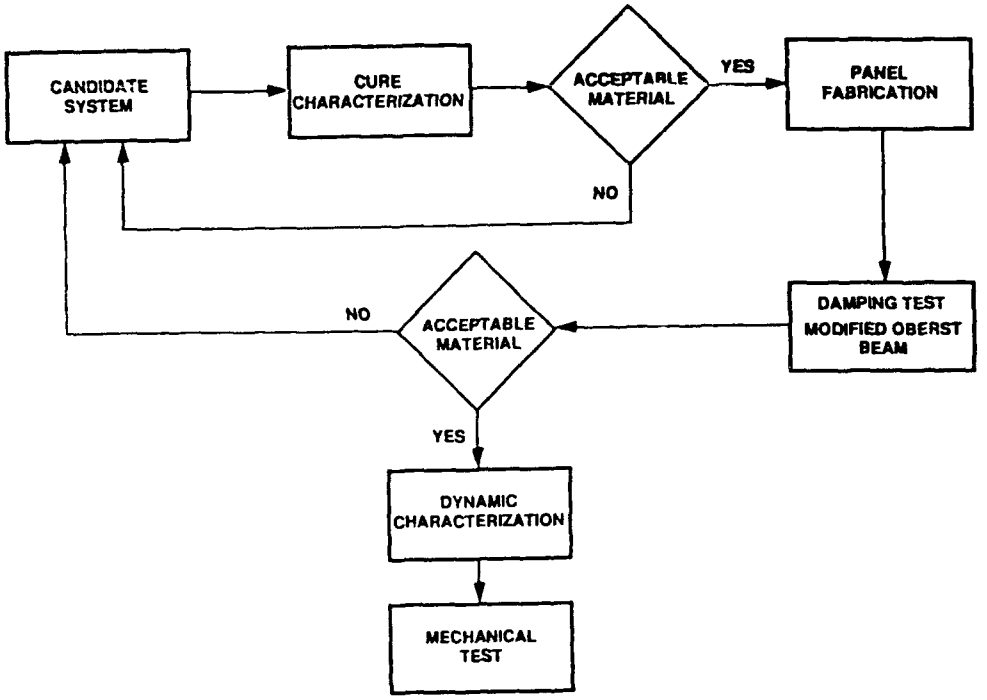

Figure 2 Damping Material Development Flow Plan

Figure 3 Modified Oberst Beam

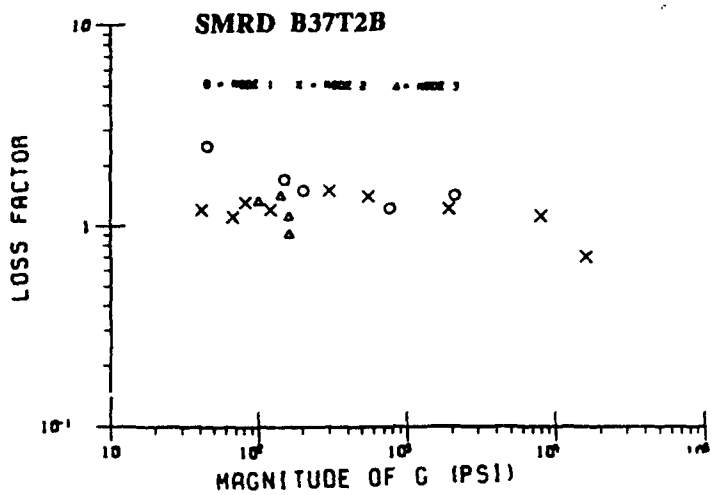

Figure 4 Wicket Plot for B37T2B Modified Oberst Beam Test Data

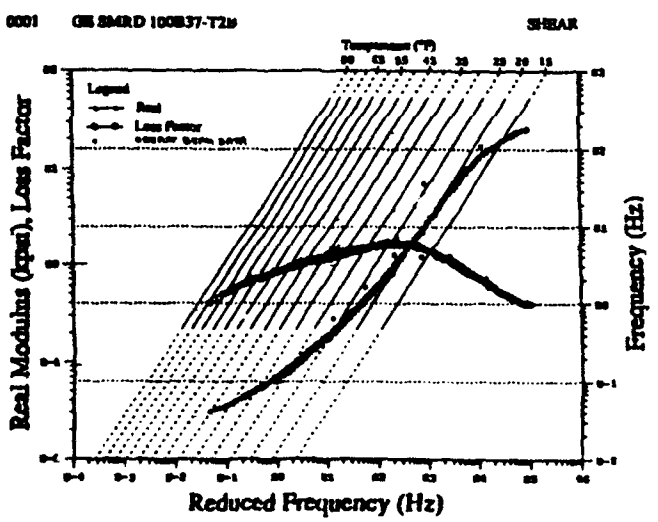

Figure 5 Complex Stiffness Test Results for B37T2B

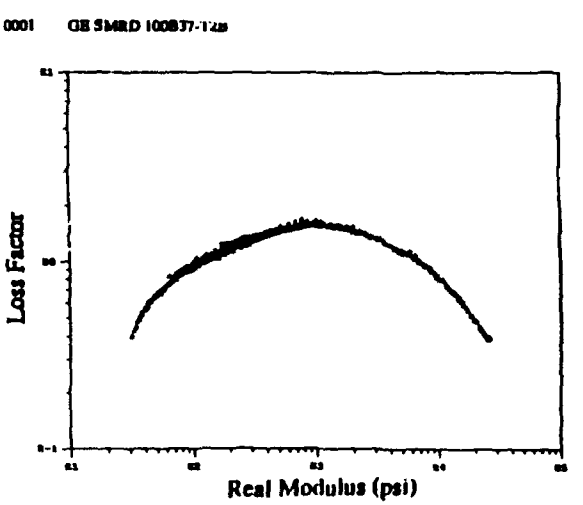

Figure 6 Wicket Plot for B37T2B Complex Stiffens Test Data

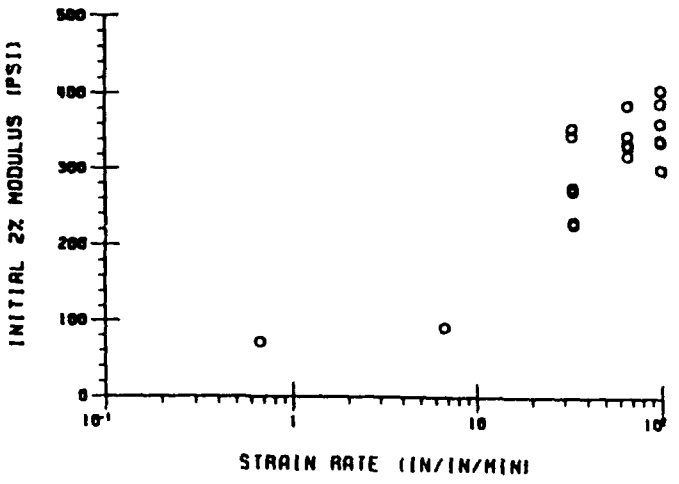

Figure 7 Variation of B37T2B Young's Modulus With Strain Rate

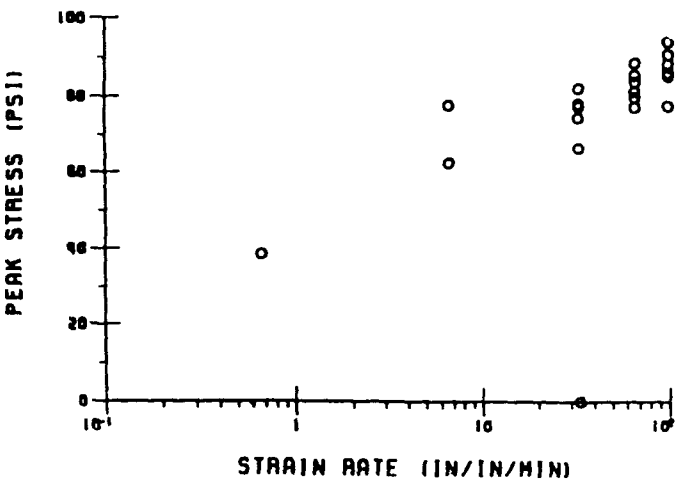

Figure 8 Variation of B37T2B Ultimate Stress With Strain Rate

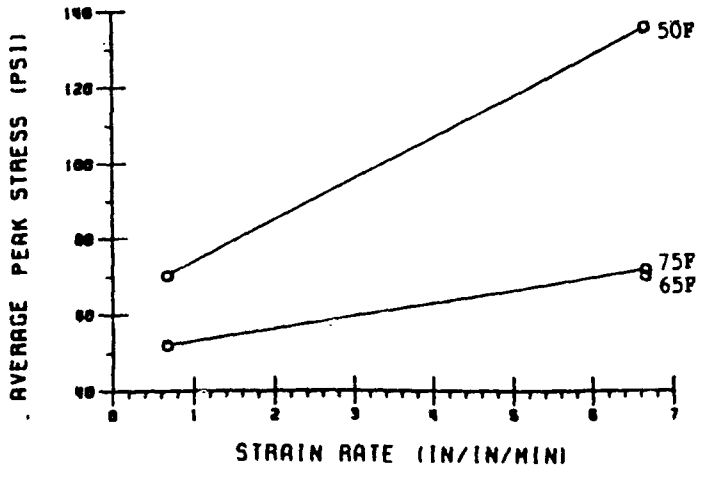

Figure 9 Variation of B37T2B Ultimate Stress With Temperature

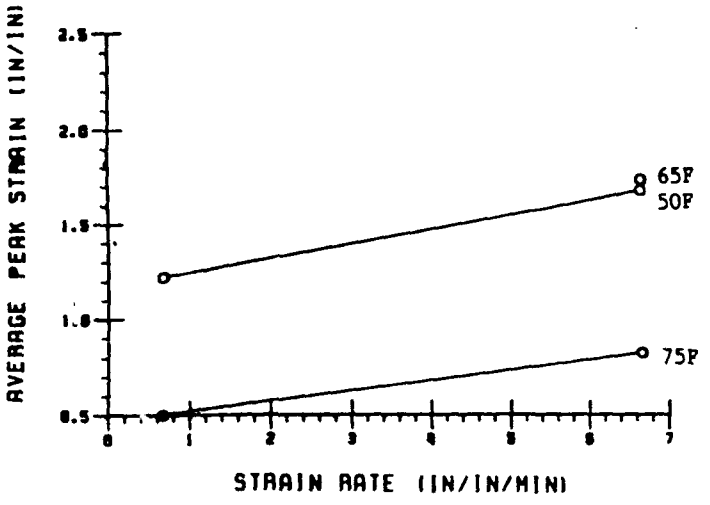

Figure 10 Variation of B37T2B Ultimate Strain With Temperature

COMPLEX STIFFNESS TEST DATA FOR THREE VISCOELASTIC MATERIALS BY THE DIRECT COMPLEX STIFFNESS METHOD

B. R. Allen
CSA Engineering, Inc.
560 San Antonio Rd.
Palo Alto, CA 94306-4682

E. D. Pinson
Lockheed Missiles & Space Company, Inc.
Space Systems Division
1111 Lockheed Way
Sunnyvale, CA 94089-3504

An integral part of the Damping and Metal Matrix for Precision Structures (DAMMPS) program involves the acquisition and dissemination of complex stiffness data for several viscoelastic material (VEM) specimens. Three such specimens have been tested by the Lockheed Missiles and Space Company, Inc. DAMMPS team: 3M Y-966, Soundcoat DYAD-606, and 3M ISD-112. These particular materials were chosen to demonstrate usable loss factor amplitudes which span the anticipated frequency and temperature range of operation for the structure studied under the contract. Future testing will characterize these and other selected specimens in more detail to provide an accurate material properties database for the detailed design task. Test data were collected very efficiently utilizing the Direct Complex Stiffness (DCS) method and manipulated/reduced using the VEMINT program. In this paper, salient aspects of the test and data reduction procedures are presented, as well as several forms of the complex modulus data.

INTRODUCTION

This paper documents the test, data reduction, and characterization of three viscoelastic materials performed under the current phase of the Damping and Metal Matrix for Precision Structures (DAMMPS) program. The three materials were 3M's Y-966, Soundcoat's DYAD-606, and 3M's ISD-112. The materials were tested using a Direct Complex Stiffness (DCS) method, and the data were reduced using a state-of-the-art characterization method. A more complete description of the test methodology, hardware, and characterization software is found in other technical papers [1,2].

The objective of the preliminary testing under this task was to screen the properties of three viscoelastic materials (VEMs) for potential incorporation into the Demonstration Structural Article (DSA) identified for study and proof-of-concept exercises in the DAMMPS program [3]. These engineering data were collected over temperature and frequency ranges particular to the expected operational environment of the structure. In general, the volume and breadth of the data obtained in this phase of testing is less than what will be produced for the next phase of the DAMMPS effort, where testing will lead to more complete characterizations, resulting in complex modulus data over broader temperature and frequency ranges.

Raw data were obtained using a testing system developed by CSA Engineering which operates on the principle of DCS measurements, a nonresonant technique. The VEM specimens were tested in shear and their properties were measured directly, not inferred indirectly, from the raw data. Although nonresonant methods place more stringent requirements on the instrumentation, it has been shown to be more accurate and versatile than the resonant testing options.

Since it is impractical to test a VEM at every combination of temperature and frequency, specimens are tested at discrete temperatures and frequencies, and a relationship is developed which characterizes the material at all other combinations of temperature and frequency. This process, referred to as characterization, was performed on the material test data by using a state-of-the-art characterization program which is currently under development. The characterization process employed the "Spline Fit of Slope" temperature shift function and the "Ratio of Factored Polynomials (Collocation)" complex modulus model [4].

DIRECT COMPLEX STIFFNESS TEST METHOD

The DCS test method, often called the impedance technique, is a nonresonant test method that uses a simple test specimen, called a lay-up, as shown in Figure 1. Transducers measure input force and the resulting displacement of the center block directly. Input and response signals are digitized and processed, usually by discrete Fourier transform methods, to obtain the impedance at the force input point. After subtracting the inertia contribution due to the known mass of the center block, this quantity is normalized by the specimen stress area and thickness to obtain the complex modulus of the VEM as a function of frequency and temperature.

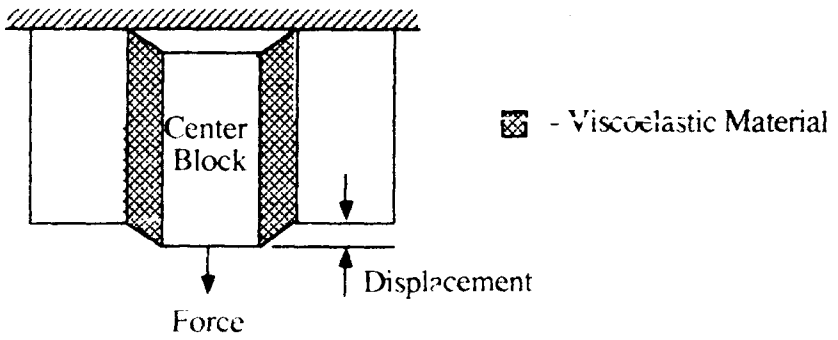

Figure 1 - Direct Complex Stiffness Testing Method

Direct stiffness methods require much care in the design of the apparatus to insure that fixture resonant frequencies are as high as possible. Likewise, operator experience is important in lay-up assembly and in interpretation of data to identify and correct any anomalies immediately. When done properly, measurements can be accurate and repeatable for frequencies from about 0.01 Hz. to an upper limit dictated by the dynamic of the fixture. Advantages with respect to speed, accuracy, temperature control, frequency range, frequency resolution, data format, and specimen generality make the direct complex stiffness technique the method of choice for most applications.

The test system used to perform the complex modulus tests described herein was designed and built by CSA Engineering. Using the principles of DCS measurements, a known dynamic force (usually a

random burst) is applied in such a way that shear deformation is produced in a small VEM specimen which is held at a known temperature. The force and resulting shear are transduced, and the frequency response between input force and output displacement is calculated by means of a discrete Fourier transform. This complex function of frequency is then processed to obtain the complex shear modulus of the material.

DATA COLLECTION

A single specimen of each of the three VEMs was used to acquire the preliminary material data for each material. Since any DCS test system can accommodate only a finite range of specimen stiffnesses, each VEM specimen can only be used when the associated stiffness is compatible with the dynamic range of the machine. Accurate measurements of the complex modulus are complicated by the large changes in stiffness which occur in the transition region, since specimen stiffness varies directly with modulus. Judgement is required to estimate the room temperature modulus of each material and its approximate location within the transition regions (e.g., glassy, rubbery, or transition). For example, if a material is known to be in the rubbery region at room temperature and target frequencies, area and thickness values would be chosen to minimize specimen stiffness so that temperatures could be decreased to approach transition without exceeding the stiffness range accommodated by the test apparatus. In the worst case, extra specimens must be made to accommodate the wide stiffness variations of transition and/or inaccurate estimates of material stiffness and transition regions.

Specimen stiffness limitations are controlled by two phenomena. The upper limit for specimen stiffness on the test equipment is limited by the absence of sufficient transducer output and/or the rigidity of the test fixture. Conversely, lower stiffness limits are controlled by the increased ratio of inertia to the total force. The latter limitation occurs when the decreasing specimen stiffness causes resonant frequencies of the constant-mass center block on the VEM "spring" to shift down near the measurement band.

Nearby resonances violate the assumptions of DCS tests since force-deflection properties are determined by inertia as well as stiffness. The intent of this and any direct stiffness test is to measure the stiffness properties of a specimen, not the inertia effects produced by a nearby resonance. At some point, the analytical mass correction will not be able to nullify the increasing inertia forces. For the testing under consideration here, inertia force magnitudes were tracked and recorded during data acquisition. Unwanted or inaccurate data were purged during characterization since this process presents additional methods of error identification.

VISCOELASTIC DATA REDUCTION AND PRESENTATION

The preceding section described the test method that was used to obtain shear modulus and loss factor data at a number of temperatures and frequencies. Because of the impracticality of testing a viscoelastic material at every combination of temperature and frequency, a relationship is developed which characterizes the material at any combination of temperature and frequency. This process is referred to as characterization. The data are "shifted" using a temperature shift function and "fitted" using a complex modulus model.

For the data reduction presented in this test report, the "Spline Fit of Slope" temperature shift function (α_T) was used to reduce experimental data [4]. In this method, the slope of α_T is defined by a spline

fit through "knots" at N evenly spaced temperature intervals.

Once α_T has been obtained, complex modulus (G^*) curves are superimposed upon the reduced data in the International plot. The following "Ratio of Factored Polynomials" model was used to draw these curves.

$$G^* = G_e \prod_{k=1}^{N} \frac{1 + \left(\frac{2\pi j f_R}{r_k e^2}\right)^{1/2}}{1 + \left(\frac{2\pi j f_R}{r_k e^2}\right)^{1/2}}$$

where G^* = complex modulus,
G_e = storage modulus rubbery asymptote,
G_g = storage modulus glassy asymptote,
$f_R = \alpha_T f_i$ = reduced frequency,
r_k = breakpoint reduced frequency, and
$e = (G_g/G_e)^{\frac{1}{2N}}$

Once the material is characterized, the program provides a superset of the plots and data described in reference 5. These are listed below and presented for each of the tested materials in the following sections.

1. Plots of $\log(G^*_R(f,T))$ and $\log(\eta)$ vs. reduced frequency with constant temperature lines and an experimental frequency axis (International plot) in both English and S.I. units,
2. Plots of $\log(\eta)$ vs. $\log(G^*_R(f,T))$ (Wicket plot) in English and S.I. units,
3. A plot of $\log(\alpha_T)$, $d(\log(\alpha_T))/dT$, and apparent activation energy vs. temperature,
4. Plots of log(frequency) vs. temperature in English and S.I. units,
5. A plot of $\log(G^*_R(f,T))$ and $\log(\eta)$ vs. temperature, and
6. An updated tabulated data file.

3M ISD-112 CHARACTERIZATION DATA

This material is an acrylic pressure sensitive adhesive, not marketed as a stand-alone damping material. It is generally sold as a part of a final 3M-designed damping solution. The test specimen was obtained from Lockheed Missiles & Space Company, Inc., Space Systems Division, identified by the manufacturer as 2105 NVB TYPE 1205 on the packing slip and 2105 1NVB964A3618 (label affixed to the roll itself). Prior to testing, the material was exposed to approximately 40% relative humidity (RH) at 75°F for one month. This environment also represents ambient test conditions. (Published information indicates a one year shelf-life at 50% RH and 70°F.) Since the test specimen was only 0.005 in. thick, special care was taken to ensure that the bonding substrates associated with the test fixture were flat to within 0.001 in. over the entire specimen area. The surfaces were then degreased with a solvent (e.g., trichloroethane or toluene). The test specimen was constructed by bonding the material between aluminum blocks at 75°F with a pressure of between 2 to 5 psi, applied for only a

few seconds, since bonding occurred instantaneously. An initial specimen was constructed with area and thickness of 0.99 in^2 and 0.0113 in., respectively. Handling may have damaged the article since it was too compliant, necessitating the construction of a second specimen with an area of 6.00 in^2 and thickness of 0.0105 in. Only data from the second article are presented in this report. This second series of tests commenced at CSA Engineering on October 1, 1990, using a proprietary DCS method test system coupled with a Zonic 6080/6081 FFT Analyzer. Although a strain linearity check was not performed, strain levels during testing were maintained at approximately 2% and the maximum loss factor observed was 1.25 (32°F < T < 96°F - eight discrete values, and 0.9 Hz. < f < 1000 Hz.). Figures 2 - 6 provide final detailed characterization data.

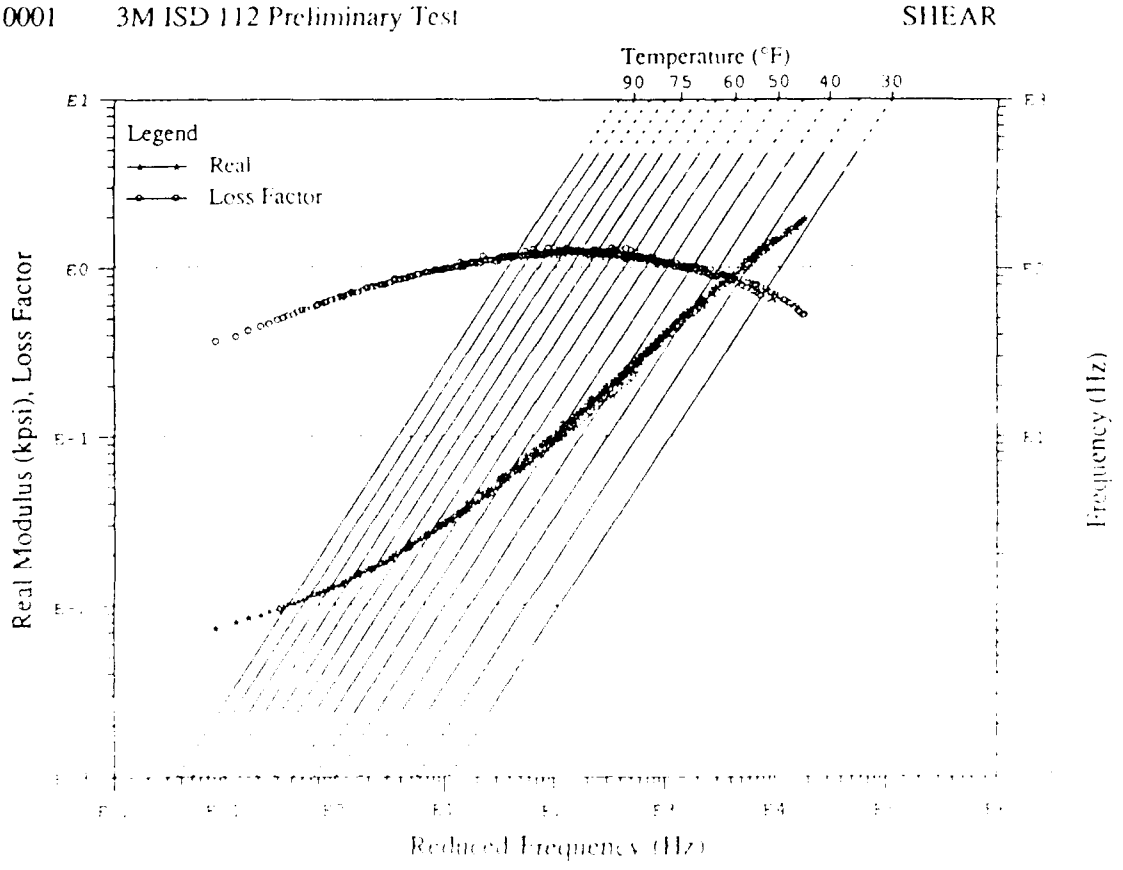

Figure 2. International plot for 3M ISD-112 (English units)

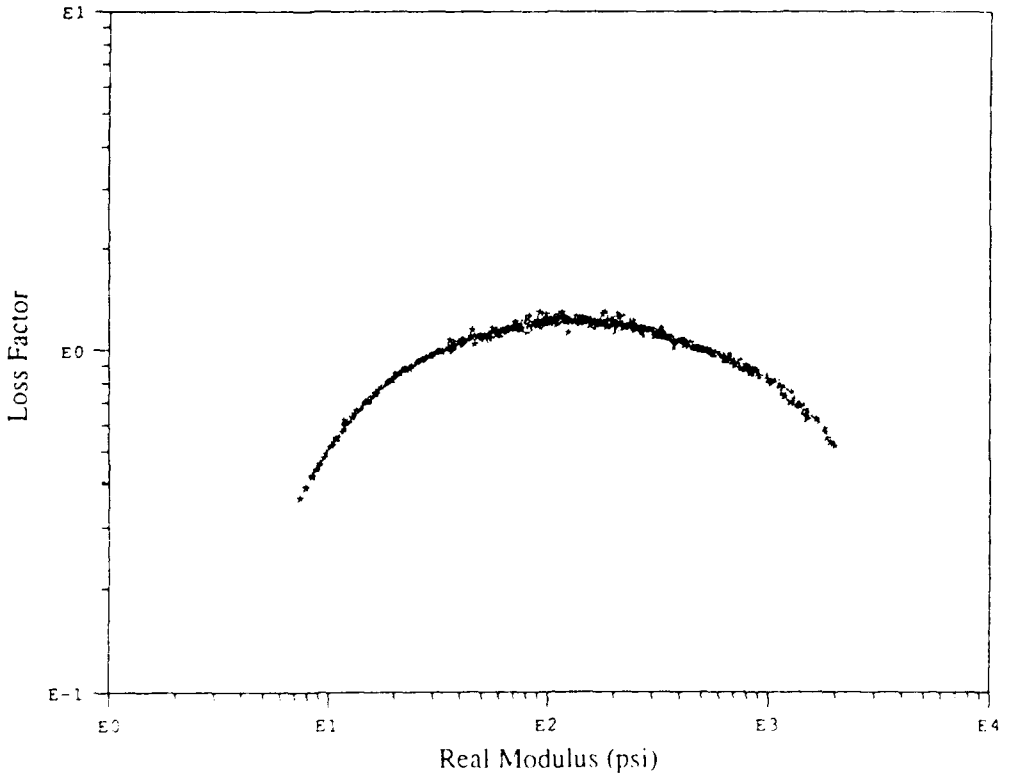

Figure 3. Wicket plot for 3M ISD-112 (English units)

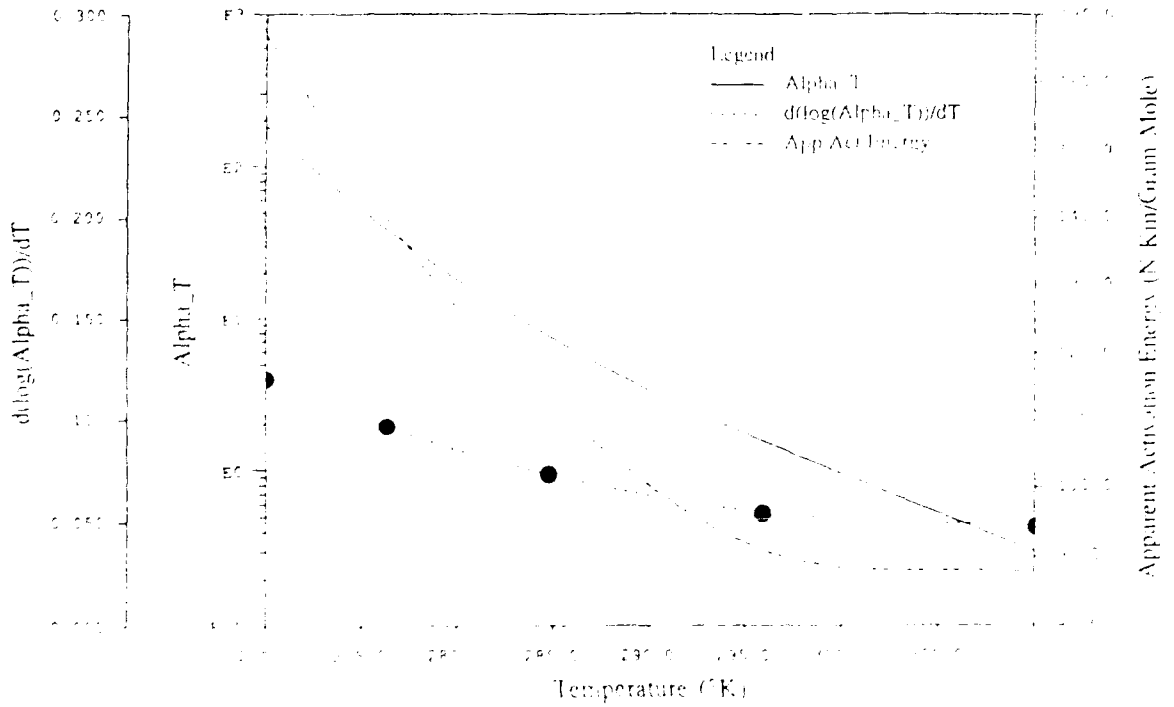

Figure 4. $Log(a_T)$, $d(log(a_T))/dT$, and apparent activation energy vs. temperature for 3M ISD-112

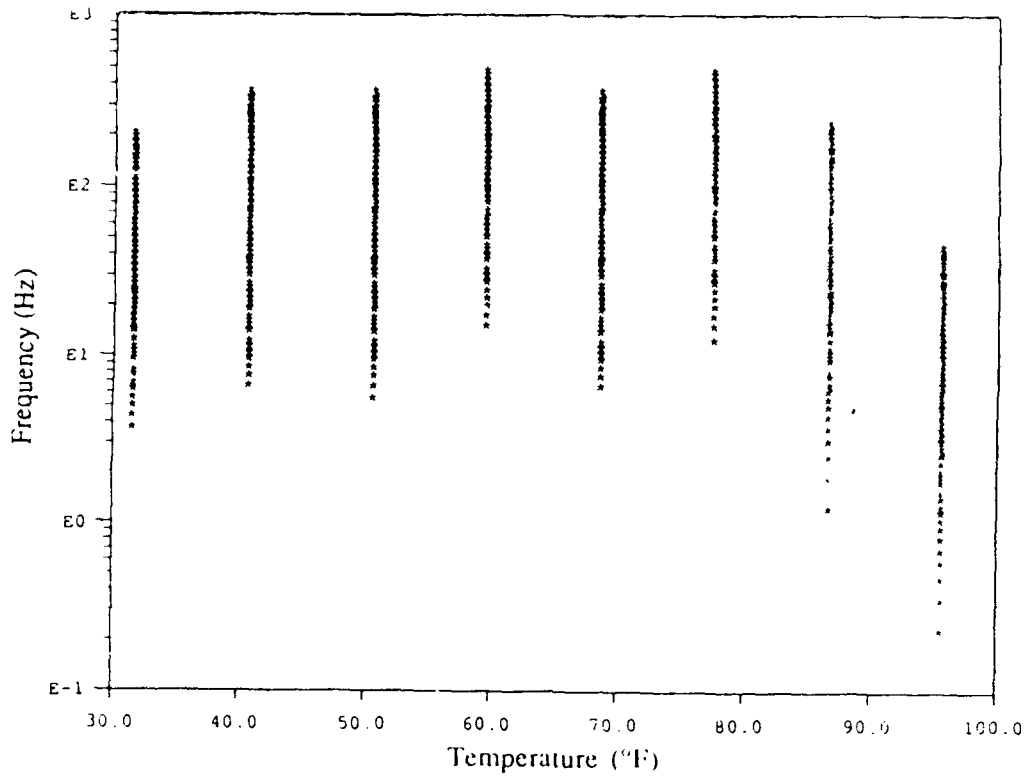

Figure 5. Log(frequency) vs. temperature for 3M ISD-112 (English units)

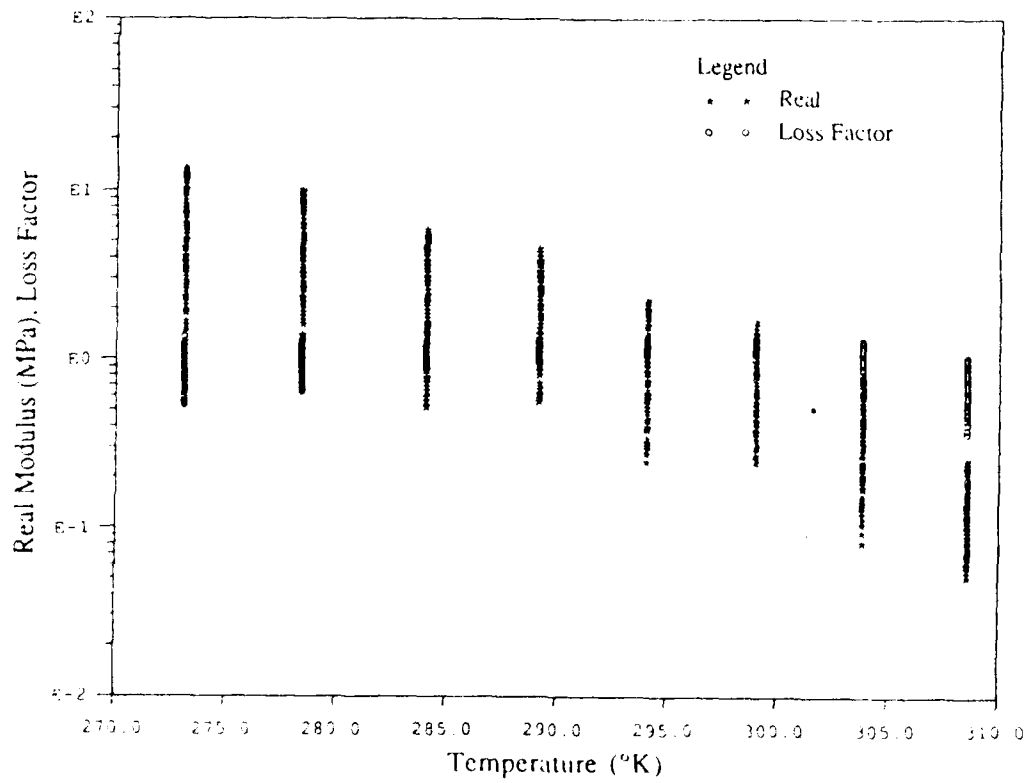

Figure 6. $\log(G^*_R(f,T))$ and $\log(\eta)$ vs. temperature for 3M ISD-112 (S.I. units)

3M Y-966 CHARACTERIZATION DATA

This material is also an acrylic pressure sensitive adhesive, obtained from the sales office of R.S. Hughes, Sunnyvale, CA. The ambient test environment and published shelf-life is identical to that of ISD-112. Since this test specimen was also very thin, similar precautions were exercised to ensure the flatness of the bonding substrates. The surfaces were degreased with a solvent, and the material was bonded to the fixture blocks. This material is generally sold with a nominal thickness of 0.002 in. To decrease the stiffness of the layup (and thus extend the upper end of measurable frequencies), the VEM was doubled to obtain a thickness of 0.0046 in. The total VEM area was 2.32 in^2. Testing was performed on September 25, 1990, using the fixturing and data acquisition system described above. Strain levels during this battery of tests were maintained at approximately 5% and the maximum loss factor observed was 1.27 ($59°F < T < 113°F$ - eight discrete values, and $0.1 Hz. < f < 1000 Hz.$). Figures 7 - 11 provide final detailed characterization data.

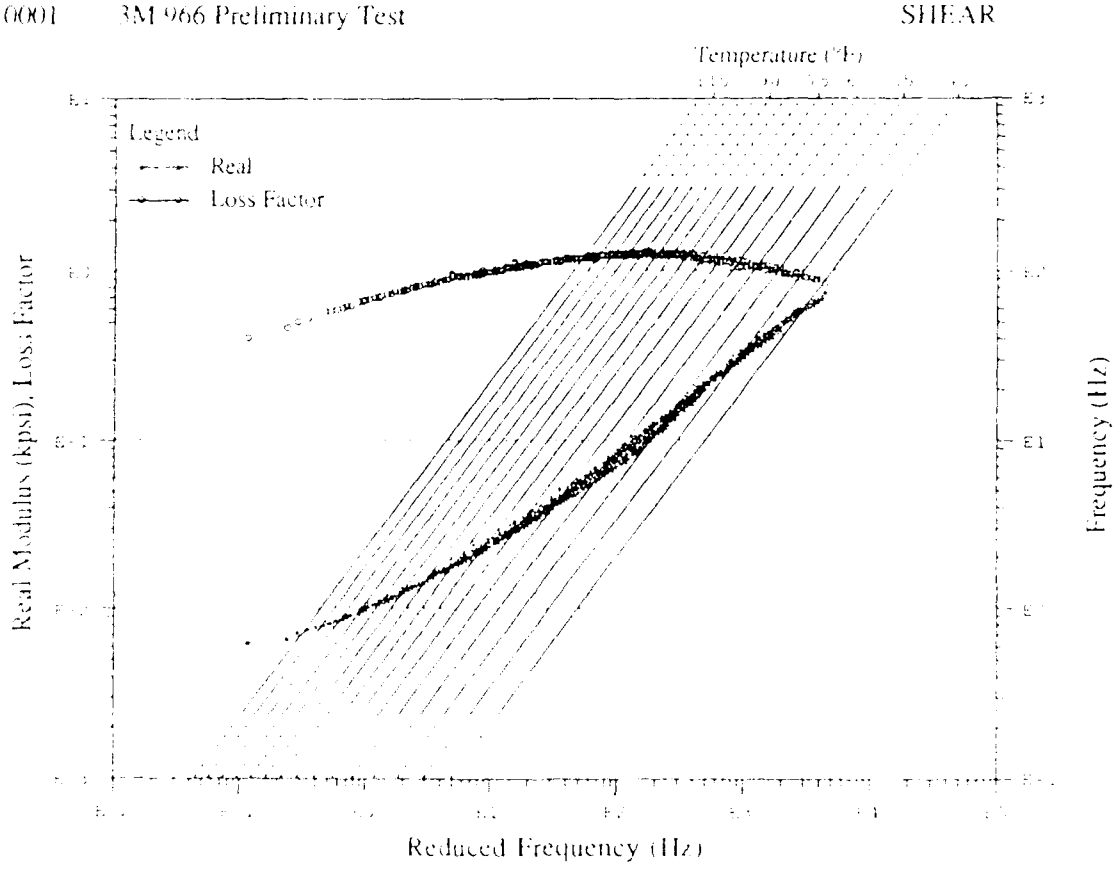

Figure 7. International plot for 3M Y-966 (English units)

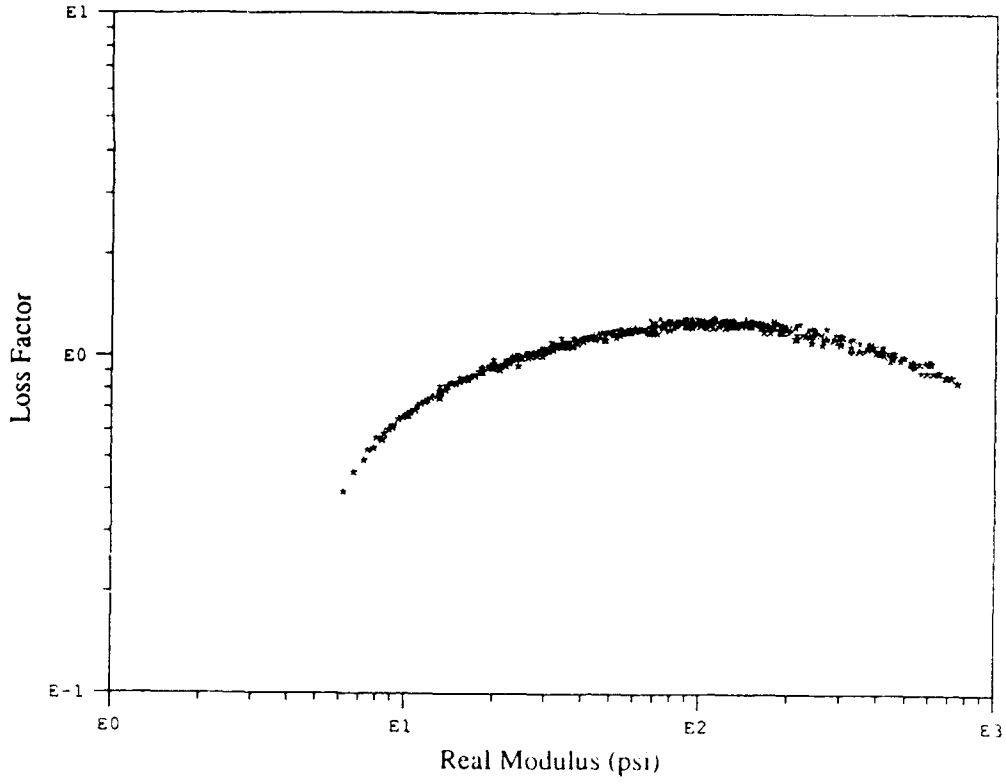

Figure 8. Wicket plot for 3M Y-966 (English units)

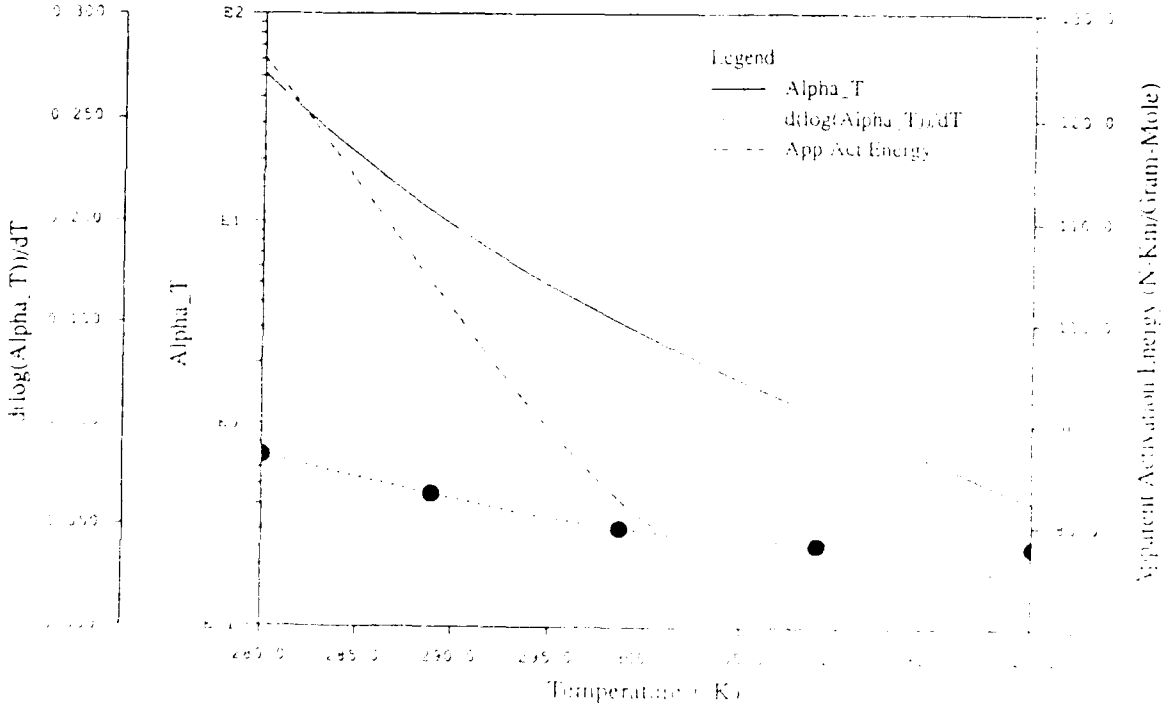

Figure 9. Log(α_T), d(log(α_T))/dT, and apparent activation energy vs. temperature for 3M Y-966

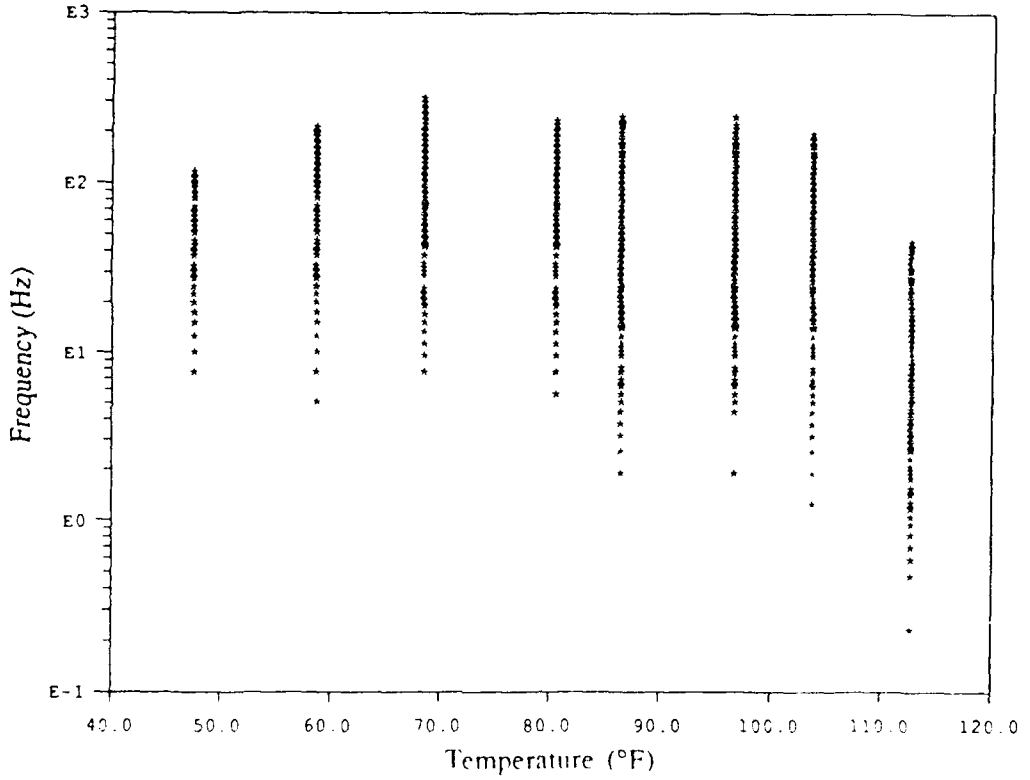

Figure 10. Log(frequency) vs. temperature for 3M Y-966 (English units)

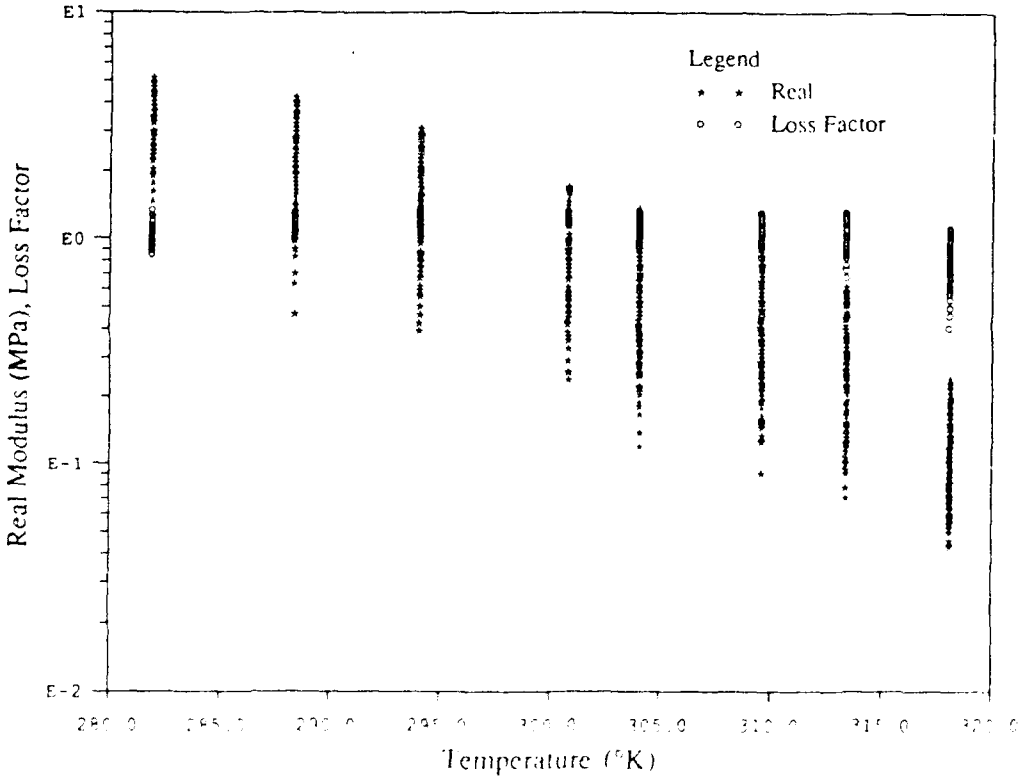

Figure 11. $\log(G^*_R(f,T))$ and $\log(\eta)$ vs. temperature for 3M Y-966 (S.I. units)

SOUNDCOAT DYAD-606 CHARACTERIZATION DATA

The third material test was performed on DYAD-606, a polyurethane manufactured by Soundcoat and obtained directly from their sales office in Santa Ana, CA. It is sold pre-cast in sheet form specifically for vibration damping applications. The test specimen was constructed by bonding the material to degreased aluminum blocks with 3M-1838 epoxy, which was allowed to cure at 75°F for two days. The final specimen area was 3.76 in^2 with a thickness was 0.050 in. Testing was performed on October 2, 1990, utilizing the fixturing and data acquisition system as before. Strain levels during this battery of tests were maintained at approximately 0.4% and the maximum loss factor observed was 1.06 (80°F < T < 126°F - six discrete values, and 0.2 Hz. < f < 1000 Hz.). Figures 12 - 16 provide final detailed characterization data.

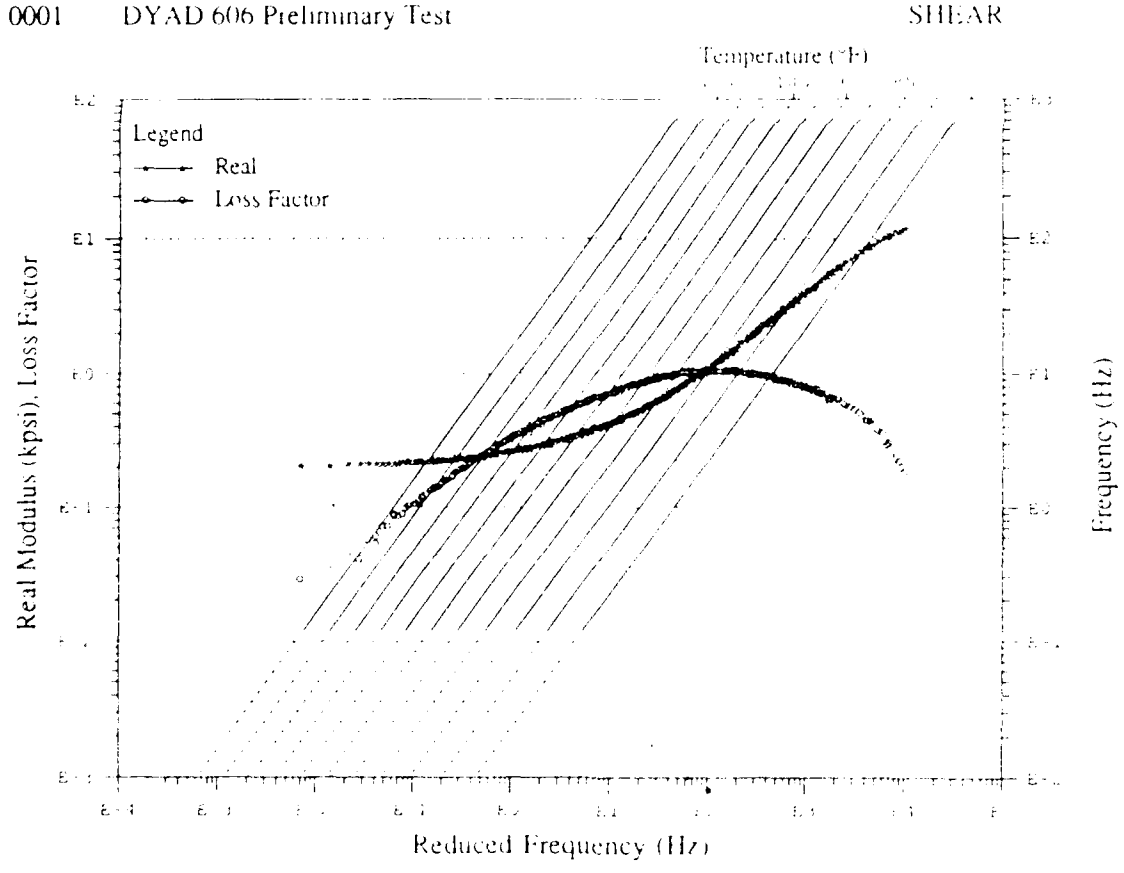

Figure 12. International plot for DYAD 606 (English units)

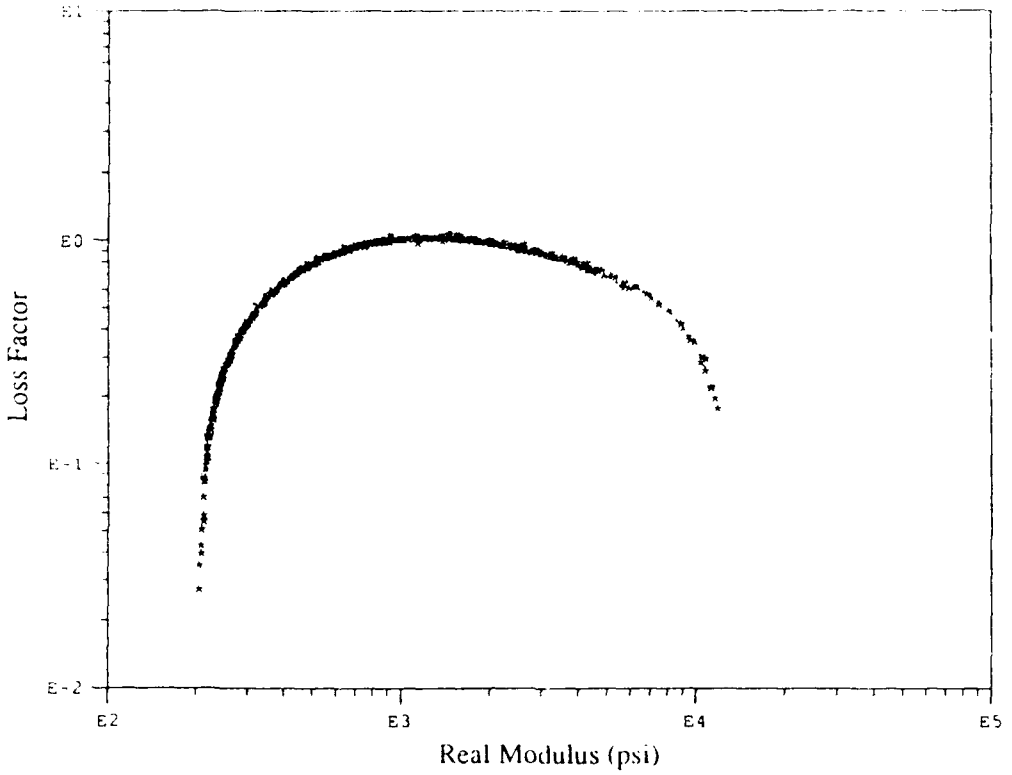

Figure 13. Wicket plot for DYAD 606 (English units)

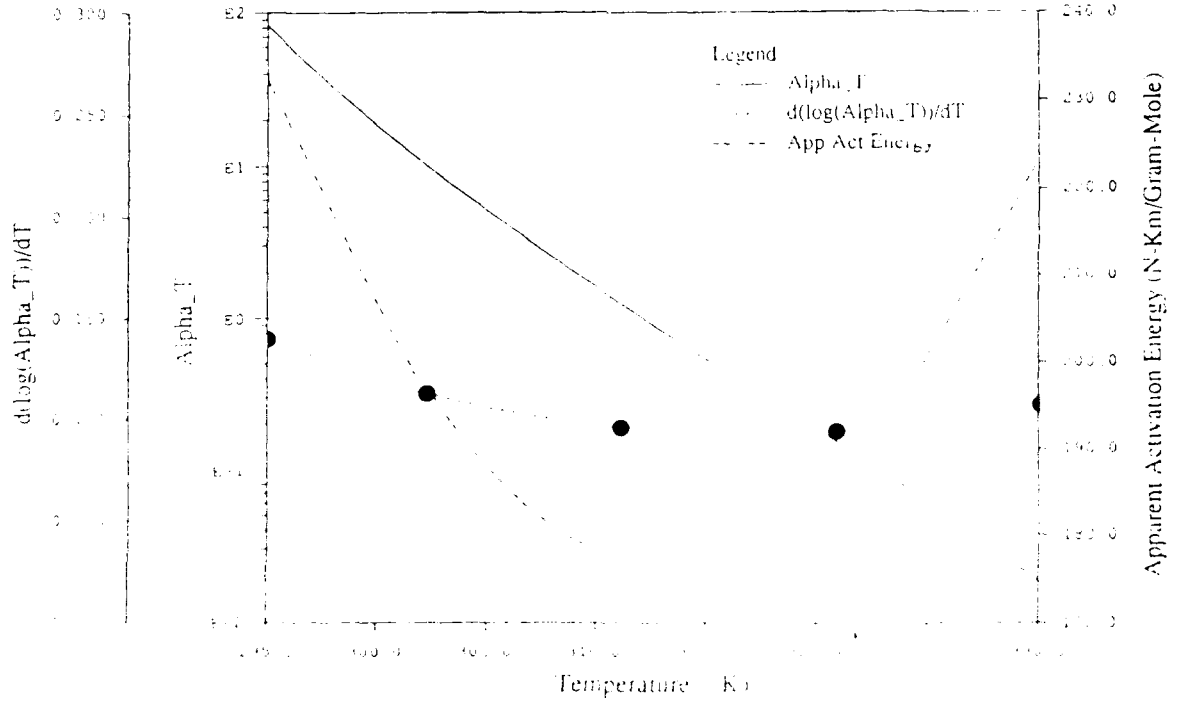

Figure 14. Log(α_T), d(log(α_T))/dT, and apparent activation energy vs. temperature for DYAD 606

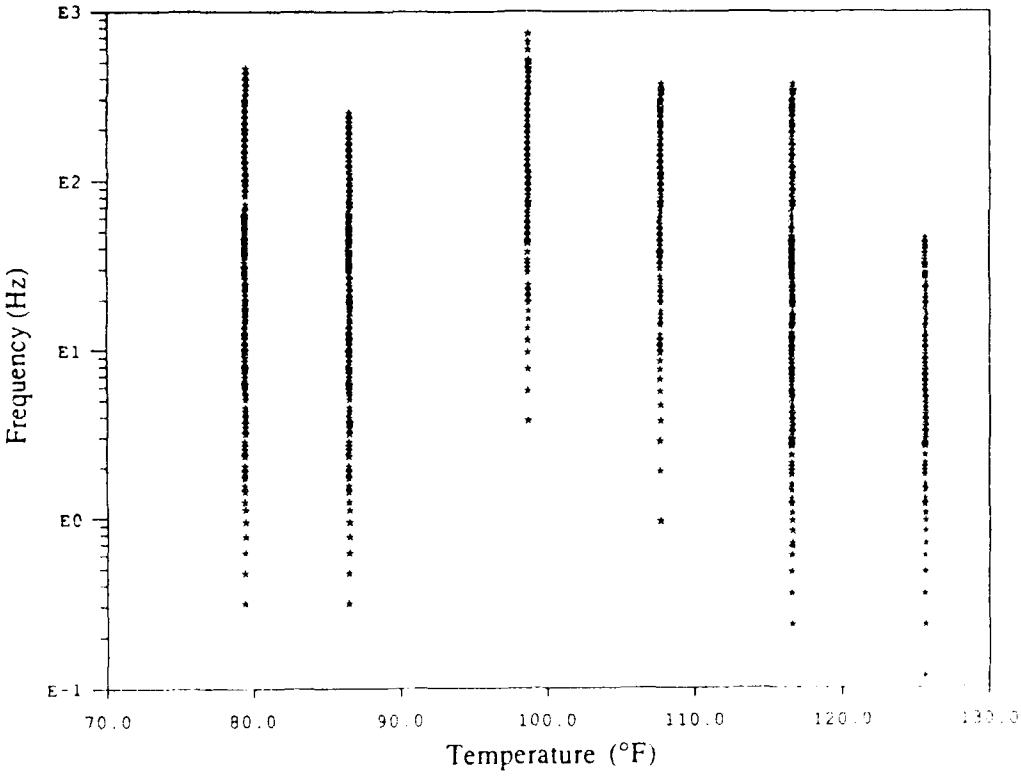

Figure 15. Log(frequency) vs. temperature for DYAD 606 (English units)

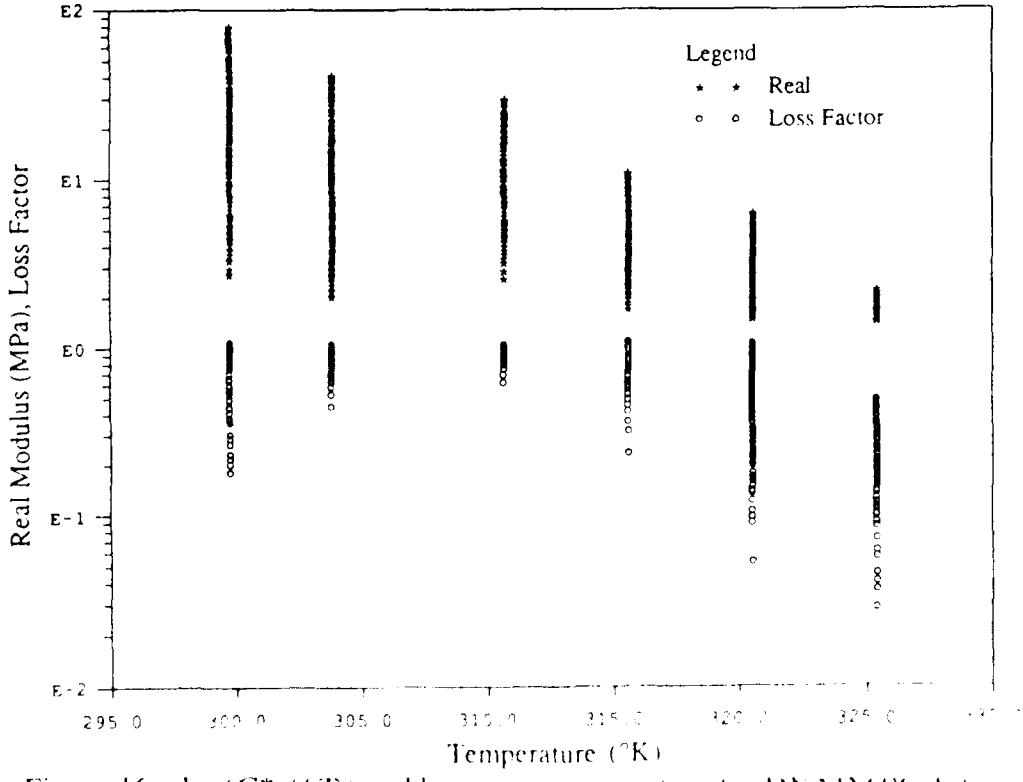

Figure 16. $\log(G^*_R(f,T))$ and $\log(\eta)$ vs. temperature for DYAD 606 (SI units)

ACKNOWLEDGEMENTS

The testing described in this paper was performed in association with the DAMMPS (Damping and Metal Matrix for Precision Structures) program, which is sponsored by the Flight Dynamics Directorate of the Wright Laboratory. The authors wish to thank Mr. B.L. Fowler for his significant efforts in the characterization process and for his expertise in data transfers, facilitating the preparation of this paper.

REFERENCES

1. Allen, B.R., "Measurement of the Mechanical Properties of Viscoelastics by the DCS Method," Presented at the Damping '91 Conference, San Diego, CA, February 13-15, 1991.

2. Fowler, B.L. and Rogers, L.C., "VEM Characterization Program," Presented at the Damping '91 Conference, San Diego, CA, February 13-15, 1991.

3. Yiu, Y.C. and Pinson, E.D., "Damping and Metal Matrix for Precision Structures - Semi-Annual Report, April 1990," Lockheed Missiles & Space Company, Inc., Document F294320-6.

4. Rogers, L.C., "An Accurate Temperature Shift Function and a New Approach to Modelling Complex Modulus," Presented at 60th Shock and Vibration Symposium, Virginia Beach, VA, November 14-16, 1989.

5. Rogers, L.C., "Graphical Presentation of Damping Material Complex Modulus," Preposed Standard, ISO/TC108/WG13-N25, August 1987.

DIRECT MEASUREMENT OF THE DYNAMIC MATERIAL PROPERTIES OF POLYMERS FOR LOW FREQUENCIES

Presenting Author

Paul J. Macioce
Anatrol Corporation

Co-Authors

Ahid D. Nashif, Tom M. Lewis
Anatrol Corporation

ABSTRACT

This paper documents recent advances relative to the characterization of the dynamic material properties of polymers over the frequency range of 1e-4 to 1000 Hz. Discussion of the technique is included as well as data taken on a familiar material. In addition, datasets have been generated for the above material using other techniques over a wide frequency and temperature range, and are presented in a reduced frequency format for correlation of this new technique with other methods.

Anatrol Corporation, 4120 Birch Street, Newport Beach, CA, 92660
Tel: (714) 660-7051

I. INTRODUCTION

There are a number of measurement techniques which are currently used to obtain the dynamic properties of viscoelastic materials. It is commonly accepted that no one technique offers the range necessary to overcome the widely varying nature in material properties of viscoelastics. These properties vary as a function of such parameters as temperature, frequency, dynamic strain amplitude, and static preload for multiple states-of-stress. For this reason, multiple sources are needed to completely characterize a given material. In addition, confidence is established in the accuracy of the test data through correlation of the various techniques over a wide range of temperatures and frequencies. This in turn provides an assurance that the temperature-frequency superposition principle holds within the range of measurements.

Therefore, it is the goal of the data acquisition system to gather dynamic properties over as wide a test range as possible to establish an accurate characterization of materials with a high degree of confidence. The vibrating beam technique and the low-frequency impedance method, presented in this paper, allow for such a range in measurements.

It is the purpose of this paper to discuss the details of the low-frequency impedance technique developed by Anatrol Corporation. Though the development of this system is an ongoing process, this system is currently capable of performing direct material evaluations over a frequency range of 1e-4 to 100 Hz (6 decades of frequency coverage).

A brief description of the measurement techniques used to generate the material properties presented in this paper, including discussion of the merits and limitations of each, is provided with special emphasis on the impedance technique. To demonstrate the effectiveness of this new test system, measurements were made on the "Round Robin" TTPC material [1] using the vibrating beam technique to provide high frequency correlation. A sandwich-type beam specimen was used to obtain the shear properties over a temperature and frequency range of -70° to 150°F and 300 to 3000 Hz, respectively. Preliminary measurements using the impedance technique include data taken at 65°, 75°, and 85°F for frequencies ranging from 5e-4 to 100 Hz.

II. VIBRATING BEAM TECHNIQUE

The vibrating beam technique has become an industry standard for obtaining material properties of viscoelastics over a wide temperature and frequency range (ASTM E-756-80). This technique lends itself well to automated control, and is used to provide a quick characterization of a material with accurate results.

The vibrating beam technique allows for the use of a number of different types of test specimens to calculate either shear or Young's modulus. Some of these specimen configurations are presented in Figure 1.

The complete set of equations which govern this technique for the various configurations shown in Figure 1 can be found from many sources [2,3,5]. However, the sandwich beam equations used to generate the shear vibrating beam data are presented below:

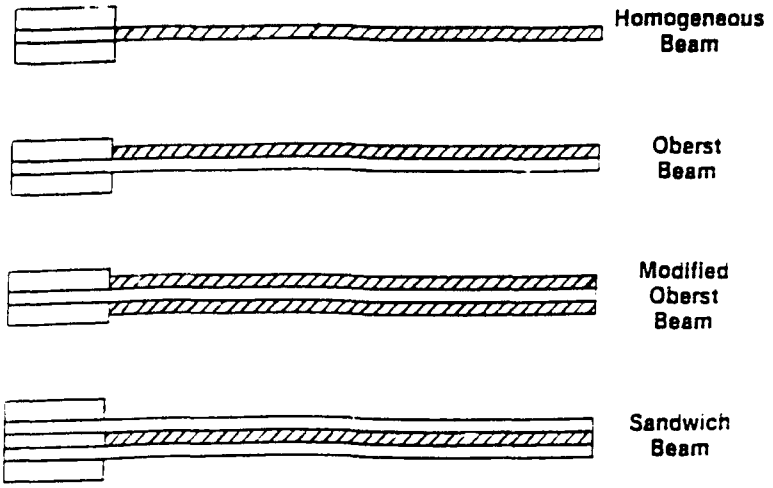

Figure 1: **Various Test Specimen Configurations for the Vibrating Beam Technique**

Sandwich Beam

$$G'(\omega) = \frac{(E_1 H_1 H_2 a_n)\left[(A - B) - 2(A - B)^2 - 2(A\eta_c)^2\right]}{L^2\left[(1 - 2A + 2B)^2 + 4(A\eta_c)^2\right]} \qquad (1)$$

$$\eta = \frac{A\eta_c}{A - B - 2(A - B)^2 - 2(A\eta_c)^2} \qquad (2)$$

where

$$A = \left(\frac{\omega_n}{\omega_{1n}}\right)^2 \left(2 + \frac{\rho_2}{\rho_1}\frac{H_2}{H_1}\right)\left(\frac{B}{2}\right) \qquad (3)$$

$$B = \frac{1}{6\left(1 + \frac{H_2}{H_1}\right)^2} \qquad (4)$$

$$\eta_c = \frac{\Delta f_n}{f_n} \qquad (5)$$

Though the vibrating beam method allows for measurements in both shear and tension/compression, it is extremely difficult to generate scatter-free data necessary to provide a precise estimate of Poisson's ratio. In addition, this technique is unable to monitor the effect of such things as dynamic non-linearities or static preload on the material's dynamic properties.

III IMPEDANCE TECHNIQUE

III.A Overview

The impedance (or forced-oscillation) technique is a direct measurement method which is not limited to the resonance of the test sample and therefore can make measurements over a wide temperature and frequency range. Of the many available systems, the test apparatus described in this paper was developed to provide measurements at extremely low frequencies. This system uses a single-degree-of-freedom model and operates at frequencies below resonance. As with all other techniques, the test apparatus is placed in an environmental chamber to monitor the effect of temperature. This system is currently able to perform automated measurements at frequencies from 1e-4 to 100 Hz and temperatures from -100° to 300°F.

Among the features of this technique, is that the effect of static preload and dynamic strain amplitude can be monitored. In addition, measurements can be made on the same sample in both shear and tension/compression states-of-stress.

III.B Test Specimens

The test specimen design used in the low frequency impedance device allows for measurements to be made in both shear and tension/compression on the same test sample in order to reduce the scatter associated with sample to sample variations. This is done by rotating the sample 90° in the fixture and applying the load from a perpendicular direction. A conceptual sketch of the test specimen is provided in Figure 2. Static preloading of the material in compression is provided by inserting spacers between the box frame of the specimen and the material sample as seen in Figure 2.

III.C Test Procedure

Once a test specimen has been fabricated, it is placed within the temperature controlled portion of the system and is oriented in a position to provide the desired state-of-stress. The box frame of the specimen is bonded in place, a temperature thermocouple is embedded within the viscoelastic material itself, and the center block spacer is attached to the mechanical actuator via a rigid stinger connection. The force and displacement transducers, as well as the actuator are located ourside of the environmental chamber. A sinusoidal input is applied to the specimen which is monitored with the force transducer connected in-line with the actuator. The resulting sinusoidal response of the sample is measured using a displacement transducer.

An FFT analyzer with programming capabilities is used to control the automated data acquisition. The user selects the frequency and temperature ranges to test over, as well as the dynamic strain level to input to the sample. The input force is varied to maintain this strain level for all measurements.

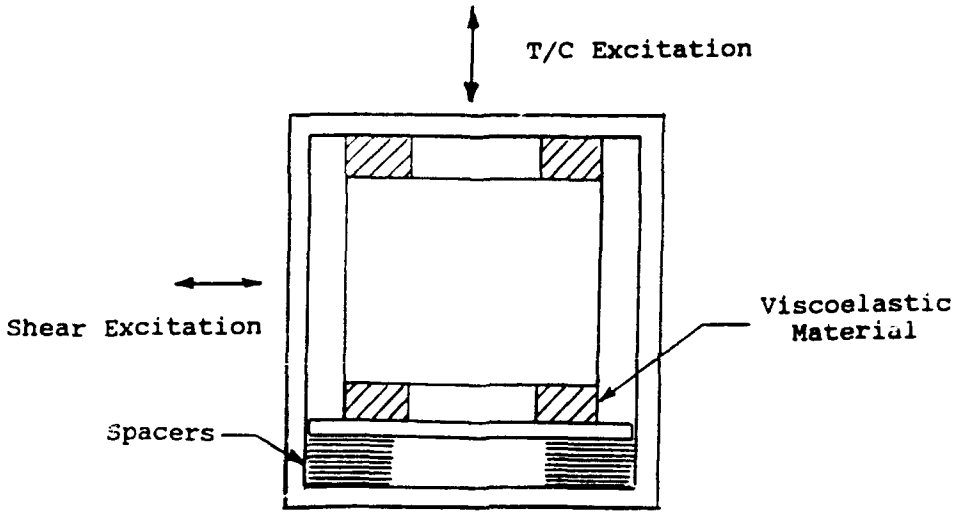

Figure 2: **Schematic Drawing of the Test Specimen Used for the Impedance Technique**

III.D Data Reduction

The impedance technique is based on a single-degree-of-freedom model in which a complex spring element is used. The imaginary portion of the modulus is calculated from the area within the hysteresis loop generated for the input stress on the sample versus the resulting strain of the material as a function of time. The specific equations used are given below:

Shear

$$G'(\omega) = \sqrt{\left(\frac{\sigma_o}{\epsilon_o}\right)^2 - G''(\omega)^2} + \frac{m\omega^2 t}{A_L} \tag{6}$$

$$G''(\omega) = \frac{A_H}{\pi \epsilon_o^2} \tag{7}$$

$$\eta = \frac{G''(\omega)}{G'(\omega)} \tag{8}$$

Tension/Compression

$$E'(\omega) = \sqrt{\left(\frac{\sigma_o}{\epsilon_o}\right)^2 \frac{1}{(1+\beta s^2)^2} - E''(\omega)^2} + \frac{m\omega^2 t}{A_L(1+\beta s^2)} \tag{9}$$

$$E''(\omega) = \frac{A_R}{\pi \epsilon_o^2} \tag{10}$$

$$\eta = \frac{E''(\omega)}{E'(\omega)} \tag{11}$$

III.E Precautions

As is the case with all test techniques, special care must be taken in fabricating the test sample, not only to ensure that proper adhesion is obtained, but also that the pad geometry of the sample is properly designed.

One limitation that is true with all impedance techniques is that testing can not be performed when the sample stiffness approaches the fixture stiffness. This happens at higher frequencies and cold temperatures, or when testing in tension/compression with pads having large shape factors. On the other end of the spectrum, if the test specimen is designed to be too weak, a poor signal-to-noise ratio problem will result with the force transducer when testing in shear at extremely low frequencies and high temperatures. Since this technique covers such a wide range of modulus values, it is difficult to design one sample that will provide clean and accurate data for both extremes. For this reason it may be necessary to design multiple samples of differing geometries.

However, a good rule of thumb is to define the maximum allowable stiffness of the test apparatus, and design the sample to approach this stiffness at the highest test frequency and coldest temperature desired. The vibrating beam technique can be used to provide initial dynamic modulus values needed to calculate the sample stiffness at a given temperature and frequency.

Once the sample has been designed, it is important to ensure that good adhesion is obtained throughout the data acquisition. For those materials which are not self-adhering, a thin layer of structural epoxy is used to bond the material in place without the adhesive "short circuiting" the viscoelastic links or contaminating the edge of the pad. It is favorable to cure the epoxy at room temperature when time will allow to ensure that the material's dynamic properties are not altered in any way due to exposure at high curing temperatures.

It is also good practice to perform measurements at room temperature three times during the testing process; once at the beginning of the test, and again after both the lowest and highest test temperatures. If the same material properties are not obtained after the cold temperature leg of the testing, it is a good indication that the sample has become disbonded. If differences are seen after high temperature testing, it is likely that the material has been heat aged, and irreversible damage has been done to the sample.

In addition to the above precautions, it is important to ensure that proper alignment of the sample with the stinger is achieved, and that all unwanted static preloads are removed before testing is commenced. To obtain accurate results, the sample should be allowed much time to reach an equilibrium

temperature, and that the sample is allowed several loading cycles to reach a steady-state condition. An additional concern is to be aware of where the sample resonance occurs and to restrict testing to frequencies well away from it.

IV. PRESENTATION OF DATA

To demonstrate the effectiveness of this technique, a familiar material was selected, namely the "Round Robin" TTPC [1], and tested over the entire range of frequencies currently available. Measurements were restricted to only a few temperatures, emphasizing the advantage of a wide frequency testing capability. To supplement this low frequency data, the vibrating beam technique was used over a wide temperature range.

Figure 3 represents a plot of temperature versus frequency for the two datasets showing the range in measurements conducted. It can be seen from this plot that the combined dataset spans 7 decades of frequency coverage over a temperature range of -70° to 155°F. Since the beam test is restricted to the linear region of the material, measurements made using the impedance technique were also tested in the linear range. To ensure that this was the case, a linearity check of the material was performed by measuring the dynamic properties for various dynamic strain levels input to the sample. Figures 4 and 5 are the direct shear storage modulus and loss factor values as a function of strain amplitude.

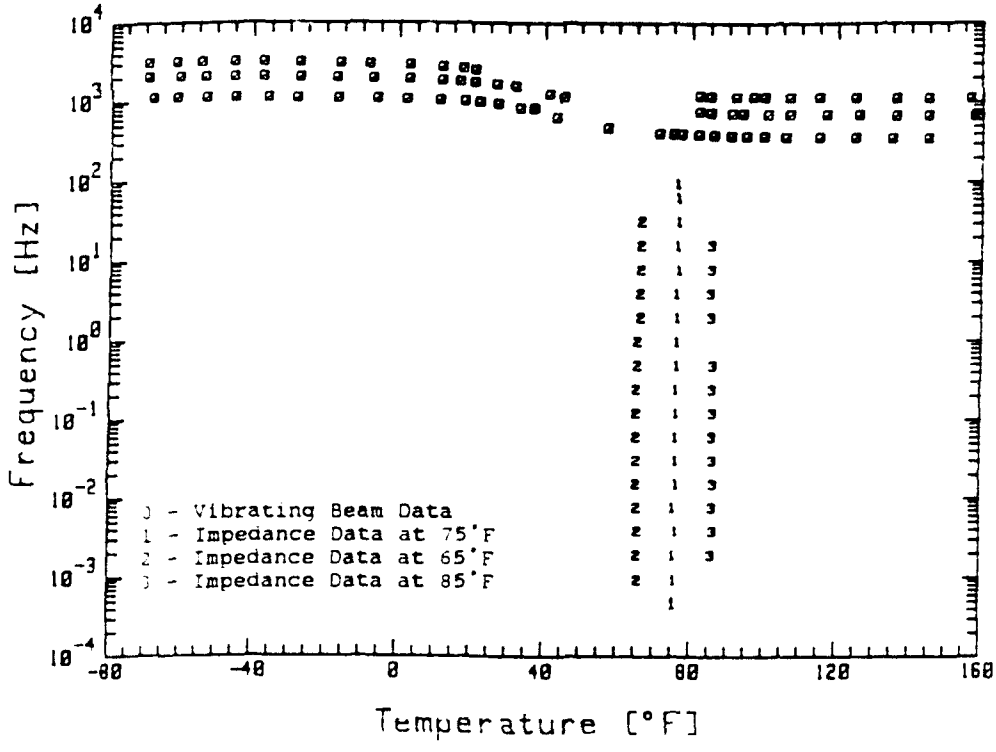

Figure 3: Range of Testing Performed in Shear Using the Impedance and Beam Techniques

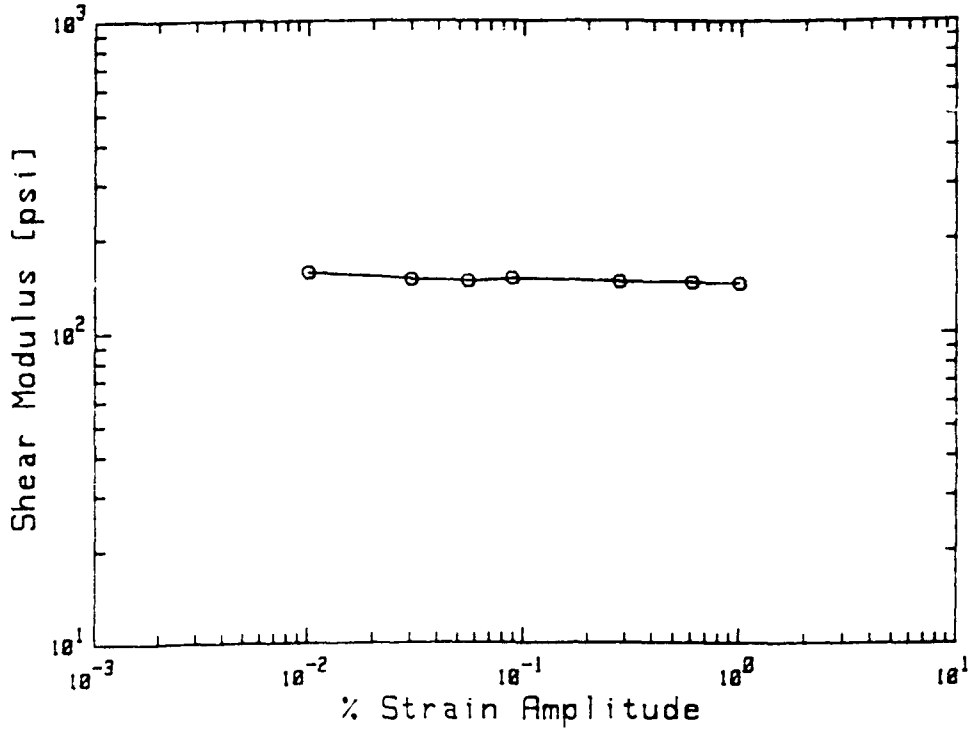

Figure 4: Effect of Various Dynamic Strain Levels on Shear Storage Modulus of the Material

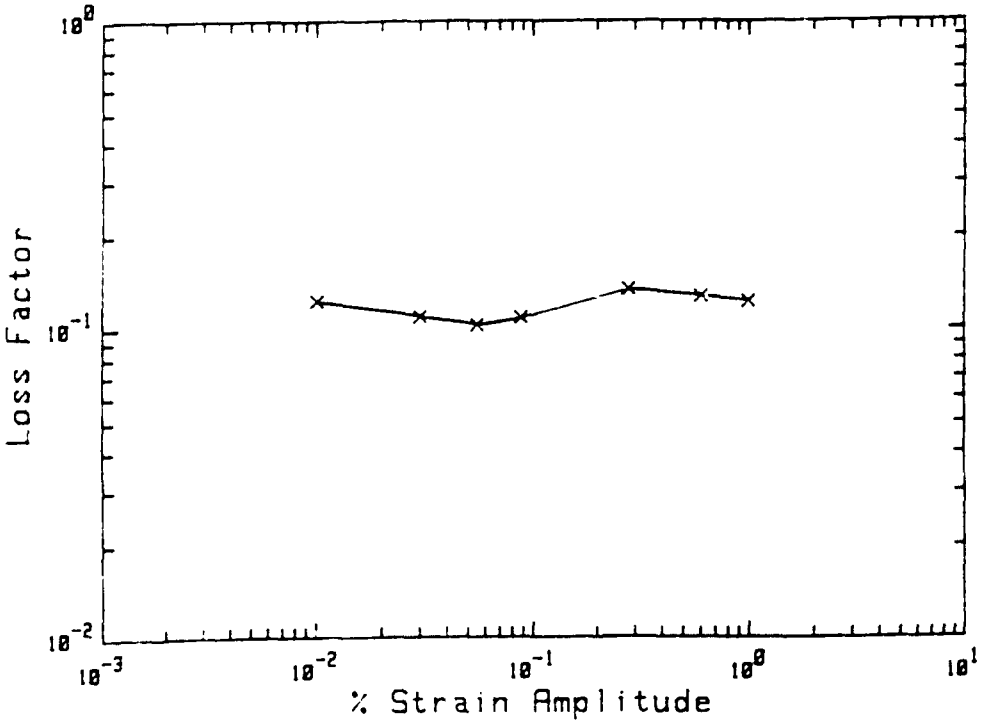

Figure 5: Effect of Various Dynamic Strain Levels on Loss Factor of the Material

In order to display all the material test results in one format, the reduced frequency nomogram is used by applying a shift factor equation to the data. More specifically, the Arrhenius shift factor equation was employed, and found to provide a good representation of the combined datasets of the vibrating beam and impedance techniques. The reduced frequency nomograms are provided for these datasets both separately and combined in Figures 6 through 8.

To qualify the accuracy and consistency of the data, the wicket plots of Figures 9 and 10 were used, plotted in log(storage modulus) versus log(loss modulus) and log(modulus magnitude) versus log(loss factor), respectively. It can be seen from these plots that the data points fall into one smooth and continuous curve, either hook-shaped (Figure 9) of bell-shaped (Figure 10), which is characteristic of the wicket plot.

The remaining nomogram shown in Figure 11 represents a combined display of both shear and tension/compression data. Contained in this plot is the vibrating beam data tested in both states-of-stress, and the impedance data in shear. The obvious missing piece of information is the impedance data in tension/compression. These measurements are currently being performed, and once completed, will allow accurate estimates of Poisson's ratio to be made. However, even with this incomplete dataset, it is interesting to note that Poisson's ratio for this material appears to be a real quantity given by the overlap in the loss factor between the two states-of-stress.

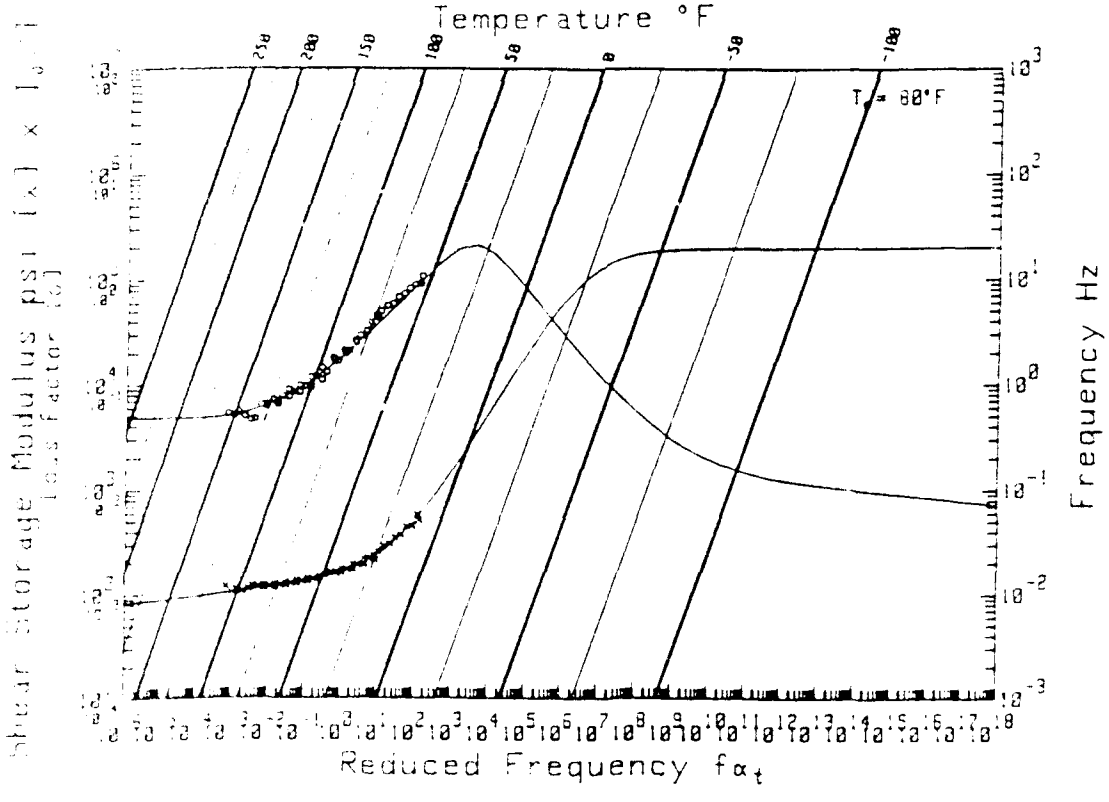

Figure 6: Reduced Frequency Nomogram for the Material Tested in Shear Using the Impedance Technique

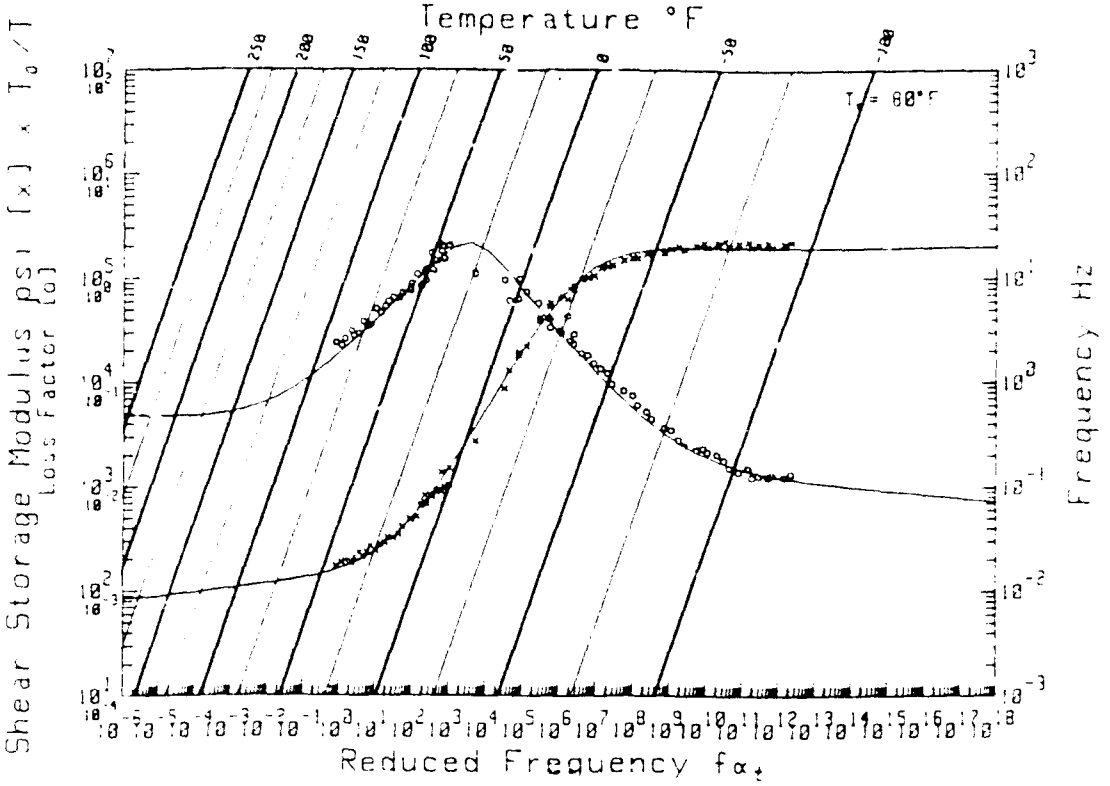

Figure 7: Reduced Frequency Nomogram for the Material Tested in Shear Using the Vibrating Beam Technique

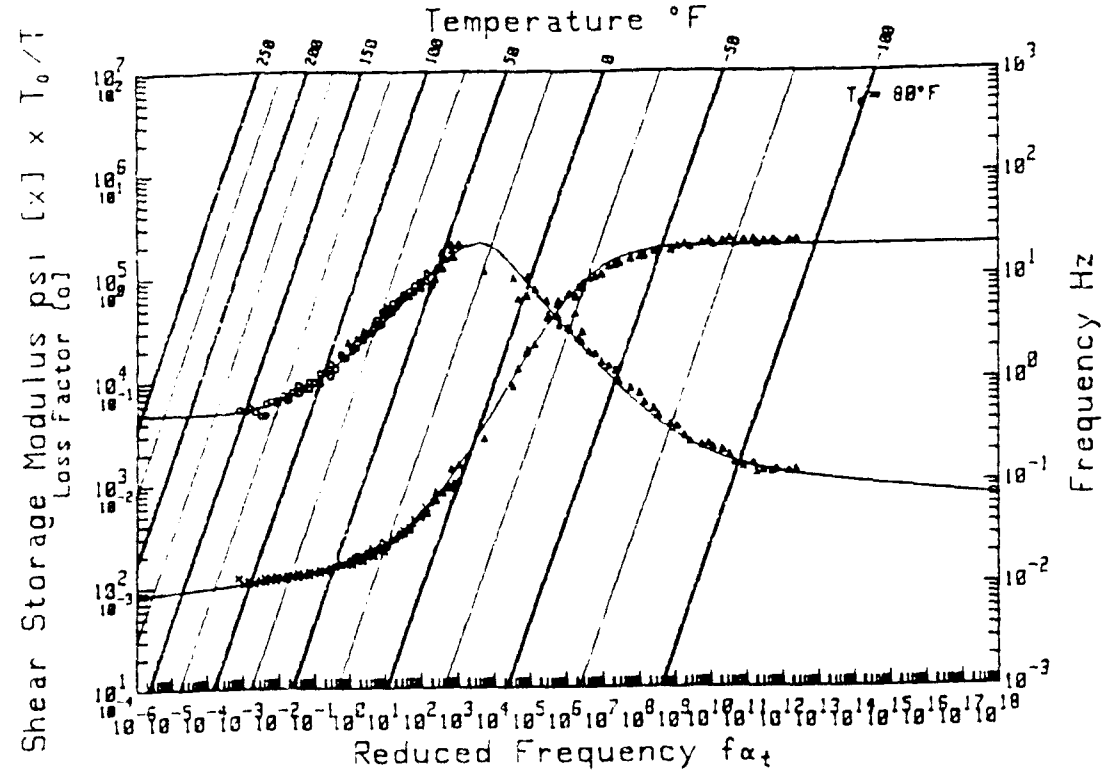

Figure 8: Reduced Frequency Nomogram for the Material Tested in Shear for Both the Impedance and Vibrating Beam Techniques

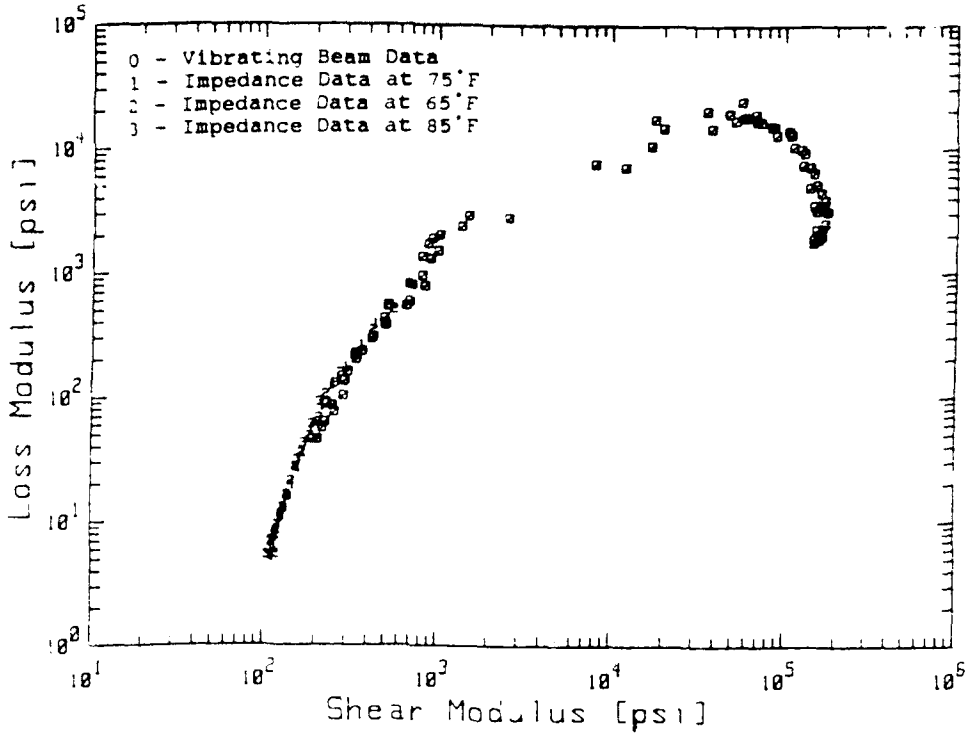

Figure 9: Qualification of Combined Shear Data Using the Wicket Plot in Loss Modulus vs. Storage Modulus Format

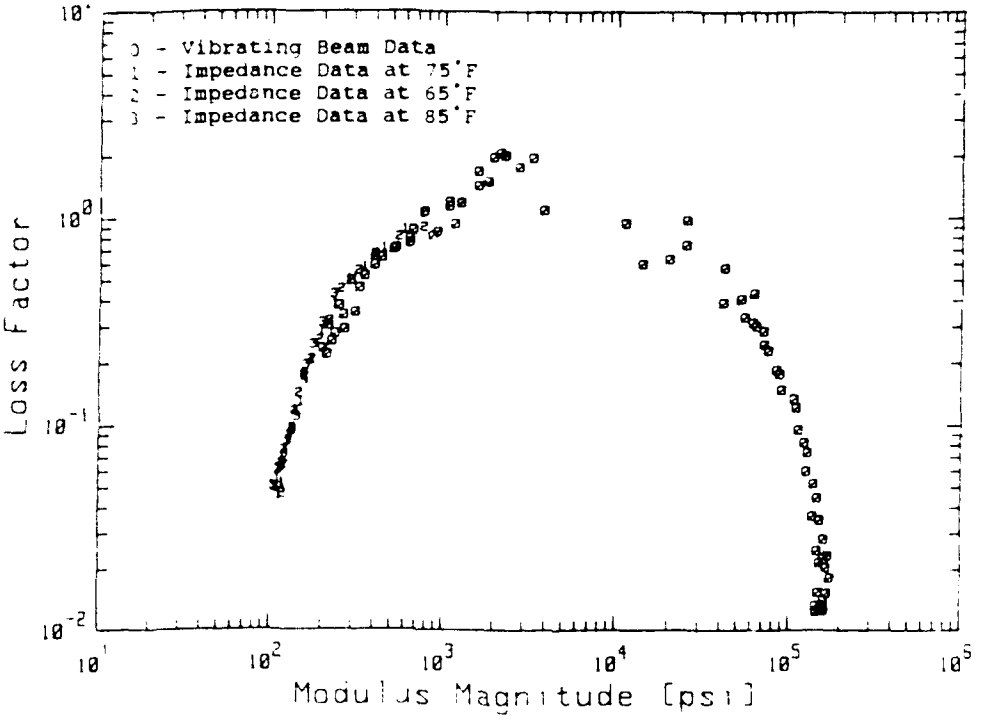

Figure 10: Qualification of Combined Shear Data Using the Wicket Plot in Loss Factor vs. Modulus Magnitude Format

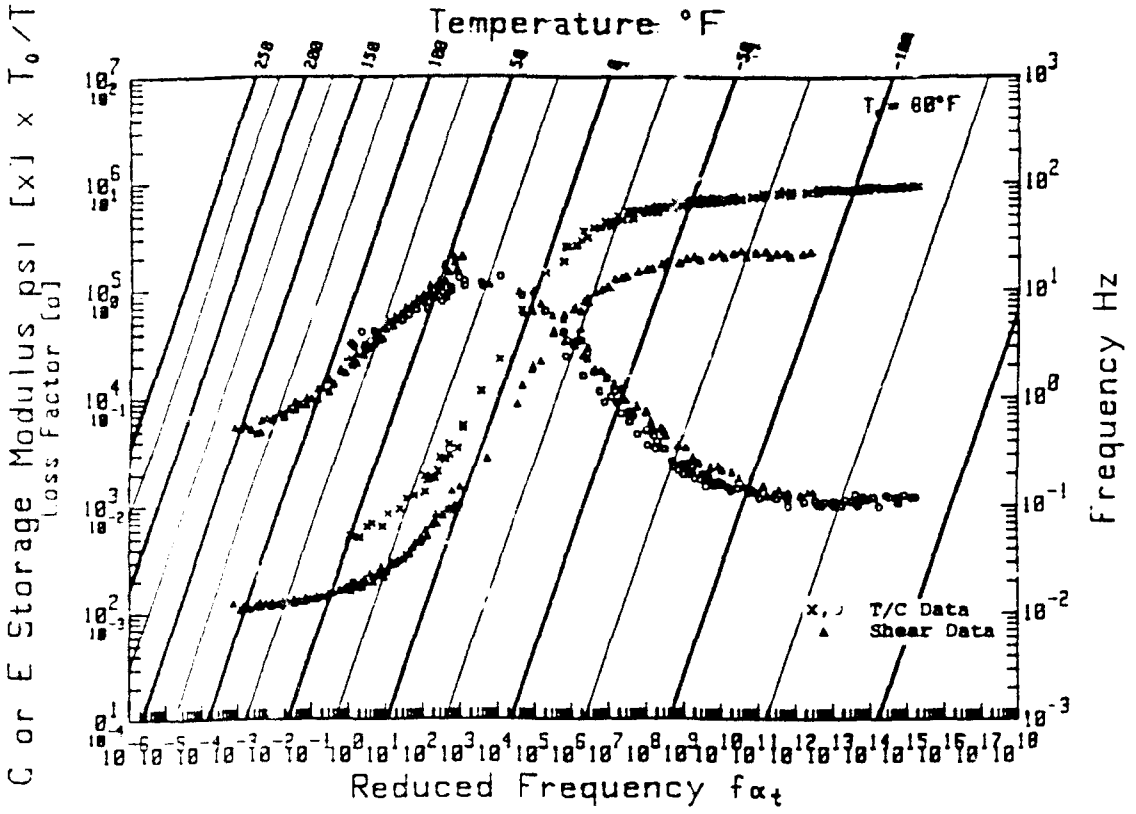

Figure 11: Reduced Frequency Nomogram for the Material Tested in Shear and Tension/ Compression Using Various Techniques

V. FUTURE INVESTIGATIONS

Some of the areas that will be focussed on to make improvements to the range and accuracy of this low-frequency impedance technique are discussed below:

(1) Expand the effective frequency range in which measurements can be performed, both on the high and low end of the spectrum. Theoretically, it should be possible to make measurements above the sample resonance, as well, assuming there are no other modes that interfere with the phase between the force and displacement. However, structural modes of the test fixture itself exist below 1000 Hz. In order to improve the performance on the high end, it will be necessary to increase the rigidity of the stinger and support structure, pushing the system resonances higher in frequency.

The actuator that is used is capable of producing low frequency sine waves down to DC. The limitations on the low frequency end lie in the source generator used, and the practical limits in allowable time which can be invested in making these measurements. Currently, it takes approximately 3 to 4 hours to produce clean waveforms at a frequency of 5e-4. This assumes there are no interruptions that contaminate the measurement traces. Frequencies much lower than this may be possible, but not practical. An achievable goal is however to consistently produce valid measurements down to 1e-4. This would require running the test at night over a 8 to 12 hour time period.

(2) Make estimates of Poisson's ratio by performing measurements in both shear

and tension/compression on the same test specimen.

(3) Select measurement transducers which cover a wider range of operation. At the present time, several transducers are used to cover the wide range of operation demanded by this technique. Displacement transducers have the capability to make measurements from 1e-5 to 4e-2 inches. Unfortunately, two force transducers are required to cover the wide range of allowable frequency measurements.

It is anticipated in the near future to have a system which is capable of generating extremely low scatter data for both shear and tension/compression over a frequency range of 1e-4 to 1000 Hz (7 decades), and at temperatures ranging from -100° to 300°F. However, as the data presented in this paper would indicate, this system is currently able to produce valid data over a wider frequency scale, and at lower frequencies than is available with other impedance systems on the market.

REFERENCES

1. D.I.G. Jones, "Results of a Round Robin Test Series To Evaluate Complex Moduli of a Selected Damping Material",Damping '91, San Diego, CA, 1991.

2. "Standard for Measuring Vibration Damping Properties of Materials", American Society for Testing and Materials, E-756-80.

3. M.L.Parin, A.D.Nashif, T.M. Lewis, "Relsat Damping Material Data", AFWAL-TR-86-3093, Vol. I, pp. AD-1 to AD-80.

4. T.M.Lewis, D.Legros, "Measurement of Polymer Complex Modulus Properties Using Several Techniques", 118th Meeting of the Acoustical Society of America, St. Louis, MO, 1989.

5. T.M.Lewis, A.D.Nashif, "Frequency-Temperature Dependance of Polymer Complex Modulus Properties", Vibration Damping Workshop, 1989.

6. A.D.Nashif, D.I.G.Jones, J.P.Henderson, Vibration Damping, Wiley Interscience, 1985.

LIST OF SYMBOLS

$G'(\omega)$ Shear Storage Modulus
$G''(\omega)$ Shear Loss Modulus
$E'(\omega)$ Young's Storage Modulus
$E''(\omega)$ Young's Loss Modulus
A_H Area of Hysteresis Loop
A_s Loaded Area of Damping Material
A_n Eigenvalue of nth Mode
E_b Young's Modulus of Metal Beam
f_n nth Natural Frequency
Δf Half Power Bandwidth
H_b Thickness of Metal Beam
H_d Thickness of Damping Material
L Length of Beam
m Added Mass of Test Sample

S	Loaded Area-to-Unloaded Area Ratio
β	1.5 for Filled Elastomers/2.0 for Non-Filled Elastomers
ϵ_o	Maximum Strain Amplitude
σ_o	Maximum Stress Amplitude
η	Loss Factor of Damping Material
η_c	Loss Factor of Composite Beam
ω	Circular Frequency ($2\pi f$)
ω_n	Circular Frequency of nth Mode
ω_{1n}	Circular Frequency of nth Mode of Metal Beam
ρ_1	Density of Metal Beam
ρ_2	Density of Damping Material

CORRELATION OF COMPLEX MODULUS DATA BY DIRECT STIFFNESS AND INDIRECT RESONANT BEAM TECHNIQUES

by

David I.G. Jones[1]
Flight Dynamics Laboratory, WPAFB, Ohio

Mona Khouri[2]
DCAN Toulon, Toulon, France

Tom Lewis[3]
Anatrol Corporation, Cincinnati, Ohio

ABSTRACT

Complex modulus data as a function of frequency and temperature for a typical viscoelastic polymer (SNPE Nepurane) have been measured by a direct stiffness technique and by means of the ASTM standard resonant sandwich beam technique. Systematic differences between the two data sets are noted at high values of the damping material shear modulus, at low temperatures. These differences are accounted for through the finite stiffness of the measurement system. Estimates of this stiffness are obtained, which are of the same order of magnitude as those for commercial force gages, and a simple correction is evaluated. The implications from the point of view of obtaining valid data in the glassy region of a polymeric material are discussed.

1. Wright Laboratories, WL/FIBGD, WPAFB, Ohio. Tel: (513) 255-5236.
2. DCAN Toulon, B.P. 77, 83800 Toulon Naval, France. Tel: (33) 94-02-47-74.
3. 10895 Indeco Drive, Cincinnati, Ohio 45241. Tel: (513) 793-8844.

INTRODUCTION

Most of the commercial complex modulus test systems are basically direct stiffness systems in which the specimen is placed in series with a force measuring transducer, a driving force is applied at the other end and the force transducer is attached to a very stiff member. The displacement of the free end of the specimen is measured by a suitable transducer, and the specimen stiffness is calculated from the measured displacement and force signals, usually varying harmonically with time. Such systems are recommended for use when the specimen stiffness is much lower than the stiffness of the remainder of the load chain, but at low temperatures when the specimen is in the glassy state, this condition is not usually met. The resulting error is not obvious, and has often been missed when tests are conducted on stiff specimens, as they inevitably are. The purpose of this investigation was to quantify this error source and demonstrate the care which must always be taken when conducting direct stiffness tests to determine complex moduli.

APPLICABILITY OF VARIOUS TEST TECHNIQUES AND SYSTEMS

At the present time, a wide variety of commercial systems for measuring the complex modulus properties of polymeric materials are offered for sale. These, along with a wide variety of custom made systems, are producing large quantities of dynamic data for various applications, including the monitoring of cure cycles in polymer, plastic and composite production, measurement of linear and nonlinear stress-strain behavior of elastomers and measurement of linear complex modulus properties of polymers over wide frequency and temperature ranges, to name a few. Some of these applications require only a qualitative assessment of the change of specimen or sample stiffness and damping behavior with time, so no question of absolute accuracy arises. For other situations, such as the application of complex modulus data in design of damped systems, the need for accuracy is much more pressing. No commercial or custom made system can measure the complex modulus properties of a polymeric sample at all arbitrary temperatures and frequencies, in part because the stiffness of the specimen may vary by four or more orders of magnitude and also because of changes in the static and dynamic behavior of the test system itself over sufficiently wide ranges of conditions.

Test systems for measuring complex modulus properties of polymers are generally divided into two classes, namely the "direct measurement techniques" and the "indirect measurement techniques", although in reality all measurement techniques are to some extent indirect, because stresses are applied and the resulting specimen deformations over time are observed, and these are never measured directly but must be inferred from other observations.

DIRECT STIFFNESS TECHNIQUES

Typically, the direct measurement techniques involve the application of a force to a polymeric material specimen, measured using a force gage or an impedance head, observing the resulting deformation, using an accelerometer, proximity probe or optical device, and then deducing the complex shear or Young's moduli or the parameters in some other model [1-3]. Fig. 1, for example,

illustrates in extremely simplified form a direct measurement system using (a) measured transfer impedances and (b) measured driving point impedances.

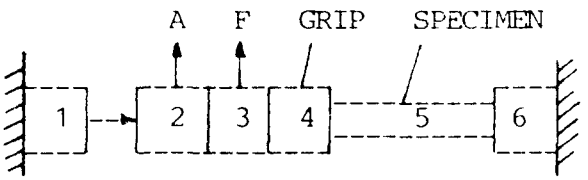

(a) Driving point impedance system

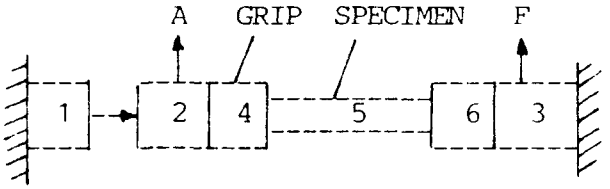

(b) Transfer impedance system

1 - Driver

2 - Accelerometer

3 Force Gage

4,6 - Grips

5 - Specimen

Figure 1. Some direct measurement techniques for measuring complex moduli

Even the simplest models of these systems may be quite complicated, as shown in Fig. 2. Here, the drive system is idealized as a pure force F(t), acting on a mass M_2, which includes the effective mass of the drive system (for example the mass of the excitation coils of an electrodynamic shaker), and the push rod connecting the shaker to the force gage (driving point impedance) or the grip (transfer impedance). The force gage is a device of finite stiffness, including the stiffness of the piezoelectric crystal (k_d) and the flanking stiffness of the case (k_f). The other end of the specimen is connected to a heavy mass M_5, which represents the connection to ground, through the grip stiffnesses k_6 and k_7. The mass M_5 is large but not infinite. It is not surprising that erroneous measurements can arise, such as those which occur when system resonances overlap the frequency range of the test, or when the specimen is very soft or very stiff, or when the forces or accelerations are too large or too small to be accurately measured.

CORRECTION FOR FINITE TEST SYSTEM STIFFNESS

For both the transfer and driving point impedance test systems, some simplification of the approximate analysis may be attained by assuming that mass M_5 is infinite, masses M_2, M_3 and M_4 are zero and that all the stiffnesses in series with the specimen may be combined into a single equivalent stiffness k_o. In this case, which is often approximately the true situation, the specimen stiffness $k_s(1+i\eta_s)$ and k_o may be added as stiffnesses in series to give the apparent specimen stiffness $k_e(1+i\eta_e)$ in the form:

$$\frac{1}{k_e(1+i\eta_e)} = \frac{1}{k_o} + \frac{1}{k_s(1+i\eta_s)} \qquad (1)$$

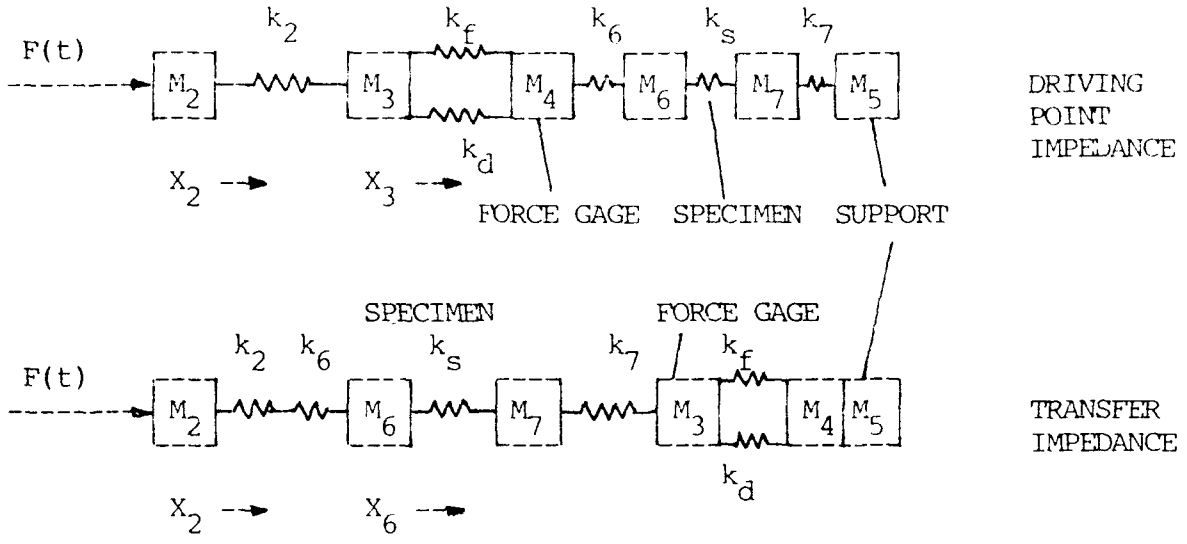

Figure 2. Simple models of direct measurement systems

Note that when k_s is larger than k_o, as happens when the temperature is low and the modulus of the specimen material is large, the limiting value of k_e is equal to k_o. Therefore, the true modulus of the specimen material is underestimated. Equation (1) may be used to estimate k_s and η_s from measured values of k_e and η_e, and a known value of k_o, obtained by measurement or other means. However, the exact value of k_o will depend on the manner in which the specimen is held in the grips and may vary significantly from test to test unless great care is taken.

VIBRATING BEAM TEST TECHNIQUES

Indirect measurement techniques include the various vibrating beam systems illustrated in Fig. 3 [2,3]. The boundary condition of choice is usually the clamped-free system, with the clamped end having a massive root and placed in a massive support structure. Free-free boundary conditions are very attractive in principle, but are difficult to achieve in practice for operationally "user-friendly" systems. From time to time, however, efforts are made to achieve this goal and it may be more readily attainable at the present time, as compared to the past, because of the much improved systems for control and measurement now available. In any case, the indirect measurement systems also have their problems. For example, great care must be taken to ensure uniformity of the test beams, the polymeric material and the bond line on to or between the beams. Also, if the dimensions are not well chosen, excessive magnification of errors arises when the polymeric material is soft and does not influence the layered beam system strongly enough for the complex modulus properties to be accurately deduced from the observed dynamic behavior. More specifically, errors can be expected when the parameter Z^2-1, defined in equation (2) below, approaches zero.

$$Z^2 = (1+\rho_2 h_2/N\rho_1 h_1)(f_n/f_{on})^2 \qquad (2)$$

where N=1 for the Oberst beam, 0.5 for the modified Oberst beam and 2.0 for the

sandwich beam. The subscript 2 refers to the polymeric layer(s), while the subscript 1 refers to the metal beam(s). The resonant frequency of the damped system is f_n while that of each metal beam is f_{no}.

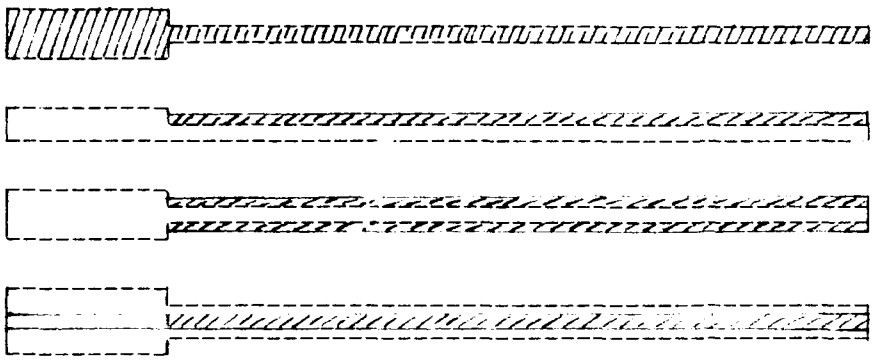

Figure 3. Vibrating beam test systems

USEFUL RANGES FOR VARIOUS TEST SYSTEMS

It may be claimed without exaggeration that the possibilities for producing numbers, representing complex modulus properties, which are in error, often by great amounts, far exceed the possibilities for producing accurate data unless very great care is taken. This applies for any apparatus, and is the crux of the problem. Each apparatus or specific test configuration is bounded, for example, by the temperature range over which internal stresses do not interfere with measurement accuracy or the indicated temperature is not close to the true specimen temperature. The useful frequency range is bounded on the low side by sensitivity of detection devices and on the high side by internal resonances which give readings having nothing to do with specimen behavior. And extremely low values of the specimen stiffness make it difficult to measure the force, while high values of the specimen stiffness interfere with measurement by interacting with the now comparable stiffnesses of various parts of the test system. Therefore, each system or configuration usually provides accurate data over a limited range of conditions. Fig. 4 illustrates, very broadly, the typical ranges for a number of test techniques [4]. The direct measurement techniques generally cover the frequency range from, typically, 0.001 Hz to 1000 Hz and moduli from 10 psi to 10000 psi. These numbers relate to the possible range for several types of system, no one of which covers the entire range, and measurements outside this range would typically involve unusual specimen sizes or equipment configurations, greatly increasing the cost. The beam techniques typically apply from about 100 Hz to 10000 Hz, and moduli from 10 to 100000 psi. At any given temperature, the modulus of a polymer varies according to the curved lines A-G, H-M or N-R. It is seen that no one technique can be used over the whole range, but that different techniques come into play as one moves from the low modulus end to the high modulus end.

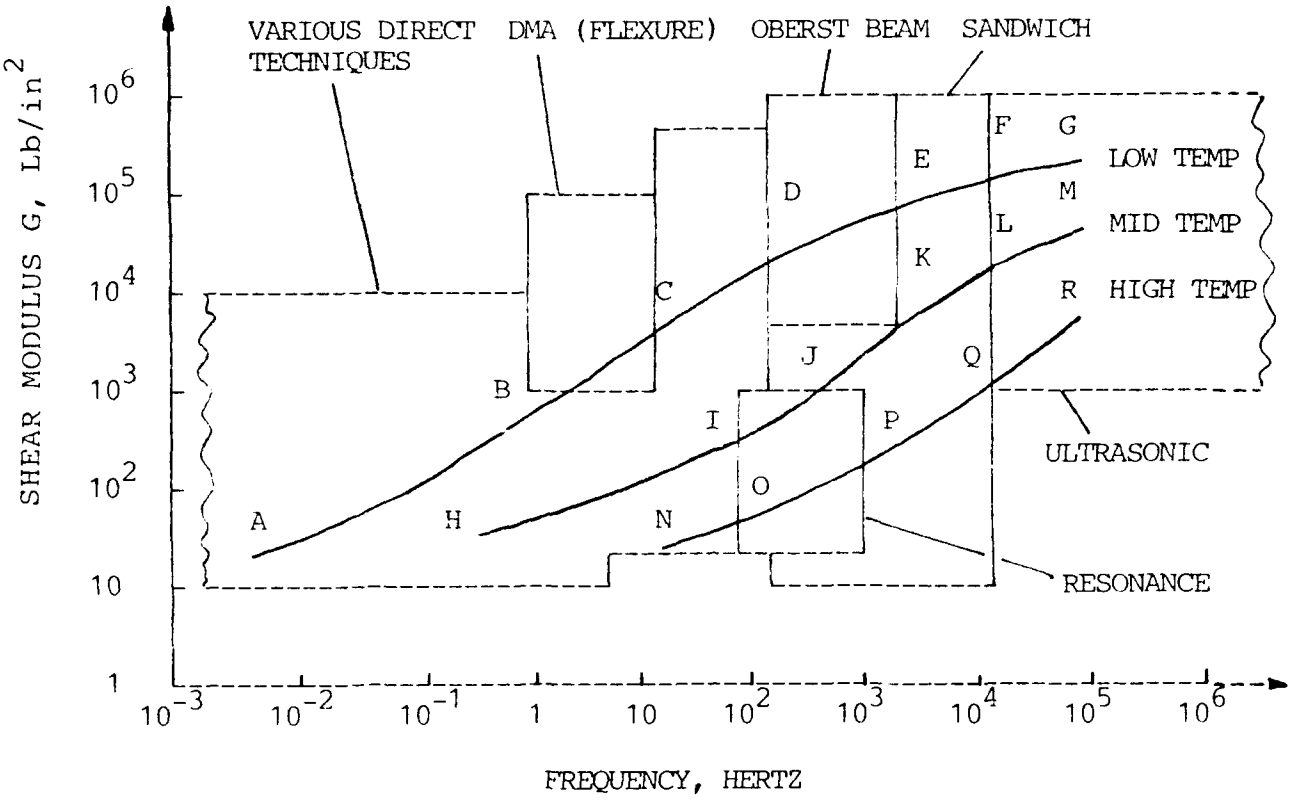

Figure 4. Zones of applicability of various test techniques

Therefore, to obtain accurate complex modulus data over the full range for a material, it is usually desirable, and often necessary, to use several test techniques and combine the data so obtained. Even when one test technique appears to cover the entire range, it is strongly recommended that other techniques also be used to verify that major systematic errors have not arisen from applying the first technique over too broad a range. Such checks can greatly increase one's own confidence in the data, as well as that of other users.

THE WICKET PLOT FOR QUALIFICATION OF COMPLEX MODULUS DATA

When one has obtained a set of complex modulus data for a specific material for a sufficiently wide range of frequencies and temperatures, one often has not had the opportunity to examine all possible sources of error. The plot of log(loss factor) versus log(modulus), known as the Wicket Plot, has become the Occam's Razor of test data evaluation, since potentially erroneous data often stands out extremely clearly. Fig. 5 illustrates an idealized Wicket plot. In this plot, the main sequence of data, if good, will tend to outline a unique relationship between loss factor and modulus. Points, or sets of points, which are well away from the main sequence are subject to question. For example, test data obtained by direct stiffness techniques often have a tendency to drop away from the main sequence for high modulus values because of the finite specimen stiffness approaching or exceeding the measuring system stiffness, and data obtained by indirect techniques, such as the resonant beams, will often tend to deviate above the main sequence at low modulus values because of error magnifications.

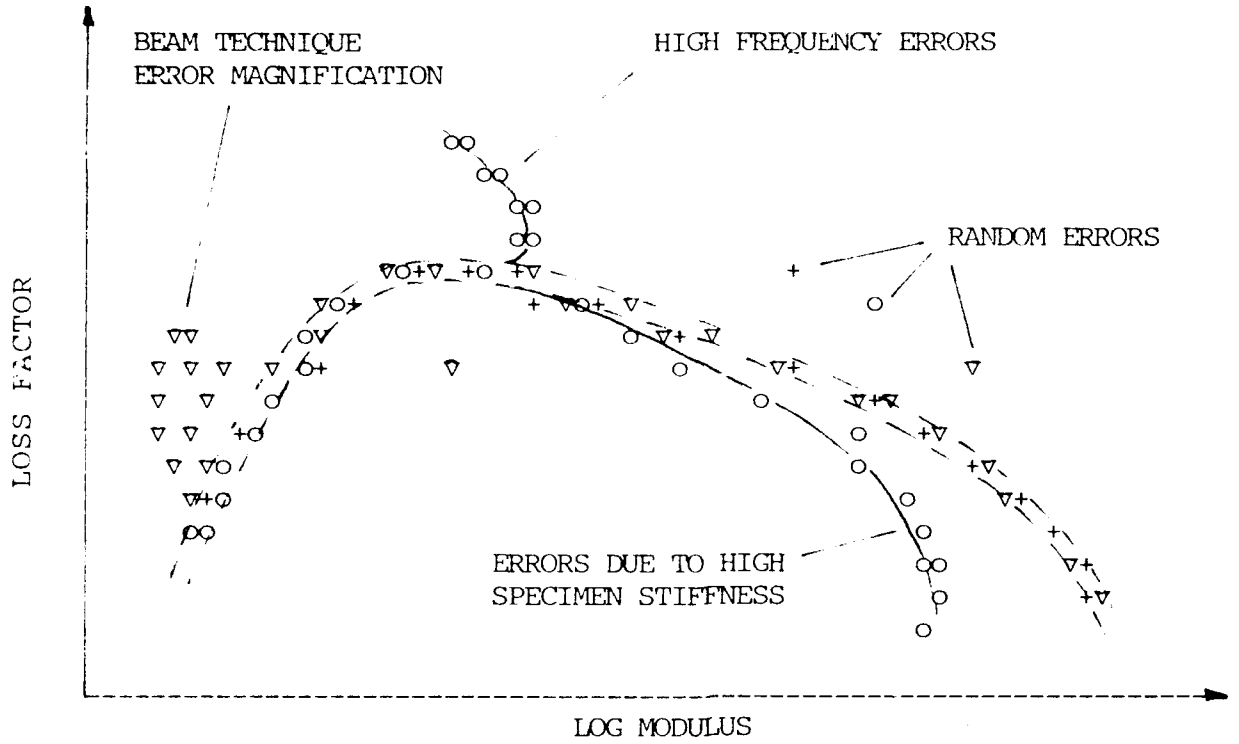

Figure 5. Idealized Wicket Plot for a Polymeric Material

Analysis of the suspect points in the test data will often provide sufficient justification for rejecting those particular points. Sometimes, individual points will deviate from the main sequence for no apparent reason, and must be rejected even without documented cause unless one is fortunate enough to have an extraordinarily complete record of the original tests. When such data is available, such points are often found to be due to isolated resonances superimposed on the main resonance (especially for indirect techniques), distorted signals in the measurement system, occasional errors in writing down the data when taken manually (not so common these days) etc. Unless one is extremely unfortunate, a sufficient number of points will remain to conduct frequency-temperature analysis of the data with a fair degree of confidence that the method of reduced variables will lead to satisfactory master curves in the well known manner.

MEASUREMENT OF COMPLEX MODULI OF SNPE NEPURANE POLYMER [5]

DIRECT STIFFNESS SYSTEM

The complex moduli of the test material were evaluated in shear using a single lap shear specimen having thickness h = 2.00 mm, width b = 5.75 mm and length l = 5.80 mm. The tests were conducted at several temperatures from - 30°C to + 70°C, and over a frequency range from 7.8 Hz to 500 Hz, by means of a Metravib Viscoanalyzer system [6]. The measured stiffnesses were converted to shear moduli by a specimen factor bl/h = 59.97 m. The test results are summarized in Table 1.

RESONANT BEAM TESTS

After the direct stiffness tests had been completed, difficulties arose in applying frequency-temperature analysis in the glassy region [8], and it was believed that these might be ascribed to measurement errors arising from temperature control and insufficiently stiff grips. The resonant beam tests, conducted to provide more reliable data in the glassy region, in particular, were carried out on a steel sandwich cantilever beam of length l = 254 mm, core thickness h_2 = 1.77 mm and the two external beam thicknesses were h_1 = 1.60 mm, as shown in Figure 3. The test data was obtained at discrete temperatures from - 17°C to + 80°C and discrete frequencies from about 100 Hz to 2000 Hz. The test results are summarized in Table 2.

WICKET PLOT ANALYSIS

The Wicket plot for the test data is shown in Figure 6. The tendency for the direct stiffness technique data to "fall off" at high values of the shear modulus is clearly seen, and is without doubt the reason for the difficulties encountered in applying frequency-temperature analysis in the glassy region.

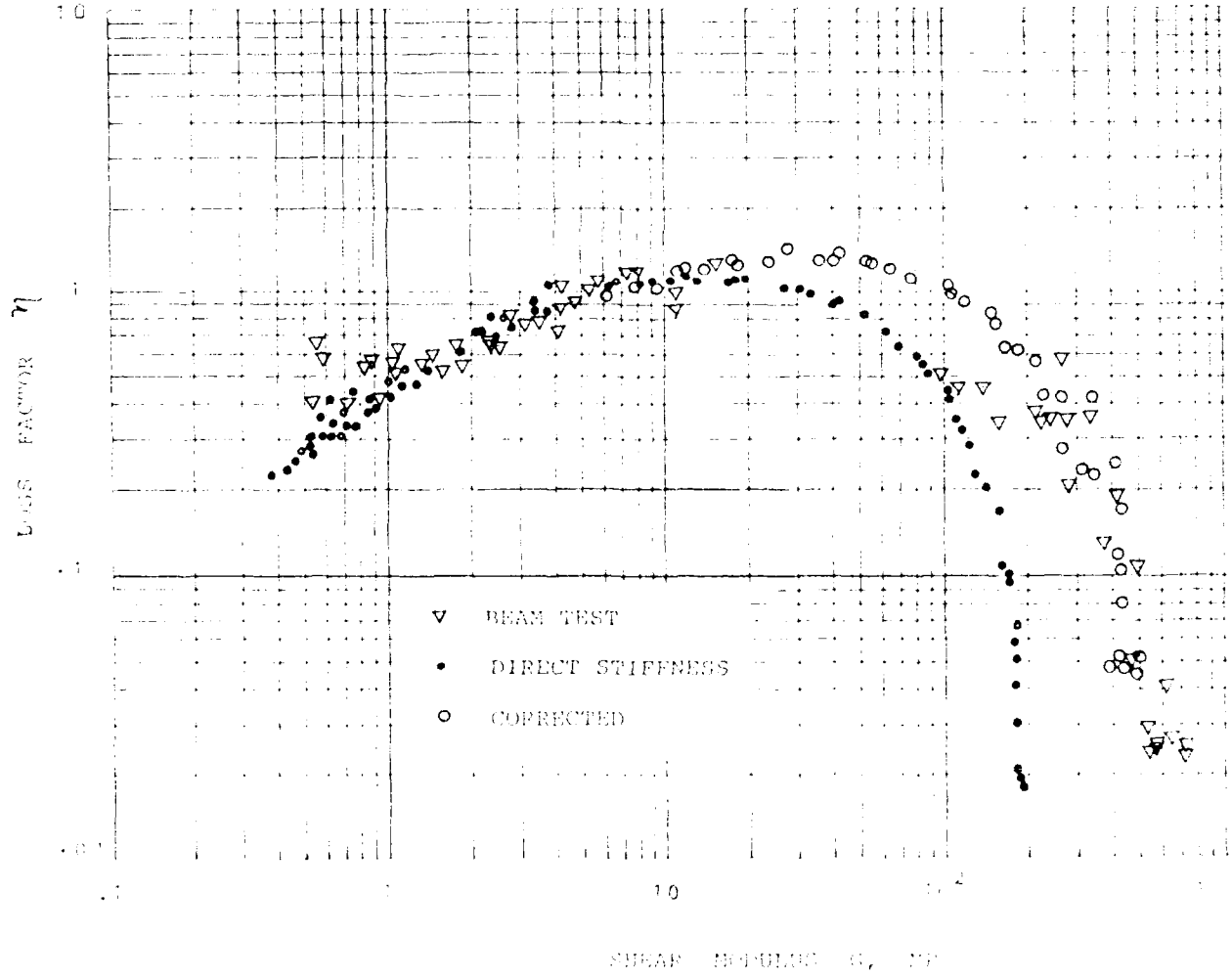

Figure 6. Wicket Plots for SNPE Nepurane

The value of the series stiffness k_o required to "move" the apparent asymptotic value of the shear modulus, G_e = 2E2 MPa, to the value of about 5E2 MPa, indicated by the beam tests, is about 5E6 N/m, as calculated by means of equation (1) with a specimen factor bl/h= 59.97 m. This is a little less than the value of about 1E7 N/m often quoted for the stiffness of commercial force gages, perhaps because of the additional series stiffness of the grips. Note that this correction may be difficult to apply in general because k_o is not known a-priori and must be determined by comparisons, as with the beam data.

The "corrected" values of G and η for the direct stiffness method, allowing for this value of k_o and the specimen factor of 59.97 m, is calculated also using equation (1) to give:

$$G = \frac{59.97\ [k_e^{-1} - 2E\text{-}7(1+\eta_e^2)]}{(k_e^{-1} - 2E\text{-}7)^2 + (2E\text{-}7\,\eta_e)^2} \qquad (2)$$

$$\eta = \frac{\eta_e}{k_e\ [k_e^{-1} - 2E\text{-}7\ (1+\eta_e^2)\ ]} \qquad (3)$$

with k_e = 59.97 G_e, G_e being the apparent modulus and η_e the apparent loss factor, not corrected for k_o. The "corrected" points are plotted in the Wicket plot, Figure 6. The agreement with the beam data is good. Additional evidence of the significance of this is seen in Figure 7, where a set of typical plots of G and η versus frequency are compared at a specific temperature.

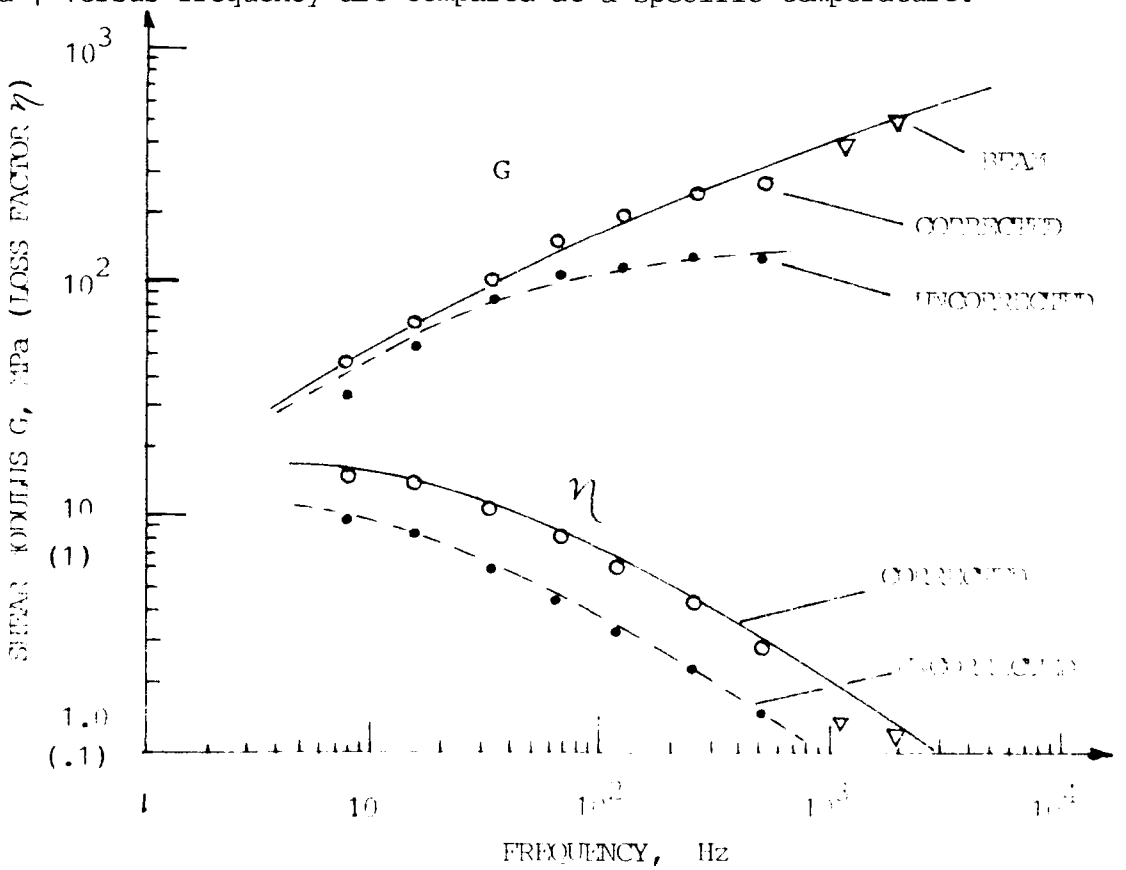

Figure 7. Plots of G and η versus frequency at -10°C

REDUCED FREQUENCY MASTER PLOTS

The corrected values of G and η for the direct stiffness technique and for the resonant beam technique agree quite well for all temperatures where comparisons can be made. Figure 8 shows the reduced frequency master curve obtained by using appropriate shift factors, with reference temperature T_o = 0°C (32°F), as shown in Figure 9. It is seen that the two data sets do not agree completely and lead to somewhat different shift factor behavior as well. The available data is insufficiently precise to allow complete resolution of the matter. However, the need for care to be taken with direct stiffness measurement techniques at high specimen stiffness values is clearly demonstrated.

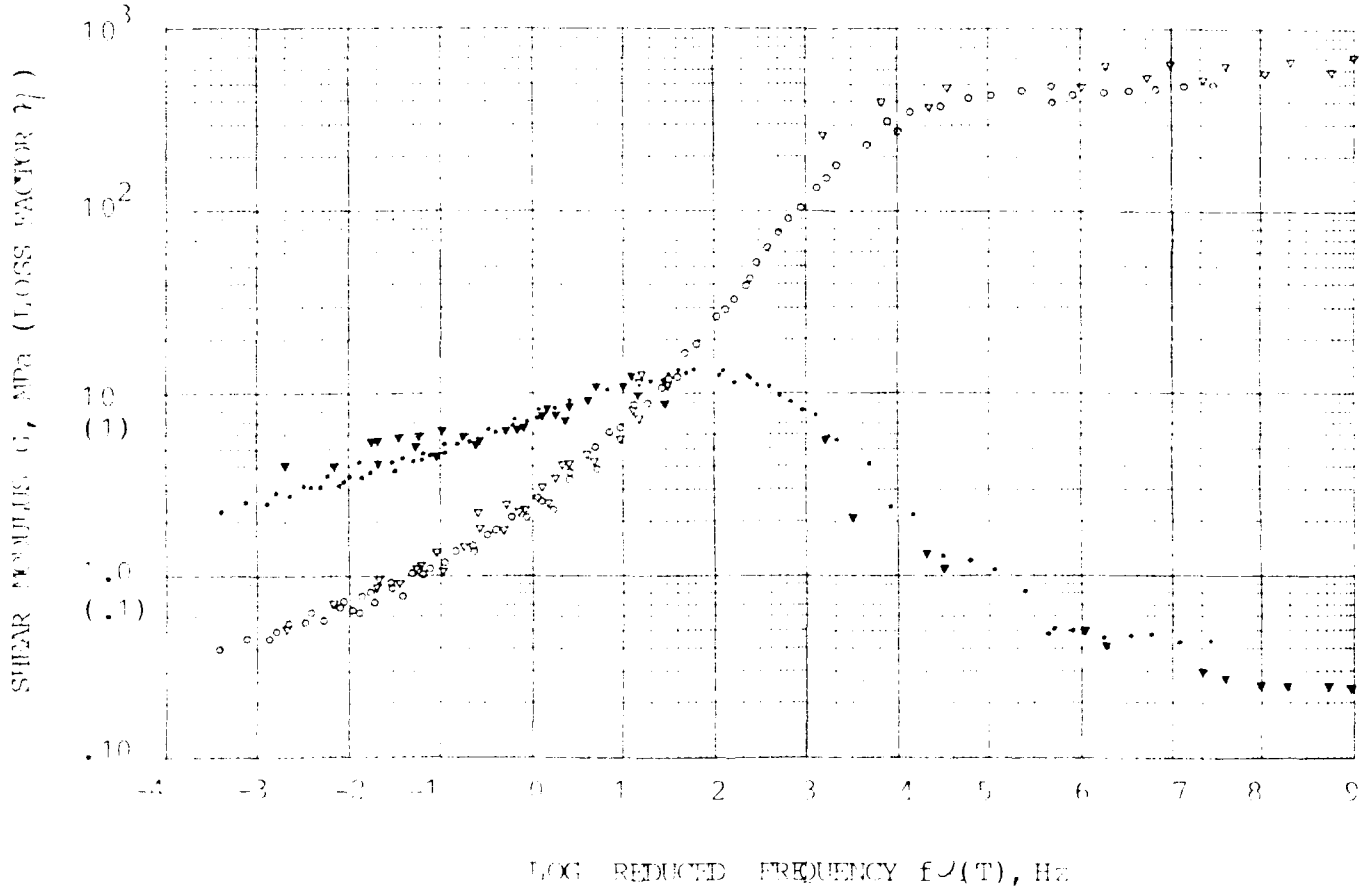

Figure 8. Reduced-frequency Master Curve

DISCUSSION AND CONCLUSIONS

The analysis of the measured complex modulus values obtained by the direct stiffness method shows that a postulated correction for the finite stiffness of the measurement chain can be determined by comparison of the apparent values in the Wicket plot with those obtained by the resonant beam technique. Such a correction, while interesting and perhaps promising for the future, must be used with caution because in the absence of other data for comparison the correction cannot be determined a-priori, and may in any case vary with grip configurations

and tightness. Users of direct stiffness systems should be aware of this feature, and may perhaps be able to develop such corrections from dynamic measurements of the test system, but in any case must check whether or not the correction is constant or depends on specimen and grip configurations. At a minimum, great care must be taken when direct stiffness techniques are used to measure complex modulus behavior at low temperatures.

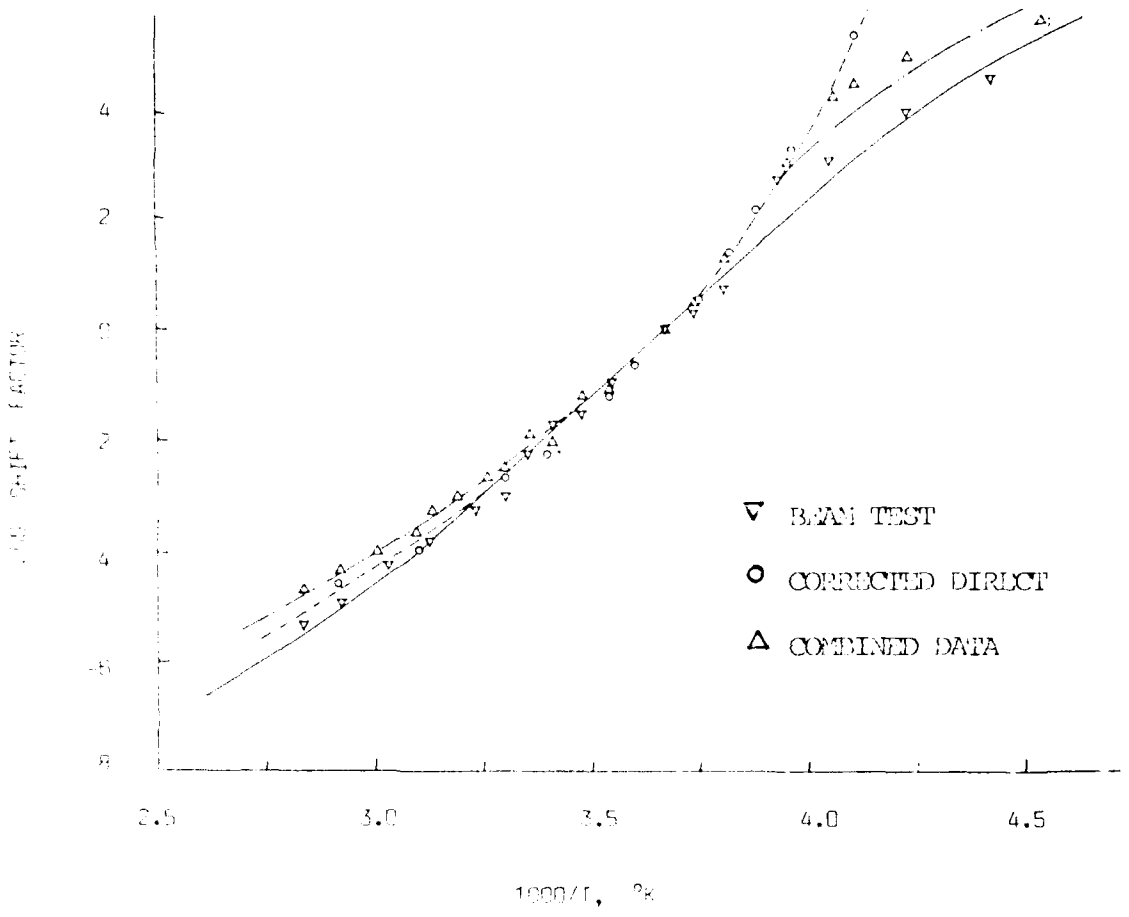

Figure 9. Log shift factor versus 1/T for test material

REFERENCES

1. C. Chesneau and B. Duperray, "Selected complex modulus data", Proc. DAMPING '86, AFWAL-TR-86-3059, Vol. I, pp AG1-28, May 1986.

2. M.L. Parin, A.D. Nashif and T. Lewis, "RELSAT Damping material data", Proc. DAMPING '86, AFWAL-TR-86-3059, Vol. I, pp AD1-80, May 1986.

3. M.L. Parin, A.D. Nashif and T. Lewis, "PACOSS Damping Material Measurements", Proc. DAMPING '86, AFWAL-TR-86-3059, Vol. I, pp AE1-56, May 1986.

4. D.I.G. Jones, "Critique of complex modulus test methods", Proc. DAMPING '86, AFWAL-TR-86-3059, Vol. I, pp A11-56, May 1986.

5. M.J. Ghaleb and M. Khoury, "Classification in the frequency-temperature range of viscoelastic materials for damping of flexural waves in sandwich structures with various boundary conditions", Proc. DAMPING '89, WRDC-TR-89-3116, Vol. 3, pp JAB1-28, Nov. 1989.

6. Societe Metravib, Ecully, France (Company literature).

NOMENCLATURE

A	Acceleration
f	Frequency (Hz)
f_n, f_{no}	Resonant frequencies of damped and bare beams, respectively
F, F(t)	Force
G, G_e	Shear modulus and apparent shear modulus, respectively
h	Thickness (various subscripts)
k	Stiffness (various subscripts)
k_s, k_e	Specimen stiffness or apparent stiffness, respectively
k_o	Stiffness of test system, assumed in series with specimen
M	Mass (various subscripts)
Q	Activation energy
R	Universal Gas constant
T, T_o	Absolute temperature and reference temperature, respectively
T_A	Activation temperature (=Q/R)
X	Displacement (various subscripts)
Z	Nondimensional parameter governing error magnification in beam tests
ρ	Density (various subscripts)
α (T)	Shift factor
η , η_e	Loss factor, apparent loss factor, respectively

TABLE 1. VALUES OF G AND η FOR DIRECT MEASUREMENT SYSTEM

1-apparent G, N/m^2; 2-apparent η; 3-corrected G, N/m^2; 4-corrected η; *-error

TEMP°C	FREQUENCY, Hz							
	7.8	15.6	31.3	62.5	125	250	500	
-30	1.71E8	1.76E8	1.79E8	1.81E8	1.83E8	1.85E8	1.87E8	/1
	.021	.021	.019	.019	.019	.017	.017	/2
	3.97E8	4.25E8	4.44E8	4.56E8	4.69E8	4.82E8	4.96E8	/3
	.049	.051	.047	.048	.049	.044	.045	/4
-20	1.56E8	1.65E8	1.69E8	1.74E8	1.78E8	1.83E8	1.86E8	
	.116	.098	.059	.052	.042	.031	.019	
	3.15E8	3.57E8	3.83E8	4.11E8	4.35E8	4.68E8	4.89E8	
	.245	.221	.136	.124	.104	.080	.050	
-15	8.39E7	1.10E8	1.32E8	1.48E8	1.67E8	1.77E8	1.82E8	
	.570	.414	.291	.203	.173	.100	.068	
	9.70E7	1.48E8	2.09E8	2.70E8	3.46E8	4.17E8	4.55E8	
	.906	.726	.557	.418	.406	.248	.174	
-10	3.33E7	5.29E7	8.03E7	1.06E8	1.20E8	1.36E8	1.46E8	
	.979	.819	.598	.449	.323	.224	.146	
	3.25E7	5.34E7	9.10E7	1.38E8	1.78E8	2.31E8	2.74E8	
	1.251	1.161	.940	.731	.579	.428	.290	
- 5	1.08E7	1.75E7	2.78E7	4.14E7	6.15E7	8.88E7	1.12E8	
	1.111	1.118	1.039	.926	.729	.523	.350	
	1.07E7	1.71E7	2.70E7	4.05E7	6.45E7	1.07E8	1.59E8	
	1.208	1.287	1.287	1.245	1.063	.840	.603	
0	6.46E6	9.01E6	1.32E7	1.99E7	3.08E7	4.41E7	7.00E7	
	1.021	1.107	1.167	1.159	1.032	.900	.647	
	6.45E6	8.93E6	1.29E7	1.92E7	2.97E7	4.34E7	7.67E7	
	1.068	1.186	1.302	1.372	1.310	1.226	.967	
10	2.16E6	2.82E6	3.73E6	5.03E6	6.45E6	9.08E6	1.28E7	
	.675	.754	.857	.972	1.076	1.134	1.222	
	2.17E6	2.83E6	3.74E6	5.03E6	6.42E6	8.98E6	1.24E7	
	.682	.765	.876	1.005	1.128	1.218	1.368	
20	1.17E6	1.40E6	1.71E6	2.10E6	2.68E6	3.41E6	3.96E6*	
	.473	.53[illegible]	.618	.713	.821	.913	1.115	
	1.17E6	1.41[illegible]	1.72E6	2.11E6	2.69E6	3.42E6	3.95E6	
	.475	.539	.623	.721	.834	.932	1.149	
30	8.76E5	1.03E6	1.20E6	1.46E6	1.71E6	2.09E6	2.35E6	
	.374	.420	.471	.541	.601	.705	.810	
	8.78E5	1.03E6	1.20E6	1.47E6	1.72E6	2.09E6	2.36E6	
	.375	.422	.473	.544	.606	.712	.821	

TABLE 1. VALUES OF G AND η FOR DIRECT MEASUREMENT SYSTEM (CONT'D)

TEMP°C	FREQUENCY, Hz						
	7.8	15.6	31.3	62.5	125	250	500
40	6.86E5	7.93E5	9.01E5	1.02E6	1.19E6	1.43E6	-
	.319	.348	.384	.441	.523	.563	-
	6.87E5	7.95E5	9.03E5	1.02E6	1.19E6	1.43E6	-
	.320	.349	.385	.443	.526	.567	-
50	5.43E5	6.31E5	7.12E5	7.97E5	8.84E5	1.02E6	-
	.277	.308	.331	.376	.422	.481	-
	5.44E5	6.32E5	7.14E5	7.99E5	8.86E5	1.02E6	-
	.278	.309	.332	.377	.423	.483	-
60	4.65E5	5.25E5	5.85E5	6.52E5	7.00E5	7.78E5*	-
	.255	.287	.308	.342	.384	.445 *	-
	4.66E5	5.26E5	5.86E5	6.53E5	7.01E5	7.80E5	-
	.255	.288	.309	.343	.385	.446	-
70	3.98E5	4.49E5	4.91E5	5.33E5	5.70E5*	6.26E5*	-
	.225	.242	.277	.308	.358 *	.416 *	-
	3.99E5	4.50E5	4.92E5	5.34E5	5.71E5	6.27E5	-
	.225	.242	.277	.309	.359	.417	-

TABLE 2. VALUES OF G AND η FROM SANDWICH BEAM TESTS

TEMP°C	MODE	FREQ, Hz	G, N/m^2	η
- 53	3	1116	5.73E8	.025
	4	2027	7.19E8	.024
- 37	3	1108	5.54E8	.026
	4	2008	6.93E8	.026
- 27	3	1098	5.30E8	.030
	4	1986	6.62E8	.028
- 19	3	1080	4.79E8	.050
	4	1951	6.09E8	.041
- 10	3	1037	3.80E8	.131
	4	1861	4.91E8	.110
- 5	2	389	1.63E8	.357
	3	989	2.97E8	.207
	4	1778	4.02E8	.194
0	2	358	9.97E7	.504
	3	922	2.10E8	.373
	4	1629	2.62E8	.588
9	2	198	1.13E7	.980
14	2	182	7.99E6	1.261
	3	429	1.07E7	.846
20	2	164	5.26E6	1.009
	5	1260	1.63E7	1.377
25	2	151	3.43E6	.786
	3	382	4.13E6	1.082
	4	731	5.84E6	1.125
	5	1188	7.30E6	1.242
31	2	145	2.50E6	.639
	3	373	3.03E6	.774
	4	716	4.04E6	.871
	5	1167	4.83E6	.927
37	2	140	1.94E6	.547
	3	367	2.35E6	.643
	4	704	2.61E6	.825
	5	1160	4.09E6	.714
47	2	136	1.40E6	.455
	3	361	2.27E6	.536
	4	697	1.86E6	.624
	5	1144	2.35E6	.651

TABLE 2. VALUES OF G AND η FROM SANDWICH BEAM TESTS (CONT'D)

TEMP°C	MODE	FREQ,Hz	G,N/m^2	η
58	2	133	9.69E5	.410
	3	356	1.09E6	.510
	4	689	1.09E6	.629
	5	1135	1.49E6	.588
69	2	130	7.04E5	.399
	3	353	8.27E5	.558
	4	687	8.98E5	.581
	5	1130	1.10E6	.587
80	2	129	5.40E5	.403
	3	351	5.54E5	.662*
	4	683	5.96E5	.599*
	5	1126	8.71E5	.575*

CONSTITUTIVE MODELING OF NONLINEAR DAMPING MATERIALS

Jerome L. Sackman
James M. Kelly*
Department of Civil Engineering
University of California at Berkeley
Berkeley, CA 94720

and

Ahmad E. Javid
IBM Corporation
5600 Cottle Road
San Jose, CA 95193

Abstract

Many of the damping materials that have been developed recently are used under transient conditions at levels of strain where their response is highly nonlinear (e.g., to improve the seismic performance of buildings and other structures in earthquake-prone regions). Transient analysis of these nonlinear materials cannot be done using Fourier or other transform methods; real time analysis is needed. In this study these materials are treated as viscoelastic and their nonlinear constitutive relations are constructed in the time domain using internal variables to account for inelastic behavior and damage. This is an approach which is popular in modern constitutive theory and has many advantages. It leads to a formulation in terms of a system of first-order nonlinear ordinary differential (or differential-functional) equations, which is computationally convenient. Furthermore, if the analyst has physical insights into the micromechanical processes that are producing the inelastic deformation and damage, then the internal variable formulation provides a means for mathematically expressing this information in the structure of the constitutive relation. Some prototypes are constructed and employed to predict hysteresis loops.

*Tel.: 415/642-3564

INTRODUCTION

The use of polymeric materials in engineering systems is ubiquitous. The large variety of desirable properties these materials possess makes them beneficial in many kinds of applications. In particular, because of their dissipative properties, some of them are employed to damp the motions of mechanical and structural systems which are undergoing either steady-state or transient vibrations. Frequently, to properly design a system employing such materials for this purpose, it is essential to have a quantitative description of their thermomechanical properties. As a matter of analytical and computational convenience, these materials are usually idealized, with good accuracy, to be viscoelastic. Several different constitutive characterizations of viscoelastic materials are possible. Generally, that one is chosen which is the most convenient for the task at hand.

The standard model for the viscoelastic response of damping materials has been the complex modulus formulation. This model, which is very popular and well understood, has proved to be an accurate and convenient technique for the vast majority of damping analyses. The complex modulus model readily allows for the incorporation of test results from steady state sinusoidal testing, permitting frequency dependence and temperature dependence to be included in a relatively simple way. It is easy to use in predicting the response of damped systems to disturbances with well defined frequencies. When it is applied to the transient response of impulsively loaded or seismically loaded systems, the prediction of the response is made using transform techniques which are intrinsically linear.

However, in certain applications the material may be used at quite large strains where the assumption of linear response is unwarranted. An example is the use of damping materials in the form of add-on viscoelastic damping devices to improve the seismic performance of sub-standard buildings and other structures in earthquake prone regions. If viscoelastic dampers were used to rehabilitate these structure, it might be possible to economically improve their dynamic behavior so that they could conform with the performance requirements of current seismic building codes. The dampers could considerably reduce the number of cycles of large deformation to be sustained by the structure and could also reduce the level of inter-story drift. Both would contribute to the ability of the structure to survive moderate earthquakes with negligible damage and survive large earthquakes without collapse.

The verification of the design of such a rehabilitated structure will require time history analysis that includes modeling of the viscoelastic dampers to permit transient, large strain response. The subsequent transient analysis of the nonlinear viscoelastic materials in the add-on damping devices that will be required cannot be performed using Fourier or other transform methods; real time analysis must be used. It is also known from testing that the first application of a sinusoidal load to a previously unloaded damping device produces, particularly at large strains, hysteresis loops that are larger than subsequent loops. The material in the device reaches a steady state only after several cycles of loading. Clearly, this is a manifestation of nonlinear action. More specifically, this kind of behavior is associated with damage that is being done to the material by the deformation to which it has been previously subjected. In seismic applications, it could be crucial to include this transitory nonlinear behavior in predicting the response of the damped structure. It is for problems of this kind that the models described in this paper have been developed.

In the sequel, the construction of constitutive relations for nonlinear polymers (which, of course, includes linear behavior as a special case) in the time domain using internal variables to account for inelastic behavior will be considered. Such relations can be applied to describe the strain (or stress) response to transient and oscillatory stress (or strain) excitations. This is an approach which is popular in modern constitutive theory and has many advantages. It leads to a

formulation in terms of a system of first order (usually nonlinear) ordinary differential (or differential-functional) equations. From the point of view of computation, this is convenient. Furthermore, if the analyst has physical insights of the micromechanical processes that are producing the inelastic deformation, then the internal variable formulation provides a means for expressing this information in the mathematical structure of the constitutive relation. Thus, this methodology is particularly useful for introducing damage mechanisms into constitutive equations.

The paper ends by considering some examples of constitutive relations constructed by the internal variable formulation. Numerical integration of the system of nonlinear ordinary differential (or differential-functional) equations representing these models is employed to predict the hysteresis loops that would be produced if they were subjected to a sinusoidal oscillating strain input. It is seen that when appropriate modeling is achieved, hysteresis loops produced by the numerical simulations are close in form to those observed in tests performed on commercially available viscoelastic dampers.

DERIVATION OF CONSTITUTIVE EQUATIONS FOR A NONLINEAR POLYMER VIA INTERNAL VARIABLES

A powerful methodology for constructing constitutive relations for nonlinear viscoelastic materials is the use of internal variables. This method starts from first principles of mechanics of continua and non-equilibrium thermodynamics to deduce a general mathematical structure of the constitutive relations which does not violate any physical principles. This general structure can then be specialized to obtain a large variety of possible behavior.

Consider an arbitrary portion of a solid body made of a polymeric material. The arbitrary portion of the body occupies some region R of space and has a boundary surface B. The unit vector normal to the surface B at a generic point on B is denoted by $\boldsymbol{n}$. The traction vector acting across B is given by $\boldsymbol{t}$, the heat flow vector across B by $\boldsymbol{h}$, the body force vector per unit of volume by $\boldsymbol{f}$, and the particle velocity vector by $\boldsymbol{v}$. It is assumed that the local thermodynamic state of the material exists and is uniquely given by the strain tensor ϵ (with Cartesian components ϵ_{ij}, $ij = 1,2,3$), the entropy per unit volume S, and a set of internal variables q_α ($\alpha = 1, \ldots n$) which are represented by the column matrix $\boldsymbol{q}$. The internal variables are used to introduce the influence of microstructural effects into the constitutive relations. For example, for general materials, they may be components of the internal strain or dislocation loop density. Or, they might be the extent of phase transformation or chemical reaction; concentration of lattice imperfections; parameters characterizing changes in molecular conformation, grain size, hardening, damage, coiling and bending of long chain molecules in polymers; etc. Thus, the local internal energy per unit of volume, U, is written as

$$U = U(\epsilon, S, q) \tag{1}$$

Now, consider the balance of thermal and mechanical energy for the arbitrary portion of the body. (In the following, attention is restricted to infinitesimal deformation theory. The results obtained here may be extended to large deformation theory by introducing proper measures of strain and stress and interpreting all quantities defined as per unit of volume as per unit of volume in the reference state.) The rate of work done on the body by the surface forces is

$$\int_B \boldsymbol{t} \cdot \boldsymbol{v} \, ds \tag{2}$$

The rate of work done by the body forces is

$$\int_R \boldsymbol{f} \cdot \boldsymbol{v} \, ds \tag{3}$$

and the rate of energy added to the body because of heat flow is

$$-\int_B \boldsymbol{h} \cdot \boldsymbol{n} \, ds \tag{4}$$

where the usual dot notation has been employed for the inner product. Assuming no internal heat sources, the sum of these energy rates must be equal to the rate of change of the total energy of the body. The total energy of the body is the sum of the internal energy and the kinetic energy. Thus,

$$\frac{d}{dt}\int_R \left(U + \frac{1}{2}\rho \boldsymbol{v} \cdot \boldsymbol{v}\right) dV = \int_B [\, \boldsymbol{t} \cdot \boldsymbol{v} - \boldsymbol{n} \cdot \boldsymbol{h}] \, ds + \int_R \boldsymbol{f} \cdot \boldsymbol{v} \, dV \tag{5}$$

where ρ is the mass density of the material.

Utilizing the balance of mass principle, the left-hand side of this equation may be written as

$$\frac{d}{dt}\int_R \left(U + \frac{1}{2}\rho \boldsymbol{v} \cdot \boldsymbol{v}\right) dV = \int_R (\dot{U} + \rho \dot{\boldsymbol{v}} \cdot \boldsymbol{v}) \, dV \tag{6}$$

where a superposed dot represents differentiation with respect to time. Recalling that the traction vector may be written in terms of the symmetric stress tensor $\boldsymbol{\sigma}$ (with Cartesian components σ_{ij}) as

$$\boldsymbol{t} = \boldsymbol{n} \cdot \boldsymbol{\sigma} \tag{7}$$

the first integral on the right-hand side of Eq. (5) takes the form

$$\int_B [\boldsymbol{t} \cdot \boldsymbol{v} - \boldsymbol{n} \cdot \boldsymbol{h}] ds = \int_B \boldsymbol{n} \cdot [\boldsymbol{\sigma} \cdot \boldsymbol{v} - \boldsymbol{h}] ds \tag{8}$$

The right-hand side of Eq. (8) can be converted to a volume integral by use of the divergence theorem, yielding

$$\int_B \boldsymbol{n} \cdot [\boldsymbol{\sigma} \cdot \boldsymbol{v} - \boldsymbol{h}] ds = \int_R \nabla \cdot [\boldsymbol{\sigma} \cdot \boldsymbol{v} - \boldsymbol{h}] dV \tag{9}$$

where ∇ is the gradient operator. Thus, Eq. (5) can be written as

$$\int_R [(\nabla \cdot \boldsymbol{\sigma} + \boldsymbol{f} - \rho \dot{\boldsymbol{v}}) \cdot \boldsymbol{v} - (\dot{U} - \sigma_{ij} \dot{\epsilon}_{ij} + \nabla \cdot \boldsymbol{h})] dV = 0 \tag{10}$$

where the summation convention is in effect, and use has been made of the fact that the scaler inner product of a symmetric tensor with an antisymmetric tensor is zero.

From the balance of linear momentum, the quantity within the first set of parentheses vanishes. Since the balance of energy holds for any region $\boldsymbol{R}$ of the body, then assuming that the

integrand is continuous, it must vanish at every point in the region occupied by the body. This gives the local equation of balance of energy (the first law of thermodynamics) as

$$\dot{U} = \sigma_{ij}\dot{\epsilon}_{ij} - \nabla\cdot\boldsymbol{h} = \frac{\partial U}{\partial \epsilon_{ij}}\,\dot{\epsilon}_{ij} + \frac{\partial U}{\partial q_\alpha}\,\dot{q}_\alpha + \frac{\partial U}{\partial S}\,\dot{S} \tag{11}$$

or

$$\left(\sigma_{ij} - \frac{\partial U}{\partial \epsilon_{ij}}\right)\dot{\epsilon}_{ij} - \frac{\partial U}{\partial q_\alpha}\,\dot{q}_\alpha - \frac{\partial U}{\partial S}\,\dot{S} - \nabla\cdot\boldsymbol{h} = 0 \tag{12}$$

If T is taken to be the local absolute temperature, then the second law of thermodynamics can be written as the local Clausius-Duhem inequality

$$\dot{S} + \nabla\cdot(\boldsymbol{h}/T) \geq 0 \tag{13}$$

Combining Eqs. (12) and (13) gives

$$\left(T - \frac{\partial U}{\partial S}\right)\dot{S} + \left(\sigma_{ij} - \frac{\partial U}{\partial \epsilon_{ij}}\right)\dot{\epsilon}_{ij} - \frac{\partial U}{\partial q_\alpha}\,\dot{q}_\alpha - \frac{1}{T}\boldsymbol{h}\cdot\nabla T \geq 0 \tag{14}$$

Assuming that the $\dot{q}_\alpha$ are independent of $\dot{S}$ and $\dot{\boldsymbol{\epsilon}}$, and recalling that $\dot{S}$ and $\dot{\boldsymbol{\epsilon}}$ can be specified arbitrarily, their coefficients must vanish, so that

$$T = \frac{\partial U}{\partial S} \tag{15}$$

$$\sigma_{ij} = \frac{\partial U}{\partial \epsilon_{ij}} \tag{16}$$

and

$$\frac{\partial U}{\partial q_\alpha}\,\dot{q}_\alpha + \boldsymbol{h}\cdot\nabla T/T \leq 0 \tag{17}$$

But, since U and $\dot{q}_\alpha$ are independent of ∇T, it follows from Eq. (17) that

$$\frac{\partial U}{\partial q_\alpha}\,\dot{q}_\alpha \leq 0 \tag{18}$$

Now, the left-hand side of Eq. (18) represents that part of the rate of change of U that is due to the changes in the internal variables. Thus, Eq. (18) states that *internal processes reduce the internal energy.*

It is convenient at this point to introduce an alternative thermodynamic potential by the use of a Legendre transformation from the internal energy. The Gibbs free energy (or the complementary free energy) G is given by

$$G = \sigma_{ij}\epsilon_{ij} - U + TS = G(\boldsymbol{\sigma},T,\boldsymbol{q}) \tag{19}$$

with, from Eqs. (15)-(17), the properties that

$$S = \frac{\partial G}{\partial T} \tag{20}$$

$$\epsilon_{ij} = \frac{\partial G}{\partial \sigma_{ij}} = \epsilon_{ij}(\sigma, T, q) \tag{21}$$

$$\frac{\partial G}{\partial q_\alpha} \dot{q}_\alpha \geq 0 \tag{22}$$

The pair of equations (20) and (21) is a set of thermomechanical constitutive equations for the material. Constitutive equations must also be specified for the internal variables; then Eq. (22) is a restriction on the form that these constitutive equations can take.

The rate of dissipation of energy by the material, d (power per unit of volume), is given by the difference between the rate of work done by the stresses, $\sigma_{ij}\dot{\epsilon}_{ij}$, and the rate of change of the internal energy (at constant entropy), $\dot{U}$. Thus

$$d = \sigma_{ij}\dot{\epsilon}_{ij} - \dot{U} = \sigma_{ij}\dot{\epsilon}_{ij} - \frac{\partial U}{\partial \epsilon_{ij}} \dot{\epsilon}_{ij} - \frac{\partial U}{\partial q_\alpha} \dot{q}_\alpha \tag{23}$$

Using (16), (19), and (22), this gives

$$d = \frac{\partial G}{\partial q_\alpha} \dot{q}_\alpha \geq 0 \tag{24}$$

Thus, the inequality expressed in (22) is just the statement that the rate of dissipation is non-negative, as is to be expected on physical grounds.

The total strain rate may be obtained by taking the time derivative of (21):

$$\dot{\epsilon}_{ij} = \frac{\partial^2 G}{\partial \sigma_{ij} \partial \sigma_{kl}} \dot{\sigma}_{kl} + \frac{\partial^2 G}{\partial \sigma_{ij} \partial q_\alpha} \dot{q}_\alpha + \frac{\partial^2 G}{\partial \sigma_{ij} \partial T} \dot{T} \tag{25}$$

The tensors $\partial^2 G / \partial \sigma_{ij} \partial \sigma_{kl}$ and $\partial^2 G / \partial \sigma_{ij} \partial T$ are, respectively, the instantaneous elastic compliance tensor and the instantaneous thermal strain tensor. In the sequel, attention will be restricted to *isothermal processes* so that $\dot{T} = 0$, and then (91) becomes

$$\dot{\epsilon}_{ij} = \alpha_{ijkl} \dot{\sigma}_{kl} + \frac{\partial^2 G}{\partial \sigma_{ij} \partial q_\alpha} \dot{q}_\alpha \tag{26}$$

where $\alpha_{ijkl} = \partial^2 G / \partial \sigma_{ij} \partial \sigma_{kl}$ is the instantaneous compliance tensor. It is natural to interpret the first term on the right-hand side of (26) as the elastic strain rate, and the second term as the inelastic strain rate.

It is an observed experimental fact that the instantaneous compliances are largely independent of the internal variables, i.e., that

$$\frac{\partial}{\partial q_\alpha} (a_{ijkl}) = \frac{\partial^3 G}{\partial q_\alpha \partial \sigma_{ij} \partial \sigma_{kl}} = 0 \tag{27}$$

The structure of G can be found by integrating (27) to obtain

$$G(\sigma,q;T) = G^*(\sigma;T) + b_{ij}(q;T)\sigma_{ij} + c(q;T) \tag{28}$$

where, for isothermal responses, the temperature T plays the role of a simple parameter. For simplicity of notation, explicit mention of T will be suppressed in what follows.

G^* is independent of q_α, and thus can be thought of as the elastic part of the complementary free energy. Thus

$$\epsilon_{ij} = \frac{\partial G}{\partial \sigma_{ij}} = \frac{\partial G^*}{\partial \sigma_{ij}} + b_{ij}(q) = \epsilon_{ij}^{el} + \epsilon_{ij}^{inel} \tag{29}$$

and

$$\begin{aligned} d = \frac{\partial G}{\partial q_\alpha}\dot{q}_\alpha &= \left(\frac{\partial b_{ij}}{\partial q_\alpha}\dot{q}_\alpha\right)\sigma_{ij} + \frac{\partial c}{\partial q_\alpha}\dot{q}_\alpha \\ &= \dot{\epsilon}_{ij}^{inel}\sigma_{ij} + \frac{\partial c}{\partial q_\alpha}\dot{q}_\alpha \end{aligned} \tag{30}$$

If in Eq. (26) the range of α is restricted so that $\alpha = 1$, and if q_1 is interpreted in such a manner that the last term on the right hand side of (26) is taken to be the inelastic strain rate of the material, then (26) can be looked upon as the constitutive relation of a nonlinear Maxwell model. With that interpretation, and with the assumption that all of the dissipation is caused by the inelastic strain rate, then $c(q)$ can be neglected. Then, Eq. (26) reduces to

$$\dot{\epsilon}_{ij} = a_{ijkl}(\sigma)\dot{\sigma}_{kl} + \lambda_{ij}^{\alpha}(q)\dot{q}_\alpha \tag{31}$$

and

$$d = \left(\lambda_{ij}^{\alpha}(q)\dot{q}_\alpha\right)\sigma_{ij} \geq 0 \tag{32}$$

where

$$\lambda_{ij}^{\alpha}(q) = \frac{\partial b_{ij}(q)}{\partial q_\alpha} \tag{33}$$

For more general modeling, where Eq. (26) has an interpretation not restricted to a Maxwell model, $c(q)$ can *not* be neglected, and the dissipation rate is given by the more general expression (24) or (30), rather than the more restrictive one, (32).

It remains to specify the constitutive equations on the internal variables. Usually, these are taken as rate equations, or equations of evolution; that is, the time derivative of each internal variable is determined by the present state. In the simplest form, it is only the thermodynamic state variables (i.e., those which determine any one of the thermodynamic potentials U or G) which determine the rate; for example,

$$\dot{q}_\alpha = f_\alpha(\sigma,T,q), \quad \alpha = 1,2,\ldots n \tag{34}$$

For isothermal processes, T is just a parameter, and its appearance in f_α will be suppressed in the sequel. Thus, the constitutive relations for the material (undergoing an isothermal process) which relate stress, strain, and the internal variables are given by Eqs. (31) and (34), with the restriction given by (32). If attention is restricted to a uniaxial stress-strain relation, these equations reduce to

$$\dot{\epsilon} = \frac{\dot{\sigma}}{E(\sigma)} + \lambda^{\alpha}(q)\dot{q}_{\alpha} \tag{35}$$

$$\dot{q}_{\alpha} = f_{\alpha}(\sigma,q) \qquad \alpha = 1,2,\ldots,n \tag{36}$$

with

$$\sigma\left[\lambda^{\alpha}(q)\dot{q}_{\alpha}\right] \geq 0 \tag{37}$$

(or the more general dissipation constraint, Eq. (24)) where $E(\sigma)$ is the instantaneous elastic modulus.

A type of equation more general than (34) can be used for the constitutive equations of the internal variables. For example, instead of the rate of evolution of the internal variables depending only on the current value of the thermodynamic state variables, they can be taken to depend also on the past history of these variables. Such a relationship would be expressed by means of a differential-functional equation, which is just a generalization of Eq. (34)

$$\dot{q}_{\alpha}(t) = \overset{\tau=t}{\underset{\tau=-\infty}{\mathcal{F}_{\alpha}}}\,[\sigma(\tau),T(\tau),q(\tau)], \qquad \alpha = 1,2,\ldots n \tag{38}$$

where $\mathcal{F}$ is a *functional* rather than an ordinary function. For the special case of a uniaxial stress-strain relationship for a material undergoing an isothermal process, Eq. (36) would become

$$\dot{q}_{\alpha} = \overset{\tau=t}{\underset{\tau=-\infty}{\mathcal{F}_{\alpha}}}\,[\sigma(\tau),q(\tau)], \qquad \alpha = 1,2,\ldots n \tag{39}$$

In practice, special cases of (39) can also be useful. Equation (36) is one such case. Another is when $\mathcal{F}$ is taken to be a functional of q but an ordinary function of σ. Use will be made of that form in the next section.

If the uniaxial form of the constitutive equations is considered, with α restricted to 1, we get from Eqs. (35)-(37)

$$\dot{\epsilon} = \frac{\dot{\sigma}}{E(\sigma)} + \lambda(q)f(\sigma,q) \tag{40}$$

$$\dot{q} = f(\sigma,q) \tag{41}$$

with

$$\sigma[\lambda(q)\dot{q}] \geq 0 \tag{42a}$$

or the more general form, from (24),

$$d = \frac{\partial G}{\partial q}\,\dot{q} \geq 0 \tag{42b}$$

For simple forms of λ and f, this constitutive equation can be interpreted as that associated with a nonlinear Maxwell material or model, as mentioned previously, where $E(\sigma)$ is the stress-dependent modulus of elasticity of the nonlinear spring, and $\lambda(q)f(\sigma,q)$ is the nonlinear inelastic strain rate of the dashpot. If $E(\sigma)$ and $\lambda(q)$ are taken to be constant ($E(\sigma) = E$, $\lambda(q) = \lambda$), and $f(\sigma,q) = \sigma$, then the model is a *linear* Maxwell body with modulus of elasticity E and

viscosity = $1/\lambda$ (i.e., fluidity = λ). Notice that for the linear case, the constraint that $d \geq 0$ requires λ to be nonnegative.

If $E(\sigma) = E$, a constant, $\lambda(q) = 1$, and $f(\sigma,q) = \sigma/E\tau - q/\tau_1$, where E, τ and τ_1 are positive constants, then the resulting model is a standard linear solid with the constitutive relation

$$E\left(\dot{\epsilon} + \frac{1}{\tau_1} G\right) = \dot{\sigma} + \frac{1}{\tau} \sigma \tag{43}$$

where τ_1 and τ are the retardation and relaxation times of the model, respectively. Thus, it is seen that the constitutive relations given by (40) and (41), with the constraint (42) can lead to a rich variety of linear and nonlinear viscoelastic models. By utilizing more than one internal variable, this richness can be greatly increased, as is also true if functionals rather than functions are used in (41). In the next section, some numerical illustrations of the constitutive equations (40) and (41) are given.

EXAMPLES

The examples described below are simulations of a hysteresis test in which the imposed excitation is a sinusoidal oscillatory strain history. The material model chosen to illustrate applications of the theoretical methodology described above is a nonlinear Maxwell body with a viscosity that can degrade, depending on the maximum magnitude of the inelastic strain (the maximum magnitude of strain in the dashpot). This model displays a variety of behavior, depending on the values of the parameters controlling the magnitude of the fluidity (which is the reciprocal of the viscosity), the elastic modulus, and the amplitude and frequency of the imposed strain history. For certain values of the parameters, a steady-state is established quickly, yielding unchanging hysteretic loops. Other values produce a stress response that takes many cycles before a steady-state is reached. This gives a stress-strain diagram in which the hysteresis loops continually change until a constant loop evolves.

The model employed is described by Eqs. (40) and (41) with $\lambda(q) = 1$ and

$$f[\sigma,q] = F[\sigma(t),q(t)] \cdot \left|\frac{\sigma}{E}\right|^c \cdot \left(\frac{\sigma}{E}\right) \tag{44}$$

where $F[\sigma,q]$ may be thought of as the fluidity of the nonlinear dashpot of the Maxwell model. The viscosity is taken to decrease (i.e., the dashpot becomes damaged) with the maximum magnitude of the strain it experiences. Thus, the fluidity is an increasing function of the maximum absolute value of the inelastic strain. In particular, in this study the fluidity function was taken to be

$$F[\sigma(t),q(t)] = \max_{0\leq\tau\leq t}\left[F_1 + F_0\left|\frac{q(\tau)}{q_o}\right|^b\right] \tag{45}$$

where b, c, F_o, F_1 and q_o are constants. These constants were given different values in the course of the investigation to see how they affected the response of the model to a sinusoidal oscillatory test (i.e., a hysteresis test) with $\epsilon(t) = A \sin t/T$, where A is the maximum strain amplitude imposed and $2\pi T$ is the period of the imposed oscillation.

It should be noted that by choosing $F_o = 0$, damage is eliminated. The response of the model to the sinusoidal input was obtained by a numerical integration of the first order system of Eqs. (40) and (41). Quiescence is assumed to exist for $t < 0$.

For the first example, the parameters were chosen such that $A = 1$, $T = 1$, $F_o = 0$, $F_1 = 0.8$, $q_o = 1$, $b = 0$ and $c = 0$. This corresponds to a linear Maxwell material with no damage. The normalized results are shown in Fig. 1. Because this model is linear, the normalized results are independent of the magnitude of A. The form of the results is typical of linear dissipative behavior. The stress leads the strain, and, after a brief transient passes (which takes less than a full cycle), is of sinusoidal form. The hysteresis loops quickly reach a steady-state and they all fall on a single tilted ellipse. Because there is no damage, the fluidity remains constant.

In the second example, $A = 1$, $T = 1$, $F_o = 0$, $F_1 = 0.8$, $q_o = 1$, $b = 0$ and $c = 1$. This corresponds to a nonlinear Maxwell material with no damage. The normalized results are shown in Fig. 2. Because this model is nonlinear, the normalized results depend on the magnitude of A. Again the stress leads the strain, and, after a transient of less than a full period, attains a steady-state form. However, it is not sinusoidal. The hysteresis loops again quickly reach a steady-state and collapse onto a single closed, convex curve, which is clearly not an ellipse.

If, in the above example, A is increased to 4, then the results in Fig. 3 are obtained. They are similar to those shown in Fig. 2, but the nonlinear features are more apparent. The greater nonlinear action which occurs in this model when the maximum amplitude of the imposed sinusoidal oscillatory strain, A, is increased from 4 to 1, results in a more distorted shape for the stress history, a greater phase shift between the stress and the strain, and a steady-state hysteresis loop which has associated with it a greatly decreased stiffness.

In the last example, $A = 1$, $T = 1$, $F_o = 5$, $q_o = 1$, $b = 4$ and $c = 1$. This is a nonlinear Maxwell material with damage. It is seen that due to the damage, the fluidity increases over several cycles before a steady-state value is attained. This results in a stress history which leads the strain, has a non-sinusoidal form, and which takes several cycles before it attains a steady-state periodic behavior. The hysteresis loops are far from being elliptical in form, and do not collapse onto a single closed, convex curve until the passage of several cycles. This is due to the damage. These results are of the type actually observed in hysteresis tests performed in the laboratory on many types of polymers undergoing large strain cycles.

CONCLUDING REMARKS

In order to determine the response of a nonlinear polymer to transient excitation, a proper constitutive relation is required. In this paper the method of internal variables was explored as a means of providing such a relation. It is seen that this is a very rich approach. By the use of this method, constitutive relations valid for transient phenomena could easily be generated that predict the kind of behavior for a sinusoidal oscillatory test (hysteresis test) that is actually observed in the laboratory.

A fundamental practical problem associated with this method is the determination of the forms of the functions and the values of the parameters appearing in those forms. This leads to the study of inverse problems or identification. How from sinusoidal oscillatory tests can these forms and parameters be determined? Indeed, what other types of tests should be utilized to that end? A good deal of research has been done in the general area of inverse and identification

problems, and there is a large body of literature available. This material should be perused to determine what portions of it are relevant to the problem at hand.

Many problems associated with modeling by means of internal variables need further investigation. The use of more than a single internal variable should be examined. Employment of internal variables to represent damage of the material and the introduction of the formal concepts of damage mechanics should be attempted. In the constitutive equations of the internal variables, the use of functional (rather than function) relationships should be explored. Attempts should be made to introduce physics at the microstructural level as a basis for developing the constitutive equations governing the evolution of the internal (and damage) variables. The implementation of the methodology of internal variables should be broadened to include thermal effects (heat generation and conduction, and thermal expansion). Finally, an extension to deal with three-dimensional states of stress and strain ought to be considered; this would probably introduce the notion of loading surfaces (similar to those employed in plasticity theory) in order to ensure positive dissipation.

It is evident that much work remains to be done in this interesting and practical problem area.

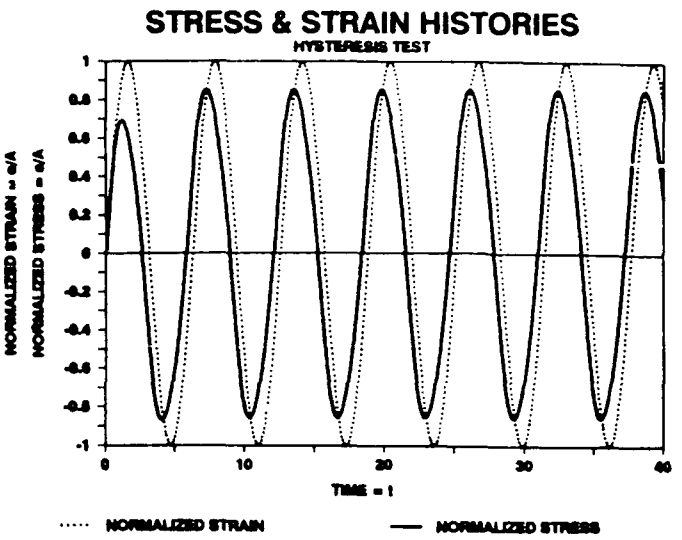

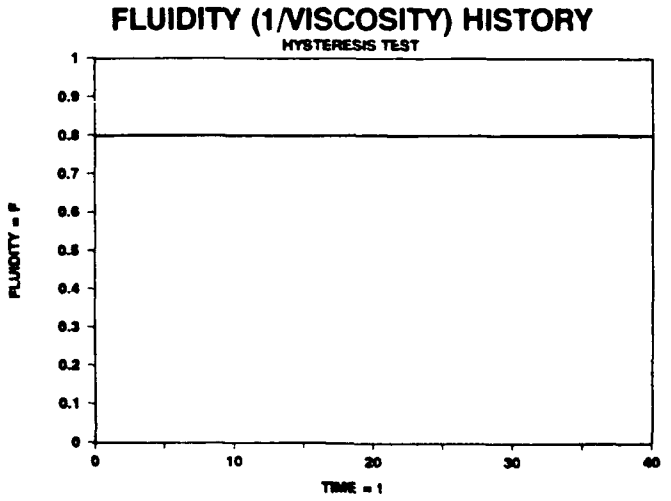

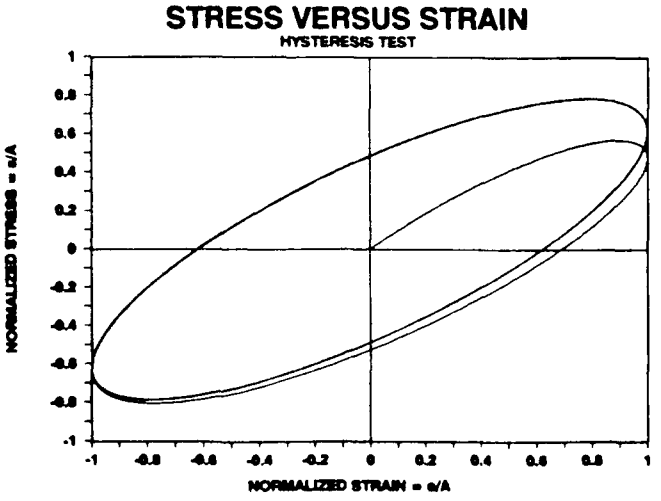

FIGURE 1: HYSTERESIS TEST ON A LINEAR MAXWELL MATERIAL

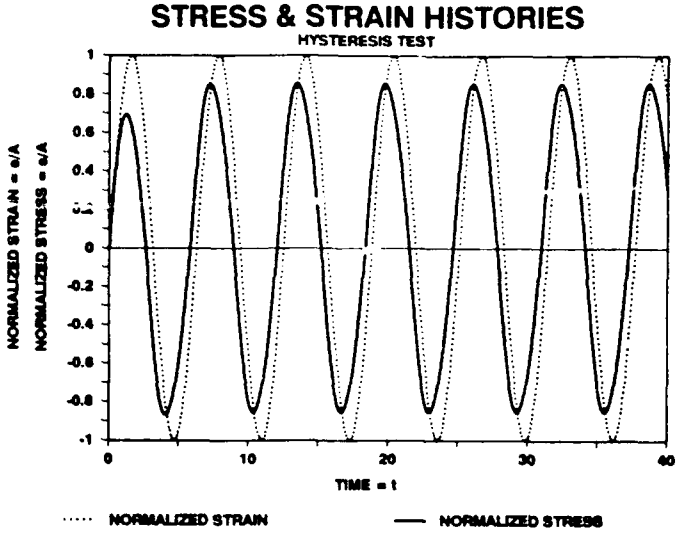

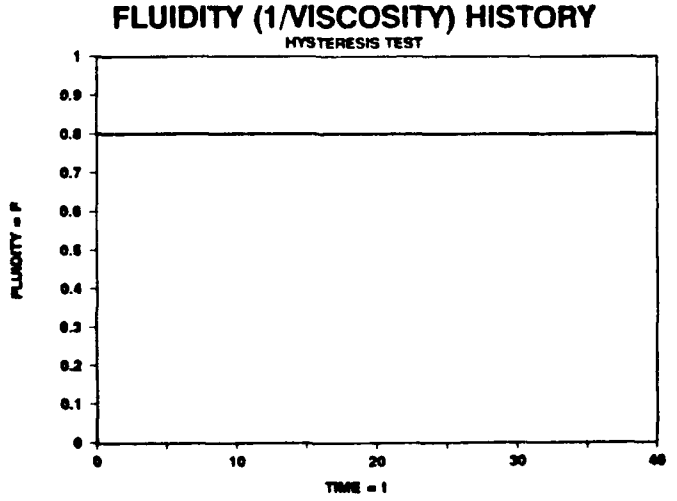

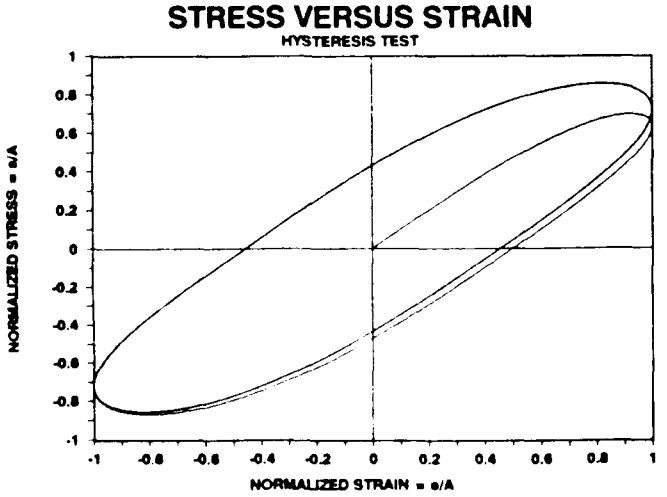

FIGURE 2: HYSTERESIS TEST ON A NONLINEAR MAXWELL MATERIAL, A = 1

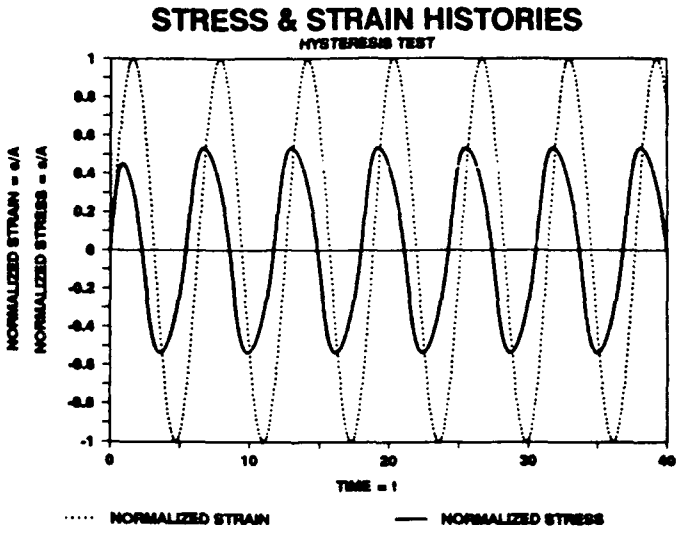

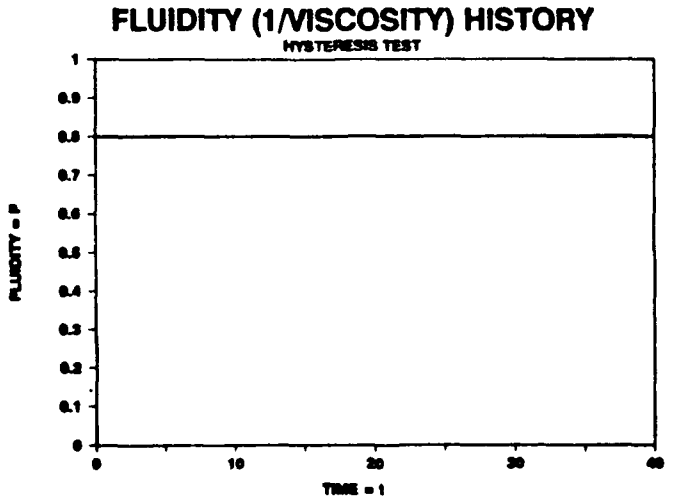

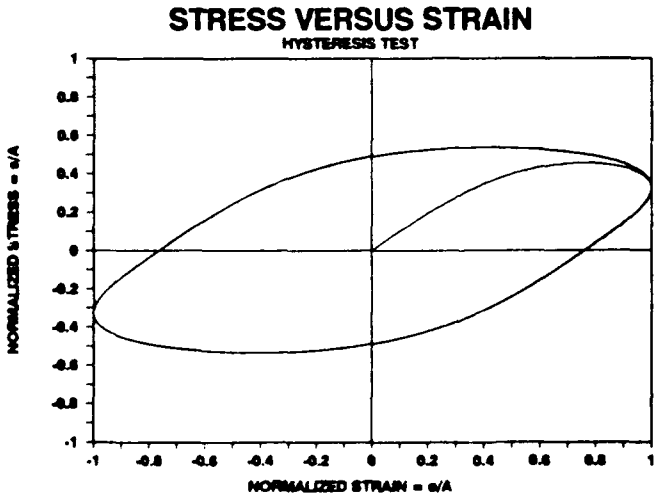

FIGURE 3: HYSTERESIS TEST ON A NONLINEAR MAXWELL MATERIAL, A = 4

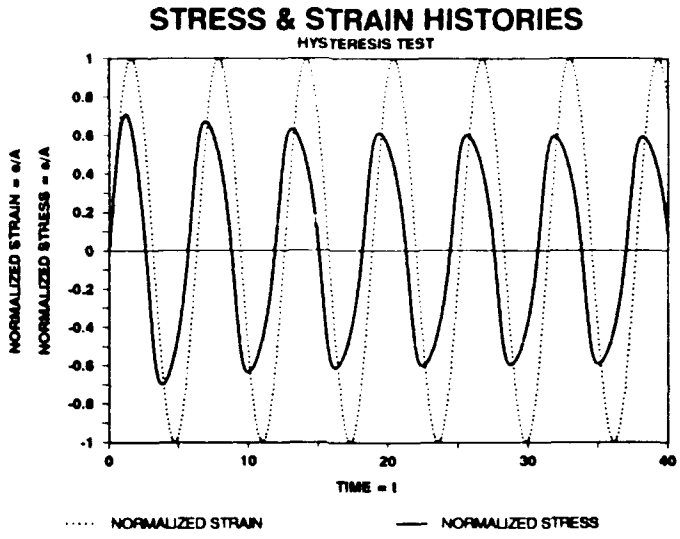

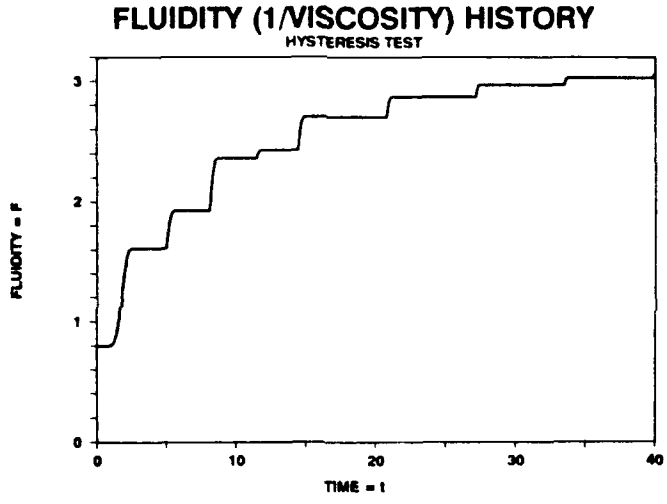

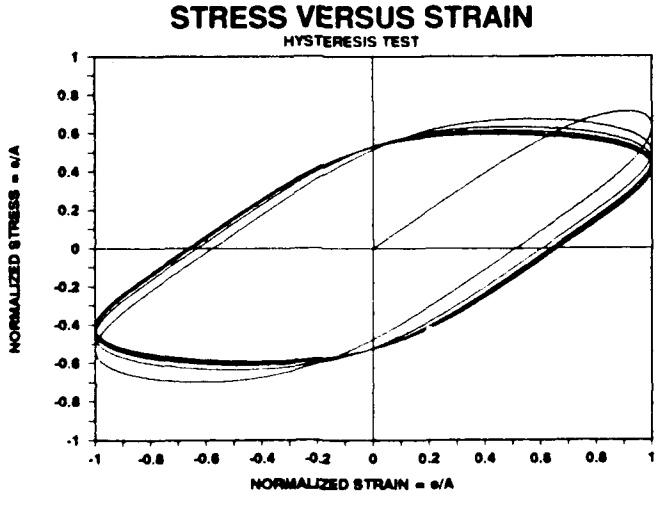

FIGURE 4: HYSTERESIS TEST ON A NONLINEAR MAXWELL MATERIAL WITH DAMAGE

RESULTS OF A ROUND ROBIN TEST SERIES TO EVALUATE COMPLEX MODULI OF A SELECTED DAMPING MATERIAL

by

David I.G. Jones
Flight Dynamics Directorate
Wright-Patterson AFB, Ohio

ABSTRACT

A Round Robin test series was conducted to establish the current state of the art in the measurement of complex moduli of polymeric damping materials as functions of frequency and temperature. Several laboratories participated, using a variety of test systems, providing data over the temperature range from -50°C to +100°C, and the frequency range from 1E-5 Hertz to over 10000 Hertz. The paper briefly describes the selection of the test material, the test methods used, and the means used to establish the accuracy of each data set and identify random and systematic errors. The results show the manner in which data from different test techniques can differ and sources are identified for some of these differences. Frequency-temperature analysis of the data is discussed.

Flight Dynamics Directorate (WL/FIBGD), Wright Laboratories, Wright-Patterson AFB, Ohio 45433. Tel: (513) 255-5236.

INTRODUCTION

In recent years it has become apparent that the routine process of measuring the complex modulus properties of polymeric materials has been conducted far too frequently without sufficient care and attention to ensuring that the data was free of errors. The outcome has been particularly unfortunate for those concerned with the application of existing data to the design of damped structures, but it has affected other users too, such as those interested in relating the observed behavior of the complex modulus properties with molecular structure. Clearly, if the data being used for comparison is erroneous, the conclusions of the research may also be erroneous. It was against this background that the Round Robin test series was organized. Round Robins have been conducted before, and have rarely been completely successful. This one may have been somewhat more successful than most, and some of the conclusions are interesting and may be of value to those concerned with improving the accuracy of future complex modulus testing.

ORGANIZING THE ROUND ROBIN

The Round Robin was organized by the author, then at the Materials Laboratory, Wright Patterson Air Force Base, Ohio, in conjunction with an international cooperative program. Many organizations in the USA and abroad were contacted, initially through a government to government cooperative program and later on a more informal basis. These organizations are summarized in Table 1. The material selected for the testing was a commercial polymer based damping material, available in sheets of various thicknesses from which various specimen geometries could be accomodated from EAR Corporation, Indianapolis, Indiana. The material identity (EAR C-1002) was not divulged to the participating organizations, though doubtless many could recognize the material. Each laboratory was requested to provide their specimen size requirements and cut specimens approximating those sizes were sent to each participant, along with limited guidelines concerning the test conditions. The main requirements are summarized in Table 2. The tests were conducted by each laboratory, as resources and time permitted, and the results were returned to the author for analysis and evaluation. Some results are still awaited, so the analysis described, in part, in this paper is still incomplete. Further analysis, and the writing of the final report, is yet to be accomplished.

ANALYSIS OF THE TEST DATA

The test data provided by each laboratory covered a wide range of test systems, as summarized on an anonymous basis in Table 3, and over a wide frequency range, as illustrated in Figure 1. The very wide frequency range provided a unique basis for evaluating the accuracy of the various data sets.

WICKET PLOT ANALYSIS

The first task was to evaluate the accuracy of each data set. This has not been a simple task in the past, but the relatively recent emergence of the Wicket Plot as a means of identifying possible errors has greatly simplified the matter. The Wicket Plot is a graph of log (loss factor)

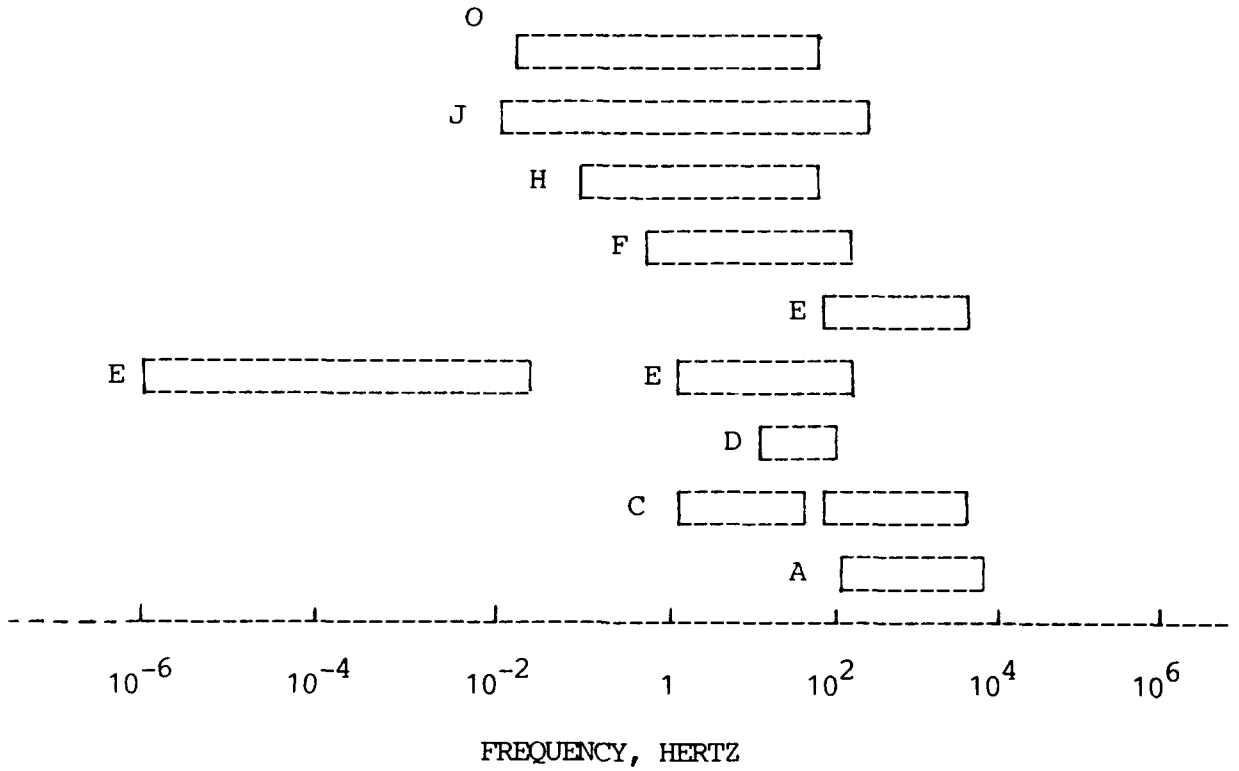

Figure 1. Frequency ranges evaluated by each laboratory

versus log (modulus) and differs from the Cole-Cole plot, which is a linear scale plot of imaginary modulus versus real modulus, in that the use of the logarithmic scale effectively accomodates the very wide range of values of the shear or Young's modulus exhibited by most polymeric materials. A linear scale may display one, or even two decades, of modulus values but only a logarithmic scale can effectively display the four or five decades often encountered. The Wicket plot is, theoretically, a unique curve for each polymer provided that no non-stationary, or time dependent, processes are taking place, and the material complex modulus behavior is thermorheologically simple, so any deviations from such a unique curve must be due to errors or time-dependent effects and in this way one may determine whether frequency-temperature analysis (reduced variables) is likely to be useful before expending often considerable effort in vain.

Representative wicket plots, for some of the test data, are shown in Figures 2 to 17, for Laboratories A,C,D,E,F,H,M,N and O in the shear and extensional modes of deformation. Each figure illustrates the types of error which may arise for the various test systems. These include random scatter, especially for the beam tests conducted by Laboratory A, deviations from the main sequence due to high specimen stiffnesses in direct stiffness test systems (Laboratories C,D,E,F,H,J,M,N and O) and deviations due to high frequency (inertia) effects in direct stiffness systems.

VARIATION OF COMPLEX MODULI WITH FREQUENCY

The Wicket Plot is the Occam's razor of complex modulus data quality analysis, in the sense that an inadequate Wicket plot at once implies that the data is suspect. However, to pass the Wicket plot test is not to guarantee the quality of the data, since temperature and frequency have been eliminated in the Wicket plot and any errors in these dimensions must also be checked. Figures 18 and 19 show typical plots of modulus and loss factor versus frequency, again on a log-log scale, at - 10°C and - 20°C, respectively. It is seen that some of the errors highlighted in the Wicket plots are reflected here also, and are in some cases more clearly seen. These plots, along with data for other temperatures, form the basis for constructing master plots of modulus and loss factor versus reduced frequency. Figure 20 shows such a master plot, generated by manual estimates of the shift factors. While the scatter is evident, the agreement between results for so many laboratories is quite remarkable. The corresponding shift factors are plotted against 1/T in Figure 21. The results lie fairly close to an Arrhenius shift relationship, of the form $\log a_T(T) \propto 1/T$, but the small deviations may be significant. The scatter, unfortunately, is too great to provide a definitive settlement of the matter.

CONCLUSIONS

The purpose of this paper has been to present the interim conclusions of a major Round Robin test series to measure the complex modulus properties of a commercial damping material sample by several test techniques, at several test locations, over wide frequency and temperature ranges. Many laboratories participated, and several more are expected to complete their tests in the near future. It is clear that all the test techniques used can produce accurate data over specific ranges of modulus and frequency, but that outside of these ranges major errors can readily be encountered. The Wicket Plot has emerged as an effective tool for detecting some of these errors. It is recommended that more than one test technique be used if data is required over a wide range of moduli, as would occur over any temperature range wide enough to encompass the rubbery, transition and glassy regions of the material behavior. A full report of all the Round Robin tests will be issued when all testing and analysis has been completed.

NOMENCLATURE

A	Load carrying area (direct stiffness tests)
E	Young's Modulus (MPa)
G	Shear Modulus (MPa)
h	Thickness of shear specimen (direct stiffness tests)
h_1	Thickness of metal beams (beam tests)
h_2	Thickness of polymer layer (beam tests)
L	Length of extensional specimen (direct stiffness tests)
Q	Activation energy
R	Universal Gas Constant
T	Absolute temperature (°K)
T_A	Activation temperature (=Q/R,°K)
η	Loss factor
$a_T(T)$	Shift factor

TABLE 1. PARTICIPATING ORGANIZATIONS

Admiralty Research Establishment, Holton Heath, Poole, England (J.R. House)
Anatrol Corporation, Cincinnati, Ohio (A.D. Nashif)
CSA Engineering Inc., Palo Alto, California (C. Johnson)
DCAN Toulon, Toulon Naval, France (M. Khoury)
Dow Corning Corporation, Midland, Michigan (N. Langley)
Institue of Sound & Vibration Research, Southampton, England (R.C. Drew)
Lehigh University, Bethlehem, Pennsylvania (L. Sperling)
MTS Corporation, Minneapolis, Minnesota (K. Biegler)
National Physical Laboratory, Teddington, England (G. Dean)
Naval Underwater Systems Center, New London, Connecticut (W. Maciejewski)
Polymer Laboratories Inc., Amherst, Massachusetts (J.C. Duncan)
TA Instruments, Cincinnati, Ohio (J. Schilthuis)
Tufts University, Medford, Massachusetts (D. Walker)
University of Dayton Research Institute, Dayton, Ohio (M.L. Drake)
University of Manchester, Manchester, England (G.R. Tomlinson)
Wright Laboratories, Materials Laboratory (D.I.G. Jones)
Wright Laboratories, Flight Dynamics Directorate (L.C. Rogers)

TABLE 2. ROUND ROBIN TEST REQUIREMENTS

Temperature range	: -20°C to +90°C in steps of 10°C (later amended to -50°C low temperature)
Frequency range	: Tester's option
Temperature soak	: At least 30 minutes before testing at each temperature.
Test condition	: Isothermal
Pre-strain	: None (preferably)
Strain amplitude	: Less than 0.1 percent (linear range)
Test methods	: Testers option
Units	: SI (preferably)
Bonding	: Tester's option

TABLE 3. TEST SYSTEMS USED BY ROUND ROBIN PARTICIPANTS

LAB	TEST SYSTEM	COMMENTS
A	7 in. Oberst Beam (E) 7 in. Sandwich Beam (G)	Limited range for extensional data at low moduli. Random scatter in shear data.
B	Direct Stiffness (E)	Resonances in test range. No usable data.
C	Direct Stiffness (HFSMA)(G) Polymer Labs DMTA (E)	Errors in dual cantilever configuration.
D	Direct Stiffness (G,E)	Some scatter at low moduli
E	10 in. F-F Homogeneous beam(E) 10 in. Oberst beam (E) 6 in. C-F homogeneous beam(E) 10 in. C-F sandwich beam (G) Resonance (E,G) Direct stiffness (G,E) Metravib Viscoanalyzer (G,E) Creep/Relaxation(G,E) Low frequency impedance	Round Robin test program within the main test program. Widest temperature and frequency ranges.
F	Direct stiffness (G)	Limited number of temperatures and limited data at high modulus values.
G	None	Analysis only.
H	Polymer Labs DMTA (G,E)	Scatter at low moduli, high modulus offset and limited range of Young's moduli.
I	No test data yet received.	
J	MTS 831.50 Elastomer Test system	High modulus offset, some discrepancies, and limited temperature range.
K	None	Analysis only.
L	Fitzgerald system	Testing in progress
M	Metravib Viscoanalyzer (E,G)	Some scatter and high modulus offset for extensional and shear data.
N	Direct stiffness systems	Testing completed
O	Rheometrics RDA2 system (G) Rheovibron (E)	High modulus offset and some erroneous data at low modulus values. Considerable scatter at low moduli, high modulus offset, and only two test frequencies.
P	No data yet received.	
Q	No data yet received	

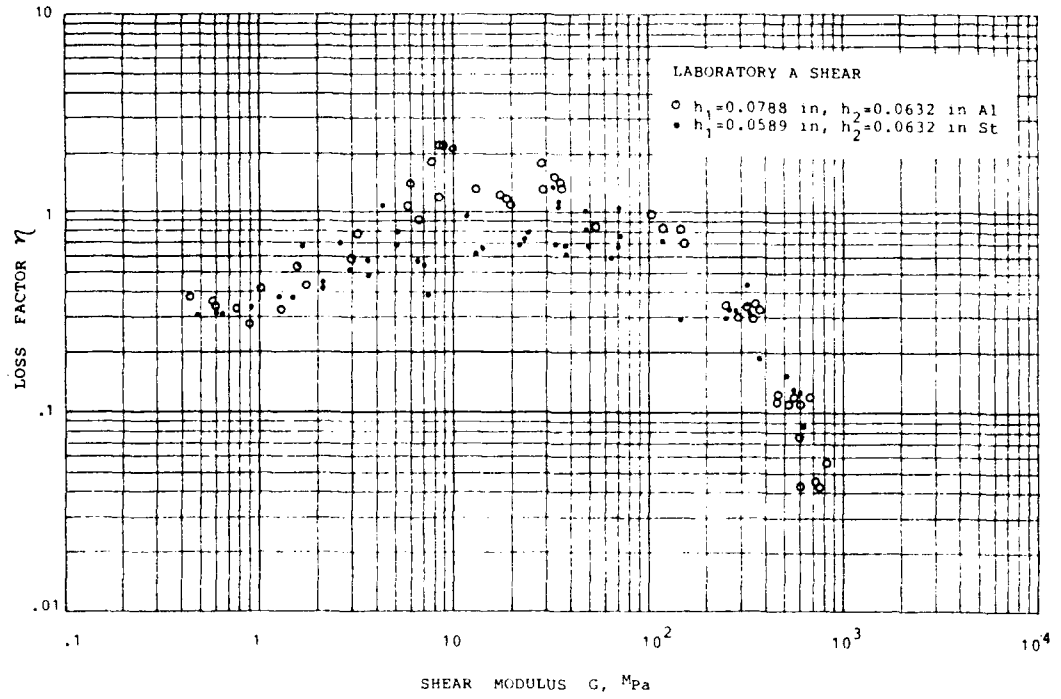

Figure 2. Wicket Plot for Laboratory A Shear Data (○ h_1 = 2 mm, h_2 = 1.61 mm, Aluminum; • h_1 = 1.50 mm, h_2 = 1.61 mm, Steel)

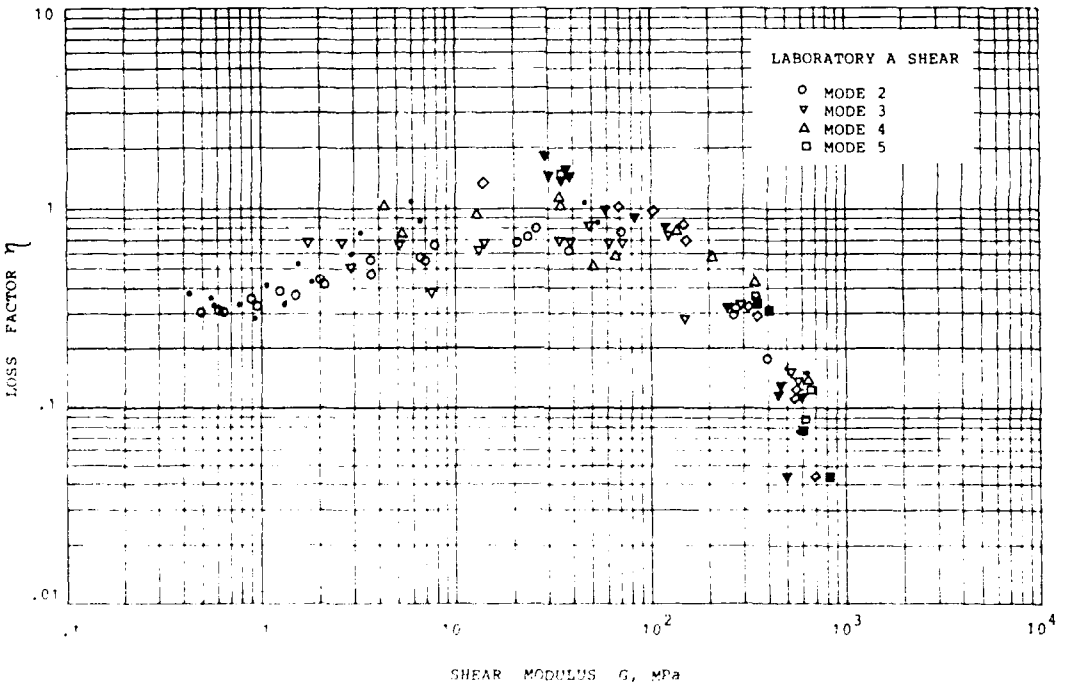

Figure 3. Wicket Plot for Laboratory A Shear Data (○ Mode 2, ▽ Mode 3, △ Mode 4, □ Mode 5)

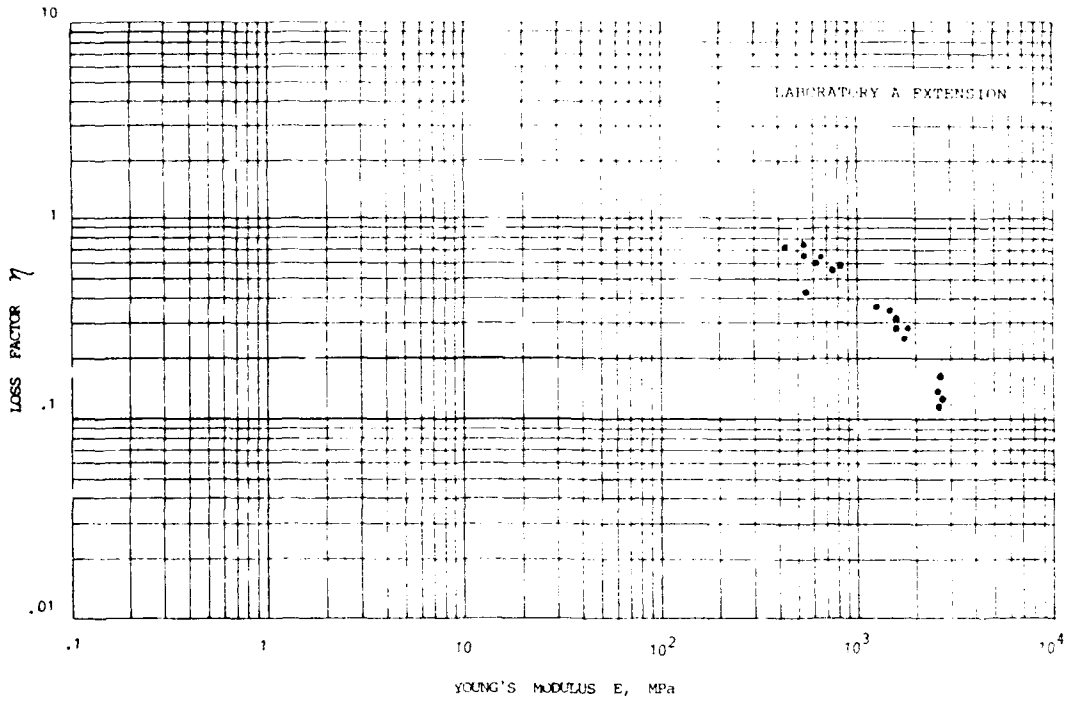

Figure 4. Wicket Plot for Laboratory A Extensional Data (h_1 = 1.52 mm, h_2 = 1.61 mm, Steel Oberst Beam)

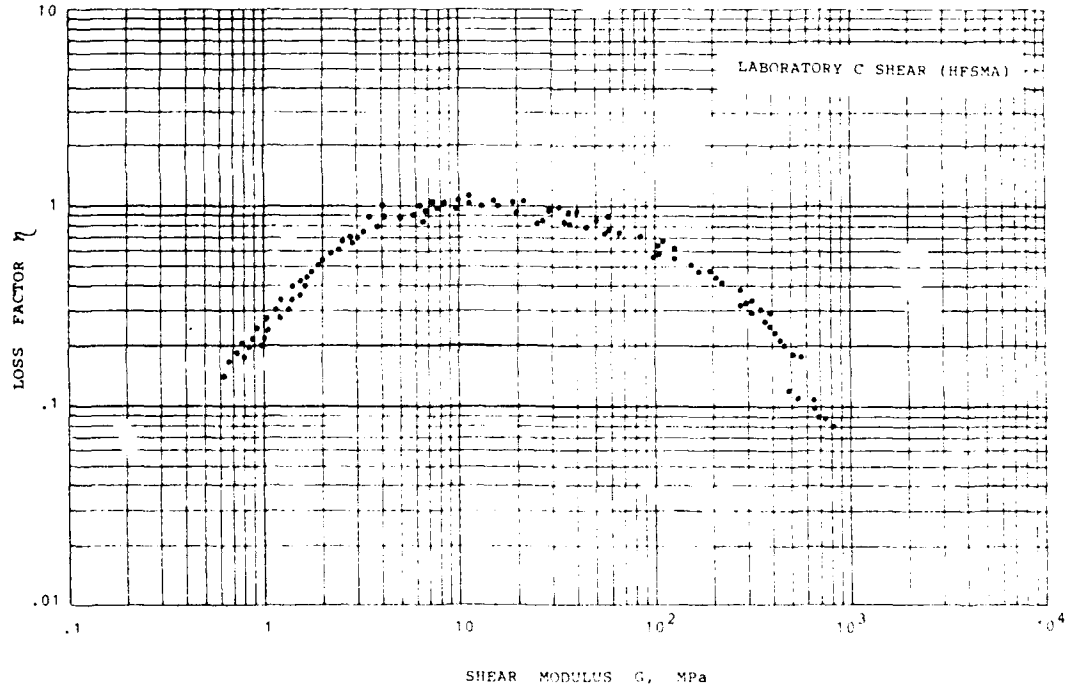

Figure 5. Wicket Plot for Laboratory C Shear Data (Direct Stiffness Method/HFSMA, thickness = 1.9 mm, diameter = 10 mm, A/h = 41.34 mm)

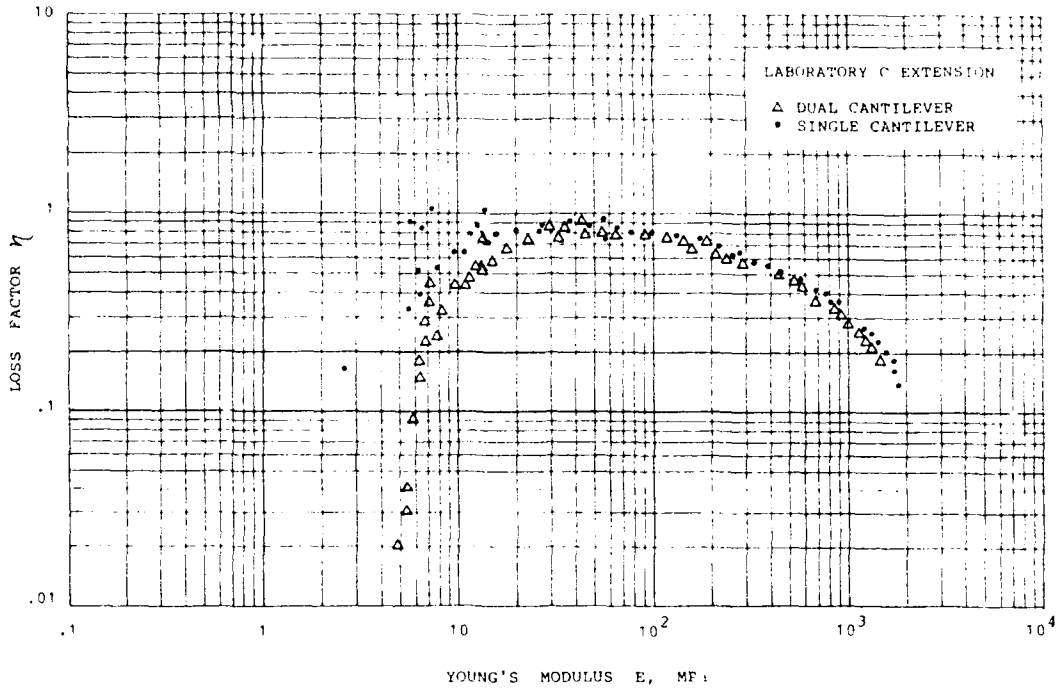

Figure 6. Wicket Plot for Laboratory C Extensional Data (Direct Stiffness Technique/PL DMTA, flexural mode, 1.24 x 12.21 x 8 mm sample)

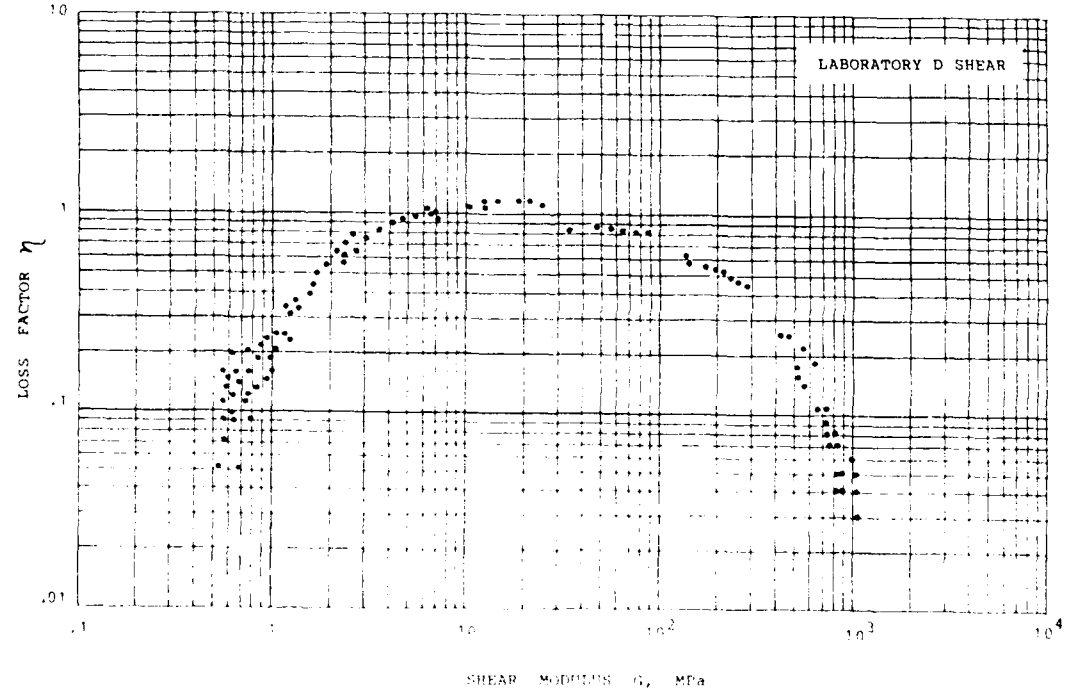

Figure 7. Wicket Plot for Laboratory D Shear Data (Direct Stiffness Method/Double Lap Shear Specimen, thickness = 12 mm, Net Area = 321.86 mm^2, A/h = 26.82 mm)

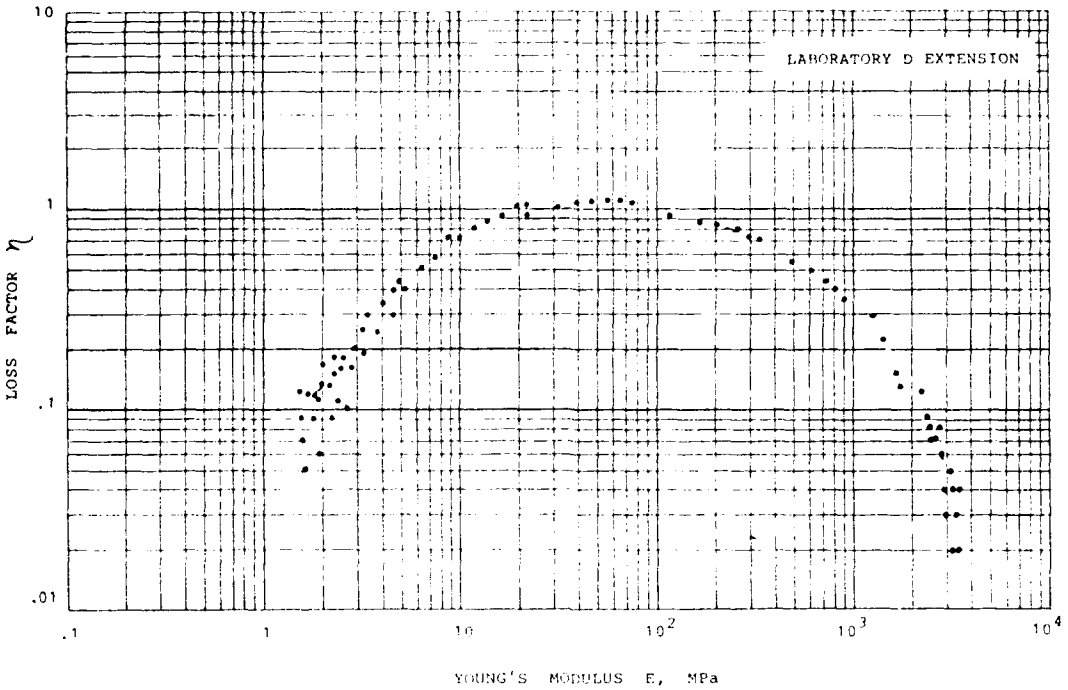

Figure 8. Wicket Plot for Laboratory D Extensional Data (Direct Stiffness Method, Length = 17.5 mm, area = 160.93 mm^2, A/h = 9.20 mm)

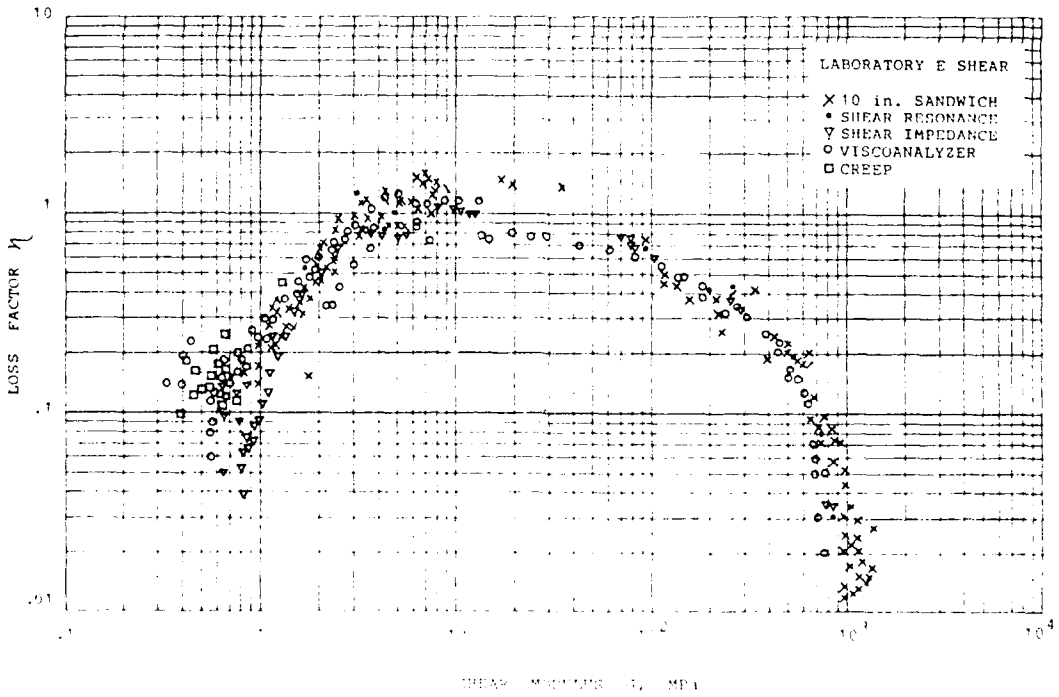

Figure 9. Wicket PLot for Laboratory E Shear Data (X 10 inch sandwich Cantilever, • Resonance, ∇ Impedance, O Viscoelasticimetre, □ Creep)

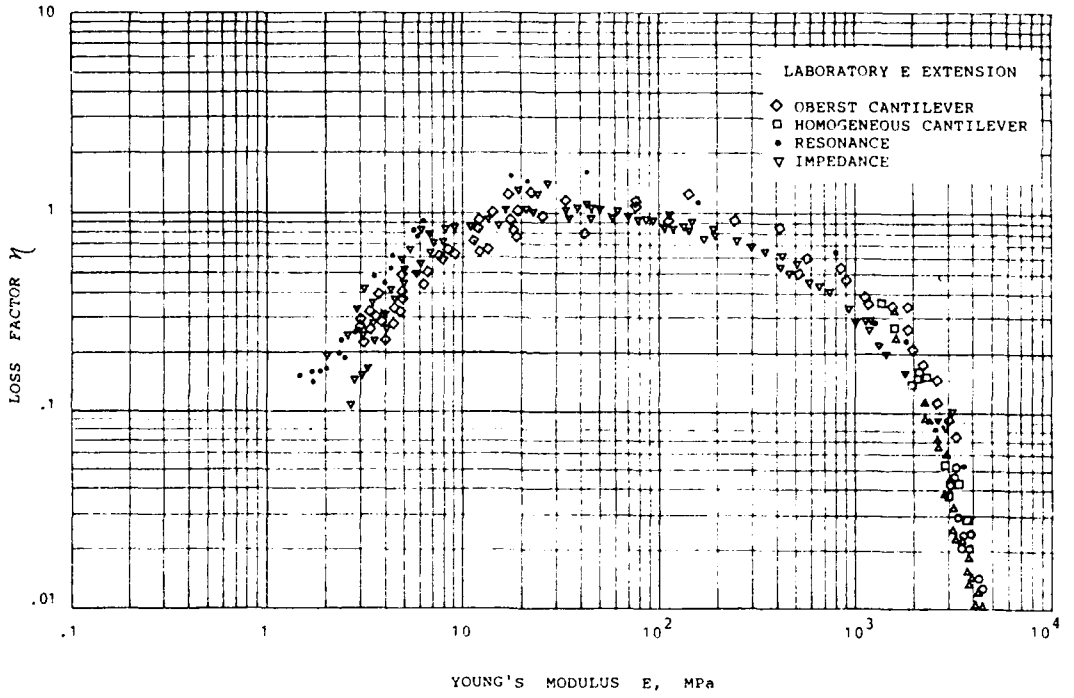

Figure 10. Wicket Plot for Laboratory E Extensional Data (◇ Oberst Cantilever, □ Homogeneous Cantilever, Δ Homogeneous Free-Free, • Resonance, ▽ Impedance: L = 44 mm, Area = 196.63 mm^2, A/L = 4.47 mm)

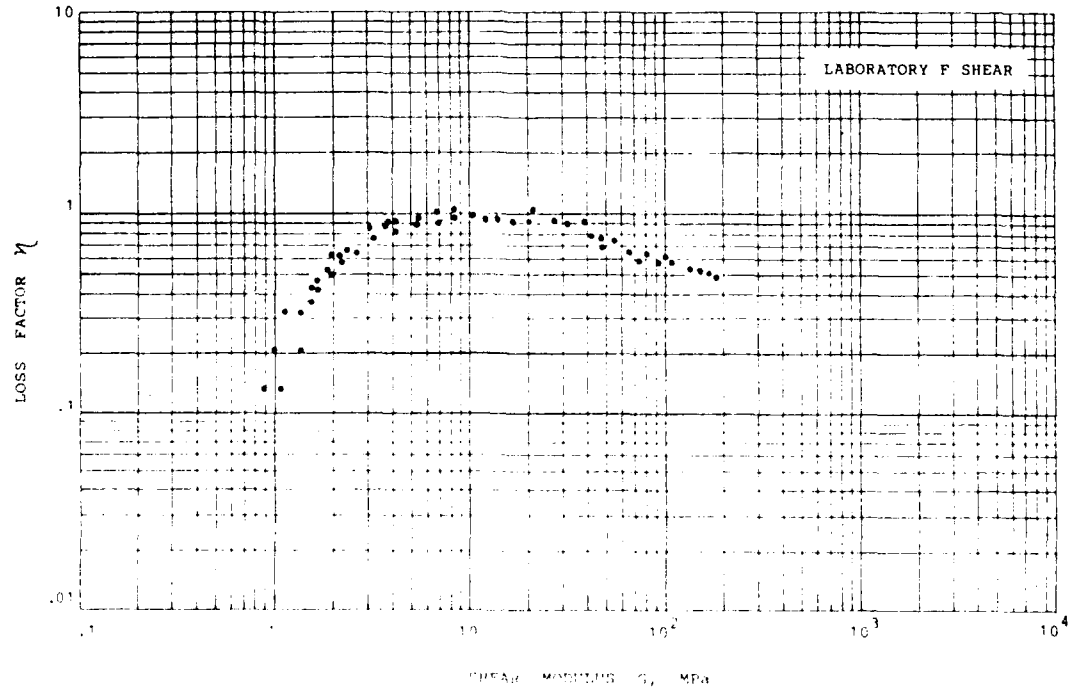

Figure 11. Wicket Plot for Laboratory F Shear Data (Direct Stiffness)

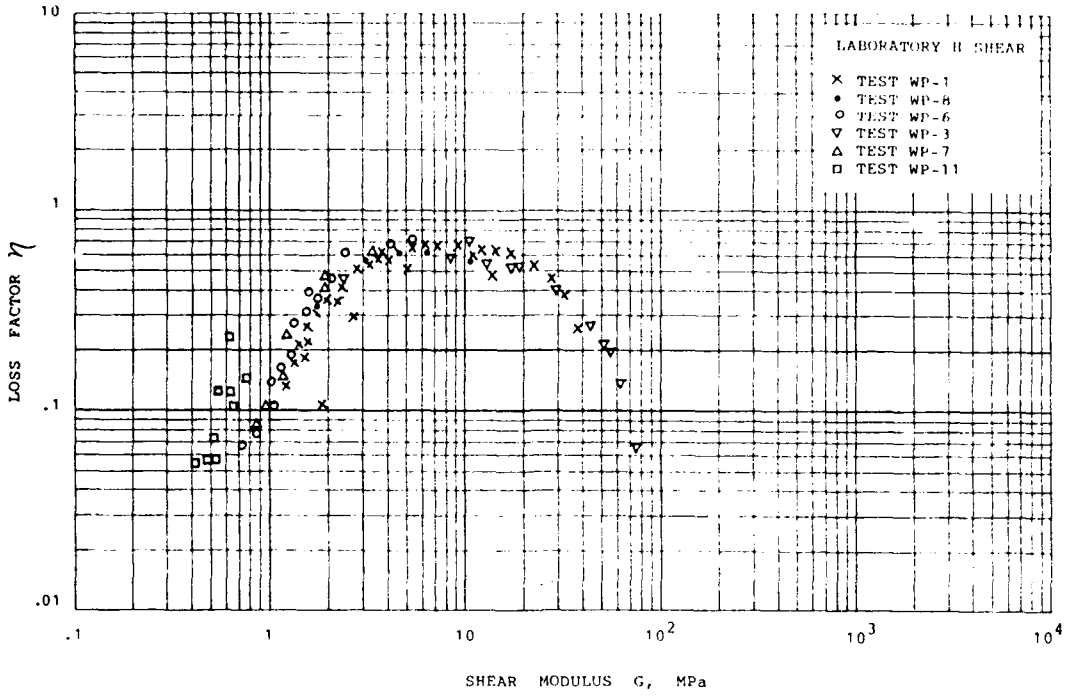

Figure 12. Wicket Plot for Laboratory H Shear Data (Direct Stiffness Method/PL DMTA, X Test WP-1, • Test WP-8, O Test WP-6, ∇ Test WP-3, Δ Test WP-7, □ Test WP-11)

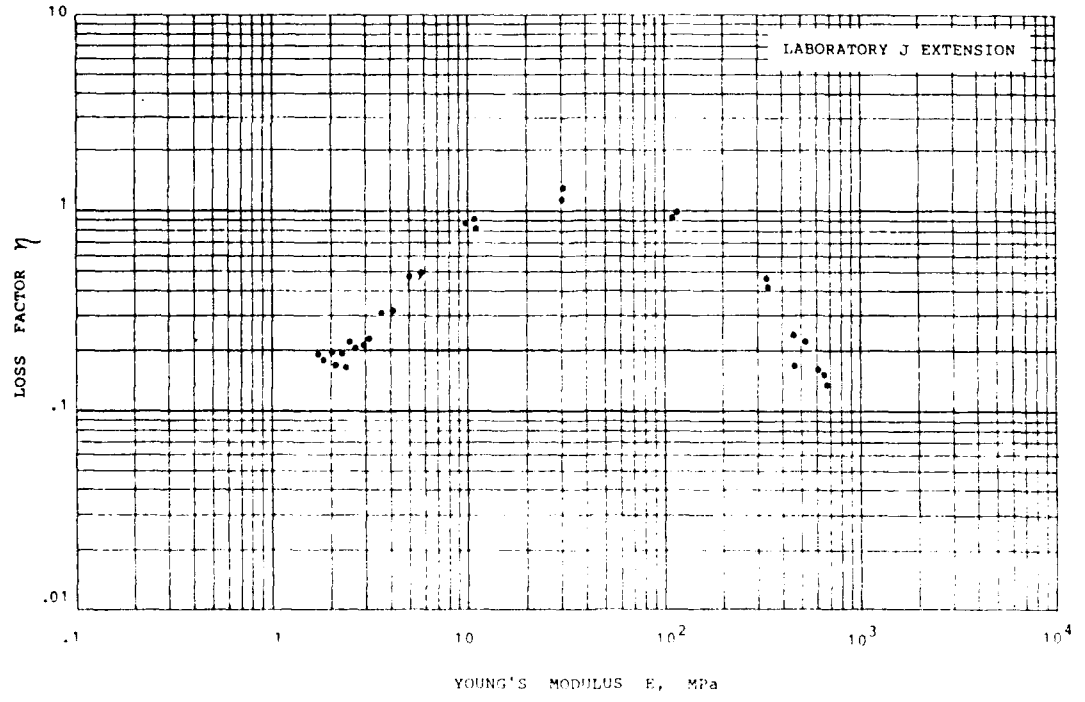

Figure 13. Wicket Plot for Laboratory J Extensional Data (Direct Stiffness Method, thickness = 12.4 mm, Area = 490.0 mm^2, A/h= 35.59 mm)

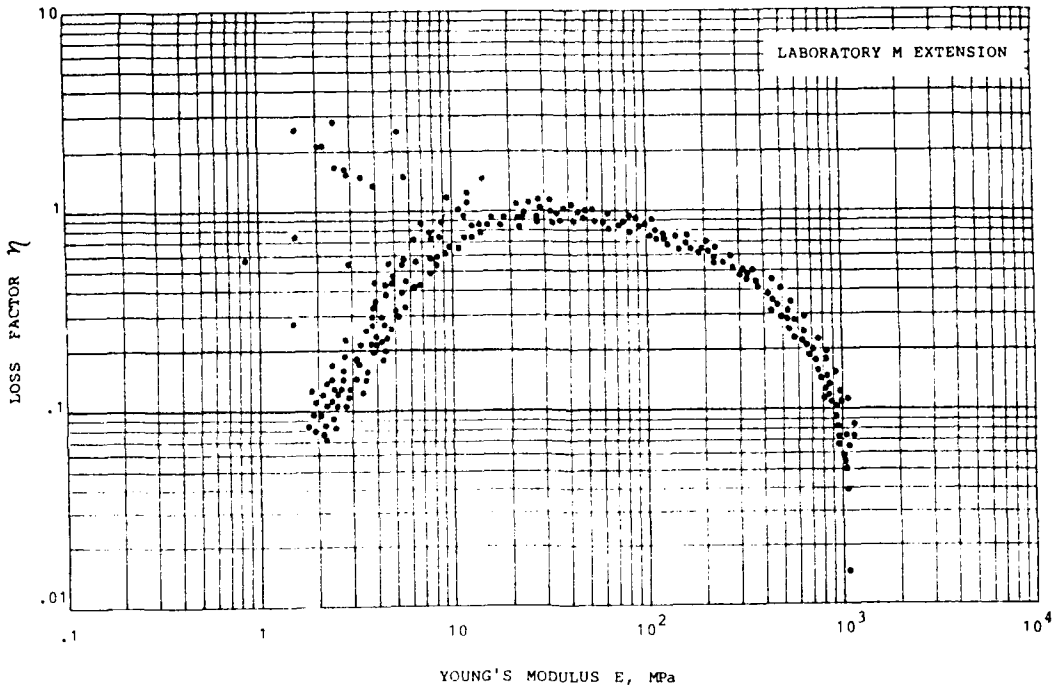

Figure 14. Wicket Plot for Laboratory M Extensional Data (Direct Stiffness Method/Viscoelasticimetre, length = 31.28 mm, Area = 447.08 mm^2, A/h = 14.29 mm)

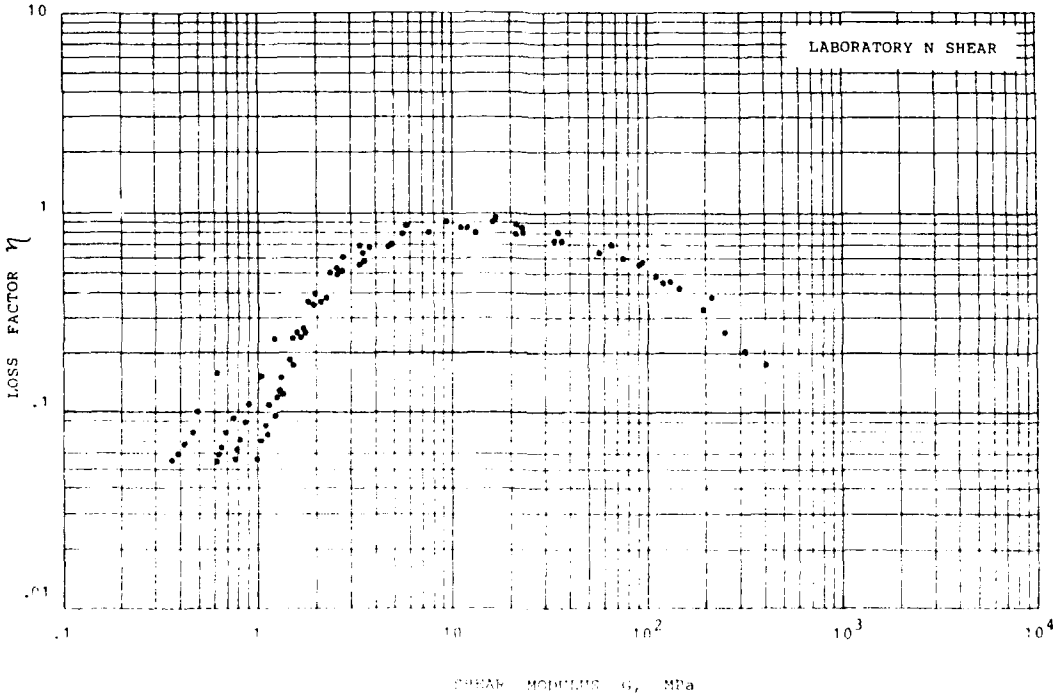

Figure 15. Wicket Plot for Laboratory N Shear Data (Direct Stiffness)

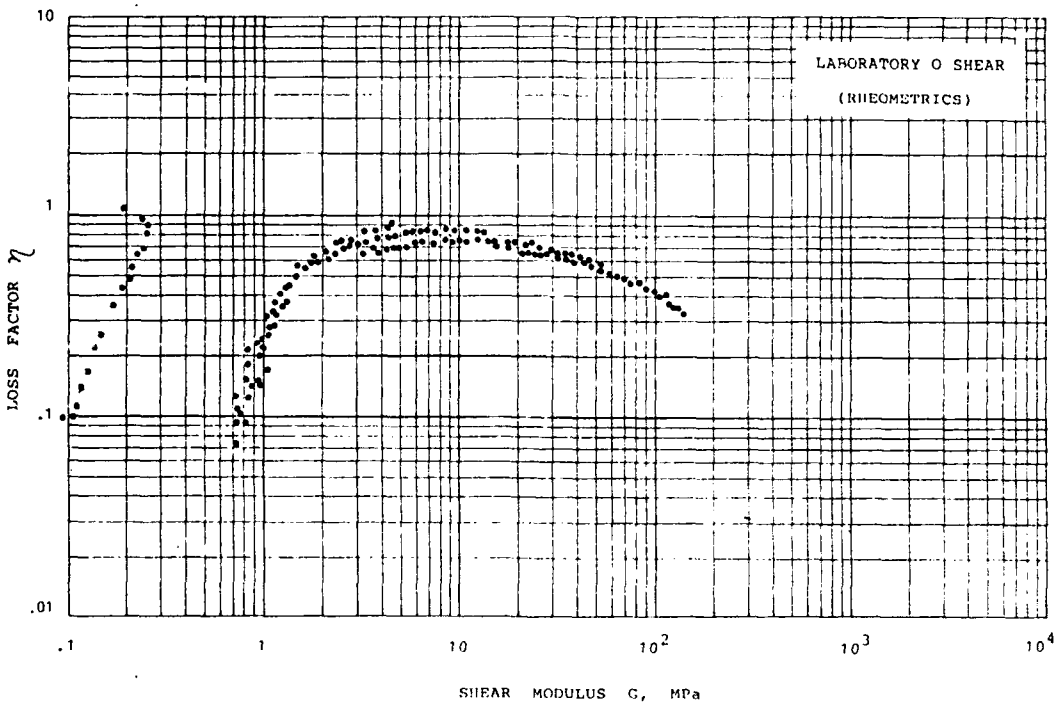

Figure 16. Wicket Plot for Laboratory O Shear Data (Rheometrics Analyzer thickness = 3 mm, Area = 49.02 mm^2, A/h = 16.43 mm)

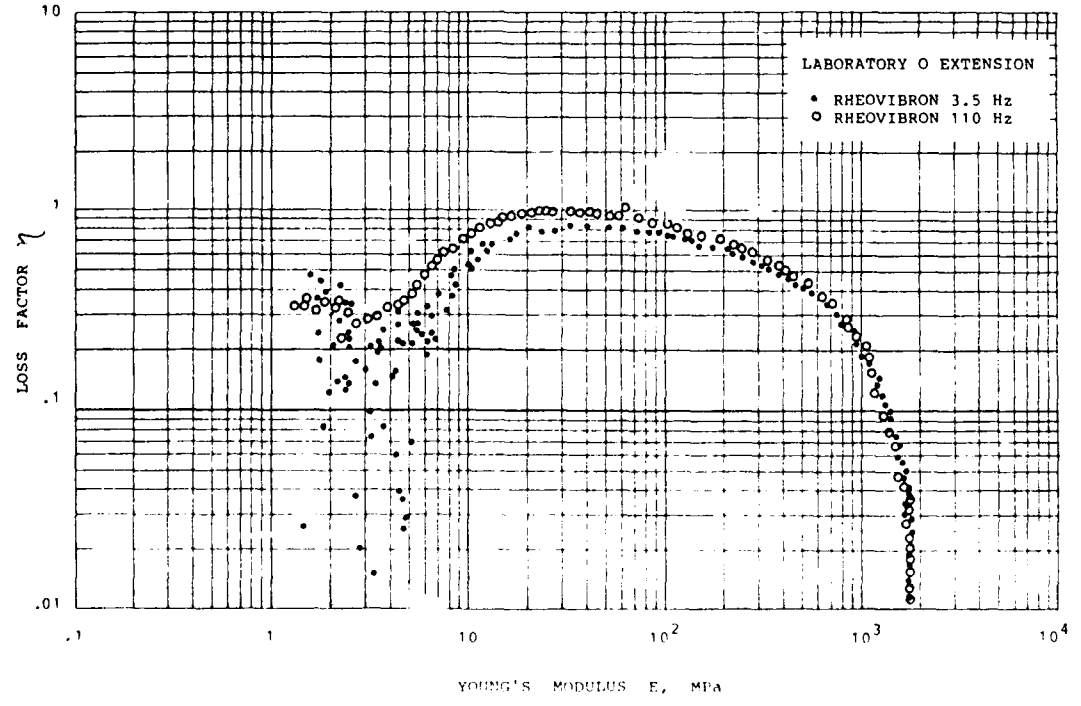

Figure 17. Wicket Plot for Laboratory O Extensional Data (Rheovibron Test System, L = 16.52 mm, Area = 24.36 mm^2, A/L = 1.47 mm)

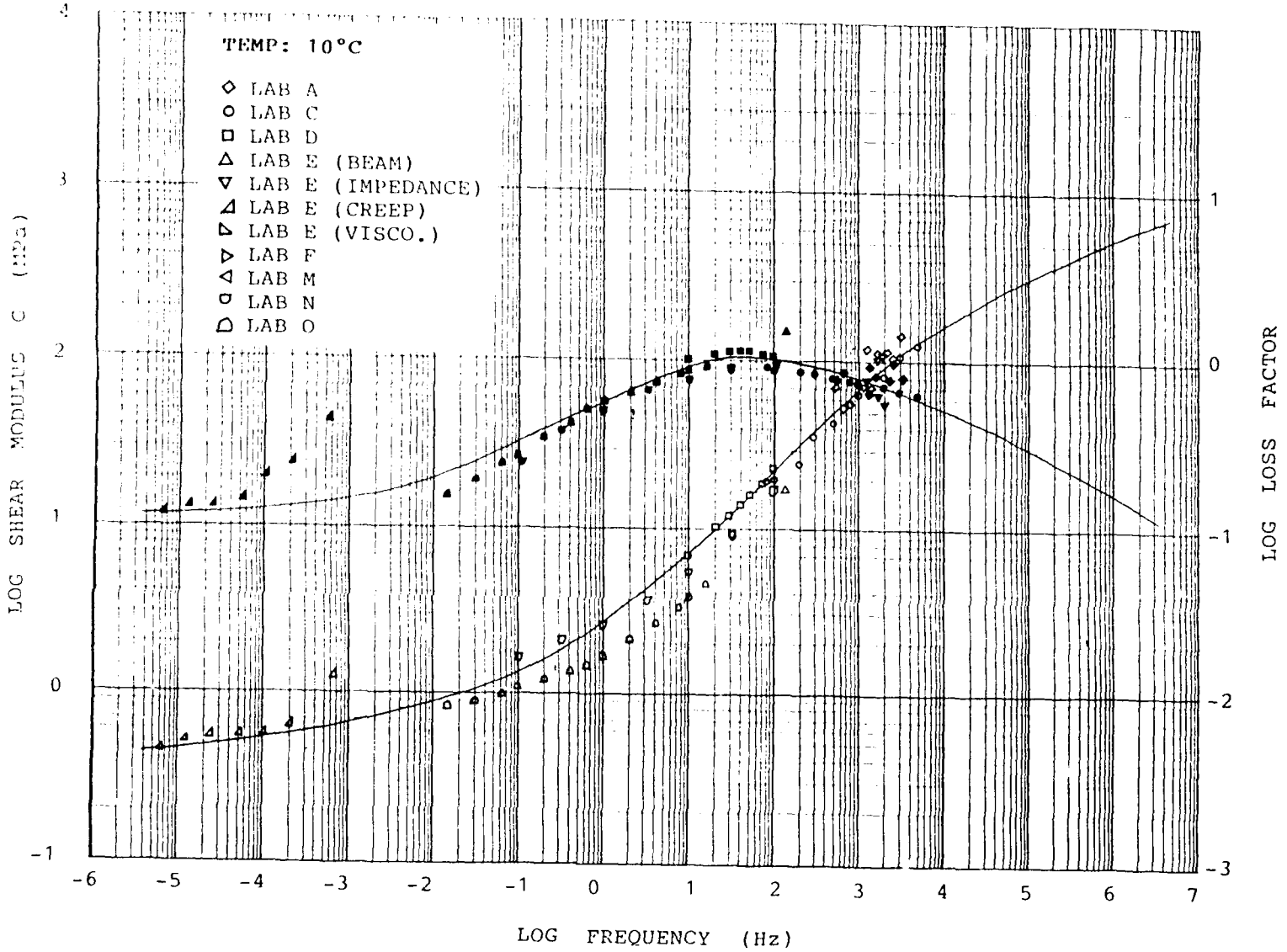

Figure 18. Plot of Shear Modulus and Loss Factor versus Frequency at + 10° (◇ Lab A, ● LabC, □ Lab D, △ Lab E (beam), ▽ Lab E (Impedance), ◁ Lab E (Creep), △ LabE (Viscoelasticimeter), ▷ Lab F, ▽ Lab N, ◁ Lab M, △ Lab O)

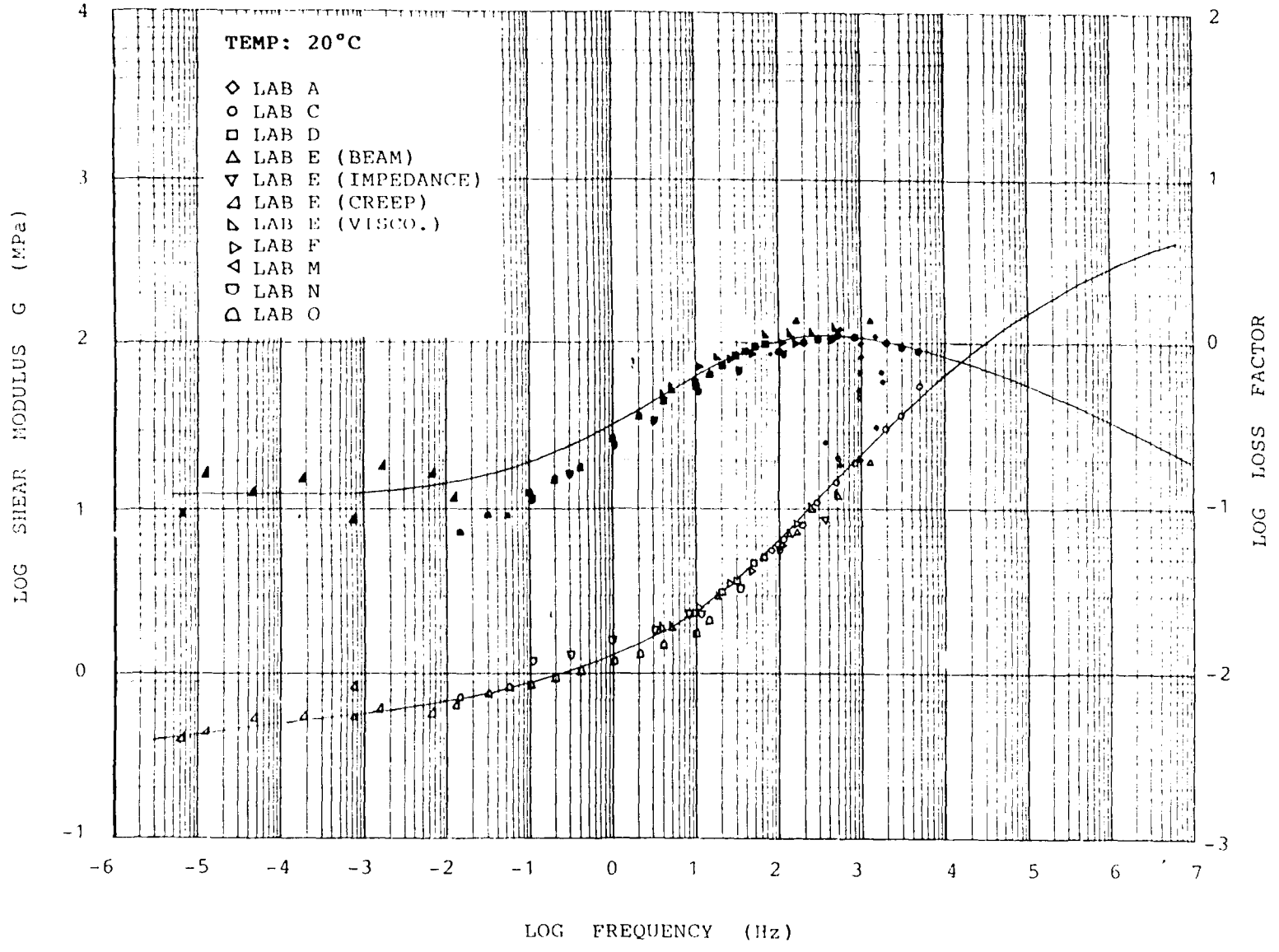

Figure 19. Plot of Shear Modulus and Loss Factor versus Frequency at + 20° (◇ Lab A, ○ LabC, □ Lab D, △ Lab E (beam), ▽ Lab E (Impedance), ◿ Lab E (Creep), ◺ LabE (Viscoelasticimeter), ▷ Lab F, ▽ Lab N, ◁ Lab M, ⏢ Lab O)

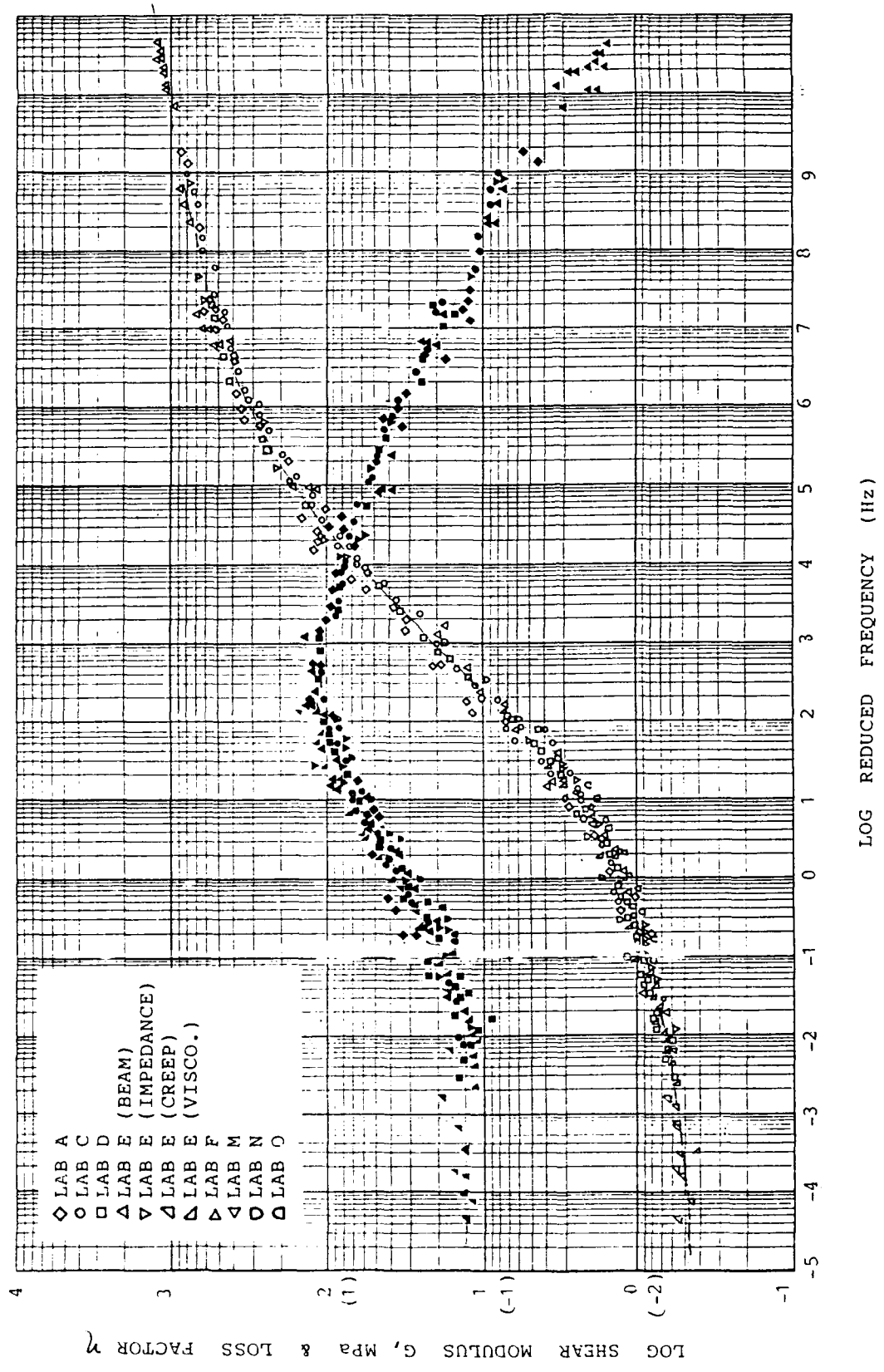

Figure 20. Master plots for All Laboratories (Shear)

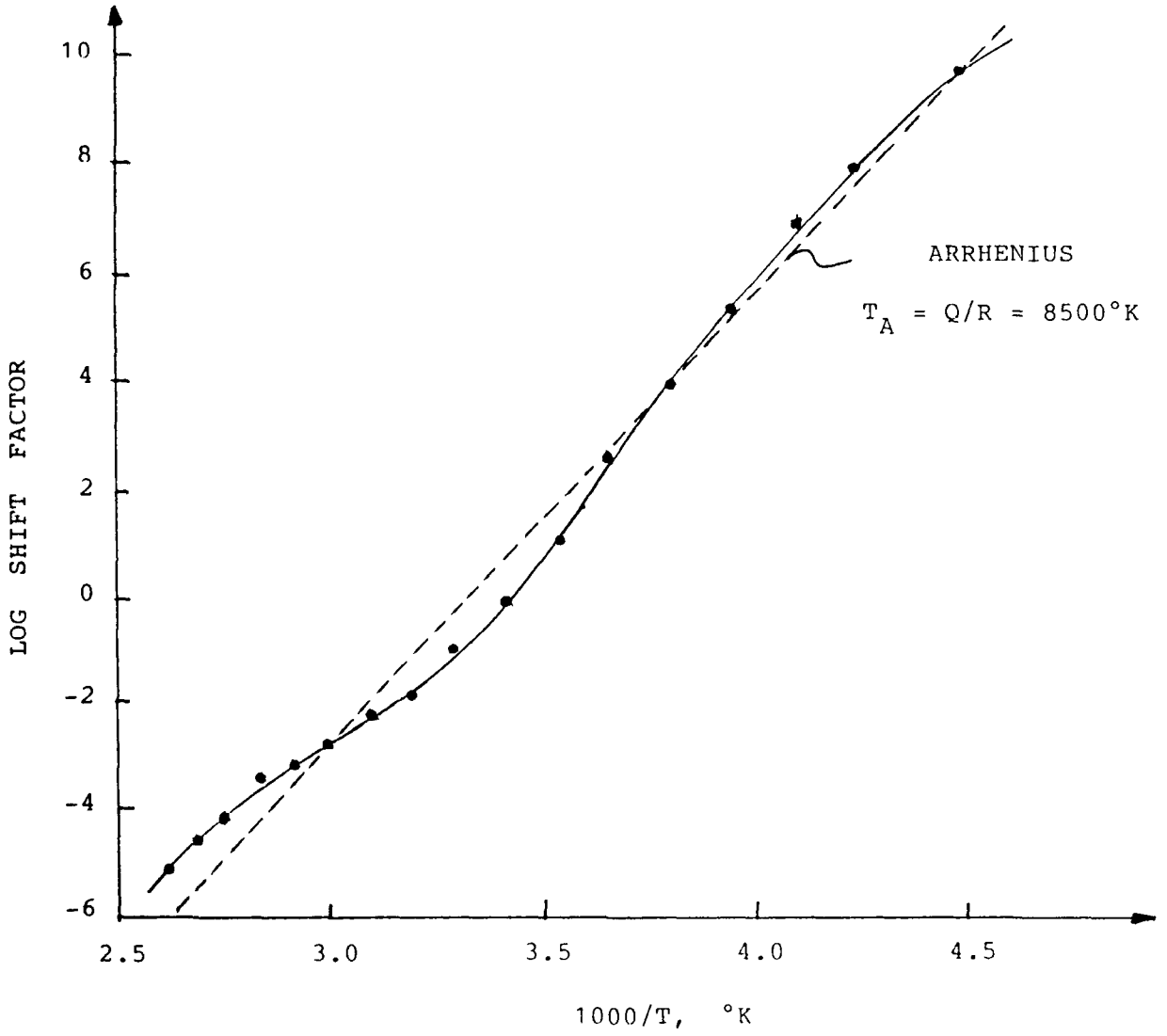

Figure 21. Plot of Log (Shift Factor) versus 1000/T

A MATHEMATICAL FRAMEWORK FOR THE STUDY OF INDIRECT DAMPING MECHANISMS

David L. Russell[1]
Virginia Polytechnic Institute and State University
Blacksburg, VA

ABSTRACT

Indirect damping, as it applies to a linear oscillator $\dot{x} = Ax$, induces energy decay through coupling of this system with an auxiliary dissipative system, rather than through insertion of dissipative terms in the original equation. Familiar physical examples lead one to distinguish (at least) two types of indirect damping; the *velocity coupled dissipator* and the *displacement coupled dissipator*. While these induce energy decay through quite distinct physical processes, we are able to show that they are mathematically equivalent. We go on to develop the mathematical properties of these models and to explore sufficient conditions under which frequency proportional damping rates may be expected. A number of examples, taken from familiar physical contexts, are cited.

FULL PAPER NOT AVAILABLE FOR PUBLICATION

[1]Virginia Tech., Department of Mathematics, 418 McBryde Hall, Blacksburg, VA 24061, (703) 231-6171

TECHNIQUES IN DESIGN AND USING VE DAMPERS

M. Tong, Z. Liang, and G. C. Lee

412 Bonner Hall
State University of New York at Buffalo
Amherst, NY 14260
Tel. (716) 636-2771

ABSTRACT

The efficiency of energy dissipation through dampers has been the major concern of damper design. This consideration is based on the assumption that the structure being worked on is proportionally damped. However, most real multi-degree-of-freedom structures are actually non-proportionally damped. For such structures, dampers not only dissipate energy but also transform energy. In this paper, some new dimensions of identifying and using dampers are investigated. A new method of design and re-design of visco-elastic dampers is suggested. Such a method is applicable to many non-proportionally damped systems.

INTRODUCTION

Minimizing excessive vibrations of structures induced by earthquake ground motions or other dynamic loadings has been a major research topic in recent years. To control such vibrations, systemic modifications of the structure's damping ratio by means of incorporating VE dampers into the system have achieved considerable success. Many recent studies as reported in the literatures contain one common restriction that the systems considered are classically damped. Since in engineering practice we often deal with non-classically damped systems, there is a need to develop approaches for non-classically damped systems. This paper presents an approach which can be used for both classically and non-classically damped systems.

Consider the fundamental equation of motion

$$\mathbf{M}\,\ddot{X}(t) + \mathbf{C}\,\dot{X}(t) + \mathbf{K}\,X(t) = F(t) \tag{1}$$

where **M**, **C** and **K** are mass, damping and stiffness matrices; They are symmetric in general. $X(t)$, $\dot{X}(t)$ and $\ddot{X}(t)$ are displacement, velocity and acceleration vectors. $F(t)$ is a forcing function. Equation (1) can be written in a monic form

$$\ddot{Y}(t) + \tilde{\mathbf{C}}\,\dot{Y}(t) + \tilde{\mathbf{K}}\,Y(t) = \tilde{F}(t) \tag{2}$$

by using the following notations

$$\begin{aligned} Y(t) &= \mathbf{M}^{-1/2}X(t) \\ \tilde{\mathbf{C}} &= \mathbf{M}^{-1/2}\mathbf{C}\,\mathbf{M}^{-1/2} \\ \tilde{\mathbf{K}} &= \mathbf{M}^{-1/2}\mathbf{K}\,\mathbf{M}^{-1/2} \end{aligned} \tag{3}$$

Next, we introduce a matrix product

$$\tilde{\mathbf{K}}^{1/2} = (\mathbf{M}^{-1/2}\,\mathbf{K}\,\mathbf{M}^{-1/2})^{1/2} = \mathbf{M}^{-1/4}\,\mathbf{K}^{1/2}\,\mathbf{M}^{-1/4}$$

which will not be discussed in detail in this paper. However, it is worth while to note that $\tilde{\mathbf{C}} = 2\,\xi\,\tilde{\mathbf{K}}^{1/2}$ is a damping representation and this representation plays a special role in VE damper design.

Examine the following case. In traditional viscous-elastic (VE) damper design, damping ratio is given by Equation (4)

$$\xi = \frac{W_d}{4\pi\,W_p} \tag{4}$$

where W_d is energy dissipated during a cycle. W_p is the maximum potential

energy (or maximum kinetic energy) before the cycle. An extension of this SDOF formula can give the i^{th} damping ratio of a proportionally damped MDOF system (see Zhang (1986))

$$\xi_i = \frac{W_{di}}{4\pi W_i} = \frac{\sum_j \gamma_{ij}^2 G_1 V_j}{2 Q_i^T \tilde{K} Q_i} \qquad (5)$$

where the subscript i indicates the formula is for the i^{th} mode. j indicates the quantity is related to the j^{th} VE damper. Q_i is the corresponding system eigenvector and V_j is the volume of the damper. With the damping ratios given as in (5), damping coefficient matrix $\tilde{C}$ can be obtained by

$$\tilde{C} = Q \, \mathrm{diag}(2 \xi_i \omega_i) \, Q^T \qquad (6)$$

Suppose damping ratio ξ_i = constant for i = 1, ... ,n. Then

$$\xi_i = \frac{W_{di}}{4\pi W_i} = \frac{(G_1 A / t)\pi Q^T \tilde{K} Q / a}{4 \pi Q^T \tilde{K} Q / 2} = \frac{G_1 A}{2 t a} = \text{constant} \qquad (7)$$

where A is the area of the VE material, t is the corresponding thickness, V = At; and a is a proportional coefficient. Thus

$$\tilde{C} = Q^T \mathrm{diag}(2 \frac{G_1 A}{2 t a} \omega_i) Q = \frac{G_1 A}{ta} Q^T \mathrm{diag}(\omega_i) Q = 2\xi \tilde{K}^{1/2} = \delta \tilde{K}^{1/2}$$

where the proportional coefficient $\delta = \frac{G_1 A}{ta} = 2 \xi$.

From the above explanation we can see that, if a system is *strictly-proportionally damped*, (i.e. ξ_i = constant for all i), then its damping matrix is proportional to $\tilde{K}^{1/2}$ with a coefficient of 2 ξ .

A GENERAL METHOD FOR EVALUATION OF THE DAMPING COEFFICIENT MATRIX

Among the three coefficient matrices, mass **M**, damping **C** and stiffness **K**, of the dynamic system (1), **K** and **M** are comparatively easy to determine. For example, we can use the finite element method to construct the mass and stiffness matrices respectively. In general we do not have explicit formula for damping matrices. This is why we consider matrix representation (6). In the following, we will show that, if mass and stiffness matrices of the structures and loss factors or loss modulus of damping materials are known, we can establish a method to determine the damping matrix within sufficient accuracy.

GENERAL PROPORTIONALLY DAMPED SYSTEMS

For a strictly-proportionally damped system, the damping matrix is

$$\tilde{\mathbf{C}} = 2\,\xi\,\tilde{\mathbf{K}}^{1/2}$$

Note that $\tilde{\mathbf{K}}$ has the eigen-decomposition

$$\tilde{\mathbf{K}} = \mathbf{Q}\ \text{diag}\ (\omega_i^2)\ \mathbf{Q}^T$$

and $\mathbf{Q} = [Q_1, Q_2, \ldots Q_n]$. Thus

$$\tilde{\mathbf{C}} = 2\,\xi\,\mathbf{Q}\ \text{diag}\ (\omega_i)\ \mathbf{Q}^T = 2\,\xi \sum_{j=1}^{n} \omega_j\, Q_j\, Q_j^T \qquad (8)$$

From Equation (8) we see that, for a strictly-proportionally damped system, the damping matrix is the sum of the outer product of mode shapes Q_i and modal damping coefficients $2\xi\omega_i$. This representation of damping matrix is very useful because it can be extended to both proportionally damped and non-proportionally damped systems. To understand this idea, we try to obtain Equation (8) by a force-method. This method is different from the energy-method used earlier to obtain $\tilde{\mathbf{C}} = 2\,\xi\,\tilde{\mathbf{K}}^{1/2}$. The energy-method is often employed to determine stiffness matrices (see Timosinko (1982)), but for a system with complicated energy interactions it can not produce the general damping matrix. Without loss of generality, we use the monic equation again. For simplicity in notations, we omit the overhead bar ~.

$$\ddot{X}(t) + \mathbf{C}\,\dot{X}(t) + \mathbf{K}\,X(t) \quad 't)$$

If we can find a forcing function F(t) su[illegible] inertia force $\ddot{X}(t)$ constantly cancels the spring force $\mathbf{K}X(t)$, [illegible] ave

$$\mathbf{C}\,\dot{X}(t) = F(t) \qquad (9)$$

and from Equation (9), we may be able to deter[illegible]ne damping matrix $\mathbf{C}$. For the easiest case of strictly-proportionally damped system, it can be seen that such a force corresponding to the i^{th} mode of the system can be given by

$$F_i(t) = 2\,\xi\,\omega_i^2\,Q_i\,\cos\,(\omega_i t)$$

Since

$$X(t) = Q_i \sin\,(\omega_i t),\ \text{and}\ \ddot{X}(t) = -\omega_i^2\,Q_i \sin\,(\omega_i t)$$

so

$$\mathbf{K}\,X(t) = \omega_i^2\,Q_i \sin\,(\omega_i t) = -\,\ddot{X}(t)$$

and

$$\mathbf{C}\,\dot{X}(t) = \mathbf{C}\,\omega_i\,Q_i \cos(\omega_i t) = 2\,\xi\,\omega_i^2 Q_i\,\cos(\omega_i t) = F_i(t).$$

Now let the forcing function be

$$F(t) = \sum_{i=1}^{n} F_i(t) = \sum_{i=1}^{n} 2\,\xi\,\omega_i^2\,Q_i\,\cos\,(\omega_i t)$$

Then

$$X(t) = \sum_{i=1}^{n} Q_i\,\sin\,(\omega_i t)$$

$$\mathbf{C}\,\dot{X}(t) = F(t) = \sum_{i=1}^{n} 2\,\xi\,\omega_i^2\,Q_i \cos\,(\omega_i t) \qquad (10)$$

Therefore, for the strictly-proportionally damped systems, the damping matrix **C** must be in the form of Equation (10). For a more general case of proportionally damped systems, the damping ratios are not necessarily identical. However, since the damping matrix must have the same eigenvector matrix as the stiffness matrix, so

$$\mathbf{C} = \mathbf{Q}\,\mathrm{diag}\,(2\,\xi_i\omega_i)\,\mathbf{Q}^T = \sum_{j=1}^{n} 2\,\xi_j\omega_j\,Q_j\,Q_j^T \qquad (11)$$

Equations (8) and (11) appear to be trivial for proportionally damped systems. However, if all the modal damping ratios ξ_i are known, then this representation of damping matrix is unique.

NON-PROPORTIONALLY DAMPED SYSTEMS

In the case of non-proportionally damped systems, the damping matrix may still be expressed in the form

$$\mathbf{C} = \mathbf{P}\,\mathrm{diag}\,(2\,\eta_i\omega_i)\,\mathbf{P}^T = \sum_{j=1}^{n} 2\,\eta_j\omega_j\,P_j\,P_j^T$$

where **P** is the system eigenvector matrix, which is now different from **Q**, the eigenvector matrix of **K**. The quantities η_i are also different from ξ_i, the i^{th} damping ratio of the system. Generally speaking, we can no longer find all P_i by the same approach described in the previous section. For the time being, we will not discuss how to overcome this difficulty which is left to the next section. Let us now examine the force-method again in a more general setting, by considering a simple damper shown in Fig. 1.

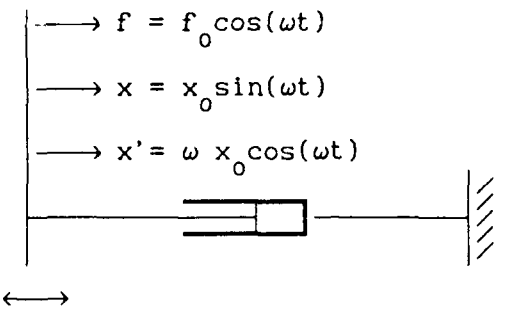

Fig. 1 A damper fixed at one end

If work is done on this damper by external force $f = f_0\cos(\omega t)$, then the forced displacement will have 90° phase difference from the given force. The velocity will be in phase with the force, that is $x = x_0\sin(\omega t)$ and $\dot{x} = \omega x_0\cos(\omega t)$. The subscript o denotes amplitude, ω denotes the driving frequency. Work W_f done by the external force in one cycle $0\text{-}2\pi/\omega$ is given by

$$W_f = \int_0^{2\pi/\omega} f\,dx = \int_0^{2\pi/\omega} f_0\cos(\omega t)\ \omega\ x_0\cos(\omega t)\,dt$$

$$= \int_0^{2\pi/\omega} f_0\ x_0\cos^2(\omega t)\,d\omega t = f_0\ x_0/2\ (\omega t + \sin(\omega t)\cos(\omega t))\Big|_0^{2\pi/\omega}$$

$$= \pi\ f_0\ x_0 \qquad (12)$$

Now consider a 3-DOF system shown in Figure 2, where k_i and $c_{(i)}$ are the stiffness and damping between the $(i-1)^{th}$ and the i^{th} floors respectively. Suppose the structure itself is damping free and the system damping si entirely provided by the added dampers, each has an identical value. Then $c_{(i)}$ is the number of dampers mounted in between the $(i-1)^{th}$ and the i^{th} floors. If both k_i and $c_{(i)}$ are constant, or the ratios $k_i/c_{(i)}$ are constants for all i, then the system is proportionally damped. Otherwise, it is non-proportionally damped.

By using the force-method, we can determine the damping matrix of the structure. The procedures are: (1) Create a sub damping matrix for each mode with natural frequency ω_i. Denote the matrix by C_i. (2) By applying the properties of lightly damped systems, add all sub matrices C_i together. The result will be the damping matrix C, i.e.

$$C = C_1 + C_2 + C_3$$

Note that, for a general damped system, without determining the damping matrix, we can not obtain the exact values of natural frequencies. However, if the system is lightly damped (see Liang et al 1991), we can use ω_{n1}, the square root of the corresponding eigenvalue of generalized stiffness matrix $\tilde{\mathbf{K}}$, to approximate the natural frequency ω_1. The error in such an approximation is negligibly small. Now, consider the first mode, with natural frequency ω_1.

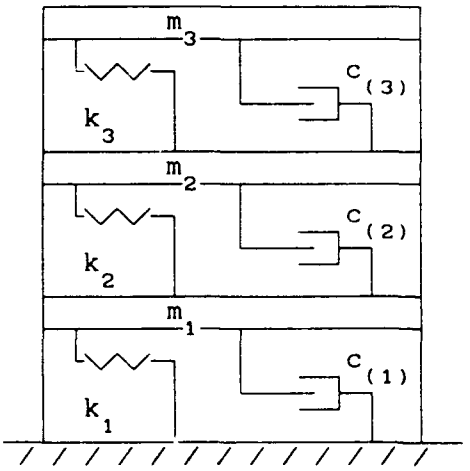

Fig. 2 3-DOF system with springs and dampers

Assume first that the second and third floors are fixed, and only the first

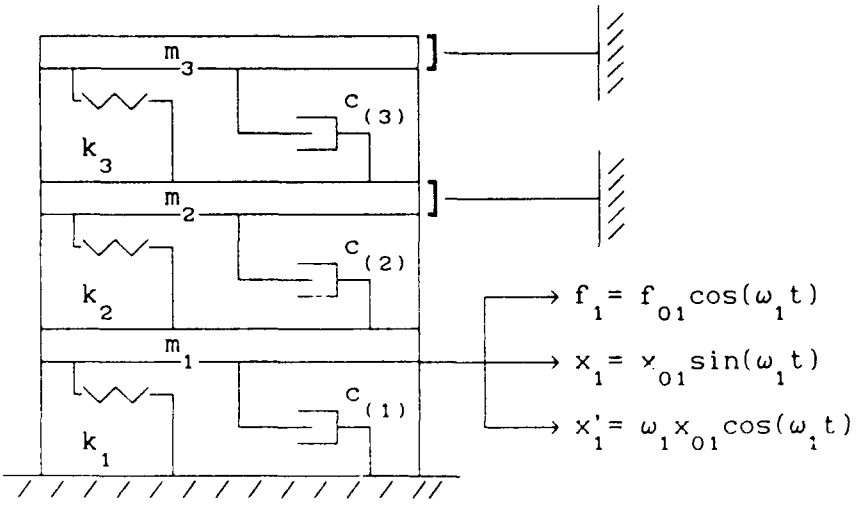

Fig. 3 3-DOF system with 2nd and 3rd floors fixed

floor may vibrate under loading $f_1 = f_{01}\cos(\omega_1 t)$. In a stabilized state, there is an instant when the inertia and the spring forces cancel each

other. Say at t_{01}, the damping force exerted on mass No.1 equals to the external loading. Namely,

$$c_{11}^{(1)} \dot{x}_1(t_{01}) = f_1(t_{01}) \tag{13}$$

Here the damping coefficient c_{ij} is quantitatively equal to the amount of force exerted on the i^{th} mass if the j^{th} mass is moving with a unit velocity and all other masses have zero velocity. The superscript (i) is used to denote the damping effect caused by the i^{th} natural frequency. Therefore, we can write

$$c_{11}^{(1)} = f_1(t_{01}) / x_1'(t_{01}) = f_{01} / (x_{01}\omega_1) = f_{01} \Big| x_{01}\omega_1 = 1$$

Note that, within one cycle, the work done by the external force f_1 is equal to the energy dissipated in the damper. That is $W_f = W_d$. In a later section it will be shown that in certain cases such as VE damper design, (the loss modulus G" and total volume V of the damping material are given), the energy dissipated in a cycle can be calculated by

$$W_d = \pi \bar{\beta} \gamma^2$$

where γ is the strain caused by deformation of damping material, $\bar{\beta}$ is a *proportional coefficient*. If the damper is a shear-resisting damper, as in the above example, then

$$\gamma = x_0 / t$$

where t is the thickness of the damping material. Thus, we have

$$f_0 x_0 \pi = W_f = W_d = \pi \bar{\beta} \gamma^2 = \pi \bar{\beta}/t \; x_0^2 \tag{14}$$

or,

$$f_0 = \beta x_0$$

where the proportional coefficient $\beta = \bar{\beta}/t$. Denote the coefficient β of the damping $c_{(1)}$ by β_1. We refer to β_1 as the *damping factor*. We then have

$$f_{01} = \beta_1 x_{01} \tag{15}$$

With the help of Equation (15), damping coefficient $c_{11}^{(1)}$ can be determined by

$$c_{11}^{(1)} = f_{01} / (x_{01}\omega_1) = f_{01} \Big| x_{01}\omega_1 = 1 = (\beta_1 + \beta_2)/\omega_1$$

Following the same procedure, we can have

$$c_{12} = -\beta_2/\omega_1$$

and

$$c_{13} = 0$$

since there is no relative motion between the second floor and the third floor.

Next let us assume the first floor is fixed and the second floor is free, as shown in Fig. 4

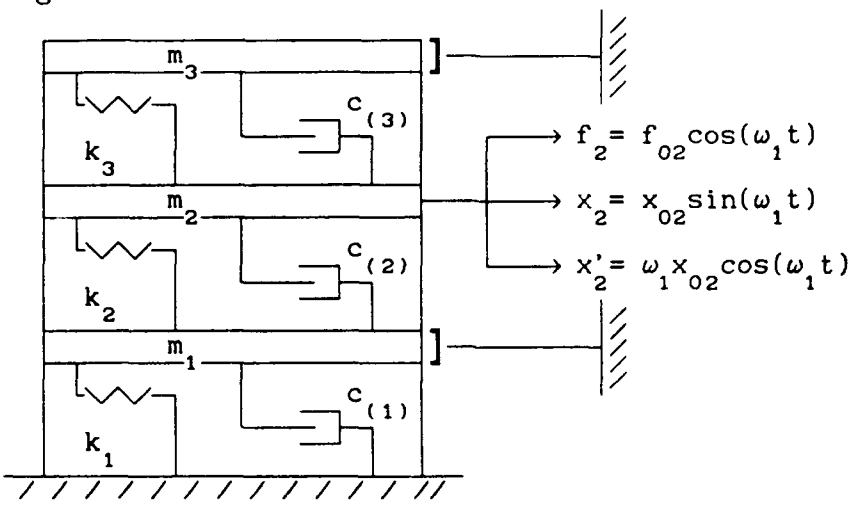

Fig 4 3-DOF system with 1st and 3rd floors fixed to grounds

Similar to the first case, we have

$$c_{21} = -\beta_2/\omega_1 \quad , \quad c_{22} = (\beta_2 + \beta_3)/\omega_1 \quad , \quad \text{and } c_{23} = -\beta_3/\omega_1$$

Finally, we free the third floor and fix the second floor, as shown in Fig. 5

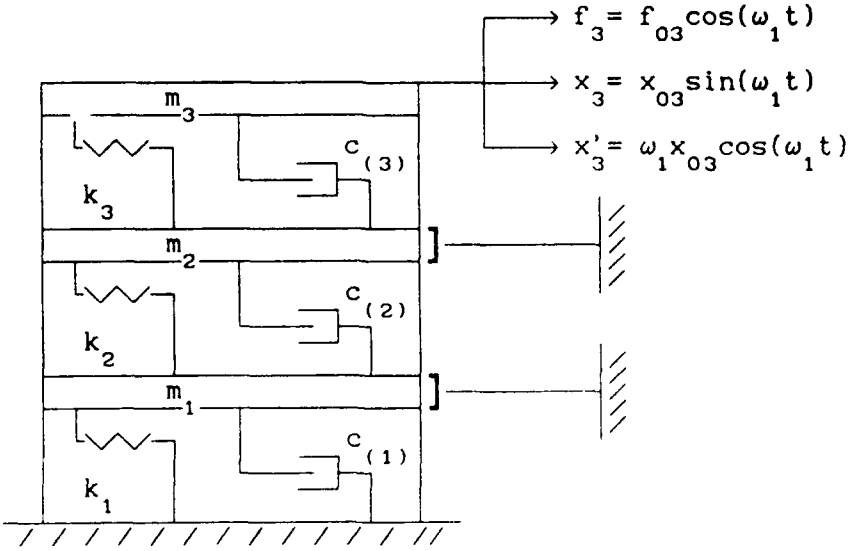

Fig. 5 3-DOF system with 1st and 2nd floors fixed to grounds

We know $c_{31} = 0$, $c_{32} = -\beta_3/\omega_1$ and $c_{33} = \beta_3/\omega_1$. Therefore, for harmonic driving frequency ω_1, we have

$$C_2 = \begin{bmatrix} \beta_1 + \beta_2 & -\beta_2 & 0 \\ -\beta_2 & \beta_2 + \beta_3 & -\beta_3 \\ 0 & -\beta_3 & \beta_3 \end{bmatrix} / \omega_2$$

Similarly, for harmonic driving frequency ω_2, we have

$$C_3 = \begin{bmatrix} \beta_1 + \beta_2 & -\beta_2 & 0 \\ -\beta_2 & \beta_2 + \beta_3 & -\beta_3 \\ 0 & -\beta_3 & \beta_3 \end{bmatrix} / \omega_3$$

By adding up all the components, The damping matrix is obtained

$$C = C_1 + C_2 + C_3 = \begin{bmatrix} \beta_1 + \beta_2 & -\beta_2 & 0 \\ -\beta_2 & \beta_2 + \beta_3 & -\beta_3 \\ 0 & -\beta_3 & \beta_3 \end{bmatrix} (1/\omega_1 + 1/\omega_2 + 1/\omega_3)$$

This idea can be extended to n DOF systems, without loss of generality, we write

$$C = \sum_{i=1}^{n} C_i = B \sum_{i=1}^{n} 1/\omega_i \qquad (16)$$

where **B** is the damping factor matrix

$$B = \begin{bmatrix} \beta_1 + \beta_2 & -\beta_2 & \cdots\cdots & 0 \\ -\beta_2 & \beta_2 + \beta_3 & -\beta_3 \ \cdots & 0 \\ & \cdots\cdots\cdots\cdots & & \\ 0 & & -\beta_n & \beta_n \end{bmatrix}$$

The above procedure is further explained by using the following example.

EXAMPLE

Consider again the structure shown in Fig. 1. Assume that the mass matrix is **I**, and the stiffness matrix is

$$K = \begin{bmatrix} 600 & -200 & 0 \\ -200 & 300 & -100 \\ 0 & -100 & 100 \end{bmatrix}$$

First, incorporate a number of dampers on the structure to make the system

proportionally damped with the damping ratio 0.0625. Denote the corresponding damping matrix by C_0 . Then add two sets of same dampers between the first floor and the ground. Add another set of the same dampers of the original kind between the first and the second floors. Denote the damping matrix regarding to these added dampers only by C_1. Now, let us try to determine C matrix. According to the earlier discussion, if the system is lightly damped, we have

$$C = C_0 + C_1$$

lhe eigenvector matrix of **K** is

$$Q = \begin{bmatrix} .1706 & -.4317 & .8857 \\ .4732 & -.7526 & -.4579 \\ .8643 & .4973 & .0759 \end{bmatrix}$$

and $\omega_1 = 6.7268$, $\omega_2 = 15.8539$, $\omega_3 = 26.5218$. Therefore

$$(1/\omega_1 + 1/\omega_2 + 1/\omega_3) = .2494$$

$$C_0 = Q \ \mathrm{diag}(2 \times .0625 \times \omega_1)\ Q^T$$

$$= \begin{bmatrix} 2.9947 & -.6330 & -.0786 \\ & 2.0059 & -.5129 \\ & & 1.1372 \end{bmatrix}$$

From C_0, we have $B_0 = C_0 \ / \ (1/\omega_1 + 1/\omega_2 + 1/\omega_3)$

$$= \begin{bmatrix} 12.0056 & -2.5376 & -0.3150 \\ & 8.0417 & -2.0564 \\ & & 4.5590 \end{bmatrix}$$

So, $\beta_1 = 9.1530$ and $\beta_2 = 3.4477$.

Thus $$B_2 = \begin{bmatrix} 21.7536 & -3.4477 & 0 \\ & 3.4477 & 0 \\ & & 0 \end{bmatrix}$$

$$C_1 = \begin{bmatrix} 5.4262 & -0.8600 & 0 \\ & 0.8600 & 0 \\ & & 0 \end{bmatrix}$$

Thus $$C = \begin{bmatrix} 8.4209 & -1.4930 & -0.0786 \\ & 2.8659 & -0.5129 \\ & & 1.1373 \end{bmatrix}$$

Table 1 lists complex damping ratios of each cases.

Table 1 Complex Damping Ratios

system with	1st mode	2nd mode	3rd mode
C_0 only	.0625 + .0000j	.0625 + .0000j	.0625 + .0000j
C_1 only	.0157 + .0005j	.0294 + .0016j	.0971 - .0022j
$C_0 + C_1$	.0782 + .0005j	.0920 + .0017j	.1597 - .0022j

From Table 1, we know that for i = 1, 2, 3, approximately

$$\xi_i(C) = \xi_i(C_0) + \xi_i(C_1)$$

and

$$\zeta_i(C) = \zeta_i(C_0) + \zeta_i(C_1)$$

With non-proportional damping C, we can calculate the natural frequencies ω_1 = 6.7303, ω_2= 15.8804 and ω_3= 26.4637. Compare the results with that of the corresponding proportionally damped system, we know the errors are small.

FORMULA FOR DESIGN OF VISCOUS-ELASTIC DAMPERS

In the previous section, we showed the procedure of how to determine the sub damping matrix when the system is not proportionally damped. In this section, we discuss a remaining issue of how to determine the damping factor β_i. For a given material, it is usually difficult to determine the damping factors. However, for certain damping materials, such as visco-elastic (VE) material, since the loss modulus are known, the damping ratios can be calculated by equation

$$\xi_i = \frac{W_{di}}{4\pi W} = \frac{\sum_j \gamma_{ij}^2 G_i V_j}{2 Q^T \tilde{K} Q} \qquad (17)$$

For more detailed information of this formula, readers may refer to Lin and Liang (1989). Now, for the case of certain proportionally damped system, Equation (17) can be used together with Equation (7) to determine the damping matrix.

In general cases, Equation (17) may not be valid. However, the energy dissipated by a damper during one cycle, W_d can be calculated by

$$W_d = \pi G''(\omega) A/t x_0^2$$

Comparing with Equation (8), we know that

$$\beta_i^{(j)} = G''(\omega_j)\ A_i / t_i \qquad (18)$$

where the subscript i denotes the i^{th} damper, and j denotes the j^{th} mode or driving frequency. Note that, for VE material, the loss modulus G" is a function of frequency, denoted by $G''(\omega_j)$. Therefore, the global damping matrix for VE damper design can be written as

$$C = \sum_{i=1}^{n} C_i \qquad (19a)$$

$$C_i = \begin{bmatrix} \beta_1^{(i)} + \beta_2^{(i)} & -\beta_2^{(i)} & \cdots & 0 \\ -\beta_2^{(i)} & \beta_2^{(i)} + \beta_3^{(i)} & -\beta_3^{(i)} & \cdots \\ & \cdots\cdots\cdots & & \\ 0 & & -\beta_n^{(i)} & \beta_n^{(i)} \end{bmatrix} / \omega_i \qquad (19b)$$

CONCLUSION

The procedure described in this paper is the first attempt to develop a way of design VE dampers for non-proportionally damped systems. Also the procedure provides a good approach to identify the system's damping matrix. It is hoped that actual applications of this method can bring out its practical meanings.

ACKNOWLEDGEMENT

Funding for the research reported in this paper has been provided jointly by the State University of New York at Buffalo and the National Science Foundation through the National Center for Earthquake Engineering Research under master contract number ECE86-07591.

REFERENCES

Caughey, T.K. and O'Kelly, M.M.J. "Classical Normal Mode in Damped Linear Dynamic Systems" J. of Appl. Mech. ASME Vol 32, pp.583-588, 1965.

Clough, R. W. and Penzien, "Dynamics of Structures," McGraw-Hill, New York, 1975.

Ibrahim, S.R., Mikulcik, E.C. "A Method for the Direct Identification of Vibration Parameters from the Free Response", the shock & Vib. bulletin 47

Sept. 1977.

Inman, D. "Vibration with Control, Measurement and Stability", Prentice-Hall, Englewood Cliffs, 1989.

Kozin, F. and Natke, H.G. (1986). "System Identification Techniques", Structural Safety, Vol.#, pp.269-316.

Liang, Z. and Lee, G.C. "On Complex Damping of MDOF Systems" Proc. of IMAC-8, 1990, pp.1048-1055.

Liang, Z. and Lee, G.C. "Representation of Damping Matrix", J. of Eng. Mech. ASCE., May 1991 (to appear).

Liang, Z., Lee, G. C. and Tong, M.(1991) "On A Theory of Complex Damping" Proc. of Damping '91, Feb. 13-15 1991, San Diego, CA., Sponsored by Wright Laboratory, Flight Dynamics Directorate, Wright-Patterson Air force Base.

Liang, Z., Lee, G. C. and Tong, M.(1991) "A Strong Criterion For Testing Proportionally Damped Systems" Proc. of Damping '91, Feb. 13-15 1991, San Diego, CA., Sponsored by Wright Laboratory, Flight Dynamics Directorate, Wright-Patterson Air force Base.

Liang, Z., Lee, G. C. and Tong, M.(1991) "On A Linear Property of Lightly Damped Systems" Proc. of Damping '91, Feb. 13-15 1991, San Diego, CA., Sponsored by Wright Laboratory Flight, Dynamics Directorate, Wright-Patterson Air force Base.

Lin, R.C., Liang, Z., Soong, T.T. and Zhang, R.H. "An Experimental Study of Seismic Structural Response With Added Viscoelstic Dampers", Technical report NCEER-88-0023. 1988.

Shinozuka, M., Yun, C-B. and Imai, H. (1982). "Indetification of Linear Structural Dynamic Systems", J. of Structural Engineering, ASCE, Vol. 108, No. EM6, pp.1371-1390.

Singh, M. D. and Ghafory-Ashtiary, M. (1986) "Modal Time History of Non-classically Damped Structures For Seismic Motions". Earthquake Engineering and Structural Dynamics, Vol 13. pp133-146.

Tong, M., Liang, Z. and Lee, G. C. (1991) "On an Application of Complex Damping Coefficients" Proc. of Damping '91, Feb. 13-15 1991, San Diego, CA., Sponsored by Wright Laboratory, Flight Dynamics Directorate, Wright-Patterson Air force Base.

Vold, H; Rocklin, G. "The Numerical Implementation of a Multi-Input Modal Estimation Method for Mini-Computer," Proc. of IMAC-1, 1982, pp.542-548.

Zhang, R. H., Soong, T.T. and Mahmoodi, D. "Seismic Response of Steel

Frame Structures with Added Visco-elastic Dampers" Earthquake Eng. Struct. Dyn. 1989 18(3) pp389-396.

Timoshenko, S. et al, "Vibration Problems in Engineering" 4^{th} ed., John Wiley & Sons Inc. 1974.

Modeling of Constrained Layer Damping in Trusses

Joseph C. Slater*
Daniel J. Inman†
W. Keith Belvin§

Mechanical Systems Lab
1012 Furnas Hall
State University of New York at Buffalo
Buffalo, NY 14260

ABSTRACT

This work reexamines the use of constrained layer damping for controlling the lower modes of vibration of a large flexible truss. The device used to suppress vibrations is a "viscoelastic strut". The design, modeling and experimental verification of the viscoelastic strut as well as the three longeron truss with and without the constrained layer treatment is presented. A complete finite element analysis (FEA) and experimental verification will be presented. The experimental results are represented by examining transfer functions and modal damping ratios as well as a video presentation of the effectiveness of the viscoelastic approach for vibration suppression.

*Graduate Research Assistant, Mechanical Systems Lab, Department of Mechanical and Aerospace Engineering

†Professor and Department Chair, Mechanical Systems Lab, Department of Mechanical and Aerospace Engineering

§Aerospace Engineer, NASA Langley Research Center, Space Craft Dynamics Branch

INTRODUCTION

Viscoelastic damping of large space structures shows promise of providing high loss factors with low cost in additional weight and no moving parts. Although many methods have been derived which are capable of determining the damping matrix of a structure after collecting response data, prediction of non viscous damping is still quite elusive. For large space structures which cannot be ground tested, such as the space station, accurate prediction of damping is required before optimal vibration control may be implemented. The modal strain energy technique is often used to predict damping in lightly damped structures with real modes, however, the introduction of highly damped struts may make the assumption of real modes improper. The Golla-Hughes-McTavish (GHM) model for viscoelastic damping is a finite element based method which models the frequency dependant complex modulus of materials and is fully compatible with the usual linear second-order equations of motion most commonly used to model structure dynamics. In order to test this theory, a highly damped viscoelastic strut has been constructed and tested. Loss factors of the viscoelastic strut are also determined using the concept of modal strain energy. Finally, the GHM method is used to predict the equivalent modal damping ratios of a test bed and a comparison is made between experimental and predicted response when the viscoelastic strut is placed in the structure.

STRUT DESIGN

The viscoelastic strut design goals were to provide a strut which would not significantly change the natural frequencies of the test structure (i.e.. the real part of the complex stiffness should be of the same order as the undamped strut's stiffness between 10Hz and 100Hz) and to create a strut which had the typical viscoelastic characteristic of frequency dependant complex stiffness. Since proving a strut with a high stiffness could still significantly increase the damping in the structure and modeling this effect were the primary concerns, creep was not considered in the design. Tests on the actual structure showed that creep was not significant over a period of more than one week while our dynamic tests lasted only minutes, verifying our assumption that for our purposes creep was not an issue.

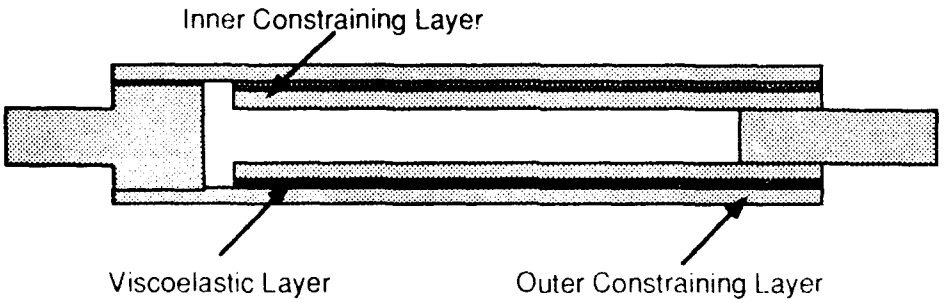

FIGURE 1: A schematic of the Viscoelastic Strut design illustrating the constrained layer configuration relative to the strut.

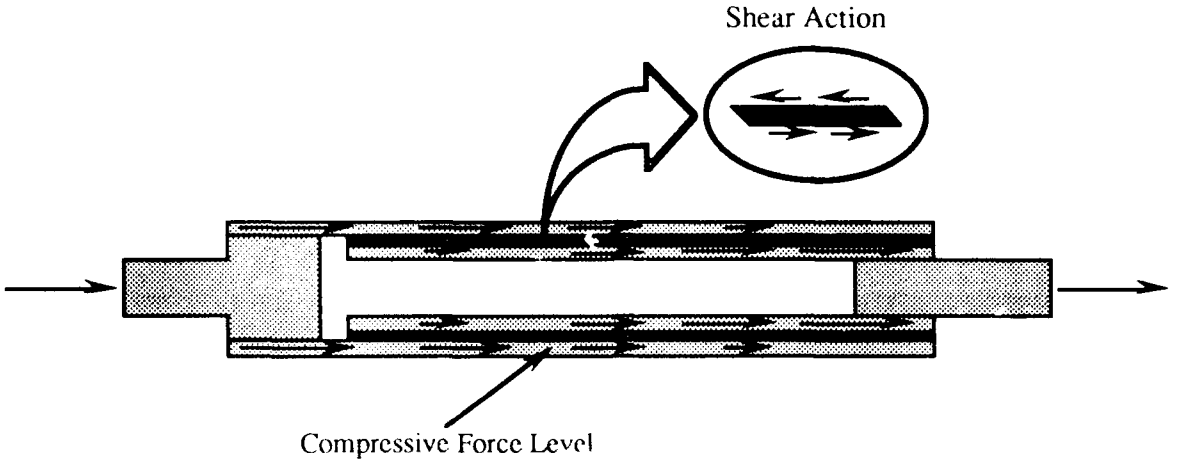

FIGURE 2: A schematic of the Viscoelastic Strut indicating the stress flow path.

The concept of the viscoelastic strut is simple in that ai er and inner layer act to shear a constrained viscoelastic layer when the strut is placed in sion or compression (Figure 1). The constraining layers are T-6061 aluminum on the order of .05 inches while the viscoelastic layer is .005 inch thick Scotchdamp™ SJ-2015X Type 112 viscoelastic material. Due to the fact that the viscoelastic layer is so thin the majority of the deflection takes place in the constraining layers. However, the high loss factor of the viscoelastic material maintains a high overall loss factor for the strut in the frequency range of interest.

STRUT "LOCAL" MODEL

The strut was modeled using discretized extensional springs for the constraining layer and discretized shear springs for the viscoelastic layer. With one end of the strut in a clamped condition, the model used was a 29 degree of freedom model similar to the one shown in Figure 3. The variables K_i and K_o are the discretized inner and outer stiffnesses and K_v is the discretized stiffness of the viscoelastic layer. Note that this model neglects shear deformation in the constraining layers as well as other less significant effects. The modulus $G'(\omega)$ for the viscoelastic layer was taken from manufacturer produced charts at room temperature. Due to the dependance of the complex shear modulus of the viscoelastic layer on frequency, K_v is also frequency dependant. At selected intervals, the stiffness of the strut and the percent strain energy in the viscoelastic layer relative to the strain energy in the entire strut were found using the shear modulus of the viscoelastic layer at that frequency. Using the principle of modal strain energy, the loss factor of the strut at a given frequency is given by

$$\eta(\omega)=\eta_v(\omega)\frac{V_v(\omega)}{V(\omega)}$$

where $\frac{V_v(\omega)}{V(\omega)}$ is the fraction of elastic strain energy in the viscoelastic layer at the frequency ω and $\eta_v(\omega)$ is the loss factor of the viscoelastic material.

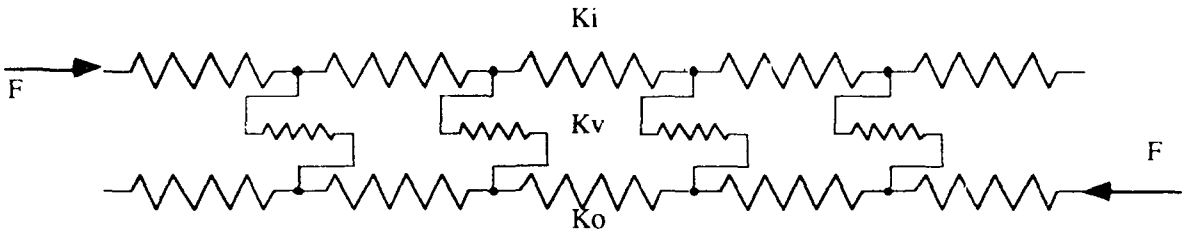

FIGURE 3: A schematic of the discretized spring model of Viscoelastic Strut of Figures 1 and 2.

These calculations give a complete characterization of the complex stiffness of the viscoelastic strut over the frequency range of 1-100 Hz.

THE GHM VISCOELASTIC MODEL FOR A MASSLESS ROD

The GHM viscoelastic model is a linear transfer function method for modeling frequency dependant complex modulus. Curve fitting the GHM transfer function to complex material data over a frequency range of interest creates a linear model which is compatible with standard finite elements. Using transformations described by McTavish[2] viscoelastic finite elements can be easily derived. The GHM transfer function is

$$K(s) = \frac{F(s)}{X(s)} = \hat{K}^0 \left[1 + \sum_{n=1}^{k} \hat{\alpha}_n \frac{s^2 + 2\hat{\zeta}_n \hat{\omega}_n s}{s^2 + 2\hat{\zeta}_n \hat{\omega}_n s + \hat{\omega}^2_n} \right]$$

where the hatted variables $\hat{\alpha}$, $\hat{\zeta}$, $\hat{\omega}$, and $\hat{K}^0$ are free variables for curve fitting (The transfer function is shown in terms of the rod stiffness. The references show the more general case for a material modulus). The number of terms in the expansion is dependant on the accuracy of the curve fitting desired, the frequency range size, and the degree of frequency dependance of the viscoelastic material. For a viscoelastic material which does not exhibit creep, $\hat{K}^0$ would be the static stiffness of the strut. However, since no static stiffness is assumed, this variable is also free for curve fitting. The linear second order matrix realization of this transfer function for a rod with k=1 is

$$\tilde{K} = \hat{K}^0 \begin{bmatrix} 1+\hat{\alpha} & -(1+\hat{\alpha}) & \hat{\alpha}\sqrt{2} \\ -(1+\hat{\alpha}) & 1+\hat{\alpha} & -\hat{\alpha}\sqrt{2} \\ \hat{\alpha}\sqrt{2} & -\hat{\alpha}\sqrt{2} & \hat{\alpha}2 \end{bmatrix} \qquad \tilde{D} = \hat{K}^0 \begin{bmatrix} 0 & 0 & 0 \\ 0 & 0 & 0 \\ 0 & 0 & 4\frac{\hat{\alpha}\hat{\zeta}}{\hat{\omega}} \end{bmatrix} \qquad \tilde{M} = \hat{K}^0 \begin{bmatrix} 0 & 0 & 0 \\ 0 & 0 & 0 \\ 0 & 0 & 2\frac{\hat{\alpha}}{\hat{\omega}^2} \end{bmatrix}$$

Setting $\hat{\alpha} = 0$ in these matrices reduces them to the ordinary finite element rod matrices except for the third coordinate. The third coordinate represents a dissipation coordinate which has no physical significance except perhaps as a state estimator. The static properties of the strut element are not effected by this coordinate. These additional coordinates add overdamped 'false' modes to the model which are easily identifiable, as demonstrated in references 1 and 2.The curve fitting was done on the complex stiffness

data found from the discretized spring model. The results of the curve fitting are shown in Figure 4.

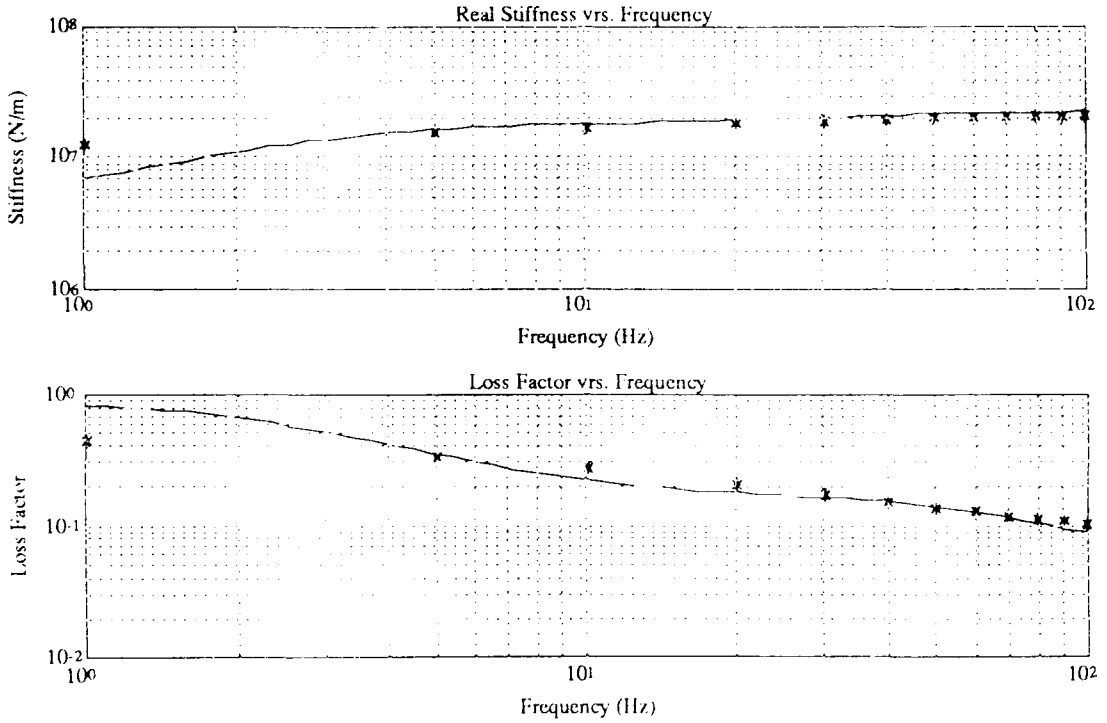

FIGURE 4: Strut model data points and GHM approximation. The line represents the curve fit of the GHM transfer functions to the data points represented by the '*'.

TEST BED

The test bed (Shown in Figure 5) is an eight bay triangular meroform truss cantilevered off of a 2000 lb steel and concrete monolith. It exhibits 5 modes below 100 Hz. The modes targeted for damping were the first and fourth modes, which were the first two modes in the vertical plane similar to those of a cantilevered beam. The second and fifth modes are horizontal bending modes similar to cantilevered beam modes while the third mode is a torsional mode.

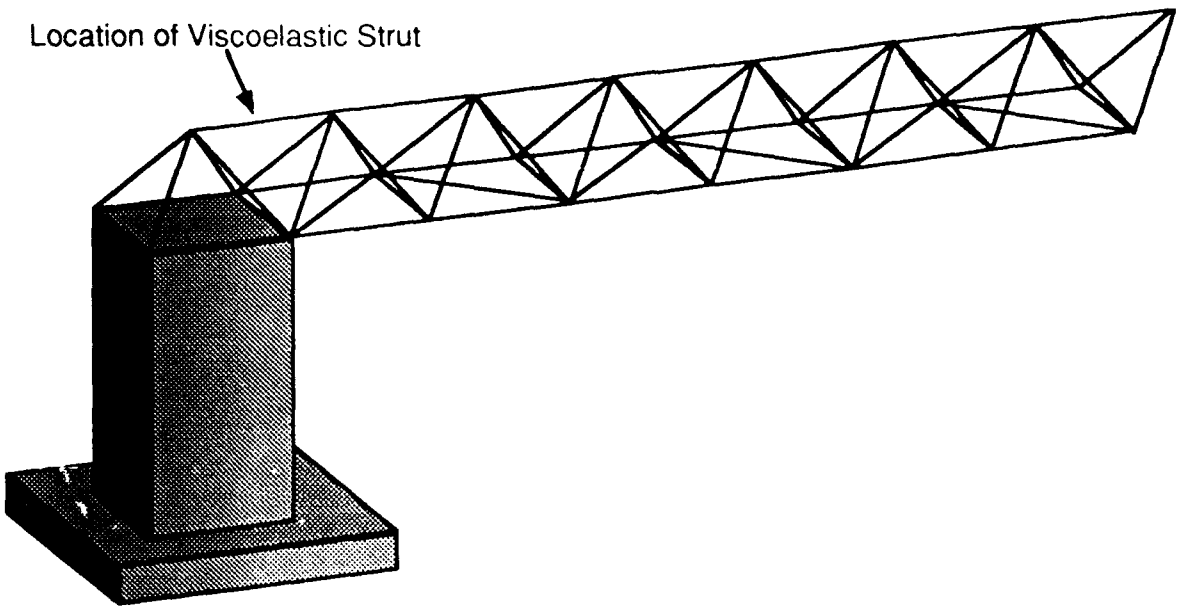

FIGURE 5: The test bed arrangement illustrating the monolith with the eight bay truss cantilevered off the top.

The truss was modeled using Euler-Bernoulli beam/rods. The damping matrix of the original undamped structure was constructed using equivalent modal damping factors from tests of the structure. The reason for assuming an original damping matrix is that the objective of this experiment is to model the change in equivalent modal damping due to the introduction of viscoelastic damping to the structure. Homogeneous, clean (without joint damping) aluminum structures tend to have damping ratios on the order of .17%. It will be shown this was the case for this truss as well, therefore predicting the truss internal damping effect is not of concern. Compliance in the monolith was accounted for by using spring to ground instead of clamped boundary conditions at the base of the truss. The viscoelastic strut was situated in the horizontal position on the top of the truss nearest the base. This provided maximum damping effect in the first mode. The Euler-Bernoulli beam/rod element in this position was replaced with the GHM rod element to model the installed viscoelastic strut. The results of the models and tests are shown in Figure 6,7 and 8.

Mode	Original Structure		FEM of Original Structure		Structure With Visco-Strut		FEM with GHM model	
	ω_d (Hz)	ζ (%)	ω_d (Hz)	ζ (%)	ω_d (Hz)	ζ (%)	ω_d (Hz)	ζ (%)
1	13.22	.18	12.88	.18	13.37	2.00	13.29	1.37
2	19.25	.17	18.82	.17	19.25	.17	18.32	.17
3	49.25	.17	50.38	.17	49.25	.17	50.30	.17
4	76.75	.17	77.82	.17	77.58	.57	77.22	.25
5	95.00	.17	97.83	.17	95.00	.17	97.75	.17
6	136.0	.17	134.8	.17	136.5	.36	136.0	.34

FIGURE 6: Experimental verses theoretical results indicating the damped natural frequencies and equivalent modal damping ratios.

Without Viscoelastic Strut

With Viscoelastic Strut

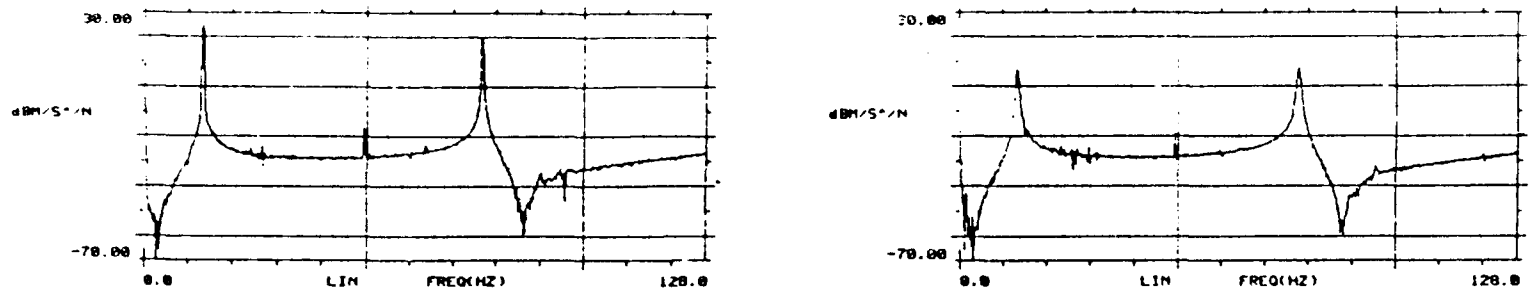

FIGURE 7: Experimental frequency response of structure with and without viscoelastic strut.

Without Viscoelastic Strut

With Viscoelastic Strut

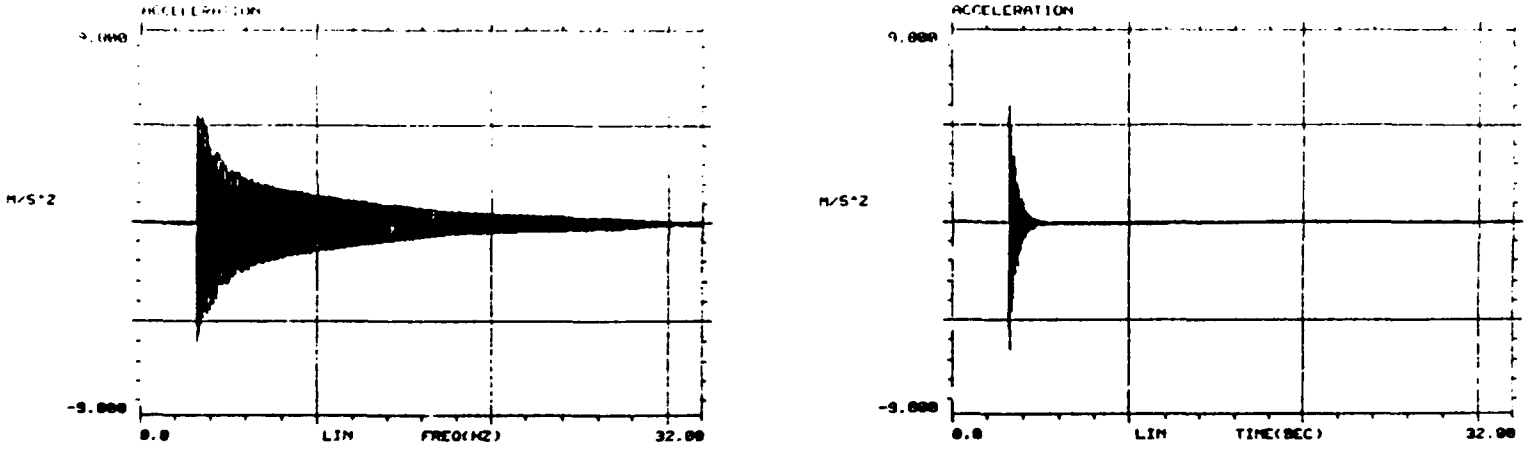

FIGURE 8: Experimental time response of structure with and without viscoelastic strut.

A number of results are presented in this table. First, note that the natural frequencies of the structure did not significantly change, although the viscoelastic strut has no real static strength. Secondly, the damping ratios of the targeted modes increased by a factor of ten in the first mode and a factor of 3.3 in the fourth. However, the prediction of the increase in damping was errant by 35% in the first mode and 75% in the second. Two effects may partially explain this. The viscoelastic material samples used in the viscoelastic strut had a thickness tolerance of ± 20% which can lead to obvious model error. The discretized spring model, although simple to use, is probably not sophisticated enough to properly model the deformation in the strut. Ideally, test data for the viscoelastic strut would be used in the GHM modeling instead of the data derived from any FEM or discretized spring model.

CONCLUSION

Viscoelastic struts introduced into flexible trusses can significantly increase the inherent damping of the structure without significantly changing the natural frequencies of the structure. The procedure for modeling the effect of viscoelastic struts using the GHM technique has been outlined. Accurate knowledge of the complex stiffness characteristics of the viscoelastic strut is vital and test data for the complex stiffness should be used if at all possible.

REFERENCES

[1]Golla, D. F., and Hughes, P. C., "Dynamics of Viscoelastic Structures - A Time Domain, Finite Element Formulation.", *Journal of Applied Mechanics*, V0l. 52, Dec. 1985, pp 897-906.

[2]McTavish, D. J.,"The Mini-Oscillator Technique: A Finite Element Method fo the Modeling of Linear Viscoelastic Structures, "University of Toronto Institute for Aerospace Studies, Toronto, Ontario, UTIAS Report Number 323, March 1988.

[3]Nashif, A. D., Jones, I. G. and Henderson, J. P.,*Vibration Damping*, Wiley, New York, 1985.

[4]Johnson, C. D. and Kienholz, D. A., "Finite Element Prediction of Damping in Structures with Constrained Viscoelastic Layers," *AIAA Journal*, vol. 20, no. 9, Sept 1982 pp. 1284-1292.

[5]Ungar, E. E. and Kerwin E. M. Jr., "Loss Factors of Viscoelastic Systems in Terms of Energy Concepts," *Acoustic Society of America*, Vol. 34, 1962, pp 954-957.

A STRONG CRITERION FOR TESTING PROPORTIONALLY DAMPED SYSTEMS

Z. Liang, M. Tong, and G. C. Lee

412 Bonner Hall
State University of New York at Buffalo
Amherst, NY 14260
Tel. (716) 636-2771

ABSTRACT

To check whether a structural system is proportionally damped in dynamic analysis, Caughey advanced criterion to examine if the generalized damping and stiffness matrices of the system commute. This criterion depends on the data of generalized damping which are not directly measurable. This is a sever restriction. In this paper, we present an alternative criterion to determine the proportionality of damping which is rigorous and dynamically flexible. In particular, it can be used in both forward and inverse problems.

INTRODUCTION

Modal analysis is a rapidly-growing field, both in theory and in engineering applications. In recent years, the theoretical basis of modal analysis has progressed extensively from the level of one-degree-of-freedom systems to the level of multi-degree-of-freedom systems by many individuals including: Frazer (1946), Foss (1956), Lancaster (1966), Clough (1975), Meirovitch (1980), Vold (1982), Ewins (1984), Juang (1985) and Mitchell (1990), et al. etc. In dealing with an MDOF system, the simplest model is one that can be decoupled into a group of SDOF systems. Such an MDOF system has great advantage over other MDOF systems in that it can be easily treated by using various techniques developed for SDOF systems. For some time, it was not obvious on how to identify the decoupleable system until Caughey and O'Kelly published a necessary and sufficient criterion (1965) that states: A system of the form

$$I_n\ddot{X} + C_1\dot{X} + K_1X = 0$$

possesses a complete decoupling, if and only if the matrix C_1 and K_1 commute, i.e.

$$C_1K_1 = K_1C_1.$$

Based on this criterion, the notion of *proportional/non-proportional damping* was introduced. A system is said to be proportionally damped if and only if the above expression holds.

Caughey and O'Kelly's criterion is a widely accepted approach in modal analysis. However, the criterion depends on the data of generalized damping which are not directly measurable. Such a limitation restricted the further applications of the criterion in many areas of modal analysis such as system identifications, forward and inverse problems. In this paper, we present an alternative criterion which in many aspects is better than the Caughey criterion in a dynamic context.

FUNDAMENTAL VIBRATION SYSTEMS AND THEIR MODES

Consider an n dimensional free vibration system described by the following matrix equation.

$$M\ddot{X} + C\dot{X} + KX = 0 \qquad (1)$$

where **M**, **C**, **K** are the mass, damping and stiffness matrices of size n×n such that **M** and **K** are positive definite, and **C** may be positive semi-definite. X, $\dot{X}$ and $\ddot{X}$ are the displacement, velocity and acceleration vectors. In general, we also require $(C^2 - 4K)$ to be negative definite, (see Inman, 1989). Since **M** is non-singular, it is easy to see that Equation (1) is equivalent to

$$I_n \ddot{X}_1 + M^{-1/2} C M^{-1/2} \dot{X}_1 + M^{-1/2} K M^{-1/2} X_1 = 0 \qquad (2)$$

where $M^{-1/2}$ is the square root of the inverse of **M**, and I_n is the identity matrix of size n; and $X_1 = M^{1/2} X$. Let C_1 and K_1 denote $M^{-1/2} C M^{-1/2}$ and $M^{-1/2} K M^{-1/2}$ respectively. Then we can write

$$I_n \ddot{X}_1 + C_1 \dot{X}_1 + K_1 X_1 = 0 \quad . \qquad (3)$$

Note that matrices C_1 and K_1 have the same definiteness as those of **C** and **K** respectively. And, both C_1 and K_1 are symmetric.

Let $X_1 = X_0 e^{\lambda t} = \begin{bmatrix} x1 \\ x2 \\ \vdots \\ xn \end{bmatrix} e^{\lambda t}$ and substitute it back in (3). We have

$$(I_n \lambda^2 + C_1 \lambda + K_1) X_0 = 0 \quad . \qquad (4)$$

In the case of proportional damping, it is known that C_1 and K_1 commute (i.e. $C_1 K_1 = K_1 C_1$). So there exists an orthogonal matrix **Q** such that $Q^T Q = I_n$, and it diagonalizes C_1 and K_1 simultaneously.

$$Q^T C_1 Q = \begin{bmatrix} c_{11} & & & \\ & c_{22} & & \\ & & \ddots & \\ & & & c_{nn} \end{bmatrix} = \Lambda_c, \qquad Q^T K_1 Q = \begin{bmatrix} k_{11} & & & \\ & k_{22} & & \\ & & \ddots & \\ & & & k_{nn} \end{bmatrix} = \Lambda_k.$$

It follows that Equation (4) can be further modified to have the form

$$Q (I_n \lambda^2 + \Lambda_c \lambda + \Lambda_k) Q^T X_0 = 0 \; . \qquad (5)$$

Let P denote $Q^T X_0$. Then multiplying Q^T to Equation (5) from the left, we get

$$(I_n \lambda^2 + \Lambda_c \lambda + \Lambda_k) P = 0 \; . \qquad (6)$$

We define this as the characteristic equation of a Λ_c-Λ_k system. Since the determinate $|I_n \lambda^2 + \Lambda_c \lambda + \Lambda_k|$ equals

$$\begin{vmatrix} \lambda^2 + c_{11}\lambda + k_{11} & & \\ & \ddots & \\ & & \lambda^2 + c_{nn}\lambda + k_{nn} \end{vmatrix} = \prod_{i=1}^{n} (\lambda^2 + c_{ii}\lambda + k_{ii}),$$

with $(\mathbf{C} - {}^2\mathbf{4K})$ negative definite, we can solve $|\mathbf{I}_n\lambda + {}^2\Lambda_c\lambda + \Lambda_k| = 0$ for n pairs of conjugate roots $\lambda_1, \bar{\lambda}_1; \lambda_2, \bar{\lambda}_2; \ldots \lambda_n, \bar{\lambda}_n$; where λ_i is defined as the i^{th} system eigenvalue (eigenfrequency). They can be further expressed as

$$\lambda_i = -\xi_i\omega_i + j\sqrt{1-\xi_i^2}\,\omega_i$$

where ξ_i and ω_i are the i^{th} damping ratio and undamped natural frequency of the system. In the following, we may omit the subscript i of λ_i, P_i and ω_i, etc., for simplicity. Note that in the normal mode case, ω_i^2 are also the eigenvalues of the matrix $\mathbf{K}_1$.

Corresponding to each λ_i there is a system eigenvector $\mathbf{e}_i$ (the unit vector at i^{th} direction in an n dimensional space) which satisfies

$$(\mathbf{I}_n\lambda_i^2 + \Lambda_c\lambda_i + \Lambda_k)\mathbf{e}_i = 0$$

$$(\mathbf{I}_n\bar{\lambda}_i^2 + \Lambda_c\bar{\lambda}_i + \Lambda_k)\mathbf{e}_i = 0 .$$

Write

$$\Lambda = \begin{bmatrix} \lambda_1 & & \\ & \lambda_2 & \\ & & \ddots \\ & & & \lambda_n \end{bmatrix} \quad \text{and} \quad \mathbf{P}_I = \begin{bmatrix} 1 & & \\ & 1 & \\ & & \ddots \\ & & & 1 \end{bmatrix}.$$

We call Λ and $\mathbf{P}_I$ the *eigenvalue* and *mode shape* matrices respectively. It is now clear that the system has been completely *self-decoupled.* (A more rigorous definition of self-decoupled system will be introduced later.)

In the case of non-proportional damping, we know that $\mathbf{C}_1\mathbf{K}_1 \neq \mathbf{K}_1\mathbf{C}_1$. So the above analysis is no longer valid. However, there still exists an orthogonal matrix Q that diagonalizes $\mathbf{K}_1$. Applying the matrix Q to Equation (4), we have

$$(\mathbf{I}_n\lambda^2 + \mathbf{Q}^T\mathbf{C}_1\mathbf{Q}\,\lambda + \Lambda_k)\mathbf{P} = 0. \qquad (7)$$

Next denote a symmetric matrix by

$$D = Q^T C_1 Q = \begin{bmatrix} d_{11} & d_{12} & \cdots & d_{1n} \\ d_{12} & d_{22} & \cdots & d_{2n} \\ & & \cdots & \\ d_{1n} & d_{2n} & \cdots & d_{nn} \end{bmatrix}.$$

Note that, in equation (7), the diagonal matrix Λ_k has the same form as equation (5). Therefore, we have

$$(I_n \lambda^2 + D\lambda + \Lambda_k)P = 0. \qquad (8)$$

This equation is called the *characteristic equation* of the $D\text{-}\Lambda_k$ system. The $D\text{-}\Lambda_k$ system has similar eigenproblem as system (1), that is, they both have the same eigenvalues and their eigenvectors are related by the formula

$$P = Q^T X_0 = Q^T M^{-1/2} X$$

where P, X_0 and X denote the eigenvector matrices of Systems (8), (3) and (1) respectively.

Because of the above mentioned property of the $D\text{-}\Lambda_k$ system simplifies the eigenproblem, we refer this system as a *fundamental vibration system* (FVS) or *canonical vibration system*. Fig 1 shows a 3 degree-of-freedom FVS.

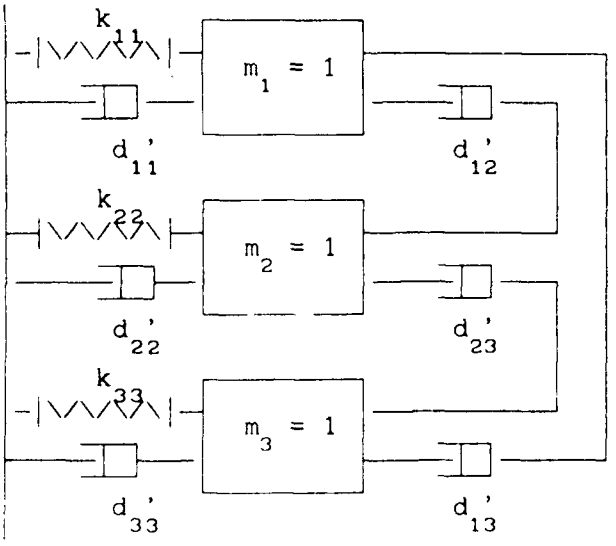

Fig. 1 A 3-DOF FVS

Comparing Fig. 1 with Equation (8), we see that

$$d_{11} = d'_{11} + d'_{12} + d'_{13}\ ,\ d_{12} = -d'_{12}\ ,\ d_{13} = -d'_{13}\ ,\ \text{etc.}$$

It is noted that the previously mentioned proportional damping model is a

special case of the FVS. Following the procedure descried above in dealing with the Λ_c-Λ_k system, we can similarly obtain an eigenvalue matrix and a mode shape matrix. However, in order to understand the properties of these two matrices, some new concepts will first be introduced.

DEFINITION: A non-zero system eigenvector P is said to be *true-complex* or *strongly-complex* for the corresponding eigenvalue λ if

$$(I_n\lambda^2 + D\lambda + \Lambda_k)P = 0$$

holds and P can not be expressed as a complex linear combination of the real-valued eigenvectors of Λ_k. A system eigenvector P is *weakly-complex* if it is not true-complex.

It is clear that a proportionally damped system has only weakly-complex system eigenvectors. Hence the system has a real-valued mode shape matrix.

LEMMA 1: Given an FVS. If P is a system eigenvector such that

$$(I_n\lambda^2 + D\lambda + \Lambda_k)P = 0$$

for some λ, and P is weakly-complex, then the corresponding eigenvalue λ satisfies $\lambda\bar{\lambda} = k_{ii}$ for some i = 1, ..., n, (where k_{ii} is the i^{th} diagonal element of Λ_k).

COROLLARY 1: Suppose λ is a system eigenvalue of a given FVS such that $\lambda\bar{\lambda} \neq k_{ii}$ for all i = 1, 2, ..., n. Then its corresponding eigenvector P is strongly-complex.

LEMMA 2: Given an FVS, if P is a system eigenvector, then the following conditions are equivalent.

(1) P is an eigenvector of the damping matrix D.

(2) P is an eigenvector of the stiffness matrix Λ_k.

(3) P is weakly-complex.

LEMMA 3: Given an FVS. If there is a vector P such that P is an eigenvector of both D and Λ_k, then it is also a system eigenvector. Moreover, P is weakly-complex.

A CRITERION FOR DETERMINING PROPORTIONALLY DAMPED SYSTEMS

In this section we present a theorem for determining a proportionally damped systems. Before starting with the theorem itself we need to consider a lemma of Rayleigh quotient.

LEMMA 4: For any Hermitian matrix $\mathbf{A} \in \mathbb{C}^{n\times n}$, denoting its first (smallest) and last (largest) eigenvalues by a_1 and a_n respectively. Then the Rayleigh quotient equals a_1 or a_n, i.e.

$$\frac{X^H \mathbf{A} X}{X^H X} = a_1 \tag{9}$$

or

$$\frac{X^H \mathbf{A} X}{X^H X} = a_n \tag{10}$$

if and only if its corresponding non-zero vector $X \in \mathbb{C}^n$ is the first or last eigenvector of **A**. Here the superscript H denotes the Hermitian transpose, $\mathbb{C}^{n\times n}$ and $\mathbb{C}^n$ stand for the set of all n×n matrices and vectors, real or complex, respectively, (see Ortega, 1987).

DEFINITION : For an FVS, if the damping matrix **D** is of the following form, then we say that the system is *self-decoupled* into two subsystems.

$$\mathbf{D} = \left[\begin{array}{ccc:ccc} d_{11} & \cdots & d_{1t} & & & \\ & \cdots & & & \mathbf{0} & \\ d_{1t} & \cdots & d_{tt} & & & \\ \hdashline & & & d_{t+1} & \cdots & d_{t+1,n} \\ & \mathbf{0} & & & \cdots & \\ & & & d_{t+1,n} & \cdots & d_{nn} \end{array}\right] .$$

An FVS with diagonal **D** is self-decoupled into n subsystems. In this case, the system is said to be *completely self-decoupled.*

DEFINITION : Two FVS $D_1 - \Lambda_{k1}$ and $D_2 - \Lambda_{k2}$ are said to be *equivalent* if there exists an orthogonal matrix **T** such that

$$T^T D_1 T = D_2$$
$$T^T \Lambda_{k1} T = \Lambda_{k2} .$$

THEOREM 1: For a given FVS, all the system eigenvectors are weakly-complex, if and only if, there exists an one-one correspondence between the system eigenvalues λ_i and the eigenvalues k_{ii} of Λ_k such that

$$\lambda_i \bar{\lambda}_i = k_{ii} \qquad i = 1, \ldots, n.$$

PROOF: Sufficiency.

First, we discuss the case where all the eigenvalues of Λ_k are distinct. Consider the smallest k_{ii}, say k_{11}. Let P_1 be a system eigenvector whose eigenvalue satisfies $\lambda_1 \bar{\lambda}_1 = k_{11}$. By the characteristic equation

$$P_1^H (I_n \lambda^2 + D\lambda + \Lambda_k) P_1 = 0$$

we have

$$\lambda_1^2 + \frac{P_1^H D P_1}{P_1^H P_1} \lambda_1 + \frac{P_1^H \Lambda_k P_1}{P_1^H P_1} = 0 . \qquad (11)$$

Since the Rayleigh quotients $\frac{P_1^H D P_1}{P_1^H P_1}$ and $\frac{P_1^H \Lambda_k P_1}{P_1^H P_1}$ are real, it follows that both λ_1 and its conjugate $\bar{\lambda}_1$ are roots of Equation (11). We know that a real quadratic equation has a unique irreducible expression in the real field. Thus $\frac{P_1^H \Lambda_k P_1}{P_1^H P_1} = \lambda_1 \bar{\lambda}_1 = k_{11}$. By Lemma 4, P_1 must be the first eigenvector of Λ_k. Namely, $P_1 = p e_1$, where p is a scalar. Then from

$$(I_n \lambda_1^2 + D \lambda_1 + \Lambda_k) p e_1 = 0$$

we have

$$\begin{aligned} \lambda_1^2 p + d_{11} p \lambda_1 + k_1 p &= 0 \\ 0 + d_{12} p \lambda_1 + 0 &= 0 \\ \cdots\cdots & \qquad (12) \\ 0 + d_{1n} p \lambda_1 + 0 &= 0 . \end{aligned}$$

Equations (12) imply that

$$d_{1m} = 0 , \qquad m = 2, \ldots, n.$$

Note that D is symmetric. So it must be of the following form

$$D = \begin{bmatrix} d_{11} & 0 & \cdots & 0 \\ 0 & d_{22} & \cdots & d_{2n} \\ & & \cdots & \\ 0 & d_{2n} & \cdots & d_{nn} \end{bmatrix} .$$

Therefore, the D-Λ_k system is self-decoupled into two independent subsystems each forms a D-Λ_k model with lower dimensions.
Now apply the same procedure to the subsystem with n-1 dimension we can show that the damping matrix D can be further divided. Hence it must be in the following form

$$D = \left[\begin{array}{cc:ccc} d_{11} & 0 & & & \\ 0 & d_{22} & & \mathbf{0} & \\ \hdashline & & d_{33} & \cdots & d_{3n} \\ & \mathbf{0} & & \cdots & \\ & & d_{3n} & \cdots & d_{nn} \end{array}\right] .$$

Repeat the same procedure, D will finally be shown to be a diagonal matrix. Thus it is proportional damping, and the system eigenvectors are weakly-complex.

Secondly, we consider the case where Λ_k has a repeated eigenvalue k_{rr} with multiplicity r. Without loss of generality, assume k_{rr} is the smallest among all k_{11}, and Λ_k is in the form

$$\Lambda = \begin{bmatrix} k_{rr} & & & & \\ & \ddots & & & \\ & & k_{rr} & & \\ & & & k_{r1} & \\ & & & & \ddots \\ & & & & & k_{nn} \end{bmatrix}$$

Choose an orthogonal matrix T such that

$$T = \left[\begin{array}{ccc:c} t_{11} & \cdots & t_{1r} & \\ & \cdots & & \mathbf{0} \\ t_{r1} & \cdots & t_{rr} & \\ \hdashline & & & \\ \mathbf{0} & & & I_{n-r} \end{array}\right]$$

$$T^T \Lambda_k T = \Lambda_k , \quad \text{and}$$

$$T^T D T = \hat{D} = \left[\begin{array}{ccc|ccc} \hat{d}_{11} & & & \hat{d}_{1,r+1} & \cdots & \hat{d}_{1n} \\ & \ddots & & & \cdots & \\ & & \hat{d}_{rr} & \hat{d}_{r,r+1} & \cdots & \hat{d}_{rn} \\ \hline \hat{d}_{1,r+1} & \cdots & \hat{d}_{r,r+1} & \hat{d}_{r+1,r+1} & \cdots & \hat{d}_{r+1,n} \\ & \cdots & & & \cdots & \\ \hat{d}_{1n} & \cdots & \hat{d}_{rn} & \hat{d}_{r+1,n} & \cdots & \hat{d}_{nn} \end{array}\right] .$$

Now we apply the same procedure described in the previous case to this induced $\hat{D} - \Lambda_k$ system until Equation (11) is obtained. According to the assumption there are r system eigenvalues, say $\lambda_1, \lambda_2, \ldots, \lambda_r$, such that $\lambda_i \bar{\lambda}_i = k_{rr}$, $i = 1, 2, \ldots, r$. By Lemma 4, their corresponding eigenvectors P_i are eigenvectors of Λ_k with eigenvalue k_{rr}. Hence

$$P_i = \beta_1 e_1 + \beta_2 e_2 + \ldots + \beta_r e_r , \quad i = 1, 2, \ldots, r.$$

If in $\hat{D}$, $\hat{d}_{11}, \ldots, \hat{d}_{rr}$ are distinct. Then we claim P_i is of the form

$$P_i = \beta_{ij} e_j , \quad 1 \le j \le r.$$

Otherwise, if P_i is the linear combination of more than one e_j, then we find there are at least two eigen-equations, say

$$\lambda_i^2 + d_{11}\lambda_i + k_{rr} = 0$$

$$\lambda_i^2 + d_{22}\lambda_i + k_{rr} = 0 .$$

Since $d_{11} \neq d_{22}$, this will contradict the uniqueness of a real coefficient irreducible quadratic expression.

Under this circumstance, we can use the same argument given in (12) and thus see that

$$\left[\begin{array}{ccc} \hat{d}_{1,r+1} & \cdots & \hat{d}_{1n} \\ & \cdots & \\ \hat{d}_{r,r+1} & \cdots & \hat{d}_{rn} \end{array}\right]^T = \left[\begin{array}{ccc} \hat{d}_{1,r+1} & \cdots & \hat{d}_{1n} \\ & \cdots & \\ \hat{d}_{r,r+1} & \cdots & \hat{d}_{rn} \end{array}\right] = 0 .$$

Therefore, we have

$$\hat{D} = \left[\begin{array}{c|c} \begin{matrix} \hat{d}_{11} & & \\ & \ddots & \\ & & \hat{d}_{rr} \end{matrix} & 0 \\ \hline 0 & \begin{matrix} \hat{d}_{r+1,r+1} & \cdots & \hat{d}_{r+1,n} \\ & \cdots & \\ \hat{d}_{r+1,n} & \cdots & \hat{d}_{nn} \end{matrix} \end{array}\right] .$$

Since $\hat{D} = T^T D\, T$, by pre- and post-multiplying T and T^T to $\hat{D}$, we have

$$D = T\,\hat{D}\,T^T = \left[\begin{array}{c|c} \begin{matrix} d_{11} & \cdots & d_{1r} \\ & \cdots & \\ d_{1r} & \cdots & d_{rr} \end{matrix} & 0 \\ \hline 0 & \begin{matrix} d_{r+1,r+1} & \cdots & d_{r+1,n} \\ & \cdots & \\ d_{r+1,n} & \cdots & d_{nn} \end{matrix} \end{array}\right] .$$

It is clear that D is self-decoupled. Hence we can continue work on the subsystems and eventually show that D-Λ_k is equivalent to a D_1- Λ_{k1} system where D_1 is diagonal.

As for the case where there are some repetitions among $d_{11}, d_{22}, \ldots, d_{rr}$, say $d = d_{11} = d_{22} = \ldots = d_{ss}$, we claim that the system has a repeated eigenvalue λ with multiplicity s. Because for each P_i, $1 \le i \le s$, the eigen-equation

$$\lambda_i^2 + \frac{P_i^H \hat{D}\, P_i}{P_i^H P_i}\,\lambda_i + \frac{P_i^H \Lambda_k P_i}{P_i^H P_i} = 0$$

has the same coefficients

$$\frac{P_i^H \hat{D}\, P_i}{P_i^H P_i} = d \qquad \text{and} \qquad \frac{P_i^H \Lambda_k P_i}{P_i^H P_i} = k_{rr} .$$

Therefore, $\lambda_1 = \lambda_2 = \ldots = \lambda_s = \lambda$ and the coefficient matrix $(\lambda^2 + \hat{D}\lambda + \Lambda_k)$ has rank n-s. It follows that we can simply choose $e_1, e_2, \ldots, e_s$ as our $P_1, P_2, \ldots, P_s$. Then following the same argument we can see that $\hat{D}$ is self-decoupled and eventually reduce D-Λ_k system to an equivalent D_1-Λ_{k1} system with D_1 diagonal.

We now know that under the given condition a D-Λ_k system must be equivalent to a D_1- Λ_{k1} system where the damping matrix D_1 is diagonal.

Consequently, $D\Lambda_k = \Lambda_k D$ and the system is proportionally damped. Therefore, all the system eigenvectors are weakly-complex. Thus the sufficiency of the Theorem is proven.

Necessity.

The necessary condition of theorem 1 is implied by Lemma 1.

COROLLARY 2: Given a System (1), either it has no strongly-complex eigenvector in which case the system is proportionally damped or there are at least two strongly-complex eigenvectors in which case it is non-proportionally damped.

EXTENSION OF THE CRITERION IN DISTRIBUTED MASS SYSTEMS

For linearly distributed mass systems, a similar theorem holds just as for the discrete lumped mass systems. Let U be a variable defined in a bounded domain $\mathcal{D}$ and satisfy the equation:

$$U_{tt} + L_1 U_t + L_2 U = 0 \qquad (13)$$

with homogeneous linear boundary conditions specified on the bounding surface Γ. L_1 and L_2 are compact self-adjoint spatial operators. Suppose that the boundary conditions for a higher-order operator are derivable from a compatible set of boundary conditions associated with a lower-order operator. We begin our discussion by considering the properties of eigenfunctions.

DEFINITION: An *eigenfunction* of System (13) is a non-zero function ϕ associated with a scalar λ such that the function is differentiable by both L_1 and L_2 and satisfies

$$(\lambda^2 + \lambda L_1 + L_2)\ \phi = 0 \qquad (14)$$

and the boundary conditions attached to (13). The scalar λ is called an *eigenvalue* of System (13).

DEFINITION: An eigenfunction ϕ associated with eigen value λ is said to be *true-complex or strongly-complex* if it can not be expressed as a linear combination of the real-valued eigenfunctions of λ. If ϕ is not strongly-complex, then it is called *pseudo-complex or weakly-complex*.

LEMMA 5: For a given System (13), if Φ is an eigenfunction, then the following conditions are equivalent.

(1) Φ is an eigenfunction of the viscous damping operator L_1.

(2) Φ is an eigenfunction of the stiffness operator L_2.

(3) Φ is weakly-complex.

PROOF: (1) is equivalent to (2).

Suppose $$L_1\phi = \alpha\,\phi\ . \tag{15}$$

Substituting Equation (15) into Equation (14), we get

$$\lambda^2\phi + \lambda(\alpha\,\phi) + L_2\phi = 0.$$

So $$L_2\phi = -(\lambda^2 + \lambda\alpha)\phi.$$

Since $-(\lambda^2 + \lambda\,\alpha)$ is a scalar, ϕ is an eigenfunction of L_2.

Now, suppose $$L_2\phi = \beta\phi. \tag{16}$$

we can similarly prove (1) if (2) holds.

(1) or (2) is equivalent to (3).

Suppose ϕ is complex valued, i.e. $\phi = \psi + j\eta$, where ψ and η are real-valued functions. Then $L_1\phi = L_1\psi + j\,L_1\eta$. It is easy to see that $L_1\psi$ is real and $j\,L_1\eta$ is imaginary.

On the other hand, $L_1\phi = \alpha\phi = \alpha\psi + j\alpha\eta$. Since L_1 is self-adjoint, all of its eigenvalues must be real. Therefore, $\alpha\psi$ is real and $j\alpha\eta$ is imaginary. Comparing the above two equations, we conclude

$$L_1\psi = \alpha\,\psi, \qquad L_1\,\eta = \alpha\,\eta\ .$$

That is, both ψ and η are real-valued eigenfunctions of L_1. Since ϕ is a linear combination of ψ and η, ϕ is weakly-complex.

LEMMA 6: Given a System (13), if there is a function Φ such that Φ is an eigenfunction of both L_1 and L_2, then it is also a system eigenfunction. Moreover, Φ is weakly-complex.

PROOF: Substituting Equations (15) and (16) into (14) and denoting the left hand side by

$$a = \lambda^2\,\phi + \lambda\,L_1\phi + L_2\phi\ ,$$

we have

$$a = (\,\lambda^2 + \alpha\,\lambda + \beta\,)\,\phi\ .$$

Choosing a λ such that $(\,\lambda^2 + \alpha\,\lambda + \beta\,) = 0$, then we have the desired

result.

LEMMA 7: For any compact and self-adjoint operator L, let its smallest (greatest) eigenvalue be denoted by λ_1 (λ_n). If the Rayleigh quotient equals λ_1, i.e.

$$\frac{< \Psi , L\Psi >}{< \Psi , \Psi >} = \lambda_1 \ (\lambda_n), \tag{17}$$

where $< (.) , (.) >$ denotes an inner product, then the non-zero function Ψ is an eigenfunction of L associated with $\lambda_1(\lambda_n)$, and vice versa.

PROOF:

Since operator L is compact and self-adjoint, there is a complete set of eigenfunctions for L, i.e. for any function f in a Hilbert space,

$$f = \sum_{i=1}^{\infty} <f, \ \phi_i> \ \phi_i$$

and

$$Lf = \sum_{i=1}^{\infty} L < f, \ \phi_i > \phi_i = \sum_{i=1}^{\infty} < f, \ \phi_i> \lambda_i \phi_i$$

where λ_i is associated eigenvalues. Suppose λ_1 is the smallest eigenvalue. Consider $< \Psi , L\Psi > = \lambda_1 < \Psi, \Psi >$. We also have

$$\Psi = \sum_{i=1}^{\infty} < \Psi, \ \phi_i > \phi_i$$

and

$$L\Psi = \sum_{i=1}^{\infty} < \Psi, \ \phi_i > \lambda_i \phi_i$$

Therefore

$$< \Psi, \ L\Psi > = \sum_{i=1}^{\infty} < \Psi, \ \phi_i>^* < \Psi, \ \phi_i>\lambda_i = \lambda_1 \sum_{i=1}^{\infty} < \Psi, \ \phi_i>^* < \Psi, \ \phi_i>$$

Or

$$\sum_{i=1}^{\infty} < \Psi, \ \phi_i>^* < \Psi, \ \phi_i> (\lambda_i - \lambda_1) = 0 \tag{18}$$

where * denotes the complex conjugate of functions.

Since λ_1 is the smallest eigenvalue, $(\lambda_i - \lambda_1) \neq 0$ when $i \neq 1$. This fact forces $<\Psi, \ \phi_i> = 0$, for all $i \neq 1$ and $< \Psi, \ \phi_1 > \neq 0$ due to non-zero Ψ. Here subscript 1 denotes the eigenfunction being associated to λ_1. we therefore conclude $\Psi = < \Psi, \ \phi_1>\phi_1$. This proves that Ψ is an eigenfunction of L associated with the smallest eigenvalue λ_1. In a similar fashion, we can show the case for λ_n, the greatest eigenvalue.

THEOREM 2: For a given System (13), all the system eigenfunctions are weakly-complex, if and only if, for any system eigenvalues λ_i, we can find an eigenvalues β_i of operator L_2 such that

$$\lambda_i \lambda_i^* = \beta_i \tag{19}$$

PROOF. Necessity.

Consider an eigenfunction ϕ_i associated with eigenvalue λ_i. Suppose it is weakly-complex. From

$$\lambda_i^2 \phi_i + \lambda_i L_1\phi_i + L_2\phi_i = 0$$

and using the Equations (15) and (16) with the subscript i, we have

$$(\lambda_i^2 + \lambda_i \alpha_i + \beta_i) \phi_i = 0 .$$

Since $\phi_i \neq 0$, so

$$(\lambda_i^2 + \lambda_i \alpha + \beta) = 0 .$$

Note that both α_i and β_i are real, so Equation (19) holds.

Sufficiency.

We only prove the case that all eigenvalues are distinct. For the case with repeated eigenvalues, the proof is similar but more complicated. Consider the smallest eigenvalue β_1 of L_2.

$$\lambda_1 \lambda_1^* = \beta_1$$

with the corresponding eigenfunction ϕ_1 and its associated system eigenvalue λ_1, that

$$\lambda_1^2 \phi_1 + \lambda_1 L_1\phi_1 + L_2\phi_1 = 0.$$

Taking the inner product of the above equation with ϕ_1, we get

$$\langle \phi_1, \lambda_1^2\phi_1 \rangle + \langle \phi_1, \lambda_1 L_1\phi_1 \rangle + \langle \phi_1, L_2\phi_1 \rangle = 0.$$

Then

$$\lambda_1^2 + \lambda_1 \left\{ \frac{\langle \phi_1, L_1\phi_1 \rangle}{\langle \phi_1, \phi_1 \rangle} \right\} + \left\{ \frac{\langle \phi_1, L_2\phi_1 \rangle}{\langle \phi_1, \phi_1 \rangle} \right\} = 0$$

Note that the terms in above $\{ \, . \, \}$ are real scalars since $\{ \, . \, \}^* = \{ \, . \, \}$ for both L_1 and L_2 are self-adjoint. Therefore,

$$\left\{ \frac{\langle \phi_1, L_2\phi_1 \rangle}{\langle \phi_1, \phi_1 \rangle} \right\} = \lambda_1 \lambda_1^* = \beta_1 .$$

β_1 is the smallest eigenvalue of L_2. Thus ϕ_1 is an eigenfunction of L_2. From Lemma 5, we know that ϕ_1 is weakly-complex. Now we show that ϕ_1 is an eigenfunction of L_1. Since L_1 is compact, it has a complete set of orthogonal base $\text{Span}_{i=1}^{\infty}\{\psi_i\}$. So ϕ_1 can be represented in $\text{Span}_{i=1}^{\infty}\{\psi_i\}$. Also L_1 is closed on $\text{Span}_{i=2}^{\infty}\{\psi_i\}$ and L_2 is closed on $\text{Span}_{i=2}^{\infty}\{\psi_i\}$. It follows that for any scalar λ, $S(\lambda) = (\lambda^2 + \lambda L_1 + L_2)$ is a closed operator on $\text{Span}_{i=2}^{\infty}\{\psi_i\}$ and $\text{Span}\{\phi_1\}$. Consider the second smallest

$$\lambda_2 \lambda_2^* = \beta_2.$$

Let ϕ_2 be the eigenfunction of $S(\lambda_2)$, i.e. $S(\lambda_2)\phi_2 = 0$. Then ϕ_2 can be express ϕ_2 as

$$\phi_2 = a_1 \phi_1 + a_2 \Psi$$

where $\Psi \in \text{Span}_{i=2}^{\infty}\{\psi_i\}$. Let $S(\lambda_2)$ acts on ϕ_2.

$$S(\lambda_2)\phi_2 = S(\lambda_2)(a_1\phi_1 + a_2\Psi) = a_1 S(\lambda_2)\phi_1 + a_2 S(\lambda_2)\Psi = 0$$

Since ϕ_1 is orthogonal to Ψ, we have $a_1 S(\lambda_2)\phi_1 = 0$ and $a_2 S(\lambda_2)\Psi = 0$. But

$$S(\lambda_2)\phi_1 \neq 0$$

because ϕ_1 is not an eigenfunction associated with λ_2. Therefore we have $a_1 = 0$ and

$$\phi_2 = a_2 \Psi . \qquad (20)$$

From Equation (20), we know that $\phi_2 \in \text{Span}_{i=2}^{\infty}\{\psi_i\}$, so we can repeat the same procedure for the case

$$S(\lambda_2)\phi_2 = 0$$

and show that ϕ_2 is weakly-complex as was shown for ϕ_1. This eventually gives the proof that all ϕ_i are weakly-complex.

ACKNOWLEDGEMENT

Funding for the research reported in this paper has been provided jointly by the State University of New York at Buffalo and the National Science Foundation through the National Center for Earthquake Engineering Research under master contract number ECE86-07591.

REFERENCES

Bellman, R. "Introduction to Matrix Analysis" 2nd ed. New York McGraw-Hill 1970.

Caughey, T.K. and O'Kelly, M.M.J. "Classical Normal Mode in Damped Linear Dynamic Systems" J. of Appl. Mech. ASME Vol 32, pp.583-588, 1965.

Clough, R. W. and Penzien, "Dynamics of Structures," McGraw-Hill, New York, 1975.

Ewins, D.J "Modal Testing, Theory and Practice" Research Studies Press LTD. England (1986).

Foss, K. A. "Co-ordinates Which Uncouple the Equations of Motion of Damped Linear Systems," Technical Report 25-30, MIT, March, 1956.

Frazer, R. A., Duncan, W. J. and Collar. A. R. "Elementary Matrices," Cambridge Univ. Press, London, England, 1946.

Gohberg, L. et al "Matrix Polynomials " (1982) Academic Press.

Inman, D. "Vibration with Control, Measurement and Stability", Prentice-Hall, Englewood Cliffs, 1989.

Juang, J-N.; Pappa, R.S. " An Eigensystem Realization Algorithm (ERA) for Modal Parameter Identification and Model Reduction" presented at NASA/JPL workshop on identification and control of flexible space structures, J. of Guidance, Control and Dynamics, Vol. 8, No. 5, Sept-Oct. 1985, pp.620-627.

Kirshenboim, J. "Real Vs Complex Normal Mode Shapes" Proc of IMAC-5, London, pp.1594-1599.

Lancaster, P. "Lambda-Matrices and Vibrating Systems" (1966) Pergamon Press.

Li, K. and Xu, M. "From Damping Type Identification to Mode parameters Identification" Proc. of IMAC-6, 1988, pp.1265-1270.

Liang, Z. and Lee, G. C. "On Complex Damping of MDOF Systems" Proc. of IMAC-8, 1990, pp.1048-1055.

Liang, Z. Lee, G. C. and Tong, M. "On a Theory of Complex Damping", Proc. of Damping '91, Feb. 13-15 1991, San Diego, CA., Sponsored by Wright Laboratory, Flight Dynamics Directorate, Wright-Patterson Air Force Base

Liang, Z. Lee, G. C. and Tong, M. "On a Linear Property of Lightly Damped System", Proc. of Damping '91, Feb. 13-15 1991, San Diego, CA., Sponsored by Wright Laboratory, Flight Dynamics Directorate, Wright-Patterson Air Force

Base

Meirovitch, L. "Analytical Methods in Vibrations " The MacMillan Comp. 1967.

Mitchell, L. "Complex Modes: A review" Proc. of IMAC-8, 1990, pp.891-899.

Ortega, J. M. "Matrix Theory" 2nd ed. Plenum Press, 1987.

Tong, M., Liang, Z and Lee, G. C. "Techniques in Design and Using VE Dampers", Proc. of Damping '91, Feb. 13-15 1991, San Diego, CA., Sponsored by Wright Laboratory, Flight Dynamics Directorate, Wright-Patterson Air Force Base

Tong, M., Liang, Z and Lee, G. C. "On an Application of Complex Damping Coefficients", Proc. of Damping '91, Feb. 13-15 1991, San Diego, CA., Sponsored by Wright Laboratory, Flight Dynamics Directorate, Wright-Patterson Air Force Base

Vold, H; Rocklin, G. " The Numerical Implementation of a Multi-Input Modal Estimation Method for Mini-Computer," Proc. of IMAC-1, 1982, pp.542-548.

The PACOSS Dynamic Test Article

Russell N. Gehling ‡
Martin Marietta Astronautics Group

ABSTRACT

The Dynamic Test Article (DTA) developed under the Passive and Active Control of Space Structures (PACOSS) program is a test-verified laboratory system for evaluating the behavior and interaction of passive and active control strategies on dynamically complex structures. The pneumatically suspended DTA possesses high modal density in the 1 to 10-Hz frequency range, with moderate levels of passive damping (near 5% modal viscous) designed into the flexible modes. The system also includes a real time control processor, ten reaction mass actuators, 23 velocity sensors, and a host workstation. Also, 200 accelerometers suitable for modal testing are available for identification and verification of performance.

This presentation describes the DTA system components, capabilities, and overall test results. The DTA has been delivered to the Air Force Institute of Technology where it was assembled for use in further studies of controls/structures interaction and passive damping performance.

‡ P.O. Box 179, Denver, CO. 80201, Mail Stop H4330, phone: (303) 971-9388.

Introduction

- Future Large Space Systems Will Require Vibration Control
- Passive/Active Approach Is Most Effective Means
- DTA Designed As Testbed for Passive/Active Control Strategies

Future large space systems (LSS) will possess high modal density at low frequencies. Mission requirements for some LSS lead to control bandwidths overlapping many closely spaced structural modes. Therefore, some means of vibration control will be necessary to avoid excessive excitation of the flexible modes.

The Passive and Active Control of Space Structures (PACOSS) program has shown that a combined passive and active vibration control approach will result in a simpler system which can be expected to be more robust and reliable than a corresponding system utilizing active control exclusively.

The PACOSS Dynamic Test Article (DTA) was designed to serve as a laboratory testbed for passive and active structural vibration control implementation and testing.

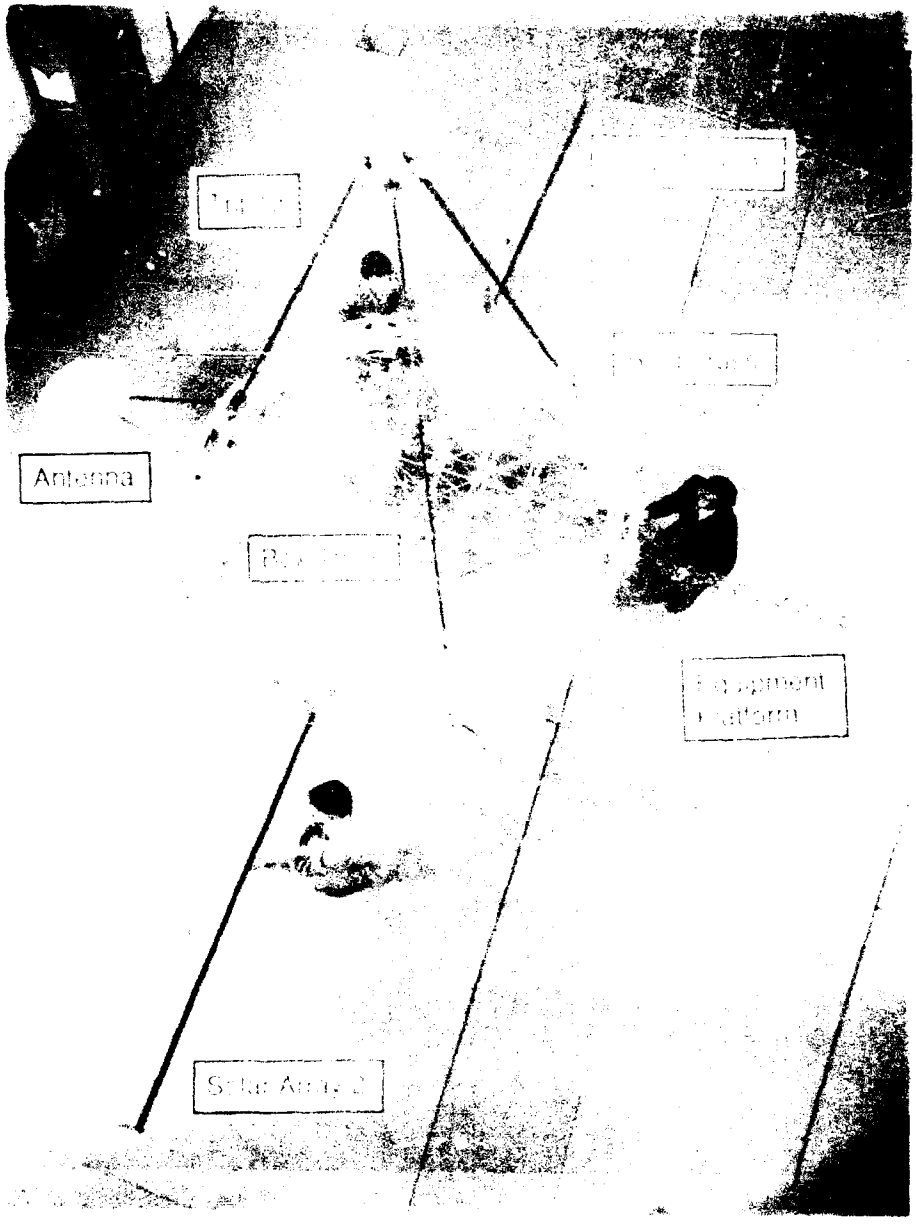

THE PACOSS DYNAMIC TEST ARTICLE

The DTA consists of seven substructures; a box truss representative of a primary reflecting surface, a tripod representing a beam expander/secondary reflecting surface, two solar array simulators, a small truss representing an equipment platform, and a communication antenna simulator. A ring truss serves as the structural backbone tying the other substructures together. All substructures, except the ring truss have passive damping treatments.

Because the DTA is a validation device, sources of inadvertent damping were kept to a minimum through the use of bonded joints and precision bolted joints. Also, to avoid the need for a complicated suspension system, the DTA was designed to withstand one-g when supported from only three suspension points on the ring truss.

DTA Summary

- **High Modal Density at Low Frequencies; 23 Major Flexible Modes between 1 and 10 Hz**
- **Moderate Passive Damping (5 to 10% Modal Viscous) Designed into Structure**
- **Versatile Active Vibration Control System**
- **Extensive Instrumentation**

The primary characteristic of the DTA is high modal density. There are 23 major flexible modes between 1 and 10 Hz. Nine of these modes are global in nature, with several separated by less than 0.2 Hz. The high modal density presents a challenging modeling and control problem, thereby making the DTA a unique testbed for vibration control research.

Passive damping was designed into the DTA to achieve 5% to 10% modal viscous damping in the structural modes which participate in the DTA performance metric, the line of sight (LOS). Also, a versatile active vibration control system was developed to allow implementation of a wide array of control laws. To date, five algorithms have been implemented;

Local Direct Velocity Feedback
Modal Space Control with a State Estimator
LQG Optimal Control with Loop Transfer Recovery
$\mathcal{H}_\infty$ (H-infinity) Control
LQG Optimal Control with Residual Mode Filtering

In addition to the active control system instrumentation, nearly 200 Kistler model 8632A5 accelerometers are installed for the purpose of modal testing. These light weight piezoelectric accelerometers are ideal for the 1 to 10 Hz frequency range of interest.

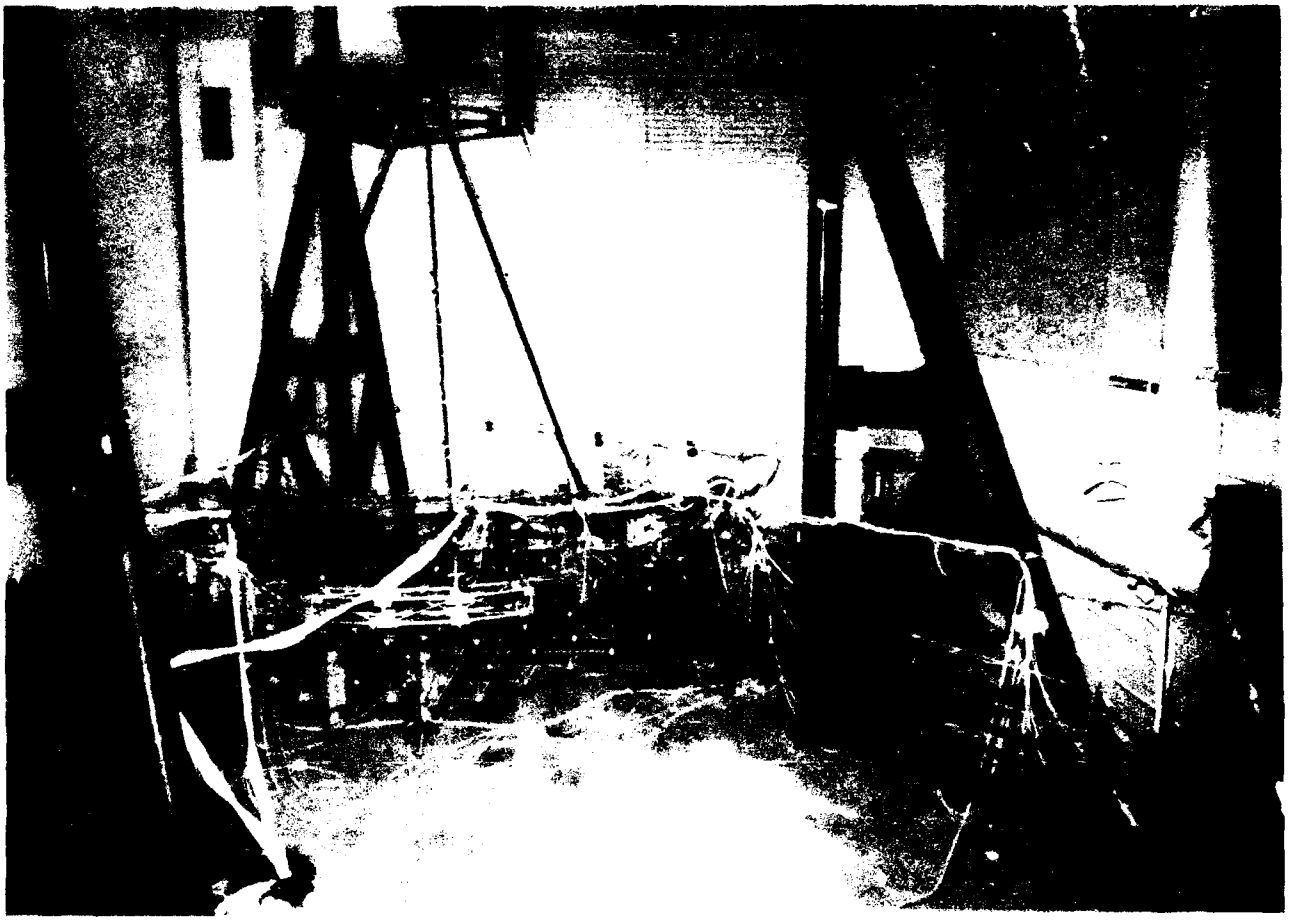

DTA TEST SETUP

This photo shows the DTA during testing in the Controls-Structures Interaction (CSI) Lab at Martin Marietta Astronautics Group's Main Plant. The lab maintains a uniform temperature within 2 degrees F, thereby allowing confident application of viscoelastic material properties (at a given temperature) in analysis of test articles.

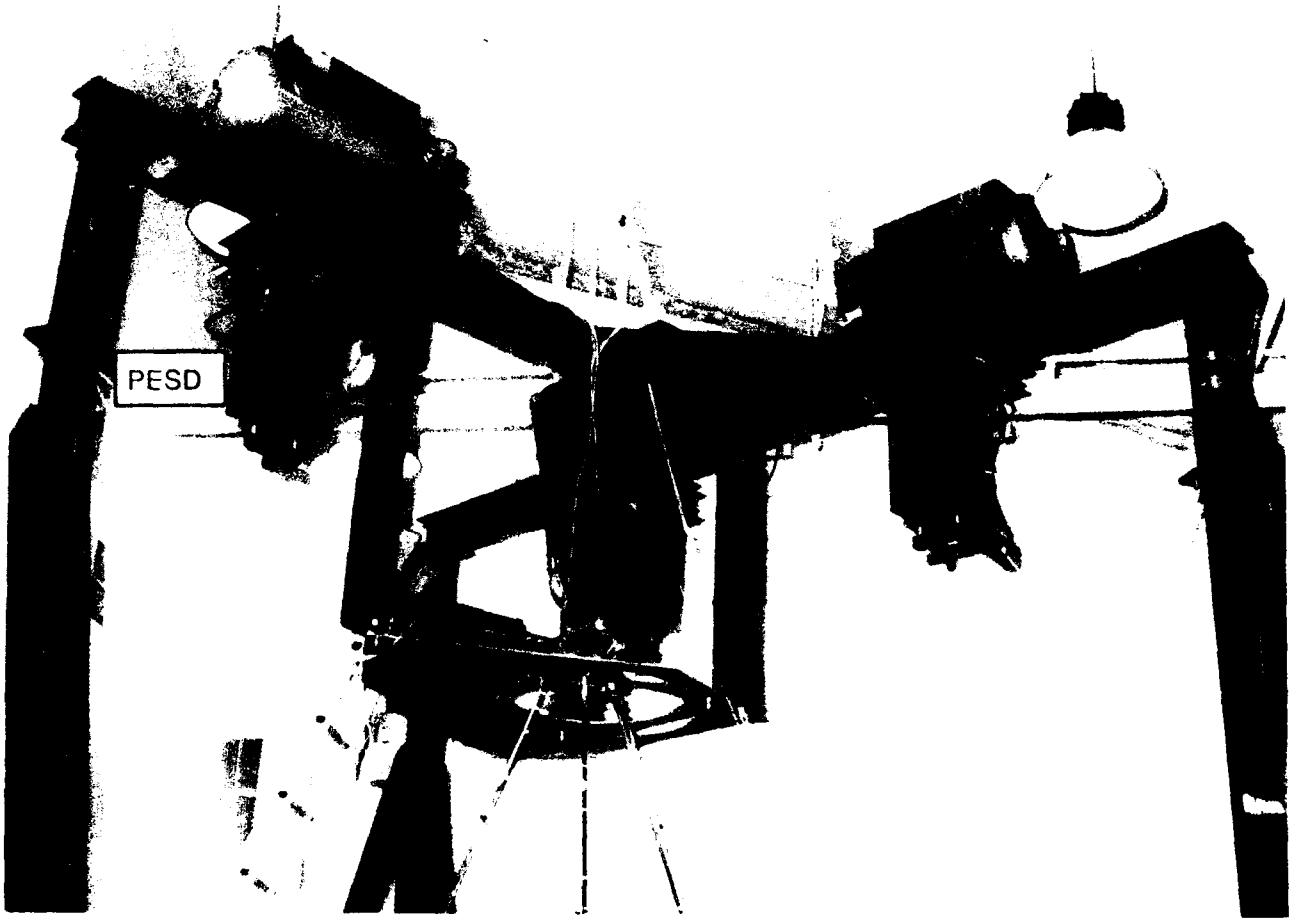

DTA PNEUMATIC-ELECTRIC SUSPENSION DEVICES

The DTA is suspended from three pneumatic-electric suspension devices recently developed by CSA Engineering Inc. The CSA devices provide a soft, virtually friction-free suspension, and are relatively easy to adjust for load ranges from 50 to 350 lbs.

Although an active centering loop is provided on each PESD, the rigid body dynamics of the DTA suspension arrangement, combined with very small restoring forces from control system and instrumentation cabling tended to keep the DTA centered without use of the active loop.

Suspension System Performance

"Roll Mode"	f_n, Hz	ζ %
With Instrumentation Cables	0.26	10
Without Instrumentation Cables	0.17	11
Predicted	0.15	?

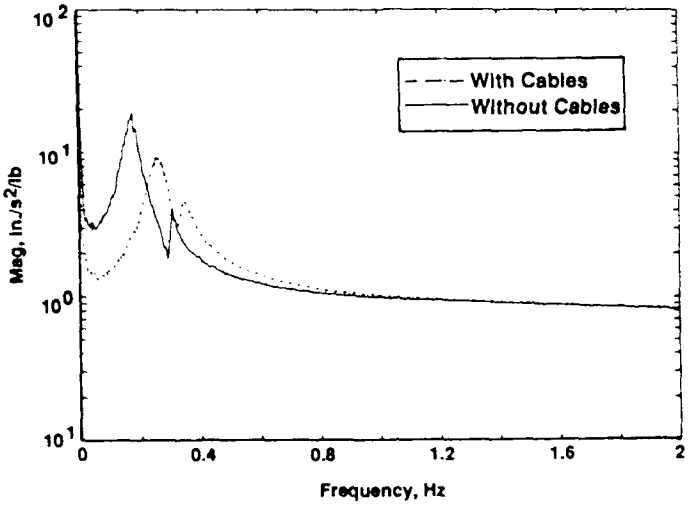

This figure shows the success of the PESDs in achieving a low frequency suspension. Also, the effect of modal survey instrumentation cables is apparent. The frequency response function (FRF) shown by the dashed line was measured with approximately 180 microdot cables attached to the Kistler accelerometers mounted on the DTA. The observed resonant frequencies were much greater than predicted by analysis including the PESD stiffness, and pendulum effects. However, as shown by the FRF denoted with a solid line, when the instrumentation cables were removed, the agreement between predicted and measured rigid body frequencies was excellent. Similar results were seen for the other suspension modes.

While there is no measurable friction in the PESDs, air movement through a 20-micron filter paper does dissipate energy, thereby giving rise to the apparent damping present in the suspension modes. However, the loss is well modeled by linear viscous damping, and is insignificant with regard to the DTA flexible modes.

DTA Passive Damping

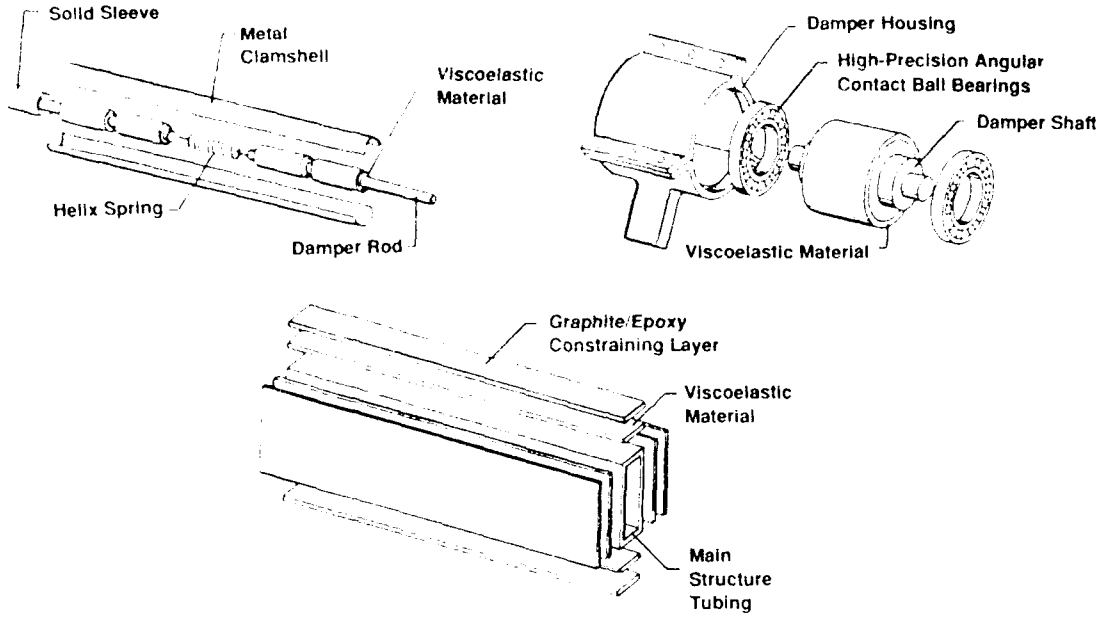

Six different types of viscoelastic damping treatments were applied to the DTA, three of which are shown in this figure. The design and placement of each treatment was based on the modal strain energy method.

Extensional shear dampers are used in the box truss and equipment platform, and are effective in damping lower truss modes. Rotational shear dampers are located at each tripod leg/secondary mirror interface to damp modes involving relative rotation between the legs and mirror. Constrained layer treatments are used on the tripod legs, antenna legs, and solar array masts. The DTA antenna dish has an integral damping treatment. Viscoelastic shear straps are used to further damp vertical bending of the solar array masts, while tuned mass dampers suppress solar array blanket modes.

DTA CONTROL SYSTEM COMPUTERS

This photo shows the DTA active control system equipment. The control processor is an Optima/3 which is based on a Motorola 68030 CPU. The Optima/3 is hosted by a Sun-3 workstation which is used to generate and download an executable control code to the Optima/3. Single-ended analog inputs are sampled by the Optima/3, processed according to the control code, and output. The input and output signal range is +/- 10 volts. DC drift of the DAC is negligible and the noise level is in the 10 to 20 millivolt range. Also shown in the photo are the signal conditioning/current drive control boxes for the actuator/sensor units.

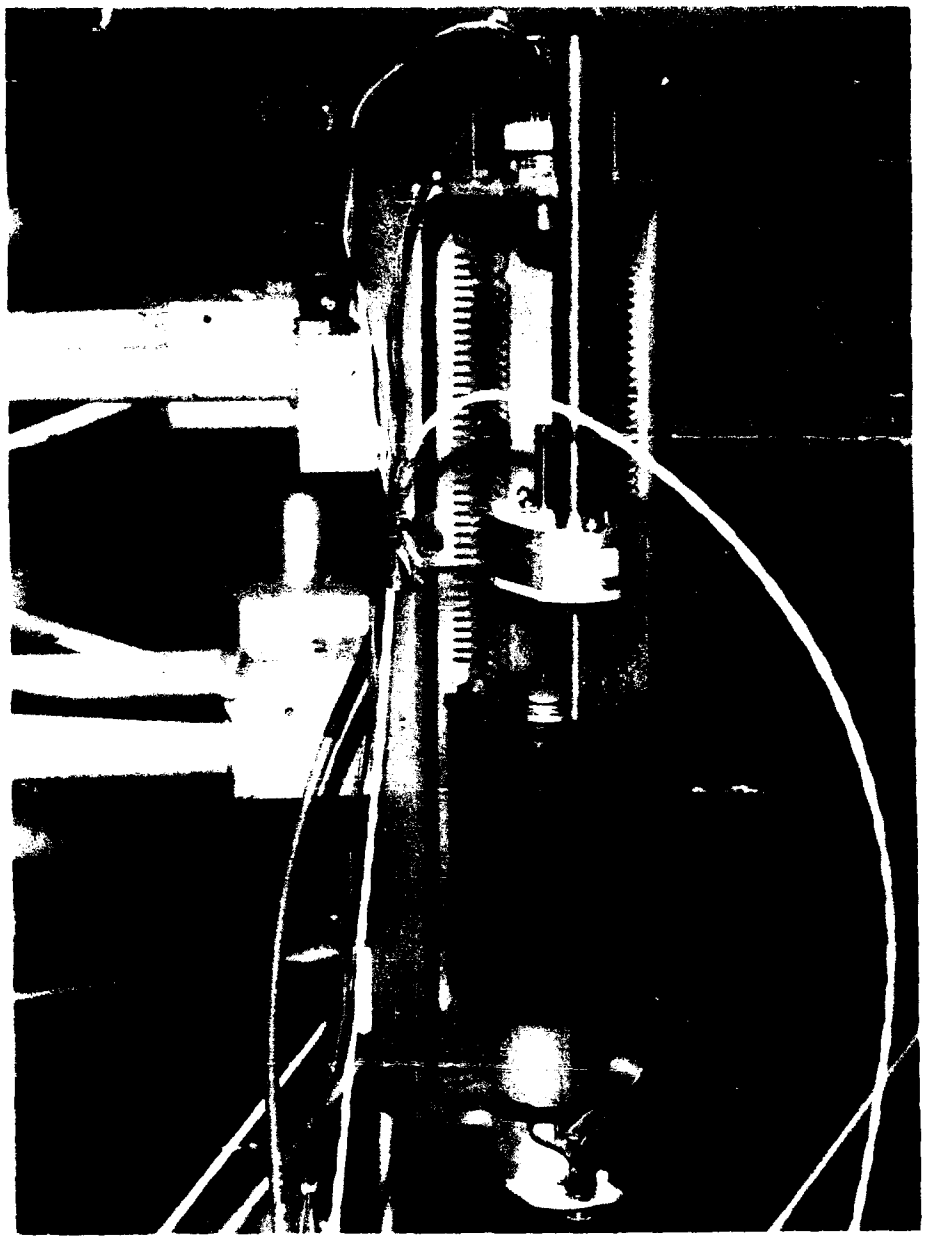

DTA REACTION MASS ACTUATOR

This photo shows an actuator/sensor unit. Each unit consists of a linear motor with a linear velocity transducer (LVT) to measure the relative velocity between the motor mass and actuator frame, and a Sundstrand QA-1400 accelerometer to measure inertial acceleration. The motor mass is supported on springs which give the actuator a 1.5 Hz natural frequency. The actuator stroke is approximately +/- 1 in. The pictured actuator is in a vertical configuration. Four DTA actuators may also be configured for horizontal operation with opposing extensional springs. In the horizontal configuration, the actuator natural frequency is about 0.7 Hz.

The QA-1400 signal is integrated in the signal conditioning electronics via an analog bi-quad filter to provide inertial velocity of the control point. The LVT signal is used to increase the damping of the actuator, and also is integrated to provide a motor mass position feedback allowing adjustment of the actuator f_n from about 1.2 to 1.8 Hz.

Control System Summary

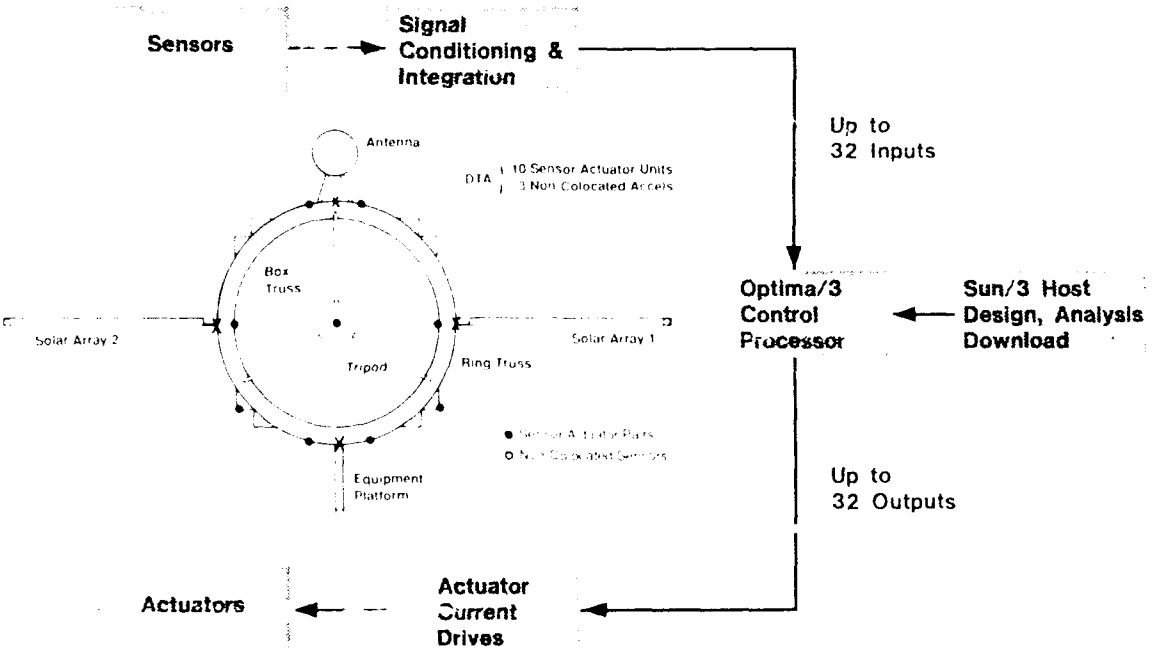

Optima/3 Processing Speed: 64 States, 23 Inputs/10 Outputs: 280 Hz

This figure summarizes the DTA active vibration control system. Each actuator/sensor unit produces two sensor signals (inertial acceleration and relative reaction mass velocity) which are fed to the analog signal conditioning electronics. Also, three non-collocated acceleration measurements are available. The inertial acceleration measurements are integrated and sent to the Optima/3 ADCs along with the LVT signals. The Optima/3 will accept up to 32 input channels, and also output up to 32 channels. In the current DTA configuration, there are 23 inputs, and 10 outputs. The Sun host workstation is used for design, analysis, and download of control algorithms to the Optima processor. Analog outputs from the Optima are sent to the actuator current drives which command a current directly proportional to the command voltage. Finally, the actuators apply a force proportional to the current command on the DTA.

The processing speed of the Optima allowed a 64 state control law with 23 inputs and 10 outputs to be processed at 280 Hz; well above the 10 to 20-Hz bandwidth of control laws applied to the DTA. Thus, it was not necessary to consider discretization effects of the control system.

DTA Analytic Model

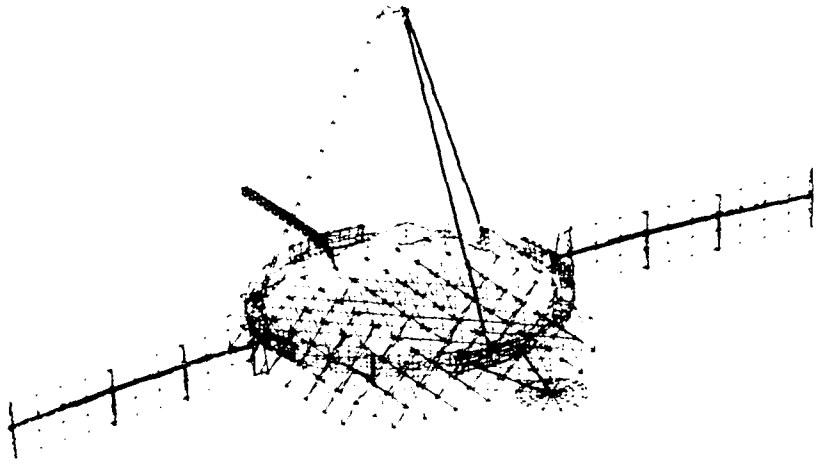

- **23 Modes Correlated with Test Results**
- **9 Global Modes**

A detailed finite element model of the DTA involving over 10,000 degrees of freedom was developed and test verified during the PACOSS program. Each substructure was modeled and test verified before the full DTA was tested. The 23 major flexible modes between 1 and 10 Hz were successfully identified in the DTA modal survey, and correlated with analytic modes.

DTA Natural Frequencies

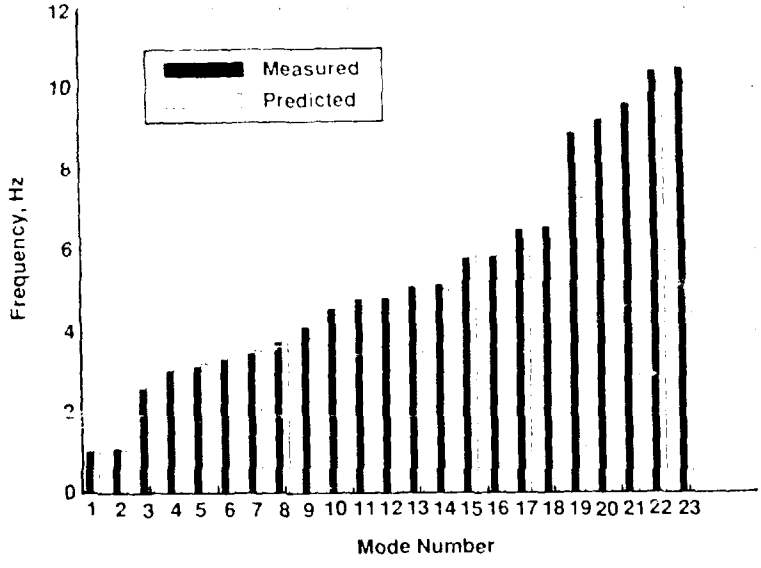

Agreement between measured and predicted natural frequencies was excellent for nearly all of the identified modes. This figure presents a bar chart to graphically depict the agreement. All natural frequencies agree to within 5% with the exception of mode 19 which is a local antenna dish mode.

DTA Modal Damping

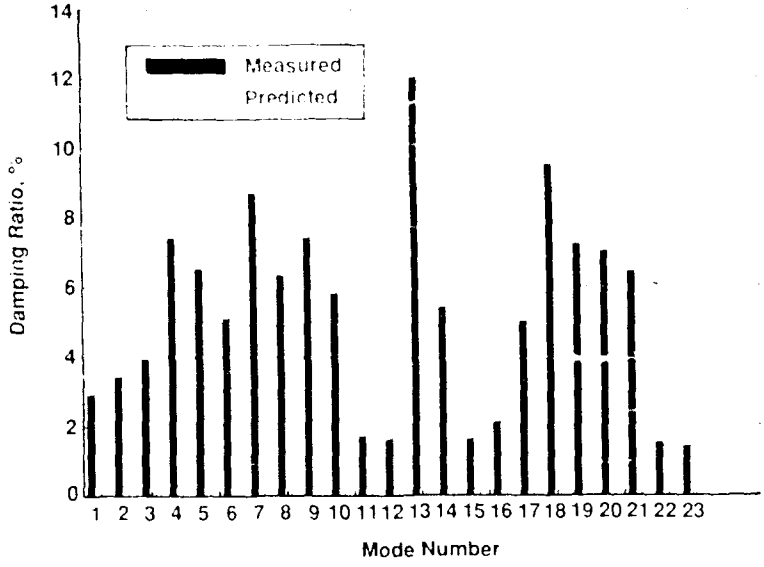

This figure presents the measured and predicted (via the modal strain energy method) modal damping ratios. The agreement is typically within 20% which is quite good considering the difficulty in determining damping ratios from the measured data. Closely spaced, highly damped modes lead to FRF measurements which cause scatter of nearly +/- 20% in identified damping ratios.

Test Setup and Analysis Validity Checks

- **Instrumentation Cable Effects**
- **Linearity**
- **Closed-Loop Analysis**

During DTA closed-loop testing, differences between the measured and predicted frequency response functions (FRF) led to an evaluation of the validity of the test setup and analysis techniques. Were the observed differences simply due to analytic model inaccuracies, or were they due to a test setup problem or the real mode model of the DTA? Three issues were investigated:

Possible instrumentation cable effects on DTA flexible modes
DTA and control system linearity
Real versus complex modes used in the DTA model.

Instrumentation Cable Effect

Typical DTA FRF

Magnitude

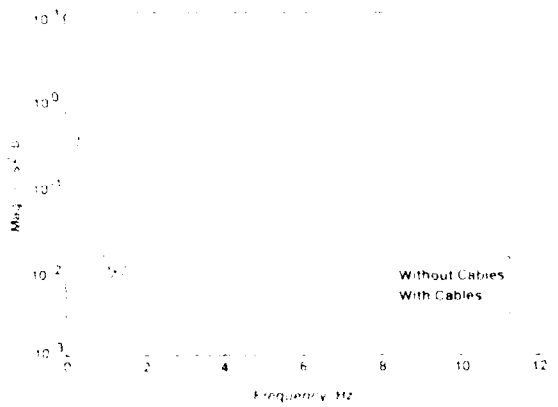

Phase Angle

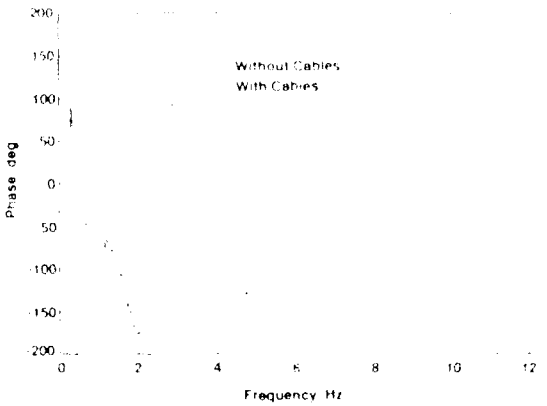

Possible instrumentation cable effects were investigated by removing nearly all of the over 180 microdot cables from the DTA. The plots shown in this figure are FRFs taken before and after removing the cables. Clearly, the instrumentation cables have a negligible effect on the DTA dynamics above 2 Hz.

Synthesized Closed-Loop FRFs

- **Form Closed-Loop FRFs from Open-Loop Measurements and Analytic Compensator**

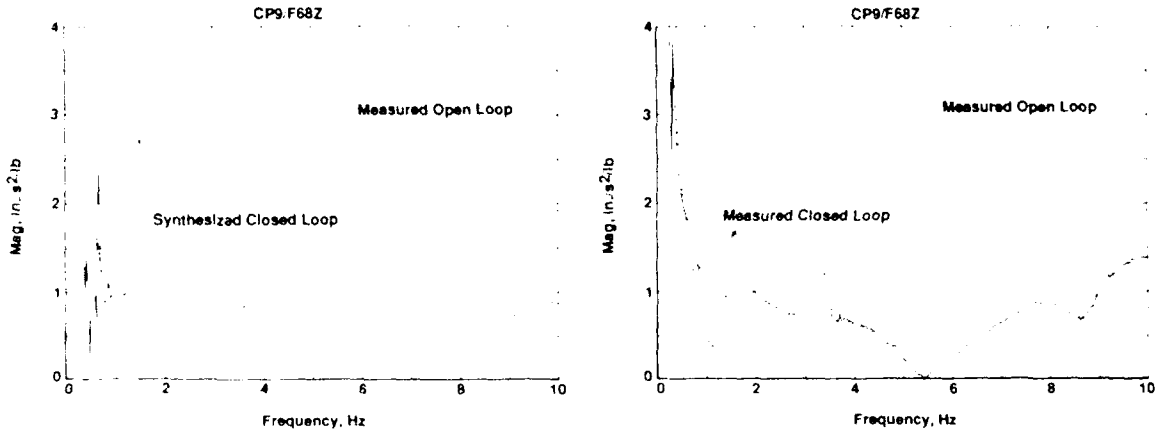

To investigate the linearity and function of the DTA control system, closed-loop FRFs were synthesized using the analytic compensator transfer functions, and measured open-loop FRFs between the DTA control points. The idea here is that if the control system is functioning as modeled, and the DTA is a linear system, the synthesized FRFs should agree with the actual closed-loop measured FRFs. This figure demonstrates good agreement between a synthesized and measured FRF using the LQG/LTR control law, thereby indicating that the control system indeed performs as designed and modeled, and that the DTA behaves as a linear system.

Complex Modes

- Couple Compensator to DTA Modeled with Real and Complex Modes

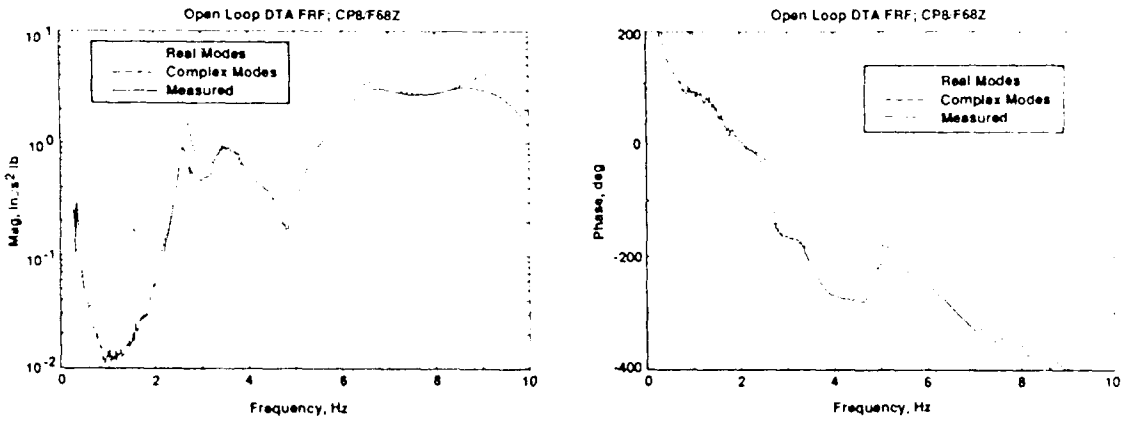

As previously mentioned, the DTA model used for control law design and analysis was generated using real modes. However, some sample studies indicated that in the presence of closely spaced modes and relatively high damping, closed-loop results can be significantly altered if complex modes are used in the plant model rather than real modes.

To investigate the effect of complex modes in the DTA analysis, complex modes for the DTA were calculated from the reduced DTA mass and complex stiffness matrices. The reduction was performed via the Guyan technique using only the real part of the stiffness matrix. The figure shows three open-loop FRF plots; an actual measurement, the corresponding analytic FRF computed using real modes/MSE approach, and the analytic FRF computed using complex modes. Note that the FRF from complex modes generally agrees better with the measurement, particularly in the 3 to 5 Hz range. Not coincidentally, the 3 to 5 Hz range possesses the highest modal density of the DTA and encompasses many global modes.

Although the open-loop agreement is improved when complex rather than real modes are used in analysis of the DTA, the closed-loop results did not change as significantly. Many of the closed-loop anomalies seen during DTA testing were not explained by using complex modes, and the overall agreement between test and analysis was not greatly improved.

Conclusion

- **DTA Exhibits Characteristics of Future LSS**
- **Analytic Model Is Quite Good**
- **Control System Behaves Linearly**
- **DTA Will Be Set Up at Air Force Institute of Technology for Further Passive/Active Research**

The DTA exhibits the dynamic characteristics expected of future LSS: high modal density at low frequencies. Passive damping designed into the structure provides a somewhat more forgiving system for investigation of active control algorithms. Also, further passive control approaches can be implemented due to the substructure assembly of the DTA. Thus, the DTA is an excellent testbed for continuing research of LSS structural vibration control, both passive and active.

The analytic model of the DTA is test verified up to 10 Hz and predicts open-loop DTA behavior relatively accurately. However, it may be insufficient for accurate prediction of the performance of high authority modern control laws. Any further model improvement would most likely involve empirical tuning, since the finite element model has been exhaustively reviewed and refined based on DTA dimensions and element tests.

The DTA control system behaves linearly and is highly versatile. While only linear constant coefficient control laws have been implemented thus far, the Optima/3 is capable of implementing any control algorithm that can be coded in "C", including adaptive control.

The DTA has been set up at the Air Force Institute of Technology for further passive/active controls research.

RETROFITTED DAMPING TREATMENT FOR A THREE STAGE BOOSTER SYSTEM

Daniel J. Segalman[1]
Sandia National Laboratories
Albuquerque, NM

E. L. Marek
Sandia Natinal Laboratories
Albuquerque, NM

ABSTRACT

A three-stage solid propellant booster system has been developed to launch a variety of payloads. A critical issue to the success of any flight is the possible interaction of the elastic vibrational modes with the control system. Modal test results indicate that damping factors may be very low ($0<0.5\%$), adversely affecting control design. To alleviate the concerns, a study of retrofitted damping application was performed. The central difficulty in designing a damping treatment was that access could be obtained to only a fraction of the straining surfaces. Thus, achieving an optimal damping design on those surfaces became essential.

FULL PAPER NOT AVAILABLE FOR PUBLICATION

[1]Sandia National Laboratories, Division 1524, P.O. Box 5800, Albuquerque, NM 87185-5800, (505) 846-1899

DAMPING DESIGN FOR A DISK DRIVE HEAD FLEXURE

Eric M. Austin[1]
James C. Goodding
CSA Engineering, Inc., Palo Alto, CA

William A. Driscoll
3M ISD Laboratory, St. Paul, MN

ABSTRACT

This paper describes the work done by 3M and CSA Engineering (under contract to 3M) that lead to the design of a high-performance damper for load beams in disk drive head suspensions.

3M has supplied dampers for such applications for the past eight years. While the current damper designs do a good job of attenuating the first bending mode of the load beam, they do only a satisfactory job of attenuating the first torsion mode and a less than satisfactory job of attenuating the sway mode. Unfortunately, disk drive design changes have caused the sway mode to become one of the more dominant modes in the load beam during operations of the drive. If excited, this is the most severe mode with regard to operation of the disk drive servo heads. After the drive is manufactured, if a resonant condition occurs in the load beam of the servo suspension, the drive is rendered useless and has to be reworked.

The purpose of this work was to design a damping treatment that attenuates all three modes in a satisfactory manner. The paper describes the four phases that are typical in the design of a damping treatment for attenuating resonant vibrations: 1) mathematical modeling of the undamped system, 2) incorporation of a damping treatment into the mathematical model, 3) arriving at the optimum design for a damping treatment, and 4) preparing and experimentally evaluating the design.

[1]Senior Engineer, CSA Engineering, Inc., 560 San Antonio Road, Suite 101, Palo Alto, CA 94306, (415) 494-7351

Damping Design for a Disk Drive Head Flexure

Eric M. Austin
James C. Goodding
CSA Engineering, Inc.

William A. Driscoll
3M / Industrial Specialties Division

Presented February 14, 1991
Damping '91, San Diego, CA

The Purpose of a Flexure Damper

Obvious benefits of adding damping to a head flexure system are that responses of the read/write head to a given excitation can be reduced. This translates into increased accuracy, fewer read/write errors, increased gain margin, and increased reliability of the drives.

Significant components of the example head suspension system shown are the load beam, slider, and flexure. The terminology for these an components often varies. For this paper, the load beam is basically a cantilevered stainless steel beam (consistent with the figure), the slider is a block containing the read/write transducer that supports the air bearing that "floats" the head above the rotating disk, and the gimbal spring is the very compliant interface between the slider and the load beam. The overall assembly is called either a head flexure or head suspension system.

The Purpose of a Flexure Damper

- Increase servo bandwidth by adding modal damping to the structure: Increase gain margin and lower access times
- Reduce read/write errors caused by head suspension structural dynamics
- Increase the reliability of the drives

The Purpose of a Flexure Damper

- Increase servo bandwidth by increasing modal damping in the structure: Increase gain margin
- Reduce read/write errors caused by head suspension structural dynamics
- Increase the reliability of the drives

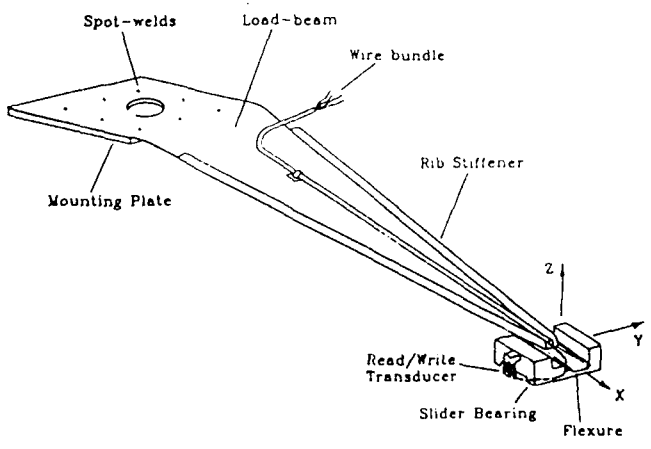

Objectives

3M currently markets several different head flexure dampers, each designed for a specific application. The end goal of this study was to reduce the number of unique flexure damper designs needed by optimizing a single design that will serve most applications. Of particular importance are treatments that perform well at typical operating temperatures near 160 deg F.

As a first step, existing designs of flexures and flexure dampers were studied using finite element analysis. Trade studies evaluated details about the viscoelastic materials, the constraining layers, and the placement of the dampers.

Objectives

- Evaluate current flexure dampers designs
  - viscoelastic materials
  - constraining layers
  - position of damping treatment
- Determine a flexure damper design with high performance for a broad range of applications
- Verify analytical predictions via a simulated in-service test, particularly at typical operating temperatures (~160° F)

Approach

The approach was dictated by the final objective: to recommend an improved design of flexure dampers to 3M. A finite element model was built to evaluate both existing and new designs for flexure dampers. As much emphasis was placed on testing resulting designs as on the analysis and design. The goals of the testing were to measure the frequency and damping in key modes and to compare this measured modal data with the analytical results.

Approach

- Develop a finite element model of the undamped flexure
- Analyze candidate damping treatments
- Make design recommendations for improving damping performance to 3M, who will subsequently fabricate the design
- Verify damping design by test
- Measure flexure modal properties, including air-bearing effects
- Qualify important mode shapes against measured modal data

Primary Modes of Interest

The modes of most interest to disk drive manufacturers are modes where the slider (read/write head) translates side to side (theta direction shown in slide).

Primary Mode of Interest
(Produces time-based error)

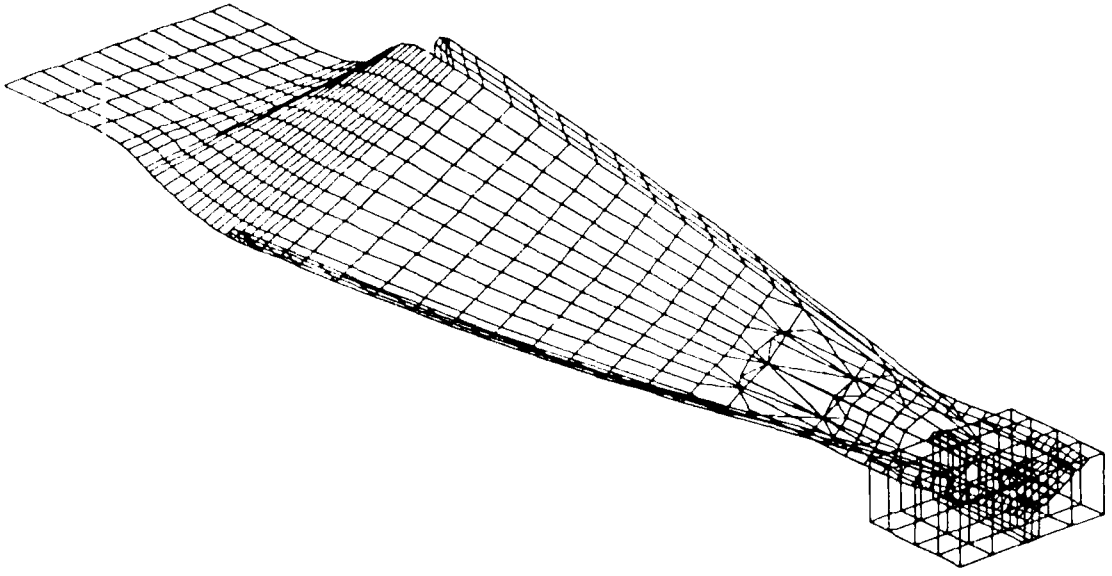

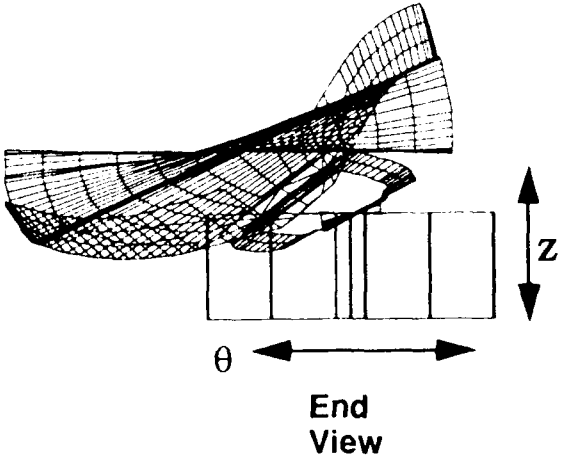

Damping Design Trade Studies

Given complete freedom, design parameters in a damping design are the location of the treatment, the constraining layer material, the constraining layer thickness, the material for the VEM layer, and the thickness of the VEM layer. However, some of these can not be changed without having a large impact on the manufacturing process and disk drive performance. For instance, the bend radius is tuned so that the slider rides at a precise height above a spinning disk. This cannot be changed by a bulky damping treatment. This restricted the constraining layer thicknesses to only 0.001" or 0.002" of stainless steel. In addition, only standard VEM thicknesses of 0.002" and 0.005" were considered. In the end, the main design parameters were the stiffness and loss factor of the VEM and the damper placement.

Damping Design Trade Studies

- There are a variety of different constraining layer damping designs used to solve resonance problems of the load beam
- Investigated VEM thicknesses of 0.002" and 0.005; investigated constraining-layer thicknesses of 0.001" and 0.002"
- Trade studies concentrated on the modulus and loss factor of viscoelastic material

Variation of VEM Strain Energy with VEM Shear Modulus

The graph shows how the modal strain energy in the viscoelastic material varies as a function of VEM shear modulus. Using the Modal Strain Energy Method, the loss factor of the mode (1/Q) is the loss factor of the VEM times this percent modal strain energy. Without going into specifics of the values, it was found that the viscoelastic materials used in most commercial head flexure dampers were much softer than the analysis identified as optimum. Ideally, the damper design should utilize VEM's who's loss factors peak near the normal operating temperatures and frequencies. The slide shows the approximate effectiveness of most current VEM's.

Variation of VEM Strain Energy with VEM Shear Modulus

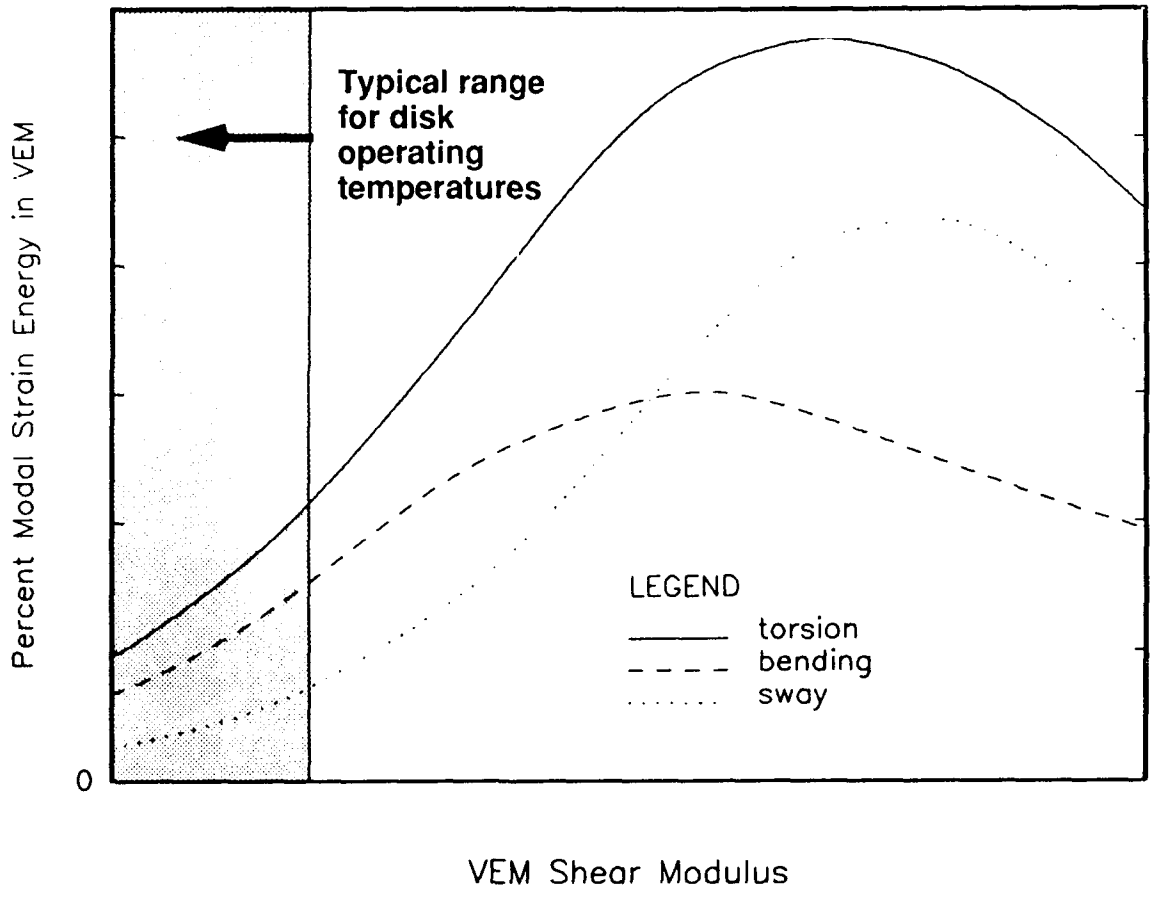

Viscoelastic Determination

Once the specification of VEM modulus and loss factor was recommended to 3M, the task of formulating the VEM commenced. Once complete, the mechanical properties of the VEM were verified (by 3M), and sample flexure dampers were prepared for testing.

Viscoelastic Determination

- Determine chemistry to produce desired material properties
- Viscoelastics prepared; three candidates with different shear moduli
- Dynamic mechanical properties measured to verify modulus and loss factor

Test Sample Preparation

Three sets of sample flexure dampers, each with a different modulus, were fabricated by 3M for testing. Each was die-cut and had a stainless steel constraining layer. They were applied to typical load beams in two slightly different configurations: one over the bend radius and the other not. The resulting damped flexures, along with two of a current configuration, were supplied to CSA for testing.

Test Sample Preparation

- Prototype flexure dampers made with three candidate viscoelastic materials (stainless steel constraining layers)
- Dampers die cut
- Applied to load beams (two locations for each candidate material)
- Supplied to CSA along with two current configurations to serve as benchmarks

Text-Fixture Design

The test fixture was designed so that the critical sway and torsion modes were sure to be excited by the base excitation. The fixturing was mounted directly on an electrodynamic shaker to provide a method to excite modes with strong theta-direction motion of the slider. Transmissibility functions were measured; the base motion sensed by an accelerometer and the response motion transduced by a noncontact optical displacement sensor. The modal properties were derived from the measured transmissibility functions.

In efforts to simulate in-service conditions as closely as possible, the air-bearing effect was simulated with by blowing air through a piece of porous bronze under the slider. In addition, the operating temperature near 160 deg F was achieved by a forced-air system.

Test-Fixture Design

- Concentrate on modes that affect disk drive performance
  - Important modes: first torsion and first sway
  - First bending normal to disk relatively unimportant
- Obtained modal properties from measured transmissibility functions
  - Input: Base motion
  - Output: Motion at points on load beam and slider
- Simulate operating conditions
  - Temperature: 158°F nominal
  - Slider support in air film bearing

Test Apparatus

The test rig was designed so that a base excitation could be applied directly to the base of the flexure in either the "Z" (producing weak-axis bending) or "theta" (producing sway and twist) directions. The optical sensor was mounted on a structure separate and vibration isolated from the shaker with a three-axis micrometer stage to position the fotonic probe accurately. The temperature was controlled by forced air and was measured with a standard thermocouple.

Test Apparatus

- Flexure-holding fixture mounted on shaker
- Fixtures to shake flexure in either Z or theta direction
- Three-axis micrometer stage to position response sensor accurately
- Measured, controlled input: Flexure base motion transduced by accelerometer
- Flexure response transduced by noncontacting optical sensor: fotonic probe
- Transmissibility measured via FFT analyzer
- Temperature control: Forced air with thermocouple

Head Flexure Test Rig

This slide shows the complete test setup on the left and a close-up view of the moving head assembly on the right. The fixturing was designed to have integral damping so that it would not corrupt the measurements by its own resonant responses. The fotonic probe, seen on top of the platform on the left, was mounted on a damped sandwich plate, using 3M's ISD 110 as the middle VEM layer. The lower plate was also a three-layer sandwich assembly.

Head Flexure Test Rig

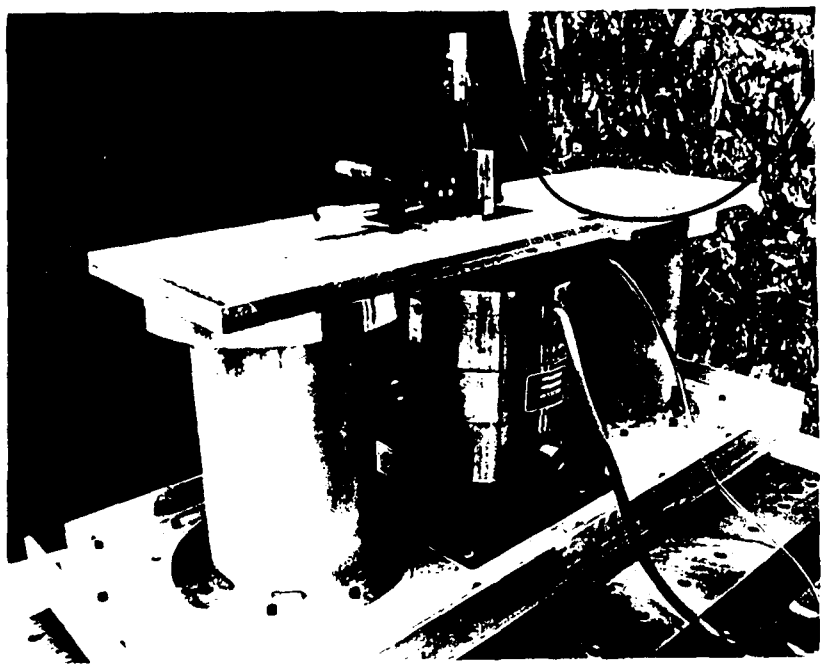

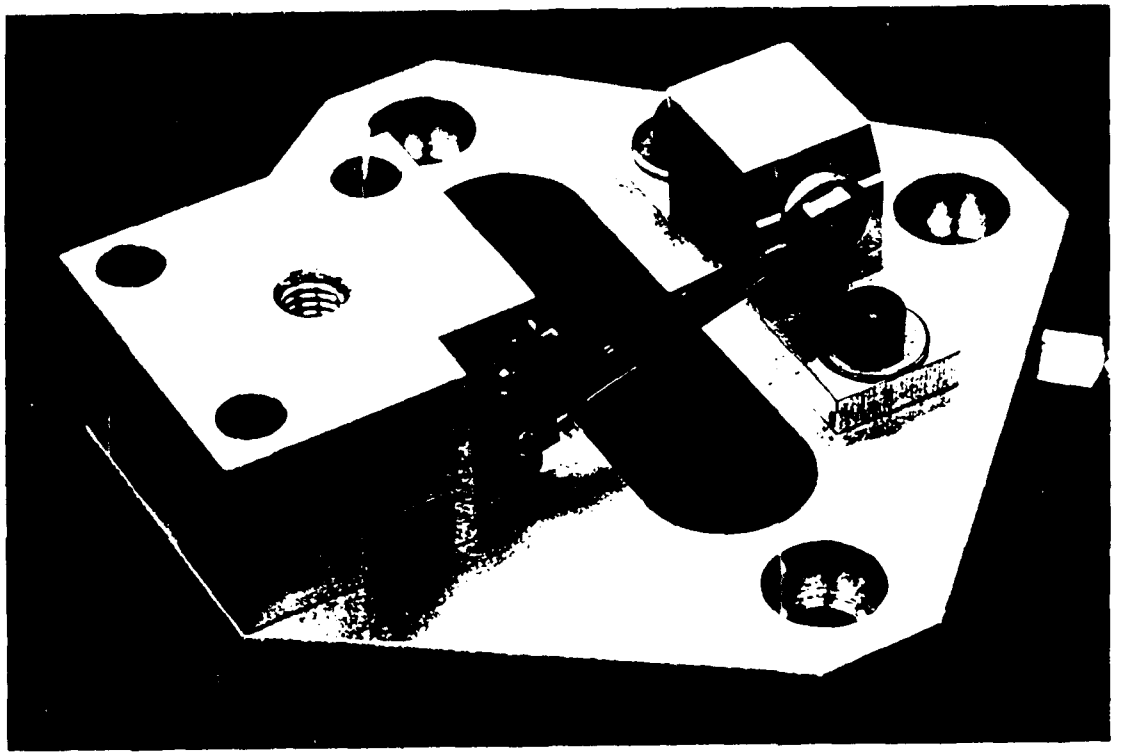

- "Backdoor vibration path" and fixture resonances major concerns
- Both shaker and fixturing are supported on vibration isolators
- Plates damped with 3M ISD 110

EA-D91-3M-12

Results

In conclusion, it was determined that damping treatments extending over the bend radius of the flexure worked better than those that did not. As reported earlier, analysis has predicted that viscoelastic material having much higher values of shear modulus are needed.

Results

- Geometric design of damper established
- Placement of damper must be over the bend at the root of the load beam in order to damp the sway mode effectively
- Both finite element and experimental analyses suggest that high-modulus viscoelastic materials will improve damping performance in torsion and sway modes
- Near-term plans are to test improved flexure dampers in actual disk drives

DAMPING JET ENGINE FRONT FRAME STRUTS

Captain Vance Johnson[1]
U.S. Air Force
Wright-Patterson AFB, OH

Dennis Murphy
General Electric Aircraft Engine Company

Kurt Nichol
Sverdrup Technology, Inc.

ABSTRACT

Throughout the development of the F110-GE-129 improved performance engine (IPE), the fabricated front frame struts experienced high stresses and associated weld cracks. Initially the cracking was attributed to poor weld penetration and benching during the manufacturing process. However, strain gages from instrumented front frames continued to indicate high stresses in a 4500 Hz natural frequency panel mode. Stiffeners and material changes were employed to break up the panel mode and provide additional strength margin. Subsequent flight testing at Edwards AFB, CA with instrumented front frames and real time monitoring of strut stresses revealed no problems. During formal qualification of the F110-GE-129 jet engine at Arnold Engineering Development Center (AEDC), however, unexpected high stresses were measured on several front frame struts. Component test data from holography, SPATE, VPI, and siren tests indicated many natural frequency panel modes with very high damping Q values existed within the 32 per revolution operating range of the fan blades. Several different damping schemes were developed and tested in March-June 1990 during actual jet engine operation at AEDC in Tullahoma, TN. The viscoelastic constrained layer damper wrap resulted in excellent stress reduction and well damped modes, however, the structural adhesive failed when tested at a high aerodynamic Q condition of Mach 2, 30K altitude with anti-ice valve failed to open. The wide waffle expandable coulomb damper configuration resulted in lowering stress amplitudes, but the frequency modes continued to exhibit high Q damping values. The narrow waffle coulomb friction damper essentially had no effect at all and the stresses remained high and the frequency modes remained very sharp. The damper design utilizing pourable RTV to fill internal strut cavities demonstrated excellent damping Q characteristics and stress amplitude reduction.

[1]U. S. Air Force, Propulsion SPO, ASD/YZEE, Wright-Patterson AFB, OH 45433, (513) 255-2596

Other damping designs were developed but not tested during engine test cell operation. The RTV damper method was chosen as the final design after qualifying at all F-16 fighter aircraft flight envelop operating conditions and further component tests to evaluate thermal and adhesion properties. In conclusion: "A little bit of damping goes a long way."

FULL PAPER NOT AVAILABLE FOR PUBLICATION

ISOLATION JOINT FOR FLEXURAL AND COMPRESSIONAL ISOLATION

Presented by: Al Wignall
Co-Author: Jeff Aron
Company: Schlumberger

Abstract:

An isolation joint was designed for an oil well logging tool operation in a downhole environment. The joint is capable of up to 1000-lb. loads and has more than 50db of attenuation for both flexural and compressional vibration in the frequency range of 500 to 20 khz.

Schlumberger Well Service - Engineering
5000 Gulf Freeway
P.O. Box 2175
Houston, Texas 77252-2175

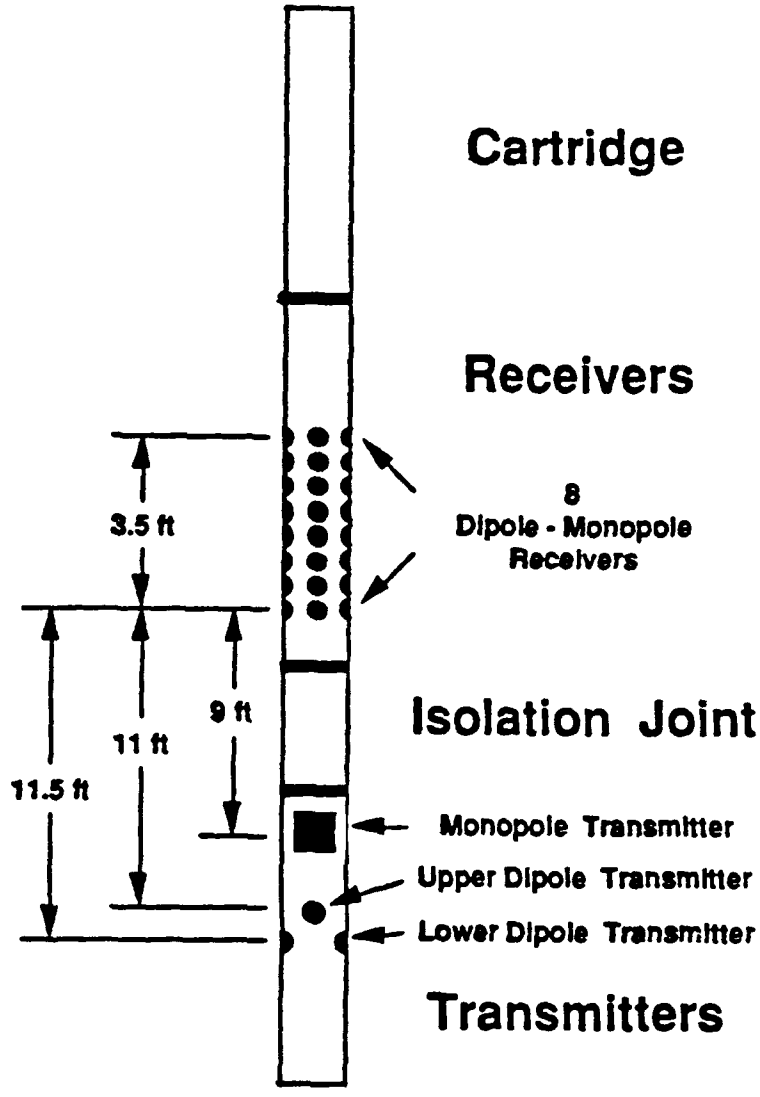

Tool Specifications

Temperature Rating	350°F (175°C)
Pressure Rating	20,000 psi (13.8 kPa)
Tool Diameter	3 5/8 in. (9.2 cm)
Tool Length	51 ft. (15.5 m)
Maximum Logging Speed	1800 ft/hr for a 8-Waveform set
Digitizer Precision	12 bits
Digitizer Sampling Interval Limits	10 µS - 32.2 mS/sample
Digitized Wave Duration Limits	15,000 samples/all waveforms
Acoustic Bandwidth	80 Hz - 5 kHz - Dipole and Stoneley 8 kHz - 30 kHz - High Frequency Monopole

FIGURE 1

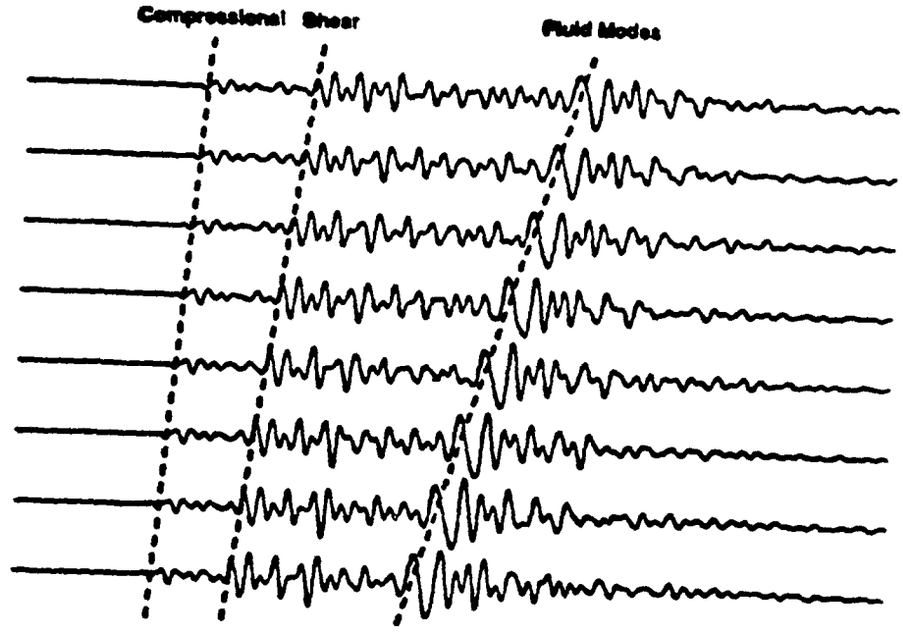

Monopole Waveforms from a Fast Formation

FIGURE 2

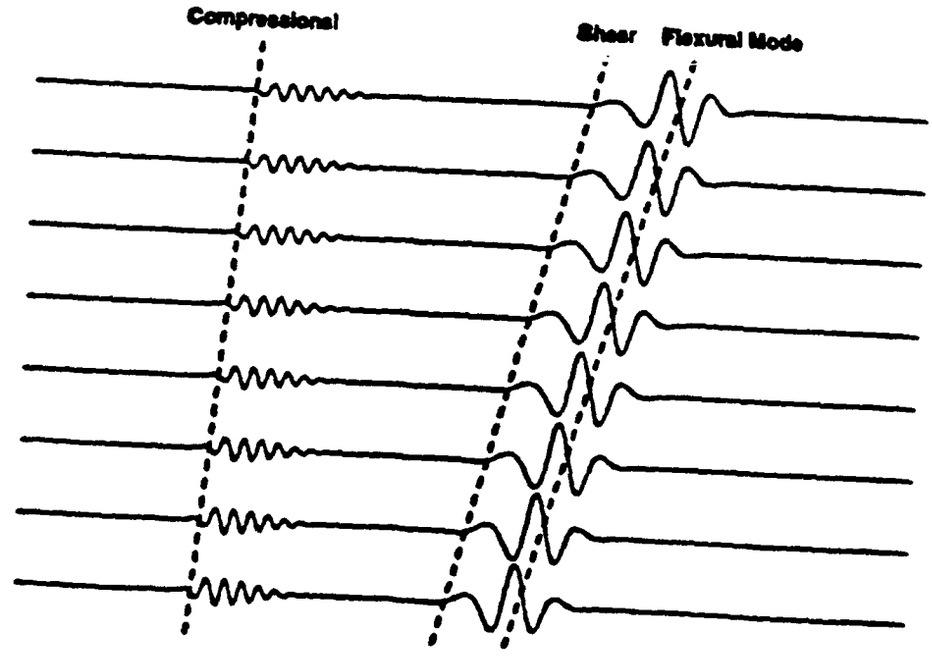

Dipole Waveforms from a Slow Formation.

FIGURE 3

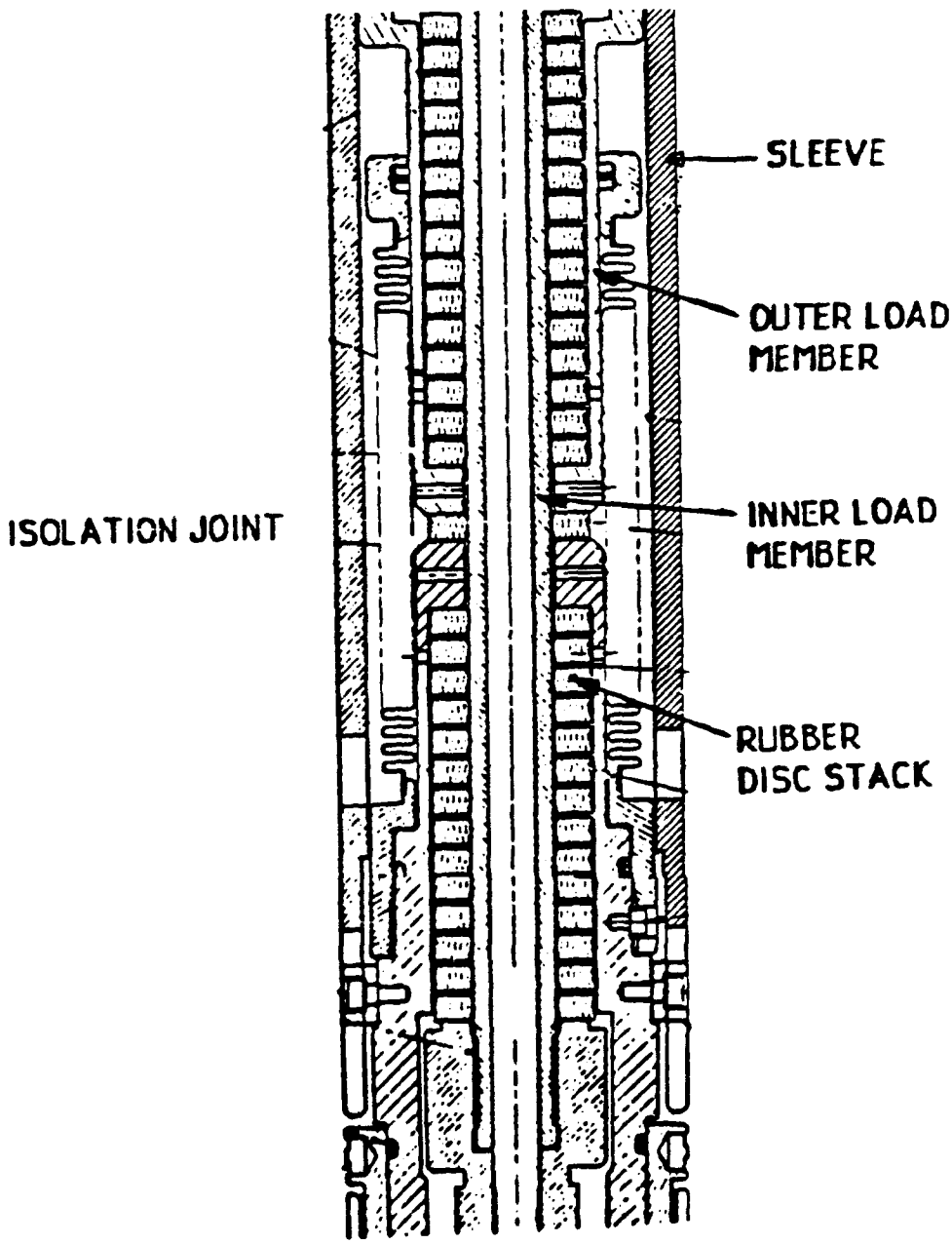
SLEEVE
OUTER LOAD MEMBER
INNER LOAD MEMBER
ISOLATION JOINT
RUBBER DISC STACK

FIGURE 4

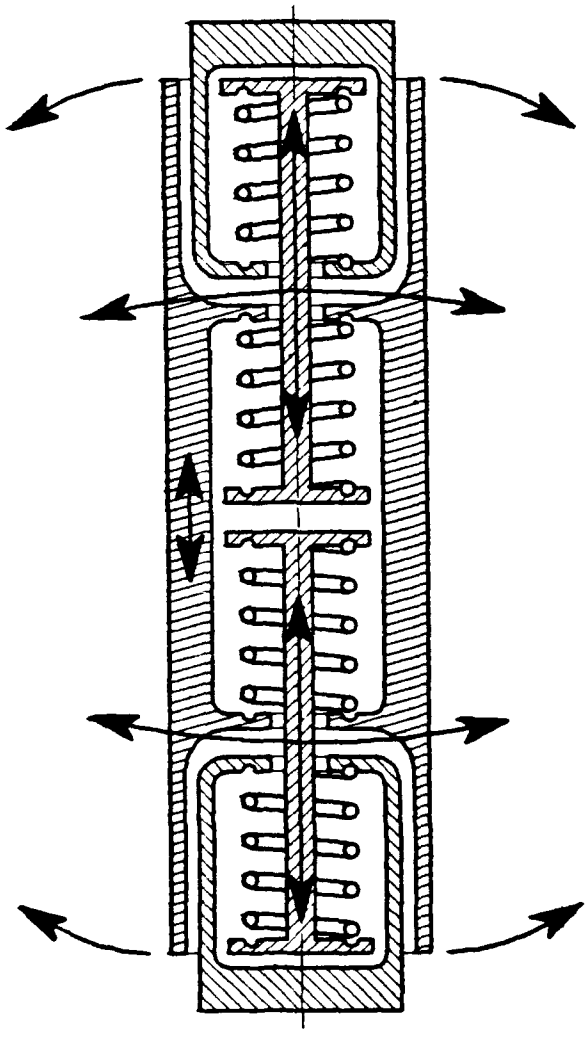

FIGURE 5

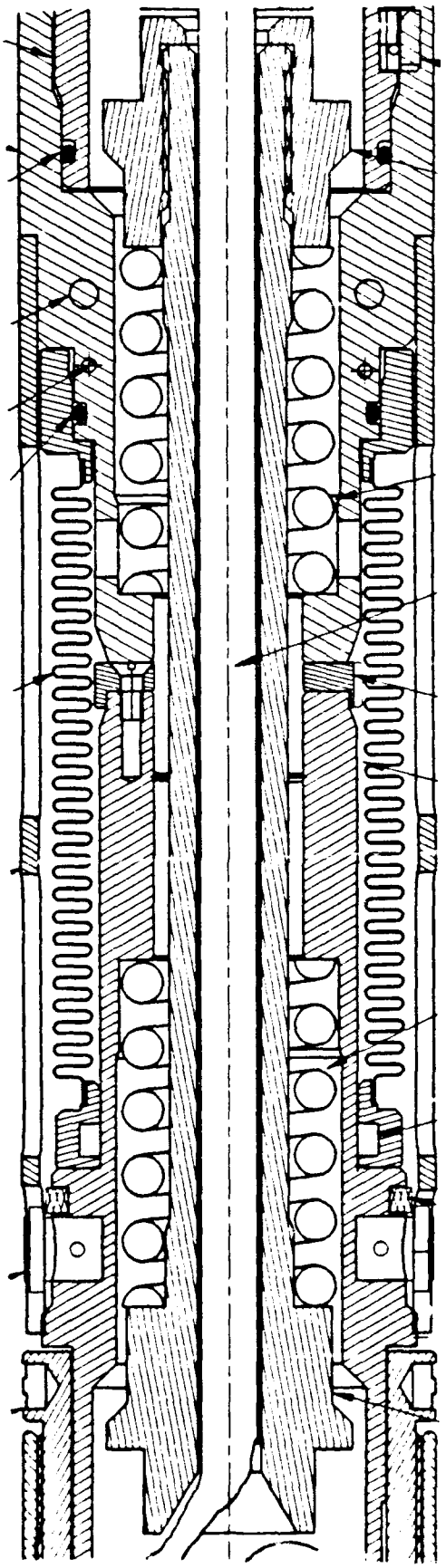

FIGURE 6

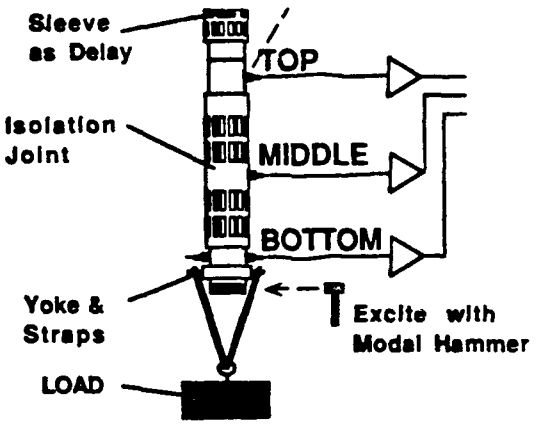
Sleeve as Delay
TOP
Isolation Joint
MIDDLE
BOTTOM
Yoke & Straps
Excite with Modal Hammer
LOAD

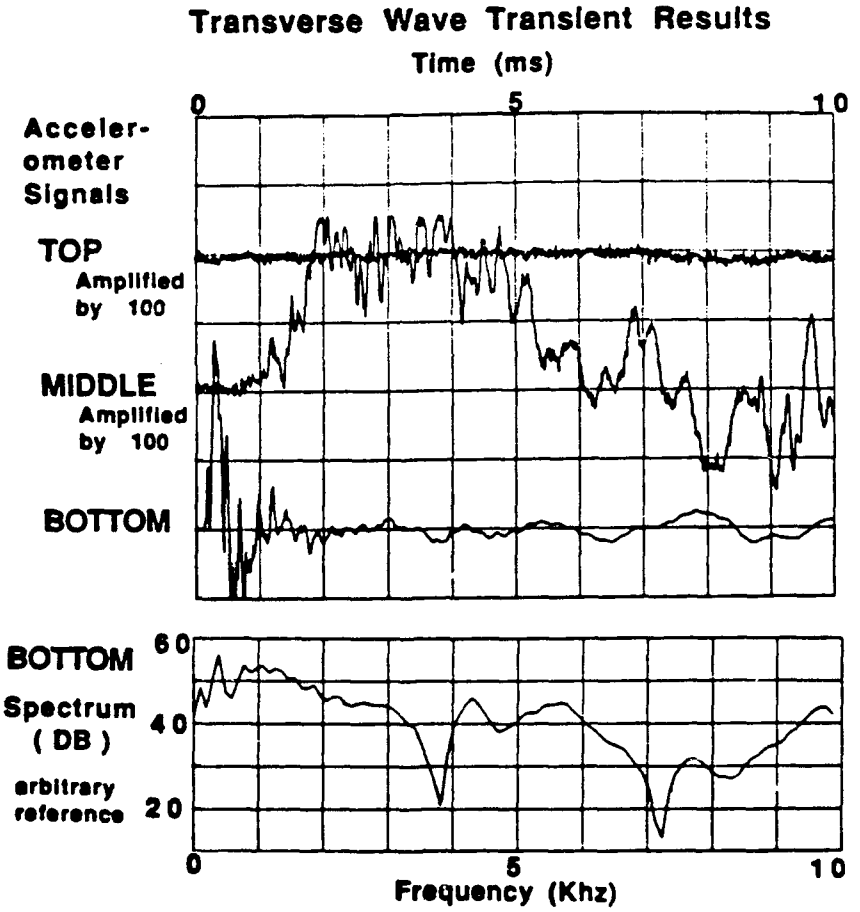
Transverse Wave Transient Results
Time (ms)
0
5
10
Acceler-ometer Signals
TOP
Amplified by 100
MIDDLE
Amplified by 100
BOTTOM
BOTTOM Spectrum (DB)
arbitrary reference
60
40
20
0
5
10
Frequency (Khz)

FIGURE 7

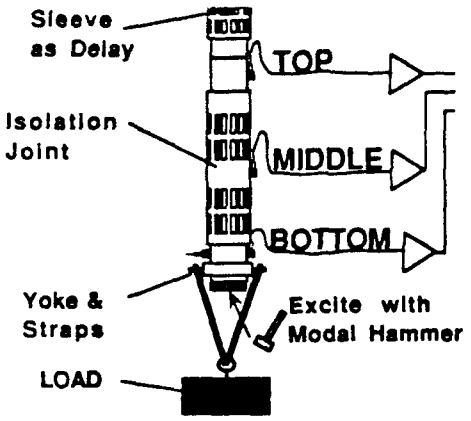
Sleeve as Delay
TOP
Isolation Joint
MIDDLE
BOTTOM
Yoke & Straps
Excite with Modal Hammer
LOAD

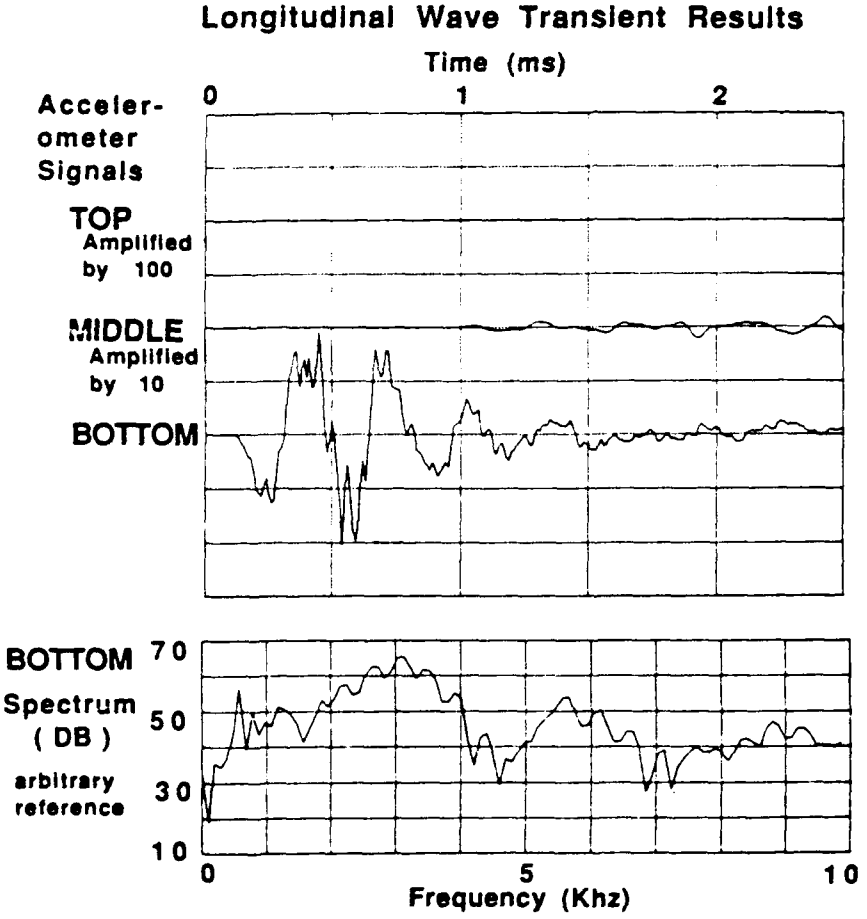
Longitudinal Wave Transient Results
Time (ms)
0
1
2
Acceler-ometer Signals
TOP
Amplified by 100
MIDDLE
Amplified by 10
BOTTOM
BOTTOM Spectrum (DB)
arbitrary reference
70
50
30
10
0
5
10
Frequency (Khz)

FIGURE 8

Characterization of Viscoelastic Damping in an Antenna Structure

James Argento
Research Assistant

Robert Carlin
Research Assistant

Ephrahim Garcia, PhD
Visiting Assistant Professor

Mechanical Systems Laboratory
State University Of New York at Buffalo
Buffalo, New York

Abstract

The dynamics of a ribbed antenna structure are examined. The symmetry of the structure generates repeated natural frequencies and hence a "beating" phenomena in the dynamic response of the structure. Two of the antenna's ribs are replaced with passively damped ribs which are treated with a constrained viscoelastic material. Since these repeated natural frequencies cannot be identified using standard frequency domain techniques, a time domain metod, the Eigensytem Realization Algorithm (ERA), is employed to measure damping in the repeated and closely spaced natural frequencies. A comparison is made between ERA and the Polyreference identified modal parameters. Consideration is given to a slight structural modification to increase the ineraction between the damped and undamped antenna ribs, thereby increasing the overall performance of the viscoelastic damping in each mode.

Characterization of Viscoelastic Damping in a Ribbed Antenna Structure

James Argento
Research Assistant

Ephrahim Garcia, PhD.
Visiting Assistant Professor

Robert A. Carlin
Research Assistant

Mechanical Systems Laboratory
State University of New York at Buffalo
Buffalo, New York

Antenna Model Schematic

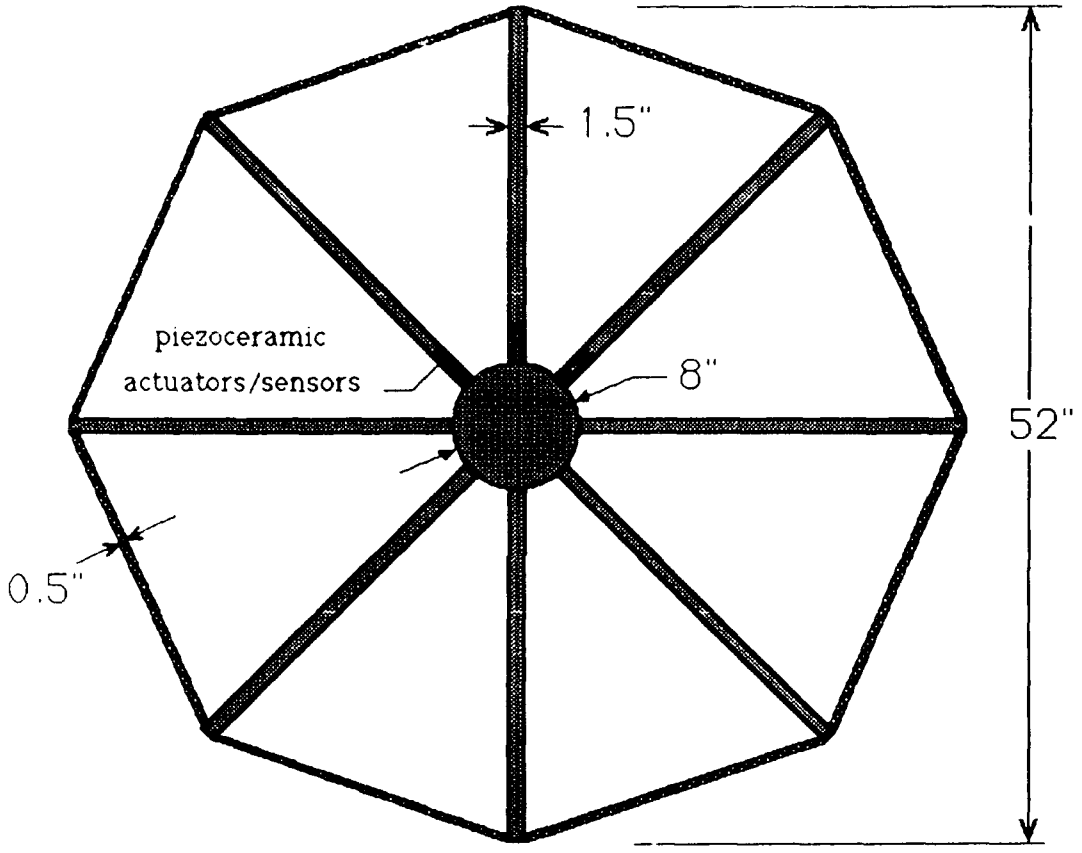

- lightweight, flexible aluminum structure
- modelled after CSI Evolutionary model, built by NASA
- why piezoceramics?
  - lightweight - negligible added mass
  - dual capabilities: actuator and sensor

Piezoceramic film elements

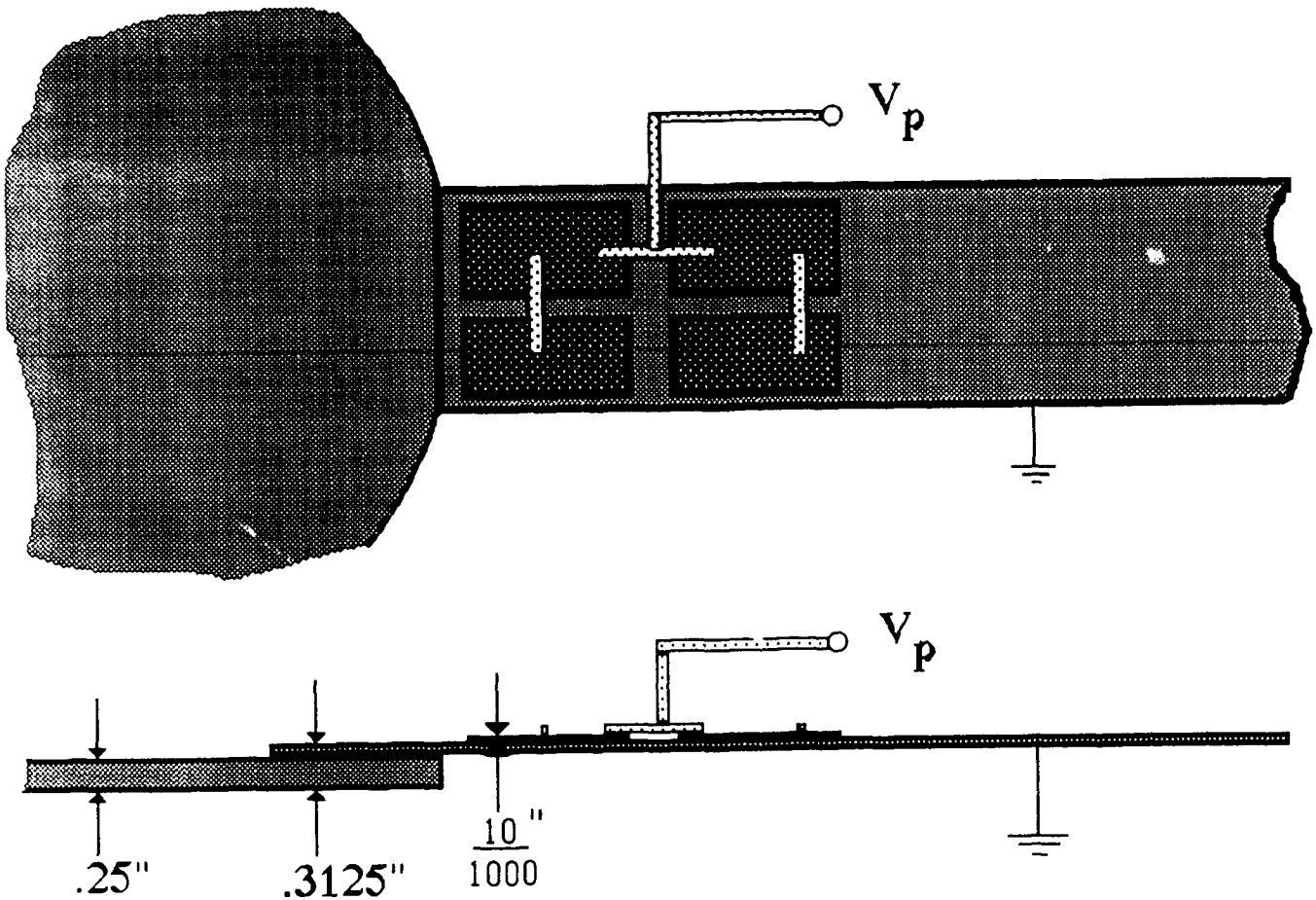

- as a sensor: strain-induced voltage as output
- as an actuator: voltage-induced strain as input

Polyreference and Analytical Modal Parameters

• Comparison of the undamped antenna model and the Polyrefence identified frequencies.

Frequency (Hz)

FEM	Polyreference
3.093	
3.314*	3.314
	3.559
4.443*	4.277
	5.595
6.686*	6.613
	7.619
8.511	8.243
	18.45
	19.16
	20.51
	21.52
22.84	22.18
23.11	22.54

* denotes repeated natural frequencies

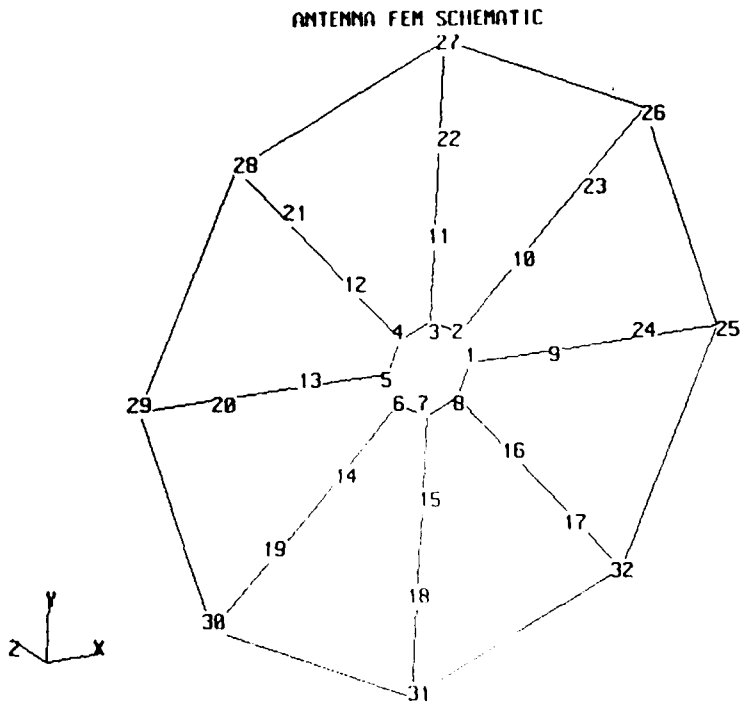

•exact symmetry of FEM yields repeated natural frequencies and orthogonal mode shapes

•inaccuracies in physical model yield closely spaced natural frequencies

Experimentally Verified Mode Shapes

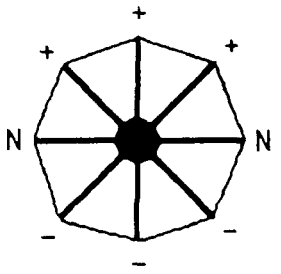

$\omega_1 = 3.3$Hz

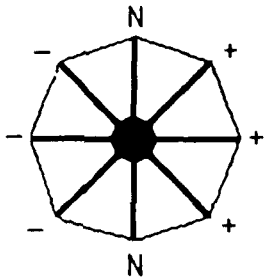

$\omega_2 = 3.3$Hz

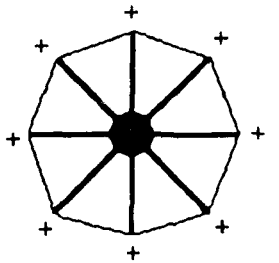

$\omega_3 = 3.6$Hz

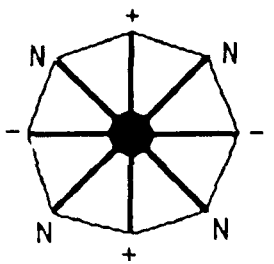

$\omega_4 = 4.3$Hz

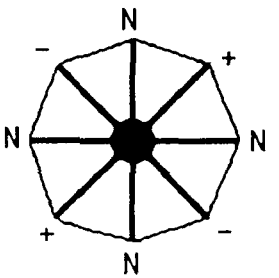

$\omega_5 = 4.3$Hz

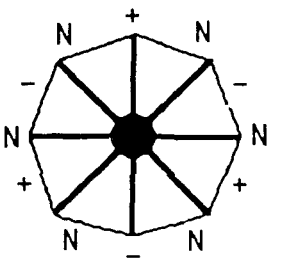

$\omega_6 = 6.5$Hz

- mode shapes exhibited by both the FEM and physical model
- symmetry yields orthogonal mode shapes and closely spaced natural frequencies

Multiple Layered Damped Antenna Rib

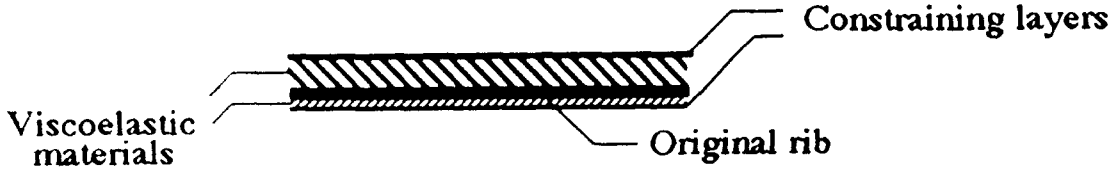

- Scotchdamp (SJ-2015X, 112) for high frequency damping
- rubber for low frequency damping

- single rib, undamped

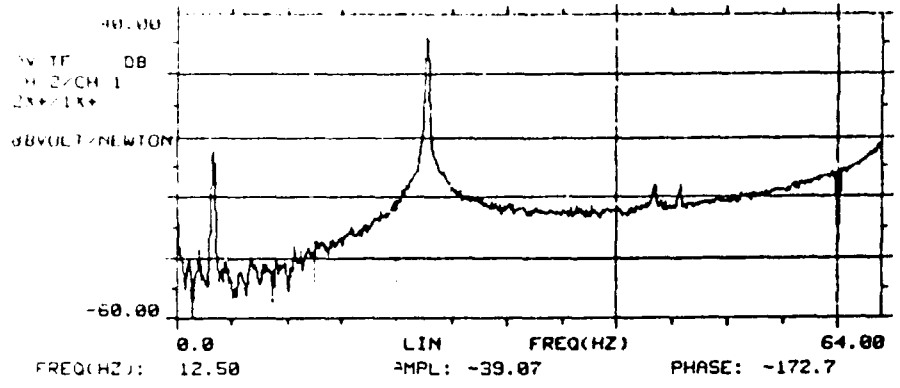

- rib w/ rubber as constraining layer

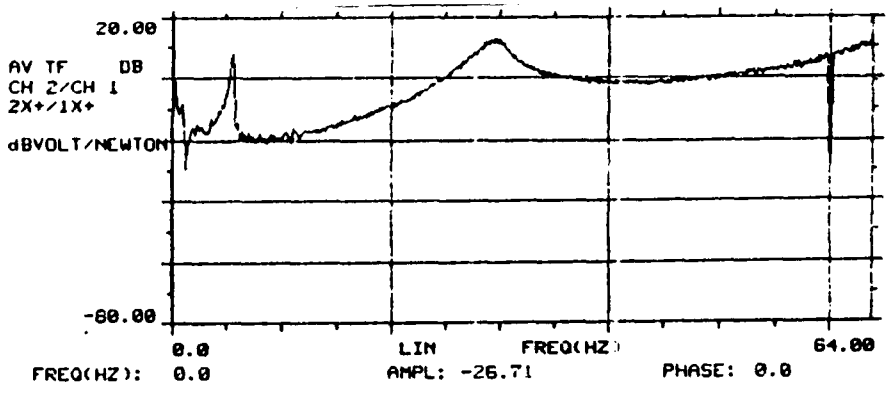

- rib w/ rubber and Scotchdamp

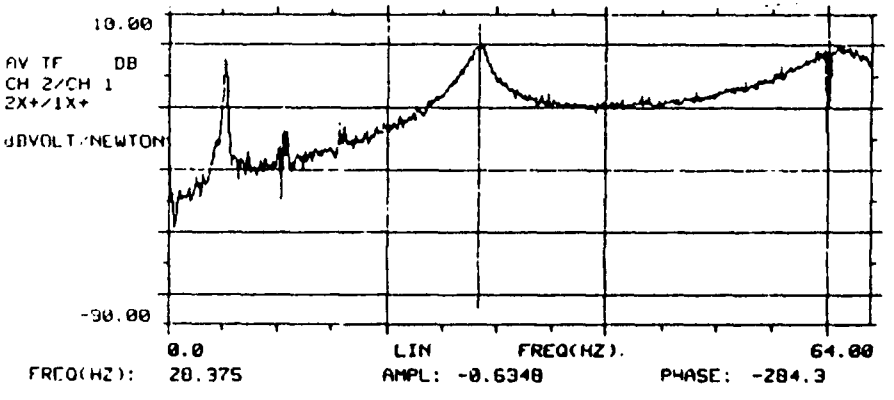

Polyreference Identified Modal Parameters

Frequency (Hz)		Damping ratio ζ (% critical)		Percent increase in ζ
Undamped	Damped	Undamped	Damped	
3.41				
4.27	4.53	0.0029	0.0067	131.
5.60	5.51	0.0018	0.0064	256.
6.61	6.94	0.0005	0.0104	1980.
7.62	7.84	0.0010	0.0042	320.
8.51		0.0013	>>	>>
18.44	18.93	0.0023	0.0031	35.8
20.51		0.0010	>>	>>
21.53	22.04	0.0016	0.0034	113.
22.18	22.38	0.0014	0.0016	14.3
22.53	22.85	0.0018	0.0023	27.8
24.30	23.65	0.0009	0.0039	333.
25.10	25.54	0.0014	0.0023	64.3
25.87		0.0014	>>	>>
27.15	26.81	0.0015	0.0018	20.0
30.17		0.0019	>>	>>
33.86	35.27	0.0011	>>	>>
37.00	37.63	0.0016	0.0060	275.
43.94	41.94	0.0013	0.0067	415.

- Effects of structure modification: two damped rib elements
  - frequency shift due to added mass
  - significant increase in global damping
  - some highly damped modes poorly identified - denoted by ">>"

Frequency Response Functions for Undamped(top) and Damped (bottom) Antenna,0-64 Hz

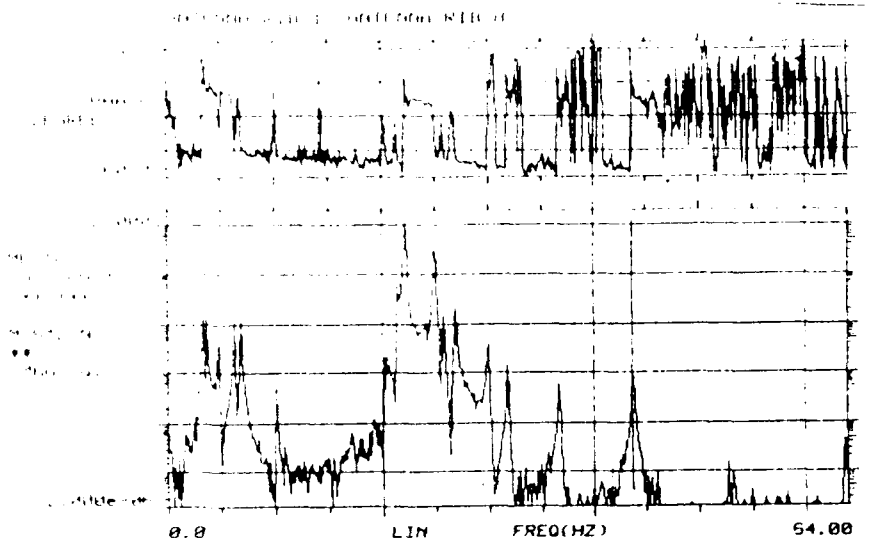

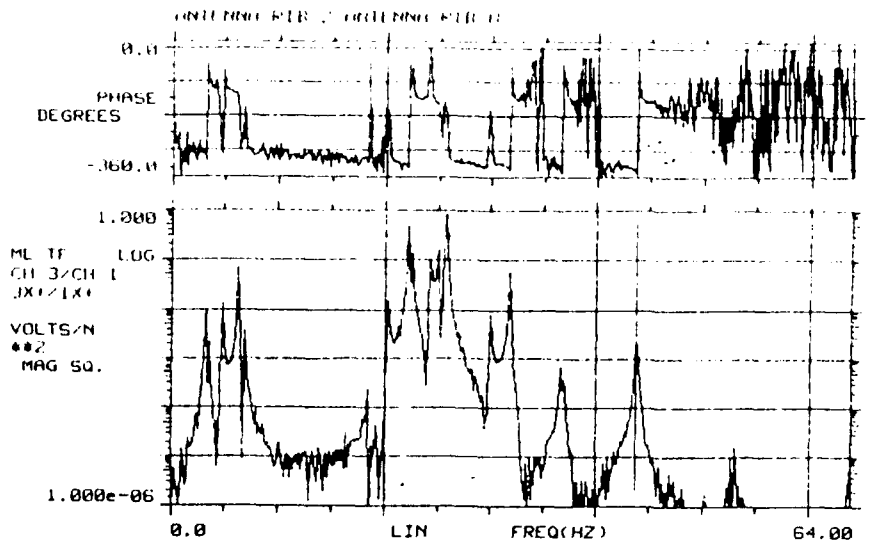

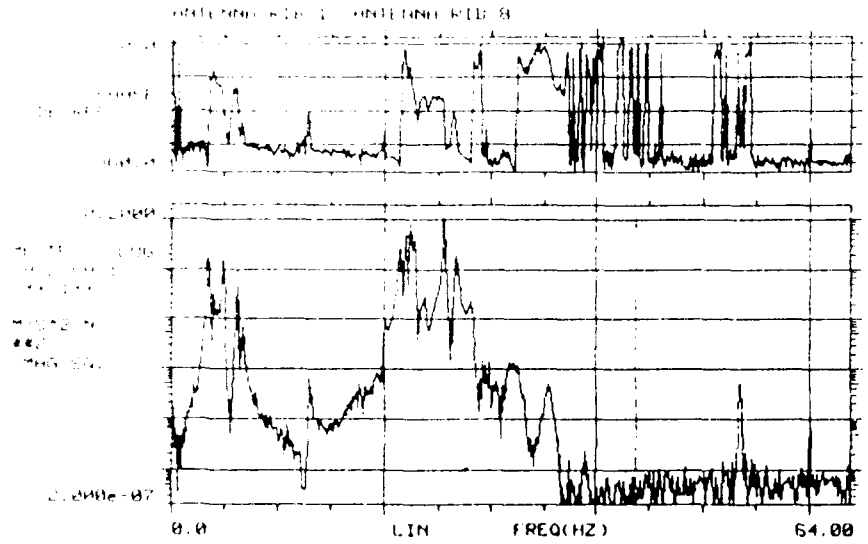

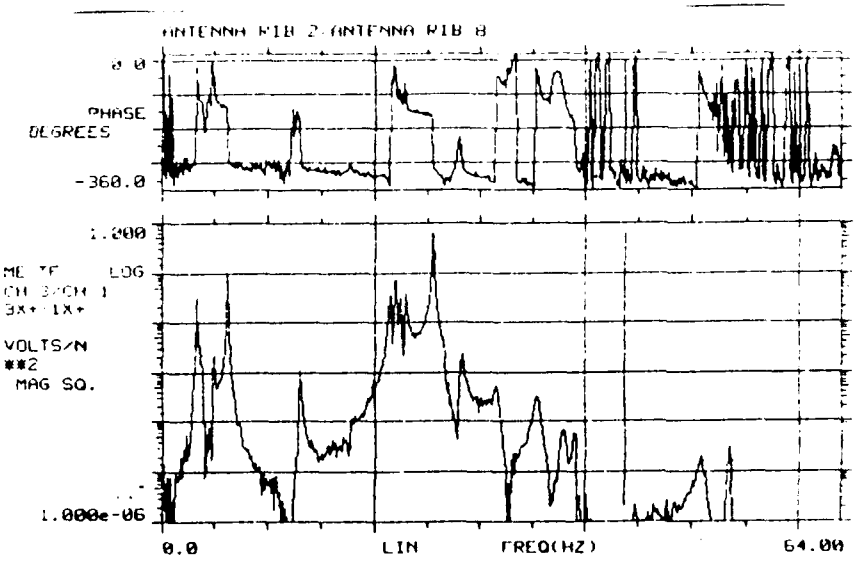

Polyreference-derived Analytical Curve Fits for Undamped (top) and Damped (bottom) Antennas, 24 - 40 Hz

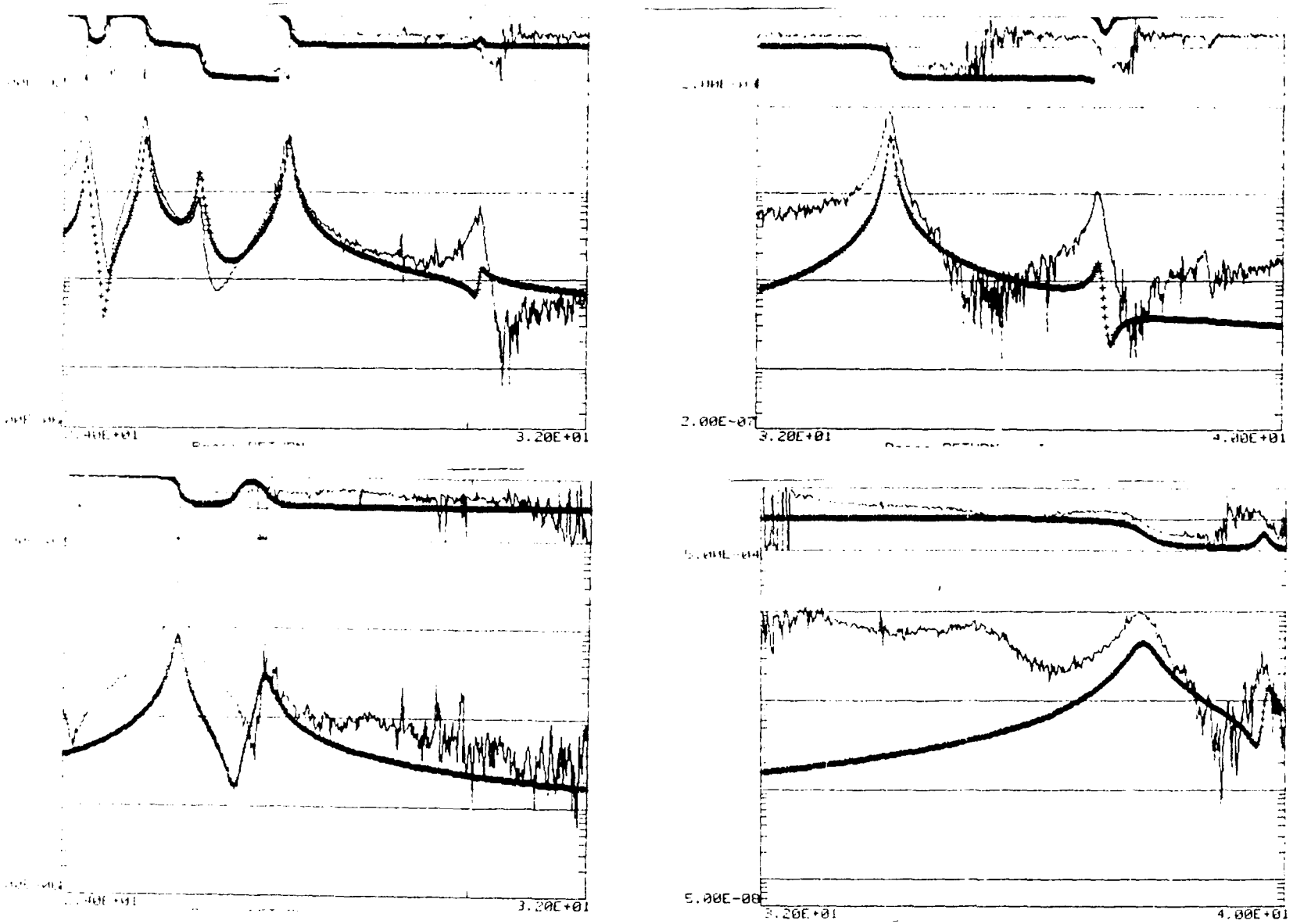

ERA Summary (Juang and Pappa, 1985)

• Impulse Response function → Markov Parameters

[Y(k) Y(k+1) Y(k+2) ...] - time histories

• Form a Block Data (Hankel) Matrix

$$H_{mn}(k) = \begin{bmatrix} CA^kB & CA^{k+1}B & \dots & CA^{k+n}B \\ CA^{k+1}B & CA^{k+2}B & \dots & \\ \vdots & & & \vdots \\ CA^{k+m}B & CA^{k+m+1}B & \dots & CA^{k+m+n}B \end{bmatrix}$$

- time domain data

• Singular Values from the SVD of the Hankel matrix are used to determine a "good" model order and a minimum order realization.

$$H_{mn}(k) = PDQ^T ; \quad D = \text{diag}[\sigma_1, \sigma_2, \dots, \sigma_n]$$

• The Eigensystem Realization Algorithm (ERA) finds a triple [A, B, C] based on the experimental data in $H_{mn}(k)$, i.e.,

$$Y(k+1) = CA^kB$$
$$= E_p^T P D^{1/2} [\, D^{-1/2} P^T H_{mn}(1) Q D^{-1/2} \,]^k D^{-1/2} Q^T E_m$$

• Eigenanalysis of the realization yields modal parameters for the system - $\{\zeta_i, \omega_i, MCF_i \text{ and } \phi_i(x)\}$.

- Typical ERA run:

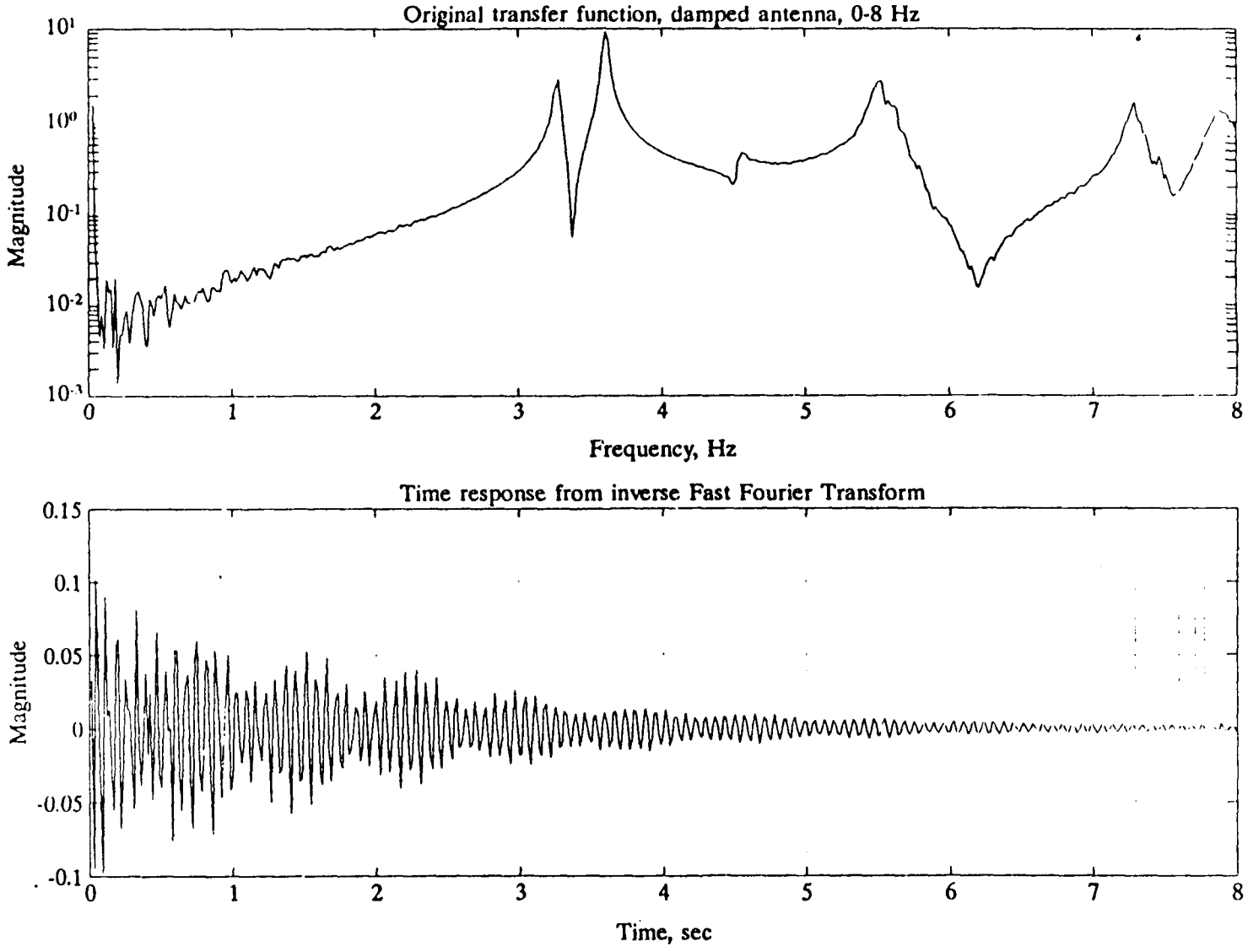

Modal Parameters: Polyreference and ERA

• Undamped, 0-8 Hz

Frequency (Hz)		Damping ratio ζ		Modal confidence factor	
Polyref.	ERA	Polyref.	ERA	Polyref.	ERA
3.31	3.31	0.011	0.003	0.912	1.000
--	3.41	--	0.002	--	1.000
3.56	3.57	0.006	0.003	0.948	1.000
4.28	4.27	0.003	0.003	0.993	1.000
5.60	5.57	0.002	0.003	0.993	1.000
6.61	6.61	0.000	0.002	0.985	1.000
7.62	7.62	0.001	0.002	0.993	1.000

•Damped, 0-8 Hz

Frequency (Hz)		Damping ratio ζ		Modal confidence factor	
Polyref.	ERA	Polyref.	ERA	Polyref.	ERA
3.26	3.27	0.003	0.006	0.995	1.000
3.60	3.60	0.003	0.006	0.999	1.000
4.53	4.54	0.007	0.019	0.993	0.932
5.52	5.51	0.006	0.007	0.996	1.000
5.73	5.69	0.000	0.011	0.973	0.979
6.94	--	0.010	--	0.834	--
7.29	7.29	0.006	0.005	0.997	1.000
7.84	7.85	0.004	0.010	0.995	0.999

- inverse Fourier transform on frequency domain data (ERA) allows comparison with time domain data (Polyreference)
- good agreement between the two methods
- modal confidence factor: ratio from 0 to 1 describing accuracy of results obtained
  - generally higher mcf's for ERA method

Closing Remarks

- Successfully applied two identification schemes to examine the effects of constrained layered damping in a model of a complex, ribbed antenna structure

- Since global modes are a sum of simpler substructure modes, "high" damping must be obtained in those fundamental modes of the substructure in order to achieve "high" damping in the global modes. The substructure modes in this structure are that of a cantilever beam. The global modes are combinations of these simpler modes.

- Viscoelastic antenna ribs improved the dynamic response slightly in the lower modes and significantly in the higher modes

LAMINAR BLADE DAMPER

Michael Koleda
15 Murray Avenue
Port Washington, NY 11050
(516) 767-2174

ABSTRACT

This device consists of multiple layers of graphite-epoxy sheets separated from each other by a film of silicone grease. The sheets are interleaved and fastened to a structure in such a way as to permit sliding motion between alternate sheets as the structure bends. Damping results as this sliding motion is resisted by the viscosity of the silicone grease.

1. Introduction

A discrete flexible vibration damping unit to co-extend with a vibratile product for sensing and damping vibrations of said product, the unit including, a framework portion means and means including, a laminar group of flexible strip members of the framework having opposed side faces directly confronting one another interiorly of the group, with there being a flexible first strip member in the group, and the laminar group and framework portion means having portions of the framework interconnected in the framework through the flexible first strip member in the group and the framework portions to be secured to the vibratile product with the unit co-extending with the product side facially of the framework toward the product, for the flexible strip members in the group to be flexed from side to side and longitudinally relatively move with reference to one another having said all other of the flexible strip members in the group remain connected with the flexible first strip member and longitudinally movably free-ended, when the group is flexed between the framework portions, and a tacky visco-elastic substance longitudinally reaching between the opposed side faces all of the flexible strip members in the group about as far as the opposed side faces of one and next of the flexible strip members in the group longitudinally co-extend directly opposing one another, and the tacky visco-elastic substance directly visco-elastically interengaging the opposed side faces with one another in the group, for the unit to have the flexible strip members in the group, flex from side to side and be retarded in the relative longitudinal movements thereof by the tacky viscoelastic substance when the flexible unit is on the vibratile product co-extending with the product side facially of the framework portions secured to the product and the unit is responding to vibrations of the product by flexing between the framework portions, with all other of the flexible strip members in the group remaining connected with the flexible first strip member in the group and longitudinally movably free-ended.

Flat-wise, edge-wise and end-to-end damping is achieved with three dimensional vibration absorbing system, adding little stiffness and small frequency change to the product.

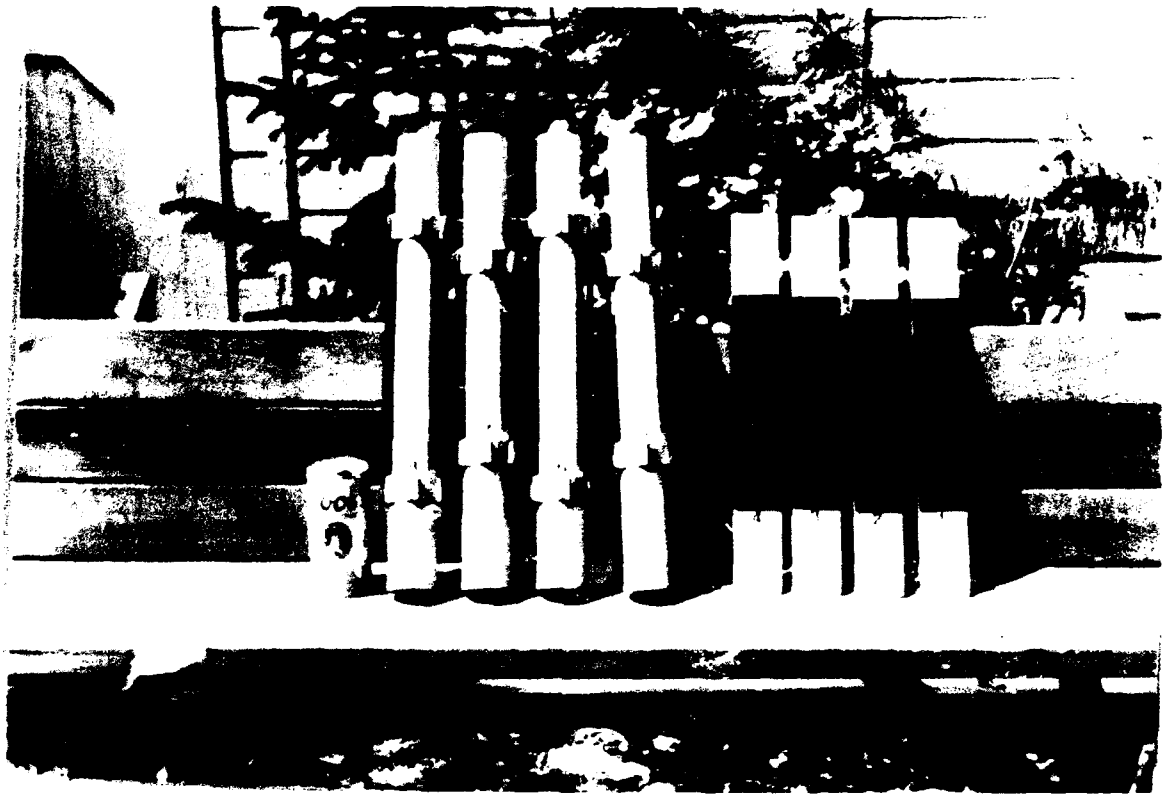

Figure 1. Two damper units fixed to segment clamps, secured to tubular specimens.

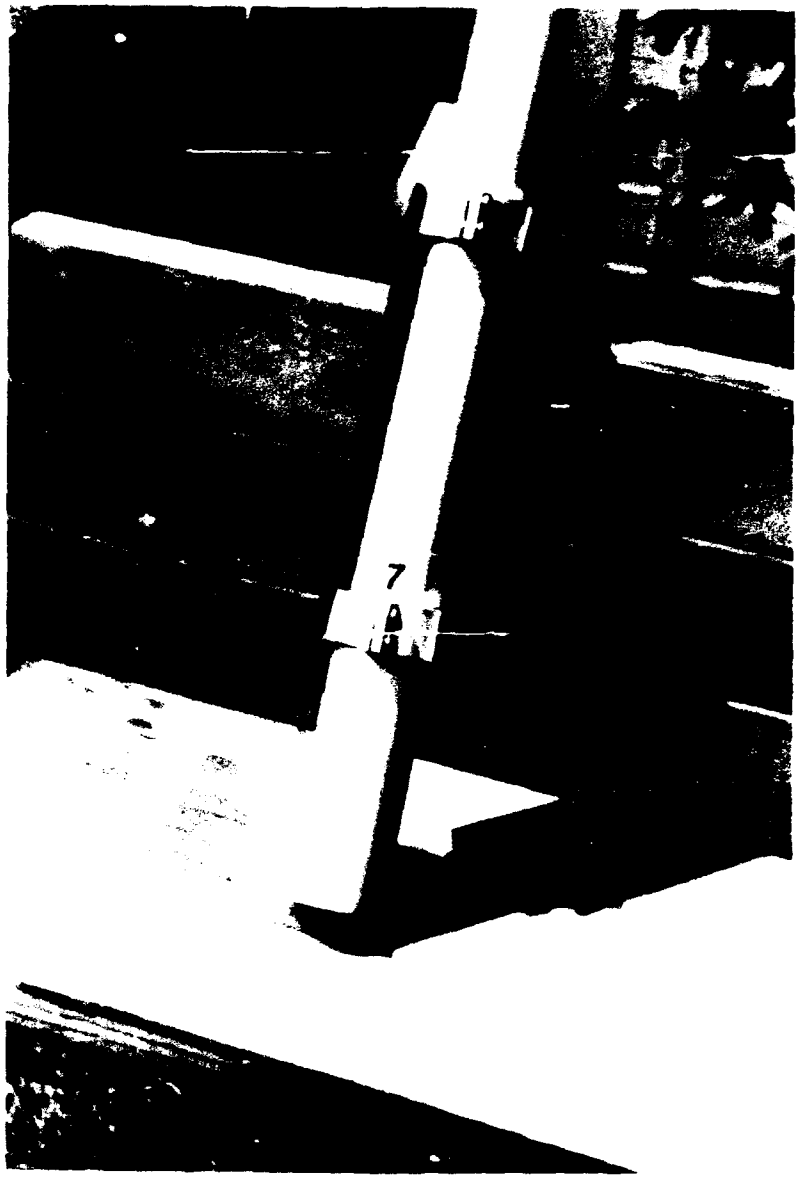

Figure 2. Two damper strips bonded to segment clamps, fixed to tubular specimen.

2. First Analytic Summary

The following seven pages indicate a damping factor of eight times.

The damper unit is 1/8 inch thick
2 inches wide
11 inches long
weight 1 and 1/2 ounce

The damper unit is bonded to "E" glass specimen 1/4 inch thick
2 inches wide
16 inches long

The specimen is clamped to a shaker table, the opposite end is weighted for these tests.

The next five pages are with damper, the two following are without damper.

TEST SETUP-ID: FLEX TEST RUN NAME: RUN2 autosave 01/10/90 10:22:46

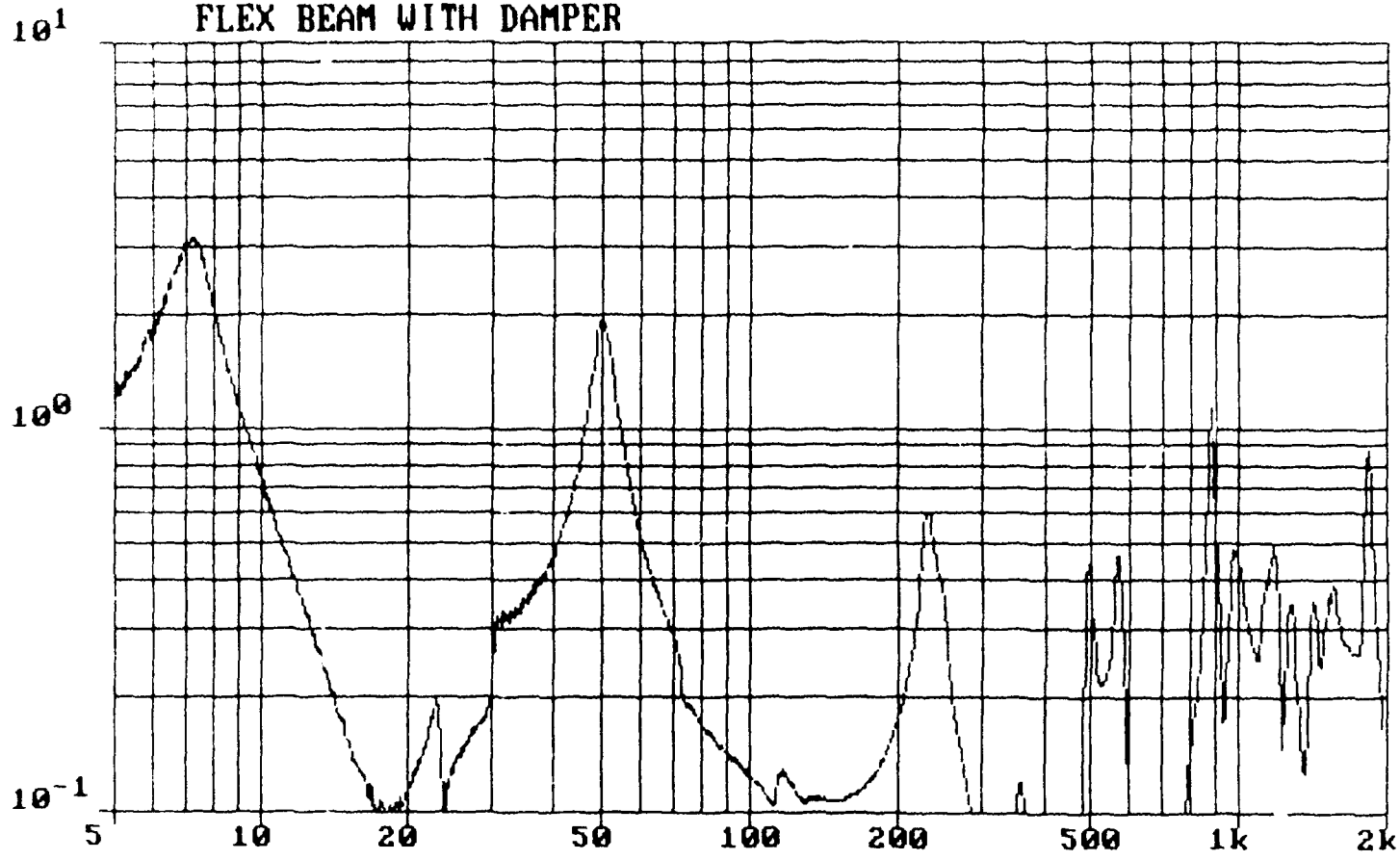

DISPLAY
C-CTRL
2-CH2
D-DRIVE
^2-2/CT
FREQ=
1998.3
CH2/CON=
0.148

REF LEV=
20.72 g
CONSTANT
ACC
LOG SWP#
1 up
of 1

10 mv/g AUTO : 00:02:52 STATUS: Finished
MAX SERV SPD 1k TOTAL: 00:03:00 SWEEP TIME: 2.9 Min CHAN 1

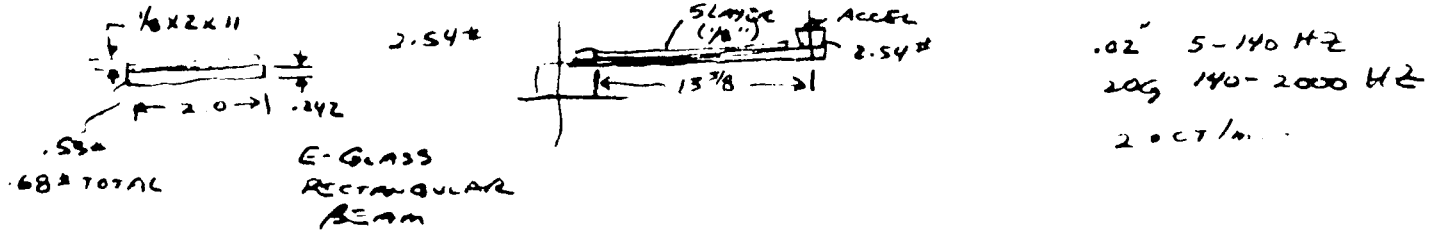

2

TEST SETUP-ID: FLEX TEST RUN NAME: RUN3 autosave 01/10/90 10:28:17

FLEX BEAM WITH DAMPER

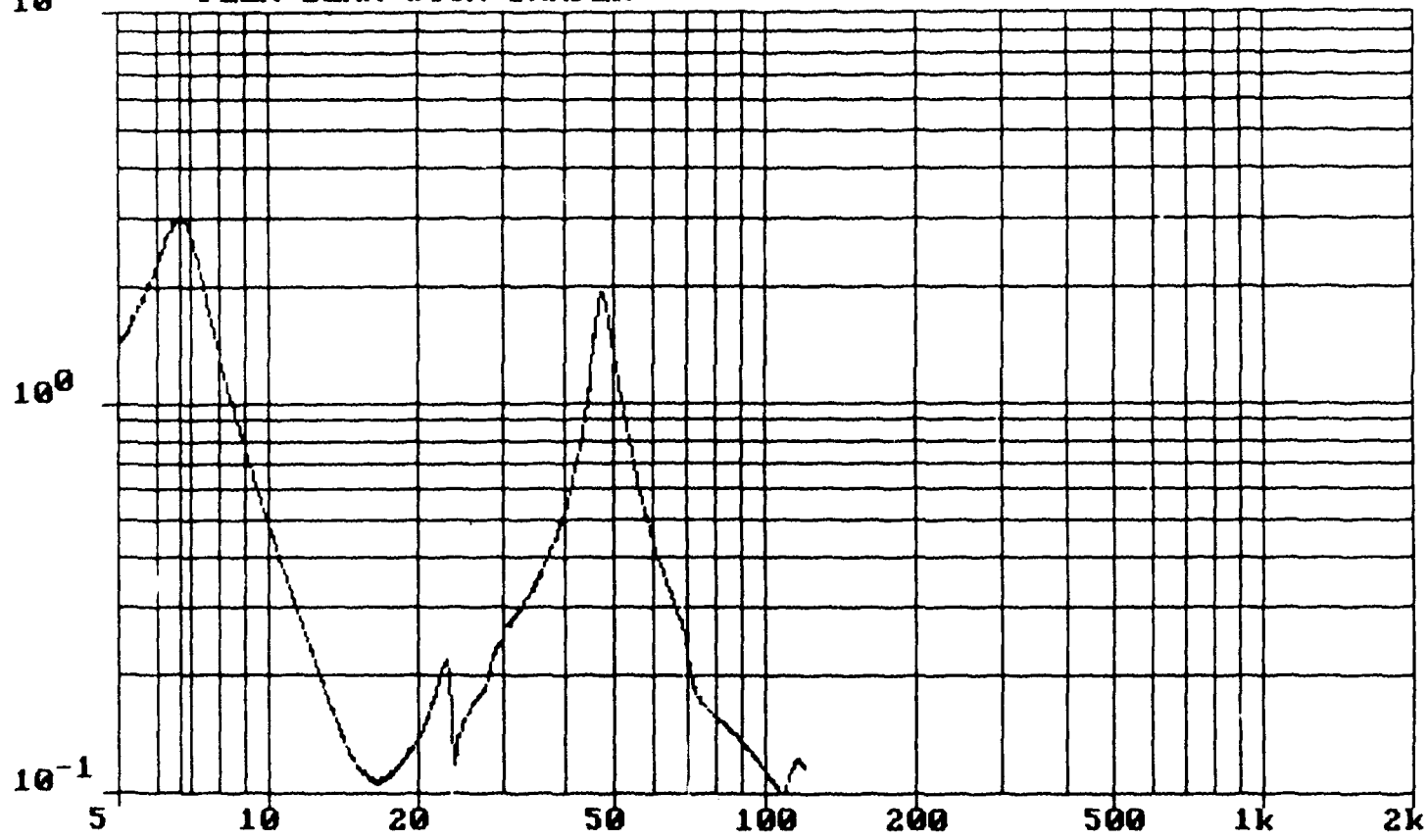

DISPLAY
C-CTRL
2-CH2
D-DRIVE
^2-2/CT
FREQ=
6.7
CH2/CON=
2.988

REF LEV=
100 mil
CONSTANT
DISP
LOG SWP#
1 up
of 1

10 mv/g AUTO : 00:01:31 STATUS: Abort - F1 pressed

MAX SERV SPD 1k TOTAL: 00:01:41 SWEEP TIME: 2.9 Min CHAN 1

.10 DA 5-63 HZ

20G 63 -

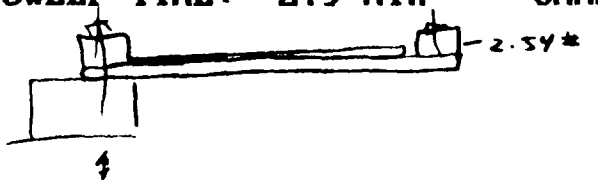

3 oct /min.

4

3

TEST SETUP-ID: FLEX TEST RUN NAME: RUN3 autosave 01/10/90 10:34:55

FLEX BEAM WITH DAMPER

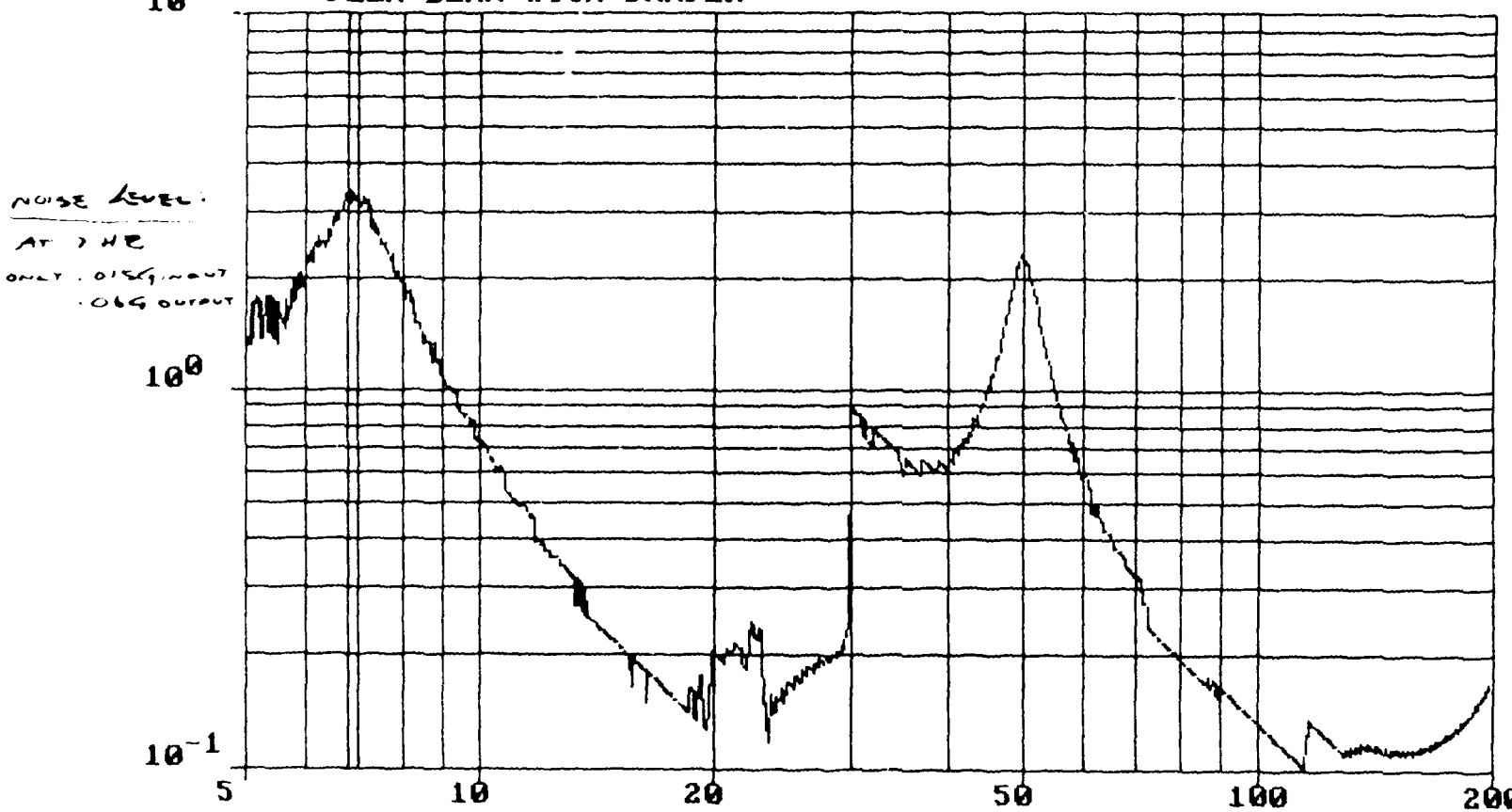

NOISE LEVEL:
AT > HZ
ONLY . 01 SIGNAL OUT
. 06 G OUTPUT

DISPLAY
C-CTRL
2-CH2
D-DRIVE
^2-2/CT
FREQ=
6.8
CH2/CON=
3.333

REF LEV=
6.00 mil
CONSTANT
DISP
LOG SWP#
1 up
of 1

10 mv/g AUTO : 00:02:52 STATUS: Finished
MAX SERV SPD 1k TOTAL: 00:02:54 SWEEP TIME: 2.9 Min CHAN 1

.006 DA - 5-250 HZ
20 G -

3 oct/min

#4

TEST SETUP-ID: FLEX TEST RUN NAME: RUN4 autosave 01/10/90 10:41:27

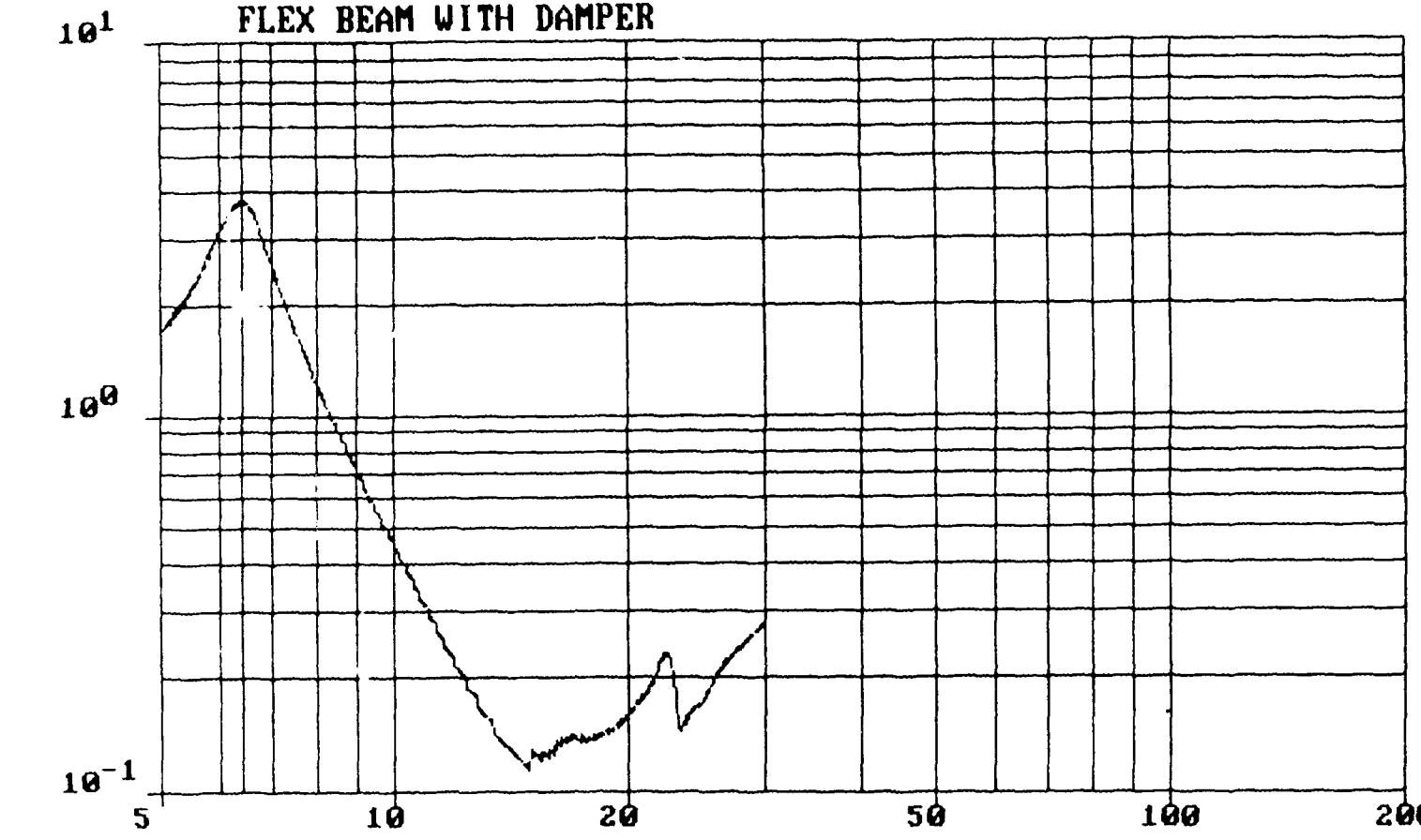

DISPLAY
C-CTRL
2-CH2
D-DRIVE
^2-2/CT
FREQ=
6.4
CH2/CON=
3.770

REF LEV=
300 mil
CONSTANT
DISP
LOG SWP#
1 up
of 1

10 mv/g AUTO : 00:01:24 STATUS: Abort 177.8 mil
MAX SERV SPD 1k TOTAL: 00:01:36 SWEEP TIME: 2.9 Min CHAN 1

.3" DA 5 - 36
20G 36 -

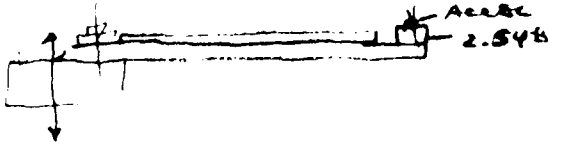

1.8 oct/min

#5

TEST SETUP-ID: FLEX TEST RUN NAME: RUN5 autosave 01/10/90 10:48:53

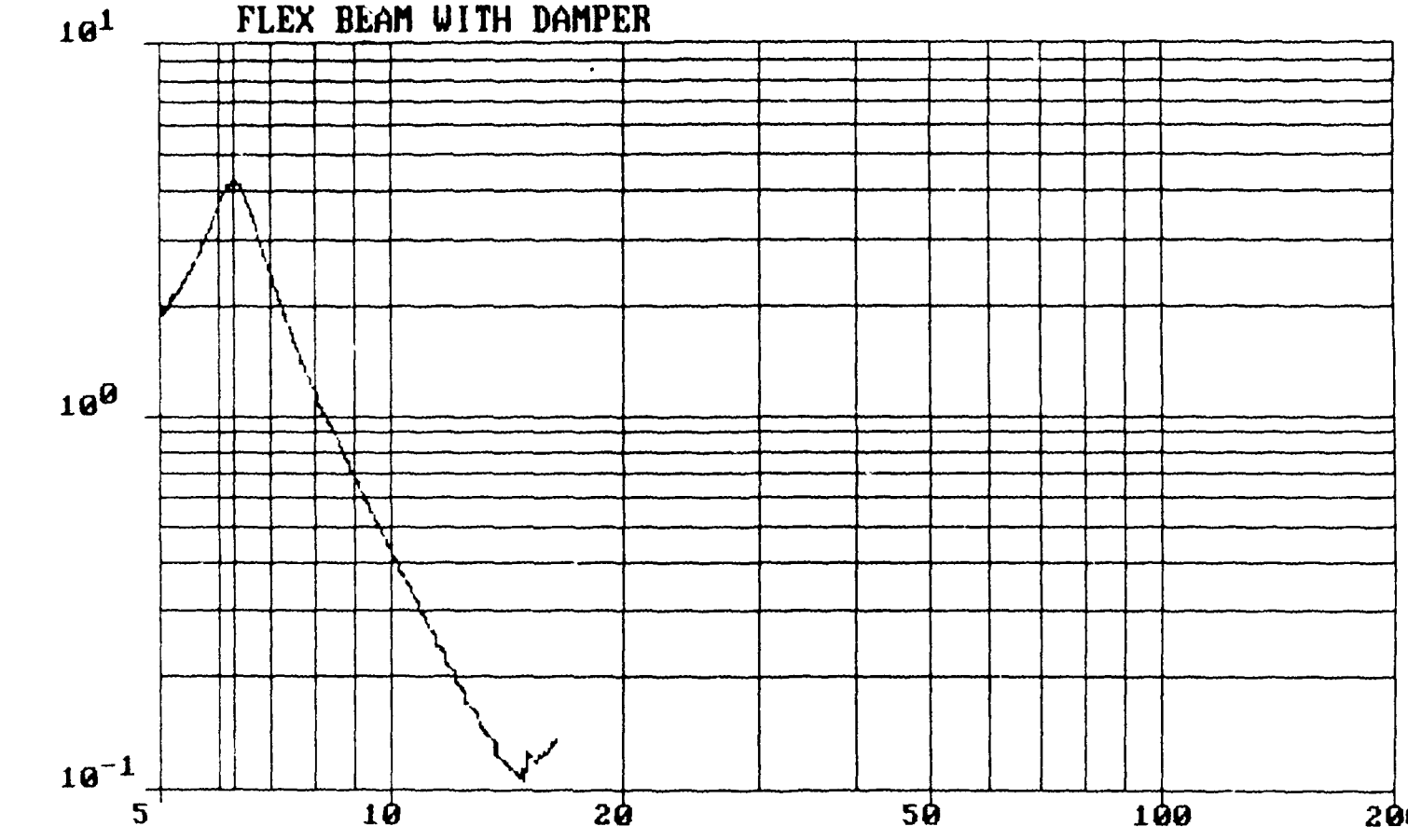

DISPLAY
C-CTRL
2-CH2
D-DRIVE
^2-2/CT
FREQ=
6.2
CH2/CON=
4.225

REF LEV=
300 mil
CONSTANT
DISP
LOG SWP#
1 up
of 1

10 mv/g AUTO : 00:03:27 STATUS: Abort - F1 pressed
MAX SERV SPD 1k TOTAL: 00:03:39 SWEEP TIME: 10.6 Min CHAN 1

.30" DA 5-36 HZ
.5 oct/min

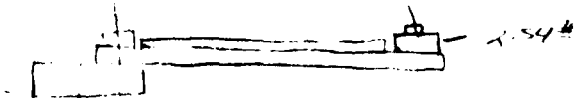

[illegible]

#6

TEST SETUP-ID: FLEX TEST RUN NAME: RUN5 autosave 01/10/90 11:01:36

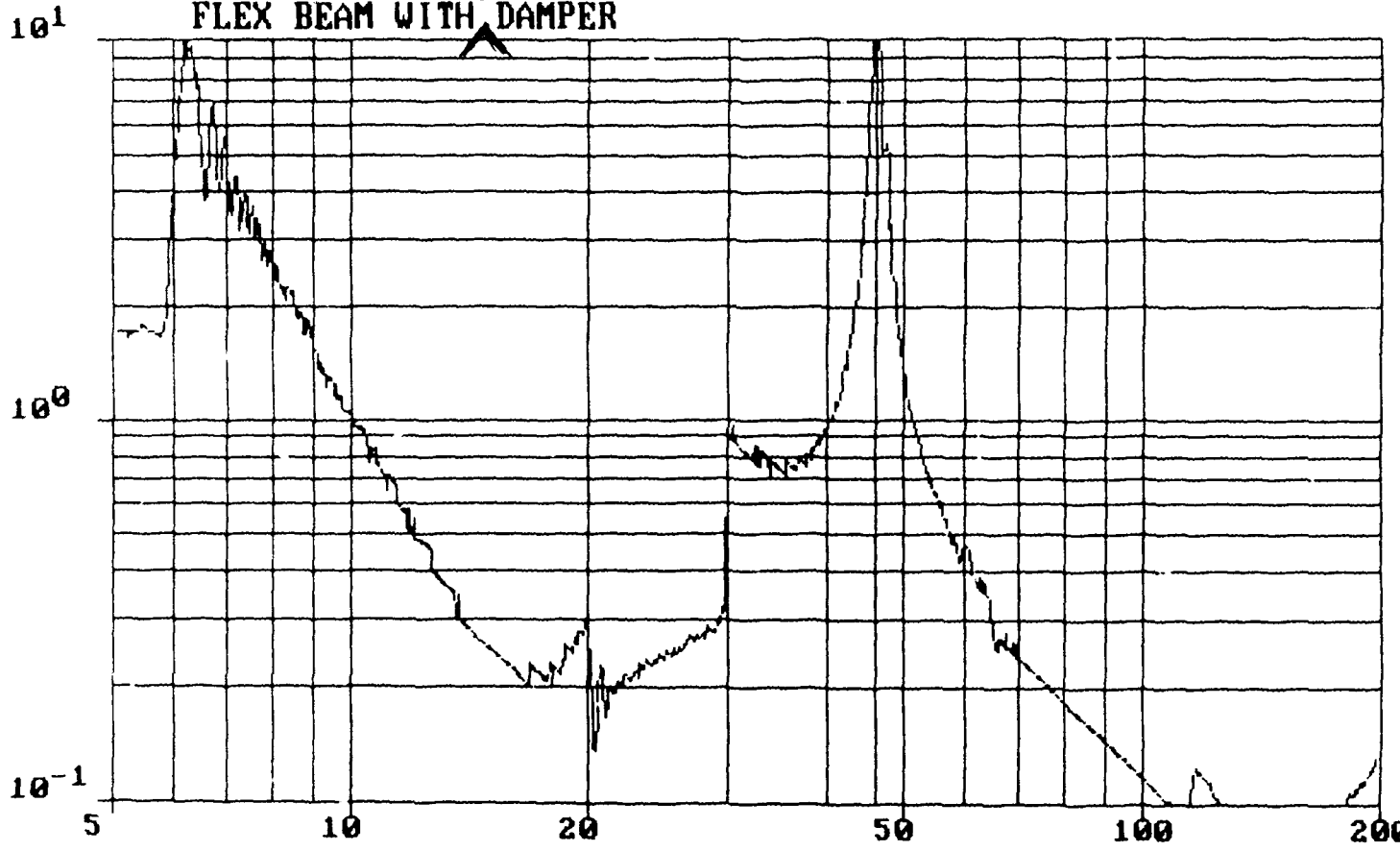

DISPLAY
C-CTRL
2-CH2
D-DRIVE
^2-2/CT
FREQ=
46.3
CH2/CON=
12.857

REF LEV=
6.00 mil
CONSTANT
DISP
LOG SWP#
1 up
of 1

10 mv/g AUTO : 00:01:46 STATUS: Finished
MAX SERV SPD 1k TOTAL: 00:01:48 SWEEP TIME: 1.8 Min CHAN 1

FLEX-11

first Peak 6.2 Hz
TR 10

0.006" DA 5-250 Hz 30CT/min

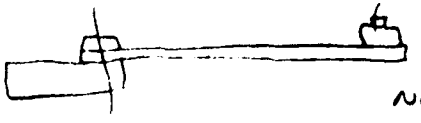

NO DAMPER

TEST SETUP-ID: FLEX TEST RUN NAME: RUN6 autosave 01/10/90 11:08:14

FLEX BEAM WITHOUT DAMPER

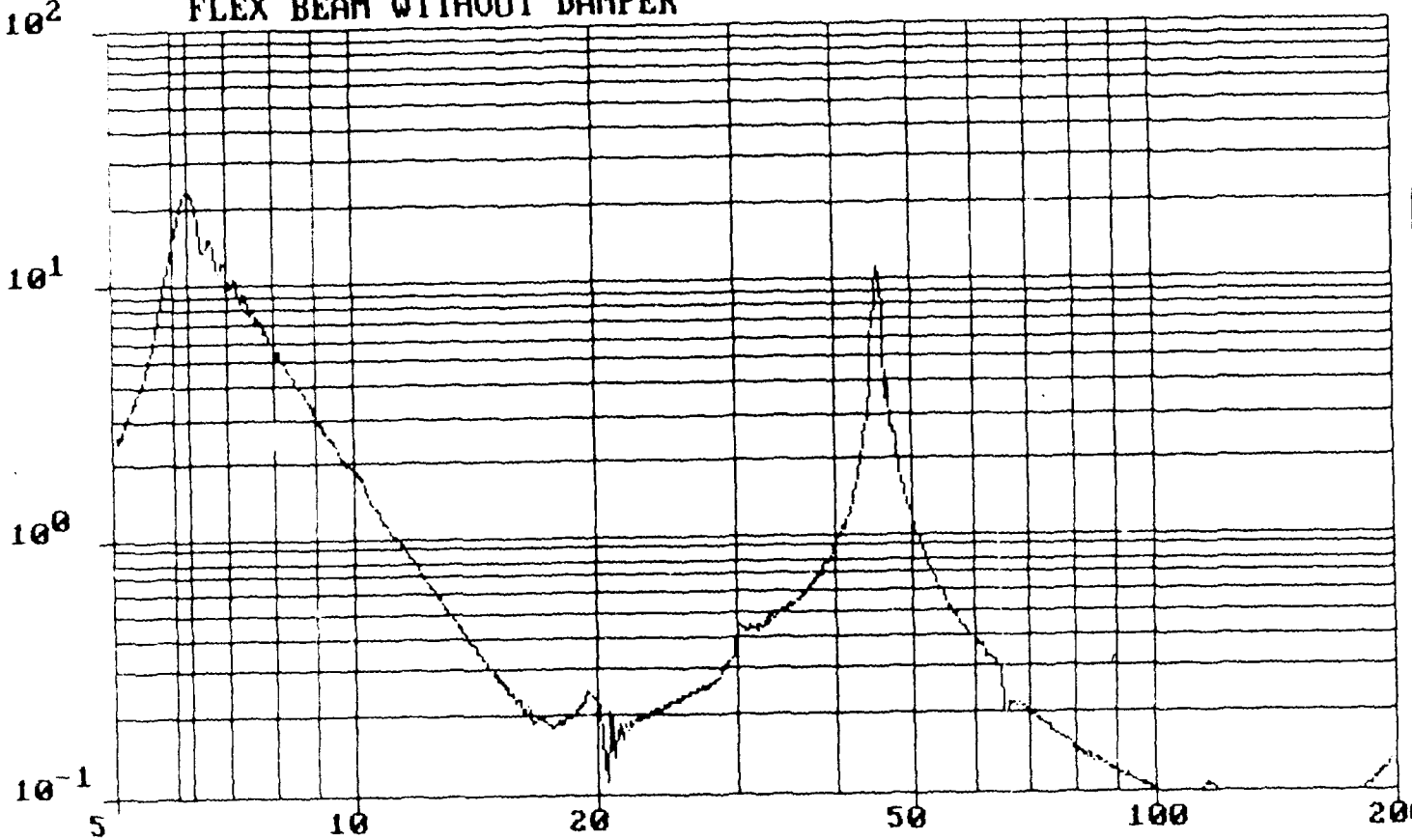

DISPLAY
C-CTRL
2-CH2
D-DRIVE
^2-2/CT
FREQ=
6.2
CH2/CON=
23.501

REF LEV=
20.0 mil
CONSTANT
DISP
LOG SWP#
1 up
of 1

10 mv/g AUTO : 00:01:46 STATUS: Finished
MAX SERV SPD 1k TOTAL: 00:01:54 SWEEP TIME: 1.8 Min CHAN 1

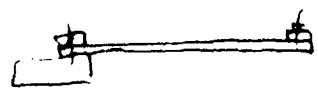

No Damping

.020 DA 5-140 Hz
20G - 140-2000 Hz

3. Second Analytic Summary

The following five pages relate to temperature and twisting of laminar damper in a flat-wise and edge-wise mode.

Single damper bonded on each side of specimen in these tests.

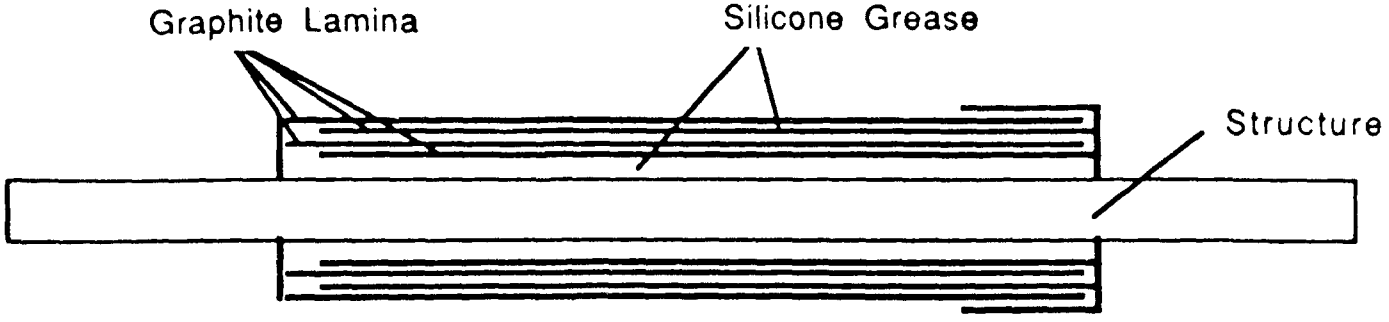

Figure 1. Cross-section of Laminar Damper

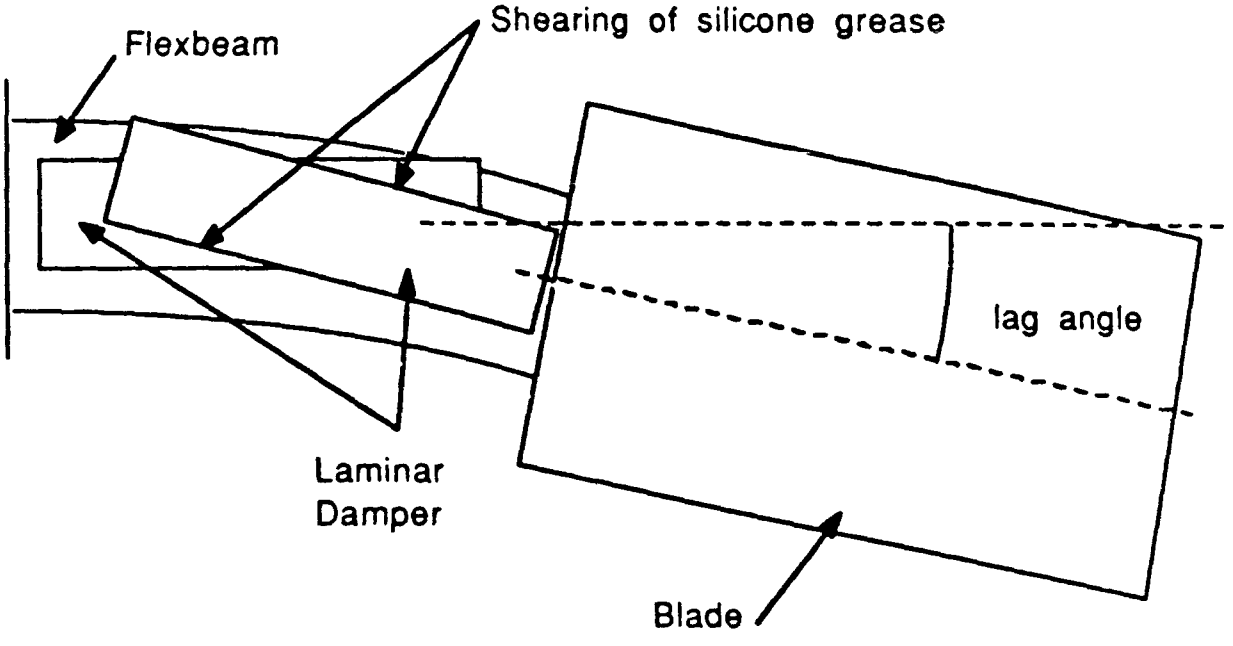

Figure 2. Action of Laminar Damper During Lead-Lag of Blade

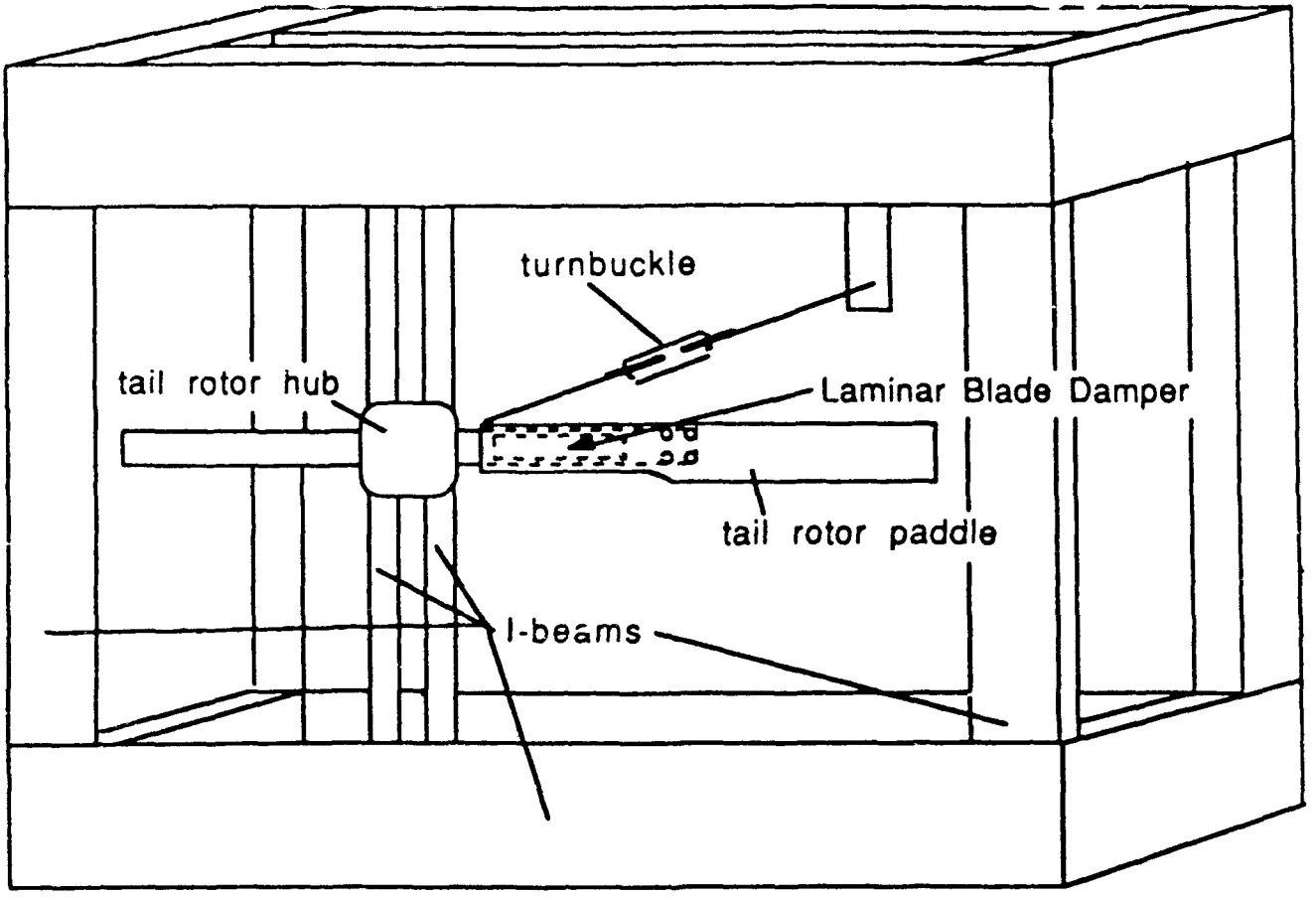

Figure 3.
Test Set-up for Determining Effect of Twist on Laminar Blade Damper Effectiveness

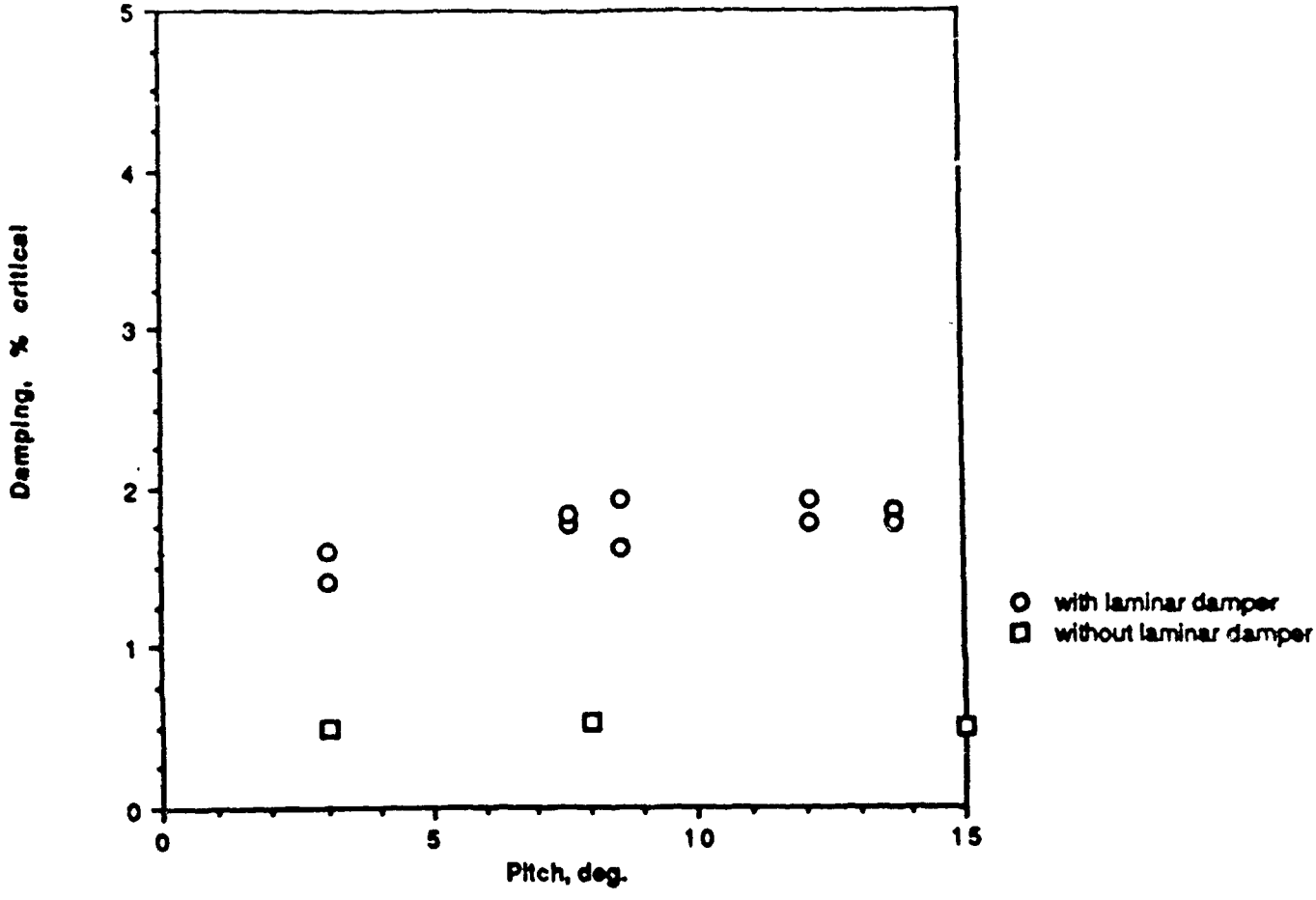

Figure 4.
Laminar Damper Damping vs Impressed Pitch
Non-Rotating Rap Test of S-76 Tail Rotor Spar

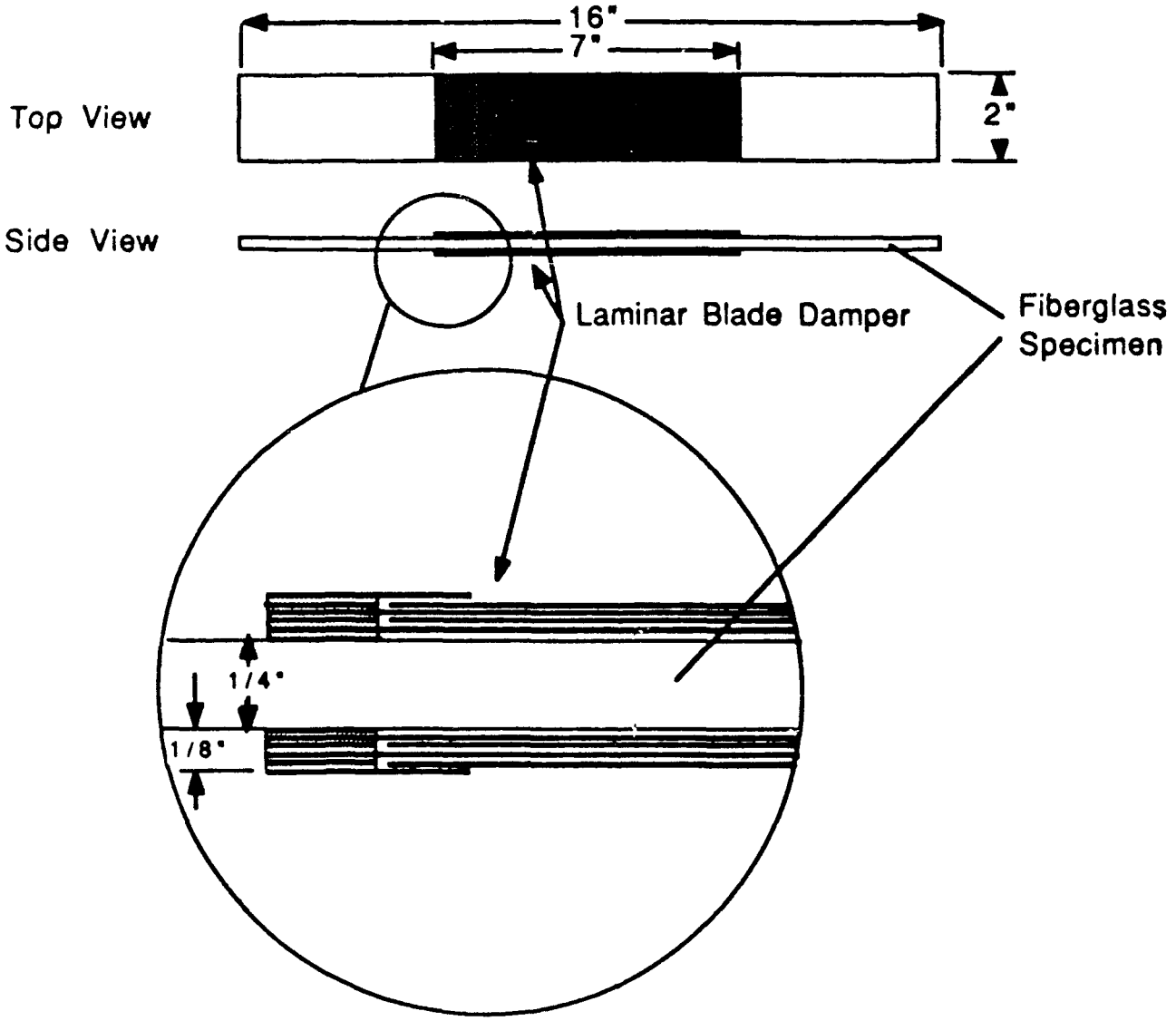

Figure 5. Second Prototype Laminar Blade Damper Mounted on Fiberglass Sample

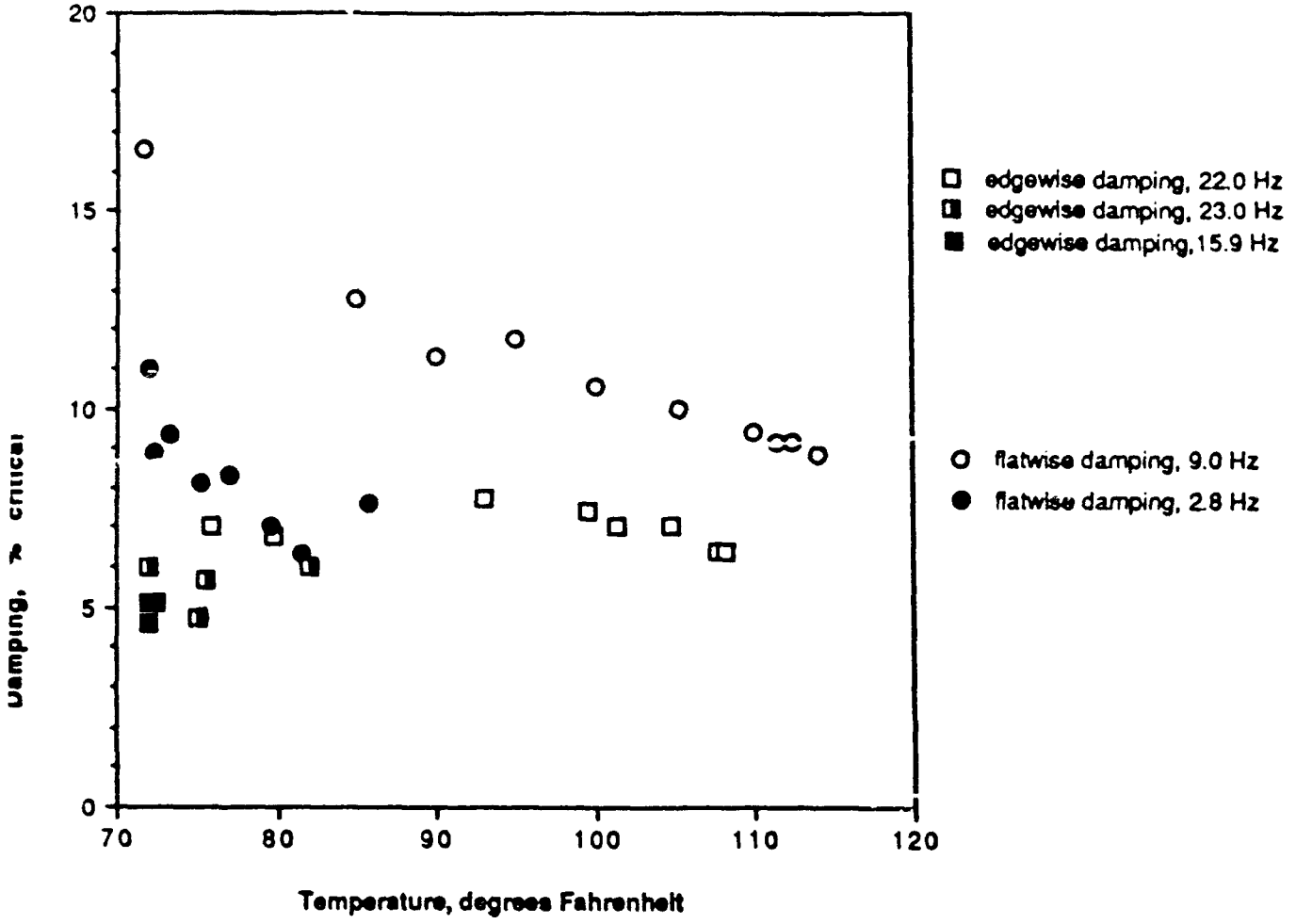

Figure 6.
Damping Variation with Laminar Blade Damper Temperature

4. Third Analytic Summary

4.1 Bang Test Results on a Tail Rotor Flexbeam

Two graphite tail rotor flexbeams and two tail rotor blades. One of these flexbeams has two dampers attached. The dampers each consist of four sheets 2-1/2 in wide and 8-1/2 in long, and were mounted on opposite sides of the flexbeam. To perform the test, the flexbeams were firmly clamped to a solid base with one end hanging down vertically. An accelerometer was then used to record the time history of the flexbeam motion in response to an impulse. A moving-block analysis was employed to calculate the damping ratio.

Bang tests were performed both with and without dampers, and with and without tail rotor blades attached for both flapwise and chordwise excitation. The damping ratio results are summarized in Table 1. The actual moving-block data is attached as Appendix B.

			Damping (% Critical)	
Figure	Description	Natural Frequency (HZ)	Without Damper	With Damper
B-1	Flapwise Excitation Blade Attached	4.0	1.19	-
B-2		4.1	-	3.23
B-3	Chordwise Excitation Blade Attached	35.6	0.77	-
B-4		33.6	-	8.43
B-5	Flapwise Excitation 1-lb Weight Attached	5.7	0.21	-
B-6		6.4	-	11.68

Table 1. Summary of Results

THE MOVING-BLOCK METHOD

On-line damping ratio data reduction was accomplished using a digital computer program based on the Fast Fourier Transform (FFT). This method, called a moving-block analysis, was applied to the time history of the transient response of the unfiltered accelerometer signal. The frequency of the mode being analyzed was identified from the frequency spectrum. Having identified the frequency, a moving-block size (time period) was selected based on the frequency accuracy required, the length of the time history, and the frequency of interest. Starting at the beginning of the transient, the FFT was performed on the block of data, and the amplitude of the frequency of interest was determined and saved. The block was then moved forward an increment in time and the process was repeated. This scheme of moving the block and FFT analysis was continued over a prescribed time period. After this process, the computer compiled a history of the transient behavior of the mode's free vibration decay. Then the logarithm of the amplitude changes was plotted against the time. A damping ratio was obtained by measuring the slope of this curve.

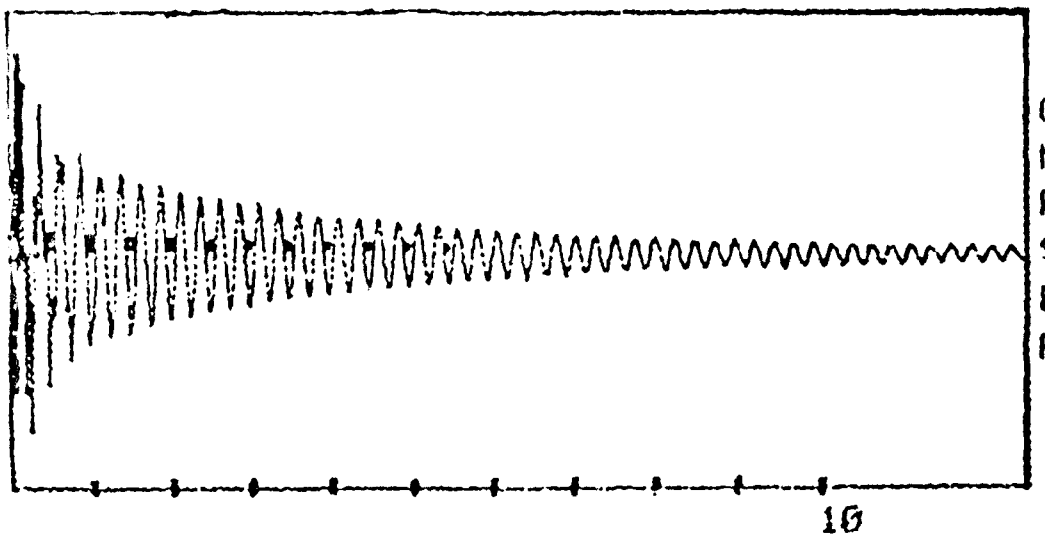

AMPLITUDE VS TIME (SECONDS)

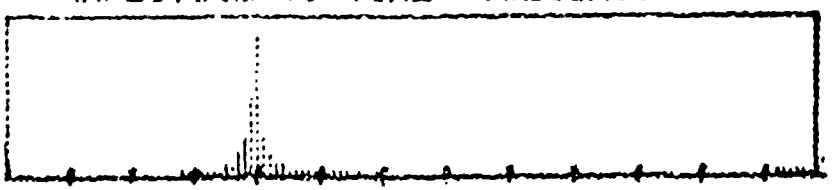

FOURIER AMPLITUDES FIRST BLOCK

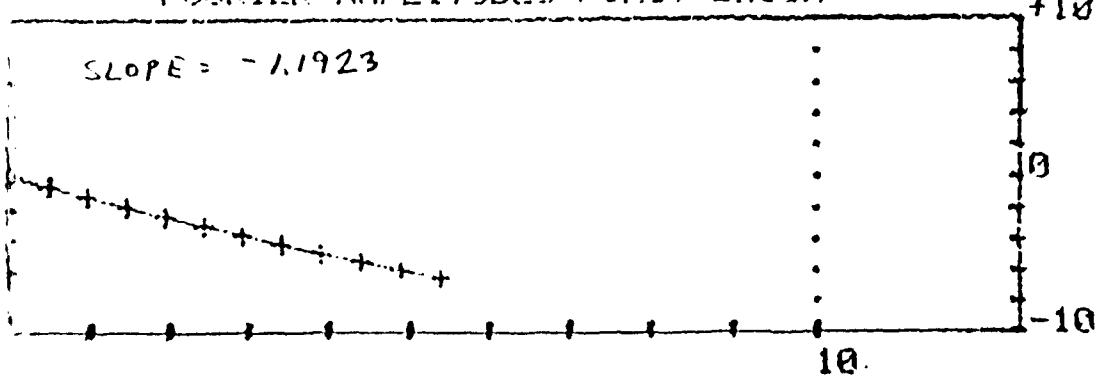

LOG DECREMENT VS TIME

BUMT
MOVING BLOCK ANALYSIS
CHANNEL NO. 2
NAME ACCEL
RUN 1 TEST POINT 3
SAMPLE RATE: 1918 SMPL/SEC
BANDWIDTH: 25.7 HZ
FREQUENCY ANALYZED: 4.0 HZ

DECREMENT RATIOS

1	+0.0
2	-0.6
3	-1.2
4	-1.9
5	-2.5
6	-3.1
7	-3.7
8	-4.3
9	-4.9
10	-5.4
11	-6.0
12	-6.5

Figure B-1

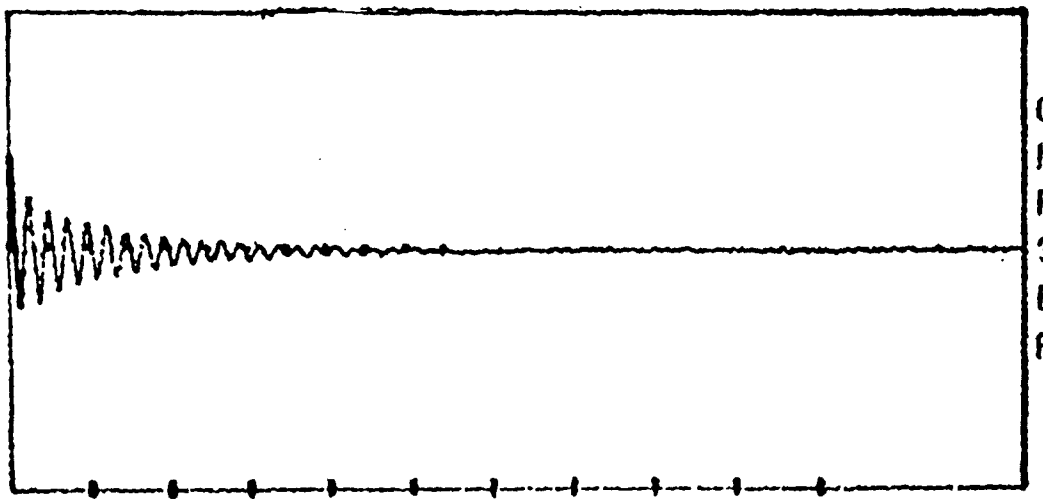

AMPLITUDE VS TIME (SECONDS)

FOURIER AMPLITUDES FIRST BLOCK

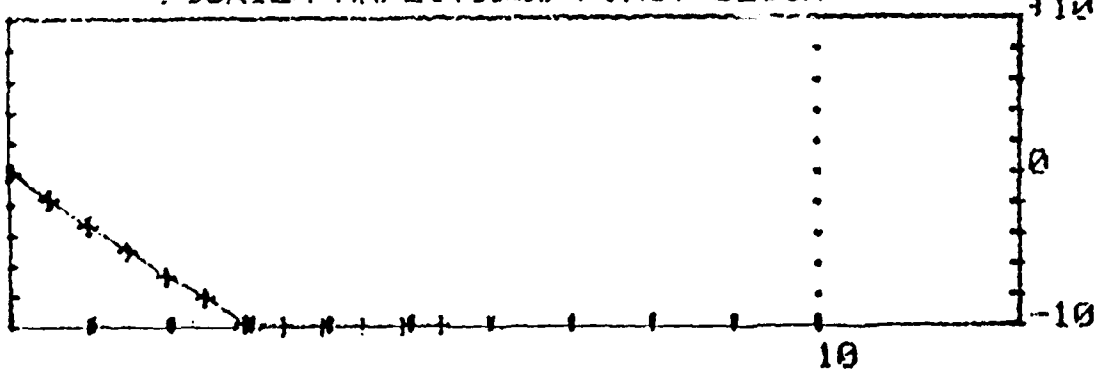

LOG DECREMENT VS TIME

BUNT
MOVING BLOCK ANALYSIS
CHANNEL NO. 2
NAME ACCEL
RUN 8 TEST POINT 1
SAMPLE RATE: 1918 SMPL/SEC
BANDWIDTH: 25.7 HZ
FREQUENCY ANALYZED: 4.1 HZ

DECREMENT RATIOS

1	+0.0
2	-1.7
3	-3.4
4	-5.0
5	-6.7
6	-8.1
7	-9.8
8	-11.2
9	-13.0
10	-15.0
11	-17.5
12	-16.6

Figure C-2

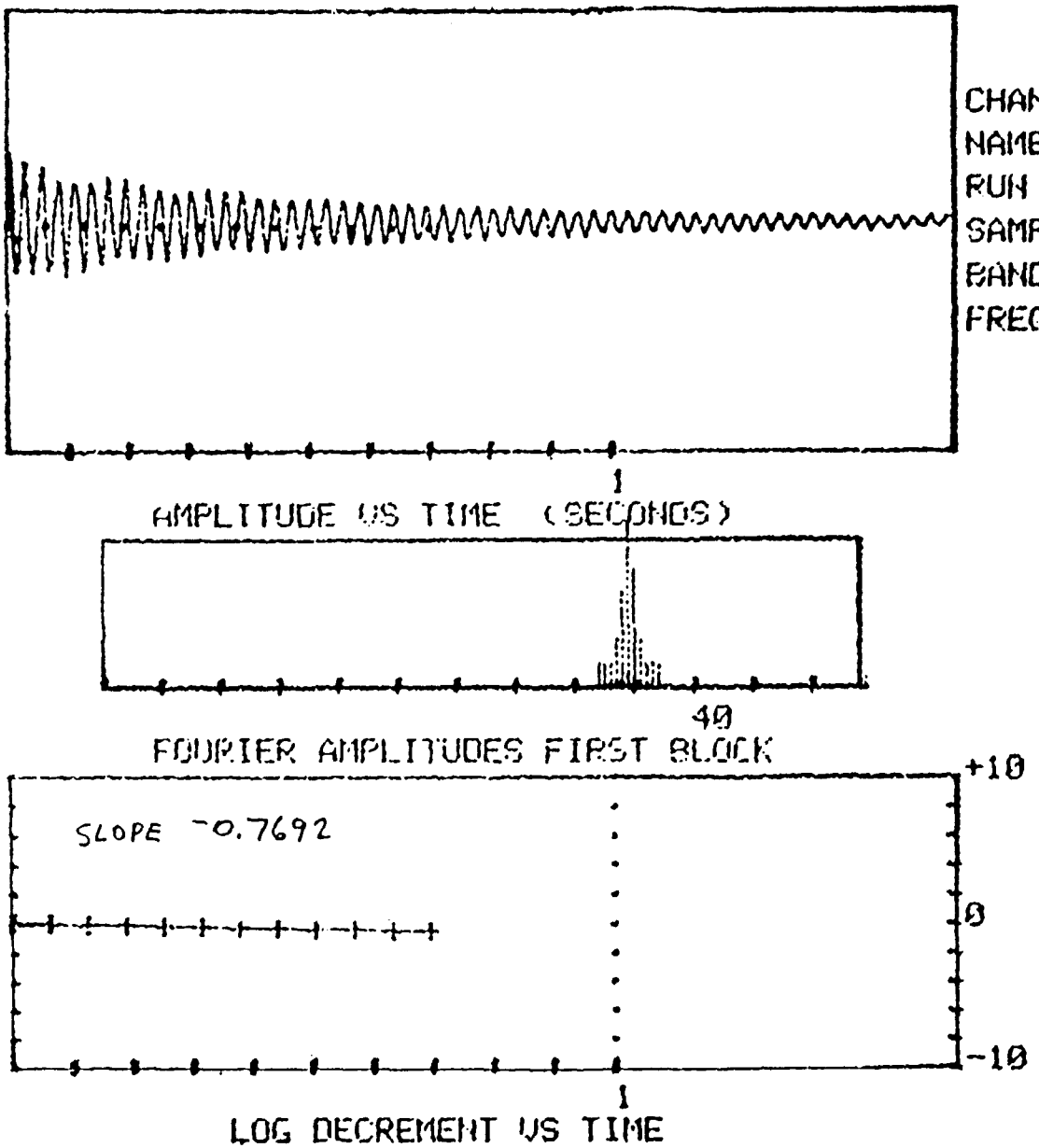

DECREMENT RATIOS

1	+0.0
2	+0.0
3	-0.1
4	-0.1
5	-0.2
6	-0.2
7	-0.3
8	-0.3
9	-0.4
10	-0.4
11	-0.5
12	-0.5

Figure B-3

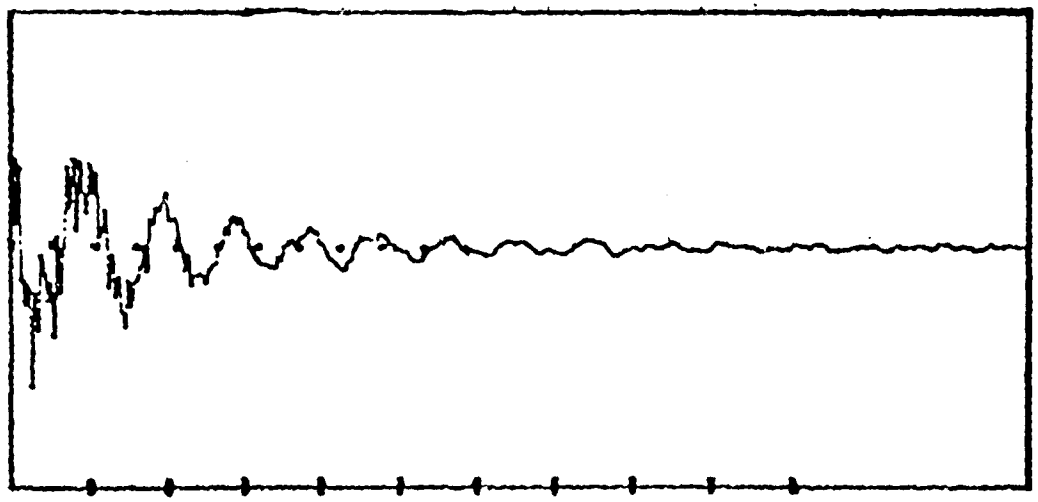

AMPLITUDE VS TIME (SECONDS)

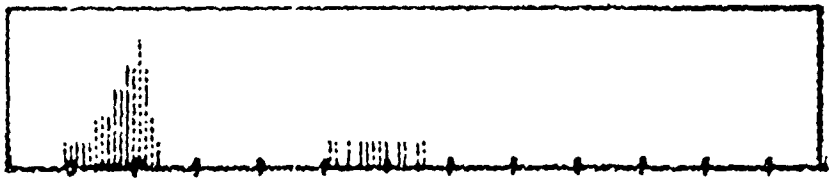

FOURIER AMPLITUDES FIRST BLOCK

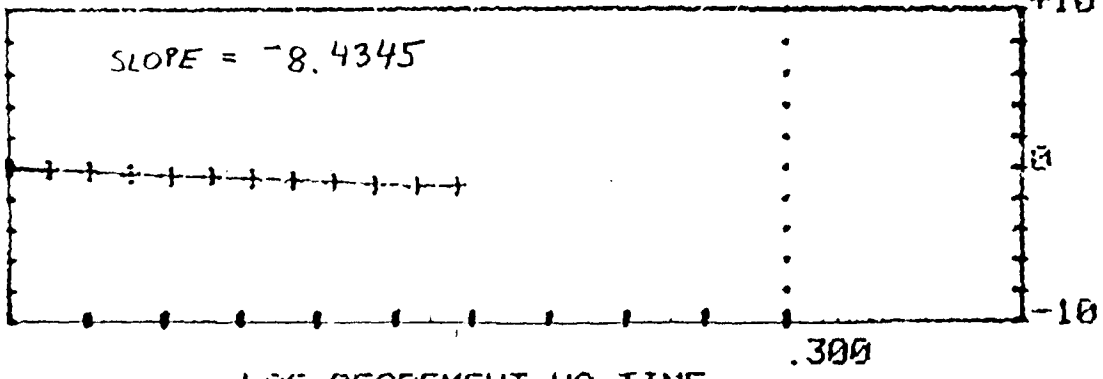

LOG DECREMENT VS TIME

BUWT
MOVING BLOCK ANALYSIS
CHANNEL NO. 2
NAME ACCEL
RUN 9 TEST POINT 2
SAMPLE RATE: 26 SMPL/SEC
BANDWIDTH: 27.2 HZ
FREQUENCY ANALYZED: 33.6HZ

DECREMENT RATIOS

1	+0.0
2	-0.1
3	-0.2
4	-0.4
5	-0.5
6	-0.6
7	-0.7
8	-0.8
9	-0.9
10	-1.1
11	-1.2
12	-1.2

Figure 8-4

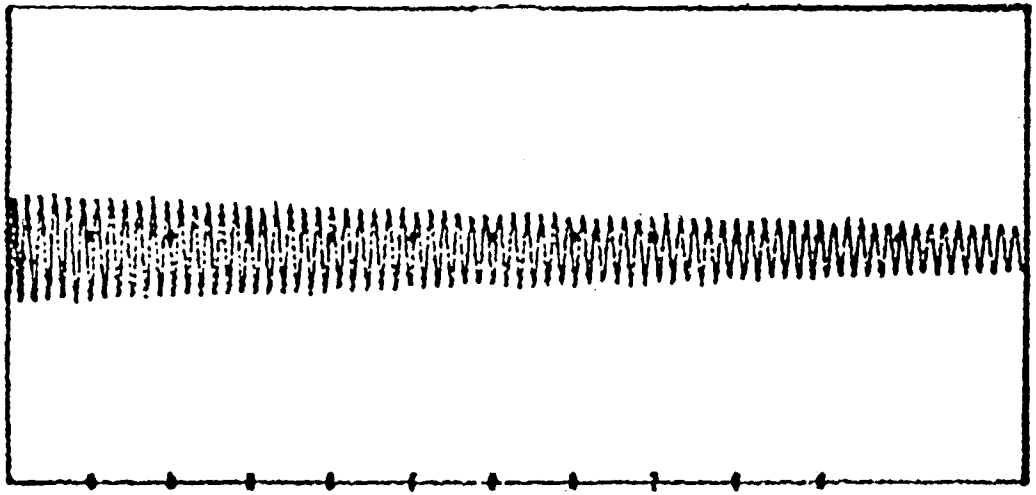

AMPLITUDE VS TIME (SECONDS)

FOURIER AMPLITUDES FIRST BLOCK

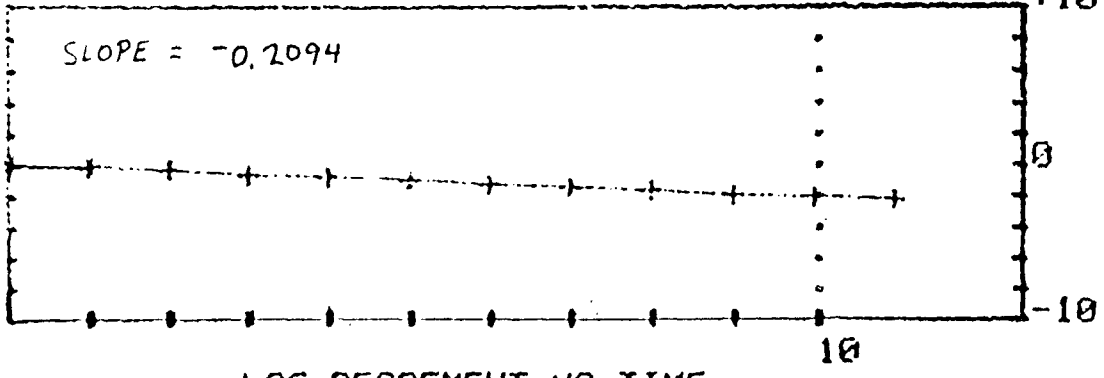

LOG DECREMENT VS TIME

BUMT
MOVING BLOCK ANALYSIS
CHANNEL NO. 2
NAME ACCEL
RUN 6 TEST POINT 2
SAMPLE RATE: 1918 SMPL/SEC
BANDWIDTH: 25.7 HZ
FREQUENCY ANALYZED: 5.7 HZ

DECREMENT RATIOS

1	+0.0
2	-0.1
3	-0.3
4	-0.6
5	-0.7
6	-0.9
7	-1.2
8	-1.4
9	-1.6
10	-1.9
11	-2.0
12	-2.2

Figure B-5

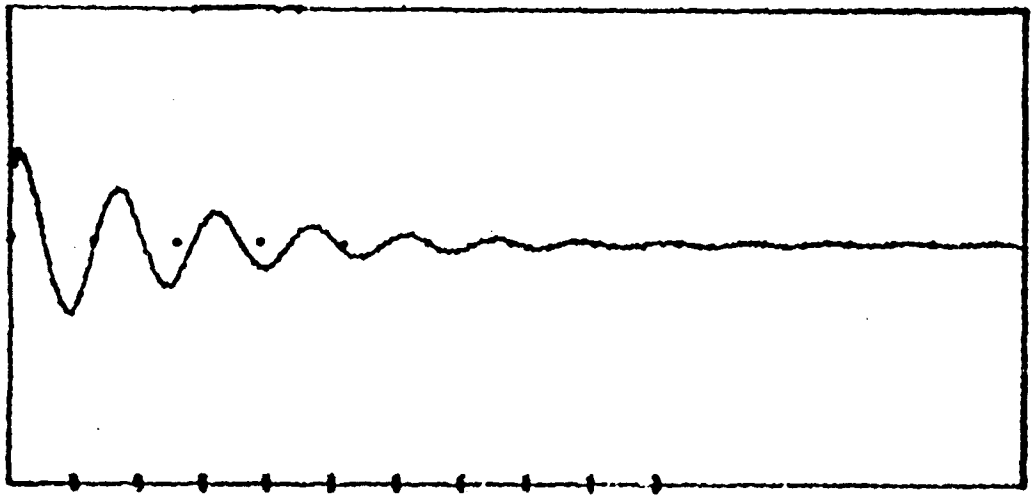

AMPLITUDE VS TIME (SECONDS)

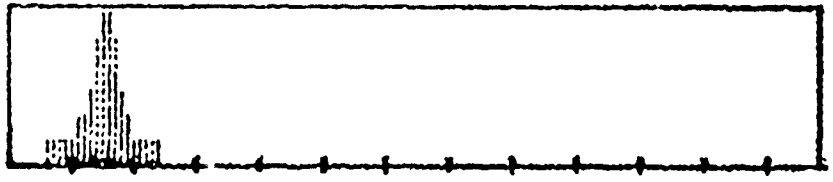

FOURIER AMPLITUDES FIRST BLOCK

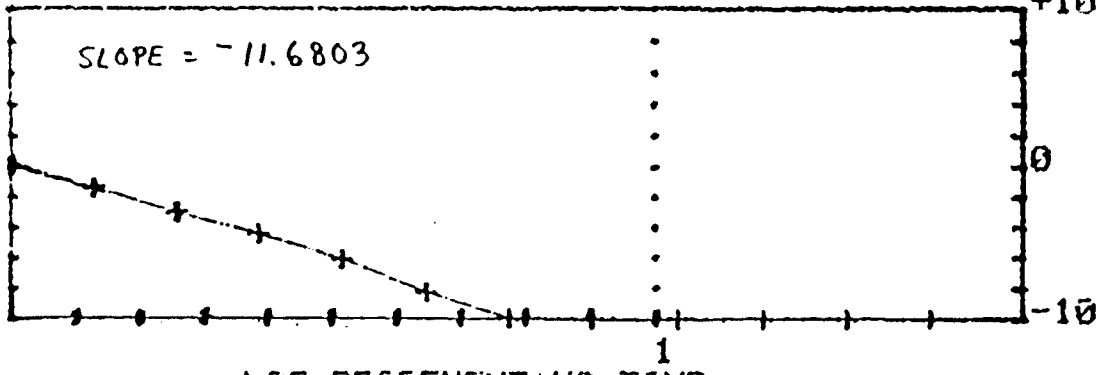

LOG DECREMENT VS TIME

BUHT
MOVING BLOCK ANALYSIS
CHANNEL NO 2
NAME ACCEL
RUN 10 TEST POINT 1
SAMPLE RATE: 209 SMPL/SEC
BANDWIDTH: 26.0 HZ
FREQUENCY ANALYZED: 6.4 HZ

DECREMENT RATIOS

1	+0.0
2	-1.4
3	-3.0
4	-4.4
5	-6.1
6	-8.3
7	-10.4
8	-11.7
9	-12.2
10	-14.4
11	-16.1
12	-14.5

Figure B-6

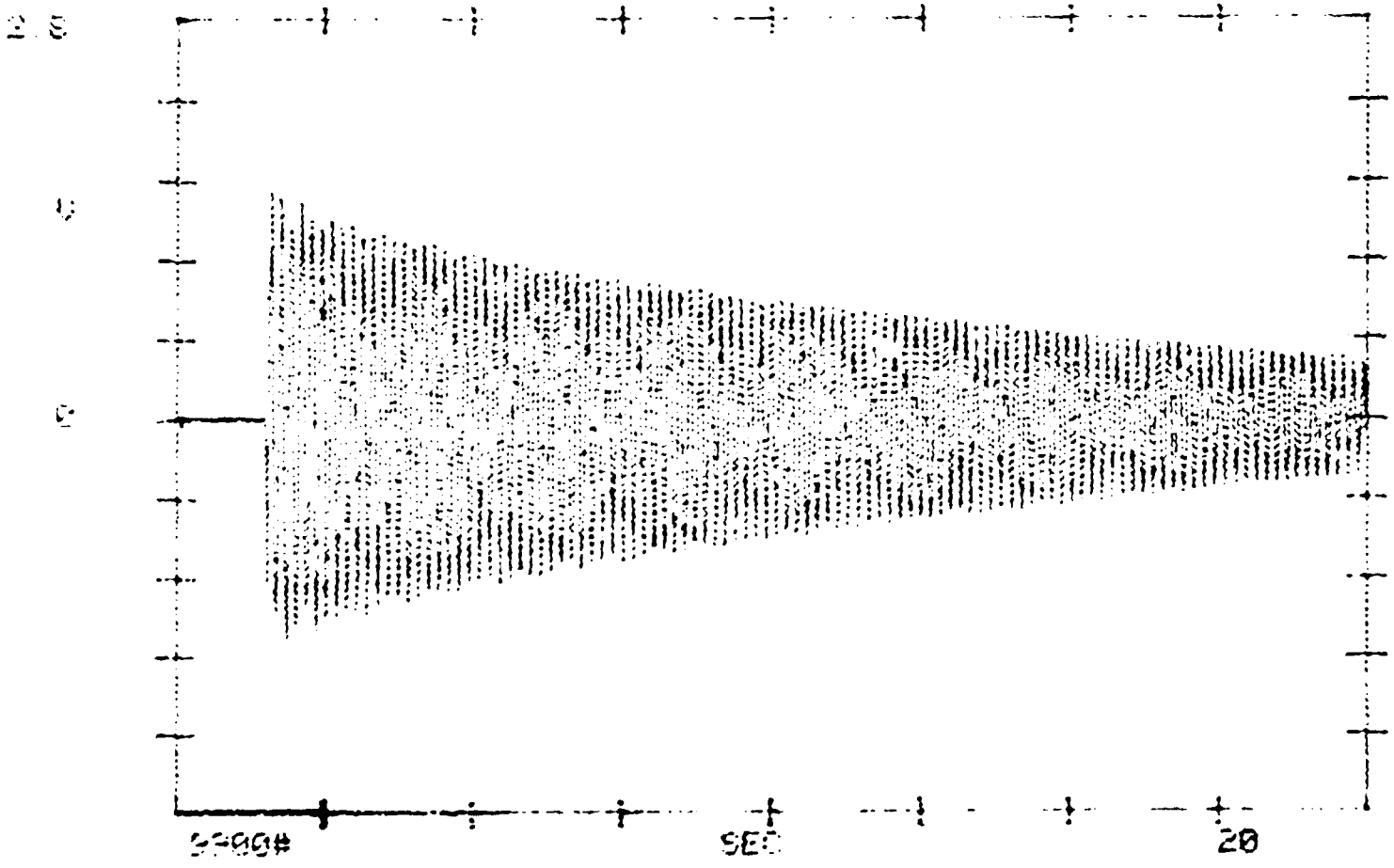

Figure R-5

2
SEC
#9868

5. References

Michael Koleda, United States Patent
France
Switzerland
West Germany
Austria

EXPERIMENTAL STUDY ON NOISE REDUCTION DUE TO DAMPING TREATMENTS

Ken Okada[1]
AT&S Tohsho Engineering Co., Ltd.
Tokyo, Japan

Junichi Kanazawa
Kobayasi Institute of Physical Research

ABSTRACT

Recently, a lot of damping material has been used for the control of structure-borne sound in electrical and automobile manufacturing, etc. in Japan. However, the accurate prediction of noise reduction by damping treatments is not easy from the catalogue data only.

In this report, the sound radiated from rectangular plates and cubes made of damped steel plates with various loss factors is examined. Sound pressure levels radiated from these testing pieces are measured on the near field and the loss factors of the complex test plates are measured by the free beam testing method. The relation between the sound pressure levels and the loss factors of the test plates is discussed with regard to these different figures of the structures.

THIS ABSTRACT PROVIDED FOR INFORMATION ONLY. ACTUAL PAPER WAS NOT PRESENTED AT THE CONFERENCE.

[1]AT&S Tohsho Engineering Co., Ltd., Konan Park Building, 2-12-26 Konan, Minato-ku, Tokyo 188 Japan, (81) 03-3471-5891

Evaluation of Damping Concepts for Precision Mounting Platforms[1]

D. Hill[2], C. Stahle, and J. Staley

General Electric - Astro Space Division

ABSTRACT

Conceptual analysis of a damped precision mounting platform with improved thermal and dynamic stability is presented. The use of metal matrix composite materials combined with viscoelastic damping materials results in uniquely stable, lightweight structures. Achievable goals for improved performance of an existing spacecraft precision mounting platform are established. Eight concepts are evaluated and ranked on damping, strength, thermal distortion, instrument mounting, and cost of fabrication. Three designs are selected for detailed quantitative analysis. Results for all three designs indicate performance goals can be met or exceeded. Thermal distortions and dynamic jitter response are both reduced by a factor of 5.

INTRODUCTION

Improved thermal and dynamic stability of spacecraft precision structures is an evolving requirement generated by the need for increased accuracy and size in the presence of more severe orbital disturbances. Remote sensing spacecraft are projected to require larger and more stable precision mounting platforms (PMPs) to support the next generation of sensors, while larger dynamic excitations caused by high instrument scanning masses and larger spacecraft guidance actuators make the platforms more susceptible to jitter. The combination of metal matrix composite (MMC) materials and passive damping using viscoelastic materials (VEM) provide uniquely stable lightweight structures suitable to the needs of future spacecraft. MMC materials are utilized to provide high stiffness, high thermal conductivity, low thermal expansion, and high specific strength. VEMs are engineered to provide high damping at desired modulus, frequency, and temperature ranges and can be used to obtain high composite loss factors on precision platforms.

A USAF Wright Research Development Center program, Damping and Metal Matrix for Precision Structures (DAMMPS), is being performed by GE Astro Space Division to develop and demonstrate a stable spacecraft PMP utilizing damping and metal matrix materials. The approach is to design, fabricate and test a Demonstration Structural

[1]This work has been performed under USAF-WRDC contract F33615-89-C-3202.

[2]Dennis Hill, GE Astro Space, 234 Goddard Blvd., King of Prussia, PA, 19406, (215) 354-6551

Article (DSA) using the design requirements of an existing platform to assure interdisciplinary design constraints are represented. The selected platform is from an existing GE-ASD spacecraft shown in Figure 1. The program utilizes the design requirements of this platform to set goals for the DSA representative of those required for the next generation of improved sensors.

The alignment critical sensors of the satellite are mounted on the PMP, located at the forward end of the spacecraft. The current design is a dip brazed aluminum egg crate structure which is kinematically mounted to the main body of the spacecraft through three struts with ball fittings at either end and a shear attachment with a ball fitting at one end. The kinematic mounting arrangement minimizes distortions due to thermal growth or distortion of the main body of the spacecraft.

The DSA design requirements and goals have been set to provide major improvements in performance including an enlarged sensor-mounting area. The DSA platform is shown in Figure 2 and the performance requirements and goals are compared in Table 1. The enlarged platform extends both axially and laterally while configured to stay within limits imposed by launch stowage of the solar array. Package locations are based on field-of-view studies. The DSA requirements are similar to the current design except for the minimum resonant frequency which has been lowered, based on control system considerations. The goals were selected based on previous experience with damped panel designs(1) and are felt to be achievable. Major performance improvements will be accomplished if these goals are met.

DESIGN CONCEPTS

The first step in the design process is the identification of concepts which should satisfy the design requirements, and goals. At this point the design goals can be regarded in general terms which fall into five categories, namely damping, stiffness and strength, thermal control and thermal distortion, support and component mounting interfaces, and ease of fabrication and cost.

Concepts which were intended to rank well in all five categories were considered as design candidates, and those in which damping is an integral part of the design were of primary interest since this is expected to provide the best damping at minimum weight. The eight concepts presented here are shown in Figure 4, and each concept is given a brief description below.

The VEM is sandwiched between two honeycomb panels in the dual honeycomb design. Each honeycomb panel consists of an aluminum core and MMC facesheets. Instruments can be mounted to inserts potted in the honeycomb panels.

The external stiffener concept has been used successfully in the past(1) to provide stiffness and damping in equipment panels on a defense communications satellite. The base panel is constructed of aluminum honeycomb core with MMC facesheets. Strips of VEM and aluminum honeycomb core with MMC facesheets are bonded to the

base panel to provide damping and added stiffness. The interior stiffener concept is a similar design with the stiffeners mounted inside the base platform. The advantage over the external stiffener design is the improved instrument mounting area.

The dual eggcrate concept evolved from the present, undamped platform design. The eggcrate core is dip brazed, then facesheets with lightening holes are dip brazed to the core. Two panels would be fabricated with eggcrate cores and MMC facesheets. These would then be bonded to the VEM layer to form the platform.

An isogrid concept is currently being used for mounting instruments on another of GE ASD's earth sensing satellites. The isogrids would be machined from MMC castings. Two isogrids would be machined and bonded to the VEM layer in the center of the platform. Instruments mount into holes at the web intersections.

The adhesive used to bond the MMC facesheets to the aluminum honeycomb core for the lower panel provides the required damping in this concept. The upper panel would be mounted to the spacecraft structure. The upper and lower panels share a common inner facesheet.

The dual honeycomb/intercostal platform is constructed of two honeycomb panels (aluminum core with MMC facesheets) connected by intercostal beams with an intermediate VEM layer. The modified intercostal concept is an offspring of the original intercostal concept. This concept cuts the number of parts by almost half. The VEM is bonded to the top and bottom flanges of the intercostals, and the honeycomb is in turn bonded to the VEM.

CONCEPT SELECTION

The five concept ranking categories in descending order of importance are ease of fabrication and cost, damping, thermal distortion, strength and stiffness, and instrument mounting. Each category is assigned a weight factor from 1 to 5 based upon relative importance. The design concepts are assigned a rank from 1 to 5 in each category. The rank in each category is multiplied by the weight factor and summed to a total. The three designs with the highest total score are selected for quantitative trade studies.

The concept ranking matrix is shown in Table 2. The highest ranked concept is the dual honeycomb concept, which received high rankings in all categories. The external stiffener concept is ranked second. It received high rankings in all categories but mounting, and the mounting category was assigned the least overall importance. The third highest ranked concept is the modified dual honeycomb/intercostal concept, which ranked higher than the original intercostal concept because of lower fabrication cost. The adhesive damped concept received the lowest ranking because of development cost, damping and strength considerations.

PLATFORM SIZING ANALYSIS

The three concepts emerging from the concept evaluation studies are the dual honeycomb, external stiffener, and modified dual honeycomb/intercostal (henceforth referred to simply as "intercostal") designs. Initial component sizes were determined based upon the 15.5 Hz minimum frequency requirement and damping goal of greater than 10 percent in all modes below 100 Hz subject to minimizing platform weight. The thicknesses of the MMC facesheets and VEM layers were limited due to manufacturing constraints. The MMC is available in thicknesses from 0.015 to 0.15 inches. The VEM can be formulated in thicknesses from 0.05 inch to 1.0 inch. The honeycomb thickness may range between 0.25 inch and 3.5 inches.

MSC/NASTRAN Finite element models (FEMs) were constructed to evaluate the stiffness and damping characteristics of the designs. The three concept FEMs are shown in Figure 3. The FEMs are composed of solid elements (HEXA) representing the VEM layers and plate elements (QUAD4) modeling the honeycomb layers. The intercostal FEM has additional plate elements representing the geometry of the intercostals themselves. An additional model of the original eggcrate structure with the same platform area, but with no damping material was constructed for comparison with the other designs.

A normal modes analysis was performed on each FEM to determine frequency and damping values for all modes less than 100 Hz. Damping was calculated using the *modal strain energy method(2), thus*

$$\eta_i = \varepsilon_v \times \eta \qquad (1)$$

were η_i is the composite loss factor, ε_v is percentage of strain energy within the VEM, and η_v is the material loss factor for the VEM. A material loss factor of 1.0 was assumed for sizing since the specific VEM was unspecified at this point and the modulus of the VEM was one of the variables subject to optimization.

The element sizing analysis is similar for all three designs and only the dual honeycomb sizing will be discussed here. The design parameters which were varied are the thicknesses of the outer facesheets, honeycomb core, and VEM, and the shear modulus of the VEM. The inner facesheet thickness was fixed at 0.015 inch because it is primarily a bonding layer, and contributes little to platform stiffness because it is close to the platform neutral axis.

An initial sensitivity study was performed to determine which parameters were effective in increasing frequency and damping. Each design variable was modified one at a time and the frequency and damping effects on each mode below 100 Hz were plotted against the change in platform weight. Results presented here are for the fundamental mode only. Different and even opposite trends occurred for the higher modes.

Results for the dual honeyccmb concept, shown in Figure 5, indicate increasing honeycomb core thickness and facesheet thickness raise the fundamental frequency while also raising piatform weight. Decreasing the VEM thickness increases the fundamental frequency and lowers the platform weight, both of which are desirable results. Unfortunately, decreasing the VEM thickness also decreases damping in the fundamental mode. Damping is increased by reducing core thickness or increasing facesheet thickness. Damping is also affected by the VEM shear modulus. Decreasing the shear modulus increases damping but reduces frequency.

The sensitivities provided insight for the 19 design iterations that were required to meet the frequency requirement and damping goal. A total of 29 and 31 sizing iterations were performed for the external stiffener and intercostal designs respectively. Progress toward the final design can be charted by defining a penalty function as follows:

$$
\begin{aligned}
PF = \; & W_p \times [1 + 0.2 \times \Sigma (10. - \eta_i) + (15.5 - f_1)]; && \eta_i < 10.\,;\, f_1 < 15.5 \\
& W_p \times [1 + (15.5 - f_1)]; && \eta_i > 10.\,;\, f_1 < 15.5 \\
& W_p \times [1 + 0.2 \times \Sigma (10. - \eta_i)]; && \eta_i < 10.\,;\, f_1 > 15.5 \\
& W_p && \eta_i > 10.\,;\, f_1 > 15.5
\end{aligned} \qquad (2)
$$

where W_P is the platform weight, and f_1 is the fundamental frequency. This function is shown for all three designs in Figure 6. While the penalty function is somewhat arbitrary, it does reflect the relative ease in achieving the design objectives, and it reduces to only the platform weight when the design goals are satisfied. The plot illustrates that the dual honeycomb design converged to a lighter configuration in fewer iterations. The dual honeycomb penalty function shows a large spike at iteration 7. This was one in a series of runs with increased modulus and stresses the importance of a low modulus VEM. As the VEM modulus was raised, the damping fell off rapidly.

The modal characteristics and weights of all three designs in the final configuration are given in Table 3. The dual honeycomb platform is 4.0 inches thick with 0.045 inch outer facesheets and 0.050 inch thick VEM. The external stiffener has a 1.0 inch thick base panel. The exterior stiffener has a 0.050 inch outer facesheet, 5.5 inches of high density honeycomb core, and a 0.125 inch VEM layer. The intercostal design has 0.030 inch outer facesheets, 2.5 inch honeycomb core, 0.125 inch VEM layers, and 1.75 inch intercostals. Only the dual honeycomb met the 10 percent damping goal for all modes. The external stiffener had one mode and the intercostal had two modes with damping values slightly less than 10 percent. Additional iterations would have increased damping in the three modes. However, the damping values were deemed sufficiently close to the goal as not to warrant further iterations during the trade study

phase of the program. The design selected for detailed design, fabrication, and test will be thoroughly optimized, and meet all damping goals.

VEM AND MMC MATERIAL SELECTION

The platform sizing analysis provided insight as to the range of VEM shear modulus which results in optimum damping. Optimum damping in all three concepts was provided by a VEM shear modulus between 50 Psi and 1200 Psi. Some latitude in the damping material modulus can be gained by examining the shear stiffness, GA/t, where G is the storage modulus of the VEM, t is material thickness, and A is the area in shear. Therefore, for a given damping material, lower stiffness can be achieved by increasing the material thickness or reducing the area in shear. However, increasing the VEM thickness increases weight and reduces through thickness thermal conductivity. Reducing the area of VEM in shear increases the stress in the material and also reduces the through thickness thermal conductivity. Then, the most desirable manner of decreasing the shear stiffness is the selection of a low modulus VEM.

Table 4 shows the shear modulus and other VEM requirements. A high material loss factor is critical to achieving the damping goal of greater the 10 percent in each mode less than 100 Hz. Outgassing criteria must be adhered to for every space qualified material. Many damping materials have high material loss factors, but also have high outgassing properties. This is undesirable in space because material lost from the VEM not only degrades platform performance, but may condense on the sensors or solar array panels causing serious degradation in satellite performance.

The material tentatively selected is one of the GE-ASD SMRD formulations, designated B37T2B. The SMRD damping material has a proven track record in space applications and the material properties can be tailored to meet stiffness requirements. This material was subjected to detailed testing as part of the DAMMPS program. The VEM properties were measured with CSA Engineering's DCS tester. The machine uses the direct complex stiffness (DCS) technique, in which a shearing force is applied across the specimen and the resulting displacement is measured and used to compute the complex modulus. The test results are shown in Figure 7. Also shown are modified Oberst beam results for comparison. The test results are in good agreement considering the accuracy of the beam test method. The material satisfies the VEM requirements for all three designs.

The metal matrix selection issues are modulus, strength, hysteresis, thermal conductivity, coefficient of thermal expansion, cost. Materials with high stiffness-to-weight and strength-to-weight ratios are desirable for light weight designs. Hysteresis should be low to minimize alignment error. The material of choice should have high thermal conductivity and low coefficient of thermal expansion to minimize thermal distortions. Low cost materials are always sought to reduce overall program costs.

The properties of the three leading candidate materials are compared with those of

aluminum in Table 5. P120/Al has the highest modulus and thermal conductivity and the lowest coefficient of thermal expansion. The modulus is three times higher than aluminum with comparable density. The thermal conductivity of P120/Al is higher than that of aluminum with a coefficient of thermal expansion which is 8 times lower. The cost of P120/Al is somewhat higher than SiCp/Al and B/Al because it is relatively new. The P120/Al material has been tentatively selected because of the outstanding properties and in spite of the increased cost.

JITTER ANALYSIS

This analysis is helpful in relating the modal characteristics of the designs to physical quantities so they may be compared on a more direct basis. The rotational response of an instrument mounted on the platform to a disturbance input is the jitter which an instrument will experience during operation on orbit. Uncontrolled jitter adversely affects instrument performance. Damping can be used to control jitter by limiting the magnitude of the instrument response and by decreasing the settling time. The settling time of the instrument response is the time taken to reach an acceptable level of jitter at which instrument performance will not be adversely affected.

The dynamic torque imposed by the primary sensor, the SSS, is the major disturbance. The sensor imposes torque pulses on the platform when the moving element reverses direction as shown in Figure 8. The Fourier analysis of the pulse train depicted in the figure shows rich harmonic content through 100 Hz. Other disturbances which must also be considered are the solar array torque, reaction wheel unbalance, and the torques resulting from the rotating dish of the SSM/I instrument.

The jitter evaluation was performed using the same FEMs developed for the modal and stress analyses. An MSC NASTRAN modal transient response analysis formed the basis for the evaluation. The worst case jitter results (including all disturbances simultaneously) are shown in Figure 9. The eggcrate model without the benefit of viscoelastic damping has the highest jitter response. The responses of the three damped designs are relatively small in comparison. The intercostal design has the smallest response, and this is probably due to the excellent damping in the first three vibrational modes.

To further investigate the effect of damping on platform stability, the response to a generic slew maneuver was determined. Figure 10 displays the superior settling time of the damped designs. It is a comparison of the slew maneuver response of the undamped eggcrate model to that of the dual honeycomb design. The results are a classic illustration of the effect of damping on settling time. The damped designs stabilized 20 times faster than the eggcrate.

THERMAL DISTORTION ANALYSIS

The thermal distortion analysis provides a basis of comparison for the thermal performance for each of the designs. In order to make a relative assessment of the

designs, it will be assumed that the same thermal control system is applied to each design. With the same heater inputs, each design will have a different thermal gradient normal to the plane of the panel. Therefore, designs with lower thermal resistance will have lower thermal gradients and lower thermal distortions. The equivalent thermal gradient across the platform can be calculated from

$$\Delta T = (\Sigma\ 1/k_i)\ /\ (\Sigma\ 1/k_j)\ \Delta T' \qquad (3)$$

where

ΔT = equivalent thermal gradient

$\Delta T'$ = reference thermal gradient

k_i = normal conductivity of the ith platform element

k_j = normal conductivity of the jth reference platform element

Then selecting the 3.96 inch thick dual honeycomb concept as the reference with the design thermal gradient of 3 C, the equivalent gradient across the 1.05 inch thick external stiffener platform is 0.76 C. Similarly, a 8 C thermal gradient is applied across the 6.88 inch thick intercostal.

The relative distortion of each design is shown in Figure 11. As indicated by the equivalent thermal gradients, the intercostal distortions are significantly higher, followed by the dual honeycomb and external stiffener thermal distortions.

SUMMARY AND CONCLUDING REMARKS

The concept analysis results at this point in the program are compared with the goals in Table 5. The weight reduction goal was exceeded in all three designs. The damping goal was satisfied in the dual honeycomb design, but damping in the other two designs fell slightly short of the goal. This does not appear to have affected the dynamic response of the platforms since all three designs far exceed the jitter reduction goal. The dual honeycomb and external stiffener designs exceeded the thermal distortion reduction goal, but the thermal distortion reduction of the intercostal design fell short of the goal. All three designs are viable candidates for the final design.

Preliminary conceptual design results have been presented for the on-going DAMMPS program. In the subsequent program phases, a detailed design will be developed for one of the three selected concepts. The design will be fabricated, and finally, ground tests will be performed to verify performance predictions. This work has established the feasibility of combining MMC and VEM materials to dramatically improve the dynamic stability of satellite sensor platforms.

ACKNOWLEDGMENT

The work reported herein was performed for the Air Force Wright Aeronautical Laboratory, Contract No. F33615-89-C-3202, "Damping and Metal Matrix for Precision Structures," under the technical direction of Michael Zeigler.

REFERENCES

1. Stahle, C.V., Staley, J.A., and Strain, J.C., "RELSAT - Reliability for Equipment in Environmental Vibration," Final Report, AFWAL, June 1990.

2. Johnson, C.D., and Kienholz, D.A., "Finite Element Prediction of Damping in Structures with Constrained Viscoelastic Layers," AIAA Journal, Vol. 20, &No. 9, Sept. 1982, pp. 1284-1290.

Table 1 DSA Requirements and Goals

DESIGN REQUIREMENTS

CONDITION/REQUIREMENT	PRESENT PLATFORM	DSA
INSTRUMENT MOUNTING · SURFACE AREA · INSTRUMENT TOTAL WEIGHT	7.7 FT^2 150 LBS	10.9 FT^2 300 LBS
PRELAUNCH/LAUNCH CONDITIONS · LIFT-OFF TRANSIENT- AXIAL/LATERAL	1.5 ± 1.8G/± 2.2G	SAME
· STAGING TRANSIENT - AXIAL LATERAL	8.9 ± 5G/± 2.8G	SAME
· QUAL PLATFORM VIBRATION - ANY SINGLE AXIS	± 15G	SAME
· ACOUSTIC NOISE	144 dB	SAME
· PLATFORM MOUNTED COMPONENT VIBRATION	0.13G^2/Hz	SAME
· TEMPERATURE EXTREMES	-5° TO 35°C	SAME
· MINIMUM RESONANT FREQUENCY	27 Hz	16 Hz
ORBITAL CONDITIONS · THERMAL GRADIENT - FACE/FACE	3°C	SAME
· OPERATING TEMPERATURE	5 ± 1 1/2°C	15 ± 1 1/2°C
ORBITAL POINTING ERRORS · ALIGNMENT	10 ARC SEC	SAME
· JITTER	30 ARC SEC IN ONE SEC	SAME
· THERMAL DISTORTION AT COMPONENT	4 ARC SEC	SAME
· PLATFORM STRUCTURAL WEIGHT	45 LBS	90 LBS

DESIGN GOALS

- REDUCE PLATFORM STUCTURAL WEIGHT BY 20 PERCENT
- PROVIDE DAMPING (2C/Cc) OF 10 PERCENT IN ALL MODES < 100 HZ
- REDUCE JITTER BY A FACTOR OF 2
- REDUCE PROBABILITY OF EXCEEDING REQUIRED JITTER BY 50 PERCENT
- REDUCE PLATFORM MOUNTED COMPONENT QUAL VIBRATION REQUIREMENT BY 6 dB
- REDUCE THERMAL DISTORTION BY A FACTOR OF 5

Table 2 DSA Concept Ranking Matrix

Performance Category	Damping	Strength/ Stiffness	Thermal Distortion	Sensor Mounting	Fabrication and Cost	Weighted Total *
Weight Factor	4	2	3	1	5	
Concept						
Dual Honeycomb	5	4	4	5	5	70
Ext. Stiffener	4	5	5	2	5	68
Int. Stiffener	2	5	4	5	4	55
Dual Eggcrate	5	4	5	4	2	57
Dual Isogrid	5	4	5	3	2	56
Adhesive Damp.	3	2	4	5	2	43
Intercostal 1	4	5	3	5	3	55
Intercostal 2	4	5	3	5	4	60

* Scale of 1 to 5 with indicated weighting factors

Table 3 Frequency, Damping, and Weight comparison

Mode	Dual Honeycomb		External Stiffener		Intercostal	
	Freq. (Hz)	Damping (prcnt)	Freq. (Hz)	Damping (prcnt)	Freq. (Hz)	Damping (prcnt)
1	16.8	10.4	15.7	10.9	15.8	22.0
2	25.2	13.7	23.2	11.9	18.8	17.1
3	40.0	15.6	47.0	17.7	27.2	22.2
4	48.3	10.7	50.0	10.5	43.2	11.5
5	56.0	14.4	63.0	8.4	50.4	12.3
6	62.9	11.4	76.0	10.1	52.3	13.3
7	66.5	13.1	91.9	12.8	55.9	9.1
8	69.1	12.0	94.7	11.8	67.8	17.7
9	80.3	12.7			71.3	16.6
10	86.3	10.1			78.0	13.9
11	88.0	12.1			80.4	13.5
12	94.8	10.2			91.4	9.6
13					96.9	10.1
Platform Weight	26 lbs		34 lbs		33 lbs	

Table 4 VEM Requirements

TEMPERATURE RANGE (F)	**40 - 75**
FREQUENCY RANGE (HZ)	**15-2000**
SHEAR MODULUS (PSI)	**50-1200**
LOSS FACTOR	**> 1.0**
STRENGTH (PSI)	**> 50**
OUTGASSING - TML (%)	**< 1.0**
OUTGASSING - CVCM (%)	**< 0.1**
THICKNESS (INCH)	**.010 - 1.0**

Table 5 MMC Requirements

Material	Volume Fraction	Laminate Geometry	Elastic Modulus	Yield Strength	CTE	Thermal Conduct.
	Percent		Msi	Ksi	10^6/F	BTU/H Ft F
SiCp/Al	40	Isotrop.	21	60	8.1	75
P120/Al(6061)	50	(0/90)NS	31.7	12	1.7	120
B/Al	50	(0/90)NS	25	12	5.6	42
Aluminum	-	-	10	35	13	85

Table 6 Analysis Summary

CATEGORY	GOAL	DUAL HC	EXTERNAL STIFF	INTERCOSTAL
WEIGHT REDUCTION (%)	**20**	**30**	**21**	**22**
>10 % DAMPING <100 HZ	**ALL**	**12/12**	**7/8**	**11/13**
THERM DIST REDUCTION	**5**	**5.5**	**13**	**3.6**
JITTER REDUCTION	**2**	**5.1**	**4.8**	**5.3**

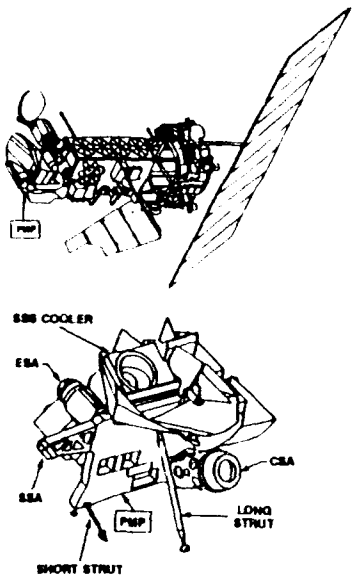

Figure 1 Remote Sensing Spacecraft and Existing Platform

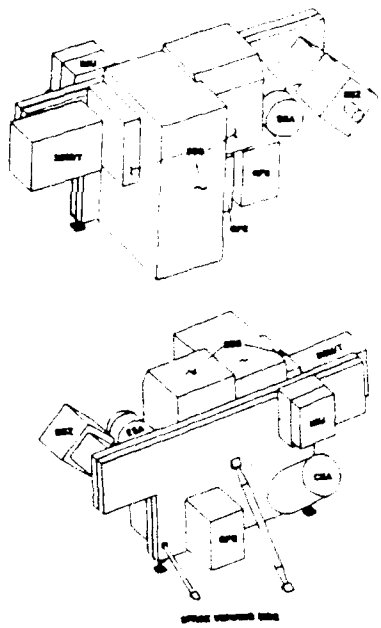

Figure 2 DSA Platform with Increased Mounting Area

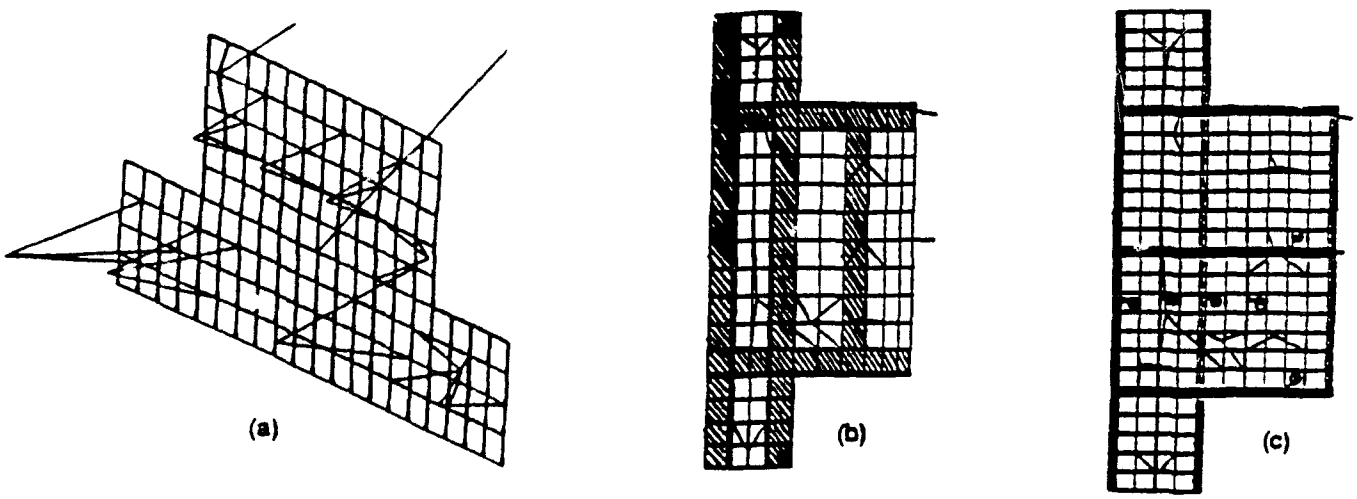

Figure 3 Concept FEMS: (a) Dual Honeycomb, (b) External Stiffener, (c) Intercostal

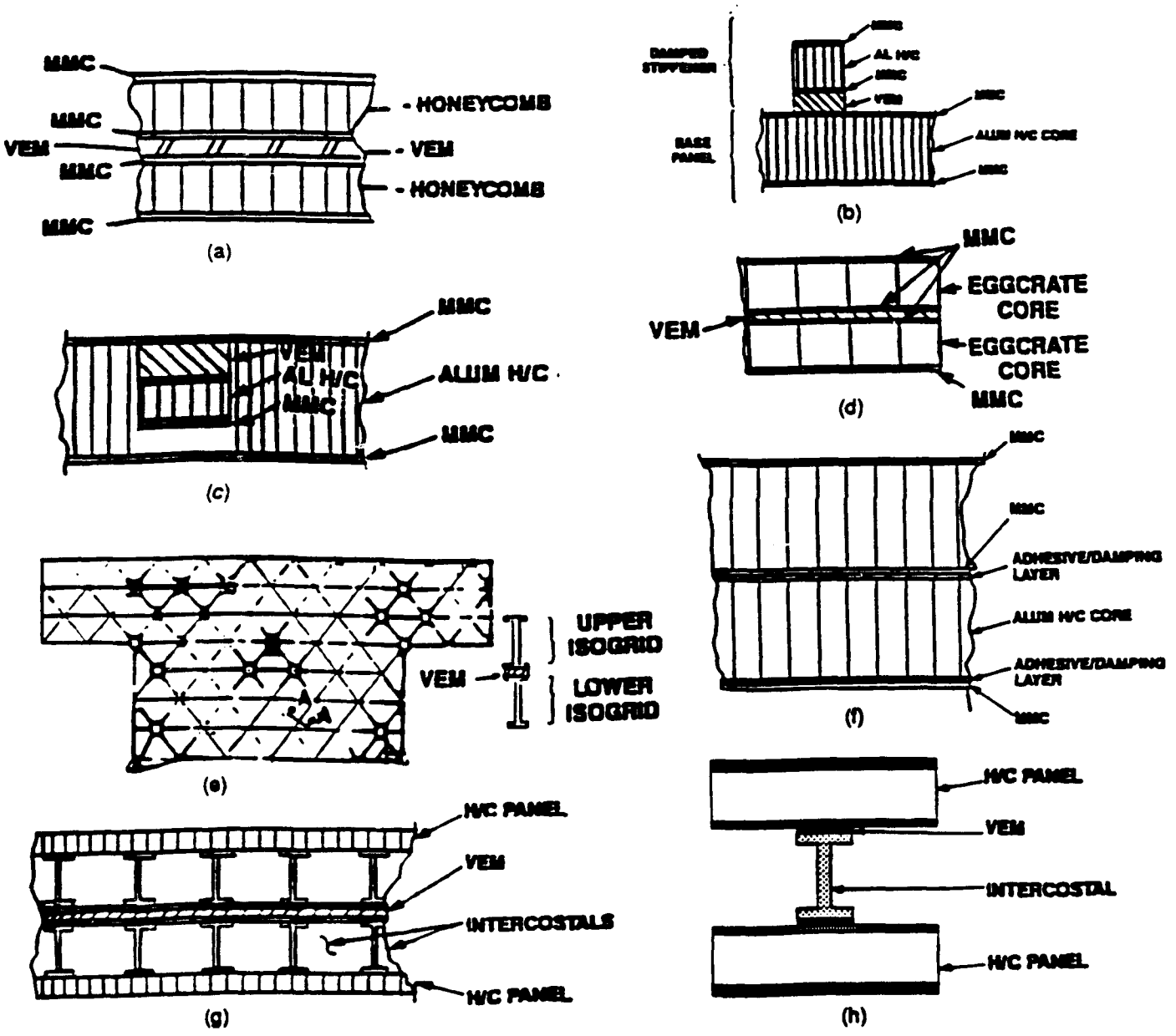

Figure 4 Eight DSA Concepts: (a) Dual Honeycomb, (b) External Stiffener, (c) Interior Stiffener, (d) Dual Eggcrate, (e) Dual Isogrid, (f) Adhesive Damping, (g) Dual Honeycomb/Intercostal, and (h) Modified Intercostal

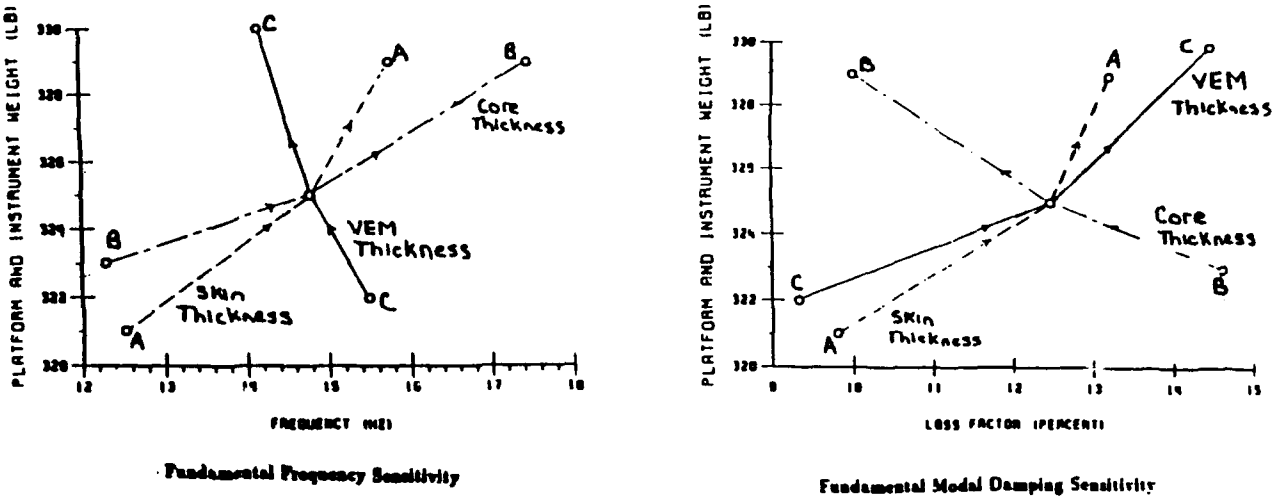

Figure 5 Frequency and Damping Sensitivity of the Dual Honeycomb Fundamental Mode

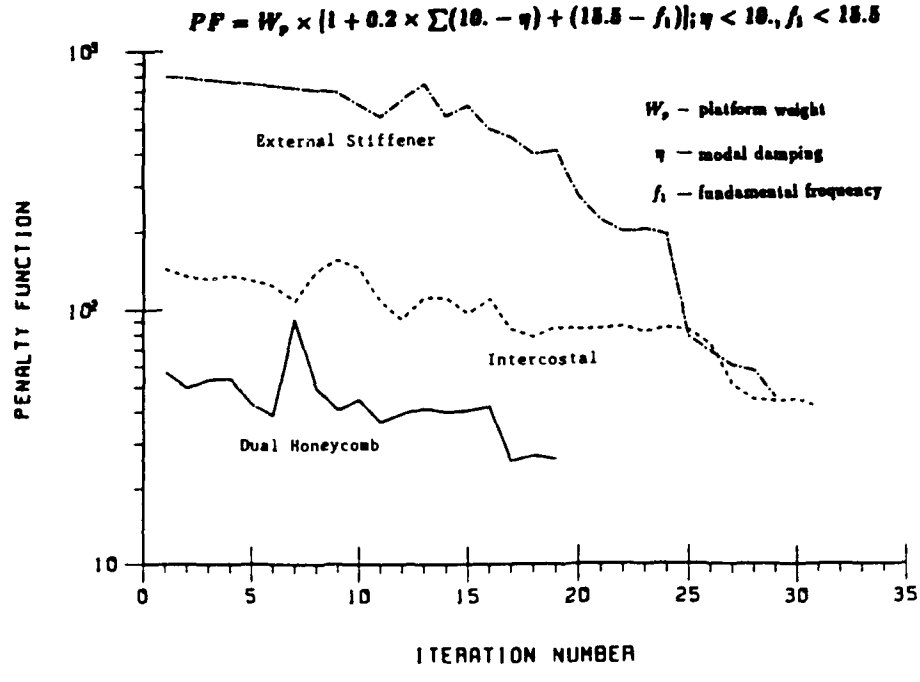

Figure 6 Penalty Function and Design Iteration History

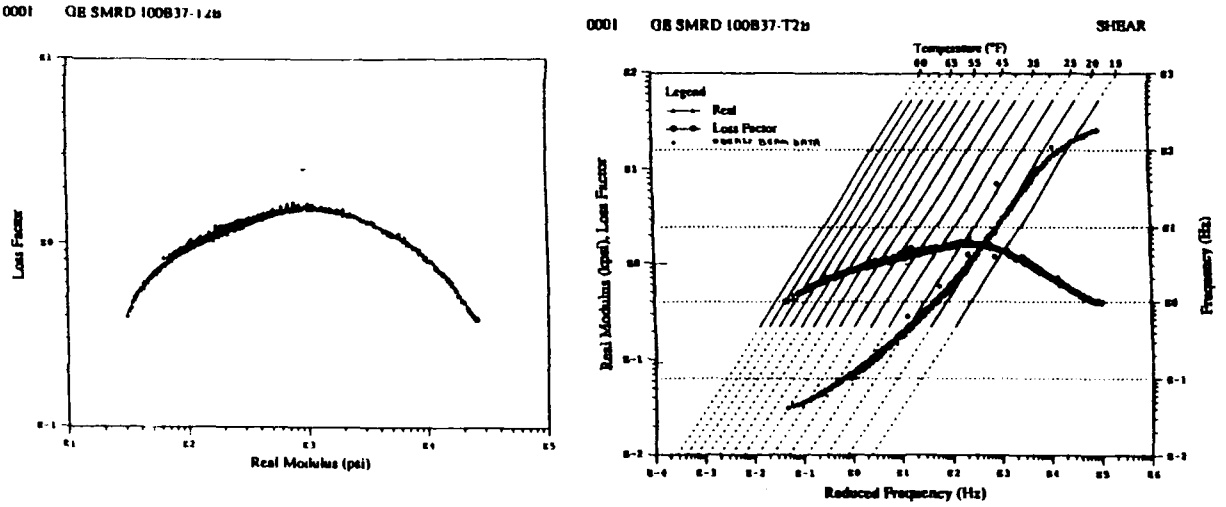

Figure 7 Storage Modulus and Loss Factor Data for SMRD B37T2B

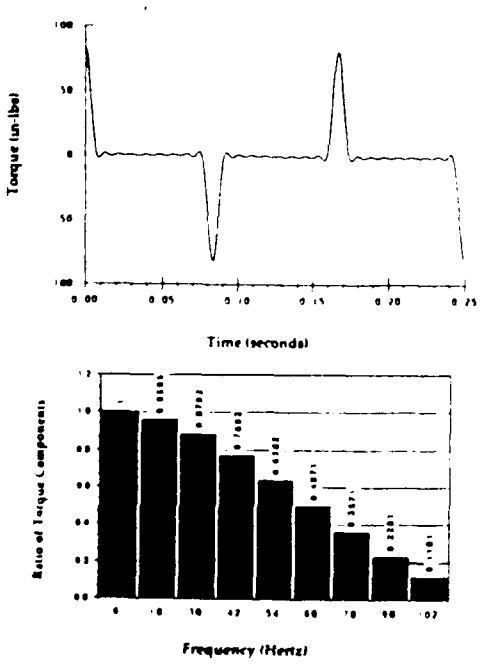

Figure 8 Input Torque Pulse Train and Fourier Components

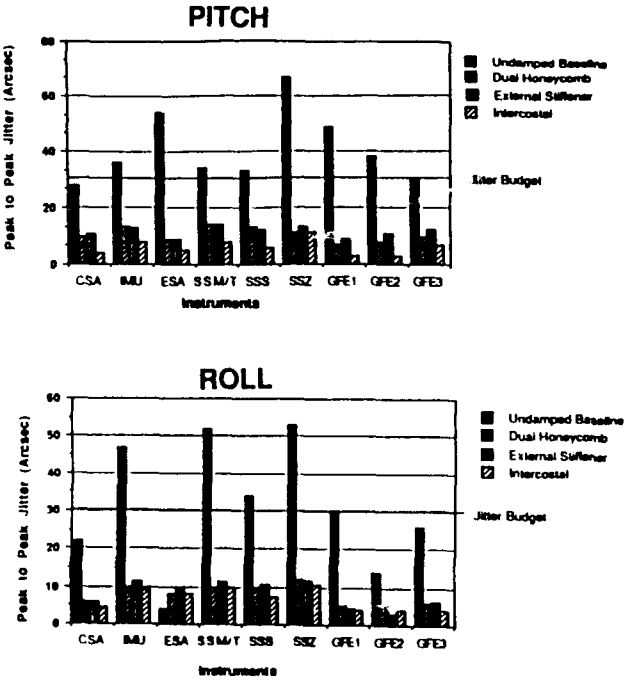

Figure 9 Worst Case Jitter Results Comparison

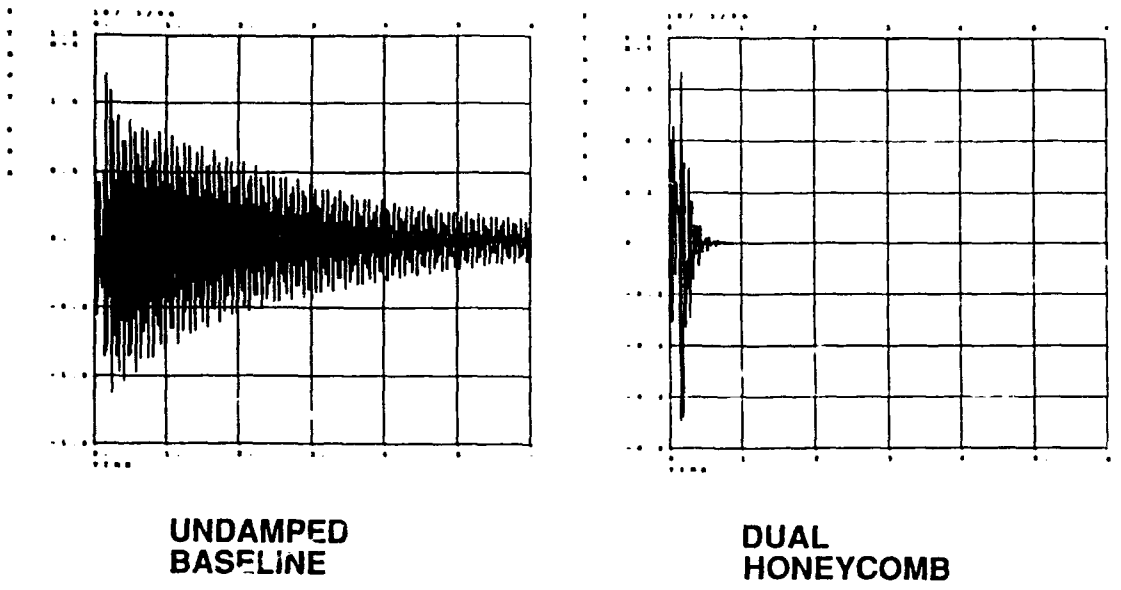

Figure 10 Settling Time Comparison - Undamped Eggcrate vs Damped Dual Honeycomb

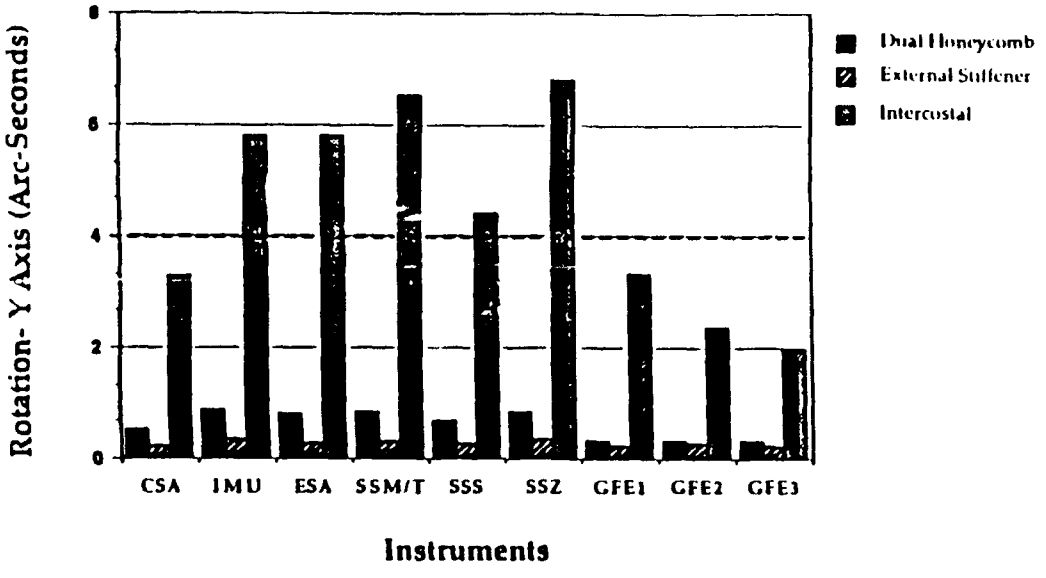

Figure 11 Thermal Distortion Comparison

SYNERGISTIC DESIGN OF PASSIVE DAMPING AND METAL MATRIX COMPOSITES

E. D. Pinson
Lockheed Missiles & Space Company, Inc.
Space Systems Division
1111 Lockheed Way
Sunnyvale, CA 94089-3504

E. M. Austin
CSA Engineering, Inc.
560 San Antonio Rd.
Palo Alto, CA 94306-4682

M. L. Zeigler
Flight Dynamics Directorate
Wright Laboratory, U.S. Air Force
Wright-Patterson AFB, OH 45433-5553

Advanced materials, such as Metal Matrix Composites, offer significant improvements in the areas of stiffness, weight, and thermal stability over most conventional materials. To further enhance the benefits afforded by these materials, integration of a passive damping concept should occupy a prominent place in the structural design process as early as feasible. To prove this synergistic approach, a simplified version of a flight-ready spacecraft attitude sensor platform has been chosen. Ultimately, two such platforms will be built, tested, and contrasted in several ways to demonstrate the performance improvements which are possible through this integrated approach. One structure will be fabricated using conventional materials and fabrication techniques, while the other will combine Metal Matrix Composite panels with a constrained-layer viscoelastic damping treatment. This paper describes the requirements, history, and design of the passively damped structure, and introduces plans for future testing and validation of analytical models.

INTRODUCTION

Present military aerospace systems, as well as those planned for future development, require increasingly stringent dimensional precision which is unattainable with reasonable extrapolations of current technology. In particular, the capabilities of systems involving radar, optical, communications, and infrared surveillance are becoming limited by structural and attitude control considerations. Deformations induced by thermal excursions and gradients make attainment of required dimensional precision extremely challenging. In addition, dynamic motions due to operational or residual vibrations often limit the ability to establish and/or maintain required pointing accuracies. These challenges are especially critical when the attitude control system itself is involved, because even small errors in sensor alignment can lead to significant misalignments of the satellite.

This paper describes the Damping and Metal Matrix for Precision Structures (DAMMPS) program, an Air Force Wright Laboratory program being performed by Lockheed Missiles and Space Co. (LMSC). The objective of this program is to demonstrate the synergistic benefits of metal matrix composites (MMC) and viscoelastic materials (VEMs). MMC technologies provide high specific stiffness, high thermal conductivity, and a low coefficient of thermal expansion, and VEM technologies provide passive vibration damping (PVD). The approach of DAMMPS is to design, fabricate, and test two Demonstration Structural Articles (DSAs) that functionally duplicate a satellite Attitude Reference Module (ARM) [1]. One of these structures will be constructed of aluminum, providing baseline data from which improvements will be measured, and the other will incorporate PVD and MMC in the design. Both structures will contain mass simulators representing inertial reference units (IRUs), horizon sensors, and an accelerometer unit.

The process of selecting an appropriate DSA began with five potential candidate structures and was based on an evaluation of several weighted criteria. Because this is an advanced development program for the Air Force with the goal of technology transition into hardware programs, the two highest weighted criteria were probability of insertion and cost. Other criteria, in descending order of weighting, were definition of environment, PVD treatment, and testing complexity. Based on these criteria, the ARM, which is currently in the hardware phase of an ongoing Air Force program, was chosen as the DAMMPS DSA because it possessed the greatest design maturity and detailed knowledge of the two environments of interest. The most unattractive aspect was the relative complexity of the structural configuration, but with subsequent simplifications, preserving all salient features, a modified version of the ARM emerged as the final choice.

The DSA design further evolved during the preliminary design phase from a simplified representation of the ARM to a detailed dynamic model with better traceability to satellite system configuration and requirements. The original design placed the two horizon sensors on the "top" of the DSA along with the accelerometer unit. Further, the size and mounting details of the simulated sensors were not precisely replicated. Following a meeting between ARM and DAMMPS personnel, it was decided to move the horizon sensors to the "bottom" of the DSA, and to scale and more closely represent actual mounting characteristics of the mass simulators. In this way, the DSA will more accurately reflect the dynamic response of the ARM. Figure 1 depicts the original ARM and the current DSA.

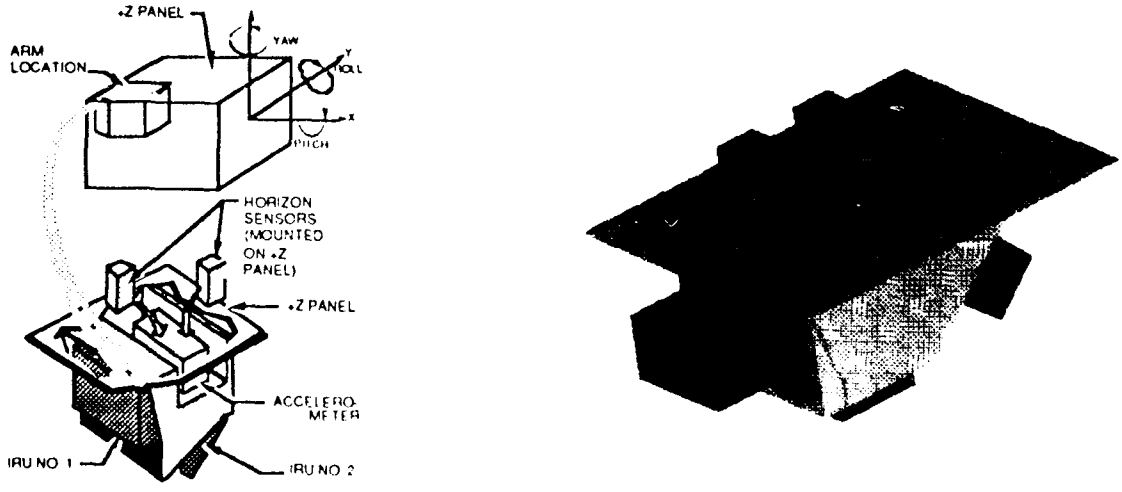

Figure 1. Traceability of the DSA to ARM

This paper provides an overview of the DAMMPS program at LMSC, including goals, technical progress, and plans. Particular emphasis will be placed on the passive damping aspects.

ARM AND DSA OPERATIONAL ENVIRONMENTS

One of the principal reasons for selecting the ARM for detailed study under the DAMMPS contract was the maturity of knowledge regarding the thermal and dynamic environments. In most instances, the level of detail available greatly exceeded that which could be efficiently utilized in the planned test program, therefore conservative simplfications were employed. Figure 2 is a comparison between the ARM thermal environment specification and the simplified temperature distributions which are designed to simulate a nominal operational loading.

Location	Hot °F	Cold °F
Horizon Sensors	82	47
IRUs	107	72
Accelerometer	98	61
ARM -Roll Axis End	103	68
ARM +Roll Axis End	101	69
ARM -Pitch Axis End	96	66
ARM +Pitch Axis End	98	62
ARM/IRU-1 Support Plate	107	67
ARM/IRU-2 Support Plate	107	68

ARM Thermal Environment Specification

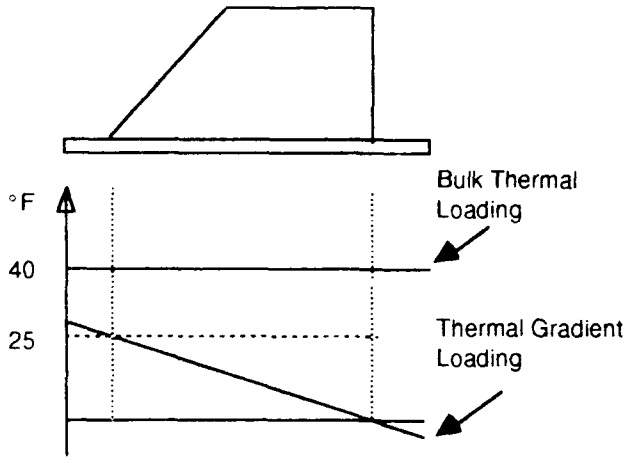

DSA Thermal Environment Simplification

Figure 2. Thermal Environments of the ARM and DSA

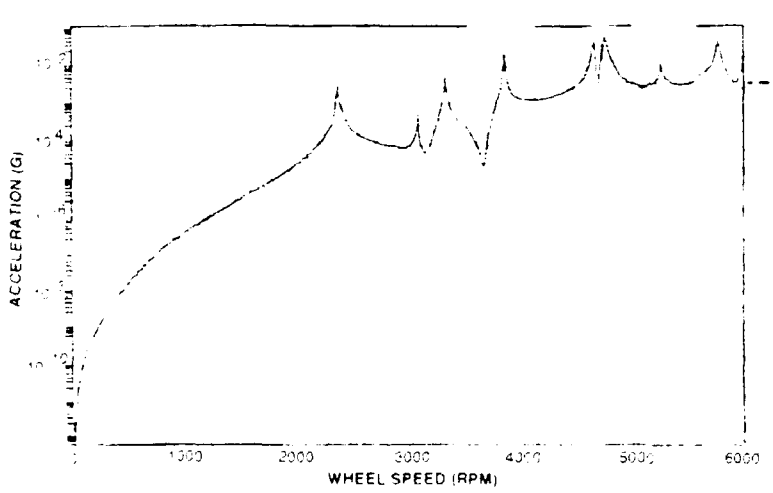

ARM Dynamic Environment Specification

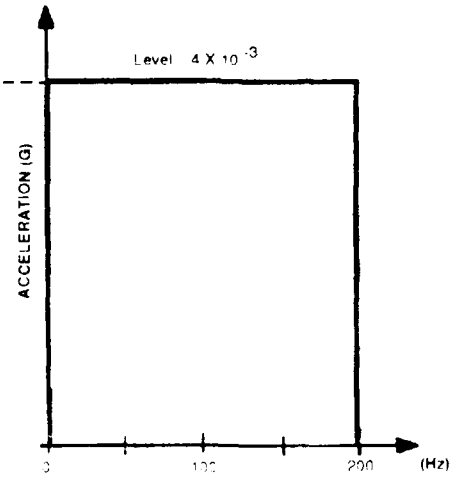

DSA Dynamic Environment Simplification

Figure 3. Dynamic Environments of the ARM and DSA

The dynamic environment of the ARM is dominated by inputs from the reaction wheel assembly (RWA) which is mounted to the spacecraft bus a short distance away. The spectrum of this excitation

source is known to be dominated by the first harmonic, and may excite the bus (hence, the ARM) in any direction. The test-derived envelope of RWA spectra, representing maximum vibration levels observed in any direction at specific wheel speeds, is shown in Figure 3. The RWAs are presently used at speeds under 3000 rpm, but growth plans involve operation to 3500 rpm (58.3 Hz., assuming first harmonic dominance). Based on these considerations, the peak dynamic excitation from the wheels (below the growth speed) is 0.004 g – assumedly steady-state, due to the nature of the excitation source. A more conservative dynamic environment (shown for comparison purposes in Figure 3) has been assumed for the DSA. This simplified spectrum is based on the peak acceleration level of the current RWAs, but extends to 200 Hz.

ARM AND DSA PERFORMANCE REQUIREMENTS

Another of the principal reasons for selecting the ARM for DAMMPS contract studies was the maturity of system-level requirements flow-downs with regard to thermally and dynamically induced error budgets. These requirements fall into two general categories: those designed to protect the sensors themselves, and those designed to yield consistent information from all sensors (alignment tolerances). Requirements from both categories are shown in Figure 4.

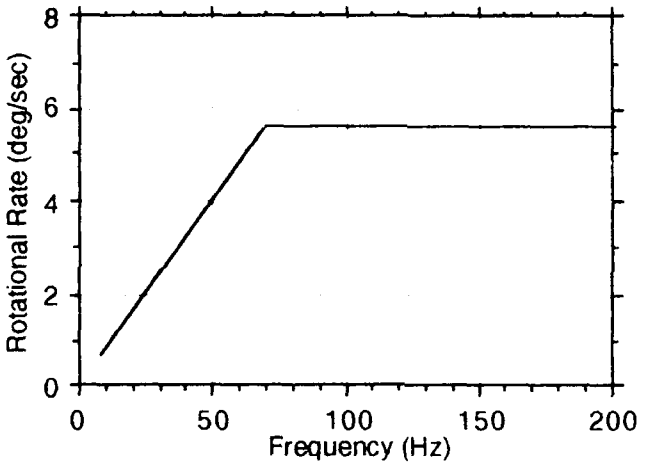

COMPONENTS	Axis	IRUs			HSs		
		Pitch	Roll	Yaw	Pitch	Roll	Yaw
Accelerometer	Pitch				120		
	Roll					120	
	Yaw			120			
IRUs	Pitch				34		
	Roll					34	
	Yaw						
HSs	Pitch	34					
	Roll		34				
	Yaw						

Units: Arc-seconc

Figure 4. ARM and DSA Rotational Rate and Alignment Requirements

DSA RESPONSE ANALYSES

During the preliminary design phase of the cotract, several finite-element models of DSA were constructed and subjected to appropriate thermal and dynamic environments. All models share the same general geometry as shown in Figure 5, which is a representative finite-element model used for dynamic response studies.

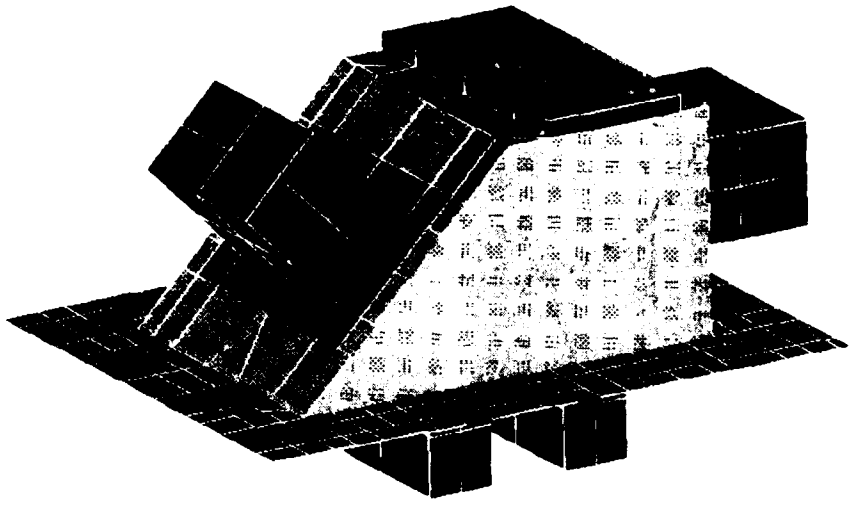

Figure 5. Representative Finite-Element Model of the DSA

For the purpose of comparison, several different material properties were substituted into geometrically similar models (see Figure 6). Standard aluminum characteristics were used to establish a baseline and coarse-tune panel thicknesses. Current plans involve the use of an aluminum sheet, folded to produce the general shape of the DSA above the baseplate. All joints will then be fastened using either sheet-metal screws or welded connections.

Two different MMC materials and shapes are required to produce the other DSA. In this case, SiC/Al structural angles (0.25 VF) and several flat P100/Al quasi-isotropic plates will be joined together to form a precision sensor base. For connections between the "upper" DSA and the baseplate, angles will be placed in exterior corners for ease of construction. Due to mounting constraints, angles to fasten the top plate to the side panels will be located on interior surfaces.

Material	Young's Modulus [psi]	Density [lb/in^3]	Coefficient of Thermal Expansion [in/in/°F]
SiC/Al (0.25 VF)	17.0	0.102	7.0 X 10^{-6}
P100/Al (Quasi-isotropic)	20.0	0.090	1.9 X 10^{-6}
Aluminum	10.0	0.098	13.0 X 10^{-6}

Figure 6. Selected Mechanical Properties of DSA Materials

The aluminum DSA was used to establish a baseline thermal performance level which was compared with that of the MMC DSA. Misalignment results for the Aluminum DSA are shown in Figure 7. Figure 8 presents the same results for the MMC DSA. While these results should be compared to each other to determine the level of improvement attainable by changing the material of the structure, these

esults should also be compared to Figure 4 – the alignment requirements. This latter comparison ndicates that neither structural configuration produces the required results, but the MMC DSA deviates rom allowable levels in only two areas (both involving IRU-2), whereas, the aluminum DSA exceeds cceptable values in several cases involving the horizon sensors and IRUs. Slight modifications to the onfiguration, presently under investigation, are available to the designer and analyst to improve these esults even further.

COMPONENTS		IRU-1			IRU-2			HS-1			HS-2		
		Pitch	Roll	Yaw	Pitch	Roll	Yaw	Pitch	Roll	Yaw	Pitch	Roll	Yaw
Accelerometer	Pitch Roll Yaw			0/0			0/0	18/2	109/36		6/6	123/6	
IRU-1	Pitch Roll Yaw							18/2	123/58		6/6	137/15	
IRU-2	Pitch Roll Yaw							18/2	34/4		6/6	21/38	
HS-1	Pitch Roll Yaw	18/2	123/58		18/2	34/4							
HS-2	Pitch Roll Yaw	6/6	137/15		6/6	21/38							

Notes: 1. Units: arc-seconds.
2. Bulk Response/Gradient Response.

Figure 7. Alignment Deviations due to Thermal Loading of the Aluminum DSA

COMPONENTS		IRU-1			IRU-2			HS-1			HS-2		
		Pitch	Roll	Yaw	Pitch	Roll	Yaw	Pitch	Roll	Yaw	Pitch	Roll	Yaw
Accelerometer	Pitch Roll Yaw			0/0			0/0	28/7	21/10		0/3	23/30	
IRU-1	Pitch Roll Yaw							28/7	11/10		0/3	10/0	
IRU-2	Pitch Roll Yaw							29/8	38/6		1/3	40/16	
HS-1	Pitch Roll Yaw	28/7	11/10		29/8	38/6							
HS-2	Pitch Roll Yaw	0/3	10/0		1/3	40/16							

Notes: 1. Units: arc-seconds.
2. Bulk Response/Gradient Response.

Figure 8. Alignment Deviations due to Thermal Loading of the MMC DSA

The DSA was designed such that salient dynamic characteristics are traceable to the ARM. To achieve this, mass simulators and panels were sized and placed to yield the first four modal frequencies near those of the ARM, though information concerning the associated mode shapes is minimal. While the finite-element models contain more element detail than needed for most basic eigenvalue analyses, there is appropriate detail for performing trade studies and predicting damping performance. Fixed boundary conditions were imposed at the edges of the baseplates to simulate mounting on a relatively stiff spacecraft bus or test fixture. The first four modes predicted for the aluminum DSA are shown in Figure 9. Their frequencies are 66.8 Hz, 77.6 Hz, 78.4 Hz, and 109.8 Hz. – acceptably close to those of the ARM.

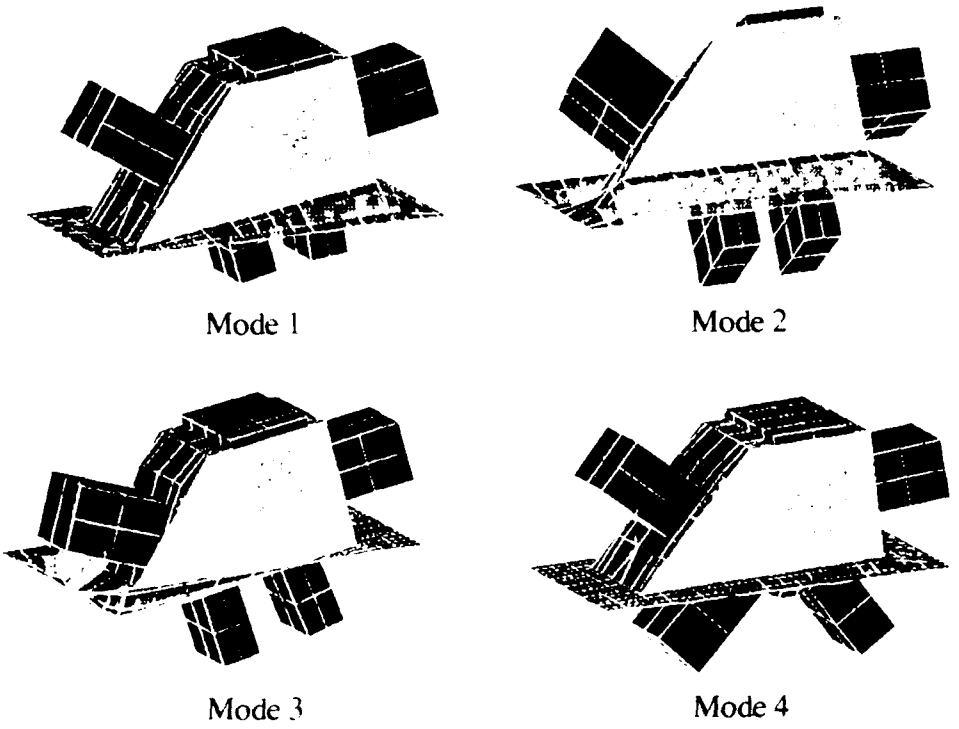

Figure 9. Four Lowest Frequency Mode Shapes of the Aluminum DSA

A baseline undamped MMC finite-element model was constructed and used as a starting point for the analogous damped structure. In this model, MMC panels were sized such that natural frequencies of the first four modes were as close possible to those of the aluminum baseline, further maintaining traceability.

Standard damping treatment design methods require identifying offending modes of the structure and performing trade studies involving various damping solutions. The target modes were those which contributed the largest percentage to base rotation rates at the IRUs and sensor misalignments – the two classes of performance requirements. At this point, the damping level normally associated with a jointed aluminum structure (e.g., 0.5% of critical) was used as a baseline for all modes to determine the level of additional damping required from a passive damping treatment. Since, by replicating known frequencies of the "as-mounted" ARM, the DSA model was designed to simulate the dynamic load path from the RWA to the ARM, excitation was applied as a base shake of the DSA from the constrained rim of the base plate. Using the assumed 0.5% damping ratio, transfer functions were calculated which related base shake inputs in the x, y, and z directions to each of the pertinent response quantities (i.e., relative alignments and IRU base rotational rates). By definition, these transfer

functions represent the dynamic responses to steady-state, unit-amplitude, sinusoidal base shake inputs. Data thus obtained were scaled to 0.004 g to determine the responses at the actual input levels.

As expected, several different analytical modes produce dominant responses, depending on the excitation frequency and direction. To determine modal damping requirements, each of the peak responses in each of the transfer functions were tabulated. A total of nineteen response quantities and three input directions yielded 57 plots which were examined in this manner. Final results indicated that the lowest four modes dominated all critical response quantities. Therefore, by linearly scaling the baseline damping level, the required damping levels for these four modes (in order) were determined to be 4.0%, 3.5%, 4.0%, and 1.2%. Implicitly, the assumption was made that only damping is used to bring the responses to a level consistent with the requirements.

PASSIVE DAMPING TRADE STUDIES

The most common classes of passive damping treatments are constrained-layer, free-layer, and discrete. Free-layer treatments consist of a layer of viscoelastic or other damping material applied directly to the base structure. In general, these treatments are heavy as well as inefficient for bending modes; thus the concept is not being considered for DAMMPS. Discrete damper concepts such as tuned-mass dampers and damped links, usually used to damp a few specific modes, are not applicable to this structure because the basic design is not readily amenable to such treatments. Constrained-layer treatments, however, are both effective and weight-efficient for damping multiple bending-dominated modes, if the bulk of the strain energy in these modes distributed over the treated area of the structure.

There are five primary characteristics of a constrained-layer damping treatment that can be varied during a trade study: location, constraining-layer (CL) thickness, CL modulus (assumed equal to that of the base material in this case), VEM thickness, and VEM modulus. The trade study undertaken for the DSA addresses each of these with an overriding goal of achieving the levels of damping outlined in the previous section while minimizing the weight of the damped platform.

Having identified the target modes damping from the dynamics requirements, the first step in the PVD design is to determine which areas of the DSA participate most in these modes. It is conclusive from both the distribution of modal strain energy (MSE, reference 2, Figure 10) and the mode shapes that damping the baseplate is necessary to achieve the goals.

	Mode 1	Mode 2	Mode 3	Mode 4	Mode 5
Frequency [Hz.]	66.77	77.60	78.45	109.8	124.9
Base Plate	81.8	61.3	82.2	13.1	51.9
Vertical Housing Plates	6.7	10.2	5.7	20.1	8.0
Sloping Housing Face	1.5	17.0	3.8	45.9	7.5
Other	10.0	11.5	8.3	20.9	32.6
Total	100.0	100.0	100.0	100.0	100.0

Figure 10. Modal Strain Energy Distribution for Target Modes

Three concepts were chosen for study to take advantage of the bending characteristics of the baseplate:

1. Make the baseplate a sandwich section, consisting of a layer of VEM between two MMC facesheets;
2. Bond the housing portion of the DSA to the baseplate with a high-loss VEM instead of a structural adhesive; and
3. Attach a pair of extruded MMC angle sections to the underside of the baseplate with a VEM.

A variation of the second candidate treatment was also studied, in which the longer two attachment brackets between the housing and baseplate were extended to the outer edge of the baseplate.

As partially enumerated before, each concept has strengths and weaknesses. In order to evaluate the relative merits of the treatments, goals were set with regard to added weight modal frequencies, and damping. The goals for weight and damping were simple: minimize the weight of the treatment and maximize the damping provided. For frequency, the goal was to fall within 15% of the baseline aluminum DSA frequency. Figure 11 summarizes the best effort arising from each concept, along with the relative score and overall ranks. The scores were normalized on a 100-point scale – higher scores being the best. For conciseness, the frequency and percent MSE of only the first mode are listed in this table, though each of the first four modes was considered in the final score. The VEM thickness was maintained at 0.006 in., with a shear modulus of 140 psi for each of these runs. This corresponds to the 3M Y-966 tested under DAMMPS evaluated at room temperature and 70 Hz. [3]. The loss factor of the Y-966 at room temperature is greater than 1.0 for frequencies in the approximate range of 5 to 1000 Hz., so the MSE values in Figure 11 correspond to roughly equal levels of structural loss. (In terms of structural loss, the goals for the first four modes are twice the goals for viscous damping, e.g., 8.0%, 7.0%, 8.0%, and 2.4%, respectively.)

CONCEPT	WEIGHT*	CONSTRAINING ELEMENT	MODE 1 FREQ. [HZ.]	MODE 1 MSE	FINAL SCORE	FINAL RANK
Baseline Aluminum	14.2	N/A	66.8	N/A	N/A	N/A
Sandwich Baseplate (1)	12.5	0.06" Face-sheets	49.8	8.6%	30.5	4
Structural Adhesive (2)	13.2	Housing	63.5	10.4%	56.1	3
Variation on Structural Adhesive (3)	9.3	Housing with Extended Angle Brackets	109.0	9.6%	62.5	2
Constrained Angles on Bottom (4)	8.8	1 X 1 X 0.08 Extruded Angles	48.2	20.7%	100.0	1

* Weight does not include the 62.1 lbs for the mass simulators

(1) VEM sandwiched between two 0.060"-thick MMC facesheets

(2) VEM replacing structural adhesive between housing and baseplate

(3) VEM replacing structural adhesive between housing and baseplate as well as long-direction attachment brackets extending the length of the baseplate.

(4) VEM sandwiched between baseplate and extruded angle section on the underside of the housing

Figure 11. Relative Ranking of Candidate Damping Treatments

Each of the concepts could be altered so that it met some of the goals, but adding the "constrained stiffener" treatment to the underside of the baseplate proved to be the best compromise. It provides very high levels of damping (10% viscous in the first two modes and 5% in the third and fourth) and results in a weight reduction of approximately 40% over the aluminum baseline structure.

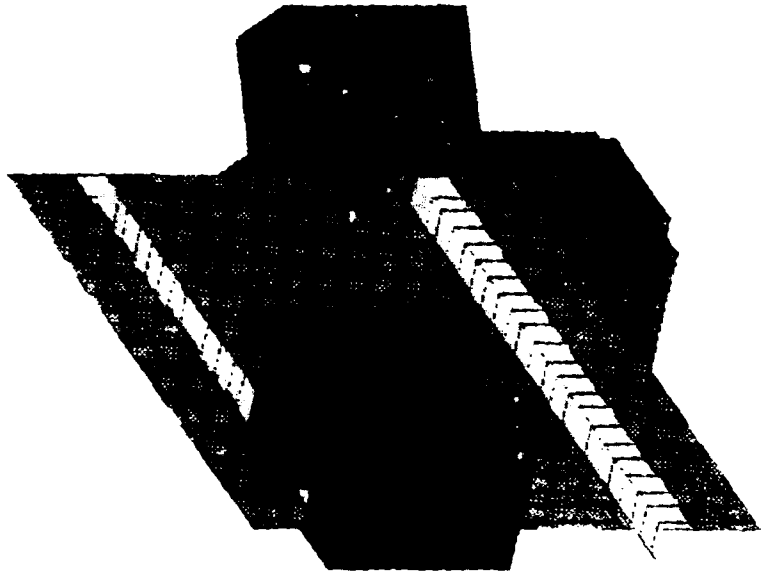

Figure 12. Selected PVD Concept

SUMMARY AND FUTURE PLANS

At this point in the study, a baseline structural configuration has been selected and modeled. Thermal analysis shows that some minor modifications and/or analytical refinements must be made to meet the requirements in the case of the undamped DSA. Further analysis will be undertaken to determine whether the damped DSA exhibits greater or lesser tendency to achieve the alignment goals for the system. If thermal conduction properties of the VEM are shown to hinder this performance, several novel concepts for optimizing this property will receive further investigation.

Purposely omitted from this paper are the ongoing activities involving design and testing of MMC coupons. This topic could not be treated adequately in conjunction with the damping studies in a discussion of reasonable length. Since the stiffness characteristics and the associated MSE distribution of the DSA are contingent on the accurate mechanical properties of MMC, the current thrust of efforts in this area is directed toward proving the accuracy and repeatability of these properties. Results from these studies will be utilized in future analyses of both the thermal and dynamic performance of the DSA.

As knowledge of MMC properties is obtained and the details of the PVD treatment converge on a viable design, component testing will begin, to prove the analytical assumptions and predictions and to fine-tune the finite-element models. Following this basic groundwork, the DSAs will be fabricated and tested at the system level.

ACKNOWLEDGEMENTS

The work described in this paper is being performed under the Damping and Metal Matrix for Precision Structures (DAMMPS) contract, sponsored by the Flight Dynamics Directorate of the Wright Laboratory. Though the efforts of several others were very important to achieving the successes summarized here, special thanks is given to Dr. Y.C. Yiu for his technical advice and service as a focal point for this phase of the program. The technical and administrative assistance of Mr. J. Warren Hoskins, Program Manager, is also gratefully acknowledged. Special thanks are also due to Mr. Kevin Napolitano for his expertise in modeling the DSA and performing several of the passive damping trade studies described herein.

REFERENCES

1. Yiu, Y.C., and Pinson, E.D., "Damping and Metal Matrix for Precision Structures - Semi-Annual Report, April 1990," Lockheed Missiles & Space Company, Inc., Document F294320-6.

2. Johnson, C.D., Kienholz, D.A., "Finite Element Prediction of Damping in Structures with Constrained Viscoelastic Layers," AIAA Journal, Vol. 20, September, 1982, pp. 1284-1290.

3. Allen, B.R., Pinson, E.D., "Complex Stiffness Test Data for Three Viscoelastic Materials by the Direct Complex Stiffness Method," presented at the Damping '91 Conference, San Diego, CA, February 13-15, 1991.

A Three Element Viscoelastic Isolator

FAC-1

Presented at : Damping '91
February 13-15, 1991
Catamaran Hotel
San Diego, CA

S. S. Simonian
14 February 1991

AGENDA

- PROBLEM
- STRUCTURE CONFIGURATION
- BASELINE RWA ISOLATOR DESIGN
- ISOLATOR CHARACTERISTICS
- SOME TEST RESULTS

PROBLEM

- EXCESSIVE SENSOR LOS DISTURBANCES
- REACTION WHEEL INDUCED DISTURBANCES
  - STATIC UNBALANCE
  - DYNAMIC UNBALANCE
  - BEARING NOISE
- LOW STRUCTURAL DAMPING

SPACECRAFT INHERENT DAMPING

- DATA OBTAINED FROM MEASUREMENTS OF 23 SATELLITES UNDER LOW EXCITATION INPUTS, MOSTLY DURING SINE DWELL MODAL SURVEY TESTS
- A TOTAL OF 290 SAMPLE DATA POINTS
- STRUCTURE FREQUENCY RANGE 0.15 - 195 HERTZ
- FURTHER DETAILS AND STATISTICAL DAMPING MODELS REPORTED IN:

S.S. Simonian, "Survey of Spacecraft Damping Measurements: Application to Electro-Optic Jitter Problems", The Role of Damping in Vibration and Noise Control, ASME Publication DE-Vol.5, September, 1987.

Low Amplitude Modal Damping Database

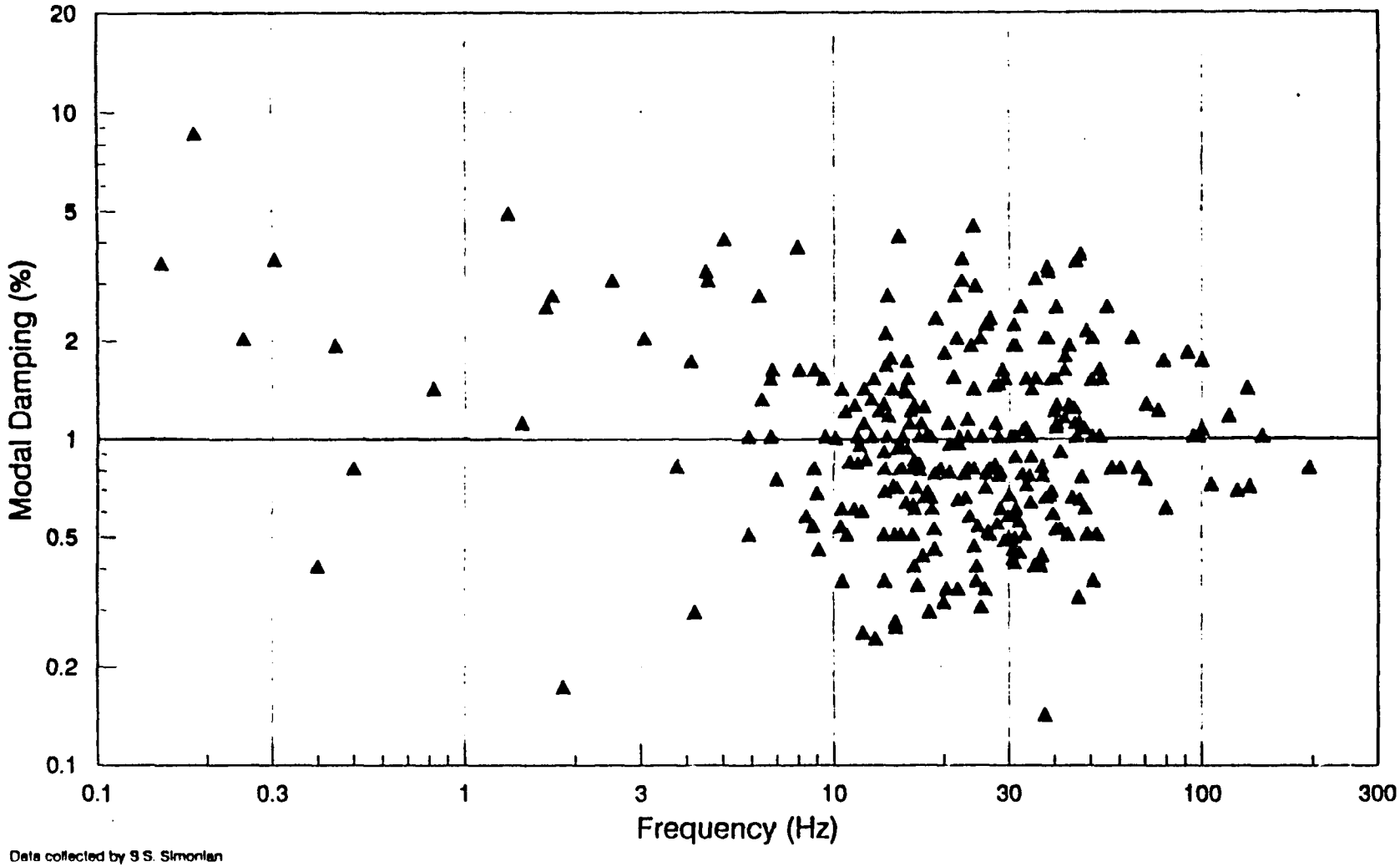

Data collected by S.S. Simonian
Several spacecraft are represented
DSP data has similar distribution

Low Amplitude Damping - Probability Density

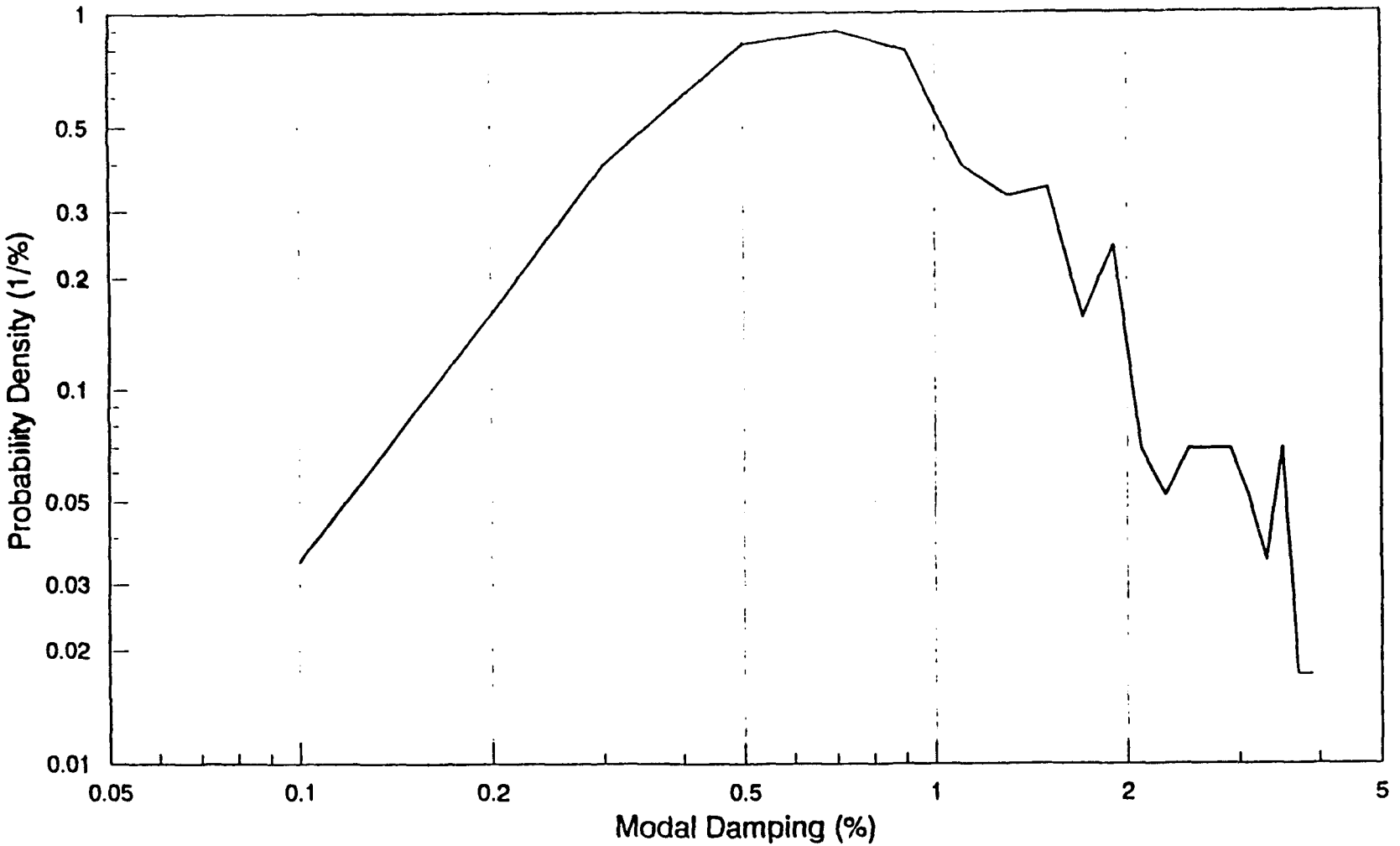

Data collected by S.S. Simonian
Several spacecraft are represented
DSP data has similar distribution

Low Amplitude Damping - Cumulative Probability

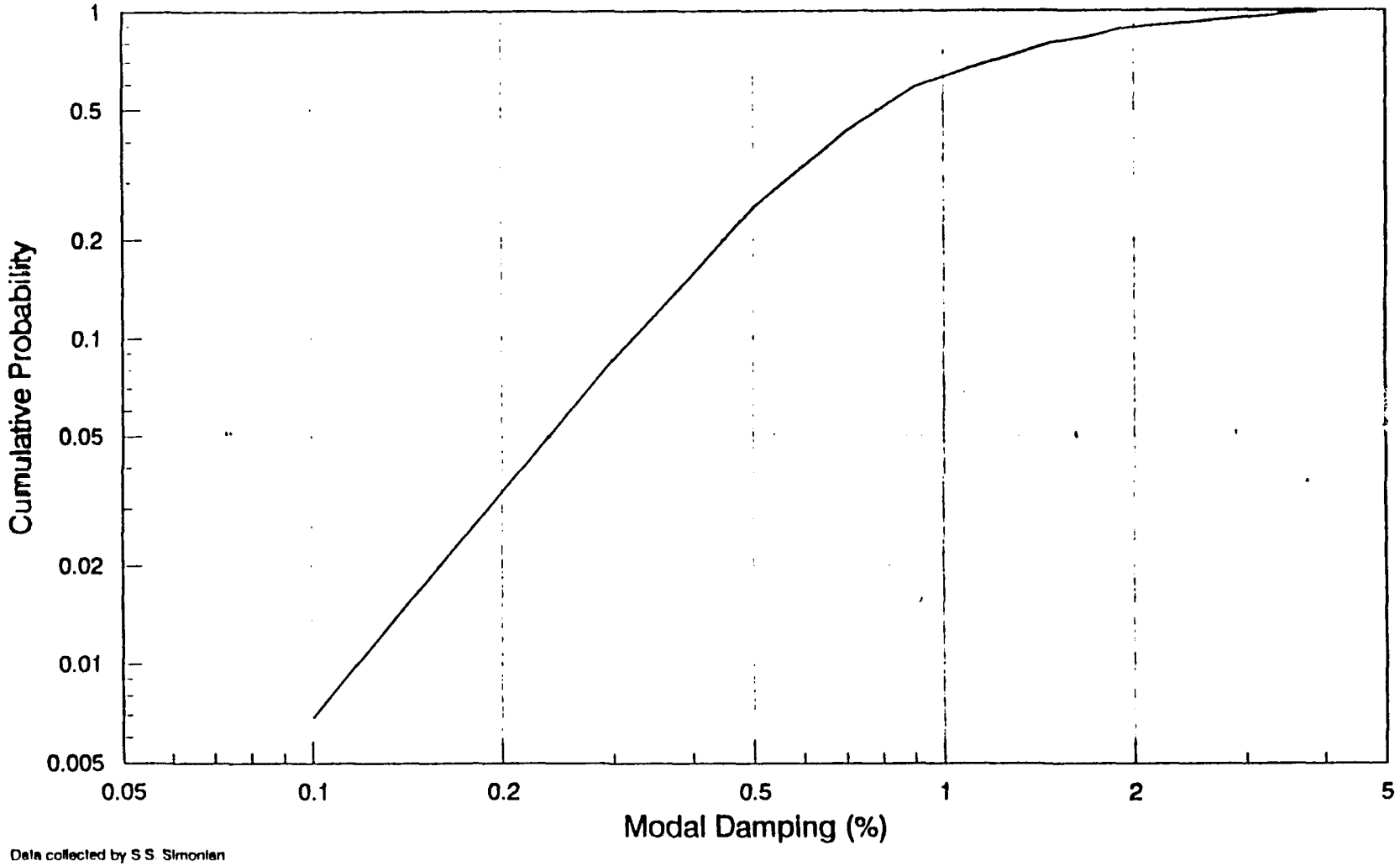

Data collected by S.S. Simonian
Several spacecraft are represented
DSP data has similar distribution

ROTOR STATIC & DYNAMIC UNBALANCE

FORCE OR MOMENT

$F = \delta . M . \Omega^2$

F = FORCE OR MOMENT (LB OR IN-LB)

M = ROTOR MASS (LB-SEC^2/IN)

Ω = WHEEL SPEED (RAD/SEC)

δ = CONSTANT OF PROPORTIONALITY (TABULATED)

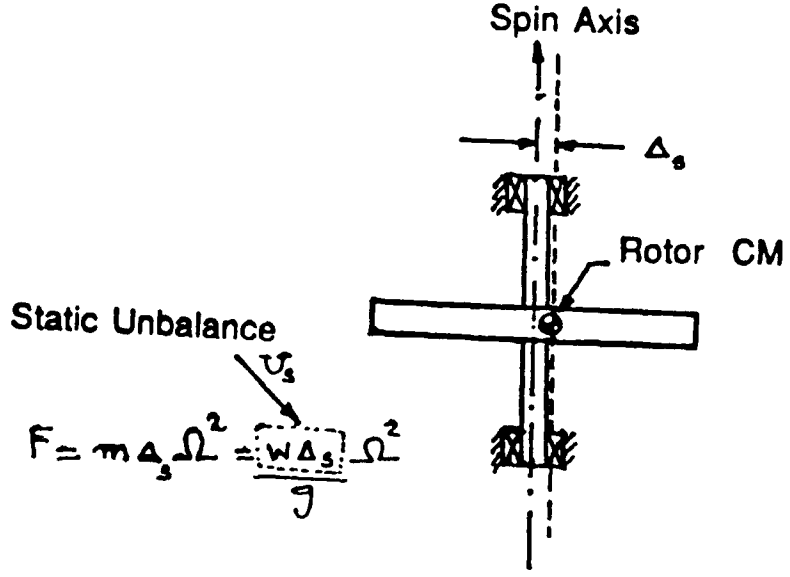

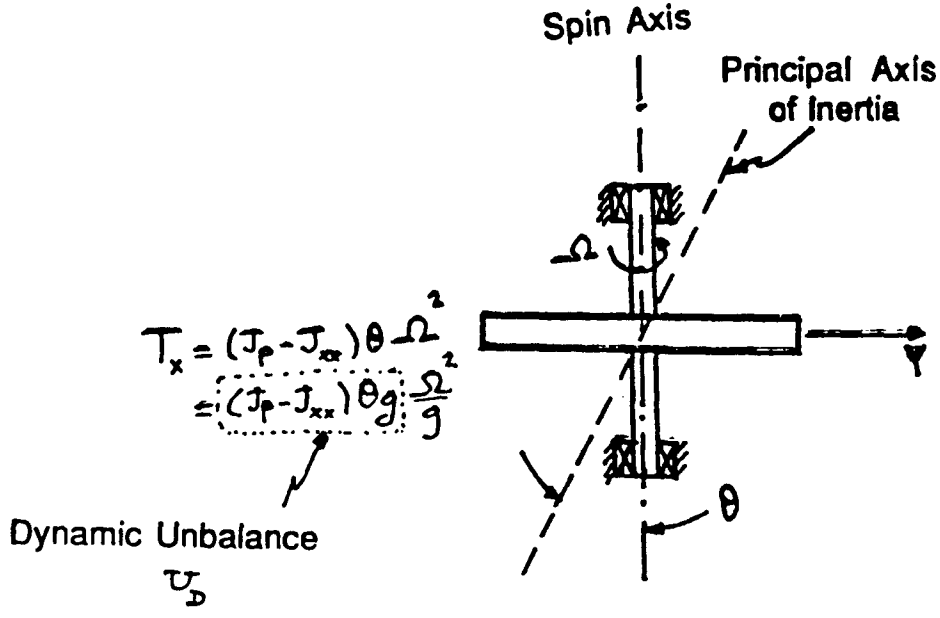

BALL BEARING DISTURBANCES

BALL BEARING GEOMETRY

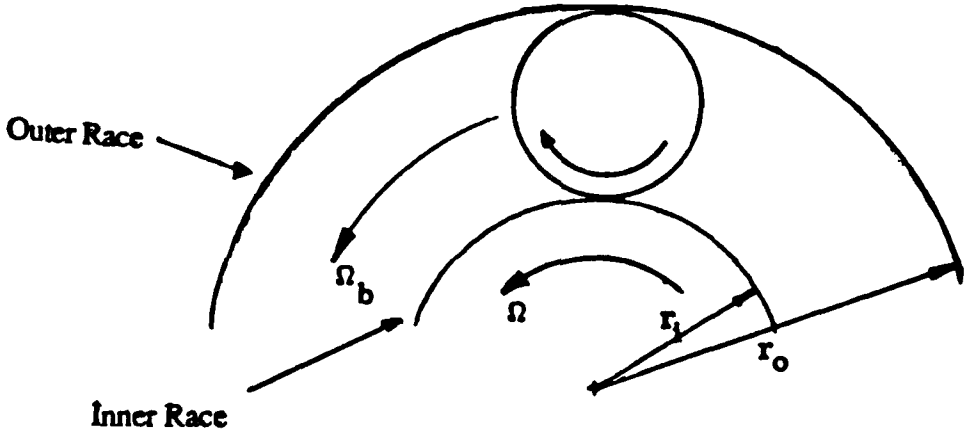

$$\frac{\Omega_b}{\Omega} = \frac{r_i}{r_i + r_o}$$

COMPONENT	SPEED
ROTOR/OUTER RACE	$N \times \Omega$
ROTOR/BALL GROUP	$N \times (\Omega - \Omega_b)$
BALL GROUP/OUTER RACE	$N \times \Omega_b$
BALLS/OUTER RACE	$N \times N_b \times \Omega_b$
ROTOR/BALLS	$N \times N_b \times (\Omega - \Omega_b)$

N_b= Number of balls

N = Harmonics of rotor speed, N = 1, 2, 3, . . .

MEASURED REACTION WHEEL DISTURBANCE MODELS

- PROPORTIONALITY CONSTANTS FOR TWO TRW REACTION WHEELS

Disturbance	Harmonic	Axial Force	Lateral Force (Y)	Lateral Force (Z)	Radial Force (avg)	Lateral Moment (Y)	Lateral Moment (Z)	Radial Moment (avg)
		$(in \cdot 10^{-6})$	$(in \cdot 10^{-6})$	$(in \cdot 10^{-6})$	$(in \cdot 10^{-6})$	$(in^2 \cdot 10^{-6})$	$(in^2 \cdot 10^{-6})$	$(in^2 \cdot 10^{-6})$
Ball Group / Outer Race	1	0.061	0.150	0.200	0.175	6.0	5.0	5.5
(0.418 x Wheel Speed)	2	0.081	0.040	0.040	0.040	1.5	5.0	3.3
	3	0.098	0.040	0.080	0.060	3.0	3.0	3.0
	4	0.175	0.150	0.200	0.175	1.5	3.0	2.3
Ball Group / Inner Race	1	0.051	0.030	0.020	0.025	2.0	2.0	2.0
(0.582 x Wheel Speed)	2	0.177	0.020	0.090	0.055	2.0	4.0	3.0
	3	0.179	0.200	0.200	0.200	4.0	4.0	4.0
Inner / Outer Race	1	13.500	1.300	1.800	1.550	550.0	500.0	530.0
(1.000 x Wheel Speed)	2	1.180	0.800	1.500	1.150	20.0	20.0	20.0

Disturbance	Harmonic	Axial Force	Lateral Force (Y)	Lateral Force (Z)	Radial Force (avg)	Lateral Moment (Y)	Lateral Moment (Z)	Radial Moment (avg)
		$(in \cdot 10^{-6})$	$(in \cdot 10^{-6})$	$(in \cdot 10^{-6})$	$(in \cdot 10^{-6})$	$(in^2 \cdot 10^{-6})$	$(in^2 \cdot 10^{-6})$	$(in^2 \cdot 10^{-6})$
Ball Group / Outer Race	1	0.015	0.500	0.500	0.500	6.0	6.0	6.0
(0.418 x Wheel Speed)	2	0.010	0.030	0.070	0.050	3.0	0.7	1.9
	3	0.091	0.090	0.110	0.100	2.0	6.0	4.0
	4	0.371	0.200	0.110	0.155	2.0	1.5	1.8
Ball Group / Inner Race	1	0.026	0.020	0.020	0.020	3.0	3.0	3.0
(0.582 x Wheel Speed)	2	0.382	0.040	0.050	0.045	4.0	4.0	4.0
	3	0.383	0.200	0.100	0.150	7.0	7.0	7.0
Inner / Outer Race	1	1.230	3.000	2.500	2.750	400.0	400.0	400.0
(1.000 x Wheel Speed)	2	1.450	0.500	0.700	0.600	10.0	10.0	10.0

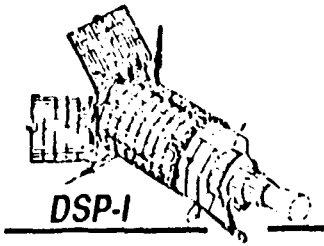

DSP Basic Structure Assembly

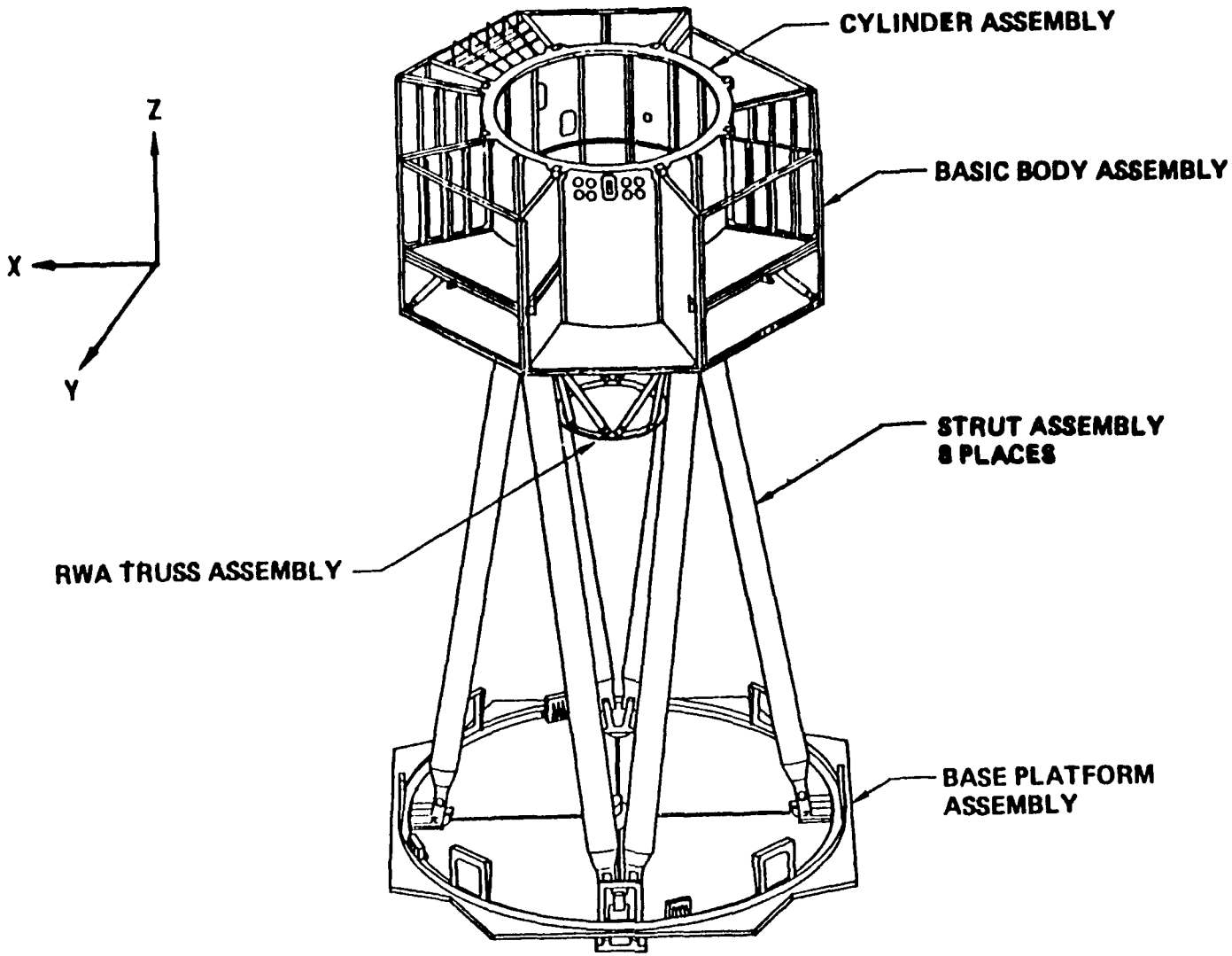

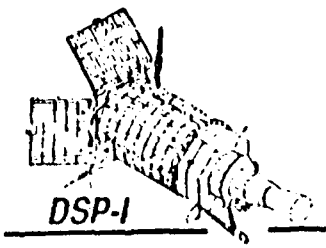

RWA and Truss Assembly

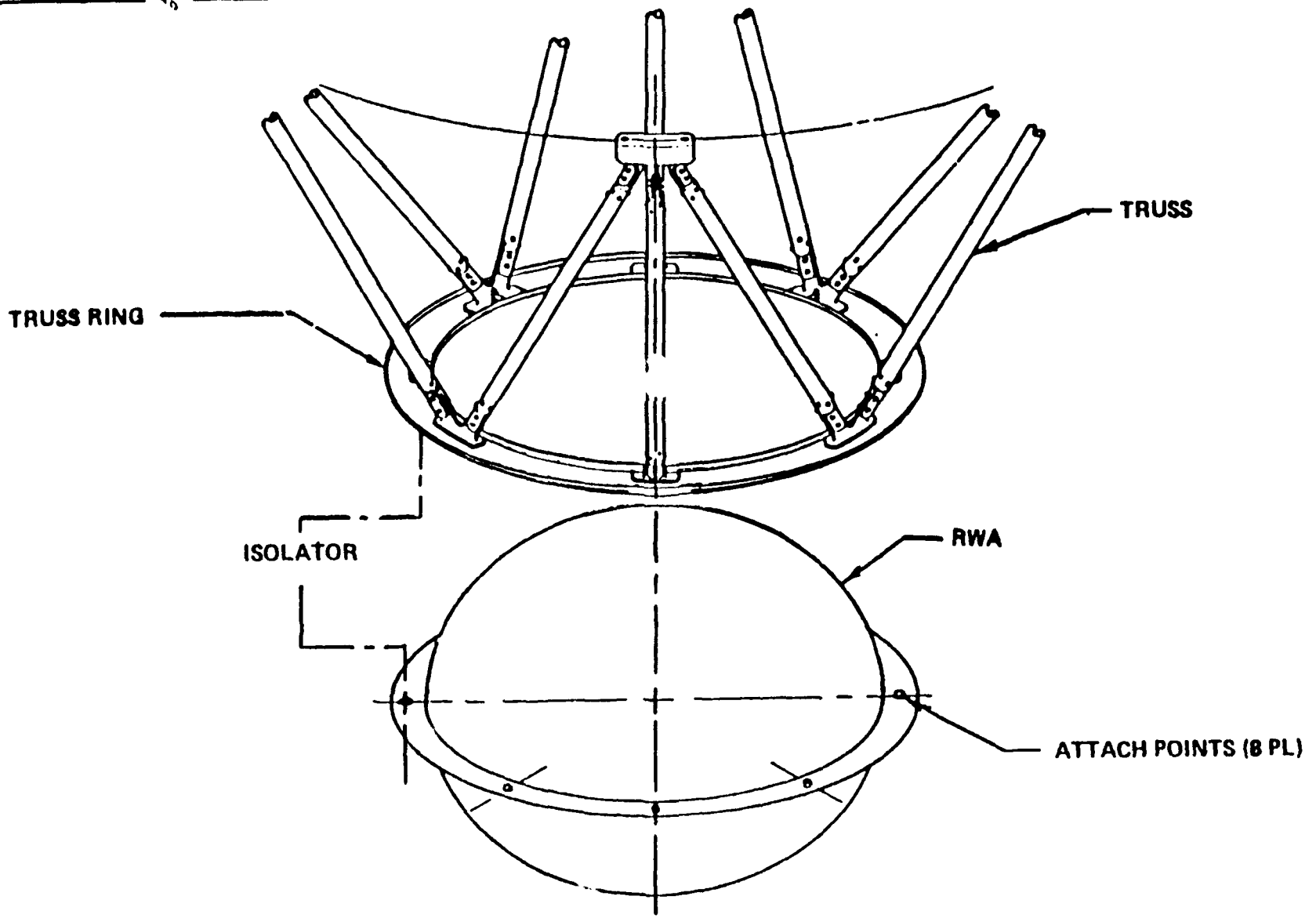

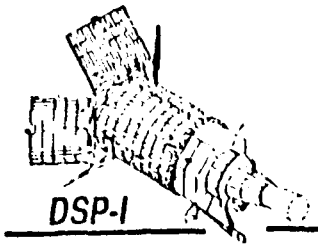

Baseline RWA Isolator Design

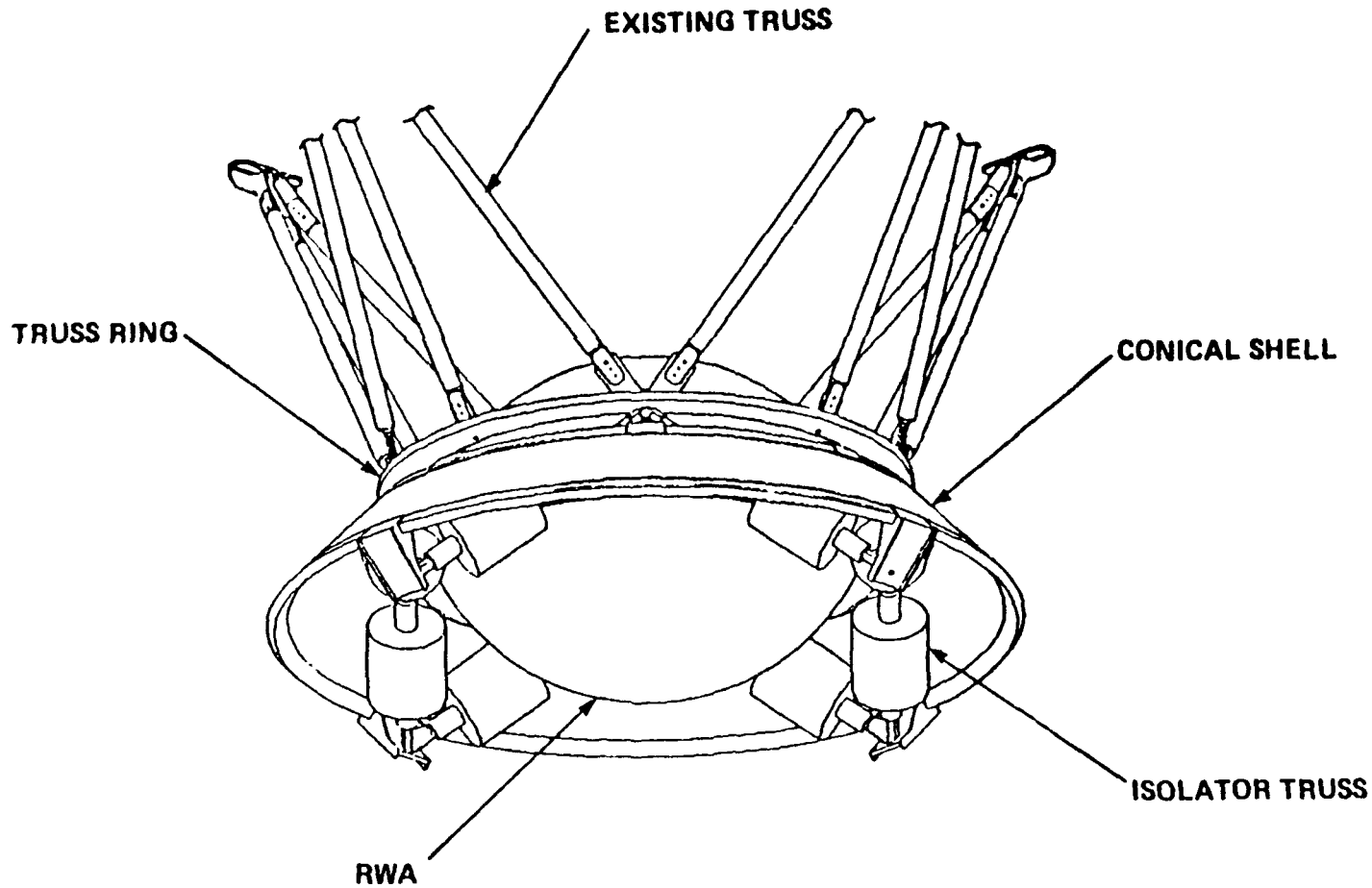

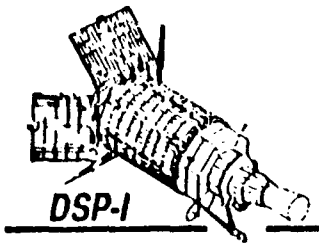

Isolator Unit Section View

- All parts are screwed together and lockwired
- Elastomer is injection molded to central cylinder and piston
- Cap has thin wall (0.043 in.) for "oil can" motion
- All parts are fabricated using standard machining practices
- 3 engineering demonstration units completed in one month

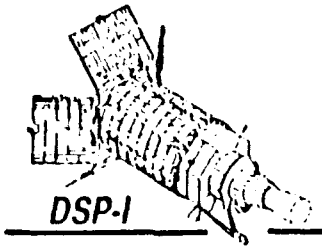

Isolator Unit Section View

TRW

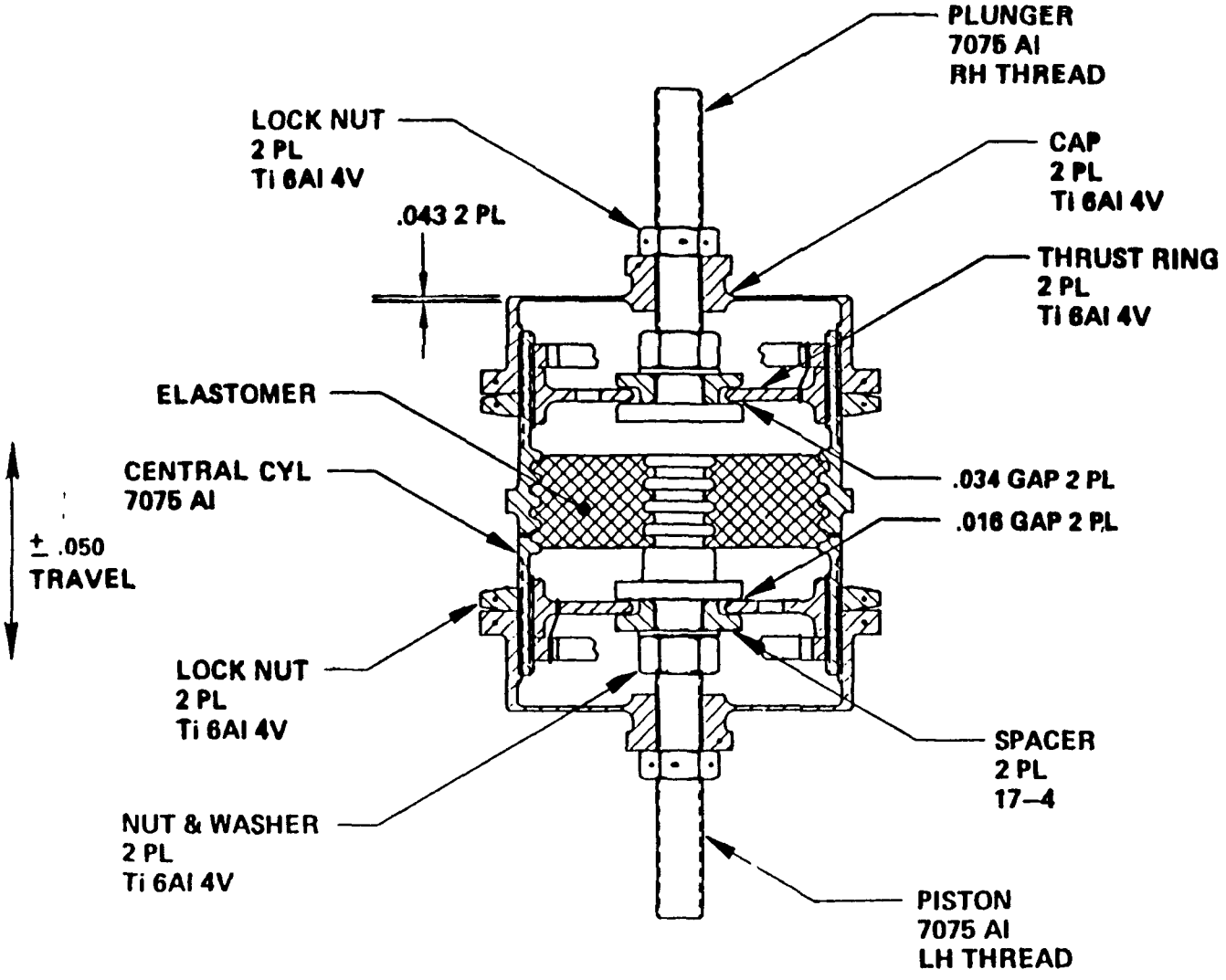

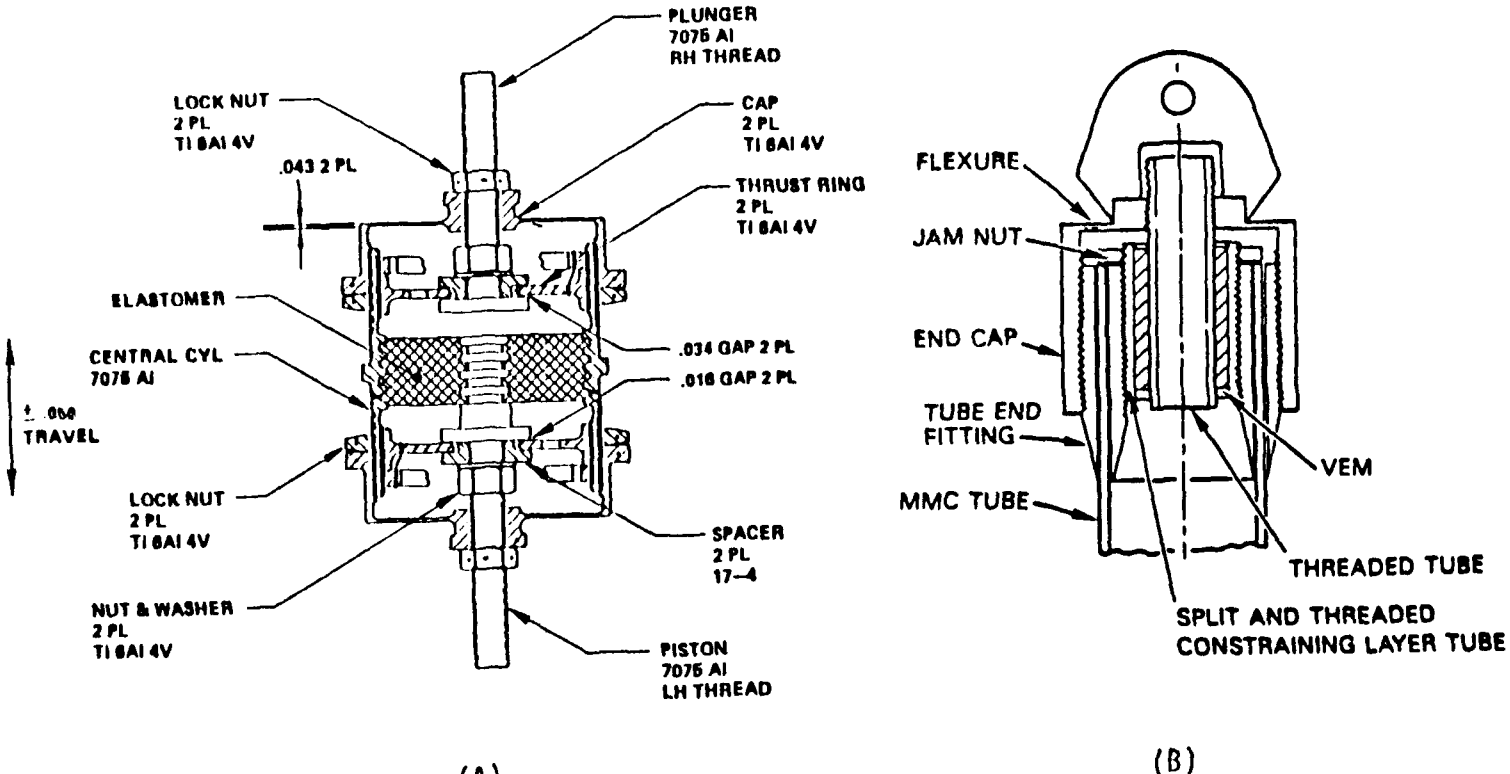

Figure 2: Comparison of A) DSP Proposed Isolator, and
B) DAMMPS JOINT Concept

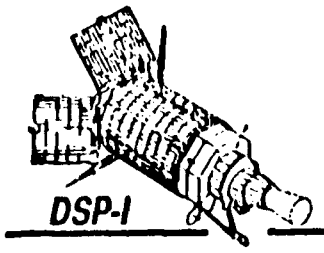

Isolator Mechanical Model (Schematic)

TRW

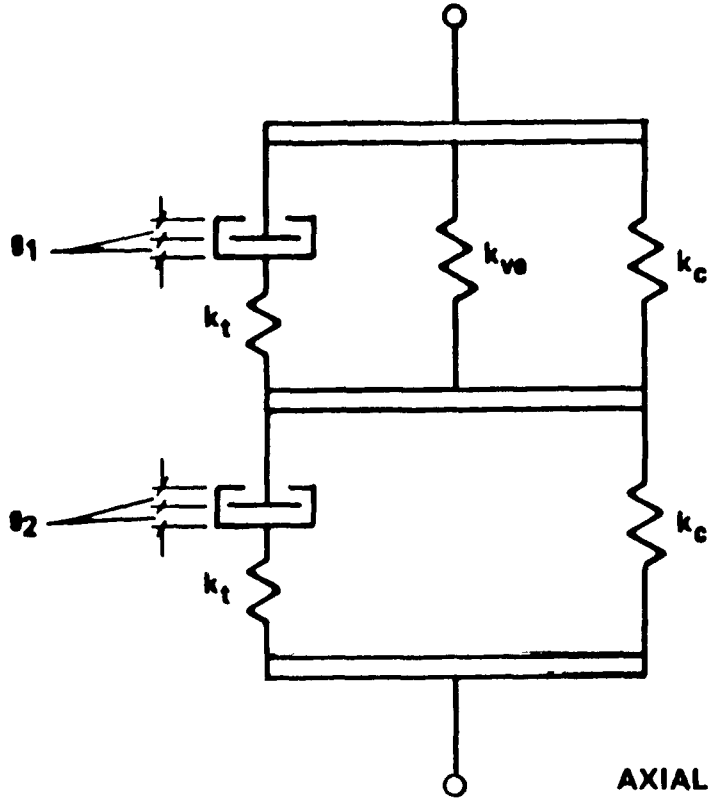

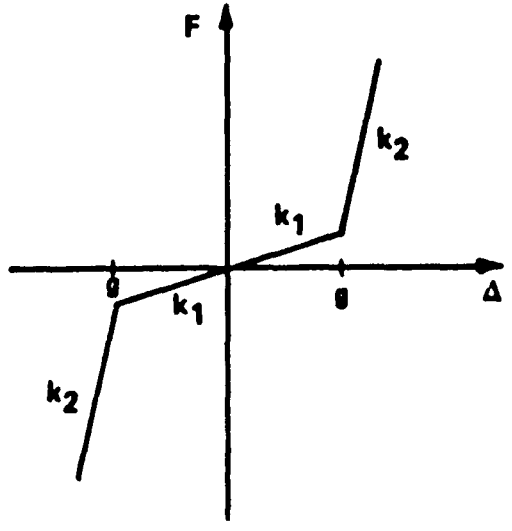

AXIAL ISOLATOR STIFFNESS MODEL:

- k_c = ISOLATOR CAP STIFFNESS
- k_{ve} = VISCOELASTIC SPRING STIFFNESS
- k_t = THRUST RING STIFFNESS
- g_1, g_2 = GAPS

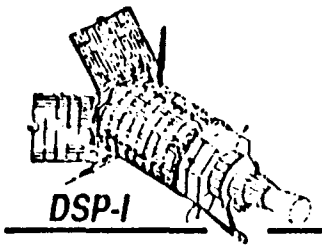

Temperature Insensitive Design

TRW

- Performance of isolator is only slightly effected by extreme changes in temperature. Operating temperature is fairly constant at about 80°F.
- Isolator axial model:

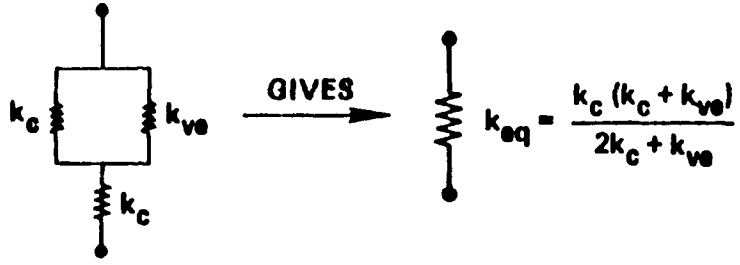

k_c = Isolator End - Cap Stiffness

k_{ve} = Viscoelastic Material Stiffn (Acts Both as a Spring and Damper)

k_{eq} = Equivalent Spring Stiffness

- Robust Stiffness K_{eq}:

If $k_{ve} \rightarrow 0, k_{eq} \rightarrow \frac{k_c}{2}$

If $k_{ve} \rightarrow \infty, k_{eq} \rightarrow k_c$

$\frac{k_c}{2} \leq k_{eq} \leq k_c$

Extreme Bounds

- Variations due to manufacturing, radiation, and fatigue are also bounded by using this analytical method

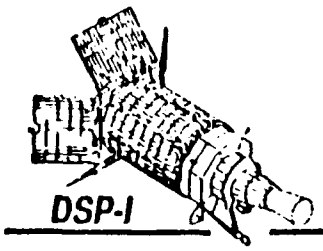

Isolator Stiffness

TRW

- Nominal 13 Hz Isolator
- Single isolator axial stiffness (total of 8 per module):

	Temp (°F)	K_c (lb/in)	K_{ve} (lb/in)	K_{eq} (lb/in)	Freq. (Hz)
Lower limit :	20	2000	135,000	1970	16
Operating :	80	2000	2000	1330	13.3
Upper limit :	185	2000	300	1070	11.8

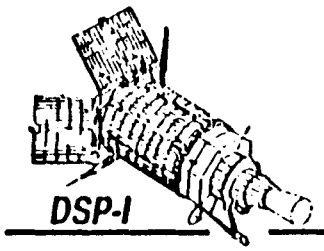

Low Outgassing Viscoelastic Material

- Specification : NASA JSC SP - R - 0022

	Requirement
— Total mass loss (%) *	≤ 1.0
— Collected volatile condensible material (%) (CVCM)	≤ 0.1

* Vendor data indicates TML of .46% for E.A. R. 's HD Isoloss and .067% for Isodamp C1002 (Tested per ASTM-E-595 modified)

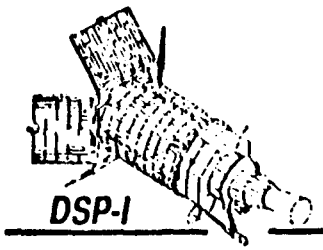

Compressive Creep

TRW

HD ISOLOSS

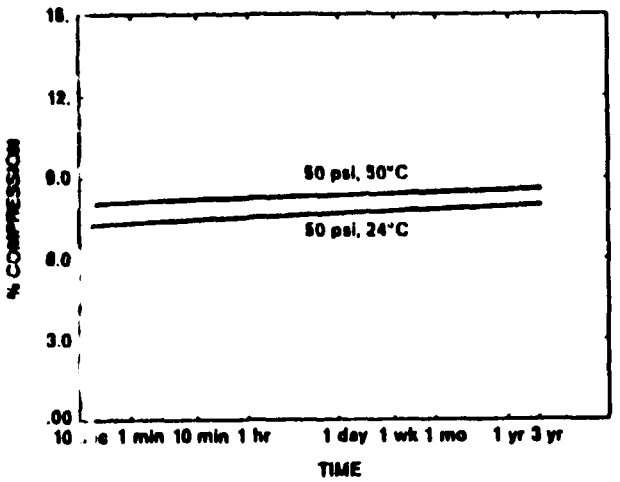

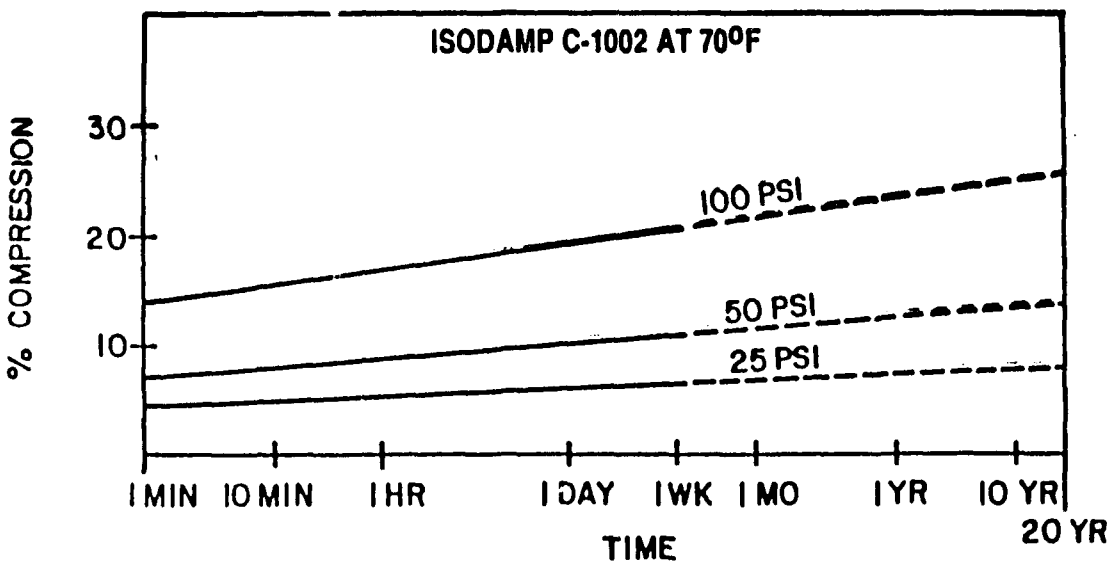

CREEP / RECOVERY TEST
(DSP ISOLATOR STUDY)

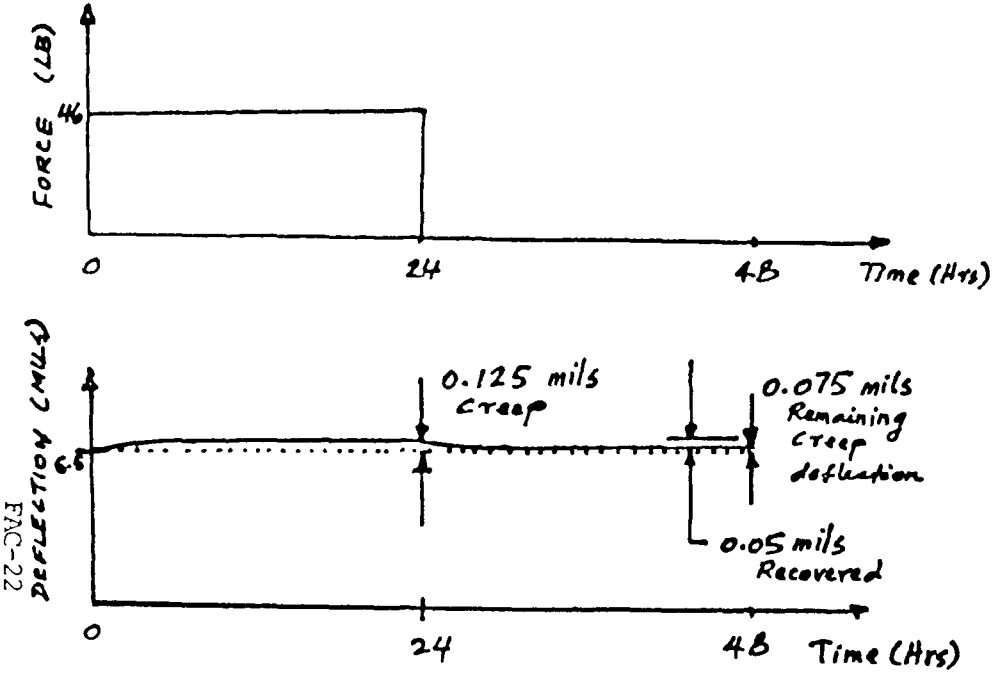

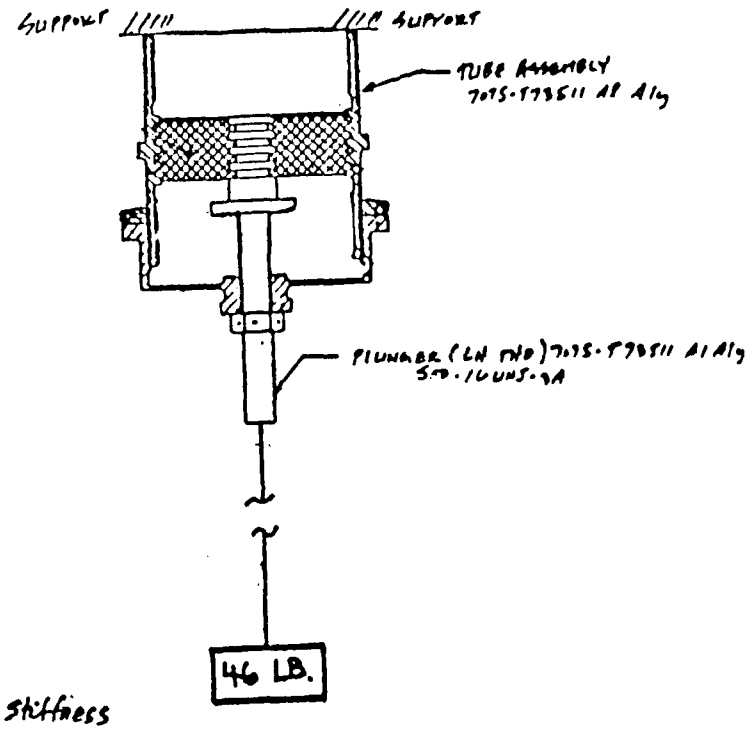

- Total Deflection (24 Hrs) = Elastic Defl. + Creep Defl. = 0.0055 in. + 0.000125 in.
  δ_{Total} = 0.005625 in.
  (Stiffness ≃ 8360 lb/in)
- Recovered Deflection (Creep part after 24 Hrs) = 0.00005 in.
- 40% of creep deflection recovered after 24 Hrs.
- COMPARISONS (ISOLOSS ND):
  - COMPRESSIVE CREEP (24 Hrs): $(\delta_{creep}/\delta_{elastic})_c$ = 0.056
  - SHEAR CREEP (24 Hrs): $(\delta_{creep}/\delta_{elastic})_s$ = 0.0227

CAP FLEXURE STIFFNESS TESTS
(DSP ISOLATOR STUDY)

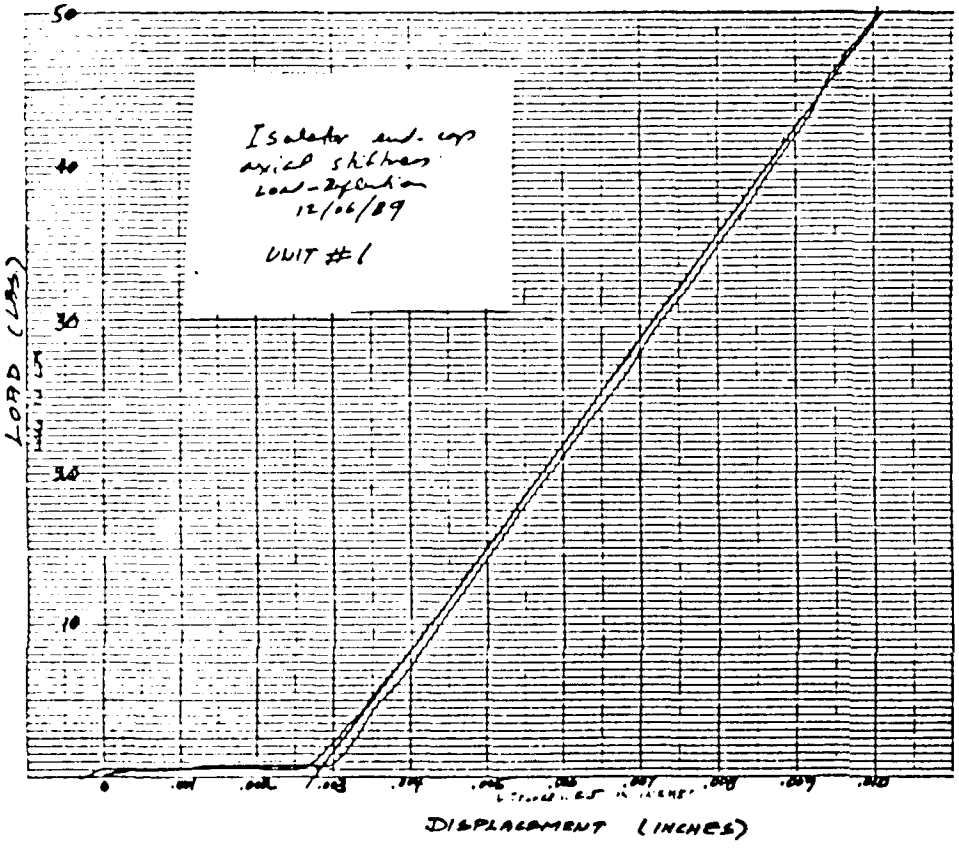

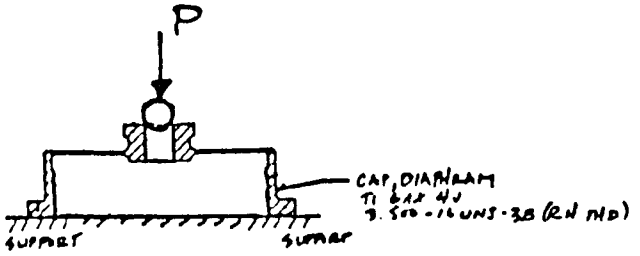

$$k = \frac{50 - 0.7}{.010 - .00275} = \frac{49.3}{.00725} = 6800 \text{ lb/in}$$

$$k \simeq \frac{50}{.0101 - .00275} = 6803 \text{ lb/in} \quad \text{OK}$$

- UNIT NO. 1 STIFFNESS $\cong$ 6800 lb/in
- UNIT NO. 2 STIFFNESS $\simeq$ 6430 lb/in

} Difference within 5.4%

- FLEXURE THICKNESS MEASUREMENTS : 0.043", 0.044", 0.044"
  (MINOT ENDICAP)
  APPROX. : 0.043" + 0.001" − 0.000"

INTEGRALLY DAMPED HONEYCOMB STRUCTURAL CONCEPTS TO INCREASE NOISE TRANSMISSION LOSS

Jefferson F. Newton*
Roy Ikegami
David J. Carbery

Boeing Aerospace & Electronics
Structures Technology
Seattle, WA

ABSTRACT

This paper describes the design, analysis, fabrication, and testing of design concepts to add passive damping to honeycomb panels to enhance the noise transmission loss in honeycomb structures. The loss factors for several damping material and panel configurations were analyzed. Statistical Energy Analyses (SEA) were then performed to predict the expected benefits of the calculated panel loss factors in terms of increased acoustic transmission loss through the panels. Based on the analyses, a honeycomb panel structural design concept was developed and three 6-ft by 6-ft panels were fabricated for acoustic testing. The first was a baseline bare honeycomb panel with no passive damping treatment, the second incorporated a NITRILE rubber material, and the third incorporated a 3M ISD 113 viscoelastic material. Acoustic testing was performed in a split reverberant/anechoic chamber at the Boeing Noise Engineering Laboratory. The results of the acoustic testing verified the predicted acoustic transmission loss and performance of the damped panels. The acoustic test results for the NITRILE damped panel showed less transmission loss than predicted indicating an apparent problem with the honeycomb core cutting into the NITRILE rubber during the fabrication of the panel. This was verified by radiographic inspection and subsequent sectioning and visual inspection of the panel.

•Correspondence and comments may be addressed to:
J.F. Newton, M/S 82-97
Boeing Aerospace & Electronics
P.O. Box 3999
Seattle, WA 98124-2499

INTRODUCTION

The trend toward the development of stiff lightweight structures in the designs of spacecraft, launch vehicles, and aircraft has made the task of protecting avionics equipment, payloads, and passengers from the acoustic environment increasingly important and demanding. For example, the design of launch vehicle shrouds, which shield the payload not only from the acoustic load, but from aerodynamic forces, thermal input, rain, sleet, and lightning, must satisfy stringent and often conflicting requirements.

It was the purpose of this research to develop and investigate design concepts that would solve or ameliorate problems of noise transmission through stiff lightweight structure, while satisfying other constraints, such as structural integrity, light weight, and low cost. One such concept, utilizing integral passive viscous damping in a honeycomb panel, is described in the following sections, along with the analyses and tests used to evaluate it.

CONCEPT DEVELOPMENT

The objectives that we set out to meet were two-fold: first, to develop stiff, lightweight structural designs to provide noise attenuation in the 50 to 200 Hz range; and second, to determine the feasibility of incorporating passive damping treatments into the design of honeycomb structures to increase noise transmission loss.

In order to understand these objectives we must examine some trends, First, there is the trend toward larger engines, or clusters of engines for both launch vehicles and aircraft. This, of course, increases the total acoustic output, thus increasing the exterior acoustic environment. In addition, as total power increases, the sound frequency at which the spectral maximum occurs tends to decrease. The effect of the above two trends is to significantly increase the exterior noise in the 50-200 Hz region of the spectrum. The other trend of significance is the decreasing effectiveness of standard, or traditional noise suppression techniques at low frequency. Absorbers, such as fiberglass blankets and sound barriers such as lead-loaded vinyl, both become largely ineffective below 100 Hz. The net effect of these trends is to create a "noise window" in the 50-200 Hz spectral region, as shown in figure 1, and explains the particular interest in the low frequency end of the spectrum.

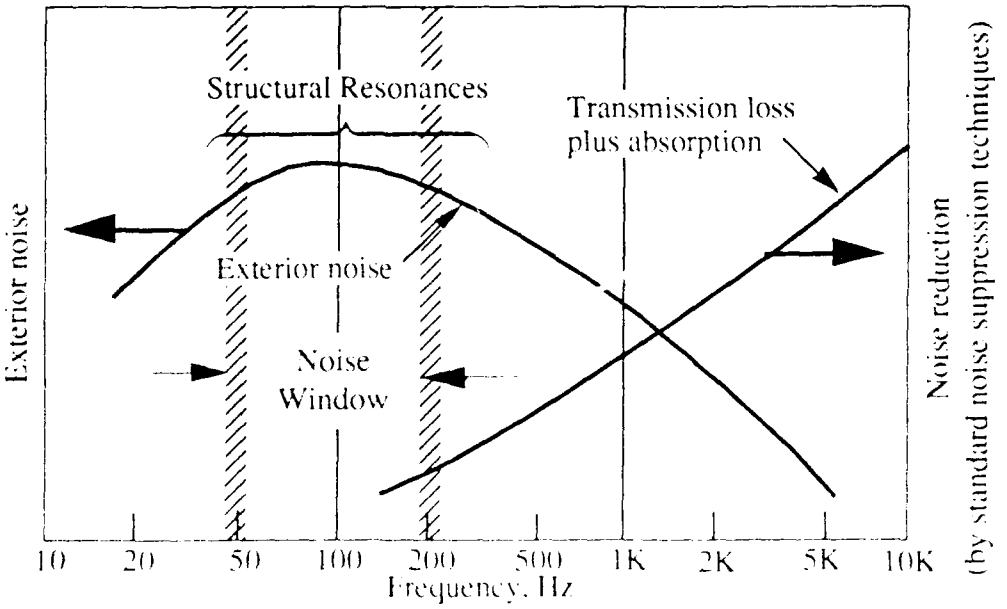

Figure 1. Launch Vehicle Noise Window

The objective of a stiff honeycomb panel is dictated by our decision to investigate integral passive viscoelastic damping. It was felt that passive damping could be integrated into a honeycomb structure with a small weight and stiffness penalty. Aluminum honeycomb was chosen for the investigation since it combines high stiffness with low weight.

Figure 2 shows the panel design corresponding to this concept. An aluminum honeycomb core is separated from the facesheet on either side by a layer of viscoelastic material (VEM). As the panel bends, due to an impressed noise field, for example, the viscoelastic layer on each side is put into shear. Damping occurs because of the strain energy converted into heat through the VEM loss factor.

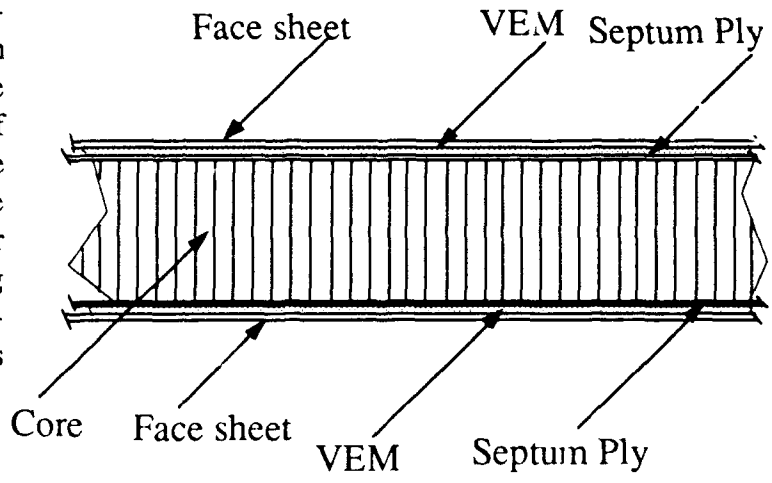

Figure 2. Damped Honeycomb Panel Design

An optional, thin epoxy fiberglass septum ply is shown in figure 2 bonded to the core and acting to transfer the shear from the core to the VEM. It can also serve to prevent the sharp edges of the core from punching through a soft viscoelastic layer.

ANALYSIS

Two analysis programs were written to act as design tools as well as to provide performance predictions for subsequent testing. The first program calculates panel loss factor as a function of frequency; the second, using loss factors obtained from the first analysis, calculates transmission loss through the panel.

DAMPING PREDICTIONS

This is programmed on SMART spreadsheet, using modal strain energy methods, for rapid parameter change and recalculation. Input parameters include: facesheet thickness, Young's modulus, and density; core thickness, shear modulus and density; VEM thickness, density, shear modulus as a function of frequency, and loss factor as a function of frequency. Loss factors can be input for the facesheets and core, as well. The program calculates strain energy for the facesheets, core and VEM, as a function frequency and deduces the composite panel loss factor. Outputs include: composite panel loss factor, stiffness, and bending wave velocity versus frequency.

TRANSMISSION LOSS PREDICTIONS

This is a simple SEA model, again programmed on SMART spreadsheet, to allow rapid change of panel input parameters and observation of their effects. The SEA model represents the test as subsequently performed in the Boeing Noise Engineering Laboratory (NEL) Anechoic/Reverberant Facility (ARF). Figure 3 shows the ARF and schematically diagrams the SEA calculation. Figures 4 and 5 are photographs of the interiors of the anechoic room and the reverberant room, respectively.

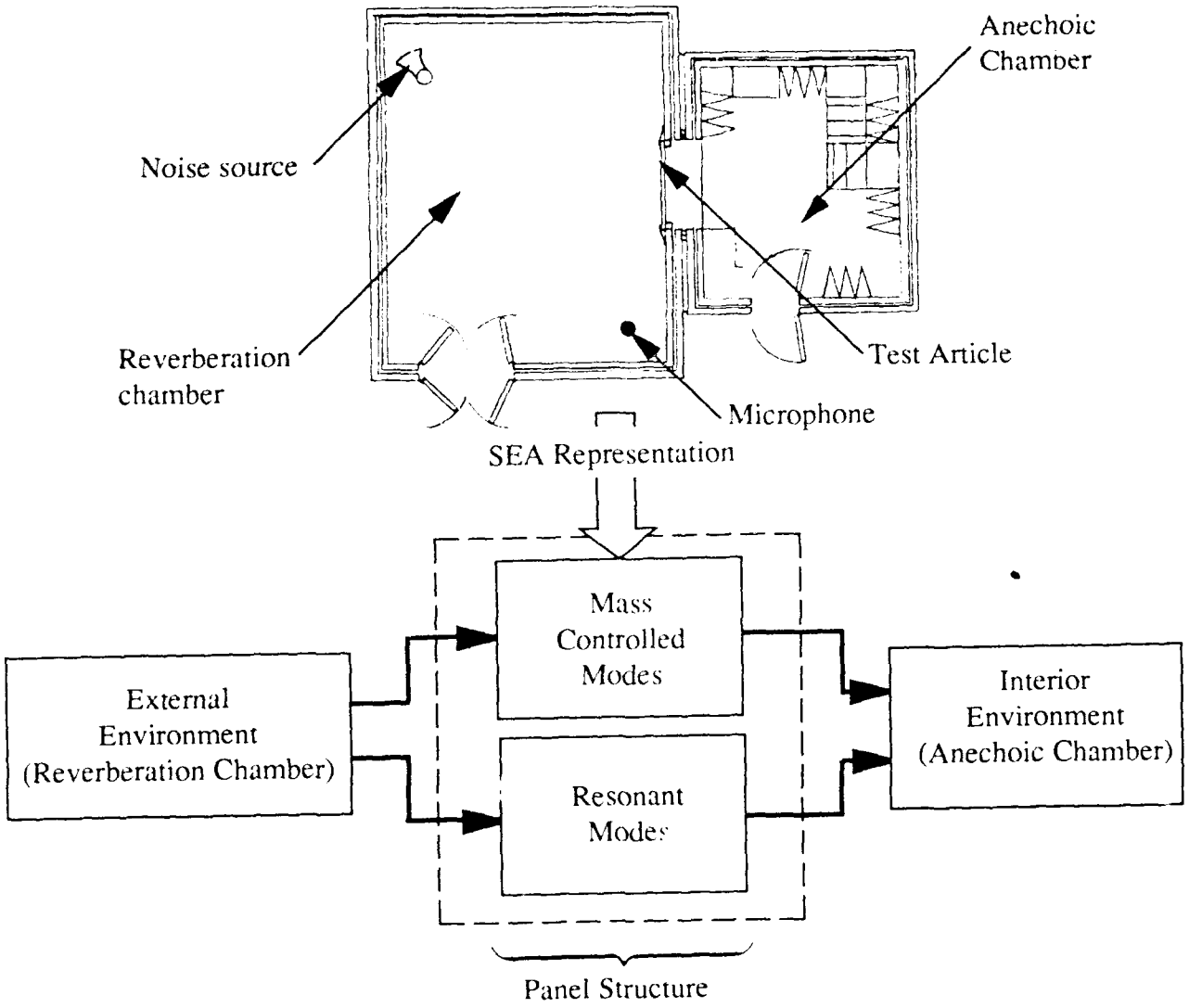

Figure 3. Anechoic/Reverb Facility With SEA Representation

Figure 4. Anechoic Room With Mounted Panel In Background

Figure 5. Reverberation Room and Rotating Microphone With Panel In Background

TEST

TEST PANELS

As a result of parametric studies done using the damping analysis and the transmission loss analysis, three test panels were designed and fabricated. All three panels were 6-ft by 6-ft in outer dimension, all had 0.050-inch aluminum facesheets, and all had identical 1.00-inch-thick aluminum honeycomb core. See figure 2. The baseline panel consisted only of the above, with the facesheets structurally bonded directly to the core. The second panel had a 1/32-inch-layer of Nitrile rubber bonded between the core and the facesheet on each side. The third panel had a 0.030-inch-thick layer of Scotchdamp ISD-113 acrylic under each facesheet. Because of the softness of the VEM, a thin septum was bonded to either side of the core, thus sandwiching the VEM between the septum and the facesheet. The septum was an 0.008-inch-thick, cured epoxy fiberglass sheet, and served to distribute the shear load from the core to the VEM, as well as preventing punch-through.

TEST PROCEDURE

Transmission loss tests were performed on all three panels using the intensity method. (Reference 1) The tests were performed at the Boeing NEL Anechoic/Reverberant Facility. The reverberant room measures 17.7-ft by 22.0-ft by 13.5-ft high and has hard, reflective walls. A speaker set acts as the noise source. Multiple reflections off the reverberation room interior surfaces ensures a diffuse sound field. A rotating boom microphone measures the spatially averaged sound pressure level (SPL). The test panel is mounted in a window separating the reverberation room from the anechoic room. Great care is taken to prevent noise leaks around the panel (flanking paths), using clay, fiberglass, and lead-loaded vinyl sheet to seal around the edge of the panel.

Noise penetrating the panel into the anechoic room (8.5-ft by 11.0-ft by 8.0-ft high, measured at the wedge tips) is measured directly, as it exits the panel, using an intensity probe. This is a relatively new procedure, made possible by the advent of the Fast Fourier Transform (FFT). It measures the sound vector intensity rather than the SPL. This method is procedurally simpler than the traditional Reverb/Reverb suite method, and is conceptually more straightforward. It has the additional advantage of allowing spatially resolved measurements over the surface of the test panel. Figure 6 shows the intensity probe being used to survey the panel. Reported transmission losses are spatial averages.

Figure 6. Intensity Probe Survey of the Test Panel Inside the Anechoic Room

Four accelerometers were mounted on the panel to assist in interpreting results. A Norwegian Electronics NE-830 analyzer was used to obtain the intensity measurements.

TEST RESULTS

The efficiency of the damping treatment is best illustrated by comparing the transmission loss of the treated panel with that of the baseline. Figure 7 shows the performance of Panel 3, the Scotchdamp ISD-113 treated panel, versus the baseline panel. Panel 2, the Nitrile panel, is not included, because examination after the test showed that the core had punched through the rubber during panel fabrication. This resulted in a transmission loss curve essentially similar to the baseline.

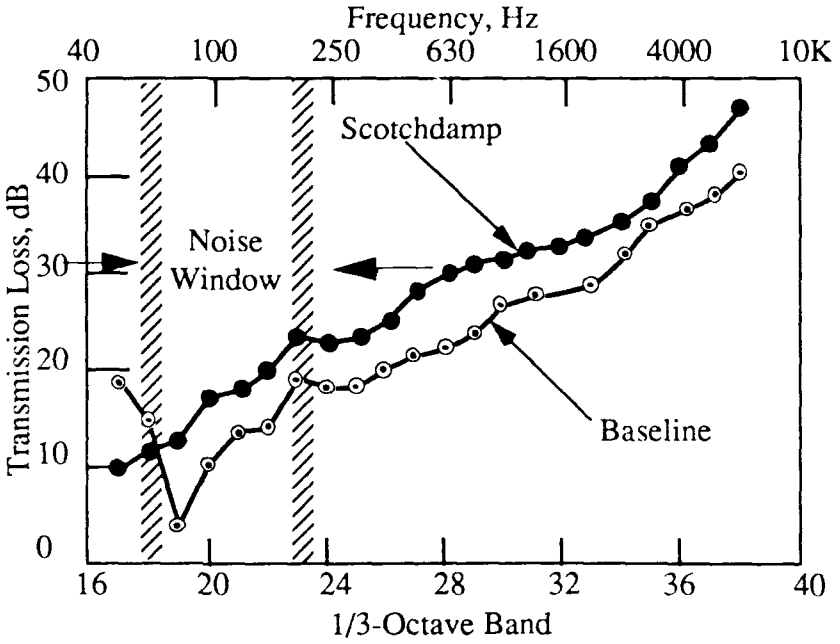

Figure 7. Noise Transmission Loss Test Results

The Scotchdamp (ISD-113) treated panel performed well, exhibiting an average improvement in transmission loss over the baseline panel of almost 6 dB (i.e. half the transmission of the baseline panel). A maximum difference of about 9 dB was obtained at 80 Hz, in substantial agreement with the pre-test predictions shown in Table 1.

• Panel transmission loss (TL) test
Average difference between baseline panel TL and "Scotchdamp" panel TL over frequency range 100-10,000 Hz

Average Transmission Loss Difference ("Scotchdamp" minus baseline)	
Analysis	Test *
6.7 dB	5.6 dB

• Beam Test

	Beam Mode	Loss Factor	
		Analysis	Test
"Scotchdamp" beam	1	37.7	46.2
(cut from test panel)	2	40.7	54.9

* Note:
The test results do not show the full difference predicted by analysis because the analysis neglects losses due to edge damping

Table 1. Comparison of Test Results with Analytical Predictions

At the conclusion of the transmission loss tests, the panels were cut into beam samples, approximately 6-inches wide by 60-inches long. These were tested at the Boeing Vibration Laboratory and the loss factor measured for the first two modes. The results of this test as well as those of the transmission loss test are shown in Table I along with the corresponding analytical predictions. It can be seen that agreement is good.

SUMMARY

The objectives of, first, developing a stiff, lightweight structural design providing noise attenuation in the 50 to 200 Hz range and second, determining the feasibility of incorporating passive damping treatments into the design of honeycomb structures to increase noise transmission loss were achieved.

The damping and transmission loss analysis programs were verified by test, giving us confidence in their future usefulness in design and prediction.

The effectiveness of the use of a septum ply to transfer the shear load from the honeycomb core to the VEM was demonstrated, as was the septum ply's efficiency in preventing punch through.

The capability of Boeing Noise Engineering Laboratory to provide fast, accurate measurements of transmission loss using the intensity method was verified.

REFERENCES

1. "Measurement of Transmission Loss of Panels by the Direct Determination of Transmitted Acoustic Intensity", Crocker et al, Noise Control Engineering, July/August, 1981.

Reduction of Acoustic Responses using Viscoelastic Damping Materials

David F. Chu*
Jong Peir
C. Stahle
J. Staley
M. McMeekin

GE/Astro Space Division

ABSTRACT

This paper presents the results of a development test conducted at GE/ASD for reduction of acoustic responses of honeycomb panels using viscoelastic damping material. The damping strip consists of viscoelastic damping material, honeycomb core, and graphite constraint layer. Acoustic tests were conducted on the undamped and damped panels. The comparison of the acoustic responses with and without damping strip are presented. Analytical prediction of the reduction factors and their comparison with the test results are also described.

*GE/ASD, P.O. Box 800, MS: 410-2-A36, Princeton, NJ. 08540

INTRODUCTION

Vibroacoustic damping material has been used successfully over the past 17 years at GE/ASD to reduce the vibroacoustic responses of spacecraft structures (References 1-5). The applicatons include printed circuit boards of electronic boxes and equipment panels. This paper discusses the analysis and test results of a damped honeycomb panel. Comparision of the analysis prediction and test results is also discussed.

TEST DESCRIPTION AND RESULTS

The acoustic test was conducted on the test panel with and without the damping strips. The panel is an aluminum honeycomb panel. Two components are attached to the panel to simulate a typical mass loaded panel for spacecraft applications. Thirteen accelerometers were installed on the panel to measure the responses. Figure 1 shows the test panel and accelerometer locations. The shaded line indicates the location of damping strips. The cross-section of the strip is shown in Figure 2. The panel is supported by a rigid frame mounted around the boundary of the panel. During the test, the panel was laid on the floor, supported by thick forms. Six microphones were located near the test panel to measure the sound pressure level.

The test panel was exposed to the protoflight acoustic level environment in the 10,000 cubic foot acoustic chamber. Two tests were conducted; one before and the other after the application of the damping material to the panel. Table 1 summarizes acoustic test levels. The first column identifies the 1/3 octave band and center frequencies and the second column gives the test specification.

The panel vibroacoustic responses which are of most significance for components mounted on the panel are those at component mounting locations. These are the responses that dictate component random vibration test requirements. Test measurements at component mounting locations for the damper and undamper panels are compared in Figure 3 for accelerometer 6Z. These responses have been scaled to a common acoustic test environment which corresponds to the test environment measured in the undamped panel acoustic test. Figure 3 shows that significant reductions of peak levels in the undamped panel random vibration due to damping.

ANALYSIS CORRELATION

Modal damping of the test panel due to viscoelastic damping is determined using modal strain energies and viscoelastic material damping properties. In this approach, the viscoelastic material is represented in a finite element model by the real part of the material shear modulus where the complex shear modulus is given by:

$$G = (1 + i\eta_v)G \qquad (1)$$

where

G = real part of complex sheet modulus

η_v = viscoelastic material composite loss factor

A NASTRAN model of the panel is used to compute the fraction of the modal strain energy in the viscoelastic material for each mode. The fraction of the modal strain energy for each mode is then multiplied by the viscoelastic material loss factor at the modal frequency and at the appropriate temperature.

The finite element model used for the damping prediction is shown in Figure 4. The model included the basic panel and the damper strips which consisted of viscoelastic damping material layer, aluminum honeycomb core, and graphite/epoxy constraining layer for each of the damper strips. The predicted damped panel modal frequencies and composite loss factor for all the panel modes up to 500 Hz are presented in Table 2 and in Figure 5. As shown in Table 2, some modes have modal loss factors which are relatively high while others are somewhat low.

To estimate the reduction of random vibration responses for the damped versus the undamped panel for the same acoustic environment, a reduction factor can be calculated based on the loss factor of undamped and damped panels. The reduction factor is defined as:

$$\text{REDUCTION FACTOR} = (QUD/QD)^2 \qquad (2)$$

where

QUD = undamped panel amplification factor

QD = 1/(.7 x LOSS FACTOR + (1/QUD))

and

LOSS FACTOR = the predicted modal composite loss factor due to viscoelastic damping only

Only 70 percent of the predicted modal loss factor due to viscoelastic damping was assumed to be effective based on previous experience with viscoelastic damped panels (Ref. 5).

Results for reduction factor based on prediction and test data are plotted in Figure 6. Six accelerometer responses at the component mounting locations were used in Figure 6. Test values are based on reductions in levels for significant peaks in the undamped panel random vibration responses. Figure 6 indicates that significant reductions in random vibration levels have been achieved and that predictions are generally conservative over most of the frequency range of interest.

SUMMARY

Comparison of predicted and test results for random vibration reductions due to viscoelastic damping for the test panel shows that:

1) Reduction of random vibration peaks seen in panel responses at component mounting points was generally greater than predicted. Reasonable agreement was obtained between analytical predictions and experimental results.

2) Significant reductions in test responses indicate that the damping design methodology is effective for honeycomb panels.

ACKNOWLEDGEMENT

The work reported herein was performed for the Air Force GPS program, Contract No. F04701-89-C-0073 .

REFERENCES

1. C.V. Stahle and W.H. McCandlises, "Controlling Vibration of Viking Lander Electronic Packages", 44th Shock and Vibration Symposium, December 1973.

2. C.V. Stahle and J.M. Medaglia, "SMRD Damping Applications", SAMPE Series Vol. 25, 1980.

3. J.M. Medaglia, "Dynamic Integrity Methods Including Damping for Electronic Packages in Random Vibration", 50th Shock and Vibration Bull., 1980.

4. J.A. Staley, and C.V. Stahle, "Damping in Support Structures for Equipment Reliability—RELSAT", Vibration Damping Workshop, Feb. 1984.

5. J.C. Strain, J.A. Staley, and C.V. Stahle, "Design and Experimental Verification of Damped Spacecraft Equipment Panels", Vibration Damping Workshop II, March 1986.

6. C.V. Stahle, J.A. Staley, and J.C. Strain, "Vibroacoustic and Shock Performance of Damped Spacecraft Equipment Panels", Vibration Damping Workshop II, March 1986.

7. C.V. Stahle, J.A. Staley, and J. C. Strain, "Analysis and Experimental Evaluation of RELSAT Damped Equipment Panels", Presented at the ASME Design Engineering Technical Conference, September, 1987.

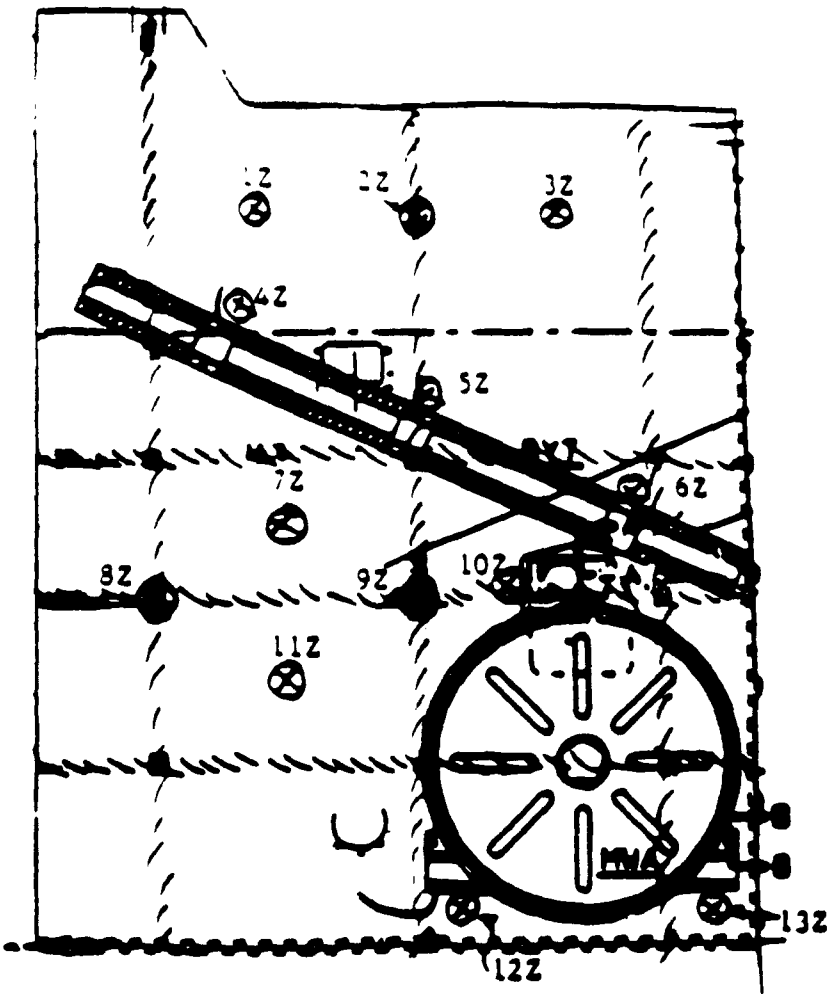

Figure 1. Test Panel and Accelerometer Locations

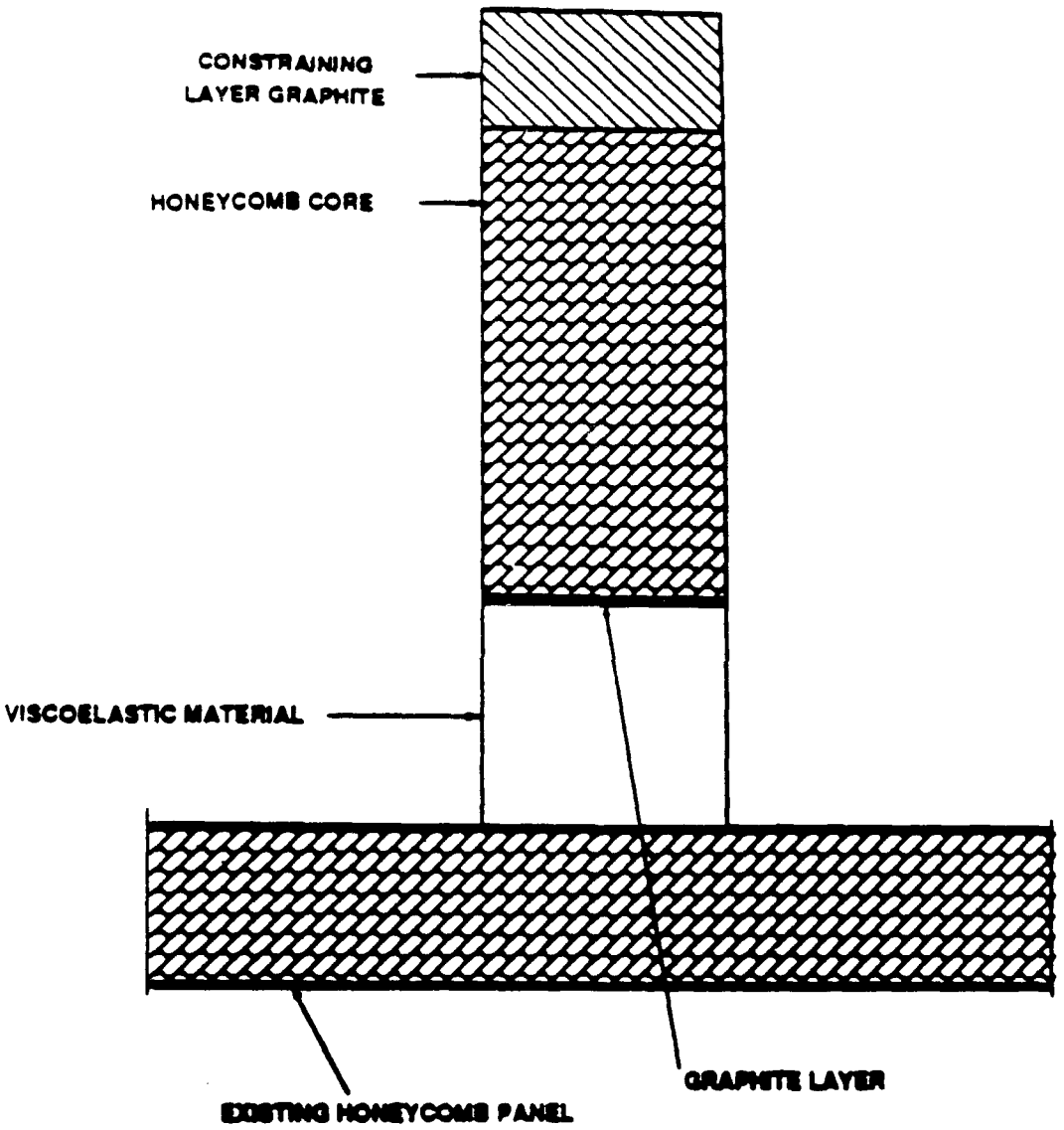

Figure 2. Damper Strip Cross-Section

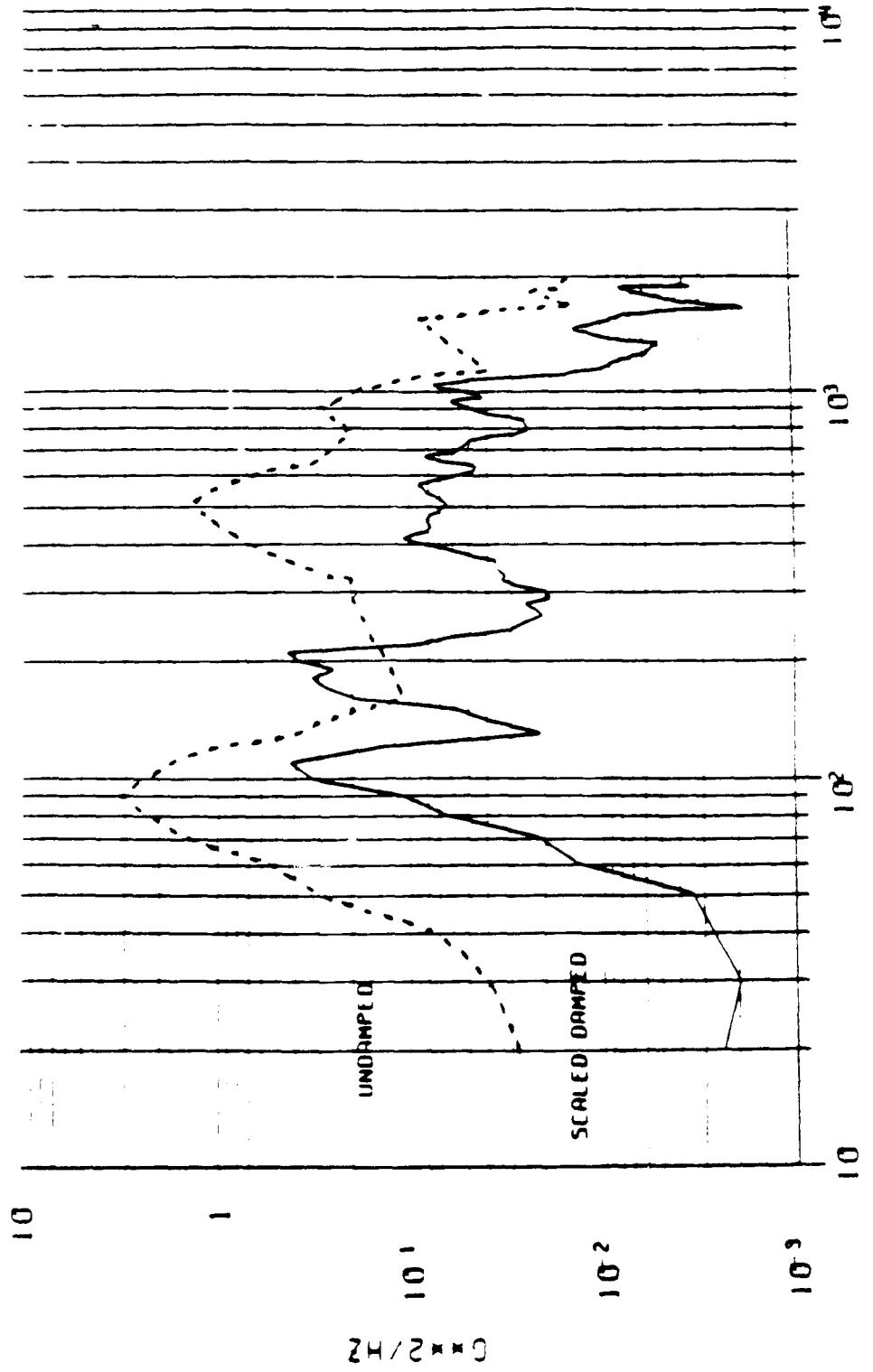

Figure 3. Damped and Undamped Panel Test Responses for Accelerometer #6Z

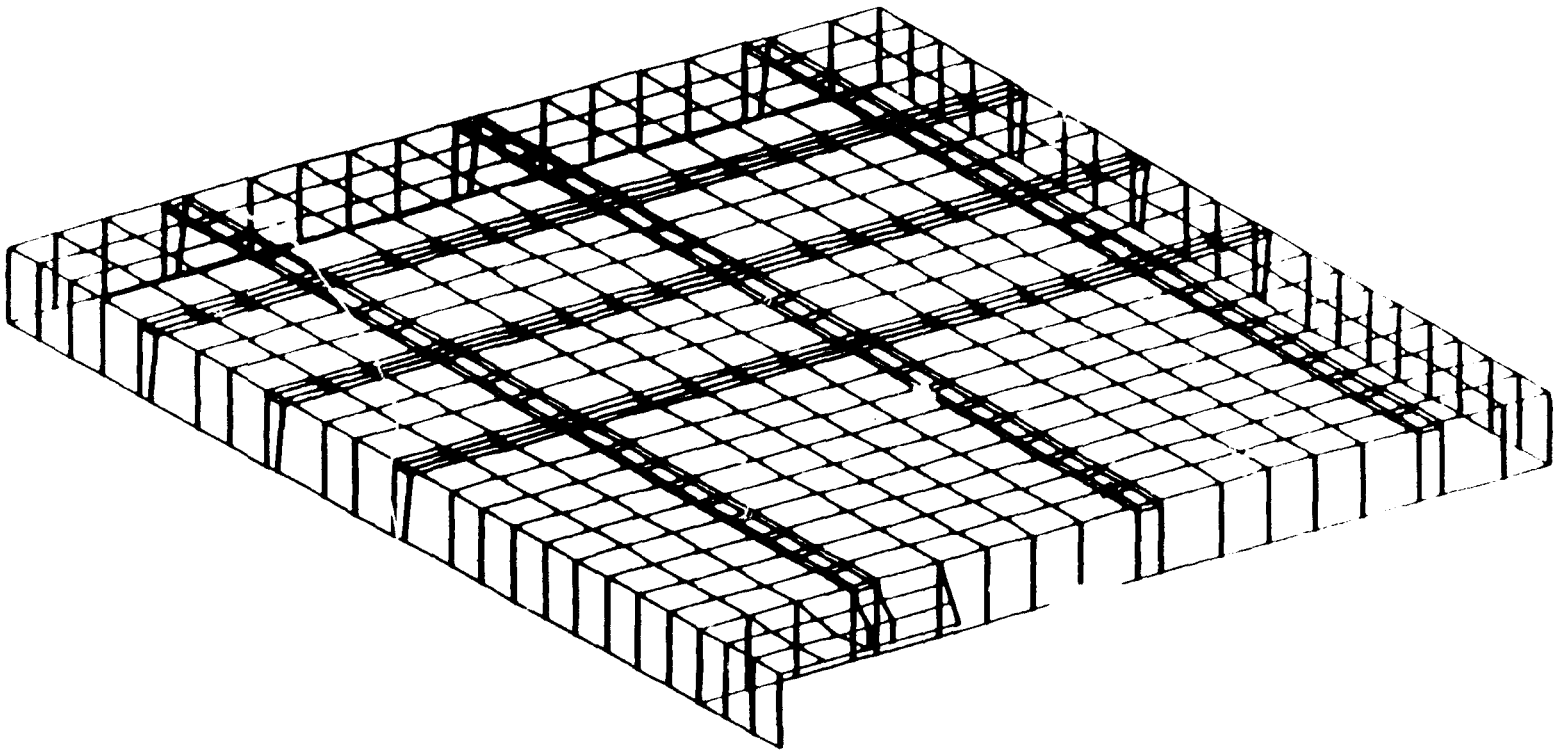

Figure 4. Damped Panel Finite Element Model

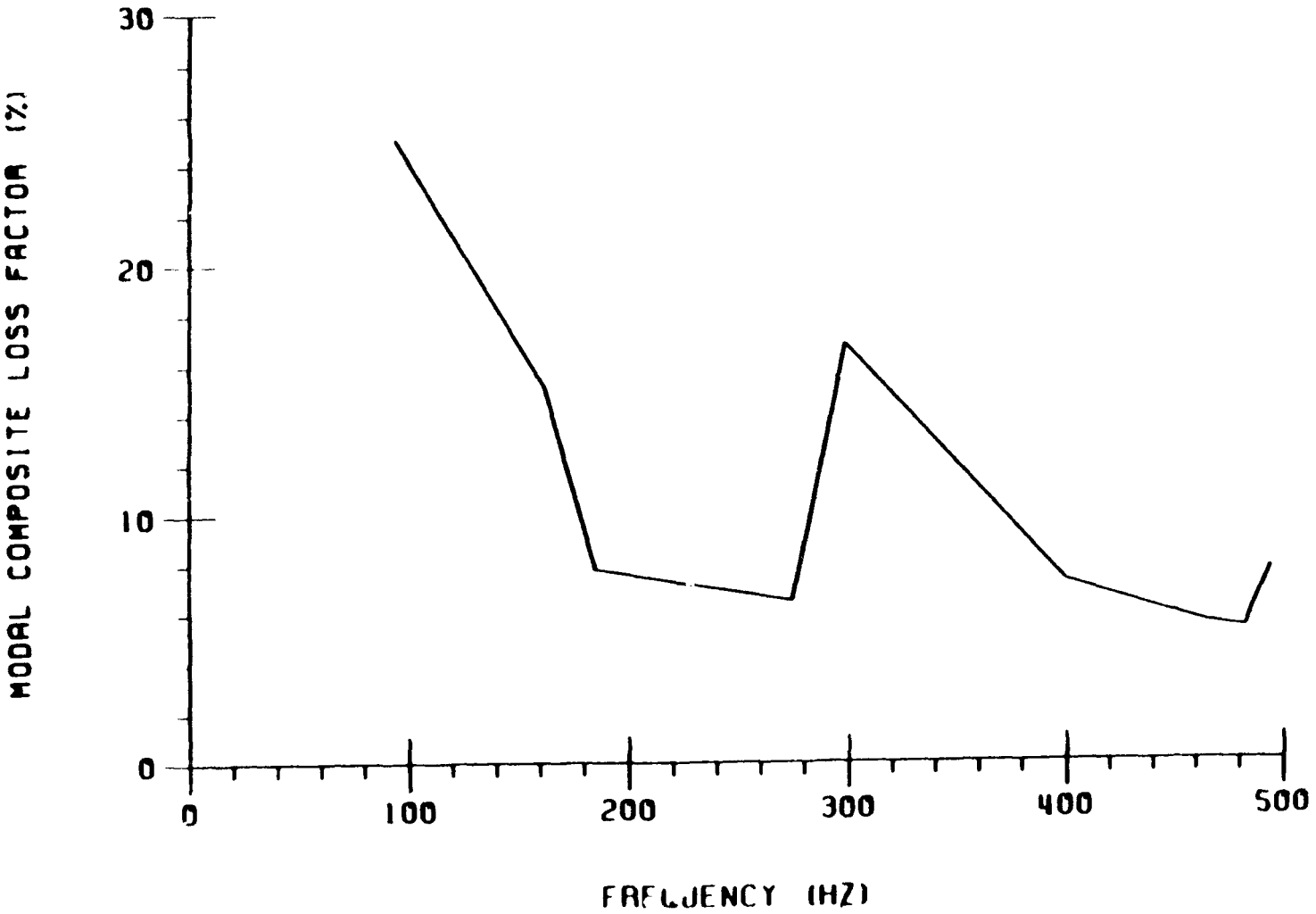

Figure 5. Predicted Modal Composite Loss Factor Vs Modal Frequency

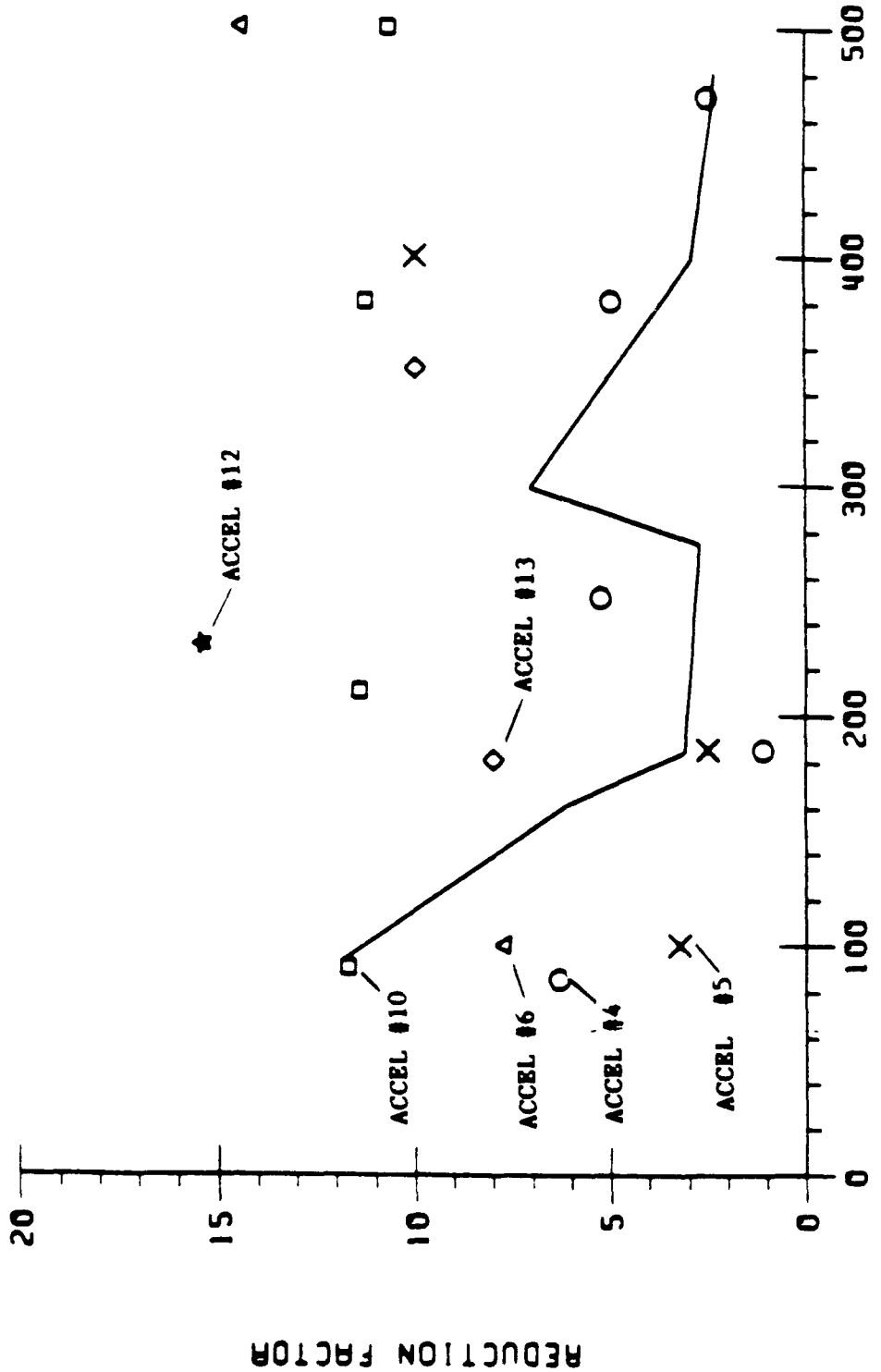

Figure 6. Reduction Factor—Prediction and Test

Table 1. Acoustic Test Level for Damping Material Test

FREQ. (Hz)	SPEC. (dB)
40	128.5
50	131.0
63	134.0
80	136.5
100	138.0
125	138.0
160	138.0
200	136.5
250	135.0
315	133.0
400	131.0
500	129.0
630	127.5
800	125.5
1000	124.0
1250	122.5
1600	121.0
2000	119.5
2500	117.5
3150	115.0
4000	113.0
5000	111.0
6300	109.0
8000	107.0
10000	105.0
Overall	146.2

Table 2. Damped Panel Predicted Modal Frequencies and Composite Loss Factors

MODE	UNDAMPED FREQ. (HZ)	FREQ. (HZ)	CLF (%)
1	57.9	92.6	25.03
2	121.1	160.7	15.12
3	155.3	184.2	7.74
4	259.2	273.8	6.51
5	269.0	297.8	16.87
6	371.9	399.1	7.28
7	441.4	463.8	5.56
8	468.6	481.4	5.35
9	481.8	493.4	7.82

AVE LOSS FACTOR = 10.8%
MAX LOSS FACTOR = 25.0%
MIN LOSS FACTOR = 5.4%

DESIGN METHOD OF DAMPING TREATMENT FOR STRUCTURE-BORNE NOISE REDUCTION

Iwao Honda[1]
Mitsubishi Heavy Ind., Ltd.
Nagasaki, Japan

Tadao Nakamura
Mitsubishi Heavy Ind., Ltd.
Nagasaki, Japan

Yoshihiko Irie
Mitsubishi Heavy Ind., Ltd.
Nagasaki, Japan

Kazuo Yamamoto
Mitsubishi Heavy Ind., Ltd.
Nagasaki, Japan

ABSTRACT

In many kinds of mechanical structures, the quietness becomes one of the important values, and the damping treatment using viscoelastic material is applied to reduce structure-borne noise. But, vibrational characteristics of viscoelastic material depend on temperature and frequency, so the systematic design of damped structures and the prediction of damping effects was difficult. This paper presents a prediction method of vibration by damping treatment applied to viscoelastic materials. The major points of this paper are as follows:

1. The iterative design procedure to determine the vibratory characteristics of a damped beam by viscoelastic material, whose properties are dependent on temperature and frequency, is shown.

2. The prediction methods of reduction in vibration, based on both modal analysis and the SEA method, are shown. Additionally, the estimated results using these methods are well in agreement with the measured results.

THIS ABSTRACT PROVIDED FOR INFORMATION ONLY. ACTUAL PAPER WAS NOT PRESENTED AT THE CONFERENCE.

[1]Mitsubishi Heavy Ind., Ltd. Nagasaki R & D Center, 1-1, Akunoura-machi, Nagasaki, 850-91, Japan. (81) 958-71-5136

EARTHQUAKE SIMULATOR TESTING OF TWO DAMPING SYSTEMS FOR MULTISTORY STRUCTURES

Ian D. Aiken, Research Engineer

and

James M. Kelly, Professor of Civil Engineering*

ABSTRACT

The use of two different types of damping devices to improve the earthquake resistance of buildings is investigated in a program of earthquake simulator testing of a 1/4-scale, nine-story, steel frame model. The devices studied are a constrained-layer viscoelastic shear damper designed using an energy approach, and a friction damper with almost perfectly rectangular hysteresis behavior, for which an iterative nonlinear analysis design method was adopted.

The model was tested with both types of energy absorbers installed and also in moment-resisting and concentrically-braced configurations. Numerous diagnostic and earthquake tests were performed. The large number of tests performed permitted numerous different comparisons of the four structural systems. Responses are compared in terms of accelerations, displacements, interstory drifts, and story shears. Floor response spectra are also evaluated for the moment-resisting frame and the two damped systems.

The damped structures were found to behave similarly to the concentrically-braced frame in terms of displacements, while having accelerations similar to those of the moment-resisting frame. Story and base shears of the damped structures were of the order of those of the moment-resisting frame, and less than those of the concentrically-braced frame. The response of the two damped systems was very similar for nearly all of the earthquake motions used.

* Earthquake Engineering Research Center, University of California, Berkeley, CA 94720, (415) 231-9480

INTRODUCTION

Conventional seismic design practice permits the reduction of forces for design below the elastic level on the premise that inelastic action in a suitably designed structure will provide that structure with significant energy dissipation potential and enable it to survive a severe earthquake without collapse. This inelastic action is typically intended to occur in especially detailed critical regions of the structure, usually in the beams near or adjacent to the beam-column joints. Inelastic behavior in these regions, while able to dissipate substantial energy, also often results in significant damage to the structural member, and although the regions may be well detailed, their hysteretic behavior will degrade with repeated inelastic cycling. The interstory drifts required to achieve significant hysteretic energy dissipation in critical regions are large and would usually result in substantial damage to non-structural elements such as in-fill walls, partitions, doorways, and ceilings. As a response to the shortcomings inherent in the philosophy of conventional seismic design a number of innovative approaches have been developed (Fig. 1).

One of these approaches involves adding energy absorbers to a structure. The use of energy absorbers to improve the dynamic behavior of structural systems is well established. There are many applications to tall buildings to reduce wind-induced vibrations. The possibility of using energy-dissipating devices to improve the earthquake resistance of buildings and other structures is a more recent development. The aim of including energy absorbers in a structure for earthquake resistance is to concentrate hysteretic behavior in especially designed and detailed regions of the structure and to avoid inelastic behavior in primary structural elements (except perhaps under the most severe conditions). Numerous different types of energy-absorbing devices have been proposed for this purpose. Devices based on the plastic deformation of mild steel were developed and extensively tested a number of years ago [1]. Friction devices of several types have been the subject of a number of test programs, and one type was recently installed in a library building in Montreal [2]. By the end of 1990, the Sumitomo-type friction dampers studied here had been incorporated in 31- and 22-story buildings, both in Japan. Viscoelastic dampers have been used in several tall buildings as wind vibration absorbers [3]. The dampers use a highly-dissipative polymeric material which has well-defined material properties and behavioral characteristics [4]. The most notable applications are the twin 110-story towers of the World Trade Center in New York City, in which the dampers have been installed for twenty years.

DESCRIPTION OF DAMPERS

The two types of devices studied were a sliding friction damper and a viscoelastic (VE) shear damper. Both types of device have already been used in a number of structural or mechanical engineering applications, however, this experimental study represented the first use of the dampers for earthquake loading conditions.

The friction damper was designed and developed by Sumitomo Metal Industries, Ltd., Japan. It is a cylindrical device, with friction pads that slide directly on the inner surface of the steel casing of the device (Fig. 2). The device was originally used for shock absorption

applications in railway rolling stock. Each of the friction devices manufactured for the test program was subjected to proof tests prior to the earthquake tests. These tests were intended to confirm the correct setting of the slip load and to identify any dependence of the force-displacement behavior on the variables of loading frequency, amplitude, temperature, or the number of loading cycles. All of the dampers performed as intended, and the effect of these factors was found to be negligible. The very good behavior of the devices has been observed in many previous tests performed by Sumitomo.

The VE damper comprises two layers of material, and was introduced in single-diagonal bracing in the test structure (Fig. 3). The VE material was manufactured by 3M Co., USA. The detailed nature of the VE material and its physical properties have been described elsewhere [4,5] and are summarized in the next section.

VISCOELASTIC MATERIAL

The VE dampers used in the earthquake simulator test program were based on a class of viscoelastic materials with certain specific characteristics. The acrylic copolymer materials are known to be very stable with good aging properties, are chemically inert and are resistant to environmental pollutants. When used as the energy absorbing components in dampers, they are normally used in the form of shear layers and the exposed surface area is very small relative to the volume of material. Thus any chemical processes that depend on diffusion, for example, moisture absorption or penetration, will be very slow.

The viscoelastic properties of these materials when used in shear are characterized by: (i) the loss modulus G'', (ii) the storage modulus G', and (iii) their ratio, the loss factor $\tan\delta = G''/G'$. The loss modulus controls the specific energy dissipation capacity of the material. This is the most important characteristic of the material for damping applications. High values of G'' mean high energy dissipation per unit volume of the material. The storage modulus G' is also important in that it will influence the change in stiffness (frequency) of the structural system to which the damper is added. The ratio $\tan\delta$ is a measure of the suitability of the material as a damping medium. The materials used in this research program have peak values of $\tan\delta$ in the range of 1 to 1.4.

These three material properties are sensitive to temperature, frequency and strain. The materials can be produced with the desired properties over a wide range of temperature and frequency. Four types of material are currently available, and of these, the material designated ISD 110 by 3M was used in the test program. The manner in which the loss modulus G'' depends on temperature, frequency, and strain is the same for all of the ISD copolymers. Thus the behavior characteristics of one material can be used to predict that of the others, provided that data points at a certain temperature, frequency and strain are available.

Tests of the materials were carried out using a standard MTS closed-loop hydraulic test machine. The primary purpose of the tests was to determine the strain sensitivity of the material properties. Material properties provided by the manufacturer in the form of data tables are based on standard tests at low levels of shear strain (< 10%) which are appropriate for vibration damping applications. For seismic applications, however, strains in the range of 10—100% or greater are needed, and tests were performed to provide performance data in this strain range.

The material tests were performed on the dampers used in the earthquake simulator test program (Fig. 3). The dampers were subjected to sinusoidal displacement signals at a range of frequencies. The test results showed that (for a given frequency) while there is a very large difference between moduli at small strains (< 10%) and those at large strains (20—150%) the sensitivity of the moduli to strain within this range is not great. This has advantages for seismic design since over the range of seismic response the damping system can be considered as linear. In contrast, a conventional structural system with equivalent damping greater than 10% must be considered to be nonlinear, and nonlinear dynamic analysis is not convenient for routine seismic design.

DESIGN OF DAMPING SYSTEMS FOR THE MODEL

(a) FRICTION DAMPERS

The size (slip force) of the friction dampers and their layout in the test structure was determined using a nonlinear time-history analysis approach. An initial slip load distribution was chosen, based closely on the results of a previous shake table study of the test structure containing another type of friction damper [6], and a series of analyses were performed for a number of different earthquakes at various input levels. The final slip load distribution was chosen as that which provided the best (lowest) structural response for all of the inputs.

(b) VISCOELASTIC DAMPERS

The method used for the design of the VE dampers for the test structure was a simplified first-mode procedure aimed at providing the structure with a specified level of damping (10%) at a nominal maximum displacement. This was done using an energy approach. A complete description of the procedure used is given in [5].

DESCRIPTION OF TEST FACILITY AND MODEL STRUCTURE

The experimental program was carried out using the earthquake simulator of the Earthquake Engineering Research Center of the University of California at Berkeley. The earthquake simulator (or shake table) measures 20 ft × 20 ft in plan and can support test specimens weighing up to 130 kips. Simulated seismic motions can be applied vertically and in one horizontal direction, with maximum accelerations of 1.0g and 1.5g, respectively.

The basic test structure was a 9-story, moment-resisting steel frame representing a section of a typical steel building at 1/4-scale. The structure was tested as a moment-resisting frame (MRF), a concentrically-braced frame (CBF), and in friction-damped (FD) and viscoelastically-damped (VD) configurations (Fig. 4). The VE dampers were added to the MRF in single-diagonal bracing, and the friction dampers were added as part of a modified chevron bracing system.

Constant stress scaling, such that model and prototype accelerations are equal, was used for the shake table tests. This required that approximately 90 kips of mass be added to the model in the form of concrete blocks and lead billets. The total test weight of the model was 100 kips. Response quantities measured during the shake table tests included floor displacements and accelerations, bracing forces and damper displacements, base shear and base overturning moment, and shake table accelerations and displacements.

DESCRIPTION OF EXPERIMENTS

The four configurations of the model structure (Fig. 4) were subjected to a number of different dynamic tests. These were free vibration (pull-back), pulse, random noise, and earthquake tests. Fundamental frequencies for the MRF and CBF of 1.95 Hz and 2.95 Hz, respectively, were identified. The dynamic characteristics of the VD and FD models were a function of the level and type of excitation, and were largely a result of whether or not the dampers were activated during the motion. From the results of the pulse tests, the fundamental frequencies of the VD (dampers activated) and the FD (dampers not activated) models were 2.30 Hz and 2.60 Hz, respectively. A more detailed presentation of the diagnostic test results is given in [5]. The remaining discussion of results is devoted to those from some of the earthquake tests.

Fourteen different earthquake motions were used in the shake table tests of the MRF, CBF, FD, and VD structures. The most extensive sequences of tests were performed for these motions:

(i) El Centro, Imperial Valley, May 18, 1940

(ii) Miyagi-Ken-Oki, Tohoku University, Sendai, June 12, 1978

(iii) Taft, Kern County, July 21, 1952

(iv) Llolleo, Chile, March 3, 1985

(v) La Union, Michoacan, September 19, 1985

(vi) Zacatula, Michoacan, September 19, 1985.

This paper discusses some of the results for the El Centro and Miyagi tests.

EARTHQUAKE TEST RESULTS

Typical hysteresis loops for the two types of dampers are shown in Fig. 5. The friction dampers exhibited outstanding behavior. The hysteretic behavior is extremely regular and repeatable. The devices showed almost no variation in slip load during earthquake motions, and from previous tests of individual dampers, their force-displacement response was known to be basically independent of loading frequency, amplitude, number of loading cycles, and temperature. In contrast to the VE dampers, the friction dampers are not activated during small excitations. Under such circumstances, the FD model behaved more as though it were a CBF.

The VE dampers exhibit elliptical hysteresis loops, typical of materials with velocity-dependent properties. The loops are regular in shape and show stable behavior. Throughout the VD model tests the maximum VE damper shear strain was 208 %. Viscoelastic dampers have no threshold or activation force level, and thus they dissipate energy for all levels of earthquake excitation. This contrasts with the behavior of the friction dampers, which for forces less than the slip force, do not slip and do not dissipate energy. The stiffness characteristics of the VE dampers are dependent on a number of factors, notably strain amplitude, frequency, and temperature. The variation of VE damper stiffness with shear strain for all of the Miyagi tests is shown in Fig. 6. Between strains of about 0 and 50 %, there is a large decrease in stiffness, but for strains in the range of about 50 to 200 %, the stiffness can be

regarded as approximately constant.

Because of the variation in VE damper stiffness with strain amplitude, the fundamental frequency of the VD model also varied with excitation level, from 2.43 Hz down to 2.00 Hz, compared with 1.95 Hz for the MRF. Low-level earthquake tests of the FD model revealed a fundamental frequency of 2.67 Hz (compared with 2.95 Hz for the CBF), while for large excitations a variation of 2.47 to 2.35 Hz was observed.

Temperature increases in the VE material during earthquake shaking were small and did not significantly affect the behavior of the VE dampers.

Shake table response comparisons of the various systems were made wherever possible. For a sequence of El Centro and Miyagi tests, the VD model generally behaved in the same way as the CBF with regard to displacements, and in the same way as the MRF with regard to accelerations. The same general trends were also seen for the FD model compared with the CBF and MRF models. FD, MRF, and CBF acceleration and displacement response profiles for the El Centro-400 tests are compared in Fig. 7. The FD floor accelerations are considerably lower than those of the CBF, and about the same as those of the MRF, while the peak floor displacements of all three structural systems are approximately the same. VD, MRF, and CBF acceleration and displacement response profiles for the El Centro-400 tests are compared in Fig. 8. For this input the VD model has peak accelerations *and* displacements less than those of the MRF and CBF. The FD and VD models responded very similarly for a large number of signals and a wide range of input levels. The FD and VD response profiles for the Miyagi-350 tests shown in Fig. 9 are typical of this close comparison.

Peak base shears of the FD, VD, and MRF models for a series of El Centro and Miyagi tests are compared in Fig. 10, where the FD and VD values are seen to be less than those of the MRF. This result, coupled with the reduced drift levels achieved by the dampers represents a significant overall improvement in response. A large number of equivalent tests were performed on the MRF, FD, and VD models. From response comparisons for the El Centro, Taft, and Miyagi sequences of inputs, drifts in both the FD and VD models were reduced by 10 to 60 % over those of the MRF, while story accelerations were reduced by 25 to 60 %. In all cases, the FD and VD responses were reduced.

Floor response spectra were also used to compare the MRF, FD, and VD models. Two percent-damped spectra for the 3rd floor of each of the models are presented in Fig. 11 for the El Centro-400 and Miyagi-400 tests. The damped structures both offer significant reductions in spectral acceleration, particularly over the range of 5 to 10 Hz. Above 10 Hz, the VD spectrum is about half that of the MRF, while the FD spectrum is less than or about the same as that of the MRF. These results, and those for many other earthquake inputs, indicate that these two types of energy absorbers do not pose problems for internal equipment in structures, and in most cases actually provide improvements over the equivalent MRF.

A comprehensive presentation of the results of the shake table tests is given in [5].

CONCLUSIONS

This experimental study has demonstrated the response improvements possible in earthquake-resistant structures through the use of energy absorbers. Separate comparisons of the FD and VD systems with the "undamped" MRF and CBF structures showed that both

damped systems behaved similarly to the CBF in terms of story drifts and similarly to the MRF in terms of story accelerations and story shears. The FD and VD systems were remarkably similar with regard to acceleration and displacement responses for a wide selection of earthquake inputs. Peak base shears of the FD and VD models were similar for a range of input levels of the El Centro, Miyagi and Taft signals. They were approximately the same as, or less than, the MRF maximum base shears. These results were achieved while simultaneously reducing the drifts to as little as one half of those of the MRF. The VE dampers supplemented the structure damping at all levels of excitation, in contrast to the friction dampers which do not operate below a threshold level of excitation. This means that VE dampers are particularly effective for low to moderate levels of seismic loading.

Floor response spectra showed spectral accelerations of both damped systems to be less than those of the MRF. Neither type of energy absorber caused undesirable high frequency response amplifications in the frequency ranges important for internal equipment or nonstructural components.

ACKNOWLEDGEMENTS

The authors are grateful to 3M Company and Sumitomo Metal Industries, Ltd., Japan, for the dampers used in the experimental study. A portion of this research was funded by the National Science Foundation. Any opinions, discussions, findings, conclusions and recommendations are those of the authors and do not necessarily reflect the views of the sponsors.

REFERENCES

[1] Skinner, R.I., Kelly, J. M., and Heine, A.J., "Hysteretic Dampers for Earthquake-Resistant Structures," *International Journal of Earthquake Engineering and Structural Dynamics*, vol. 3, no. 3, pp. 287-296 (1975).

[2] Pall, A.S., Verganelakis, V. and Marsh, C., "Friction Dampers for Seismic Control of Concordia University Library Building," *Proceedings, 5th Canadian Conference on Earthquake Engineering*, pp. 191-200 (1987).

[3] Keel, C.J. and Mahmoodi, P., "Designing of Viscoelastic Dampers for the Columbia Center Building," in *Building Motion in Wind*, N. Isyumov and T. Tschanz (eds.), ASCE, pp. 66-82 (1986).

[4] Mahmoodi, P., "Structural Dampers," Journal of the Structural Division, ASCE, Vol. 95, no. ST8, pp. 1661-1672 (1972).

[5] Aiken, I. D., "Earthquake Simulator Testing and Analytical Studies of Two Energy-Absorbing Systems for Multistory Structures," Report No. UCB/EERC-90/03, Earthquake Engineering Research Center, University of California at Berkeley (1990).

[6] Aiken, I. D., Kelly, J. M., and Pall, A. S., "Experimental Study of Friction Damp-ing for Steel Frame Structures," Proceedings, ASME PVP Conference, Vol. PVP-133, pp 95-100 (1988).

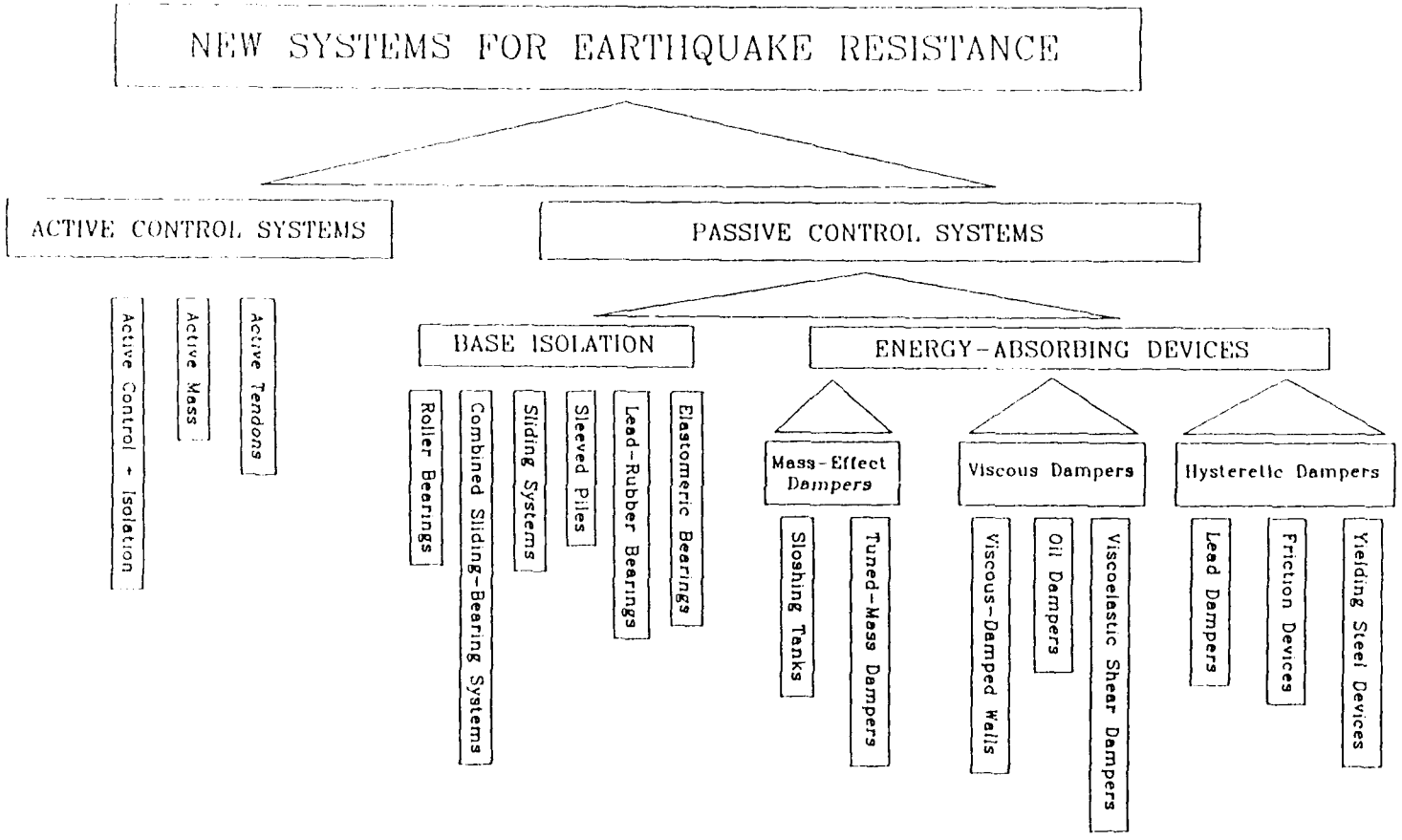

Fig. 1 New Systems for Improved Earthquake Resistance of Structures

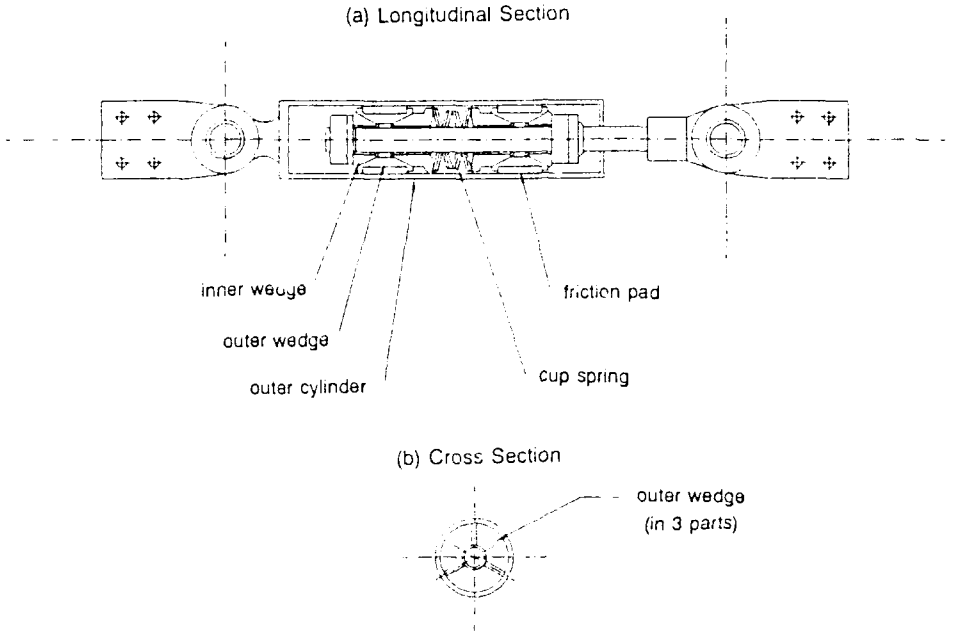

Fig. 2 Sectional Views of Friction Damper

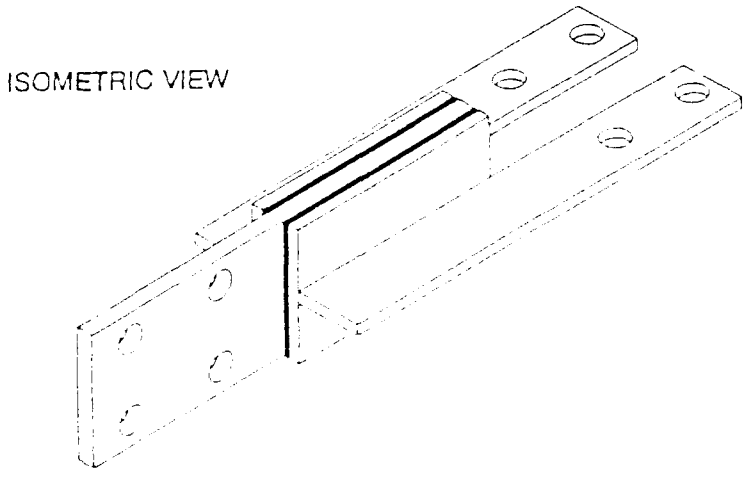

Fig. 3 Constrained-Layer Viscoelastic Shear Damper

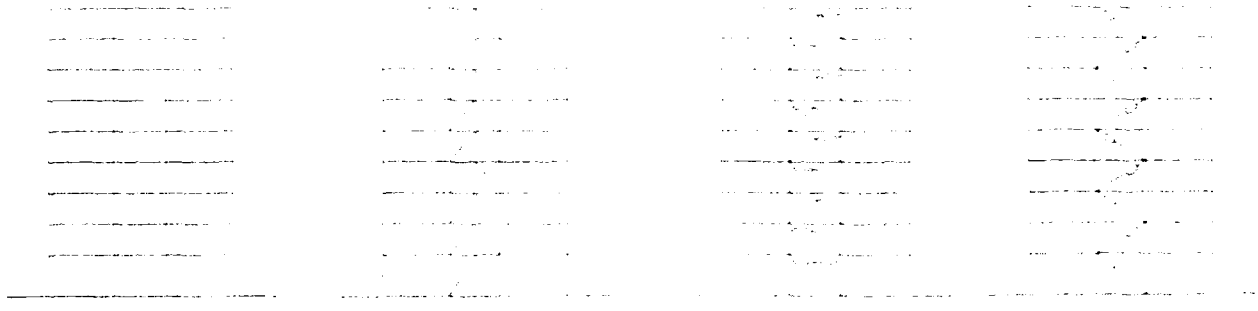

(a) MRF (b) CBF (c) FD (d) VD

Fig. 4 Test Configurations of Model Structure

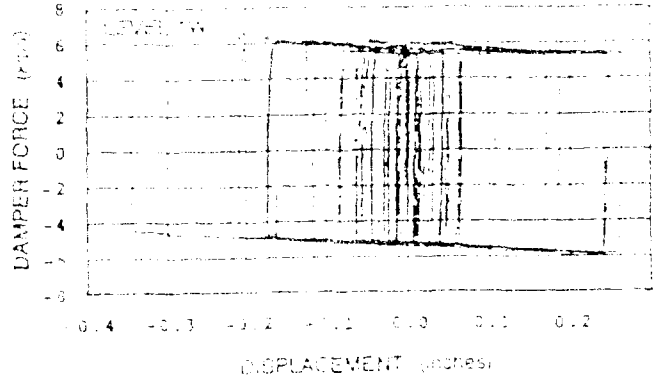

(a) Friction Damper

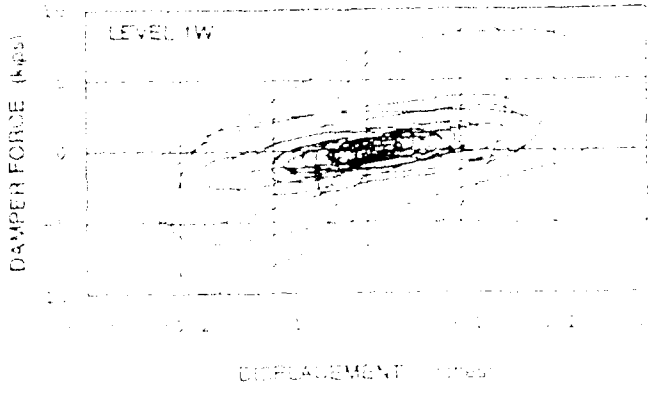

(b) VE Damper

Fig. 5 Typical Damper Hysteresis Loops for Control Tests

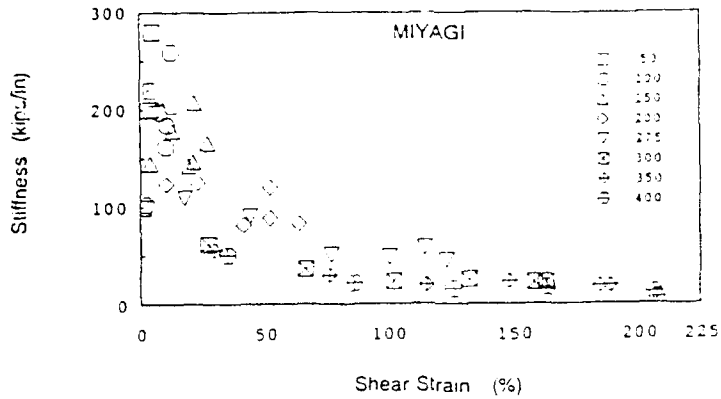

Fig. 6 VE Damper Stiffness versus Shear Strain

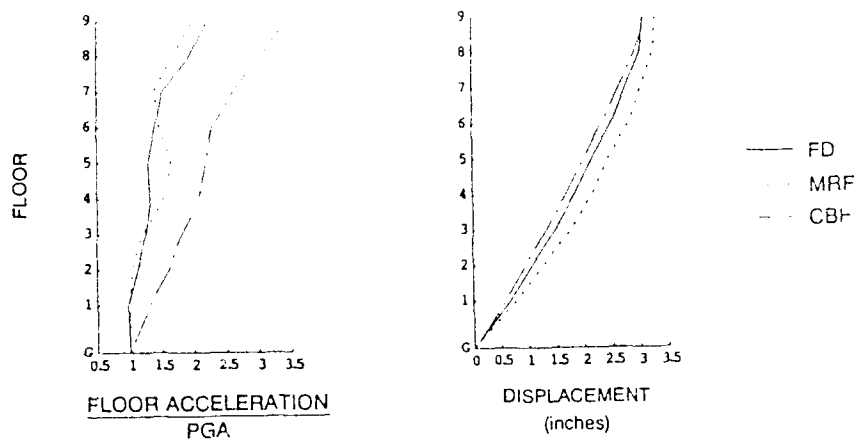

Fig. 7 FD, MRF, and CBF Acceleration and Displacement Response Profiles for El Centro-400 Tests

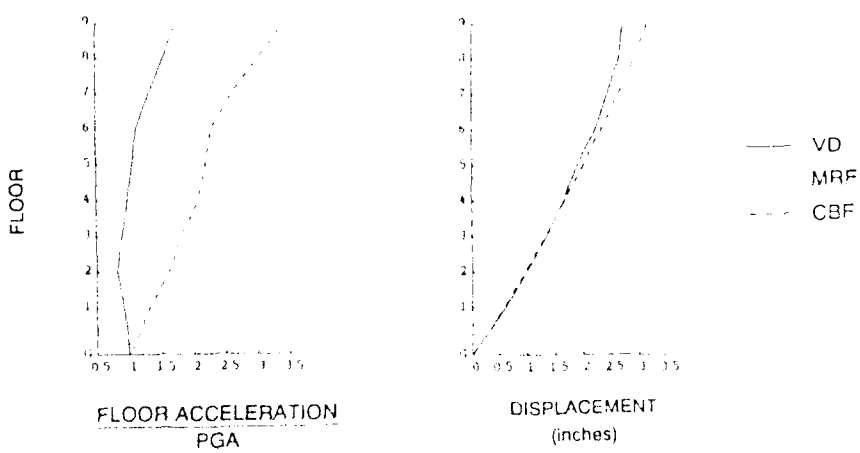

Fig. 8 VD, MRF, and CBF Acceleration and Displacement Response Profiles for El Centro-400 Tests

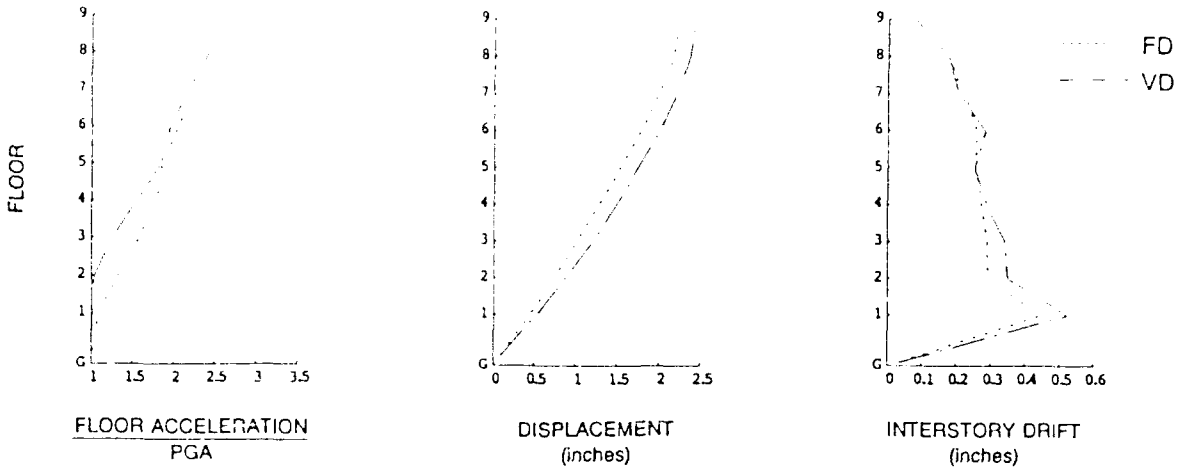

Fig. 9 FD and VD Acceleration and Displacement Response Profiles for Miyagi-350 Tests

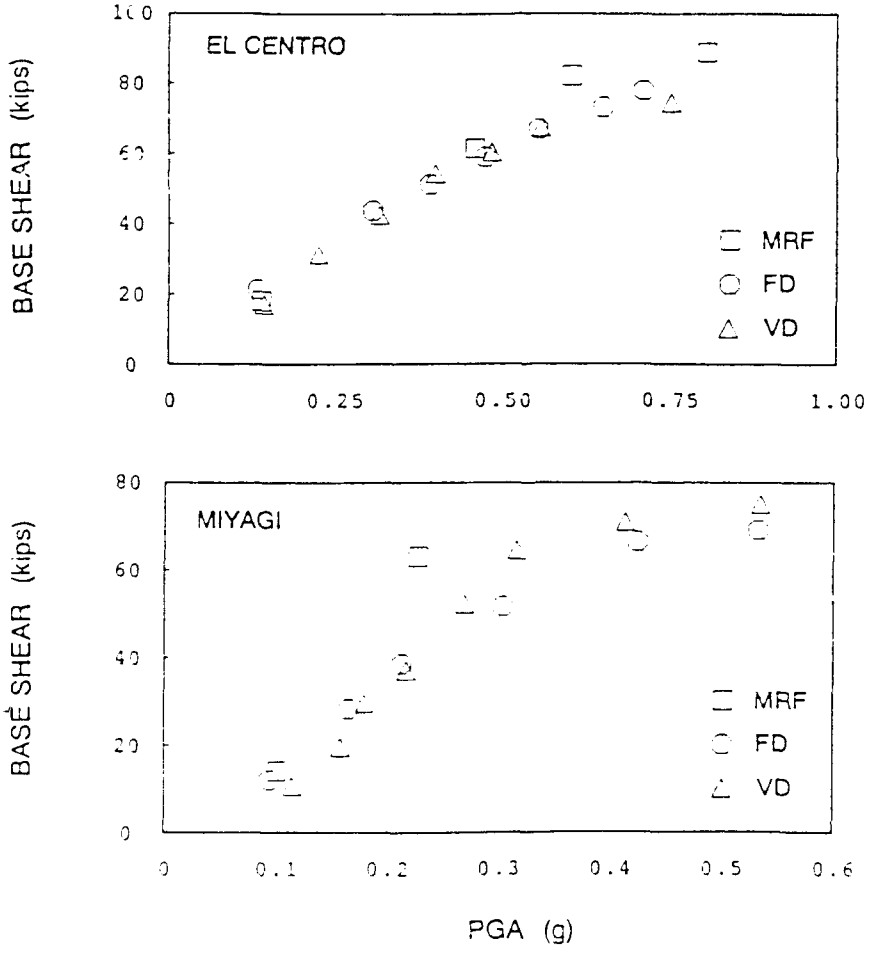

Fig. 10 FD, VD, and MRF Peak Base Shear vs. PGA for El Centro and Miyagi Tests

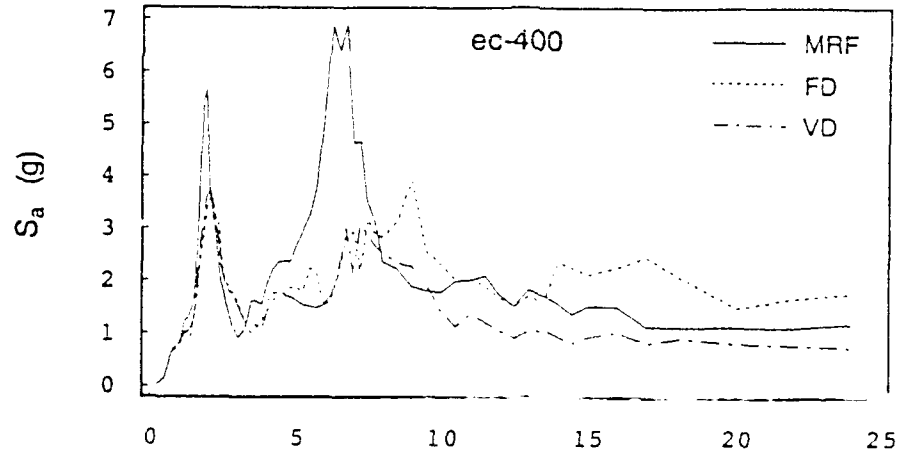

(a) El Centro-400

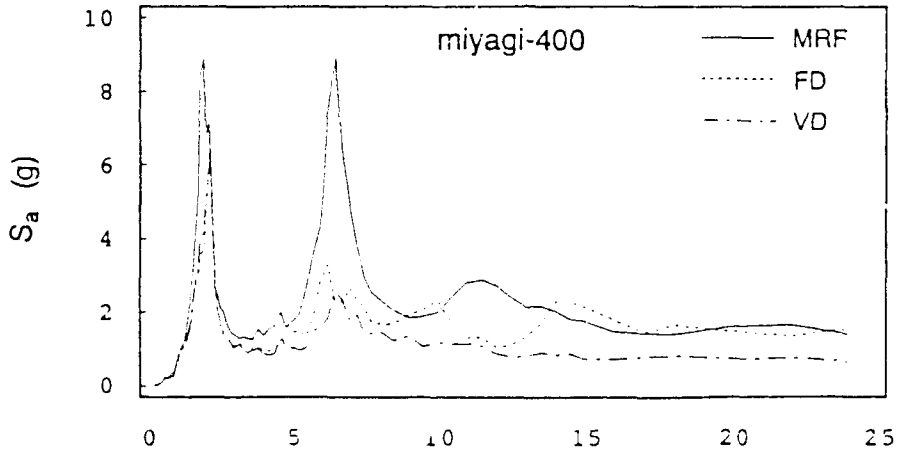

(b) Miyagi-400

Fig. 11 FD, VD, and MRF Level 3 Two Percent-Damped Floor Response Spectra, El Centro-400 and Miyagi-400 Tests

CORRELATION OF EXPERIMENTAL RESULTS WITH PREDICTIONS OF VISCOELASTIC DAMPING FOR A MODEL STRUCTURE

T. T. Soong
Department of Civil Engineering
State University of New York at Buffalo
Buffalo, NY 14260
(716) 636-2469

and

M. L. Lai
The 3M Company
New Product Department
Building 201-1N-35, 3M Center
St. Paul, MN 55144
(716) 736-0704

ABSTRACT:

Viscoelastic dampers as supplementary damping devices have been applied to building structures under wind loads. More recently, analytical and experimental results have shown that, when properly designed, they can also be effective against earthquake and other environmental forces. One of the challenging areas in research and implementation of viscoelastic dampers is to evaluate the damping effect of the dampers on structures. In this paper, the modal strain energy method in conjunction with the finite element method is used to evaluate the damping ratio of a 1/2.5 scaled steel frame building with viscoelastic dampers installed. Computed damping ratios are found to be in very good agreement with the experimental results.

INTRODUCTION

In recent years, both researchers and practicing professionals have recognized that energy dissipation devices can provide an efficient means of mitigating the building response induced by strong motion earthquakes (ATC-17 1986 and ATC-15-3 1990). By dissipating the vibratory energy in the structure, the energy dissipation devices can reduce the risk for the building of experiencing excessive deformations or accelerations. As a result, less ductility or inelastic energy demand is required.

Since the first implementation of 10,000 viscoelastic dampers in each of the two World Trade Center buildings in New York City in early the 1970's, two more buildings, the Columbia Center and the Two Union Square building, both in Seattle, have incorporated passive viscoelastic dampers. All these applications are to increase the structural damping and eventually to reduce the building response due to ambient wind loadings. Recently, the viscoelastic dampers have also been tested in scaled models on shaking tables for seismic applications (Soong and Mahmoodi 1990 and Aiken, Kelly and Mahmoodi 1990). It has been shown that passive viscoelastic dampers can very effectively attenuate the earthquake-induced structural response. It is also noted that the viscoelastic dampers behave quite linearly. This should greatly simplify the damping analysis and design for buildings

Literatures on the characterization of viscoelastic materials for passive building dampers are identified by Mahmoodi (for instance, Mahmoodi 1969 and Keel and Mahmoodi 1986). Recently, the analysis of the damping effect on buildings were attempted by Lin, *et al* (1991) and Zhang, *et al* (1989). However, no effort has been made to correlate the analytical results to the experimental results.

In this paper, analytically calculated modal damping ratios and modal frequencies are compared to experimental results.

EQUATIONS OF MOTION OF A VISCOELASTICALLY DAMPED SYSTEM

Viscoelastic dampers installed in a building may behave linearly within a range of strain of the viscoelastic material (Aiken, Kelly and Mahmoodi 1990). The dampers will contribute to the viscous damping as well as the stiffness of the building. In this case, the discretized system linear equations of motion for the building subjected to an earthquake excitation $\ddot{X}_g(t)$ may be written as

$$[m]\{\ddot{X}\} + [c]\{\dot{X}\} + [k]\{X\} = -[m]\{1\}\ddot{X}_g(t) \tag{1}$$

where $\{X\}$ is the column vector of the displacements of the nodes relative to the base; a dot represents differentiation with respect to time; $\{1\}$ is a column vector of ones; and $[m]$, $[c]$ and $[k]$ are the mass, damping and stiffness matrices, respectively, in physical coordinates.

Although the response of the building can be obtained by direct time integration of Eq. 1, it is generally more efficient to analyze the system by modal analysis techniques. The system response is then approximated by a linear combination of the lowest modes of vibration.

In conducting modal analyses, one of the main tasks is to estimate modal parameters, i.e., modal frequency, mode shape and modal damping ratio for the modes of interest. It has become a common practice to calculate the modal frequency and mode shape of buildings, for instance, using finite element methods. The modal damping ratio of a building is usually based on empirical estimates since efficient analytical predictions are hindered by the complex damping mechanisms involved

in buildings. However, by taking advantage of the fact that a viscoelastically damped building responds approximately linearly to dynamic excitations, a method based on the modal strain energy method can be used to predict the modal damping ratio.

MODAL STRAIN ENERGY METHOD

The modal strain energy method has widely been used to calculate the damping ratio of viscoelastic damped systems (Ungar and Kerwin 1962 and Johnson and Kienholz 1982). In this method, the real normal mode modal analysis is used.

In real normal mode modal analyses, the modal equations of motion for Eq. 1 can be written as

$$\ddot{Z}_n + 2\zeta_n \omega_n \dot{Z}_n + \omega_n^2 Z_n = \frac{-\{\phi\}_n^T [m]\{1\}\ddot{X}_g(t)}{m_n} \tag{2}$$

$$\{X(t)\} = \sum \{\phi_n\} Z_n(t) \qquad n = 1, 2, 3, \cdots \tag{3}$$

where Z_n is the nth modal response, ζ_n is the nth modal damping ratio, ω_n is the nth modal frequency, $\{\phi_n\}^T$ is the nth mode shape vector and is the transpose of $\{\phi_n\}$, and m_n is the nth modal mass. These quantities as well as the system response, $\{X(t)\}$, can readily be evaluated if the matrices $[m]$, $[c]$ and $[k]$ and the excitation in Eq. 1 are known.

In this paper, no attempts is committed to the evaluation of the damping matrix $[c]$ of the system. Rather, from the modal strain energy method (Johnson and Kienholz 1982), the modal damping ratio of the nth mode ζ_n can be calculated as

$$\zeta_n = \frac{\eta_v}{2} \frac{E_v}{E_s} \tag{5}$$

where η_v is the loss factor of the viscoelastic material at the modal frequency, E_s is the nth modal strain energy of the system with dampers and E_v is the energy stored in the viscoelastic dampers. These energies are calculated from

$$E_v = \{\phi_n\}^T [k_v]\{\phi_n\} \qquad \text{and} \qquad E_s = \{\phi_n\}^T [k_s]\{\phi_n\} \tag{6}$$

where $[k_v]$ is the stiffness matrix attributed to the added dampers and $[k_s]$ is the stiffness matrix of the structure when the dampers are installed.

Eq. 5 can be rewritten as

$$2\zeta_n E_s = \eta_v E_v \tag{7}$$

Eq. 7 states that the energy loss in the structure equals the energy dissipated in the dampers. In other words, only the viscoelastic dampers contribute to the damping of the structure. Other mechanisms of damping are neglected.

DAMPING RATIOS OF A VISCOELASTICALLY DAMPED 5-STORY MODEL

Viscoelastic dampers are installed in a 1/2.5 scaled single bay 5-story steel moment resisting frame model as shown in Figs. 1a and 1b. Six cases are used to verify the modal strain energy method for computing the modal damping ratio of the first mode. Experimental verifications were conducted on a shaking table. Detailed test procedures and results will be presented elsewhere.

Finite element methods are used to obtain the system mass and stiffness matrices. A spring element is used to represent the damper stiffness. Fig. 2 shows that the predicted first modal frequencies in all cases are in very good agreement with the measurements. It is also shown that by employing the dampers, the modal frequency of the structure is slightly increased.

Predicted damping ratios of the first mode for all cases using Eqs. 5 and 6 are shown in Fig. 3 along with experimental results. The prediction error is within ±5%. It is also shown that the damper placement greatly affects the modal damping ratio of the structure. In order to maximize the damping ratio, an optimum placement strategy may be warranted. However, as a rule of thumb, dampers should be placed at the locations that will experience large deformations.

CONCLUSIONS

The structural modal damping ratio is estimated using the modal strain energy method in conjunction with the finite element method. The estimated damping ratios of a 1/2.5 scaled model are verified by experiments. The viscoelastic dampers provide a very efficient way to increase the damping and survivability for buildings under earthquake excitations.

REFERENCES

Aiken, I. D., Kelly, J. M. and Mahmoodi, P. (1990). "The Application of Viscoelastic Dampers to Seismicity Resistant Structures." *Proc. 4th National Conf. on Earthquake Engineering,* Vol. 3, pp. 459-468, May 20-24, 1990, Palm Spring, CA.

ATC-15-3 (1990). *Four*th U.S.-Japan Workshop on the Improvement of Building Structural Design Practices, August 27-29, 1990. Kona, Hawaii.

ATC-17 (1986). Base Isolation and Passive Energy Dissipation. March 12-14, 1986. San Francisco, CA.

Johnson, C. D. and Kienholz, D. A. (1982). "Finite Element Prediction of Damping in Structures with Constrained Viscoelastic Layers." *AIAA Journal.* Vol. 20, No. 9, pp. 1284-1290.

Keel, C. J. and Mahmoodi, P. (1986). "Design of Viscoelastic Dampers for Columbia Center Building." *ASCE Structural Division, Building Motion in Wind,* Edited by N. Isyumov and T. Tschanz, pp. 66-82.

Lin, R. C., Liang, Z., Soong, T. T., and Zhang, R. H. (1991). "An Experimental Study of Seismic Structural Response with Added Viscoelastic Dampers." *Engineering Structures,* Vol. 13, No. 1, pp. 75-84.

Mahmoodi, P. (1969). "Structural Dampers." *Journal of Structural Division, ASCE*, 95, 1661-1972.

Soong, T. T. and Mahmoodi, P. (1990). "Seismic Behavior of Structures with Added Viscoelastic Dampers." *Proc. 4th National Conf. on Earthquake Engineering,* Vol. 3, pp. 499-506, May 20-24, 1990, Palm Spring, CA.

Ungar, E. E. and Kerwin, E. M., Jr. (1962). "Loss Factor of Viscoelastic Systems in Terms of Energy Concepts." *Journal of the Acoustical Society of America*, 34(7), 954-957.

Zhang, R. H., Soong, T. T. and Mahmoodi, P. (1989). "Seismic Response of Steel Frame Structures with Added Viscoelastic Dampers." *Earthquake Engineering and Structural Dynamics*, 18, 389-396.

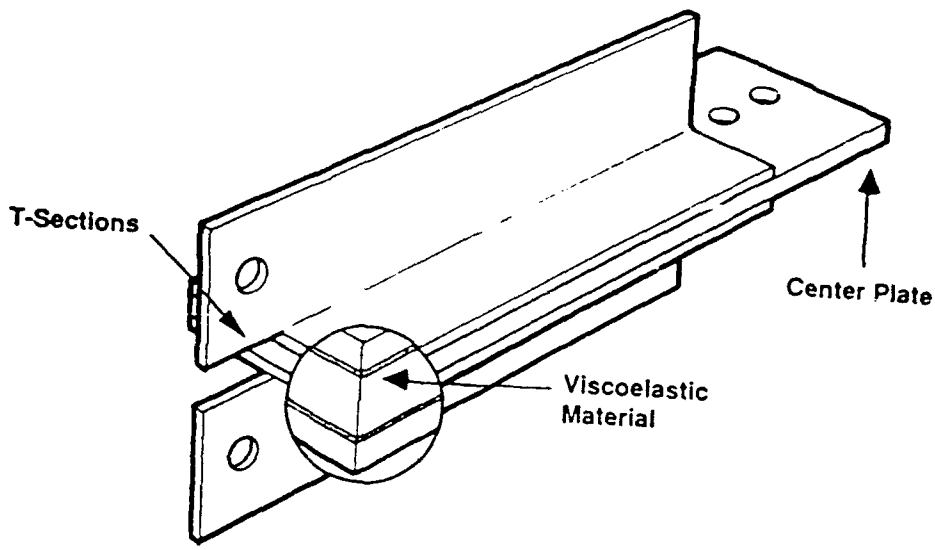

Fig. 1a A typical Viscoelastic Damper.

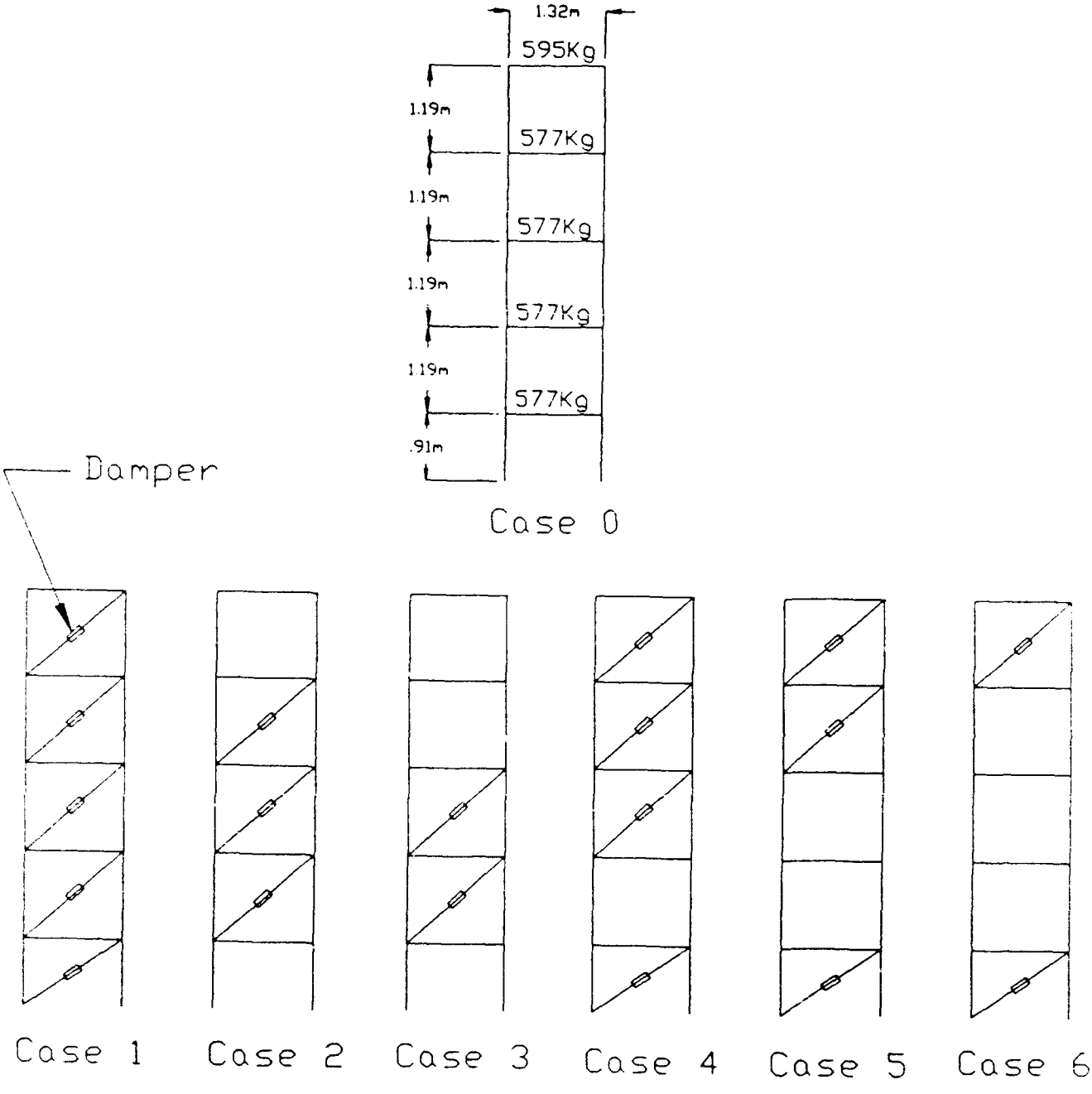

Fig. 1b **A 1/2.5 scaled structure with and without viscoelastic dampers installed.**

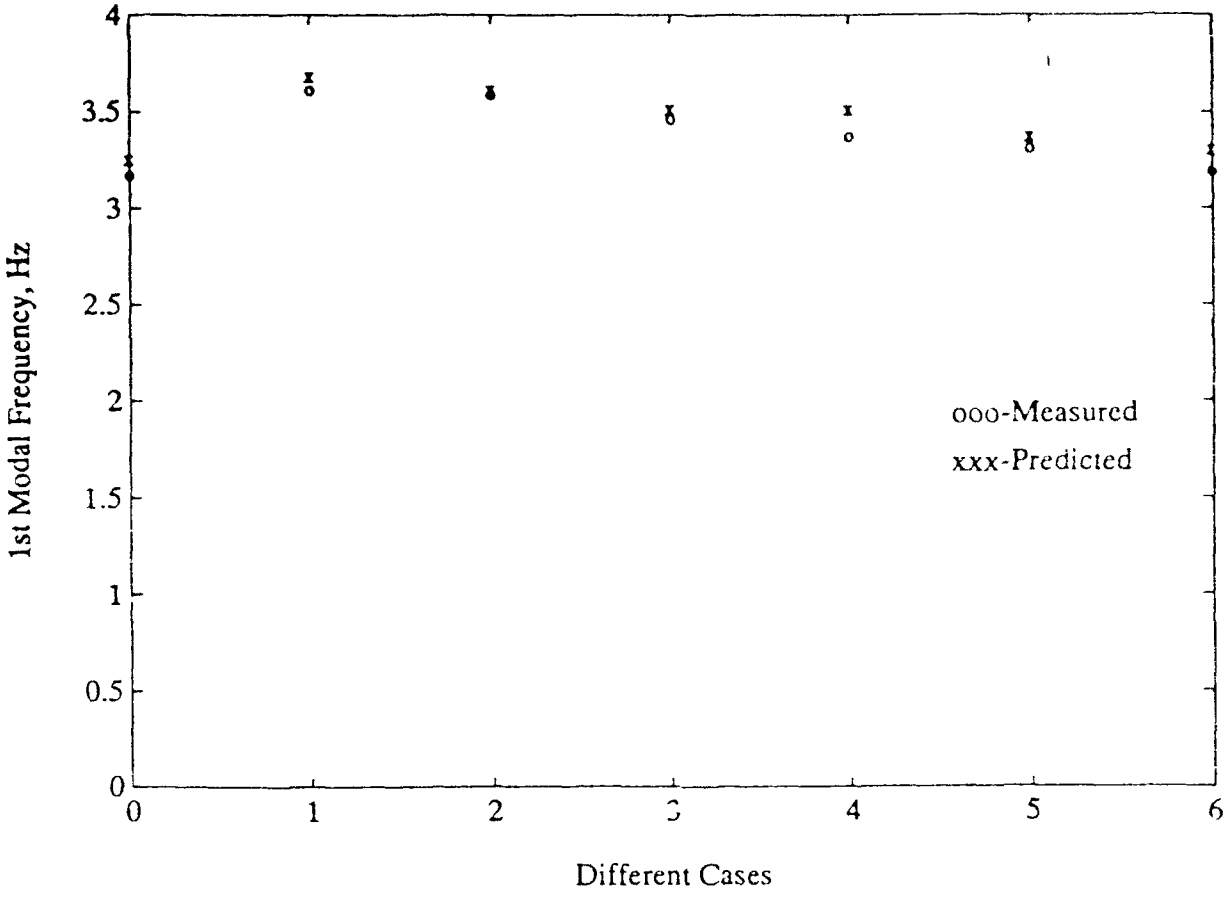

Fig. 2 Measured and Predicted 1st Modal Frequencies for All Cases.

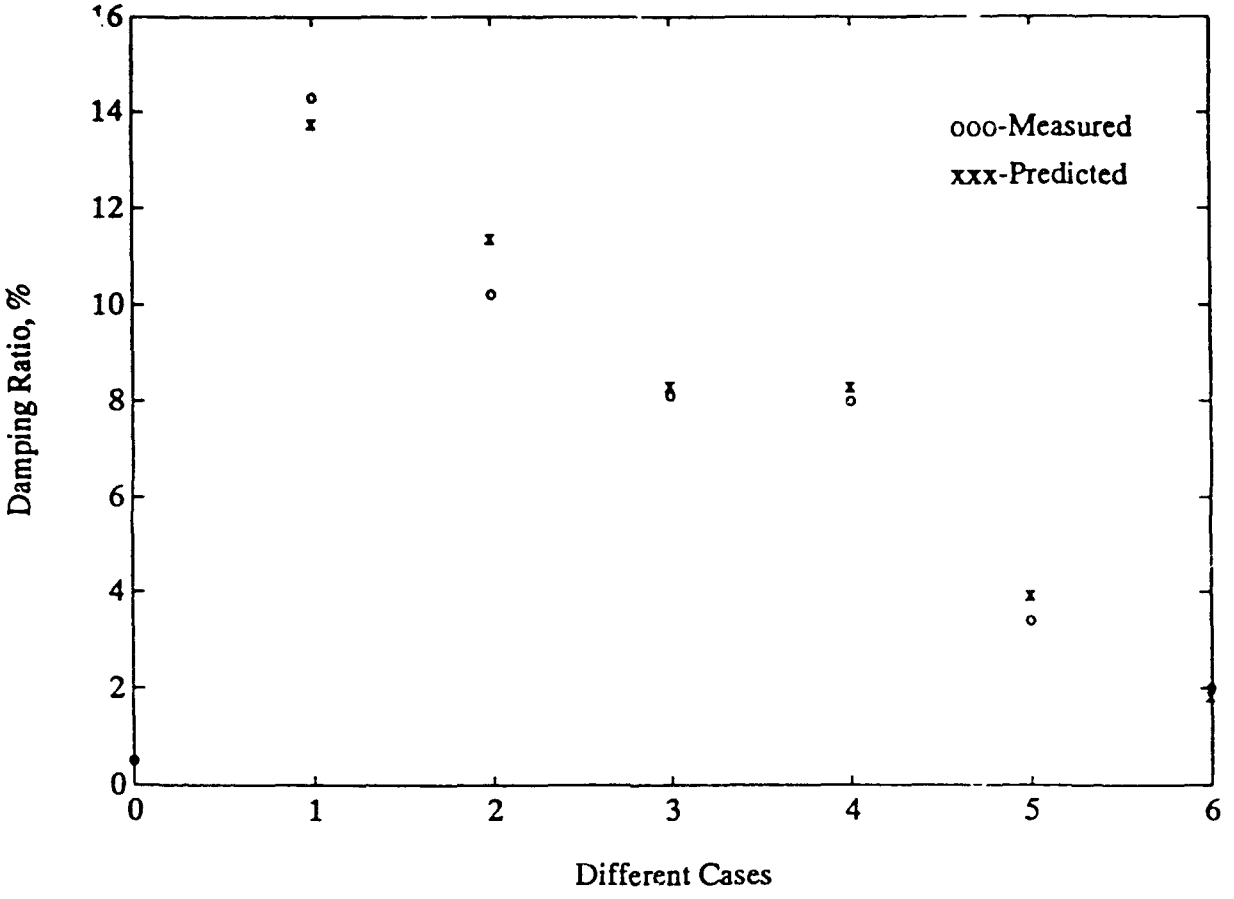

Fig. 3 Measured and Predicted 1st Modal Damping Ratios for All Cases.

DAMPING CAPACITY OF REINFORCED CONCRETE EXTERNAL BEAM COLUMN CONNECTIONS

Alexander G. Tsonos[1]
Aristotle University of Thessaloniki
Greece

Ioannis A. Tegos
Aristotle University of Thessaloniki
Greece

Georgios G. Penelis
Aristotle University of Thessaloniki
Greece

ABSTRACT

In this study experimental results are presented, obtained during an investigation on the influence of the axial load change in the eternal beam-column joints' damping capacity. Six full sized exterior beam-column joint specimens were tested. The increasing or decreasing of the load point displacement was simultaneous with the increasing or decreasing of the axial column's compression (or tension) load. It was concluded that the column's axial load change is important and causes a significant reduction in strength, stiffness, ductility and energy dissipation capacity. This effect cannot be neglected in either the analysis or design, as it may be the cause of premature instability. A new mechanism (with inclined bars) for improving the structural damping properties of earthquake resistance reinforced concrete exterior beam-column joints was examined and the results were very encouraging regarding the reduction of the unfavourable effects of the axial column load's change in the above (mentioned) structural elements.

FULL PAPER NOT AVAILABLE FOR PUBLICATION

[1]Researcher, Department of Civil Engineering, Aristotle University of Thessaloniki, Greece, 031-99-2641

EDDY CURRENT-BASED VIBRATION DAMPING FOR AEROSPACE STRUCTURES

Prepared for:

Damping '91 Conference

February 1991

ABSTRACT

A need exists for enhancing the passive damping present in proposed aerospace structures. A research program is underway to assess the feasibility of exploiting the retarding force experienced by conductors moving in the presence of a magnetic field, to provide passive damping of space-deployed structures. The characteristics of this approach are strikingly suitable for space applications: non-outgassing, relatively insensitive to temperature, noncontacting (no stiction or wear), linear, radiation tolerant, highly reliable. An eddy current-based damper could be used as the damping element in a tuned inertial reaction device (passive vibration absorber, proof mass actuator, etc.) or, alternatively, as part of a static broad-band damper. For a static damper, a flexure-based mechanism would amplify the vibratory motion of the truss member, ensuring sufficient motion of the conductor to develop adequate power dissipation. Preliminary calculations have shown that substantial modal damping ratios can be achieved at minimal weight. SatCon is undertaking an analytical, experimental and design-oriented program to assess the weight, performance, cost and reliability of this novel approach to vibration damping of space structures.

James H. Goldie
SatCon Technology Corporation
12 Emily Street
Cambridge, MA 02139
Phone: (617)661-0540 ext 204

What is basic idea?

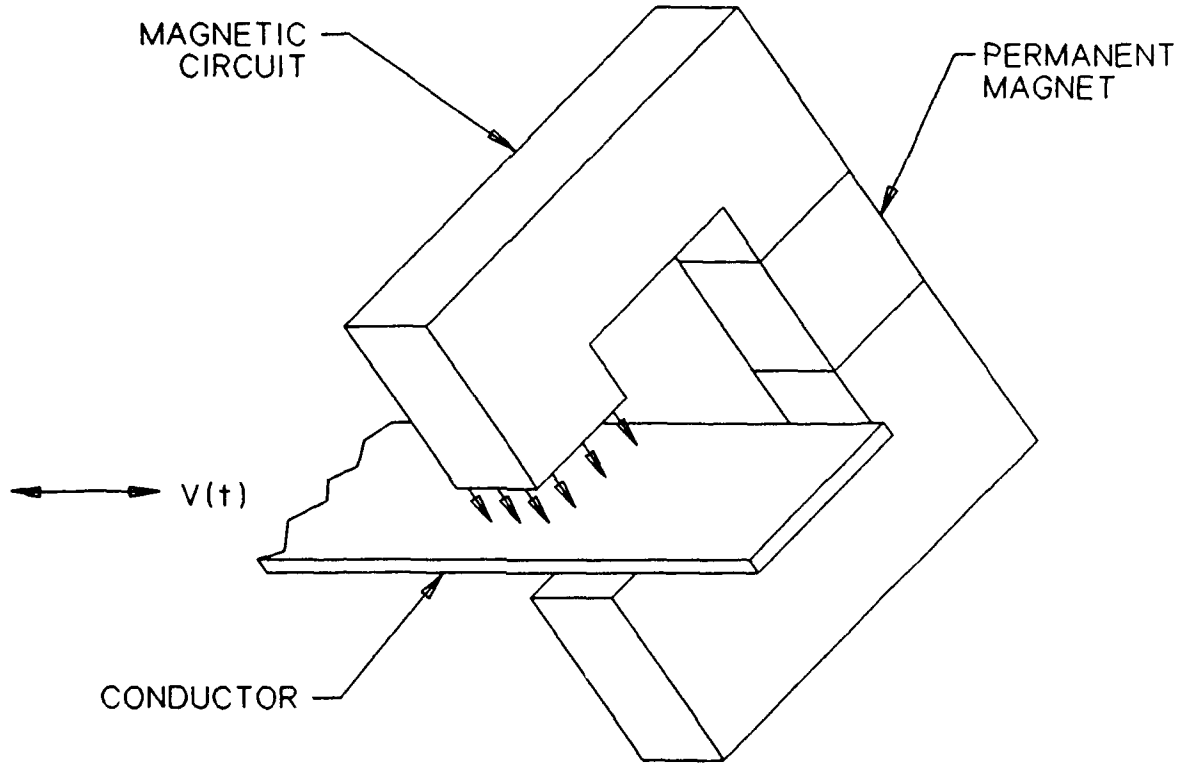

- Field can be produced by a permanent magnet
- Conductor experiences a viscous drag force
- Currents induced in moving conductor dissipate vibrational energy

It is well known that a conductor moving within a magnetic field will experience a drag force. As the conductor moves, eddy currents are induced which interact with the field present so as to resist the motion. The net result is that vibrational energy is converted to heat (produced by the dissipative losses of the caused by the eddy currents in the conductor).

The approach shown in the figure is the simplest rendition of an eddy current-based damper. A totally passive damper can be made by letting a thin conducting strip move within the field of a permanent magnet. Alternative schemes employing superconducting field magnets or electromagnets can be envisioned. A superconducting magnet would offer extremely high flux densities and the elimination of return iron. Application of electromagnets would permit the field to be actively controlled, which would allow control of the damper characteristics.

What are the benefits of eddy current-based damping?

Applications ----→ / BENEFITS:	Space	Cryogenics	Precise Positioning	Commercial Vibration Isolation
LINEAR	△			△
INSENSITIVE TO TEMP.	△	△		
NON-OUTGASSING	△			
NON-CONTACTING		△	△	
NO WEAR/FATIGUE	△			
HIGH RELIABILITY	△			
TEMPORAL STABILITY	△		△	
EASY ADD-ON	△			

SatCon is particularly excited about eddy current-based damping because of its extraordinary collection of attributes.

Its linearity under most operating conditions is attractive because of the resulting analytical simplicity and the avoidance of exciting higher modes of vibration.

Perhaps its most significant attribute is its relative insensitivity to temperature. The performance of other damping schemes involving hydraulics or viscoelastic materials is extremely sensitive to temperature. There is some sensitivity of an eddy current-based damper, due to the change in conductivity of metals with temperature. The change in conductivity, however, is relatively benign and can be tailored by the proper choice of the conducting metal and its purity. This insensitivity and tolerance to a wide temperature range is particularly beneficial for vibration damping in space or orbital applications, which experience wide temperature swings, and for cryogenic applications.

The eddy current-based damper is comprised of metals. Consequently, it will not outgas in a space vacuum.

Amongst the attributes of the eddy current damper are its noncontacting nature, and its low wear and high reliability. These attributes spring form the fact that there is no contact between the moving and stationary portions of the device. They are particularly beneficial to cryogenic, precise positioning and space applications. The noncontacting character is significant for cryogenic application, since it prevents the introduction of additional conduction paths. Applications which require precise positioning of components (such as optics) benefit since the phenomena of stiction and position hysteresis are eliminated. Finally, vibration damping applications in space benefit from the high reliability and long life offered by the eddy current-based damper.

There is no reason for the characteristics of the damper to change with time. This offers benefits for long duration space applications and precise positioning applications.

Finally, it should be added that an eddy current damper could be conveniently added to an existing structure which requires supplemental damping.

Eddy Current–Based Dampers have been used for Cryogenic Applications

- Good conductivity at cryogenic temperatures beneficial
- Alternatives such as squeeze film dampers, viscoelastic material dampers or coulomb friction dampers not practical
- Stanford Gravity Wave Experiment
- Vibration control in cryogenic turbomachinery

Eddy current-based dampers have been used in a few specialized vibration damping applications. The most important are cryogenic applications such as the Stanford Gravity Wave Experiment, where cryogenic temperatures are required to reduce Brownian motion to an acceptable level. In its latest rendition the damping scheme is inside the cryogenics and, hence, is required to work at cryogenic temperatures. Consequently, an eddy current-based damping scheme is employed in which vapor-cooled superconductors carry the induced eddy currents out of the dewar to be dissipated in a location where the resulting heat is tolerable. The eddy current damper is particularly appropriate for this application since it does not produce heat in the cryogenics, it provides damping at cryogenic temperatures and it does not introduce substantial heat conduction paths. Some research has been performed by Robert E. Cunningham at the NASA Lewis Research Center regarding the use of eddy current damping for vibration control in cryogenic turbomachinery[1]. At cryogenic temperatures common techniques employing squeeze film dampers, viscoelastic material dampers or coulomb dampers are not feasible, whereas eddy current-based dampers exhibit improved performance. Other applications have included damping of wind tunnel models and Foucault pendulum damping[2].

[1] R. E. Cunningham, "Passive Eddy-Current Damping as a Means of Vibration Control in Cryogenic Turbomachinery," NASA Lewis Research Center, NASA Technical Paper 2562, 1986.

[2] G. Mastner, et al, "Foucault Pendulum with Eddy-Current Damping of the Elliptical Motion," Review of Scientific Instruments, Vol. 55, No. 10, October 1984.

How is an eddy current-based damper analyzed?

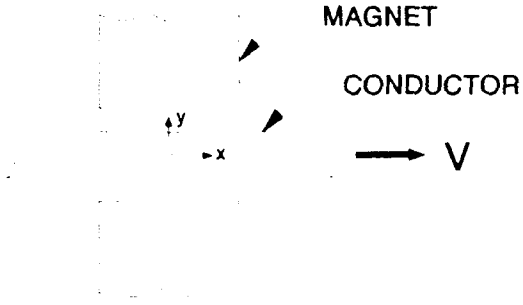

Field Problem for Eddy Current-Based Damper

- Complete 2-D model

$$\frac{1}{\mu\sigma}\left(\frac{\partial^2 B_y}{\partial x^2} + \frac{\partial^2 B_y}{\partial y^2}\right) = \frac{\partial B_y}{\partial t} + V\,\frac{\partial B_y}{\partial x}$$

Includes skin effect, end effects and nonlinearity.

- For many operating conditions and design parameters, a simple model may be used

$$J_z = \sigma V B_y$$

$$F_x = -\sigma V B_y^{\,2} \cdot (\mathrm{Vol})_{\mathrm{cond}} \qquad \text{(Lorentz force)}$$

$$b = \sigma B_y^{\,2} \cdot (\mathrm{Vol})_{\mathrm{cond}}$$

The field equations can be combined to yield a two-dimensional partial differential equation for the flux density for a conductor moving in a magnetic field. This is a challenging analytical problem, due to the nonlinearity caused by the variation of the vibrational velocity, V. In many situations the field produced by the eddy currents is small compared to the imposed field. Under these circumstances the drag force is proportional to the velocity, the conductivity and the square of the flux density.

Broad Band Supplemental Damping of Space Truss Structure

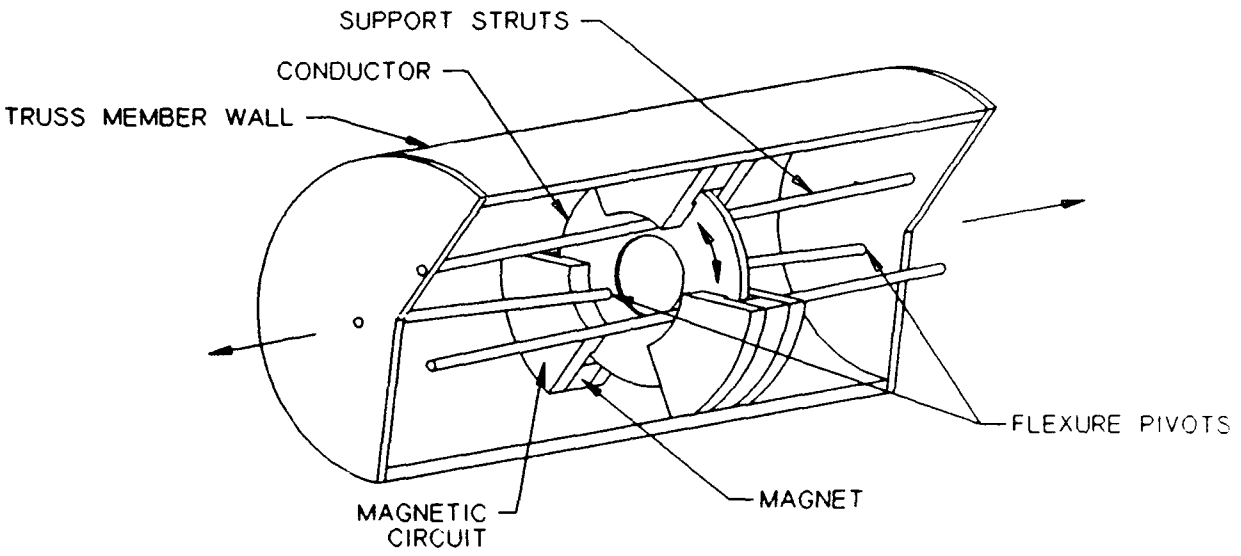

- Relatively small vibrational strains/velocities
- Damping is enhanced by use of flexure-based mechanism

$$b_{eff} = m^2 b$$

One approach envisioned by SatCon for applying an eddy current-based vibration damper to individual members of a space truss structure results in a broad-band damper that would enhance damping in much the same way that a hydraulic or viscoelastic-based damper would. The fundamental difficulty with this approach is that the vibrational strains and velocities are too small to develop significant power dissipation. In order to properly match the impedance of the damper to the structure, a flexure-based mechanism such as the one shown can be employed. It should be noted that the figure is intended to clarify the concept and, consequently, is not to scale. The helical orientation of the support struts causes the conducting disc to rotate substantially when the truss member axially deforms. The large mechanical gain developed by a mechanism of this sort allows the damper to dissipate significant vibrational energy. The use of flexures avoids the difficulties of stiction, backlash and lubrication of metal surfaces in sliding contact.

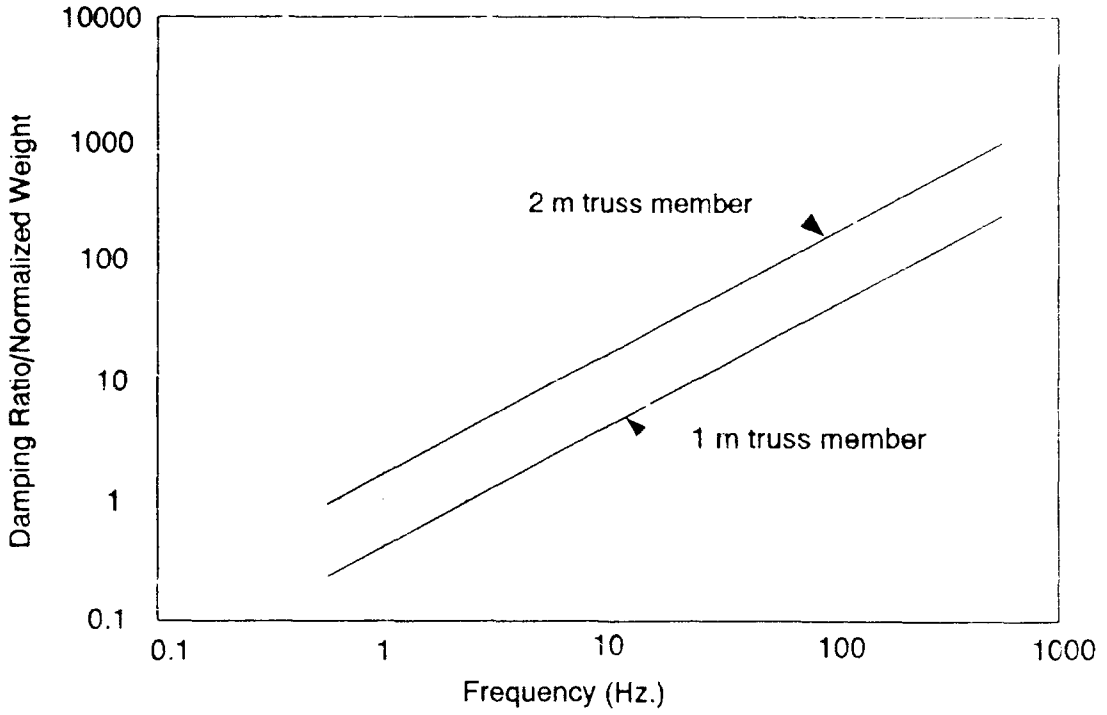

The Damping Ratio (divided by normalized weight) as a Function of Vibrational Frequency

The Damping Ratios Achieved with 1 m Struts and a Broad-band Eddy Current Damper

f(Hz)	ζ (%)	W'
1	1.0	.024
1	2.5	.061
10	5.0	.012
10	10.0	.024
100	25.0	.006

As with most engineering design, there is a tradeoff between desired characteristics. In the case of the broadband damper, there is a tradeoff between performance (i.e., damping ratio) and weight of the device. Assuming that the design shown in the figure is used, the simple model discussed above can be used to investigate this tradeoff. The plot shows the damping ratio divided by the normalized weight of the damper (weight of the damper as a fraction of the weight of the associated truss member) as a function of frequency. This calculation includes the weight of the magnetic circuit components and the conductor required and assumes that the truss member is hollow and made from graphite epoxy and that the conductor used is copper. The damping ratio is calculated as $1/4\pi$ times the ratio of the energy dissipated per cycle by the damper to the strain energy of the member at it largest axial deformation.

It is worth noting that the modal frequencies associated with the important lower modes of space-deployed truss structures are well below those of the individual truss members. Consequently, motion of an individual truss member will be predominantly static axial deformation caused by the vibrational movement of the overall structure.

As the plot indicates, the performance improves linearly with frequency and with truss member length. The improvement with length stems from the fact that practical considerations limit the mechanical gain possible independent of truss member length. Consequently, the power dissipated per cycle varies as the square of the truss member length and strain energy only linearly with length for a given maximum truss member strain.

The table gives some typical damping ratios and normalized damper weights as a function of frequency. As the table indicates substantial damping ratios can be achieved at small weights. For example, at 10 Hz. a 5% damping ratio can be achieved with a damper which is only 1.2% of the weight of the associated truss member.

Damping Element in a Tuned Passive Vibration Absorber or Proof Mass Actuator

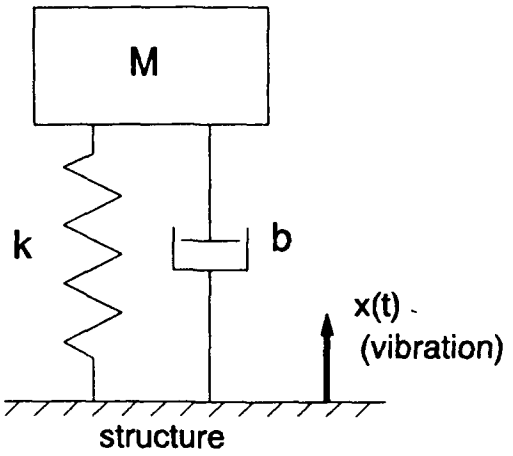

- Tuned to slightly below first structural mode
- Appropriately sized to structure
- Damping ratio chosen to maximize vibrational power dissipation

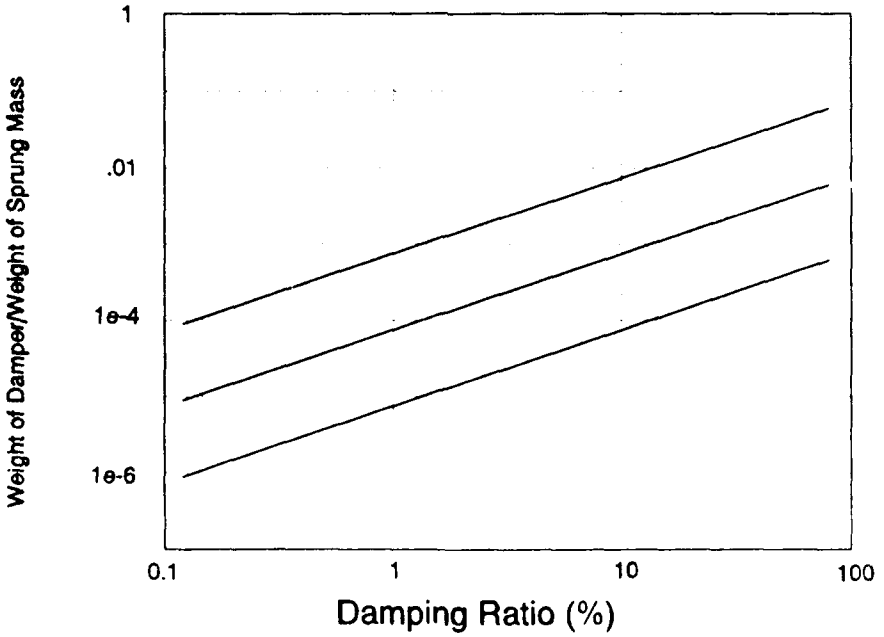

Another promising application of this technology is as the damping element for tuned passive vibration absorbers[3,4] or proof mass actuators. These devices are typically tuned to resonate at slightly below the first mode of the associated structure. They are appropriately sized to the structure to which they are attached, and their damping ratio is set to maximize vibrational power dissipation. Of course, in this case the device added to a structure includes energy storage (the spring and mass) as well as the damping element and, hence, the damping ratio is defined as $(1/4\pi)$ times the energy dissipated per cycle of the damper divided by the maximum strain energy of the damper itself.

The plot shows the ratio of the damping element weight to the weight of the sprung mass, as a function of the damping ratio for three different resonant frequencies. The plot indicates that the eddy current-based damping element is a very small portion of the overall weight of the device and, therefore, should be seriously considered for use as the damping element in these devices.

[3] J. R. Sesak, et al, "Passive Damping Augmentation for Flexible Structures," Lockheed, First NASA/DOD CSI Technology Conference, November 18–21, 1986, pp. 475–493.

[4] D.W. Miller and E. F. Crawley, "Theoretical and Experimental Evaluation of Space–Realizable Inertial Actuation for Passive and Active Structural Control," J. Guidance Control & Dynamics, Vol. 11, No. 5, Sept–Oct 1988, pp. 449–458.

How is SatCon pursuing this approach to vibration damping?

- Theoretical understanding and modelling
  - How and when is performance influenced by skin effect, end effects and nonlinearity?
  - Create models to predict performance
- Develop promising strawmen designs for specific applications
- Experimentally evaluate prototypes
- Consideration of alternative uses
  - Noise suppression (aircraft, spacecraft)
  - Precise positioning (optics)

SatCon is pursuing development of eddy current-based structural damping through a combined analytical and experimental program. The initial efforts have been aimed at developing analytical design tools which can be used to evaluate some promising strawmen designs. In addition, SatCon shall build and evaluate some prototypes for an eddy current-based damper.

SatCon believes that this approach to vibration damping offers benefits for a wide range of applications and should, therefore, be pursued aggressively.

THE ABSOLUTE VALUE MODAL STRAIN ENERGY METHOD

Daniel R. Morgenthaler *
Martin Marietta Astronautics Group
Denver, CO

ABSTRACT

The Modal Strain Energy (MSE) method has become a significant design tool in the last decade. The MSE method allows the approximate solution to a complex eigenvalue problem using the solution to a real eigenvalue problem and knowledge of element loss factors and the percentage of MSE contained in each element.

While the MSE method has been shown to be relatively accurate in many instances, particularly for design purposes, it can produce high errors even in simple cases with relatively low damping levels. This paper discusses a new MSE method which allows the approximate solution to complex eigenvalue problems while providing more accurate approximations.

The Absolute Value MSE (AVMSE) method incorporates the absolute value of the individual element impedances to form a real "stiffness" matrix. From the solution of the eigenvalue problem associated with the system mass matrix and this real "stiffness" matrix; approximate mode shapes, natural frequencies, and damping ratios may be obtained.

The new method provides greater accuracy than the standard MSE method in most instances, and more importantly provides conservative damping estimates while the standard method tend to overpredict damping ratios. The AVMSE provides more accurate results while remaining innexpensive to implement.

* Mail Stop H4330
P. O. Box 179
Denver, CO 80201
(303)-971-9387

Introduction

- **Damping Devices Can Be Modeled by Impedances**
  - **Viscoelastics**
  - **D-Struts**
  - **Passive Piezoceramic Members**

- **Impedance Is a Frequency-Dependent Complex Quantity**

$$Z(s) = Z_R(s) + i\,Z_I(s)$$

- **Rearranging the Impedance Results In a Frequency-Dependent "Complex Stiffness"**

$$\equiv K_d(s) \cdot (1 + i\,\eta_d(s))$$

- **Modes of Systems That Contain Damping Devices Are Complex**

Passive damping applied to structures for vibration control has become an accepted practice in the past decade. Passive damping devices are efficiently modeled by their mechanical impedance for incorporation into structures. Such devices include viscoelastic members, viscous damping members, piezoceramic passive devices, and many others.

Mechanical impedance is a frequency dependent complex quantity which describes the relationship between an applied force to a member and the resulting displacement.

By writing the impedance in the proper form, a frequency dependent complex stiffness results. This form of the impedance is typically used to model viscoelastic material, however, it can be used for other damping members. The modes of a system which incorporate damping devices with complex stiffnesses are generally complex.

Introduction (concl)

- MSE Method Is Well-Known for Approximate Solution of Damped Systems

$$(-M\omega^2 + K_R) \cdot \Phi = 0$$

$$\zeta_i = \frac{1}{2} \Phi_i^T \cdot K_I \cdot \Phi_i / \omega_i^2$$

- MSE Method Provides Insight into Damping Design Improvements
- MSE Method Can Sometimes Provide Inaccurate Results–It Tends To
  - Overpredict Damping Ratios
  - Underpredict Natural Frequencies
  - Overpredict Modal Motion across Damped Elements
- New Method That Improves Approximations Has Been Developed

The Modal Strain Energy Method is a well known method of approximating the solution of the complex eigenvalue problem using real eigenvalue problems.

In addition to the computational advantage of the MSE method as compared to the complex eigenvalue problem, it has the advantage that it provides insight in effective improvements in damping design for a particular system. However, the MSE method can sometimes provide inaccurate results. It tends to overpredict the damping ratios, underpredict natural frequencies, and overpredict the motion across damped elements.

This presentation discusses a new approximation method with improved accuracy which also has the computation advantages of the MSE method.

Typical Complex Impedance Element

- The Ratio of the Motion Across a Complex Spring to Applied Force Is the Absolute Value of the Impedance

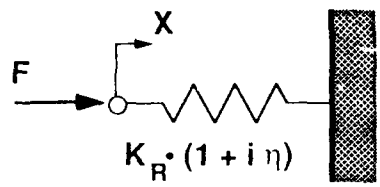

$$F e^{i\theta_F} = K e^{i \tan^{-1}(\eta)} \cdot X e^{i\theta_X}$$

$$\frac{|X|}{|F|} = K = K_R \cdot \sqrt{1+\eta^2}$$

For a typical complex impedance element, the complex spring constant describes the ratio of the displacement to applied force. The ratio of the magnitude of the displacement to the magnitude of the force is the absolute value of the impedance.

Single Degree-of-Freedom Complex System

- The Natural Frequency and Damping Ratio Are Found from the Location of the Pole

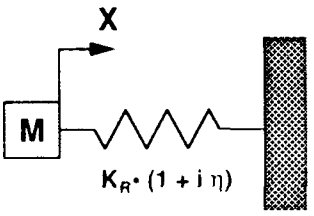

$$\lambda = \omega \cdot e^{i\left[\tan^{-1}\left(\frac{2\zeta}{\sqrt{1+\zeta^2}}\right) + \frac{\pi}{2}\right]}$$

$$\omega = \sqrt{\frac{\left|K_R \cdot (1 + i\eta)\right|}{M}}$$

$$\zeta = \sqrt{\frac{1 - \sqrt{\frac{1}{\eta^2 + 1}}}{2}}$$

For a single degree of freedom system with a complex spring, the natural frequency and damping ratio can be obtained from the location of the pole in the system transfer function. The eigenvalue can be written in terms of its magnitude and phase angle, which are a function of the natural frequency and viscous damping ratio.

Equating the pole location to the eigenvalue, we find that the natural frequency is the square root of the ratio of the absolute value of the impedance and the mass. The modal damping ratio is a function of the element loss factor.

The MSE Method

- **Assume the Real Modes Derived from the Real Part of the Stiffness Matrix Are Good Approximate Eigenvalues**

$$(-M\omega^2 + K_R)\cdot\Phi = 0$$

- **Compute the Rayleigh Quotient To Find the Eigenvalue**

$$\lambda_i^2 = \frac{\Phi_i^T\cdot(K_R + K_I)\cdot\Phi_i}{\Phi_i^T\cdot M\cdot\Phi}$$

- **Assume That the Real Part of the Rayleigh Quotient Is the Natural Frequency Squared**

$$|\lambda_i|^2 = \frac{\Phi_i^T\cdot K_R\cdot\Phi_i}{\Phi_i^T\cdot M\cdot\Phi_i} = \omega_i^2$$

- **Calculate the Damping Ratio Using the Approximation Formula**

$$\zeta_i = \frac{1}{2}\,\Phi_i^T\cdot K_I\cdot\Phi_i / \omega_i^2$$

In the well known MSE method, the real system modes which are derived from the mass matrix and the real part of the complex stiffness matrix are assumed to be accurate approximations to the complex system eigenvectors.The Rayleigh Quotient is then used to approximate the eigenvalues of the system.

As opposed to the absolute value of the Rayleigh Quotient, using the MSE method the natural frequency squared is assumed to be the real part of the Rayleigh Quotient. The damping ratio is then calculated using an approximation formula which is one half the ratio of the real and imaginary parts of the Rayleigh Quotient.

Note that the MSE method does not yield the correct result for the single degree of freedom system. It is relatively accurate, however, for small damping ratios.

The Absolute Value MSE Method

- **Assemble the Absolute Value Matrix**

$$\overline{K} = \sum_{j=1}^{NE} K_{R_j} \sqrt{1+\eta_j^2}$$

- **Find the Eigenvectors and Eigenvalues Associated with This Matrix and the Mass Matrix**

$$(-M\omega^2 + \overline{K}) \cdot \Phi = 0$$

- **Assume That These Vectors Are Approximate Eigenvectors**

- **Compute the Rayleigh Quotient To Find the Approximate Eigenvalue**

$$\lambda^2 \cong \frac{\Phi^T \cdot (K_R + iK_I) \cdot \Phi}{\Phi^T \cdot M \cdot \Phi}$$

- **Calculate the Modal Strain Energy in Each Element**

$$MSE_{ij} = \frac{\Phi_i^T \cdot K_{R_j} \sqrt{1+\eta^2} \cdot \Phi_i}{\omega_i^2}$$

A new energy method of has been developed for the approximation of the complex eigenvalue problem, which is termed the Absolute Value Modal Strain Energy (AVMSE) method. In the AVMSE method, a stiffness matrix is assembled with the absolute value of each elements impedance, which is consistent with the single degree of freedom system.

The eigenvectors and eigenvalues associated with the system mass matrix and this stiffness matrix are then computed. These eigenvectors are assumed to be a good approximation to the complex system eigenvectors. The Rayleigh Quotient is then used to determine the location of the eigenvalue.

By defining the modal strain energy in the elements of the system, in a manner similar to the standard MSE method, we can determine the eigenvalue location in terms of element real and complex energies. This provides the same insight for design development as the standard MSE method.

The Absolute Value MSE Method (concl)

- Calculate the Approximate Natural Frequency As the Absolute Value of the Rayleigh Quotient

$$\left|\lambda_j^2\right| = \left[\left(\omega_A^2 \cdot \sum_{j=1}^{NE} \frac{MSE_{ij}}{\sqrt{1+\eta_j^2}}\right) + \left(\omega_A^2 \cdot \sum_{j=1}^{NE} \frac{MSE_{ij} \cdot \eta_j}{\sqrt{1+\eta_j^2}}\right)\right] \cong \omega_A^2$$

- Use the Phase Angle of the Rayleigh Quotient To Calculate the Damping Ratio

$$\eta_j = \frac{\sum_{j=1}^{NE} \frac{MSE_{ij} \cdot \eta_j}{\sqrt{1+\eta_j^2}}}{\sum_{j=1}^{NE} \frac{MSE_{ij}}{\sqrt{1+\eta_j^2}}} \qquad \zeta_j = \sqrt{\frac{1-\sqrt{\frac{1}{\eta^2+1}}}{2}}$$

From the complex Rayleigh Quotient, the natural frequency is the square root of its absolute value. This can be shown to be approximately the eigenvalue which is computed from the real eigenvalue problem.

By defining the modal loss factor, the viscous damping ratio can be determined from the phase angle of the eigenvalue similar to the single degree of freedom system. The modal loss factor can be written in terms of the MSE in various elements and their loss factors.

A Simple Example Problem

- Simple 3-DOF System with One Complex Spring
- Vary the Spring Loss Factor
- Compute Modal Properties Using Various Methods
  - Complex Eigenproblem
  - MSE Method
  - Absolute Value MSE Method
- Compare Results

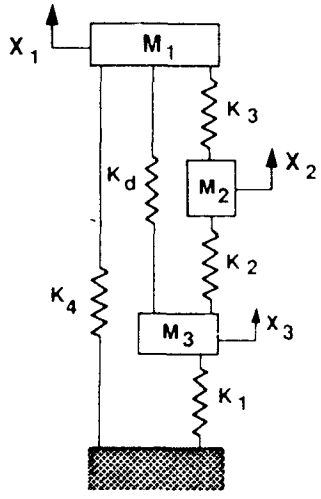

To demonstrate the behavior of the standard MSE method, the AVMSE method, and the complex eigenvalue problem, a simple system was used. This system consists of three masses interconnected by springs, one of which is complex.

For the example, the loss factor of the complex spring was varied and the modal properties were computed using the various methods, so that the results could be compared.

Fundamental Frequency vs Spring Loss Factor

- Absolute Value MSE Shows Frequency Increase with Spring Loss Factor

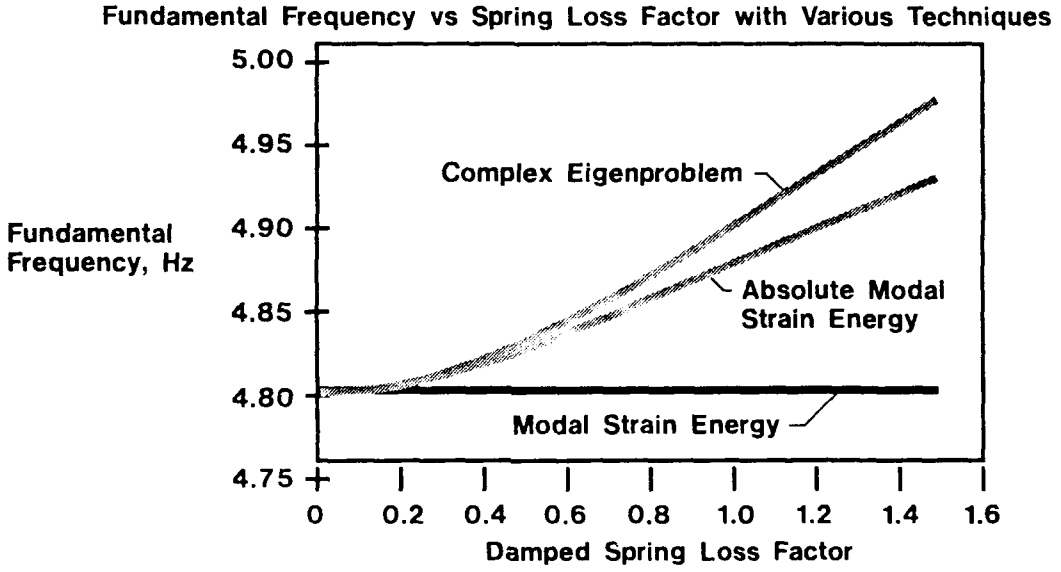

Plotted here is the variation in the system fundamental frequency with the damped element loss factor. The MSE solution, of course shows no variation in natural frequency with element loss factor. The complex eigenproblem shows a frequency increase as the loss factor of the element increases, implying "stiffer" behavior of the damped element. Similarly, the AVMSE method also shows an increase in the frequency with element loss factor, and is more accurate than the standard MSE method.

Fundamental Mode Damping vs Spring Loss Factor

- Absolute Value MSE More Accurate and Has Desirable Characteristics
  - Peak Damping at Specific Loss Factor Value
  - Conservative Damping Ratio Estimates

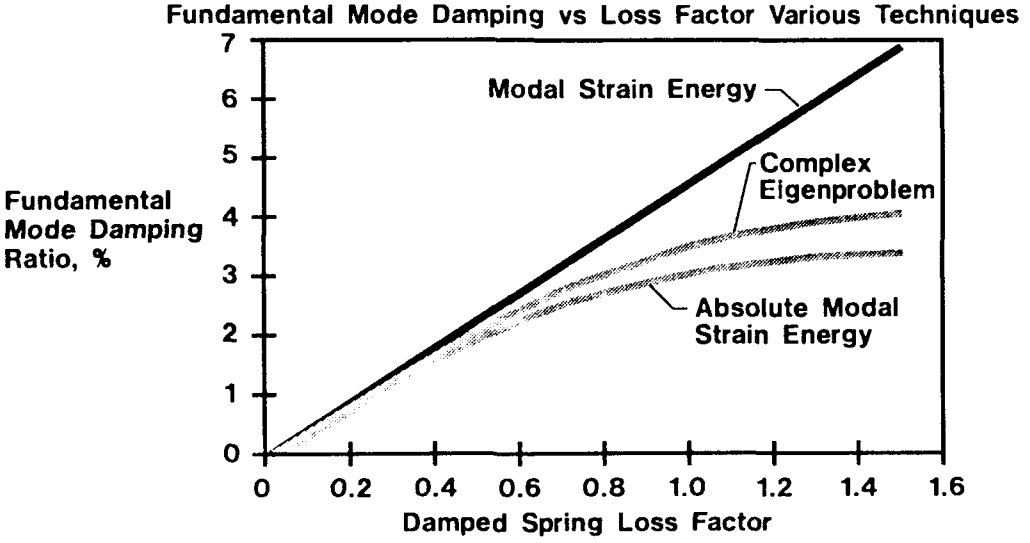

This plot shows the damping in the fundamental mode of the system as the loss factor is varied. The MSE solution predicts that the damping is linear in the element loss factor. The complex eigenvalue problem, however, shows that as the loss factor becomes large, the rate of damping increase becomes smaller. The complex eigenvalue problem also shows that if the loss factor is raised too high, the damping can actually decrease. The AVMSE solution duplicates this behavior, while providing a conservative estimate to the damping ratio. Notice that the problem was selected such that the damping ratio is low, on the order of 3%.

Frequency Response Using Various Methods

- Absolute Value MSE Provides More Accurate Frequency Response

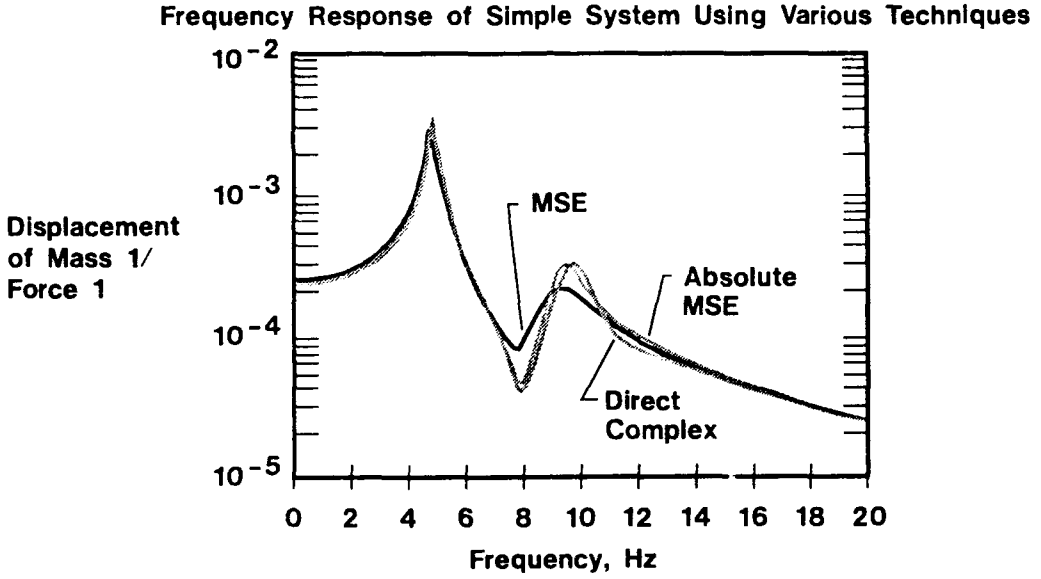

This plot compares the frequency response for displacement of the first mass for forces applied to the same mass computed using the various methods. Notice that the absolute value MSE method is more accurate for the first mode, and very much better for the two coupled modes at 9 and 11 Hz. The standard MSE method has much greater error in this frequency region.

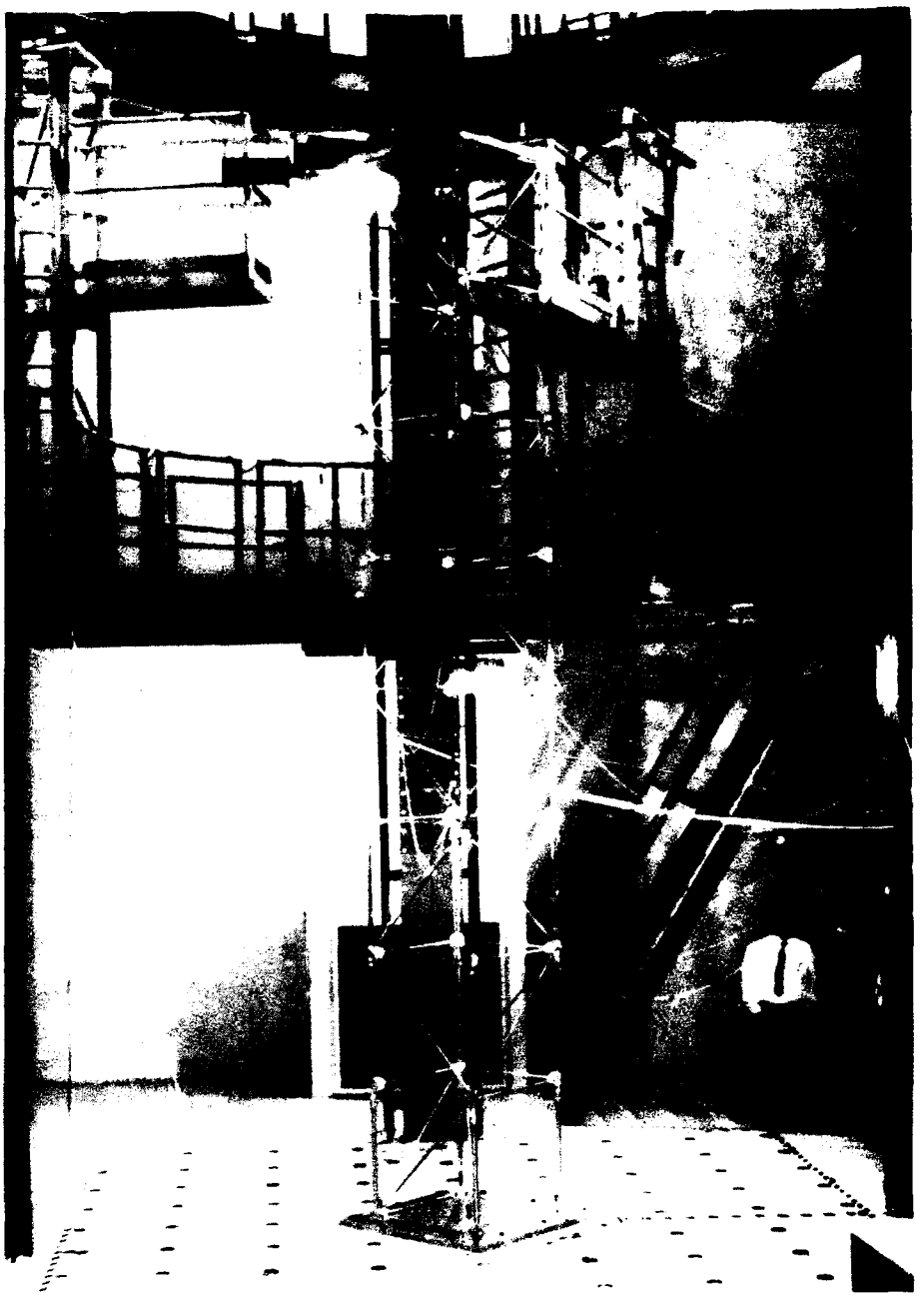

To show a comparison of the methods on a realistic problem, the PACOSS D-Strut truss was selected. This truss includes damping members which can be modeled with complex impedances. The exact solution can be generated by the solution of a viscous damping eigenvalue problem and compared with alternative solution methods.

Results of Application to D-Strut Truss Model

- Complex Modes with Complex Stiffness Matrix Provides Exact Results If Computed at Eigenvalue
- Absolute Value MSE Provides More Accurate Frequencies, Damping, and Mode Shapes than Standard MSE Method

Analysis Method	*Mode No.*	*Frequency, Hz*	*Damping Ratio*
Complex Network	1	5.493	14.93
	2	6.142	15.63
Complex Stiffness	1	5.493	14.93
	2	6.093	16.51
MSE	1	5.220	17.69
	2	5.720	18.85
Absolute MSE	1	5.457	14.10
	2	6.000	15.78

The viscous eigenvalue problem with struts modeled as networks was solved first. A complex stiffness eigenvalue problem was then solved with the strut complex stiffness computed at the first eigenvalue. Of course, the first mode of this solution agrees exactly with the viscous damping formulation. The second mode of the complex solution has some error, as the properties were not computed at this eigenvalue.

Even with the correct strut properties, the standard MSE method does not provide an accurate solution to this problem, as the first mode is predicted to have 17.7% damping while the solution is 14.9%, a relative error of 18.5%. Similarly the frequency is in error by almost 5%. The AVMSE method, however, is much more accurate. This method underpredicts the damping ratio by 5.5% relative error, and underpredicts the frequency by 0.6% relative error. This shows the much greater accuracy which can be achieved with the AVMSE method on difficult damping problems.

Conclusions

- New Method of Complex Stiffness Eigenproblem Approximation Developed
  - Uses Real Eigenproblem
  - Stiffness Matrix Is Assembled with Absolute Value of Impedance
- Absolute Value MSE Method Behaves As Complex Eigenproblem
  - Elements Appear "Stiffer" As Loss Factor Increases
  - Damping Decreases As Loss Factors Raised Too High
  - Can Model Systems with Dashpots As Only Connection between DOFs

A new method of determining approximate properties of damped structures has been developed and was presented. This method is based on a real eigenvalue problem which uses an assemblage of the absolute value of the element impedance matrices as the stiffness matrix.

The behavior of the new method is more consistent with the complex eigenvalue problem. Similar to the complex solution, elements appear stiffer as loss factors increase, and the natural frequency increases. The AVMSE method does not predict a linear relationship between element loss factors and system damping, similar to the complex eigenvalue problem.

Additionally, the new method can model systems with dashpots as the sole connection between degrees of freedom. As a dashpot has an infinite loss factor and no real part to its stiffness, the standard MSE method would not place a stiffness term in the MSE stiffness matrix. The new method places a term equal to the natural frequency multiplied by the dashpot coefficient in the stiffness matrix, and allows the approximate solution to this problem.

Conclusions (concl)

- **Absolute Value MSE Method Provides More Accurate Results for Examples**
  - **Single-DOF System**
  - **Three-DOF Example Problem**
  - **D-Strut Truss**
- **Absolute Value MSE Method Is As Easy To Implement As Standard MSE Method**
- **New Method Should Be Used for Accurate Damping Design Approximations**
  - **More Accurate**
  - **Same Expense As MSE**

The AVMSE method provides more accurate results for example problems, including a single degree of freedom system, the three degree of freedom example system, and the D-Strut truss.

The AVMSE method is as easy and inexpensive to implement as the standard MSE method, as element stiffnesses need only be raised by a factor dependent on their loss factors. Damping is readily determined from the MSE distribution.

Based on these results and conclusions, the new method AVMSE method should be used for damping design and system analysis, as it provides more accurate solutions at the same expense as the MSE method. Errors due to the AVMSE approximation tend to be conservative.

AN ANALYTICAL MODEL FOR THE VIBRATION OF VISCOELASTICALLY DAMPED CURVED SANDWICH BEAMS

Mohan D. Rao* and Shulin He**
ME-EM Department
Michigan Technological University
Houghton, MI 49931
(906) 487-2551

This paper describes an analytical model for the coupled flexural and longitudinal vibration of a curved sandwich beam system. The system consists of a pair of parallel and identical composite sandwich beams with a viscoelastic damping material forming the core. The ends of the beams may have any physically realizable boundary conditions, but, in this case are assumed to be simply-supported. The governing equations of motion for the forced vibration of the system are derived using the energy method and Hamilton's principle. Both shear and thickness deformation in the adhesive layer is included in the analysis. The solution of the governing equations for the system resonance frequencies and loss factors are obtained in closed form using the Rayleigh-Ritz method. A parametric study has been conducted to evaluate the effects of curvature, core-thickness and adhesive shear modulus on the system natural frequencies and loss factors. The implications of this parametric study on the damping effectiveness of the system along with some design guidelines are included in the paper.

* Assistant Professor
** Graduate Student

I. INTRODUCTION

The use of viscoelastic material as a core material in constrained layer and sandwich layer arrangement is an effective way of damping vibration and noise in structures subjected to dynamic loading. Many structural components such as the wing of an aircraft, body panel of an automobile are curved in shape. In the analysis and design of passive damping treatments of such panels, it has been customary to use straight beam theory approximations, because of lack of better analysis methods that are simple and accurate. The objective of this research effort is to develop simple yet accurate analysis and design procedures for passive vibration control of curved sandwich panels.

Considerable research work has been done on the vibration of straight sandwich beams. The classic work in this area is reported by Ross, Ungar and Kerwin [1], and Kerwin [2]. They have derived an expression for an effective complex flexural stiffness for the system consisting of a damping layer sandwich between two face-plates. Mead and Markus [3] have studied the forced vibration of a sandwich beam with arbitrary boundary conditions. They have derived the sixth-order differential equation of motion for the flexural vibration and obtained solutions. Rao [4] has studied the frequency and loss factors of sandwich beams under various boundary conditions using the energy approach. Miles and Reinhall [5] have described an analytical model for the vibration of laminated beams including the effects of both shear and thickness deformation in the adhesive layer. Some work has been done on the vibration of curved sandwich beams. Petyt and Fleischer [6] have investigated the free vibration of a curved homogeneous beam. Ahmed [7] has studied the free vibration of curved sandwich beams by the finite element method. Vaswani, Asnavi and Nakra [8] have derived a closed-form solution for the system loss factors and resonance frequencies for a curved sandwich beams with a

viscoelastic core by the Ritz method. But the thickness of the adhesive core was not considered in their analysis. Furthermore their analysis does not include the longitudinal inertia effects.

In this papper, the authors have used the energy method and Hamilton's principle to derive the governing equation of motion for the coupled flexural and longitudinal vibation of a curved snadwich beam system. Both shear and thickness deformations of the adhesive core are included. The longitudinal kinetic energy of the beam system is also considered. A closed-form solution of the system modal loss facotrs, resonance frequencies and mode shapes is derived for a system having simply supported ends by the Ritz method. The effects of curvature, core-thckness and adhesive shear modulus on the system natural frequencies and loss factors are also studied.

II. THEORY

Fig. 1 shows the curved sandwich beam system chosen for study. Both the upper and lower beams are constrained in the radial (transverse) direction at the two ends, and the upper beam is free to deform in the circumferential (longitudinal) direction. The governing equations of motion for the coupled flexural and longitudinal vibration under radial distribution load are derived by Hamilton's Princple. The following basic assumptions are made in the analysis.

1. Both upper and lower beams are elastic and isotropic. The adhesive core is viscoelastic whose elastic and shear moduli are modeled using the complex modulus approach.
2. Both beams and the adhesive core are assumed to be under plane stress state. The shear strain in the adhesive is proportional to $\left(\frac{R_c}{R_c + z_c}\right)$, where $-h_c/2 \le z_c \le h_c/2$, h_c being the adhesive thickness and R_c the radius of curvature of the middle surface of the adhesive layer. But

the radial deformation of the adhesive is assumed to be constant through its thickness.

3. The transverse shear strains in both beams and the longitudinal deformation of the adhesive are neglected. Furthermore, rotational kinetic energies of both beams are also neglected.

Let the transverse and longitudinal displacements of a fiber in the middle surface of the upper beam be w_1 and u_1 respectively. The same variables with subscript 2 refer to those of the lower beam. The radial and circumferential displacements of the fiber at any point $p(\theta,z_1)$ in the upper beam are given by

$$w_p = w_1 , \qquad u_p = \frac{R_1+z_1}{R_1} u_1 - \frac{z_1}{R_1}\frac{\partial w_1}{\partial \theta} , \quad -h_1/2 \le z_1 \le h_1/2 \tag{1}$$

respectively. The strain in the fiber is given by

$$\varepsilon_{1,\theta} = \frac{1}{R_1+z_1}\left(\frac{\partial u_p}{\partial \theta} + w_p\right)$$

or

$$\varepsilon_{1,\theta} = \frac{1}{R_1} u_1' + \frac{1}{(R_1+z_1)}\left(w_1 - \frac{z_1}{R_1} w_1''\right) \tag{2}$$

where $u_1' = \frac{\partial u_1}{\partial \theta}$ and $w_1'' = \frac{\partial^2 w_1}{\partial \theta^2}$.

Strain energy of the upper beam is $U_1 = \frac{1}{2}\int_{v_1} E_1 \varepsilon_{1,\theta}^2 dv_1$. As $dv_1 = (R_1+z_1)dz_1 d\theta$, for unit width, we have

$$U_1 = \frac{E_1}{2}\int_0^{\phi}\frac{h_1}{R_1}\left[\left(u_1'+w_1\right)^2 + \left(\frac{h_1^2}{12R_1^2}\right)\left(w_1+w_1''\right)^2\right]d\theta \tag{3}$$

where E_1, R_1 and h_1 are the elastic moduli, radius of curvature of the middle surface and thickness of the upper beam respectively. z_1 is the radial coordinate from the middle surface.

Kinetic energy of the upper beam is approximated as

$$T_1 = \frac{\rho_1 h_1 R_1}{2}\int_0^{\phi}\left(\dot{u}_1^2 + \dot{w}_1^2\right)d\theta \tag{4}$$

where ρ_1 is the density of the upper beam material and $\dot{u}_1 = \frac{\partial u_1}{\partial t}$, $\dot{w}_1 = \frac{\partial w_1}{\partial t}$.

Similarly, kinetic energy T_2 and strain energy U_2 of lower beam are given by

$$T_2 = \frac{\rho_2 h_2 R_2}{2}\int_0^{\phi}\left(\dot{u}_2^2 + \dot{w}_2^2\right)d\theta \tag{5}$$

$$U_2 = \frac{E_2}{2}\int_0^{\phi}\frac{h_2}{R_2}\left[\left(u_2' + w_2\right)^2 + \left(\frac{h_2^2}{12R_2^2}\right)\left(w_2 + w_2''\right)^2\right]d\theta \tag{6}$$

where E_2, R_2, h_2 and ρ_2 are the young's moduli, radius of curvature of the middle surface, thickness and density of the lower beam respectively. Also, $u_2' = \frac{\partial u_2}{\partial \theta}$, $w_2'' = \frac{\partial^2 w_2}{\partial \theta^2}$, $\dot{u}_2 = \frac{\partial u_2}{\partial t}$ and $\dot{w}_2 = \frac{\partial w_2}{\partial t}$.

The shear strain in the middle fiber of the adhesive core is approximated as

$$\gamma_{mid} = \frac{u_B - u_A}{h_c} + \frac{1}{2}\left[\frac{1}{R_1}\frac{\partial w_1}{\partial \theta} + \frac{1}{R_2}\frac{\partial w_2}{\partial \theta}\right]$$

or
$$\gamma_{mid} = \frac{1}{h_c}\left[\left(a_2 u_2 - a_1 u_1\right) + \frac{h_1 + h_c}{2}\frac{w_1'}{R_1} + \frac{h_2 + h_c}{2}\frac{w_2'}{R_2}\right] \tag{7}$$

where $a_1 = 1 + h_1/(2R_1)$ and $a_2 = 1 - h_2/(2R_2)$.

Then the shear strain of the adhesive core is

$$\gamma_c = \frac{R_c}{R_c + z_c}\frac{1}{h_c}\left[\left(a_2 u_2 - a_1 u_1\right) + \frac{h_1 + h_c}{2}\frac{w_1'}{R_1} + \frac{h_2 + h_c}{2}\frac{w_2'}{R_2}\right],\ -h_c/2 \le z_c \le h_c/2 \tag{8}$$

The radial strain of the adhesive core is $\varepsilon_{c,z} = \frac{w_2 - w_1}{h_c}$.

Strain energy of the adhesive core is $U_c = \frac{1}{2}\int_{v_c}\left[G_c^{*}\gamma_c^2 + kE_c^{*}\varepsilon_{c,z}^2\right]dv_c$, i.e.

$$U_c = \int_0^{\phi}\left\{\frac{G_c^{*}R_c}{2h_c}\left(1 + \frac{h_c^2}{12R_c^2}\right)\left[\left(a_2 u_2 - a_1 u_1\right) + \left(\frac{h_1 + h_c}{2}\right)\frac{w_1'}{R_1} + \left(\frac{h_2 + h_c}{2}\right)\frac{w_2'}{R_2}\right]^2 + \frac{kE_c^{*}R_c}{2h_c}\left(w_2 - w_1\right)^2\right\}d\theta \tag{9}$$

where $k = \frac{1}{(1-\nu)(1+\nu)}$. ν is Poisson's ratio. E_c^{*} and G_c^{*} are the complex elastic and shear moduli of the adhesive layer which are applicable only under harmonic vibration. $E_c^{*} = E_c'(1+\eta_{c1})$ and $G_c^{*} = G_c'(1+\eta_{c2})$, where E_c' and G_c' are the storage moduli, and η_{c1} and η_{c2} are the loss factors corresponding to extensional and shear deformation of the viscoelastic material. Values of E_c^{*}

and G_c^* corresponding to a frequnecy and temperature can be obtained from material data sheets supplied by the manufacturers in the form of a nomogram.

Kinetic energy of the adhesive layer is approximated as

$$T_c = \frac{1}{8}\rho_c \int_{v_c} \left[(\dot{u}_A+\dot{u}_B)^2 + (\dot{w}_A+\dot{w}_B)^2\right] dv_c, \quad \text{or}$$

$$T_c = \frac{\rho_c h_c R_c}{8} \int_0^{\phi} \left\{ \left[a_1\dot{u}_1 + a_2\dot{u}_2 + \frac{1}{2}\left(\frac{h_2}{R_2}\dot{w}_2' - \frac{h_1}{R_1}\dot{w}_1'\right)\right]^2 + (\dot{w}_1+\dot{w}_2)^2 \right\} d\theta \qquad (10)$$

where ρ_c is the density of adhesive and $\dot{w}_i' = \frac{\partial^2 w_i}{\partial t \partial \theta}$, $i = 1, 2$.

Work done by external forces is

$$W = \int_0^{\phi} w_1 q_1 (R_1 - h_1/2) d\theta \qquad (11)$$

Let $\int_0^{\phi} f d\theta = T_1+T_2+T_c-U_1-U_2-U_c+W$. Hamilton's Principle $\delta\int_{t_1}^{t_2}(T-V+W)dt = 0$ gives

$$\int_{t_1}^{t_2} \left\{ \int_0^{\phi} \delta f(u_1, u_2, u_1', u_2', \dot{u}_1, \dot{u}_2, w_1, w_2, w_1', w_2', w_1'', w_2'', \dot{w}_1', \dot{w}_2', \dot{w}_1, \dot{w}_2) d\theta \right\} dt = 0 \qquad (12)$$

From the principle of calculus of variations, we get the following governing equations of motion of the system.

$$\frac{E_1 h_1}{R_1}\left(\frac{\partial^2 u_1}{\partial\theta^2} + \frac{\partial w_1}{\partial\theta}\right) + \frac{a_1 G_c^* R_c}{h_c}\left(1+\frac{h_c^2}{12R_c^2}\right)\left[(a_2u_2 - a_1u_1) + \frac{\partial}{\partial\theta}\left(\frac{h_1+h_c}{2R_1}w_1 + \frac{h_2+h_c}{2R_2}w_2\right)\right]$$

$$- \rho_1 h_1 R_1 \frac{\partial^2 u_1}{\partial t^2} - \frac{a_1\rho_c h_c R_c}{4}\left[\frac{\partial^2}{\partial t^2}(a_1u_1 + a_2u_2) + \frac{1}{2}\frac{\partial^3}{\partial t^2\partial\theta}\left(\frac{h_2}{R_2}w_2 - \frac{h_1}{R_1}w_1\right)\right] = 0 \qquad (13)$$

$$\frac{E_2 h_2}{R_2}\left(\frac{\partial^2 u_2}{\partial\theta^2} + \frac{\partial w_2}{\partial\theta}\right) - \frac{a_2 G_c^* R_c}{h_c}\left(1+\frac{h_c^2}{12R_c^2}\right)\left[(a_2u_2 - a_1u_1) + \frac{\partial}{\partial\theta}\left(\frac{h_1+h_c}{2R_1}w_1 + \frac{h_2+h_c}{2R_2}w_2\right)\right]$$

$$- \rho_2 h_2 R_2 \frac{\partial^2 u_2}{\partial t^2} - \frac{a_2\rho_c h_c R_c}{4}\left[\frac{\partial^2}{\partial t^2}(a_1u_1 + a_2u_2) + \frac{1}{2}\frac{\partial^3}{\partial t^2\partial\theta}\left(\frac{h_2}{R_2}w_2 - \frac{h_1}{R_1}w_1\right)\right] = 0 \qquad (14)$$

$$\frac{E_1 h_1^3}{12R_1^3}\left(\frac{\partial^4 w_1}{\partial\theta^4} + 2\frac{\partial^2 w_1}{\partial\theta^2} + w_1\right) + \frac{E_1 h_1}{R_1}\left(\frac{\partial u_1}{\partial\theta} + w_1\right) - \frac{kE_c^* R_c}{h_c}(w_2 - w_1)$$

$$- \frac{G^{*}_{c} R_{c}}{h_{c}}\left(1+\frac{h_{c}^{2}}{12R_{c}^{2}}\right)\left[\frac{\partial}{\partial\theta}(a_{2}u_{2}-a_{1}u_{1})+\frac{\partial^{2}}{\partial\theta^{2}}\left(\frac{h_{1}+h_{c}}{2R_{1}}w_{1}+\frac{h_{2}+h_{c}}{2R_{2}}w_{2}\right)\right]\left(\frac{h_{1}+h_{c}}{2R_{1}}\right) + \rho_{1}h_{1}R_{1}\frac{\partial^{2}w_{1}}{\partial t^{2}}$$

$$+ \frac{\rho_{c}h_{c}R_{c}}{4}\left\{\frac{\partial^{2}}{\partial t^{2}}(w_{1}+w_{2}) + \frac{h_{1}}{2R_{2}}\frac{\partial^{3}}{\partial t^{2}\partial\theta}\left[a_{1}u_{1}+a_{2}u_{2}+\frac{1}{2}\left(\frac{h_{2}}{R_{2}}w_{2}-\frac{h_{1}}{R_{1}}w_{1}\right)\right]\right\} = \left(R_{1}-\frac{h_{1}}{2}\right)q_{1} \qquad (15)$$

$$\frac{E_{2}h_{2}^{3}}{12R_{2}^{3}}\left(\frac{\partial^{4}w_{2}}{\partial\theta^{4}}+2\frac{\partial^{2}w_{2}}{\partial\theta^{2}}+w_{2}\right) + \frac{E_{2}h_{2}}{R_{2}}\left(\frac{\partial u_{2}}{\partial\theta}+w_{2}\right) + \frac{kE^{*}_{c}R_{c}}{h_{c}}(w_{2}-w_{1})$$

$$- \frac{G^{*}_{c} R_{c}}{h_{c}}\left(1+\frac{h_{c}^{2}}{12R_{c}^{2}}\right)\left[\frac{\partial}{\partial\theta}(a_{2}u_{2}-a_{1}u_{1})+\frac{\partial^{2}}{\partial\theta^{2}}\left(\frac{h_{1}+h_{c}}{2R_{1}}w_{1}+\frac{h_{2}+h_{c}}{2R_{2}}w_{2}\right)\right]\left(\frac{h_{2}+h_{c}}{2R_{2}}\right) + \rho_{2}h_{2}R_{2}\frac{\partial^{2}w_{2}}{\partial t^{2}}$$

$$+ \frac{\rho_{c}h_{c}R_{c}}{4}\left\{\frac{\partial^{2}}{\partial t^{2}}(w_{1}+w_{2}) - \frac{h_{2}}{2R_{2}}\frac{\partial^{3}}{\partial t^{2}\partial\theta}\left[a_{1}u_{1}+a_{2}u_{2}+\frac{1}{2}\left(\frac{h_{2}}{R_{2}}w_{2}-\frac{h_{1}}{R_{1}}w_{1}\right)\right]\right\} = 0 \qquad (16)$$

The natural boundary conditions are given by

$$\left[\frac{\partial f}{\partial u'_{1}}\delta u_{1} + \frac{\partial f}{\partial u'_{2}}\delta u_{2}+\left(\frac{\partial f}{\partial w'_{1}} - \frac{\partial}{\partial\theta}\frac{\partial f}{\partial w''_{1}} - \frac{\partial}{\partial t}\frac{\partial f}{\partial \dot{w}'_{1}}\right)\delta w_{1} + \left(\frac{\partial f}{\partial w'_{2}} - \frac{\partial}{\partial\theta}\frac{\partial f}{\partial w''_{2}} - \frac{\partial}{\partial t}\frac{\partial f}{\partial \dot{w}'_{2}}\right)\delta w_{2}\right.$$

$$\left. + \frac{\partial f}{\partial w''_{1}}\delta w'_{1} + \frac{\partial f}{\partial w''_{2}}\delta w'_{2}\right]\Bigg|_{0}^{\phi} = 0 \qquad (17)$$

We will first consider the free vibration of the system and solve the above four equations to find the system loss factors, resoance frequencies and mode shapes. By using the forced and natural boundary conditions, it is possible to set up the frequency equation which is a matrix equation with complex elements. Using a numerical search technique, we can find the system resonance frequencies, loss factors, etc. The disadvantage of this method, however, is that the natural frequencies and loss factors are not obtained in closed form as it requires a numerical searching technique to obtain the results. Since we are interested in finding only the first several modes of vibration of the system, other approximate methods that are fairly accurate would yield closed form solution. One such method is the the Rayleigh-Ritz method in which the mode shapes are first assumed to set up the eigenvalue problem. The details of the application of Rayleigh-Ritz method to the present problem are presented in the following sections.

III. NUMERICAL RESULTS

To find the system resonance frequencies ω_r and the modal loss factors η corresponding to ω_r, we consider the free vibration of the system and assume $w_1(\theta,t)=W_1(\theta)e^{i\omega t}$, $u_1(\theta,t)=U_1(\theta)e^{i\omega t}$, $w_2(\theta,t)=W_2(\theta)e^{i\omega t}$ and $u_2(\theta,t)=U_2(\theta)e^{i\omega t}$, where $\omega = \omega_r(1 + i\,\eta)$. From the variational integral $\delta\int_{t_1}^{t_2}(T-V)dt = 0$, we get

$$\int_0^{\phi}\Bigg\{\bar{\omega}^2\Bigg[(U_1\delta U_1+W_1\delta W_1)+\bar{\rho}_2\bar{h}_2\bar{R}_2(U_2\delta U_2+W_2\delta W_2)+\frac{\bar{\rho}_c\bar{h}_c\bar{R}_c}{4}\Big[(a_1U_1+a_2U_2+\frac{h_2}{2R_2}W'_2-\frac{h_1}{2R_1}W'_1)(a_1\delta U_1$$

$$+a_2\delta U_2+\frac{h_2}{2R_2}\delta W'_2-\frac{h_1}{2R_1}\delta W'_1)+(W_1+W_2)(\delta W_1+\delta W_2)\Big]\Bigg] + \Bigg[(U'_1+W_1)(\delta U'_1+\delta W_1)+\frac{h_1^2}{12R_1^2}(W_1$$

$$+W''_1)(\delta W_1+\delta W''_1)+\frac{\bar{E}_2\bar{h}_2}{\bar{R}_2}\Big[(U'_2+W_2)(\delta U'_2+\delta W_2)+\frac{h_2^2}{12R_2^2}(W_2+W''_2)(\delta W_2+\delta W''_2)\Big]+\frac{k\bar{E}_c R_1 R_c}{2h_1h_c}\delta\Big(W_2$$

$$-W_1\Big)^2+\frac{\bar{G}_c R_1 R_c}{h_1h_c}\Big(1+\frac{h_c^2}{12R_c^2}\Big)\Big[a_2U_2-a_1U_1+\frac{h_1+h_2}{2R_1}W'_1+\frac{h_2+h_c}{2R_2}W'_2\Big]\Big[a_2\delta U_2-a_1\delta U_1$$

$$+\frac{h_1+h_c}{2R_1}\delta W'_1+\frac{h_2+h_c}{2R_2}\delta W'_2\Big]\Bigg]\Bigg\}\,d\theta = 0 \qquad (18)$$

where $\bar{h}_2 = \frac{h_2}{h_1}$, $\bar{\rho}_2 = \frac{\rho_2}{\rho_1}$, $\bar{R}_2 = \frac{R_2}{R_1}$, $\bar{h}_c = \frac{h_c}{h_1}$, $\bar{\rho}_c = \frac{\rho_c}{\rho_1}$, $\bar{R}_c = \frac{R_c}{R_1}$, $\bar{E}_2 = \frac{E_2}{E_1}$, $\bar{E}_c = \frac{E_c^*}{E_1}$, $\bar{G}_c = \frac{G_c^*}{E_1}$, $\bar{\omega} = \frac{\omega}{\omega_o}$ and $\omega_o = (\sqrt{E_1/\rho_1})/R_1$.

To define to mode shape of the curved sandwich beam system, it is assumed that both the lower and upper beams are simply supported in the transverse direction but the upper beam is free to move in longitudinal direction. The forced boundary conditions will then be $W_1(0) = W_2(0) = 0$, $U_2(0) = 0$, $W_1(\phi) = W_2(\phi) = 0$. Also the mode shape functions of the curved beams are approximated with the mode shape functions of straight Euler-Bernoulli beams. Then the mode shape functions can be chosen as

$$W_1(\theta) = \sum_{r=1}^{N} C_r \sin\left(\frac{r\pi\theta}{\phi}\right) \tag{19}$$

$$U_1(\theta) = \sum_{r=1}^{N} C_r \cos\left(\frac{r\pi\theta}{\phi}\right) \tag{20}$$

$$W_2(\theta) = \sum_{r=1}^{N} C_r \sin\left(\frac{r\pi\theta}{\phi}\right) \tag{21}$$

$$U_2(\theta) = \sum_{r=1}^{N} C_r \sin\left[\left(r - \frac{1}{2}\right)\frac{r\pi\theta}{\phi}\right] \tag{22}$$

which satisfy all the forced (essential) boundary conditions. The coefficient C_r for the shape functions are chosen to be the same for all four functions so that the resulting eigenvalue problem would yield the required N resonance frequencies and N loss factors of the system. Substituting the expressions of W_1, U_1, W_2 and U_2 into equation (18), we get,

$$\sum_{j=1}^{N}\left\{\frac{1}{2}\left\{\left(\frac{j\pi}{\phi}-1\right)^2+\frac{h_1^2}{12R_1^2}\left[1-\left(\frac{j\pi}{\phi}\right)^2\right]^2+\frac{\bar{E}_2\bar{h}_2}{\bar{R}_2}\left[\left(\frac{j\pi}{\phi}\right)^2\left(\left(j-\frac{1}{2}\right)^2+1\right)+\frac{h_2^2}{12R_2^2}\left(1-\left(\frac{j\pi}{\phi}\right)^2\right)^2\right]\right.\right.$$

$$\left.\left.+\frac{\bar{G}_c R_1 R_c}{h_1 h_c}\left(1+\frac{h_c^2}{12R_c^2}\right)\left[a_1^2+a_2^2-\frac{a_1 j\pi}{\phi}\left(\frac{h_1+h_c}{R_1}+\frac{h_2+h_c}{R_2}\right)+\frac{1}{4}\left(\frac{j\pi}{\phi}\right)^2\left(\frac{h_1+h_c}{R_1}+\frac{h_2+h_c}{R_2}\right)^2\right]\right\}C_j$$

$$+\sum_{i=1}^{N}\left\{\frac{\bar{E}_2\bar{h}_2}{\phi\bar{R}_2}\left[\frac{i\left(j-\frac{1}{2}\right)}{i^2-\left(j-\frac{1}{2}\right)^2}+\frac{j\left(i-\frac{1}{2}\right)}{j^2-\left(i-\frac{1}{2}\right)^2}\right]+\frac{\bar{G}_c R_1 R_c}{h_1 h_c}\left(1+\frac{h_c^2}{12R_c^2}\right)\left[\frac{a_2}{2\phi}\left(\frac{h_1+h_c}{R_1}+\frac{h_2+h_c}{R_2}\right)\left(\frac{i\left(j-\frac{1}{2}\right)}{\left(j-\frac{1}{2}\right)^2-i^2}\right.\right.\right.$$

$$\left.\left.\left.+\frac{i\left(i-\frac{1}{2}\right)}{\left(i-\frac{1}{2}\right)^2-j^2}\right)-\frac{a_1 a_2}{\pi}\left(\frac{\left(j-\frac{1}{2}\right)}{\left(j-\frac{1}{2}\right)^2-i^2}+\frac{\left(i-\frac{1}{2}\right)}{\left(i-\frac{1}{2}\right)^2-j^2}\right)\right]\right\}C_i\Bigg\}\,\delta C_j+\bar{\omega}^2\sum_{j=1}^{N}\left\{\left\{(1+\bar{\rho}_2\bar{h}_2\bar{R}_2)\right.\right.$$

$$\left.\left.+\frac{\bar{\rho}_c\bar{h}_c\bar{R}_c}{8}\left[(a_1^2+a_2^2)+\frac{a_1\pi j}{\phi}\left(\frac{h_2}{\bar{R}_2}-\frac{h_1}{\bar{R}_1}\right)+\frac{1}{4}\left(\frac{j\pi}{\phi}\right)^2\left(\frac{h_2}{\bar{R}_2}-\frac{h_1}{\bar{R}_1}\right)^2+4\right]\right\}C_j+\sum_{i=1}^{N}\frac{\bar{\rho}_c\bar{h}_c\bar{R}_c}{8}\left\{\frac{2a_1a_2}{\pi}\left[\frac{\left(i-\frac{1}{2}\right)}{\left(i-\frac{1}{2}\right)^2-j^2}\right.\right.$$

$$\left.\left.\left.+\frac{\left(j-\frac{1}{2}\right)}{\left(j-\frac{1}{2}\right)^2-i^2}\right]+\frac{a_2}{\phi}\left(\frac{h_2}{\bar{R}_2}-\frac{h_1}{\bar{R}_1}\right)\left[\frac{i\left(j-\frac{1}{2}\right)}{\left(j-\frac{1}{2}\right)^2-i^2}+\frac{j\left(i-\frac{1}{2}\right)}{\left(i-\frac{1}{2}\right)^2-j^2}\right]\right\}C_i\right\}\delta C_j = 0 \tag{23}$$

Writing the above equation in matrix form, we have

$$[K_{ij}]\{C\} = \lambda\,[M_{ij}]\{C\} \tag{24}$$

where $[K_{ij}]$ and $[M_{ij}]$ are N × N matrices, called stiffness and inertia matrix respectively. $\lambda = \omega^2 = \omega_r^2(1+i\eta)$ and $\{C\} = [C_1\ C_2\ \cdots\ C_N]^T$. Here ω_r is the system resonance frequency and η is the modal loss factor corresponding to ω_r. A computer program has been written to solve this eigenvalue problem. Numerical results were generated to observe the effects of curvture, core-thickness and adhesive shear modulus on the system resonance frequencies ω_r and modal loss factors η for the first four modes.

The adhesive shear modulus plays a very important role on the damping of the sandwich system. The variations of the normalized resonance frequency $\bar{\omega}_r$ $(= \frac{\omega_r}{\omega_0})$ and modal loss factor η with respect to the normalized shear modulus G_{c1} (= real part of $\bar{G}_c$) are plotted in Figures 2 and 3 for the first four modes. The input data used here were $\eta_c = \eta_{c1} = \eta_{c2} = 0.1$, $h_1 = h_2 = 4$ mm, $\phi = 1.0$, $h_c = 2$ mm and $R_c = 1.2$ m. It can be observed from Figure 2 and Figure 3 that when $G_{c1} < 10^{-5}$ (soft adhesive material), the system resonance frequencies $\bar{\omega}_r$ increase very slowly (or almost constant) with G_{c1}, but the system loss factors η vary almost linearly with G_{c1}. For values of G_{c1} such that $10^{-5} < G_{c1} < 10^{-3}$, both $\bar{\omega}_r$ and η increase rapidly with G_{c1}, which means we can increase the system damping capacity without sacrificing the stiffness of system. Usually this is what the designers require in the design of constrained layer damping treatment for the system. When $G_{c1} > 10^{-3}$ (hard adhesive material), the system loss factors η remain almost constant with G_{c1}, but the resonance frequencies $\bar{\omega}_r$ increase linearly with G_{c1}.

The effects of the adhesive thickness h_c on the system resonance frequencies and loss factors are also studied. The input data in this case were $G_{c1} = 10^{-4}$, $\eta_{c2} = 0.1$, $h_1 = h_2 = 4$ mm, $R_1 = 1.2$ m and $\phi = 1.0$. The thickness h_c was increased from 0.5 mm to 6 mm in steps of 0.5 mm. The variations of $\bar{\omega}_r$ and η with h_c are plotted in Figures 4 and 5. It can be seen

from these two figures that both $\bar{\omega}_r$ and η decrease with h_c. The decrease of $\bar{\omega}_r$ with h_c is obvious as the system stifness will decrease when h_c is increased. Furthermore, from section II, we know that the shear strain of the adhesive layer is mainly contributed by the term $(u_2 - u_1)/h_c)$. Hence, increasing h_c will reduce the shear deformation of the adhesive layer and thus decrease the energy dissipation capacity of the sandwich system. This concludes that an increase in adhesive thickness does not always increase the system loss factor. It is therefore the combination of G_{c1} and h_c that needs to be optimized to maximize the system damping capacity.

The third parameter which affect the system resonance frequencies and modal loss factors is the the radius of curvature R_c of the middle surface of the adhesive layer. There are two ways of changing R_c as discussed below.

In the first case, the angle ϕ is kept constant, while changing R_c. This means the total length of the sandwich beam system will change with R_c. Figures 6 and 7 shows the variations of $\bar{\omega}_r$ and η with R_c. The input data were $\phi = 1.0$, $G_{c1} = 1 \times 10^{-4}$, $\eta_c = \eta_{c1} = \eta_{c2} = 0.1$, $h_1 = h_2 = 4$ mm, $h_c = 2$ mm and $\omega_o = \sqrt{E_1/\rho_1}$. R_c was varied from 0.1 m to 2.0 m in steps of 0.1 m. It can be seen that $\bar{\omega}_r$ decreases but η increases with R_c, especially when $R_c <$ 0.7 m. The variations of $\bar{\omega}_r$ and η with R_c are obvious as the total length of the curved sandwich beam system increases with an increase in R_c.

In the second case, the total length of the curved sandwich beam is kept constant at 1.2 m, which means changing R_c will result in a change of angle ϕ. Figures 8 and 9 show the variations of $\bar{\omega}_r$ and η with R_c. G_{c1}, η_c, h_1, h_2, h_c and ω_o were kept same as case one, but $\phi = 1.2/R_c$. R_c was varied from 0.3 m to 2.2 m in steps of 0.1 m. It is observed from Figure 8 that $\bar{\omega}_r$ is almost constant with R_c. In fact the change of $\bar{\omega}_r$ with R_c is very insignifcant for the first and second mode when $R_c > 0.6$ m. For the third and fourth modes, however, $\bar{\omega}_r$ change slightly with R_c when $R_c < 0.9$ m, but after $R_c > 0.9$ m the

change of $\bar{\omega}_r$ with R_c is not very obvious. In fact, in this range, as R_c increases, the curved beam turns to a straight beam and so large values of R_c will have little effect on the system resonance frequencies. The variation of η with R_c has a somewhat decreasing trend as seen in Figure 9. In summary, when the radius of curvature R_c is relatively small, R_c has some effect on $\bar{\omega}_r$ and η, but the effects are negligible for large values of R_c.

IV. CONCLUSIONS

The coupled transverse and longitudinal vibration of a curved sandwich beam system is investigated using the energy method in this paper. A closed form solution for the system resonance frequencies and modal loss factors is derived by the Rayleigh-Ritz method. Numerical results show that high values of adhesive shear modulus will influence the resonance frequenies much more greatly than the modal loss factors. Relatively small radius of curvature of the beam system will affect the system resonance frequencies and modal loss factors. But large values of radius of curvature will have very little effect on the resonance frequencies and modal loss factors. Furthermore, an increase in the thickness of the adhesive layer will decrease both the system resonance frequencies and modal loss factors. The analytical model presented here can be used as an effective tool in the design of constrained layer damping treatments for passive vibration control of curved sandwich systems.

V. ACKNOWLEDGEMENT

The authors would like to acknowledge the Natural Science Foundation, Washington, D.C. for financial support for this project through a research grant.

VI. REFERENCES

1. D. Ross, E. Ungar and E. M. Kerwin, Jr. 1959, *Structural Damping, ASME, NewYork. ed. by J. E. Ruzicka* Damping of Plate Flexural Vibrations by

Means of Viscoelastic Laminae

2. E. M. KERWIN, Jr. 1959 *The Journal of the Acoustical Society of America* **31(7)**, 952-962. Damping of Flexural Waves by a Constrained Visco-elastic Layer.

3. D. J. MEAD and S. MARKUS 1970 *Journal of Sound and Vibration* **12(1)**, 99-112. Loss Factors and Resonant Frequencies of Encastre Damped Sandwich Beams.

4. D. K. RAO 1978 *Journal of Mechanical Engineering Science* **20(5)**, 271-282. Frequency and Loss Factors of Sandwich Beams Under Various Boundary Conditions.

5. R. N. MILES and P. G. REINHALL 1986 *Journal of Vibration, Acoustics, Stress and Reliability in Design* **108**, 56-64. An Analytical Model for the Vibration of Laminated Beams Including the Effects of Both Shear and Thickness Deformation in the Adhesive Layer.

6. M. PETYT and C. C. FLEISCHER 1971 *Journal of Sound and Vibration* **18(1)**, 17-30. Free Vibration of A Curved Beam.

7. K. M. AHMED 1971 *Journal of Sound and Vibration* **18**, 61-74. Free Vibration of Curved Sandwich Beam by Finite Element Method.

8. J. VASWANI, N. T. ASNANI and B. C. NAKRA 1988 *Composite Structures* 10, 231-245. Vibration and Damping Analysis of Curved Sandwich Beams with a Visco-elastic Core.

9. W. FLUGGE 1962 *Stress in Shells*. Springer-Verlag.

Figure 1. Configuration of the curved sandwich beam system

Figure 2. Variation of system resonance frequency with adhesive shear modulus

Figure 3. Variation of system loss factor with adhesive shear modulus

Figure 4. Variation of system resonance frequency with adhesive thickness

Figure 5. Variation of system loss factor with adhesive thickness

Figure 6. Variation of system resonance frequency with radius of curvature of the central surface of the adhesive layer (ϕ = 1.0)

Figure 7. Variation of system loss factor with radius of curvature of the central surface of the adhesive layer (ϕ = 1.0)

Figure 8. Variation of system resonance frequency with radius of curvature of the central surface of the adhesive layer ($\phi = 1.2/R_c$)

Figure 9. Variation of system loss factor with radius of curvature of the central surface of the adhesive layer ($\phi = 1.2/R_c$)

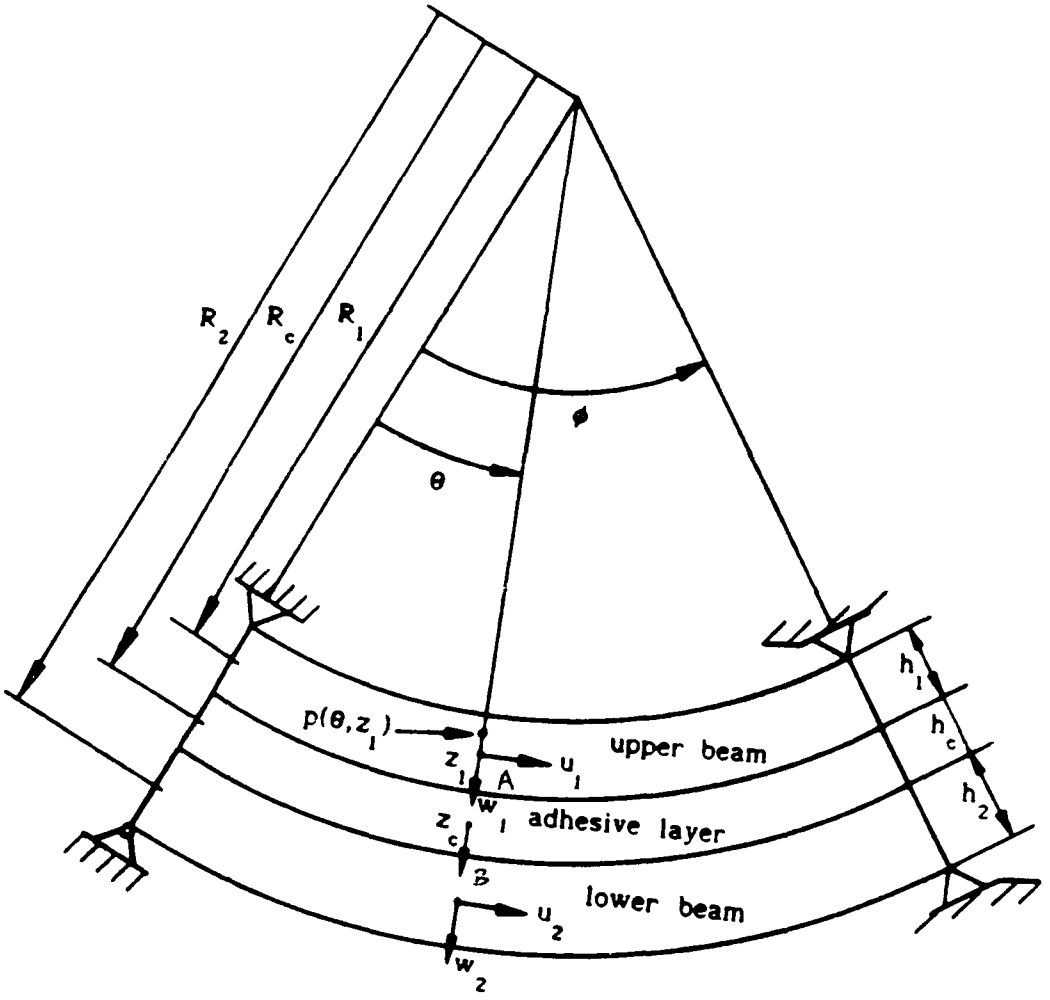
R2
Rc
R1
φ
θ
h1
hc
h2
p(θ,z1)
z1
A
u1
upper beam
w1
zc
adhesive layer
B
u2
lower beam
w2

Figure 2

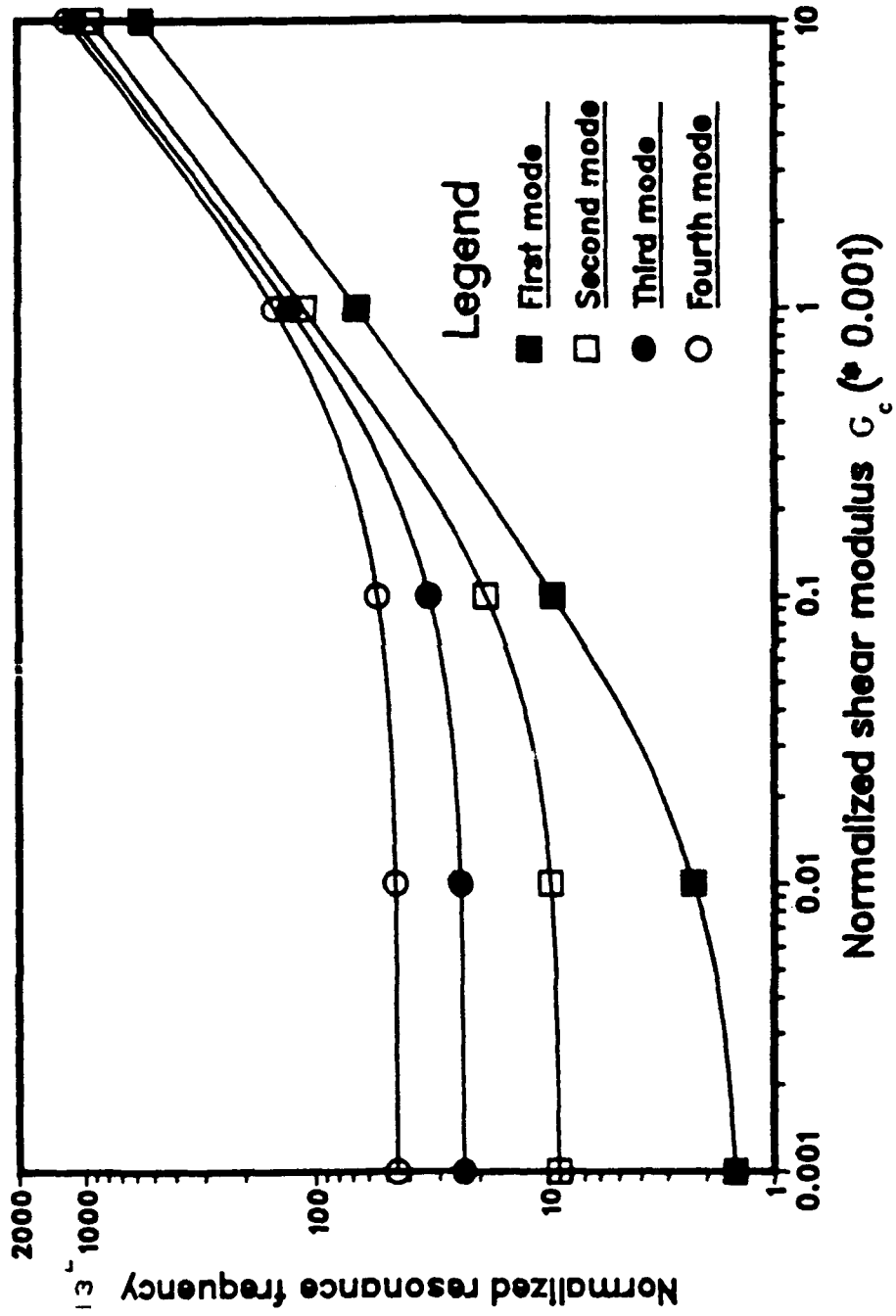
Normalized resonance frequency
2000
1000
100
10
1
0.001
0.01
0.1
1
10
Normalized shear modulus G_c (* 0.001)
Legend
First mode
Second mode
Third mode
Fourth mode

Fig. 2

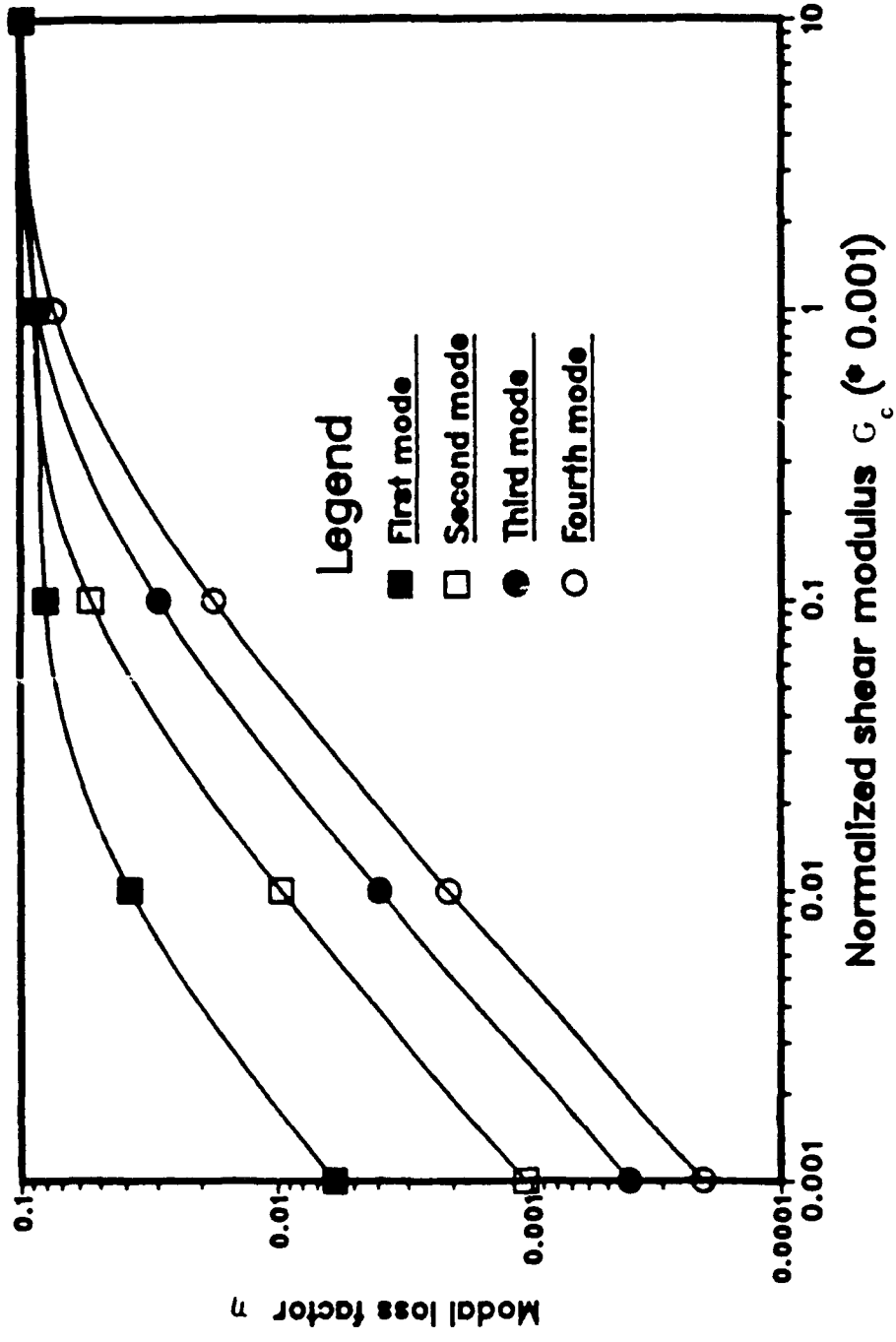
Modal loss factor η
0.1
0.01
0.001
0.0001
0.001
0.01
0.1
1
10
Normalized shear modulus G_c (* 0.001)
Legend
First mode
Second mode
Third mode
Fourth mode

Fig. 3

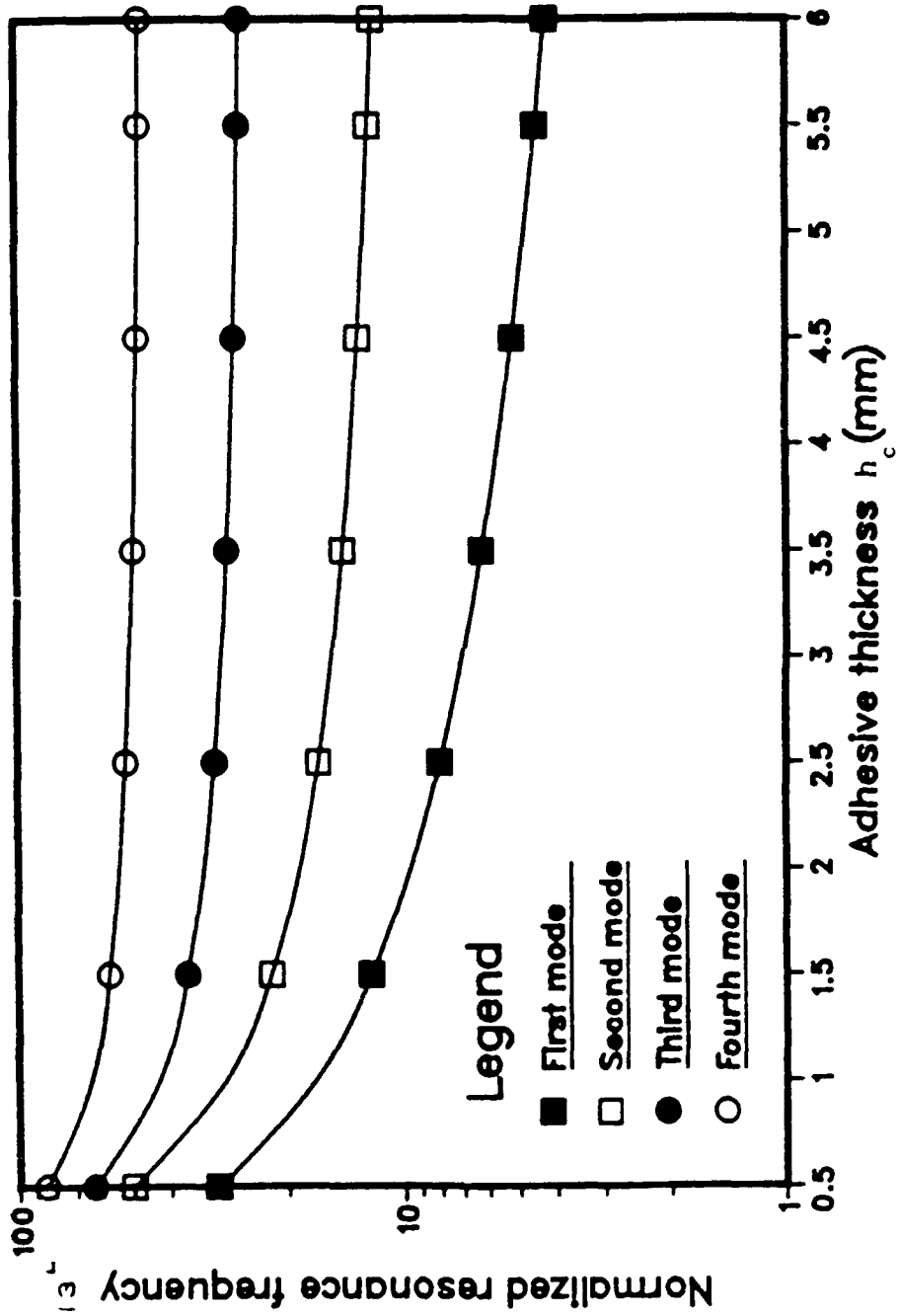
Normalized resonance frequency f_{c1}
100
10
1
0.5
1
1.5
2
2.5
3
3.5
4
4.5
5
5.5
6
Adhesive thickness h_c (mm)
Legend
First mode
Second mode
Third mode
Fourth mode

Fig. 4

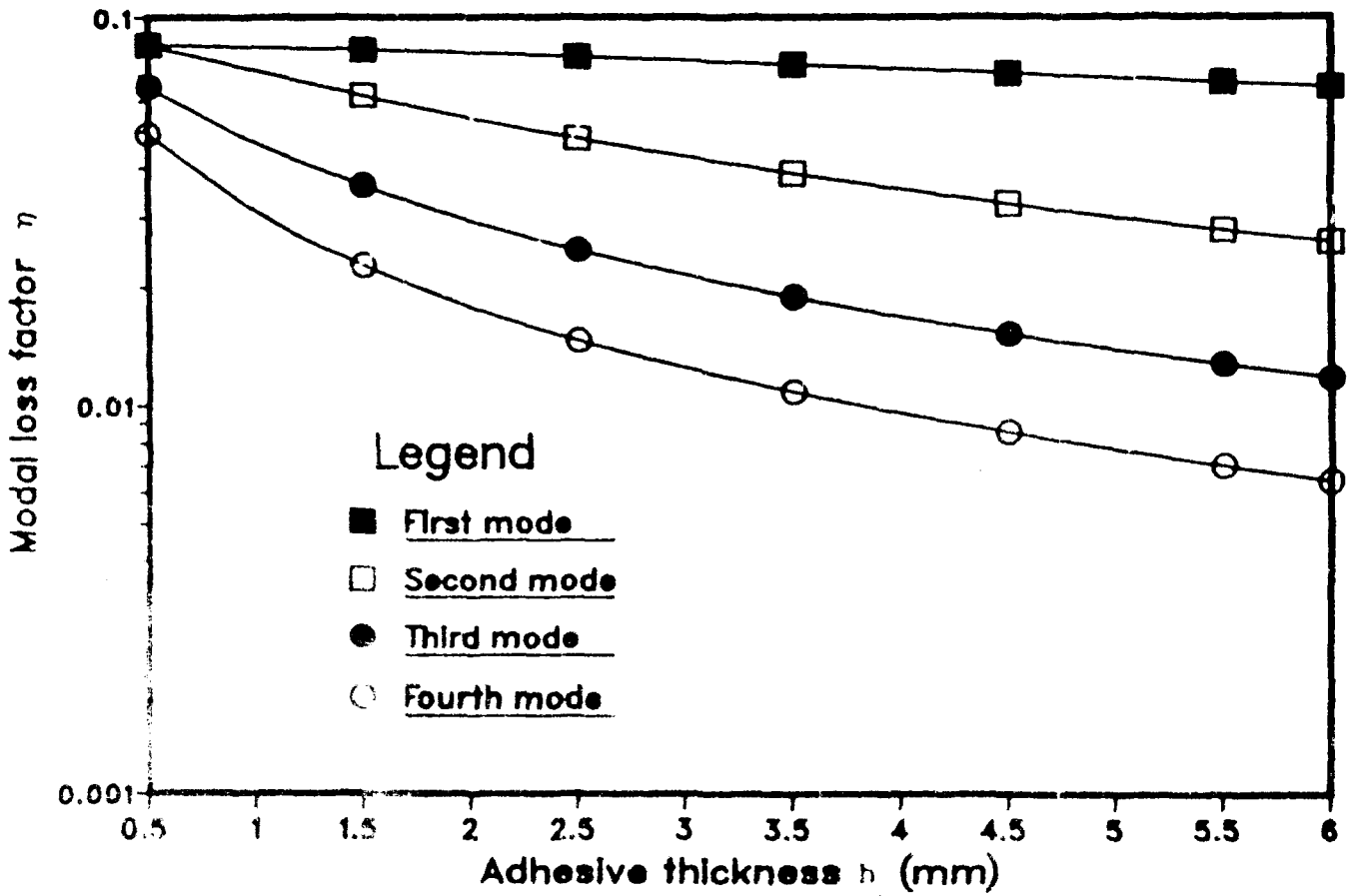
0.1
0.01
0.001
Modal loss factor η
Legend
First mode
Second mode
Third mode
Fourth mode
0.5
1
1.5
2
2.5
3
3.5
4
4.5
5
5.5
6
Adhesive thickness h (mm)

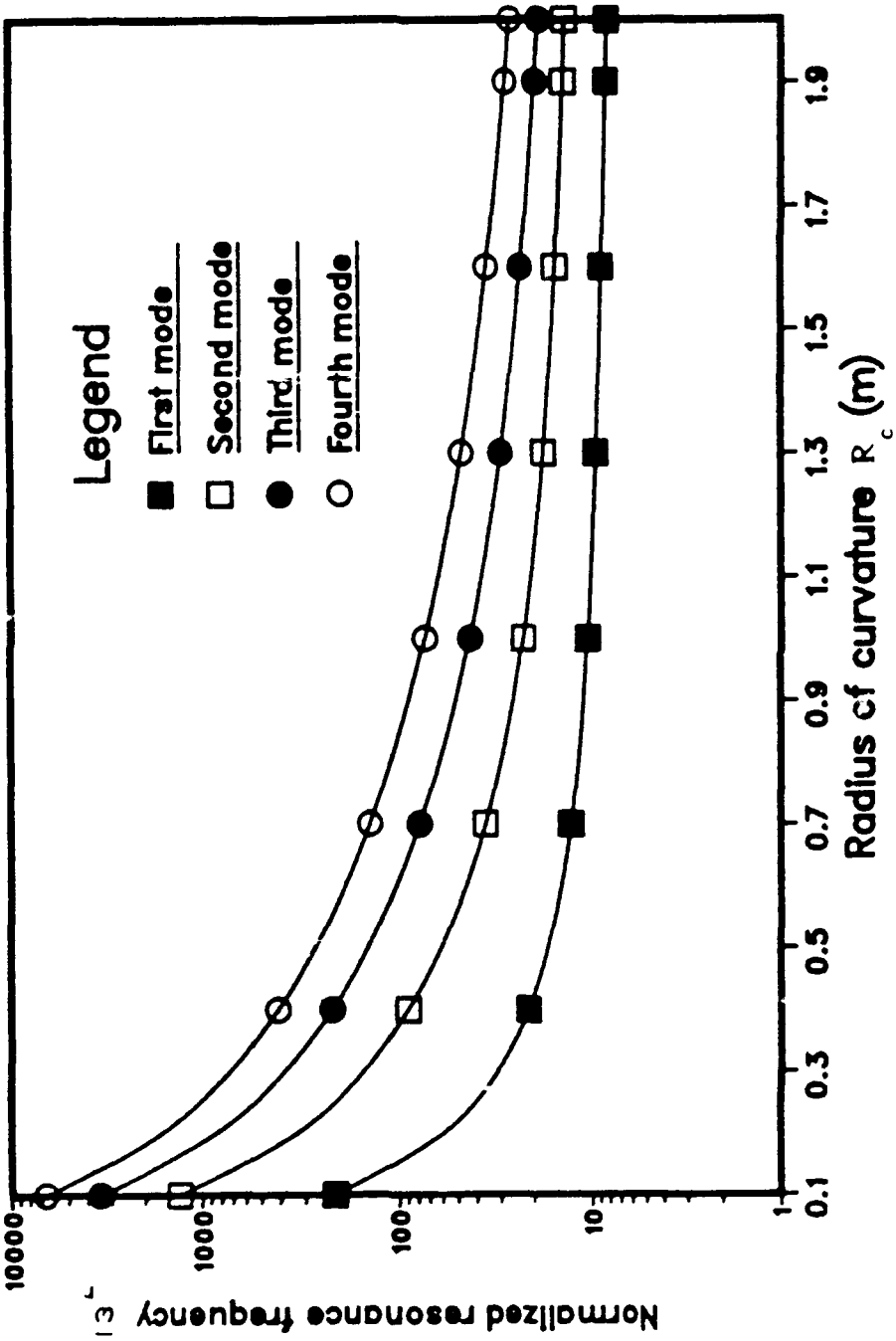
Legend
First mode
Second mode
Third mode
Fourth mode
Normalized resonance frequency $\bar{\omega}_r$
10000
1000
100
10
1
0.1
0.3
0.5
0.7
0.9
1.1
1.3
1.5
1.7
1.9
Radius of curvature R_c (m)

Fig. 6

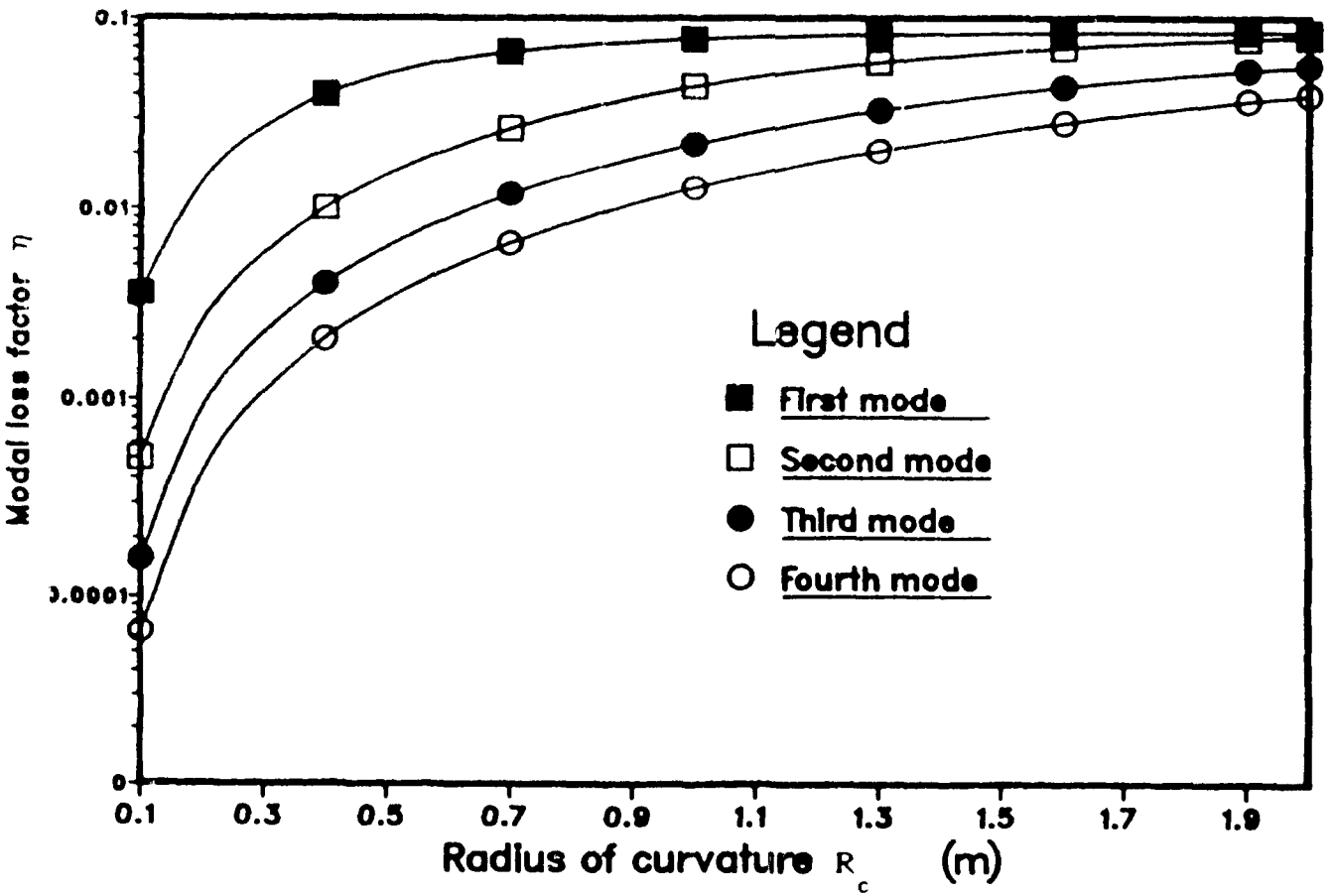
0.1
0.01
0.001
0.0001
0
Modal loss factor η
0.1
0.3
0.5
0.7
0.9
1.1
1.3
1.5
1.7
1.9
Radius of curvature R_c (m)
Legend
First mode
Second mode
Third mode
Fourth mode

Fig. 7

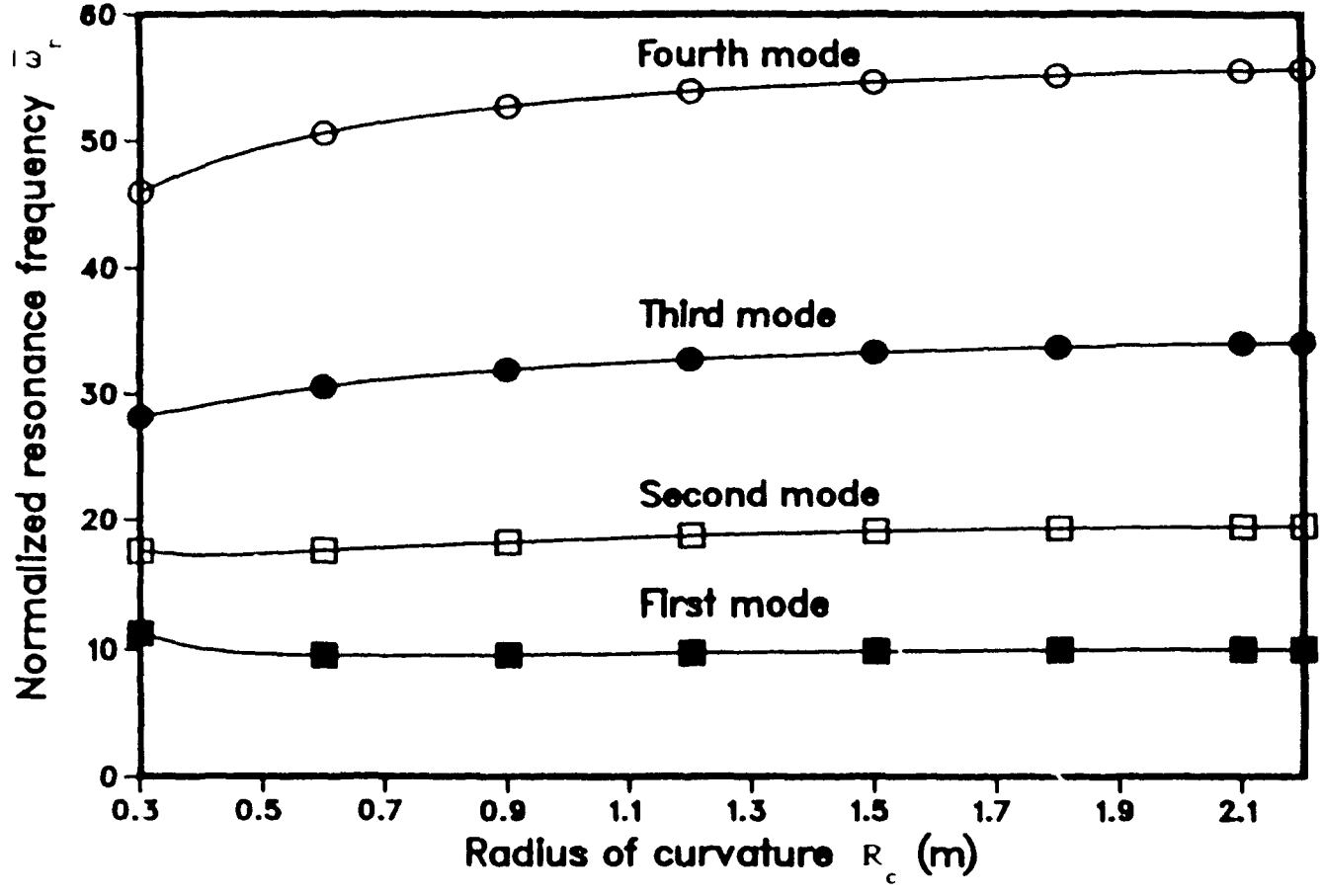
Normalized resonance frequency $\bar{\omega}$
60
50
40
30
20
10
0
Fourth mode
Third mode
Second mode
First mode
0.3
0.5
0.7
0.9
1.1
1.3
1.5
1.7
1.9
2.1
Radius of curvature R_c (m)

Fig. 8

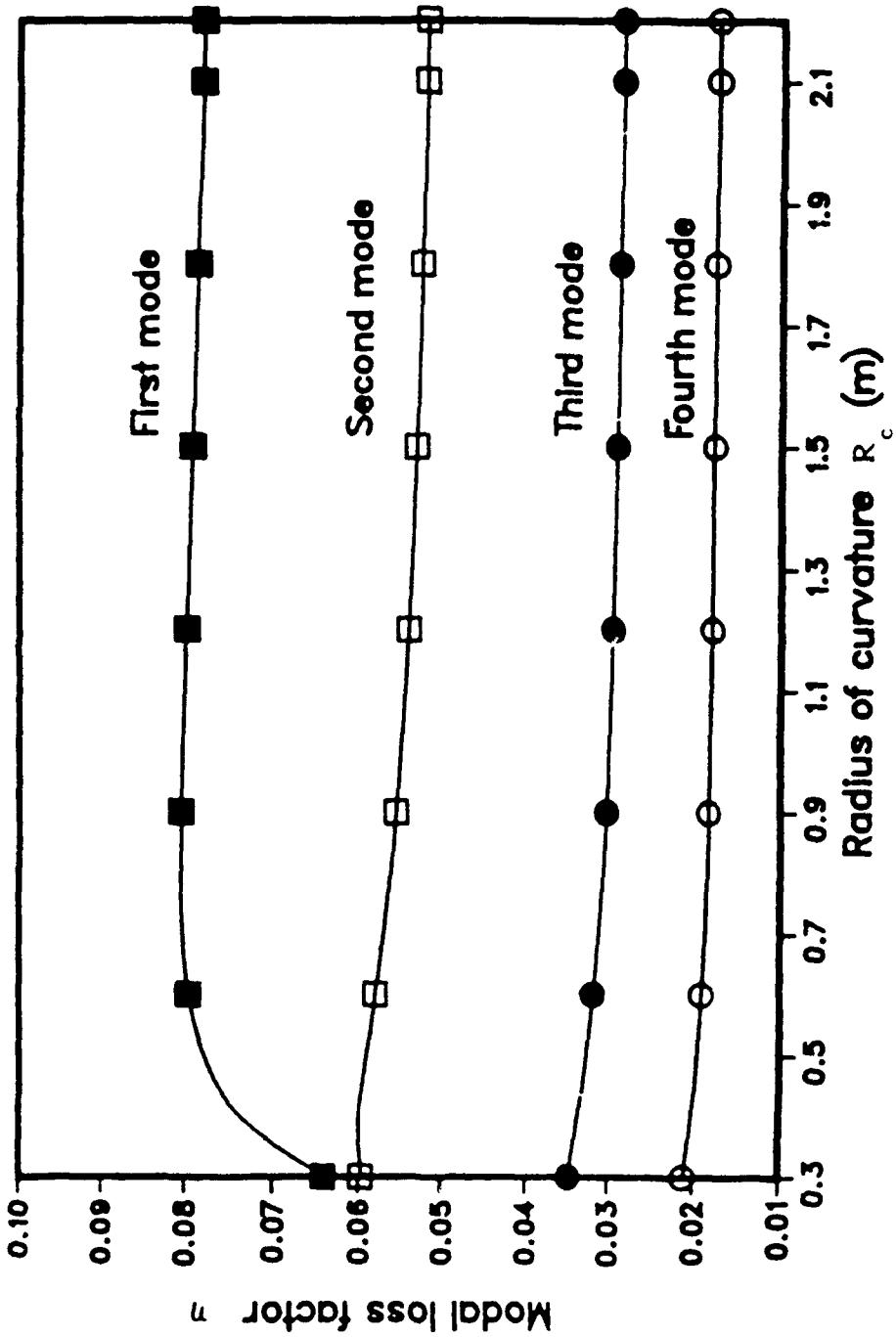
Modal loss factor η
0.10
0.09
0.08
0.07
0.06
0.05
0.04
0.03
0.02
0.01
0.3
0.5
0.7
0.9
1.1
1.3
1.5
1.7
1.9
2.1
Radius of curvature R_c (m)
First mode
Second mode
Third mode
Fourth mode

Fig 9

BIBLIOGRAPHY OF ENVIRONMENTAL DATA MEASURED IN FLIGHT

by

R.F. HAIN *
LIEUTENANT COLONEL, USAFR
Wright Laboratory/Flight Dynamics Directorate
Wright-Patterson AFB, Ohio

The increased emphasis on product reliability and maintainability has put a premium on knowing what environments, and their intensity, are experienced in flight. A bibliography is being assembled of reports that contain flight test measurements of dynamic data (acoustic, vibration, dynamic loads, flutter, etc.) and thermal data. The purpose of the bibliography is to get a better basis for estimating what the shock, vibration, acoustic and thermal environments are like for today's military aircraft. The bibliography already contains 250 entries consisting of the report number, title, source of the report, type of in-flight measurements made and the systems (A/C and avionics systems or external stores) monitored. A major goal of this project is to determine the potential need for a future systematic flight test program that will fill in gaps in the reported data.

*2810 South 299th Place,
Federal Way, Wa., 98003
(206) 941-4457 (H)
(206) 544-6707 (W)

INTRODUCTION

Increasing attention is being given to maintaining secondary structure and avionics subsystems in today's Air Force. There are several reasons for this increased interest:

- Increasing costs of
  - hardware
  - maintenance--regardless of equipment or its age

- tactical doctrine that sets as a goal the usage of austere bases with minimal maintenance facilities

INTRODUCTION

- NEED: A COMPREHENSIVE SURVEY OF ENVIRONMENTAL DATA MEASURED IN-FLIGHT
- WHY: BETTER PREDICTION OF ENVIRONMENTS
- FOR WHOM: DESIGNERS WHO MUST PREDICT SUCH ENVIRONMENTS FOR DESIGN AND ANALYSIS OF NEW COMPONENTS
- HOW: LITERATURE SURVEYS; REPORT EVALUATIONS; IF NECESSARY, FLIGHT TEST PROGRAM
- BY WHOM: LTC RAY HAIN; MAJ ALEX CORONADO; CAPT MIKE DILLARD
- WHERE: WRIGHT LABORATORY, FLIGHT DYNAMICS DIRECTORATE, WRIGHT-PATTERSON AFB, OHIO
- PROJECT SPONSOR: DR. JIM OLSEN, FLIGHT DYNAMICS DIRECTORATE CHIEF SCIENTIST

REASONS

- It seems fairly typical to design to predicted levels only to find out (from the flight testing that is done and field use) that the predictions were too low.
- Fixing broken equipment is expensive.
- A look at reliability data may well corroborate the fact that at least one of the environments was much too low, e.g., the acoustic levels seen by the B-1 Aft Equipment Bay during take-off or the A-10 gunfire acoustic levels in the nose wheel well.
- A flight test program is expensive; finding out what data is available can cut down on such testing.
- No one office is aware of all the testing done; the Navy does testing on the F-16 and AIM-9 but the Air Force may not be aware of it.

REASON FOR EFFORT

- POOR HANDLE ON WHAT ENVIRONMENTS "REALLY" ARE
- INCREASING COSTS
- INCREASING EMPHASIS ON THE "ILITIES"
- EXPENSE INVOLVED IN RUNNING A FLIGHT TEST PROGRAM
- REDUCE DUPLICATION OF EFFORT

ACCOMPLISHMENTS

- Bibliography now contains 250 entries from a wide spectrum of sources. All entries are unclassified but a few are "competition sensitive" or were at time of writing. Presumably this restriction will be (or has been) removed with contract award.
- Several offices at Wright-Patterson are interested in what we are doing: Avionics Integrity Program Office (would like to see extensive surveys); ASD/EN (Engineering) is interested; F-15 SPO could allow us collect data on some of their tests.
- A library at Wright Laboratory, Flight Dynamics Directorate, (Structural Dynamics Branch) has been established for the test reports we collect.

ACCOMPLISHMENTS

- SEVERAL LITERATURE SURVEYS ACCOMPLISHED:
  - 250 REPORTS IDENTIFIED
    - REPORTS COVER APPROXIMATELY 50 YEARS.
- DISCUSSED SURVEY WITH SEVERAL INTERESTED OFFICES AT WRIGHT-PATTERSON AFB:
  - AVIONICS INTEGRITY PROGRAM OFFICE
  - F-15 SPO
  - ASD/EN
- LIBRARY FOR FLIGHT TEST REPORTS ESTABLISHED AT WRIGHT LABORATORY, FLIGHT DYNAMICS DIRECTORATE
- END PRODUCT OF PROJECT: BIBLIOGRAPHY OF REPORTS

DATA BASE STRUCTURE

- DBASE III STRUCTURE
- 19 FIELDS OF DATA
  - THREE FOR A/C TYPES
  - THREE FOR SUBSYSTEMS TYPES
  - THREE FOR AUTHORS AND THEIR ORGANIZATIONS
  - THREE FOR DATA TYPES
  - PLUS FIELDS FOR TITLE, REPORT NUMBER, LOCATION OF COPY, ORGANIZATION OF ORIGINATION, ETC.

BIBLIOGRAPHY STRUCTURE

- USE DBASE I I I
- DATA LISTED:
  - REPORT NO.
  - REPORT TITLE
  - REPORT AUTHOR
  - SYSTEMS MONITORED
    - AIRCRAFT (UP TO THREE IN DATA BASE)
    - SYSTEMS MONITORED (E.G., RADAR, ANTENNAE, GUNFIRE DATA, EXTERNAL STORES) (UP TO THREE LISTED IN DATA BASE)
  - TYPE OF DATA (NOISE, VIBRATION, LOADS, FLUTTER, ETC.)

DATA

- Vibration data is presented in several ways:
  - Acceleration PSDs
  - RPM vs Amplitude
  - Double Amplitude displacement vs. frequency
- Acoustic data is generally presented as dB per octave band with some at smaller band widths.
  - Very little aeroacoustic noise is reported. Need more of it.
- Thermal data is at a premium. Very little of it appears in the open literature.
- Dynamic Loads data and flutter data are reported. Need more of both.

TYPES OF DATA

- VIBRATION
- ACOUSTIC
- THERMAL
- DYNAMIC LOADS
- FLUTTER

SYSTEMS

- Various combinations of aircraft systems have been monitored. Almost all systems are represented in some test or other. Generally, only one or two (occasionally three) aircraft systems are monitored. Some systems are monitored on more than one airplane.
- Extensive data for very FEW aircraft are available; the two in our data base are the F-111 and F-15.

SYSTEMS MONITORED

- AIRCRAFT
  - FIGHTERS
  - CARGO A/C
  - BOMBERS
  - HELICOPTERS
- EXTERNAL STORES
  - BOMBS AND FUSES
  - AIR-TO-AIR MISSILES
  - FUEL TANKS
- INTERNAL EQUIPMENT
  - RADAR SETS
  - VARIOUS RECEIVERS AND ANTENNAS
  - GUN DATA (VIBRATION AND ACOUSTIC)

TESTING

- Of the data collected, very little is actually reduced. There are several reasons for this: (1) only as much of the collected data as is thought necessary to solve problem is reduced; (2) lack of resources (money, manpower, or equipment); (3) lack of vision for future needs; (4) inability to read tapes because tape parameters are no longer known.

- Many different agencies run a flight test program of some type. Each is often unaware that any other test has been accomplished. Duplication of effort results.

TEST PROGRAMS

- GENERALLY USED TO SOLVE A VERY LIMITED PROBLEM
- LIMITED AMOUNT OF THE DATA COLLECTED IS ACTUALLY REDUCED
- VERY FEW SURVEYS OF ENTIRE A/C
- RUN BY MANY DIFFERENT AGENCIES

TEST ORGANIZATIONS

- Each of the services run their own tests "in-house". Some of the tests are run by several agencies within the home service.
- Other tests are run by the contractors who expect to be paid for their effort. They provide what is paid for only.
- Particular test organizations:
  - Air Force Flight Test Center • Air Force Flight Dynamics Lab
  - Air Force Special Weapons Center • Armament Division (AFSC)
  - 4950th Test Wing (WPAFB) • Federal Aviation Administration
  - NASA • Naval Air Test Center • Naval Weapons Center
  - Army's ECOM • Army Missile Command • AGARD
  - Plus many more military and civilian organizations.

TEST ORGANIZATIONS

- HOME "SERVICE" OF TEST ORGANIZATIONS REPRESENTED IN DATA BASE
  - AIR FORCE
  - NAVY
  - ARMY
  - NASA
- CONTRACTORS
  - McDONNEL DOUGLAS CORPORATION
  - GENERAL DYNAMICS
  - BOLT, BERANEK, AND NEWMAN
  - BOEING
  - PLUS ANY ONE ELSE PRODUCING MILITARY HARDWARE

FURTHER EFFORTS

- A Continuing effort is being made to collect as much additional data as possible. We are trying to add as many titles as possible to our bibliography.
- A systematic flight test program will be designed to fill as many of the gaps as possible--but only if necessary.
- Several avenues of data collection are being followed:
  - Additional literature surveys/searches
  - Letters to test organizations asking for inputs
  - Searching filing cabinets of reports
  - "Piggybacking" instrumentation on other tests (F-15 SPO may allow this)
  - "Piggybacking" instrumentation packages on training missions if MAJCOM will allow it.

CONTINUING EFFORT

- COLLECT COPIES OF AS MANY REPORTS AS POSSIBLE TO BE ADDED TO LIBRARY
- CONTINUING LITERATURE SURVEYS/SEARCHES
- LETTERS TO TEST ORGANIZATIONS ASKING FOR INPUTS
- COLLECT DATA BY:
- DESIGNING A FLIGHT TEST PROGRAM TO FILL IN GAPS IN DATA (IF NEEDED)
- PIGGYBACK ON OTHER TEST PROGRAMS
  - F-15 IS POSSIBLE
- PIGGYBACK ON TRAINING MISSIONS
  - WHEN MAJCOM WILL ALLOW IT

ADDITIONAL DATA

- Additional data and bibliographic entries are our current aim.
- Information requested includes:
  - Report number
  - Report title
  - Report authors
  - Type of data in report (i.e., vibration, noise, flutter, loads, etc.)
  - Systems monitored (i.e., A/C type, avionics components, structure)
  - Point of contact to obtain copy of report or to review report
  - Location of copy of test report
  - Source of report, i.e., the test organization

COLLECTION OF DATA

- TYPE OF DATA WANTED:
  - DYNAMIC
    - VIBRATION
    - ACOUSTIC
      - REGARDLESS OF SOURCE
    - FLUTTER
  - THERMAL
- COPY OF TEST REPORT FOR LIBRARY AT WRIGHT LABORATORY, FLIGHT DYNAMICS DIRECTORATE
- HELP FROM OTHER TEST ORGANIZATIONS:
  - SEND INFORMATION TO:

    DR. JAMES J. OLSEN
    FLIGHT DYNAMICS DIRECTORATE CHIEF SCIENTIST
    WL/FI-F
    WRIGHT-PATTERSON AFB, OHIO
    45433

THANKS

SPECIAL THANKS TO DEBBIE COTTRILL, A SUMMER INTERN AND STUDENT AT THE OHIO STATE UNIVERSITY, FOR DOING THE INITIAL DATA ENTRY IN THE DATA BASE. IT WAS A BIG CHORE WITH A LOT OF DATA TO ENTER. SHE HANDLED IT WITH APLOMB.

GENERAL MOTION OF AN INCLINED IMPACT DAMPER WITH FRICTION

C. N. Bapat
Department of Mechanical Engineering
The City College of the City University of New York
Convent Ave. at 138th St.
New York, NY 10031.

ABSTRACT

Here an exact approach to analyze the stable periodic N impacts/period motion of an inclined damper with friction and collisions on either one or both sides of a container with identical and nonidentical coefficients of restitutions is presented. The proposed theory can be easily modified for the cases of a pressurized damper mass and a damper mass oscillating on a spring supported platform. The comparison of theoretical predictions with previous results and with results obtained by numerical simulation of motion on a digital computer indicates a good agreement. Few results are presented.

1. INTRODUCTION

An impact damper is a light weight auxiliary device, which consists of a container with a loose mass. The superior effectiveness of this device as a damper has been demonstrated. Device is most effective in damping vibrations in the resonant range when damper mass moves freely in the horizontal direction and has vibroimpact motion with alternating two equispaced impacts/cycle of an external sinusoidal load. This particular motion has been studied extensively for last few decades [1,2]. However, in many practical applications damper may operate in the nonhorizontal direction and with friction and hence it is important to know its damping properties under realistic operating conditions. Few investigations which account for the effect of friction or gravity on impact damper are reported [3-6]. However, an exact analysis of the general motions of an impact damper with friction or gravity is not available. Hence such an approach was

developed.

2 THEORY

The model of an impact damper shown in Figure 1 consists of a primary mass, M, a linear spring, K, and a viscous dashpot with damping constant, C. An impact damper consists of a loose mass, m, moving in a container atached to the main mass with gap, d. The system was assumed to oscillate along a plane making an angle θ with the horizontal plane.

Governing nonlinear equations of assumed motion were developed by combining approaches used in references [2] and [6]. After lengthy algebraic manipulations and using various relations between impact velocities before and after impact and average velocity between impacts etc., the 2N nonlinear equations in 2N unknowns were obtained. These equations are generally solved iteratively for all values of N. Equations can be further simplified for a practically important case of two impacts/cycle motion. Stability of motion was studied by extending approaches presented in references [1] and [2].

When gap becomes so large that impacts occur only on side 1, then the resulting model represents the vibratory conveyor system widely used in industry; cast shake out grids and vibroimpact test rigs to name a few [7]. Impact damper with compressed air can also be studied using these equations [8].

3. RESULTS

The theoretical predictions were checked with the previous results and the agreement is good. The correctness of the newly developed elements of the stability matrix were checked by additionally comparing the theoretical and numerical simulation results.

The effect of gravity on amplitude reduction and time duration between three consecutive impact of an two unequispaced impacts/cycle motion is shown in Figure 2. Figure indicates that gravity has detrimental effect as Xmax/A increases with the angle θ. The effect is more pronounced on the time duration between impacts near the resonance.

The effect of gravity on the stability regions is shown in

Figure 3. It indicates that system just below resonance is unstable. However, above and below resonance system has reasonably sized stability regions.

The effect of nonidentical coefficients of restitution on the amplitude reduction, shown in Figure 4 indicates that the identical coefficients of restitution case is the most efficient from the point of view of amplitude reduction and a small difference in the coefficients of restitution has little effect on the amplitude reduction.

4. CONCLUSION

An exact approach to study general periodic motion of an inclined damper with friction and nonidentical coefficients of restitution is developed. The theoretical predictions are compared with the results obtained using a simulation approach and indicates a good agreement.

6. REFERENCES

1. S. F. MASRI 1969 The Journal of Acoustical Society of America, 47, 229-237. General motion of impact dampers.
2. N. POPPLEWELL, C. N. et. al Journal of Sound and Vibration, 87, 41-59. Stable periodic vibroimpacts of an oscillator.
3. H. G. KAPER 1961 Applied Science Research, Series A, 10, 369-383. The behavior of a mass-spring system provided with a discontinuous dynamic vibration absorber.
4. M. M. SADEK and B. MILLS 1970 Journal of Mechanical Engineers, 12, 268-287. Effect of gravity on the performance of an impact damper, Part 1. Steady state motion, Part 2. Stability of vibration modes.
5. W. M. MANSOUR and D. R. T. FILHO 1974 Journal of Sound and Vibration 33, 247-265. Impact dampers with coulomb friction.
6. C. N. BAPAT and S. SANKAR 1985 Journal of Sound and Vibration 103, 457-469. Multiunit impact damper-re-examined.
7. YA. F. VAINKOF 1967 Soviet Applied Mechanics 3, 69-72. The stability of motion in a two mass vibroimpact system with one-sided excitation.
8. D. L. CRONIN and N. K. VAN 1975 An ASME Publication. Paper no. 75-DET-17. Substitute for the impact damper.

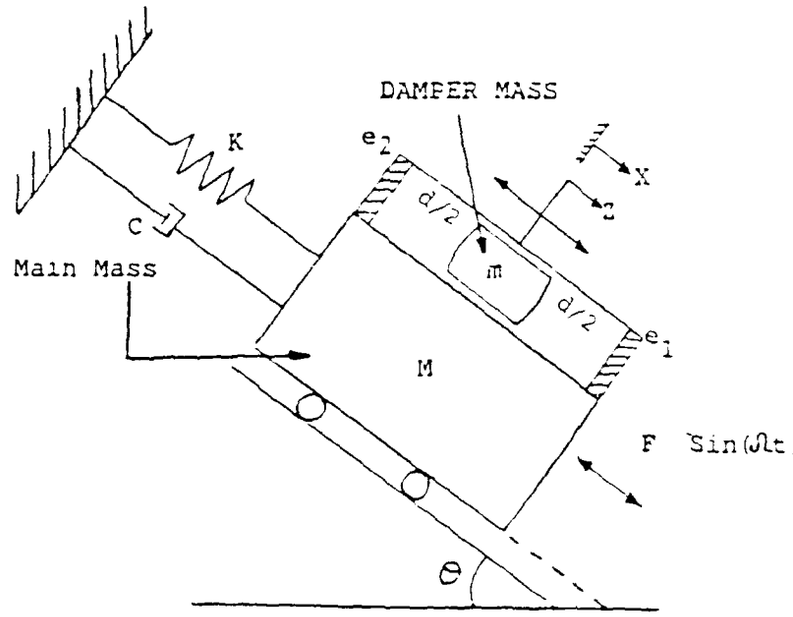

FIGURE 1. MODEL OF AN INCLINED IMPACT DAMPER.

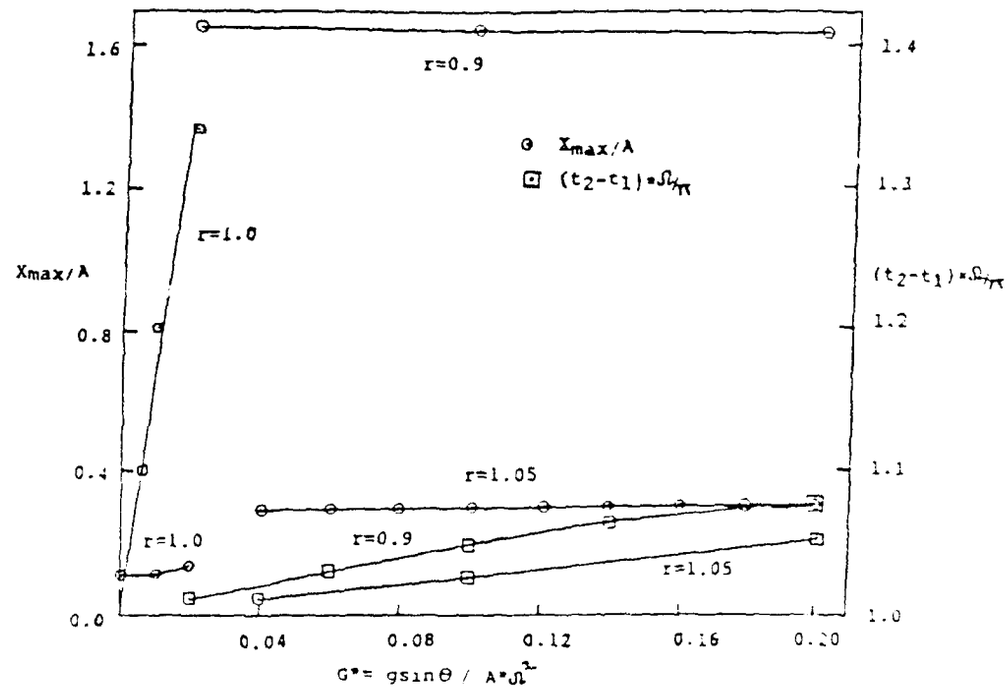

FIGURE 2. EFFECT OF GRAVITY ON AMPLITUDE REDUCTION AND TIME DURATION BETWEEN IMPACTS.
ξ =0.005, m/M =0.042, dk/F = 37, e_1=e_2=0.75.

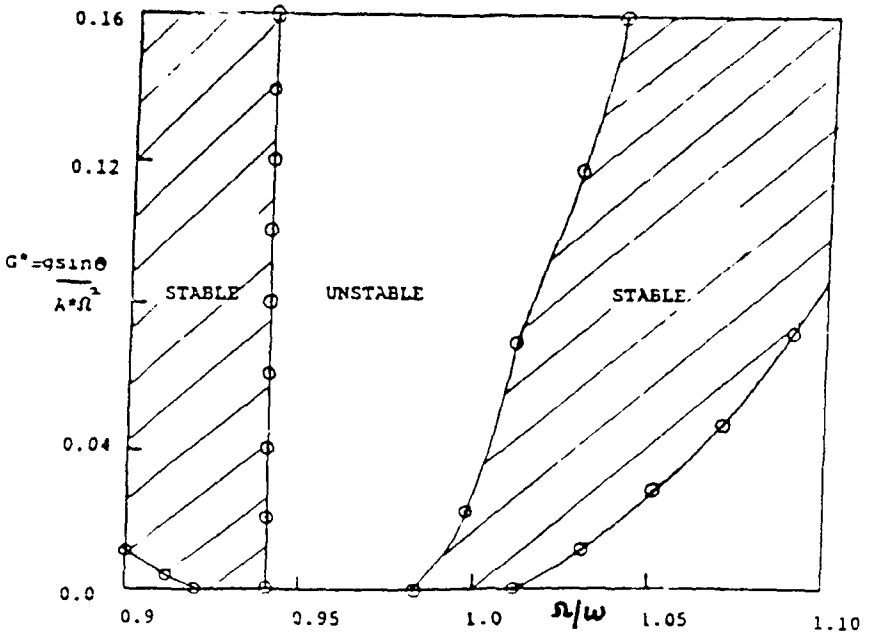

FIGURE 3. STABILITY ZONES OF TWO IMPACTS/CYCLE MOTION OF AN IMPACT DAMPER. ζ =0.005, m/M =0.042, dk/F =37, $e_1=e_2=0.75$.

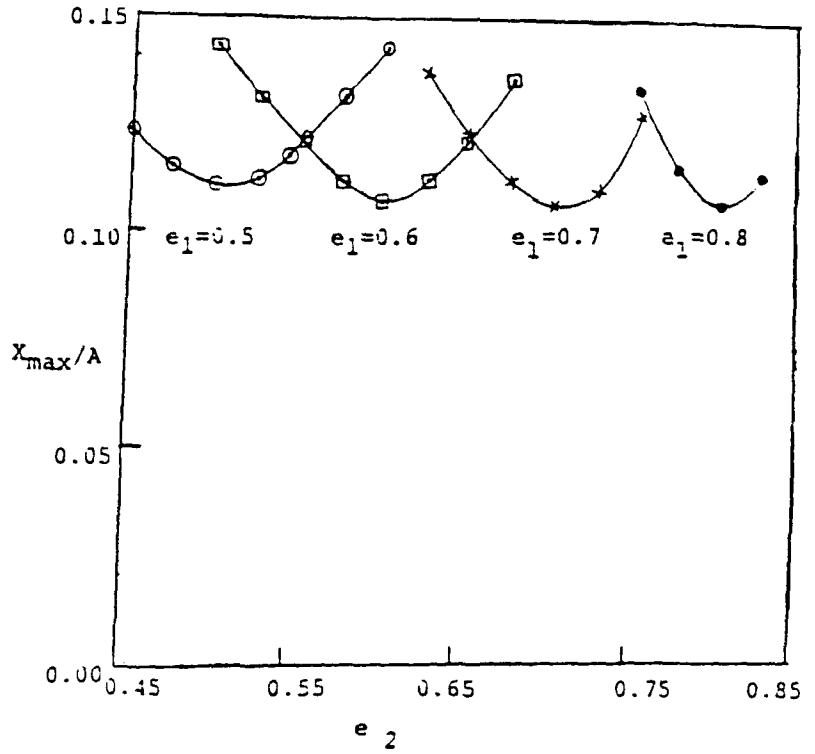

FIGURE 4. EFFECT OF NONIDENTICAL COEFFICIENTS OF RESTITUTION ON AMPLITUDE REDUCTION. r=1.0, ζ =0.005, g=0.0,dk/F=37, m/M=0.042.

SAVIAC

THE SHOCK AND VIBRATION INFORMATION ANALYSIS CENTER

PRESENTATION TO DAMPING '91 CONFERENCE, 14 FEBRUARY 1991

DISCUSSION TOPICS

- Information Analysis Centers
- SAVIAC Background
- The SAVIAC Team
- Our Goals for SAVIAC
- Core Activities
- Information System
- Auxiliary Tasks
- Interaction with Government/Private Activities
- SAVIAC Funding

INFORMATION ANALYSIS CENTERS

What is an IAC?

An IAC is an activity set up to facilitate access to technical information in specialized areas. The IAC's mission is to improve the productivity of Government and industry RDT&E personnel by serving as an effective information resource.

INFORMATION ANALYSIS CENTERS

- There are 14 IACs managed by the Defense Technical Information Center

- 10 managed by service activities

INFORMATION ANALYSIS CENTERS

What do IACs do with information?

- Collect
- Review
- Analyze
- Disseminate

INFORMATION ANALYSIS CENTERS

Sources of Information:

- Government
- Industry
- Academic Institutions
- Foreign

Typical Material Drawn Upon:

- Technical Reports
- Conference Proceedings
- Trade & Professional Journals
- Test Reports
- Work-in-Progress

INFORMATION ANALYSIS CENTERS

Products and Services:

- Current Awareness Newsletters
- Technical Journals
- Indexes
- Reference Works
- Technology Assessments
- Technical Inquiry Services
- Analytical and Technical Tasks

INFORMATION ANALYSIS CENTERS

Funding comes from:

- Core Funding
- Fees for Products and Services
- Special Tasking

SAVIAC BACKGROUND

- SAVIAC's forerunner, SVIC, was established 1946 at the Naval Research Laboratory
- SVIC disestablished October 1986
- Representatives from the three services, DoE and NASA joined to form the Technical Advisory Group (TAG) in order to maintain the Shock and Vibration Symposium and to re-establish SVIC services
- Naval Surface Warfare Center/White Oak Laboratory acted as contracting activity for TAG
- RFP issued December 1989
- Contract awarded November 1990 to Booz•Allen & Hamilton Inc. and Southwest Research Institute to operate SAVIAC

TECHNICAL ADVISORY GROUP FOR SAVIAC

Stan Wojnar, Chairman	- Naval Surface Warfare Center/White Oak
Howard Camp	- Army CECOM, Ft. Monmouth
Tommy Dobson	- 6585th Test Group, Holloman AFB
Ken Eliott	- NASA Langley Research Center
John Ferritto	- Navy Civil Engineering Laboratory
Ami Frydman	- Army LABCOM, Harry Diamond Laboratories
Howard Gaberson	- Navy Civil Engineering Laboratory
Doug Henderson	- Wright Laboratory, Wright-Patterson AFB
Dennis Kern	- NASA Jet Propulsion Laboratory
Bob McCarthy	- Naval Sea Systems Command
Robert Nichols	- Army White Sands Missile Range
Stephen Matson	- Army White Sands Missile Range
LCDR Charles Nofziger	- Defense Nuclear Agency
Michael Riley	- David Taylor Research Center/UERD
Jack Robinson	- Army Aberdeen Proving Grounds
Walter Ruh	- Army TECOM, Redstone Arsenal
David Smallwood	- Sandia National Laboratories
Paul Smith	- Los Alamos National Laboratories
Ken Stuart	- Army ARDEC, Picatinny Arsenal
Tom Tsai	- Defense Nuclear Agency
John Wafford	- Aeronautical Systems Div., Wright-Patterson AFB
John Walker	- Naval Ocean Systems Center

THE SAVIAC TEAM

- Booz•Allen & Hamilton Inc., Arlington, VA
- Southwest Research Institute, San Antonio, TX
- Senior Consultants

OUR GOALS FOR SAVIAC

- Build SAVIAC into a national resource of shock and vibration expertise
- Become the center of activity for the gathering and distribution of technical information for the shock and vibration community
- Serve as the primary forum within the community for issues of concern for the RDT&E of systems

SAVIAC CORE ACTIVITIES

- Shock and Vibration Symposium
- Shock and Vibration Technology Review
- Current Awareness Newsletter
- User Inquiries
- Information System

SHOCK AND VIBRATION SYMPOSIUM

62nd Shock and Vibration Symposium

October 29-31, 1991

Springfield, Virginia

INFORMATION SYSTEM

Databases

- S & V Symposium papers/authors index
- Referrals, "Who's Who" listing of technical experts
- Test Facilties
- Vendors/Equipment
- Training Resources

Delivery System

- Hard Copy
- Floppy Disk
- On-Line

SAVIAC AUXILIARY TASKS

- Topical Monographs
- Handbooks and Data Books
- State of the Art Reports
- Critical Reviews and Technology Assessments
- Special Studies and Tasks

INTERACTION WITH GOVERNMENT AND PRIVATE ACTIVITIES

SAVIAC maintains controls for:

- Conflict of Interest
- Proprietary Information
- Classified Information Control/Access

WHERE SAVIAC FUNDING COMES FROM

- Seed Funding $100K
- Symposium Attendance Fees
- Publication Subscriptions
- User Funding
- Special Tasks

SAVIAC USER FUNDING

SAVIAC Provides to Users:

User Funding	Research on Technical Inquiries	Bibliographic Searches and Referral Inquiries	Copies of Technology Review	Symposium Seats
$20K	300 hrs	60 hrs	5	5
$10K	150 hrs	30 hrs	2	2
$5K	75 hrs	15 hrs	1	1

NOTE: Fee schedule for individual services is also available

SAVIAC USER FUNDING SERVICE PAYMENT METHODS

Government Activities -

MIPR to Naval Surface Warfare Center/White Oak Laboratory

Commercial -

by Purchase Order to SAVIAC/Booz•Allen

SUMMARY

SAVIAC was created by the shock and vibration technical community, to serve the community.

SUMMARY

For further information, contact:
Mr. Harold Kohn, Director of Operations

The Shock and Vibration Information Analysis Center
2711 South Jefferson Davis Hwy
Suite 600
Arlington, VA 22202-4158

Phone (703) 769-7570 FAX (703) 685-6555

The Vibration Damping Effect of an Electrorheological Fluid

Stephen A. Austin

Naval Underwater Systems Center

Towed Array Exploratory Development Branch[1]

ABSTRACT

The attenuation of longitudinal vibrations in structures can be achieved through a change in the impedance of the structure. This impedance change can be produced by an electrorheological fluid. The transmission of a known vibration input along a test structure will be correlated to the impedance characteristics of the electrorheological fluid. This impedance characteristic of the fluid will be expressed in terms of the applied electric field.

The attenuation characteristics of the electrorheological fluid on longitudinal vibration have been presented through experimental and numerical results. The results of this study showed an attenuation of 4 dB in the transmissibility of acceleration from the forward to the aft ends of the test structure. This level can be increased by using a fluid possessing a lower zero state viscosity.

A secondary result of this investigation is understanding the physics of the damping mechanism in the test module when the electric field was increased from 1.2 kV/mm to the value of 1.6 kV/mm. During this increase in the electric field, the logarithmic decrement increased by more than a factor of three. The transmissibility data also shows that the resonant frequency decreased.

INTRODUCTION

The application of electrorheological (ER) fluids have been cited by many authors, such as the work of Stanway et al. (1987), Coulter et al. (1989), Duclos (1988), Stevens et al. (1984) and by Margolis and Vahdati (1989), as an effective means for vibration isolation and control. The many applications of these fluids include clutches, viscous dampers, and active engine mounts. In the vibration isolation applications, the predominant method of vibrational energy dissipation is the interaction between a plunger mechanism and the ER fluid. The fluid properties are actively altered by the magnitude of the electric field applied; thus, the response of the structure is altered and controlled.

In this paper, an application of an ER fluid to attenuate the longitudinal vibration in a flexible cylindrical structure is discussed. The attenuation of the longitudinal vibration (Figure 1) will be achieved by the relative shearing of the fluid at the inner surface of the flexible boundary and a region of fluid driven by an applied electric field.

1. NUSC, Code 2141, New London, Connecticut, 06320, (203) 440-4570

The shear interface is developed between the driven, center line, fluid posing a resistance to the zero state fluid entrained with the flexible cylinder motion. The vibrational energy in the wall of the flexible cylinder will be dissipated through the relative shearing of the driven and zero state ER fluid.

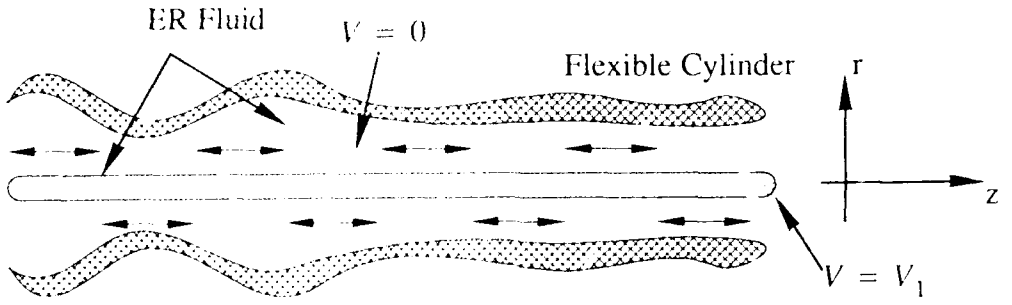

Figure 1. ER Shear Application

The results of this analysis show an increase in attenuation with an increase of the applied electric field. This analysis also shows an extreme increase (3 times) in the damping of the system as the electric field transitions in the range of $1.2 < E \leq 1.6$ kV/mm dc. This extreme increase in the system damping ratio can be explained by the results of Jaggi et al. (1989) and Tao et al. (1989) concerning a phase transition at a critical electric field.

EXPERIMENT

The objective of the experimental portion of this investigation was to determine the attenuation effect that an ER fluid has on the longitudinal vibration in a flexible structure. The geometry of the test structure is shown in Figure 2. The internal components of the ER test module consist of the ER fluid and the electric field device. The electric field device contains 190 electrodes made of copper disks. The electric field is contained within a 5mm gap between the electrodes. The test module consisted of a cylinder approximately 150 cm in length and a diameter of 7.5 cm. The electric field device was approximately 95 cm long. The diameter of the copper electrodes was 3.125 cm. This provided a gap between the inner wall of the flexible cylinder and the edge of the electrode of 2.1875 cm. It is this annulus of zero state ER fluid moving parallel and over the electrically driven ER fluid along the center line which dissipates the vibration in the flexible cylinder.

This investigation was conducted using a corn starch and mineral oil fluid mixture. The fluid was prepared in the following manner:

(1) The mineral oil was filtered to remove foreign particles (40 mesh filter).

(2) The corn starch had a water content of approximately two percent.

(3) The corn starch was added with a measuring (1 cup) cup.

(4) The starch was packed by lightly tapping the cup on the table.

(5) The starch was sifted into mineral oil (50% by volume).

(6) The starch was blended into mineral oil with electric mixer (132 ml quantities, total of 8 liters).

(7) The mixture was degassed in a vacuum chamber.

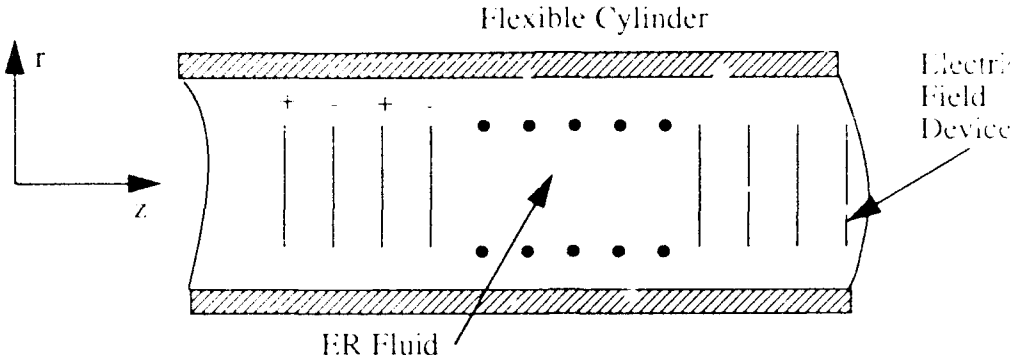

Figure 2. Electrorheological Test Module

The experimental apparatus consisted of the ER test module attached to an electrohydraulic shaker and tensioned to a force of approximately 445 N. The instrumentation included a force transducer and accelerometer at both ends of the ER test module as shown in Figure 3.

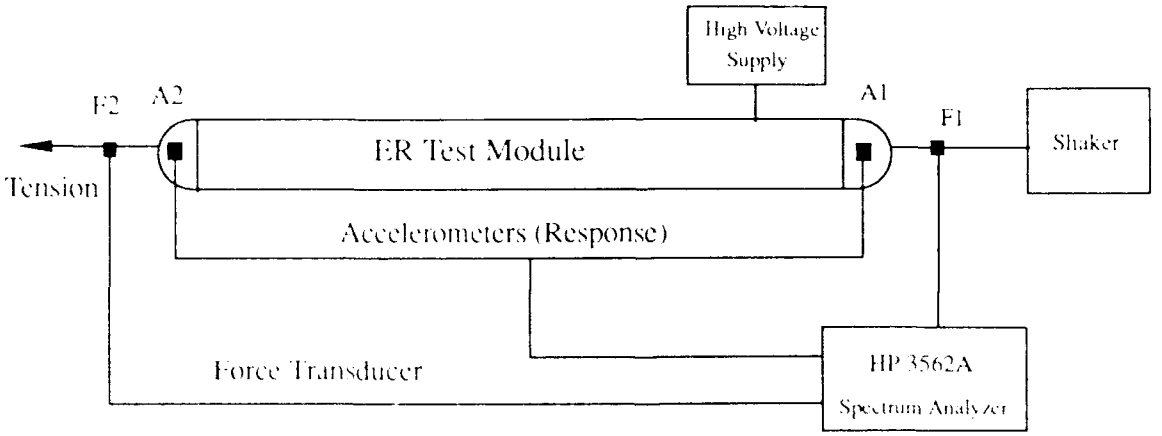

Figure 3. Configuratiuon of the Experiment

The experiments were conducted by exciting the ER test module in the axial direction with a swept sine (1 - 300 Hz) input. The data (average of three samples) was recorded in the form of frequency response functions. The use of a frequency response function is preferred since the results can be applied to predict the response of the structure to other excitation functions. The recorded frequency response functions included the ratios of the aft

acceleration to the forward acceleration, the forward force to the forward acceleration and the forward force to the aft acceleration. The data used in this paper focuses on the frequency response function of the acceleration ratio. The experiments were conducted at electric field strengths of 0.0, 0.4, 0.8, 1.2, and 1.6 kV/mm dc. This set of data was generated when the fluid was one day old. These experiments were conducted at each value of the electric field twice. The repeatability at each value of the electric field was excellent, within ±0.2dB; however, the same experiment was executed twenty four days later which generated values that differed by forty percent over the first set of experimental results. This extreme variance highlights the need for a fluid possessing a longer shelf life.

Figures 4-7 illustrate the data acquired during the first set of experiments. These figures represent the frequency response functions calculated from the ratio of the aft acceleration to the forward acceleration. The abscissa represents frequency in the units of cycles/sec (Hz). The ordinate represents the magnitude of the acceleration ratio (transmissibility) expressed in decibels (dB). Figures 4, 5, and 6 show the damping contribution of the ER fluid at 0.4, 0.8, and 1.2 kV/mm respectively. The resonant peak in these plots has been reduced without a noticeable shift in the resonant frequency. The resonant frequency may have been shifted to the right in Figures 4 - 6, but due to the resolution of the data over the given frequency range, the effect was not evident. A series of zoom measurements will be made to explore the possibility of a shift in resonant frequency at these electric field strengths. At an electric field of 1.6 kV/mm, Figure 7, the magnitude of the resonant peak as well as the resonant frequency decreased due to the ER fluid effect. From the comparison of this data there appears to be a change in the damping mechanism when the electric field is increased between 1.2kV/mm to 1.6kV/mm. This will be discussed in terms of the system damping properties in the next section.

QUANTITATIVE RESULTS

The magnitude of damping provided by the ER fluid has been quantified by the calculation of the system amplitude ratio (AR) and the logarithmic decrement (δ). These quantities depend on the calculation of the system damping ratio (ξ). The system damping ratio can be calculated from experimental data by three methods, as shown in Steidel (1979) and Nashif et al. (1985). These methods are by the half power points, the shift in frequency and from the phase angle.

The half power point method provides a good approximation to the system damping for damping values less than 0.1. Since the system damping in this case is greater than 0.1, the half power point method will generate erroneous results for the system damping coefficient at the higher electric field values. Another technique to calculate the system damping ratio from the experimental data is to use the shift in natural frequency of the damped system. The damped natural frequency will be lower than that of the undamped natural frequency. The relationship between the damped natural frequency and the undamped natural frequency is given by the following equation from Steidel (1979):

$$\xi = \sqrt{1 - \left(\frac{\omega_d}{\omega_n}\right)^2} \qquad (1)$$

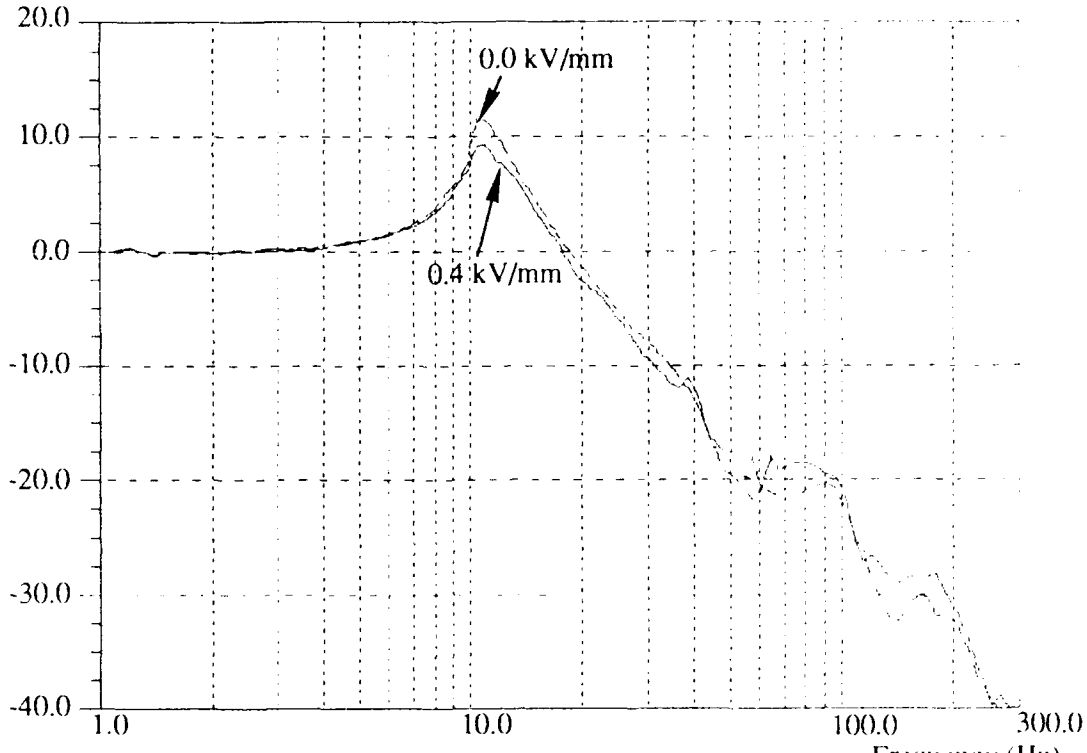

Figure 4. Magnitude of Acceleration Ratio in dB

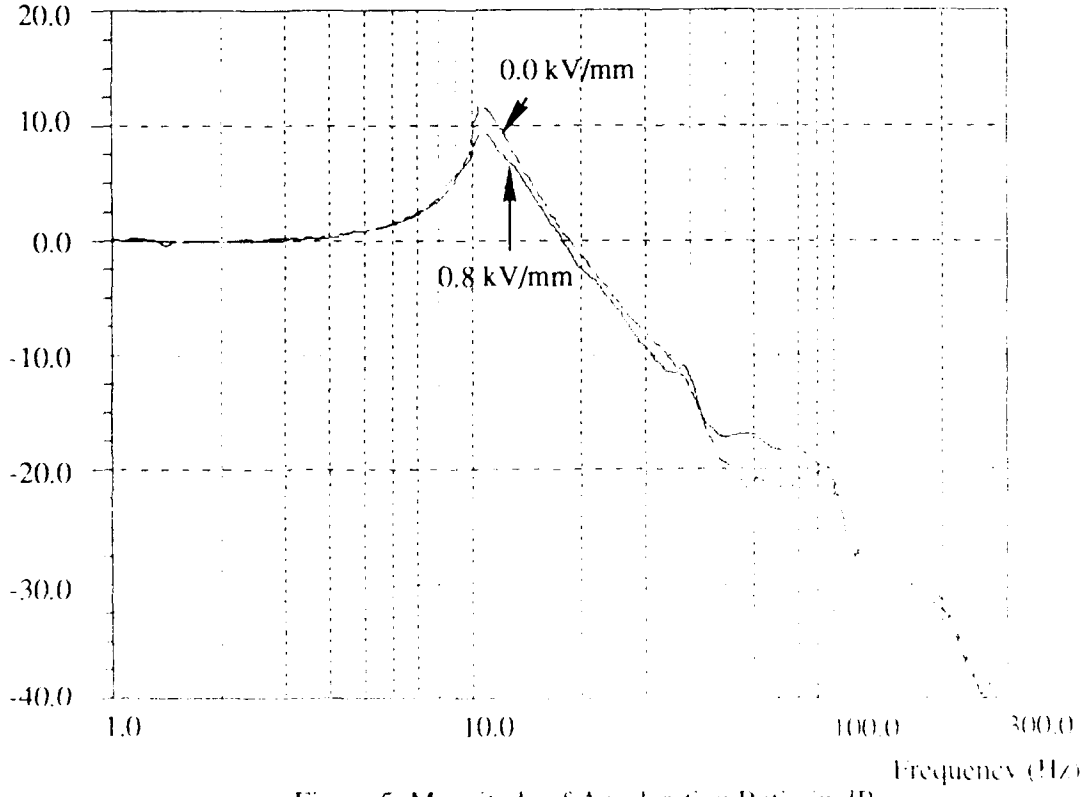

Figure 5. Magnitude of Acceleration Ratio in dB

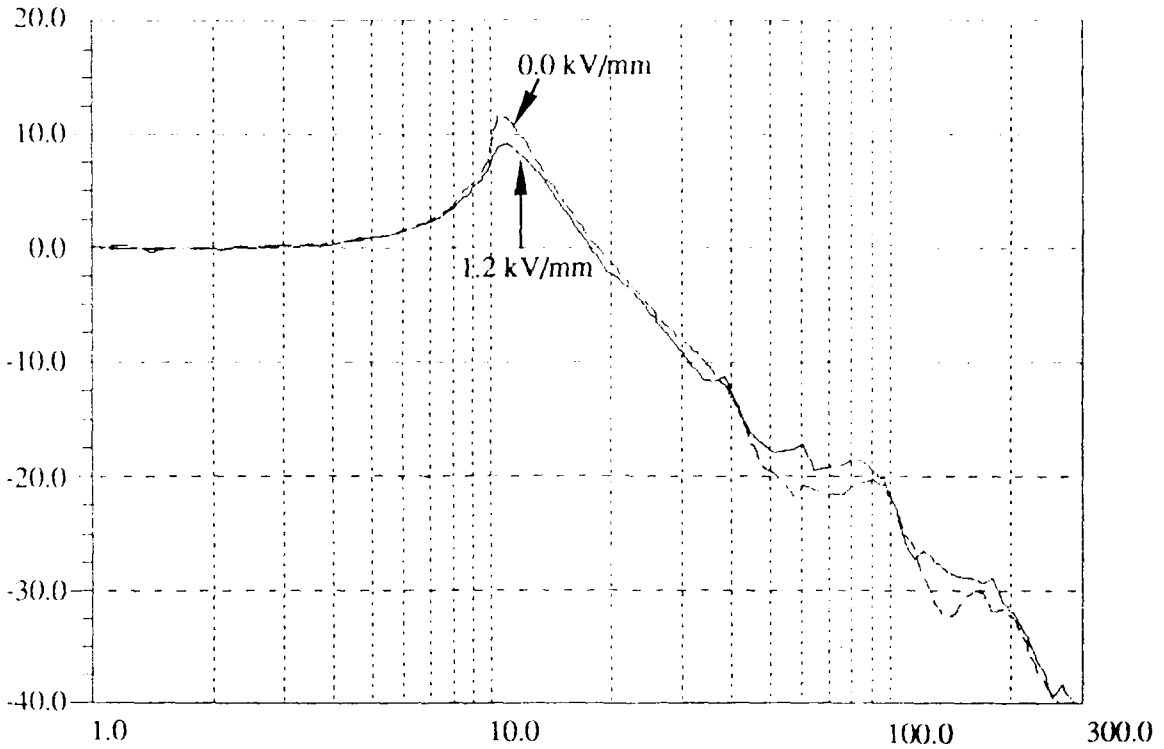

Figure 6. Magnitude of Acceleration Ratio in dB

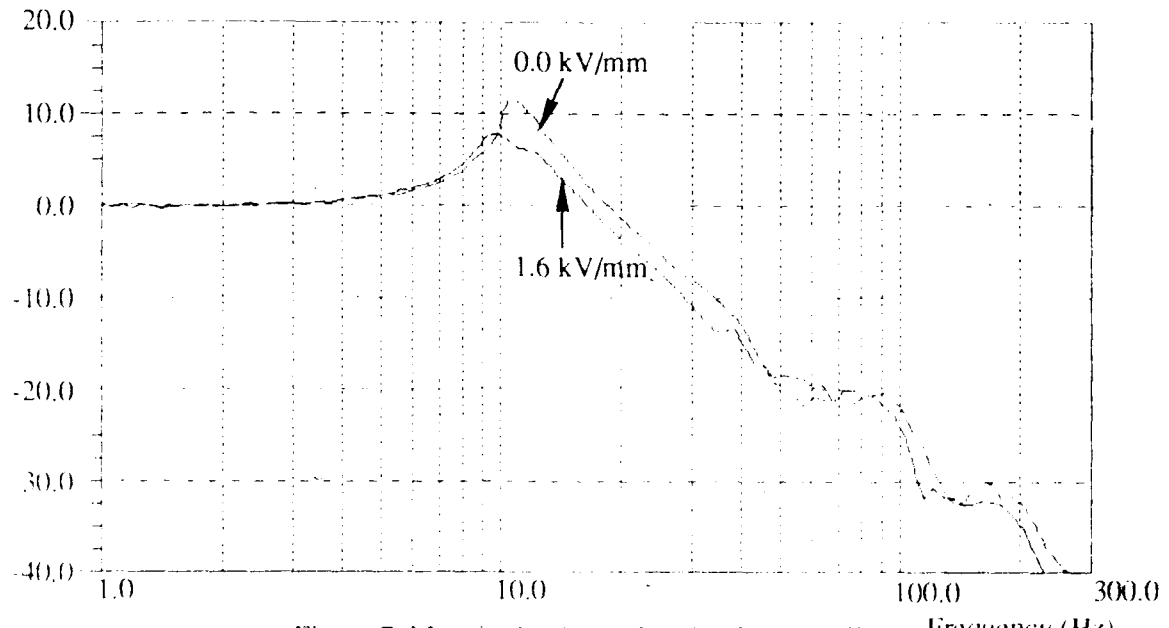

Figure 7. Magnitude of Acceleration Ratio in dB

This method was useful on the 1.6kV/mm data only since the data resolution of the other resonant frequencies did not show this shift in frequency.

The phase angle information generated can be used to estimate the damping characteristics of the system with respect to the applied electric field. If the structure contained no damping then the phase angle would be zero for all frequencies up to the resonant frequency. At the resonant frequency the phase angle would instantaneously increase to π radians and remain at this value for all frequencies (Figure 8).

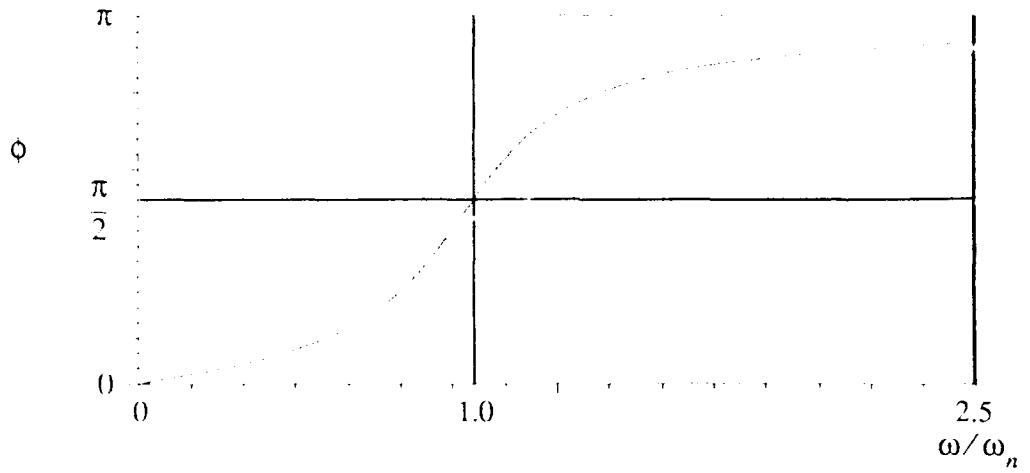

Figure 8. A Phase Angle vs Frequency Ratio Plot

The phase angle has a value between zero and π radians when damping is present in the structure. The phase angle is to equal $\pi/2$ radians at the resonant frequency. For a given value of the phase angle at a given frequency, the system damping ratio can be calculated from the following equation in Steidel (1979):

$$\xi = \frac{(\omega^2 - \omega_n^2)}{2\omega\omega_n} \tan\phi \qquad (2)$$

This expression provides a relationship between phase and frequency as a comparison of the system damping. This method is used in the calculation of the system damping ratio to represent the effect of the electric field on the ER fluid. The phase angle method is the most accurate for the given data set.

The result of the system damping ratio calculation by the phase angle method is shown in Figure 9. This figure shows the increase in the damping effect as a function of the electric field and frequency. The entries in Table I are the system damping ratios normalized by the zero state result. This normalization was performed to illustrate the effect that the electric field has on the system damping ratio. The system damping ratio values in Table I are reported at the natural frequency of 10.366 Hz

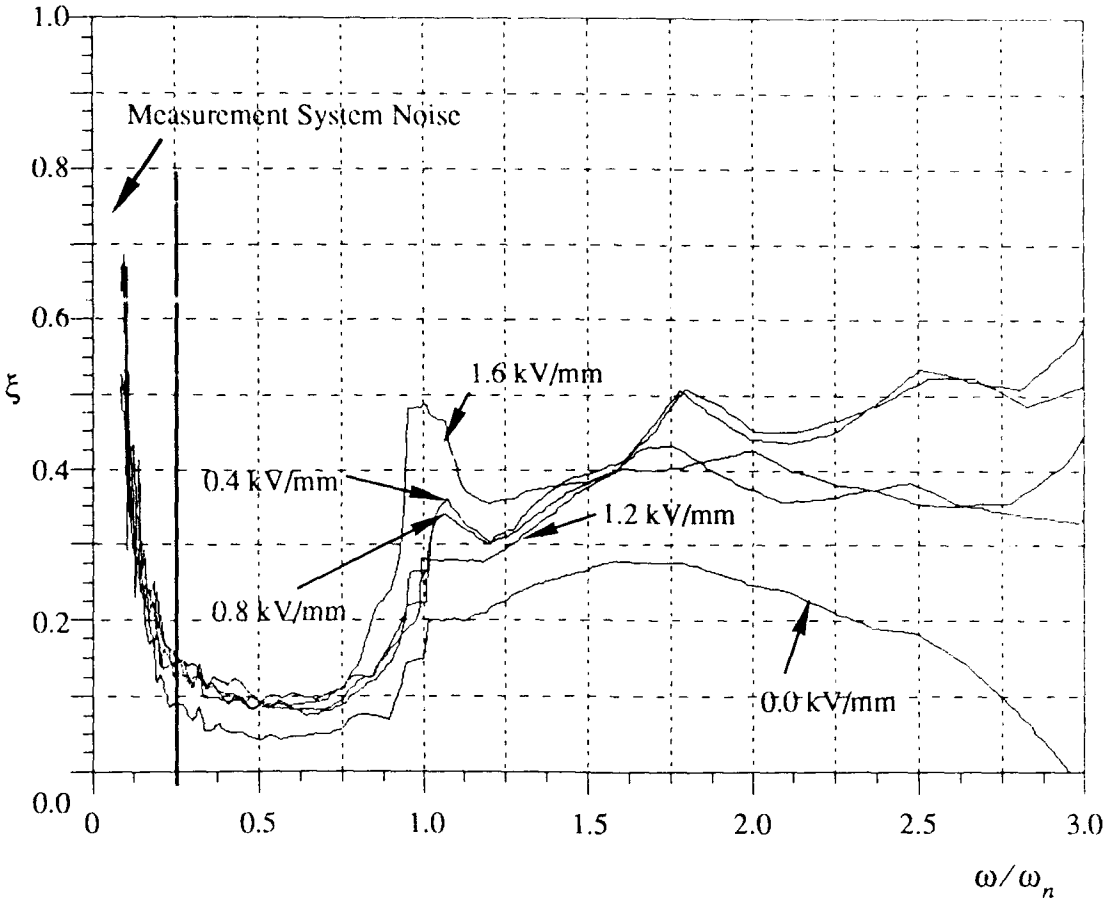

Figure 9. Damping Ratio vs. Frequency Ratio

Table I. System Damping Ratios (ξ)

Electric Field Strength	Phase Angle	Shift in Frequency
1.6 kV/mm	3.575	2.299
1.2 kV/mm	1.089	-
0.8 kv/mm	1.175	-
0.4 kV/mm	0.939	-
0.0 kV/mm	1.0	1.0

KEY RESULTS

The results of this analysis will be represented in terms of the amplitude ratio and the logarithmic decrement. The amplitude ratio provides a relative comparison of the damping effect on the system due to the applied electric field. The amplitude ratio derived for a viscous damped, single degree of freedom system excited by a harmonic forcing function can be found in Steidel (1979) as:

$$AR = \frac{1}{\sqrt{\left[1-\left(\frac{\omega}{\omega_n}\right)^2\right]^2+\left[2\xi\left(\frac{\omega}{\omega_n}\right)\right]^2}} \qquad (3)$$

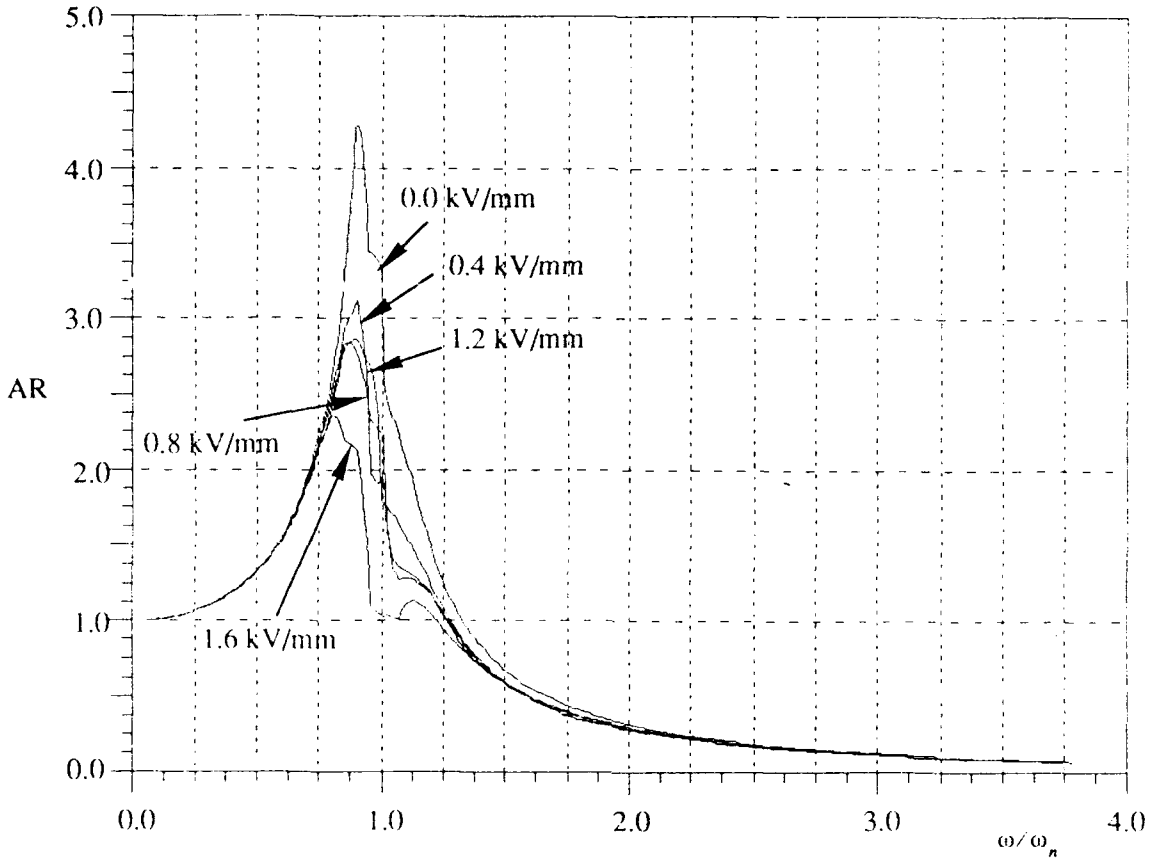

Figure 10. Amplitude Ratio vs. Frequency Ratio

By comparing the reduction of the amplitude ratio (Figure 10) at 1.6kV/mm to the zero state, an attenuation of approximately 4.0 dB is realized. The shift in the resonant frequency is also evident for the 1.6kV/mm case.

An additional measure of the system damping capacity of the ER fluid is the logarithmic decrement. The logarithmic decrement provides a measure of the amplitude reduction from cycle to cycle. This reduction in amplitude is of the form, $X_n = X_0 e^{-\delta_n}$. The logarithmic decrement is defined in Steidel (1979) as:

$$\delta = \frac{2\pi(\xi)}{\sqrt{1-\xi^2}} \tag{4}$$

The values of the logarithmic decrement calculated from equation (4) are listed in Table II. These calculations were made at the damped natural frequency, which corresponded to the particular case using the phase angle calculation for the system damping ratio.

Table II. Logarithmic Decrement

Electric Field Strength	Logarithmic Decrement
1.6 kV/mm	3.454
1.2 kV/mm	0.989
0.8 kV/mm	1.070
0.4 kV/mm	0.850
0.0 kV/mm	0.906

For comparison, the logarithmic decrement of a new automobile shock absorber is approximately 4 (Steidel (1979)). From the results in Table II, in general, system damping improves as the electric field is increased from the zero state to the value of 1.2 kV/mm. The effect of the electric field is not strong in this electric field range. When the electric field was increased to 1.6 kV/mm the logarithmic decrement dramatically increased by a factor of three. This dramatic increase in the system damping ability indicates a physical change in the damping mechanism of the structure.

CONCLUSIONS

A result of this analysis is that the vibrational input was attenuated by 4.0 dB through the use of an ER fluid. This value of attenuation is low when compared to the results of other applications (Stanway et al. (1987), Stevens et al. (1984) and Margolis and Vahdati (1989)). The results of this application depend on the relative shearing between the ER fluid along the flexible boundary and the center where the ER fluid is driven by the electric field. The zero state viscosity of the corn starch/mineral oil mixture was high (209 centipoise). A less viscid zero state fluid would provide better results in this application by producing a larger gradient between the electric field driven fluid and the outer fluid. A silicone oil based fluid (50 centipoise) will be utilized for future experimentation to prove this statement.

A secondary result, but the most interesting, is what happened inside the ER test module when the electric field increased from 1.2kV/mm to 1.6kV/mm. The quantification of the transition was attempted by taking data at smaller increments of electric field (0.1 kv/mm); however, the fluid was found to be past its usable life. A possible explanation to describe the damping mechanism could be made based on the critical electric field theory of Jaggi et al . (1989) and Tao et al. (1989). The work of Jaggi (1989) and Tao (1989) predicts a critical electric field where the onset of a phase transition in the ER fluid occurs. With the existence of a phase transition electric field, the ER fluid in the test structure would not have become a 'solid' at the electric fields below 1.2kV/mm. Since the zero state viscosity of the ER fluid was high, the difference in phase state between the fluid regions may not have been sufficient to produce an interface where the shear dissipation was to occur. At the electric field of 1.6kV/mm (or between 1.2 and 1.6kV/mm), the ER fluid driven by the field became 'solid'; thus, developing the shear interface between the fluid regions.

This will be experimentally verified in the near future by reproducing Jaggi's experiment with the fluid used in this investigation.

ACKNOWLEDGEMENTS

The author would like to thank Mr. Vinson Go, Mr. Scott Patton, and Mr. Ralph Greene for assistance and guidance in the development of the fluid, electrical application and the fabrication of the ER Test Module. I would also like to thank Mr. Greg Simonds and Mr. Matt Thompkins for their assistance with the vibration shaker tests. Finally, thanks to Mr. Kent Kasper for his assistance with the entire project but mostly the arduous task of data reduction.

REFERENCES

Coulter, J. P., Duclos, T. G., and Acker, D. N., "The Usage of Electrorheological Materials in Viscoelastic Layer Damping Applications", Proceedings of *Damping'89*, CAA1-CAA17 (1989).

Duclos, T. G., "Design of Devices Using Electrorheological Fluids", Society of Automotive Engineers Technical Paper 881134, Warrendale, Pennsylvania, (1988).

Jaggi, N. K., Woestman, J. T., and Tao, R., "Possible Phase Transition in Electrorheological Fluids", Proceedings of the *Second International Conference on ER Fluids*, 53-62 (1989).

Margolis, D. L., and Vahdati, N., "The Control of Damping in Distributed Systems Using ER Fluids", Proceedings of the *Second International Conference on ER Fluids*, 326-348 (1989).

Nashif, A. D., Jones, D. I. G., and Henderson, J. P., Vibration Damping, J. Wiley & Sons, (1985).

Stanway, R., Sproston, J. L. and Stevens, N. G., "Non-linear Modelling of an Electrorheological Vibration Damper", J. of Electrostatics, **20**, 167-184 (1987).

Steidel, R. F., Jr., Mechanical Vibrations, J. Wiley & Sons, 212-216 (1979).

Stevens, N. G., Sproston, J. L. and Stanway, R., "Experimental Evaluation of a Simple Electroviscous Damper", J. of Electrostatics, **15**, 275-283 (1984).

Tao, R., Woestman, J. T. and Jaggi, N. K. , "Electric Field Induced Solidification", Appl. Phys. Lett., **55**, 1844-1846 (1989).

MODELLING OF NONLINEAR DILATATION RESPONSE OF FLUIDS CONTAINING COLUMNS-Plastic and Shear Relaxation Considered

Bernd Wendlandt*
Department of Defence, Materials Research
Laboratory, DSTO, PO Box 50, Ascot Vale,
Victoria 3032, Australia

Abstract

The non-linear wave equation governing the propagation and scatter of dilatation waves in discontinuous media is presented and its Eulerian numerical analogue is used to study scatter of acoustic dilatation waves by columns and ducts in elastic and visco-elastic fluids. Plastic and visco-elastic relaxation mechanisms are considered. The spectral form of the wave equation is developed and used to discuss dispersion. Selected applications of the numerical analogue to simulation of scatter, propagation and echo attenuation are presented.

INTRODUCTION

A second order, partially implicit and alternating direction Eulerian numerical approximation to the parabolic, first order non-linear wave equation is used to compute scatter of dilatations from inhomogeneities in material moduli and density. Spectral analysis is used to discuss the dispersive effect material inhomogeneities have on travelling dilatational waves. The usefulness of the scheme is illustrated by simulating the propagation of a Gaussian shaped dilatational pulse around an elbow in a duct immersed and radially out of a cylinder in an elastic fluid and by computing the scatter of dilatations from air columns in elastic fluids. Finally, the reflection of dilatations from a row of double and single wedge shaped air columns in a fictitious plastic-visco-elastic medium backed by a layer of air is calculated. The scheme considers plastic relaxation and visco-elastic relaxation due to compression and shear.

MODEL

The propagation of acoustic waves is governed by the laws of conservation of momentum and mass, and equation of state which relates the stress in a medium to the associated strain through material properties. The Hookean-Kelvin model [1] provides the simplest relationship between strain and stress, which, when applied to compression and shear separately, yields a stress-strain

*5 Cumberland Ct, Annapolis, MD 21401, Telephone: (301) 267 6653.

relationship which reflects observed plastic relaxation and visco-elastic relaxation in dilatation and shear. This relationship can be written as

$$\sigma_{ij} + \beta_\sigma \frac{\partial \sigma_{ij}}{\partial t} = \lambda \left(1 + \beta_\lambda \frac{\partial}{\partial t}\right) \epsilon_{mm} \delta_{ij} + 2\mu \left(1 + \beta_\mu \frac{\partial}{\partial t}\right) \epsilon_{ij} \qquad (1)$$

where σ_{ij} is the stress tensor and ϵ_{ij} is the strain tensor. Material properties are described by λ,the first Lamé constant, and μ, the modulus of rigidity. The plastic and visco-elastic relaxation times of the material for direct and shear strains are β_σ, β_λ and β_μ respectively. The strain tensor is related to the displacement tensor u_i for small displacements by the linear expression $\epsilon_{ij} = (u_{i,j} + u_{j,i})/2$, where $u_{i,j}$ represents differentiation of tensor u_i with respect to displacement tensor x_j. This strain-displacement relationship provides an adequate description for material response to excitations when the strain is less than ab ·ut 10%. Strain can vary rapidly with respect to ·distance at material interfaces [2], particularly when the acoustic or vibrational impedance varies significantly across the interface. The strain at the interface of materials with disparate acoustic impedances is more accurately modelled by the parabolic, or first order non-linear, approximation to the strain [3] and [4], which can be expressed as $\epsilon_{ij} = (u_{i,j} + u_{j,i} + u_{k,i} u_{k,j})/2$. Incorporation of this non-linear strain into Equation 1, enables the Hookean-Kelvin stress-strain constitutive equation to accurately model material responses for strain values up to 30%, [3]. In this approximation, σ_{ij} is known as the 2nd Piola-Kirchhoff stress tensor and ϵ_{ij} is known as the Green-Lagrangian strain tensor [3]. A linearized expression for the non-linear strain can be obtained from a first order extension of Taylor expansion definition of the strain-displacement definition [5] which yields

$$\epsilon_{ij} \approx \frac{1}{2}\{u_{i,j} + u_{j,i} + \frac{\partial(u_{i,j} + u_{j,i})}{\partial x_j} \delta x_j\} \qquad (2)$$

When this expression for the strain is substituted into Equation 1, a second order approximation in u to the non-linear constitutive law is obtained.

When $\lambda \gg \mu$ the propagation of an acoustic excitation in the medium may be described by the dilatation , Θ . Dilatation is defined by the divergence of the incremental displacement of the strain. In regions where the medium is uniform, the dilatation Θ is related to the pressure by $p = -\rho c^2 \Theta$, where ρ is the density and c is the speed of sound characterizing the medium. The propagation of the dilatation can be described by a wave equation derived from divergence of the law of conservation of momentum, $\rho \frac{\partial^2 u}{\partial t^2} = \frac{\partial \sigma_{ij}}{\partial x_j}$, and mass, $\frac{\partial \rho}{\partial t} = -\rho \frac{\partial \Theta}{\partial t}$, and combined with the above approximation to the non-linear constitutive law, Equation 1 and the non-linear strain Equation 2. This non-linear wave equation can be expressed, approximately, as

$$\rho \frac{\partial^2 \Theta}{\partial t^2} \approx \nabla^2\{(\lambda^* + < \mu^* >)(\Theta + \nabla\Theta \cdot \delta\vec{x})\} + \nabla \cdot (< \mu^* > \nabla\{\Theta + \nabla\Theta \cdot \delta\vec{x}\}) + Q_s \quad (3)$$

where $\lambda^* = \lambda(1 + \{\beta_\lambda - \beta_\sigma\}\frac{\partial}{\partial t})$ and $\mu^* = \mu(1 + \{\beta_\mu - \beta_\sigma\}\frac{\partial}{\partial t})$, and $\delta\vec{x}$ is an increment of expansion of the position vector of the spatial location (x, y, z). The density, ρ at position (x, y, z) and time t is related to the initial, unperturbed

density ρ_0 from the law of conservation of mass by $\rho \approx \rho_0(1 - \Theta + \Theta^2)$, to second order in Θ, which is assumed to be zero at time $t = 0$. The $< \mu^* >$ represents the average value of μ^* over a small volume of computational cell of the numerical analogue of Equation 3. This approximation is justified through the integral form of the divergence theorem [1].

The Q_s describes the scatter of dilatation waves by material inhomogeneities and can be written as

$$Q_s \approx -\frac{\nabla\rho}{\rho} \cdot [\nabla(\lambda^* + < \mu^* >)(\Theta + \nabla\Theta \cdot \delta\vec{x}) + < \mu^* > \nabla(\Theta + \nabla\Theta \cdot \delta\vec{x})] \quad (4)$$

The Q_s is a source term for the generation of dilatation wavelets at material discontinuities [1]. Shear losses dominate when $\mu\beta_\mu \frac{\partial}{\partial t} \gg \lambda\beta_\lambda \frac{\partial}{\partial t}$.

The non-linear wave equation, Equation 3, is dispersive and a spectral analysis [6] of Equation 3 shows that as dilatational waves interact with and are scattered by material inhomogeneities they may change their nature from travelling to damped and vice versa. If the dilatation wave, Θ is represented in complex formulation, where $\imath = \sqrt{-1}$, by

$$\Theta = \Theta_0 \exp \imath(\vec{k} \cdot \vec{x} - \omega t) \quad (5)$$

where $\vec{k}$ is the momentum vector, Θ_0 is the amplitude and ω the angular frequency of the wave, the spectrum form of Equation 3 may be written as the quadratic expression $ak^2 - \imath bk - c \approx 0$. The spectrum relation [6] for the momentum vector k is then in terms of material properties and angular frequency given by

$$k(\omega) \approx \pm\frac{\sqrt{4ac + b^2}}{2a} + \imath\frac{b}{2a} \quad (6)$$

where the coefficients

$$a = \lambda_\omega + 2 < \mu >_\omega + (2\nabla[\lambda_\omega + < \mu >_\omega] + \nabla < \mu >_\omega - \frac{\nabla\rho}{\rho}[\lambda_\omega + 2 < \mu >_\omega])\hat{k} \cdot \delta\vec{x} \quad (7)$$

and

$$b \approx \left[2\nabla(\lambda_\omega + < \mu >_\omega) + \nabla < \mu >_\omega - (\lambda_\omega + 2 < \mu >_\omega)\frac{\nabla\rho}{\rho}\right] \cdot \hat{k} +$$

$$\left[\nabla^2(\lambda_\omega + < \mu >_\omega) - \frac{\nabla\rho}{\rho} \cdot \nabla(\lambda_\omega + < \mu >_\omega)\right] \hat{k} \cdot \delta\vec{x} \quad (8)$$

and

$$c = \rho\omega^2 + \nabla^2(\lambda_\omega + < \mu >_\omega) - \frac{\nabla\rho}{\rho} \cdot \nabla(\lambda_\omega + < \mu >_\omega) \quad (9)$$

Here the Lamé operators convert in frequency space to the complex parameters $\lambda_\omega = \lambda(1 + \imath\omega[\beta_\lambda - \beta_\mu])$ and $\mu_\omega = \mu(1 + \imath\omega[\beta_\mu - \beta_\mu])$. The terms $\hat{k}$ denote unit vectors of $\vec{k}$.

Inspection of the exponential representation of Θ for a wave, Equation 5, shows that Θ is a travelling wave when $\vec{k}$ is real and is damped, or decays as $\exp -\vec{\kappa} \cdot \vec{x}$, when $\vec{k}$ is complex and $\vec{\kappa}$ represents the imaginary component of $\vec{k}$.

Equation 6 has at least one complex root for $\vec{k}$, even when plasticity and viscous effects are ignored, if the material properties are inhomogeneous and $b \neq 0$. Thus travelling waves may be damped, or decay exponentially, in elastic inhomogeneous materials. Waves whose frequencies, and direction of propagation relative to material interfaces, make $b^2 > 4ac$ are completely damped and do not propagate.

NUMERICAL ANALOGUE OF WAVE EQUATION

Equation 3 assumes that the material parameters are differentiable with respect to spatial coordinates. Their use in discontinuous media may require special consideration of boundary conditions to avoid any smearing of material interfaces. However, very acceptable solution schemes for wave equations have been obtained, [7] and [2], which do not require special treatment of boundary conditions and linear approximations in Θ are able to trace the propagation of acoustic Gaussian pulses and wave- packets through water-elastomer-air-elastomer-steel-water sandwiches to an accuracy of 95 to 98 %, Figure 1 and 2 which show superimposed snapshots of Gaussian pulses reflected and transmitted across interfaces. As the problems computed are one dimensional the more familiar particle displacement rather than dilatation is shown. However,

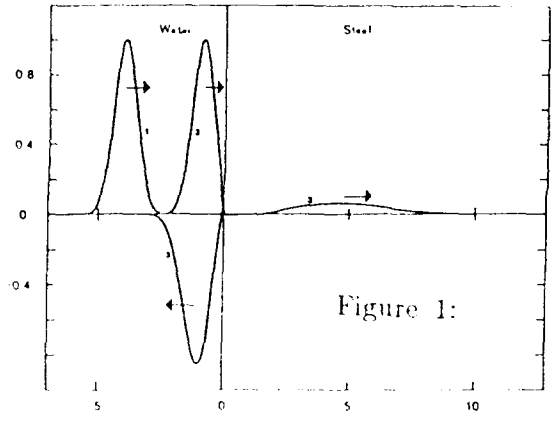

Figure 1: Snapshot of Gaussian pulse reflected and transmitted at water/steel interface

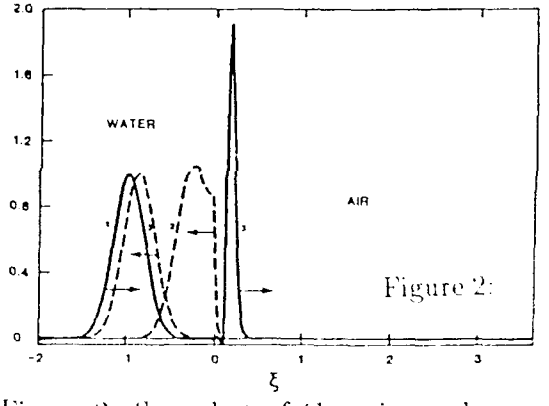

Figure 2: Snapshot of Gaussian pulse reflected and transmitted at air/water interface

close inspection of the displacement variations at the material interfaces indicates that the waves are not very well approximated at the interface, although accurately away from the interface. This ability of the linear wave equation to model reflection and refraction from material interfaces accurately, without yielding accurate values of the functional at the interface is well known [7]. The distortions shown in Figures 1 and 2 indicate that strain variations across interfaces may be greater than 10% and that a non-linear form of the wave equation, which permits dilation to be approximated by a parabolic expression, is appropriate for accurate approximation to dilatations at the material interfaces. Accurate modelling of dilatations at interfaces is important in understanding composite material delamination under vibrational loading [8].

Using second order, centered differences for the derivatives of Equation 3

a numerical analogue was written in an explicit-implicit formulation [9], which can readily be integrated using the unconditionally stable alternating direction technique, ADI [10]. The ADI time steps the analogue equation to Equation 3 implicitly, first along one space dimension , leaving all terms involving differentiation along the other space dimension and the non-linear terms at the previous time level temporarily to provide an interim approximation to Θ. This process is repeated along the other space dimension, and Θ in the non- linear terms assume the value of the interim approximation to Θ. An updated value for Θ is considered to have been obtained after the completion of this second step [10].

CASE STUDIES

To illustrate the usefulness of Equation 3, and the resulting finite difference scheme, three case studies were carried out. First the scheme was used to simulate the propagation of a Gaussian shaped dilatation pulse see Figure 3, around a curved duct immersed in water and of acoustic impedance equal to

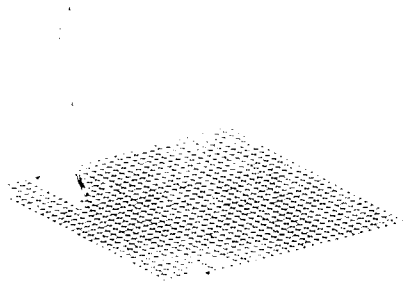

Figure 3: Initial Gaussian profile of pulse launched down duct.

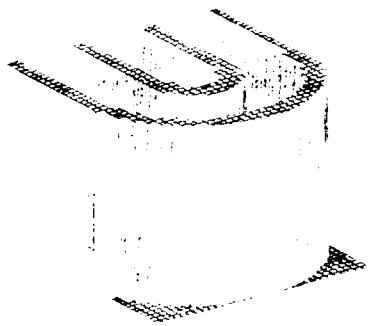

Figure 4: Density cross-section of duct elbow/water background

that of water. For ease of simulation, the density of the duct, see Figure 4

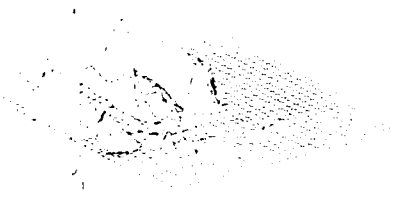

Figure 5: Snapshot of Gaussian pulse scattered in duct

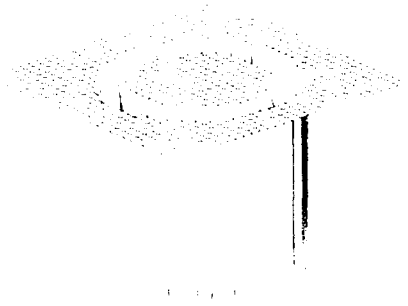

Figure 6: Speed of sound cross-section of cylinder/water background

. was taken to be four times that of water. The pulse was attenuated upon

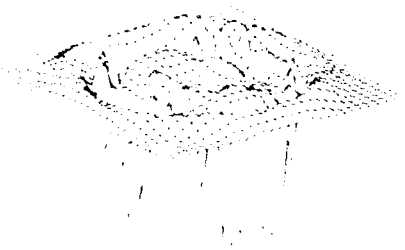

Figure 7: Snapshot of Gaussian pulse expanding through cylinder walls

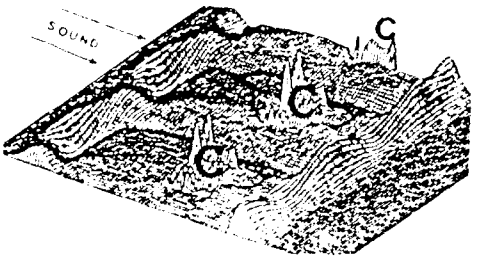

Figure 8: Snapshot of reflection and transmission of Gaussian shaped acoustic pulse by row of air filled square columns in water,pulse incident from upper left

scatter from the duct walls and very little is transmitted around the bend of the duct, see Figure 5. In the example displayed more dilatation is transmitted through the duct wall than around the duct bend at the time of the computation snapshot shown. This attenuation of the pulse is expected from the spectrum relation Equation 6. Second, the scheme was used to calculate the acoustic response of a cylinder immersed in water, and of material properties of the duct, see Figure 6, to a Gaussian pulse generated at time $t = 0$ along the axis of the cylinder. A snapshot of the radial expansion of the pulse and its penetration through and reflection from the cylinder wall is shown in Figure 7. As can be seen from Figure 7, the pulse radiates outward uniformly as expected and is partially reflected from the cylinder walls. The reflections are seen to be uneven, and rotate around the inside of the cylinder wall indicating that the reflections are not the first mode, or specular, reflections but are higher, circumferential modes. Thirdly, the scheme was used to calculate the acoustic

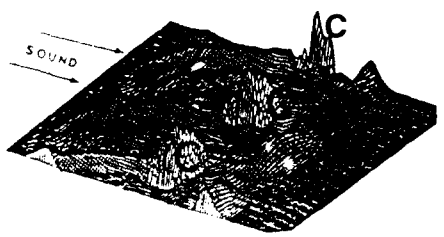

Figure 9: Snapshot of reflection and transmission of Gaussian shaped acoustic pulse by row of air filled cylindrical columns in water,pulse incident from upper left

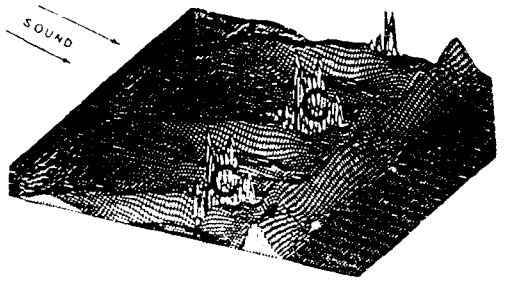

Figure 10: Snapshot of reflection and transmission of Gaussian shaped acoustic pulse by row of air filled square columns in water,pulse incident from upper left

response of rectangular, cylindrical and double wedge air columns in water to Gaussian and five wavelength sinusoidal wave-packets. To indicate a practical use of this scheme, the acoustic echo of an elastomer layer, filled with air columns and backed by air, was calculated, assuming $\lambda \gg \mu$.

The acoustic responses of the cavities to a Gaussian shaped wave-packet, are shown in scalar, or modulus, form of the dilatation in Figures 8 - 10. The Gaussian pulse is incident from the left in the figures and the time snapshots show the column responses when the pulse has passed the row of air filled cavities, C. The figures show a reflected component moving to the left and the part of the pulse not affected by the cavity to the right. A component which has been slowed at the surface of the cavities through surface relaxation is trailing the main portion of the pulse as expected from surface wave theory [1]. The rapid change in dilatation across the surface indicates that a parabolic

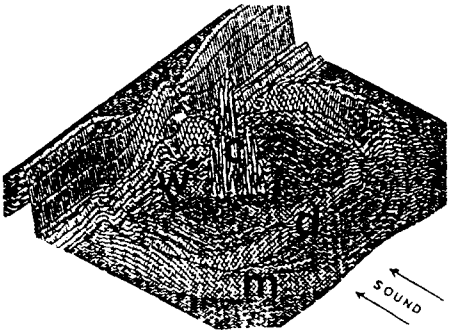

Figure 11: Snapshot of monopole, m , dipole, d, and wavelet, w, responses to Gaussian shaped acoustic pulse, incident from lower right, by air column

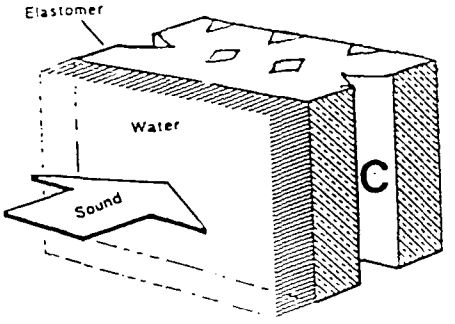

Figure 12: Layer of elastomer containing rows of double and single wedge air columns, basic cell used in computations is shown by dotted lines

approximation to the strain simulates the computed dilatation more accurately than the linear approximation.

The response of a single double wedge shaped air column in water to a Gaussian pulse is shown in Figure 11. The pulse is travelling from lower right to upper left and has passed the double wedge. The primary reflection has moved away from the air column and is followed by the dipole reflection. The corner at the back of the wedge generates a wavelet as is expected from Q_s and theory of surface waves [1]. The cylindrical radial symmetry of the reflections indicate, from consideration of Equation 3 in cylindrical co-ordinates and Equation 6, that sinusoidal waves will be reflected as a damped and a travelling wave.

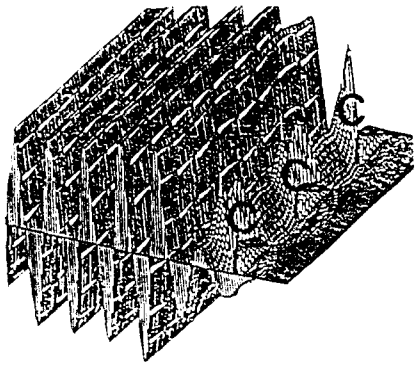

Figure 13: Snapshot of the beginning of the interaction of an acoustic excitation sinusoidal wavepacket with elastomer layer containing double and single wedge air columns

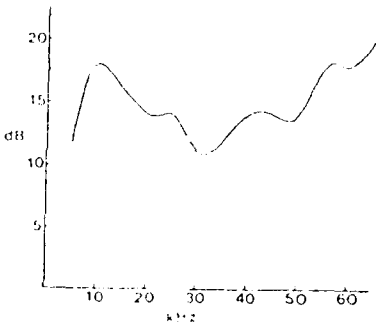

Figure 14: Echo attenuation of elastomer layer containing double and single wedge air columns

Acoustic echo calculations for a selected frequency band of a row of air filled wedges immersed in a fictitious elastomer layer loaded with water, Figure 12, are shown in Figure 13 and Figure 14. The shape, size and spacing of the double and single wedges were chosen to maximize the scatter of short wavelength waves into the coating, resonance absorption of medium wavelength waves in inter-wedge spaces and absorption of longer wavelengths around the cavities.

The reflection coefficient R, shown in Figure 14, was computed from the amplitude of the standing wave Θ_t generated in front of the layer and the amplitude of the incident wave Θ_i through $R = -20\log_{10}\{(\Theta_t - \Theta_i)/\Theta_i\}$.The material properties and layer parameters assumed in the calculations are shown in Table I.

Table I. MATERIAL PROPERTIES AND GEOMETRY OF ELASTOMER LAYER

Material	Density kg/m^3	Lamé constant kg/sm^2	Loss Tangent $\omega \quad \beta$
water	1000	2.25×10^6	0.0
air	1.29×10^{-3}	14.0	0.0
elastomer	1130	2.54×10^6	0.650
Thickness of layer	$0.050m$	Height of double wedge	$0.020m$
Width of wedge	$0.015m$	Separation of wedges	$0.015m$
ω	: angular	excitation frequency	

Analysis indicates that the echo reduction peak at $10kHz$ may be due to monopole resonance, or resonance of circumferential waves around the air column, and the small peak at $22kHz$ may be due to a dipole resonance of the

double wedge air column. The peak at $42kHz$ might be due to a resonance set up between the double wedge and the single wedge of the elastomer layer. The high echo reduction properties of the generic elastomer layer for frequencies greater than $50kHz$ may be attributed to scattering and absorption within the elastomer.

CONCLUSION

The non-linear wave-equation describing the propagation and scatter of a dilatation through piecewise continuous elastic and plastic-visco-elastic media has been presented. The wave-equation has been augmented by the corresponding spectral equation which is able to describe the attenuation and decomposition of travelling waves into damped and propagating components at material boundaries in inhomogeneous media. The numerical analogue is able to model non-linear wave/material interface and discontinuity interactions, and address problems of practical interest in noise engineering.

References

[1] A. Sommerfeld, Mechanics of Deformable Bodies,(Academic Press, New York, 1964).

[2] B. C. H. "The Acoustic Properties of Layered Coatings",MRL Report, MRL-R-1034,(DSTO, March 1988).

[3] R.S. Dunham et al. "Collapse of Various Shaped Cavities in a Pressurized Incompressible Material",ANA-89-0081, ANATECH Research Corp.,March 1989.

[4] J.L. Davis, Wave Propagation in Solid and Fluids,(Springer-Verlag, New York,1987).

[5] H.and B.S.Jeffreys, Mathematical Physics,(Cambridge University Press, Cambridge,1962).

[6] J. A. Doyle, Wave Propagation in Structures,(Springer-Verlag, New York,1988).

[7] D. L. Brown, " A Note on the Numerical Solution of the Wave Equation with Piecewise Smooth Coefficients", Math. Comp.,42, (166), 369-391 (April 1984).

[8] D.A.Sotiropoulus et al. "Quality Assessment of Composite Materials Through Dynamic Characterization",Proceedings COMPO-90,Patras,20-24 August 1990.

[9] R. D. Richtmyer and K. W. Morton, Difference Methods for Initial-Value Problems,(Interscience Publishers,New York,1967).

[10] P. Roache Computational Fluid Dynamics, (Hermosa Publishers, Albequerque,1982).

ELECTRO-RHEOLOGICAL FLUIDS CHARACTERISATION BY DYNAMIC MECHANICAL THERMAL ANALYSIS UNDER APPLIED FIELDS

Ray E. Wetton[1]
Polymer Laboratories Ltd.
Loughborough, United Kingdom

J. C. Duncan
Polymer Laboratories Ltd.
Loughborough, United Kingdom

Mike Connolly
PL Thermal Sciences Inc.
Amherst, MA

ABSTRACT

Electro-rheological fluids increase viscosity under high electric fields and are of great interest for variable mechanical torque transmission (electrical clutch) but of course have potential applications for variable controlled damping. The electro-viscous effect can be achieved in two different ways:

1. Structure build-up under electric field
2. Introducing a relaxation process of the same timescale of the motion to be coupled.

Mechanism (1) will be inherently mechanically non-linear/non Newtonian whilst (2) can in principle be linear visco-elastic.

The torsional rheometer head for the PL-DMTA has been used in this work in the oscillating mode with parallel plate geometry. The parallel plate configuration allows uniform high voltage to be applied across the sample during measurement of the visco-elastic characteristics. Cone and plate geometry does not allow application of a uniform electric field and has not been utilised in the present work. Type (1) and (2) systems have been studied as a function of temperature oscillation frequency and applied voltage. Results are reported in terms of a tan δ and shear dynamic shear moduli.

FULL PAPER NOT AVAILABLE FOR PUBLICATION

[1]Polymer Laboratories Ltd., The Technology Centre, Epinal Way, Loughborough LE11 OQ United Kingdom, 0509 233300

ON PIEZOELECTRIC ENERGY CONVERSION FOR ELECTRONIC PASSIVE DAMPING ENHANCEMENT

D. L. Edberg*
A. S. Bicos
McDonnell Douglas Space Systems Company
J. S. Fechter
McDonnell Douglas Electronic Systems Company

ABSTRACT

To meet their performance requirements, large orbiting space structures are expected to need both passive and active vibration suppression systems. Ideally these systems would replace structural members with members possessing both structural and dissipative properties.

The design and develcpment of concepts of enhanced-damping struts that employ the mechanical/electrical conversion properties of piezoelectric materials is presented. Rather than mechanically dissipating energy, the strain-induced mechanical vibration is converted to electrical energy which is shunted through a tuned electrical network. The networks use a shunted inductance which acts in concert with the inherent reactance of the piezoelectric material to maximize the current dissipated.

Because of the relatively low structural frequencies and large piezoelectric capacitance, inductances on the order of tens to hundreds of Henries are required. A means of using operational amplifiers to simulate the inductance is presented. This substitution eliminates the substantial dead weight of the inductance, and allows for fine-tuning and programming of the inductance to match variations in frequency. A means of adding damping for several frequencies is given. Finally, experimental results are presented.

*Senior Scientist, Advanced Structures and Materials, Dept. A3-Y857-13-3, 5301 Bolsa Avenue, Huntington Beach, California 92647. Tel: 1-714-896-5210

INTRODUCTION

Many types of spacecraft are expected to need shape control and structural vibration suppression systems to meet their performance requirements. Spacecraft operating conditions and on-board systems can induce unacceptable structural vibrations requiring many minutes to naturally dissipate. Systems require precise spatial positioning of their components, and such motion can result in the need to introduce some means of vibration dissipation to the structure. This dissipation can take the form of some passive damping mechanism, shape controls, an active vibration control system, or a combination of passive and active systems.

This investigation is concerned with the theoretical modelling and experimental implementation of piezoelectric struts in a generic truss structure. Our recent efforts in this area include struts currently under development using a composite material with embedded Lead Zirconate Titanate piezoelectric ceramic materials (PZTs). Using the piezoelectric effect, the embedded PZTs can act both as actuators and sensors for a shape or vibration control system. The actuators convert the electric field generated by an applied voltage into a mechanical strain, which may elongate or shorten the PZT. Conversely, the sensors convert mechanical strain due to motion into a voltage which may be used to monitor the structure's shape or vibration.

The piezoelectric struts were used to enhance the structure's dissipation. The PZT terminals were shunted with resistor or resistor/inductor networks [1,2], which dissipated the electrical voltage piezoelectrically generated by the structure's motion. Results of choosing the electric elements in the network to tune for a structure's natural frequency will be presented, and the means used to damp two modes simultaneously will be shown. A circuit consisting only of resistors, capacitors, and operational amplifiers simulating an inductance will be shown.

1. THE MDSSC CSI TRUSS

The MDSSC CSI (Control Structure Interaction) Truss has been assembled to serve as a testbed for a wide variety of CSI investigations, including various passive and active control technologies and their practical implementation. It consists of Meroform

aluminum and Plexiglass struts and steel nodes, and may consist of up to nineteen bays of rectangular trusswork with diagonal members. The Plexiglass struts may easily be moved to alter the structural frequencies, and any member may be replaced by piezoelectric active struts manufactured by MDSSC. The CSI truss is shown in Figure 1.

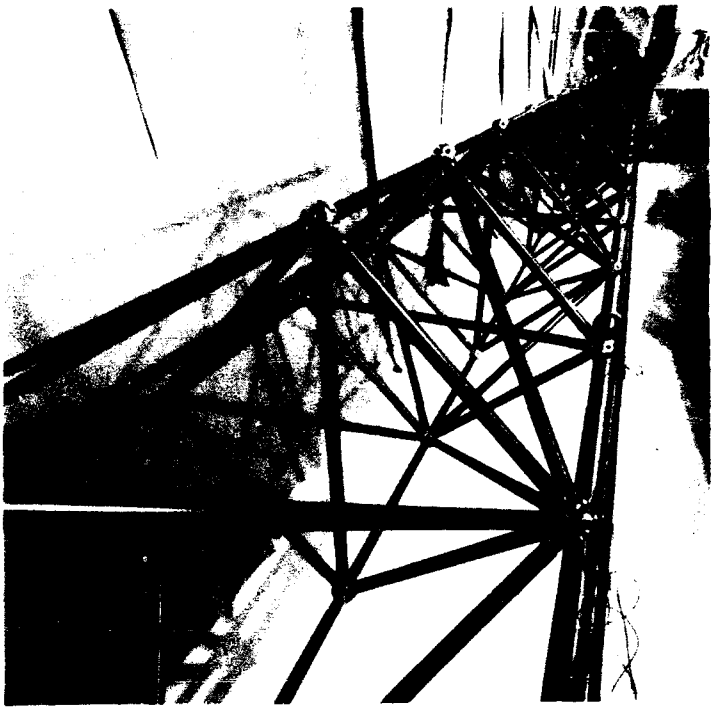

Figure 1. The MDSSC CSI Truss testbed.

The CSI truss is suspended by eight soft springs simulating a "free-free" support system. The spring supports provide pendulum modal frequencies less than 0.5 Hz for all six quasi-rigid body modes. As this is significantly lower than any of the structural mode frequencies, the suspension can be considered "zero stiffness" as far as coupling issues are concerned.

For passive and active control investigations, MDSSC fabricated a number of piezoelectric struts, each consisting of a number of lead zirconate titanate (PZT) hollow cylinder segments wrapped with a fiberglass/epoxy outer coating. The PZT segments were polarized so that an electric field applied between the outer radius and the inner radius created axial deformation. Mechanically, the segments were connected in series, and electrically all but one of the cylindrical rings were connected in parallel.

The remaining segment was electrically isolated so that it could be used independently as a strain rate sensor. Figure 2 shows the design of the MDSSC-fabricated piezoelectric struts. The design was modified from one used by researchers at MIT.

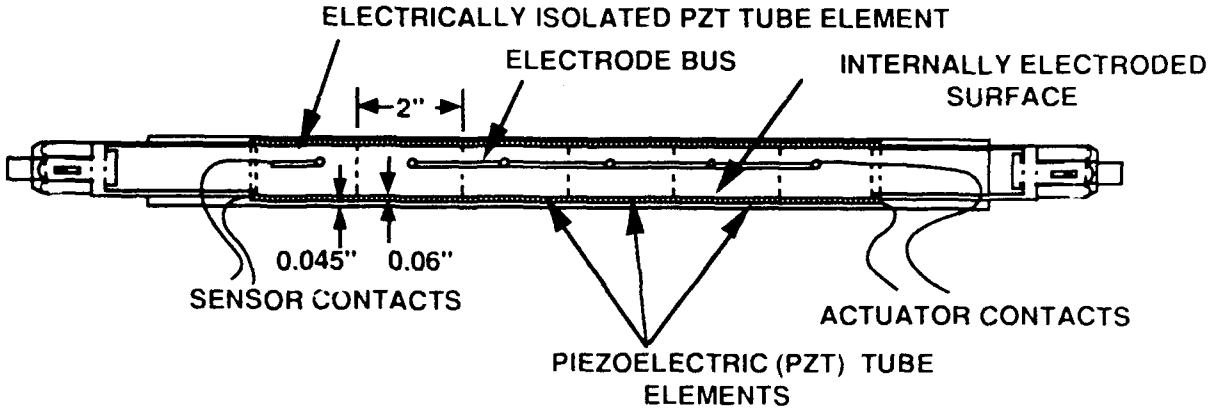

Figure 2. The MDSSC Piezoelectric Strut.

In this work, the piezoelectric functioned as a portion of a vibration dissipation system, where the PZT struts used their electromechanical conversion properties to couple vibrationally-generated energy to a tuned electronic shunt circuit to dissipate energy. A second application was to use the voltage observed at the terminals of the isolated segment of the piezoelectric members as a direct readout of vibrational amplitude. With their very high voltage output, PZTs approach the qualities of ideal sensors.

2. ENHANCEMENT OF DAMPING USING A TUNED ELECTRONIC SHUNT

When a structure is vibrating, components of the assembly are mechanically strained. Piezoelectric materials convert this mechanical strain to electric potential, which allows the addition of an electrical network to extract energy. Hagood et al [1,2] have shown the results of adding a passive shunt to a truss with piezoelectric members. Their truss was of similar construction to the MDSSC CSI truss, except that it was shorter and had twice as many piezoelectric struts. Their experimentation employed both resistive shunting and combined resistive/inductive shunting.

Piezoelectric materials under external excitation behave similar to a capacitance electrically in parallel with a voltage source (see Figure 3). A pure resistance is the only means to dissipate energy, because both capacitive and inductive elements can store energy, but not dissipate it. References [1] and [2] showed that there are optimal values for either resistive or inductive/resistive shunts, and the optima were determined by energy dissipation relationships having to do with cancelling the inductive and capacitive reactance at the structure's resonant frequencies.

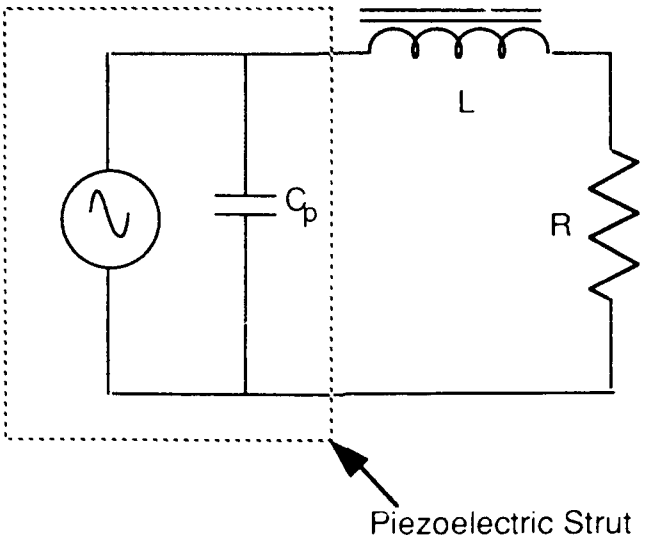

Figure 3. Equivalent Electric Circuit for a Piezoelectric Material and Shunt

Because of the low frequencies involved (from under ten to hundreds of Hertz), large values of inductance are usually required, because the natural frequencies of the attached shunt are related by the following, where L is the added inductance, and C_p is the capacitance of the piezoelectric:

$$f_n \sim (LC_p)^{-1/2} \tag{1}$$

With f_n around 10 Hz and C_p about 1 μF, the value of L computed from Eq. (1) is in the hundreds of Henries. Inductors in this size range are very heavy and possess significant internal resistance, usually higher than that for optimum dissipation. Reducing the resistance or increasing the "Q" of the inductors may be accomplished at the expense of additional mass, by increasing the gauge of the wire and the mass of the inductive material. This is contrary to mass/payload constraints for large space structures.

For this work, MDSSC designed "active" inductors using operational amplifiers and passive circuitry to replace the large mass associated with the necessary values of passive inductance necessary. This was done with a pair of integrated circuit operational amplifiers connected as a gyrator[3], which can produce values ranging from hundreds to thousands of Henries with just a few simple electronic components. Operational amplifiers and a few passive components are all that is required. The electronic circuit used to simulate a large inductance is shown in Figure 4. The value of the simulated inductance may be easily changed by adjusting the variable resistor.

One difficulty was related to the EMF generated by current through the large inductance. Voltage on the inductor may be computed by the relation

$$V = L \times di/dt \quad , \tag{2}$$

where V is the inductor voltage, L is the inductance in Henries, and di/dt is the rate of change of the current through the inductor. It may be seen from Eq. (2) that for moderate currents and inductance in the hundreds of Henries, it does not take long to exceed the normal ±15V range of a common operational amplifier. This indicates that damping performance is likely to be improved at higher current levels corresponding to higher vibration levels with the application of operational amplifiers with higher voltage characteristics.

The use of operational amplifier circuitry to replace passive inductances may mean that it is possible to have passive damping circuits monitor the frequencies to which they are subjected and alter their own characteristics in order to optimize their behavior. This idea is similar to the AFC (Automatic Frequency Control) circuitry used on FM radios to track frequency shifts in commercial broadcasting stations.

The results of applying a single-mode tuned shunt containing an active inductor to the first bending mode are shown in Figure 5. Notice that both the amplitude and frequency drop upon application of the tuned shunt, just a a mechanical system behaves with the application of a viscous damper. The amplitude drops 11 dB, corresponding to a damping ratio increase from 0.068% to 0.25% of critical.

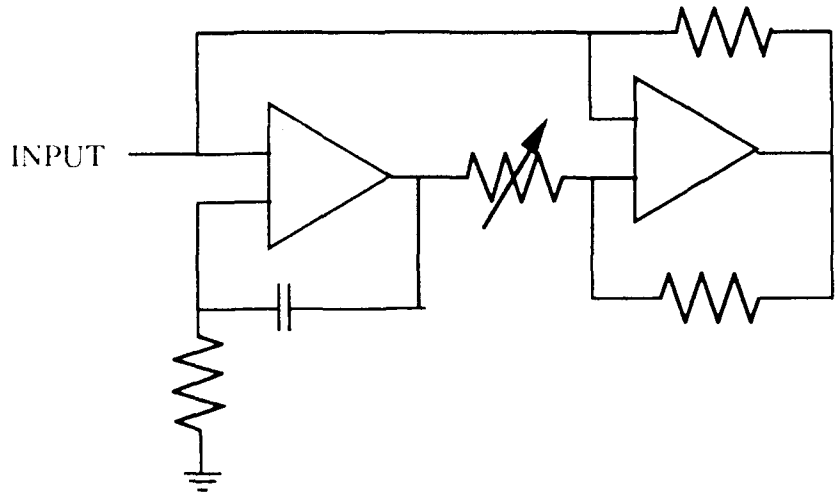

Figure 4. Operational Amplifier Simulated Inductor.

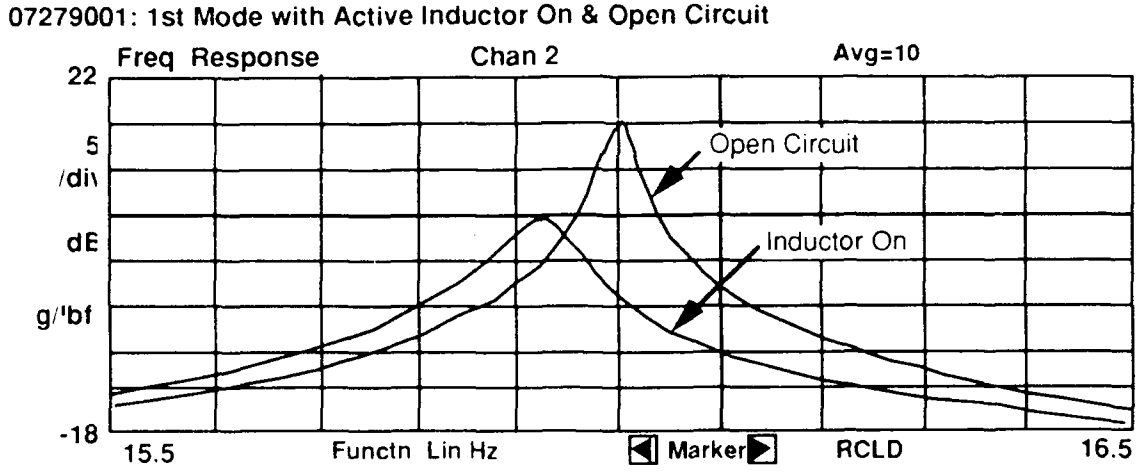

Figure 5. Damping Increase Obtained Through The Use of Simulated Inductor.

To be practical, a vibration dissipation system must work on a range of frequencies, not just a single mode of vibration. This means that added circuitry must be tuned for other modes. Because of mutual loading effects, adding a second shunt circuit "detunes" the first shunt as well as its own settings, so that these effects mst be considered in the design phase. The configuration may be analyzed somewhat easily by iteration, but an expanded theory for synthesis of multiple mode shunts is presently under development.

An example two-mode shunt is shown in Figure 6. It adds a second parallel *LC* network to the original shunt circuitry. Such a configuration simultaneously damped the first and third mode of the MDSSC CSI truss, as shown in Table I. The second mode was not targeted because the piezoelectric struts have little participation and thus effectiveness on this mode.

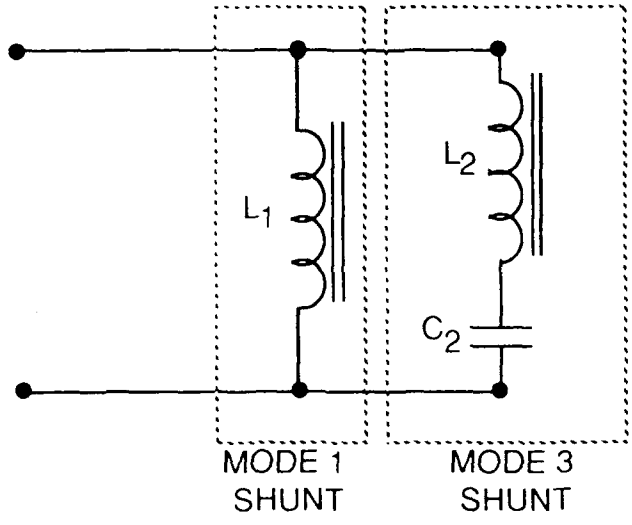

Figure 6. Electric Circuit Depiction of Two-Mode Shunt

TABLE I. RESULTS OF TWO-MODE SHUNT DAMPING EXPERIMENT

Mode	Damping Ratio (% Critical)		% Increase	dB reduction
	Unshunted	Shunted		
1	0.0397	0.146	368	11.3
3	0.0381	0.200	525	14.4

CONCLUSIONS

This paper presents several concepts that are intended to enhance the available damping created by structural members in a vibrating mechanical system The damping is enhanced by dissipating the energy created by mechanical-electrical conversion of the piezoelectric materials within an electronic circuit.

We have used the piezoelectric members of the MDSSC CSI Truss in a demonstration of various vibration dissipation techniques. In all of these techniques, one or more tuned shunts is connected to the terminals of a piezoelectric truss element and tuned to create a resonant circuit for enhanced passive damping. We have shown that heavy passive inductances may be replaced by lightweight electronic circuits, and that a tuned shunt circuit may be made to simultaneously dissipate two modes of vibration. Due to mutual loading effects between multiple shunts, there are still analysis difficulties related to their design and synthesis.

RECOMMENDATIONS

We are working to develop an active inductor circuit that can tolerate higher voltages without saturation of its operational amplifiers. This development will be coupled with the development of a more practical theory for the multiple shunt analysis that will reduce or eliminate the trial and error methods used for this study. A wideband shunt circuit will also be investigated, as will self-tuning (AFC) circuitry.

REFERENCES

1. Hagood, Nesbitt W., and Crawley, Edward F., "Development and Experimental Verification of Damping Enhancement Methodologies for Space Structures," Massachusetts Institute of Technology Space Systems Laboratory Report #18-88, September 1988.

2. Hagood, Nesbitt W., von Flotow, Andreas, "Damping of Structural Vibrations with Piezoelectric Materials and Passive Electrical Networks," Paper ICC, presented at the Damping '89 Conference, West Palm Beach, Florida, 8-10 February 1989.

3. Horowitz, P., and Hill, W., **The Art of Electronics**, Cambridge University Press, 1980.

PAPER KEYWORDS: Piezoelectric; Passive Damping; Vibration Dissipation; Tuned Shunt Circuitry; Active Inductors

THE NEED FOR PASSIVE DAMPING IN FEEDBACK CONTROLLED FLEXIBLE STRUCTURES *

A.H. von Flotow and D.W. Vos
Massachusetts Institute of Technology
Cambridge, Massachusetts

ABSTRACT

It is well established that an undamped infinite dimensional *mathematical model* of a flexible structure cannot be stabilized with finite bandwidth control; the required gain stabilization beyond the bandwidth is negated by the infinite structural gain at each resonance. Thus, even a mathematical model with no modeling uncertainty will show that passive damping is critical to enabling active control. What is less well known are the benefits of passive damping for the robust control of *real structures*. There has been a tendency, in the research literature, to define the research problem to consist of developing control approaches for the broadband control (many modes in the control bandwidth) of poorly modeled, lightly damped, modally dense structures. There is ample reason to believe that such control is practically unachievable and that the attribute "lightly damped" is one of the most easily and readily remedied characteristics of such a problem structure.

This paper reports upon the enabling effect of passive damping in the control of uncertain flexible structures, particularly with non–collocated actuators and sensors. Quantative results are all single–input single–output and the benefits of passive damping are then understandable in terms of classical ideas of gain and phase stabilization. The paper derives approximate expressions for the minimum acceptable level of passive damping in terms of modeling uncertainty and desired bandwidth. These relationships can then be interpreted as specifying either a minimum level of passive damping or a minimum level of modeling fidelity. If the requirement is not met, robust control with the bandwidth including uncertain flexible dynamics is not possible with linear time invariant (LTI) compensation.

INTRODUCTION

In this paper, "bandwidth" implies "that frequency range over which the loop transfer function magnitude ratio varies by no more than 3dB." This definition is sensible for reference command following and for disturbance rejection when the respective input command and output referenced disturbance signals are expected to be broadband. It is possible that neither condition is met in an application of feedback control to a lightly damped flexible structure. A common goal for flexible structures is disturbance rejection rather than command following. Typical output–referenced disturbances are narrow band, either because they were generated by a time periodic process (typically an operating machine) or because they have been filtered through the resonant structure. With reference to rejection of such disturbances, another definition of bandwidth may be appropriate.

This paper addresses the problem statement: "The control bandwidth must include many poorly modeled, lightly damped, closely spaced modes." This problem statement is figuratively depicted in Figure 1a. The fundamental point made in the paper is that no linear time invariant compensation exists which will robustly (in the sense of stability

* This paper is an edited version of a previous draft presented at the 61st Shock and Vibration Symposium, Pasedena, CA, Oct 1990 and in present form will be presented at the VPI+SU Conference on Recent Advances in Active Control of Sound and Vibration, April 1991 and the Air Force Damping '91 Conference, San Diego, Feb 1991.

robustness as opposed to performance robustness) achieve what is suggested by Figure 1a, unless a significant amount of passive damping is present. The required level of passive damping is sketched in Figure 1b.

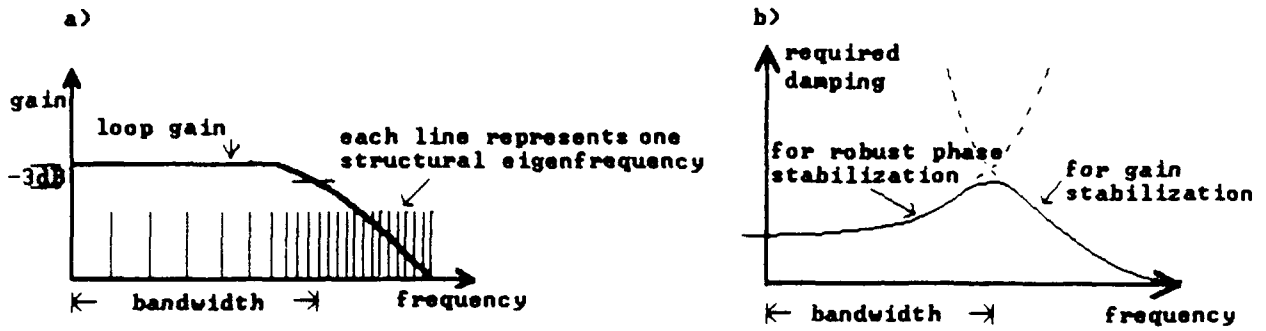

Figure 1. (a) Figurative depiction of problem statement for bandwidth to include many poorly modeled, lightly damped, closely spaced modes. (b) Required level of passive damping to meet problem specification.

The obvious approach to eliminating undesirable dynamics from the controlled plant is to generate control signals which cancel these motions [Rossi]. This "plant inversion" philosophy is what all control design techniques, both linear and nonlinear, SISO and MIMO [Williams], strive to realize when the aim is to achieve bandwidth greater than the frequency of the dominant modes. In benign systems, the effect of reasonable levels of model uncertainty is not such as to yield instability and is thus tolerable. For lightly damped oscillatory systems which typify the broadband structure control problem, however, the undesirable result of high gain/performance plant inversion, is instability of the closed loop system when sufficient model mismatch ocurs. A question which arises is how much damping is required to maintain closed loop stability if the structural dynamics are known only with a given level of uncertainty?

Some specialized literature dealing with design of controllers for uncertain lightly damped structural dynamics exists [ACC, Bryson, Bontsema, Rosenthal, Rossi, Wedell, Wie, et al], but the authors assume a plant given and unable to be modified, leading to a disregard of prescribing increased passive damping as part of the control solution. "Modern" (LQG, H_2, $H\infty$, L_1) control design techniques revolve around parameterizing of the uncertainty into the design model [Bontsema, Bryson, Wie, Wedell], often leading to rather convoluted design and robustness evaluation procedures. Notable for also ignoring passive damping is a large body of literature on combined optimal design of the structural dynamics and the active control system [JPL, Venkayya, Rao, Belvin]. Much of this literature implicitly defines structural dynamic design as the appropriate selection of stiffness and mass parameters. Passive damping levels are assumed to be very low and beyond specification by the designer. This leads to elegant mathematics and numerics, but also leads to results of questionable engineering relevance.

Novel nonlinear techniques, not LTI, such as that due to [Balas] or [Kopf], where use is made of phase–locked loops to track modal frequency and adjust compensation accordingly, also exist. These techniques may offer much promise for the broadband control of poorly modeled lightly damped structural dynamics, but are beyond the scope of this paper.

This paper makes the strong quantitative statement that sufficiently lightly damped and poorly modeled structural dynamics can never be within the bandwidth of an LTI control system. This statement is supported with some SISO case studies, which serve to quantify the level of passive damping required to permit robust phase stabilization of uncertain

structural poles. Uncertainty in eigenfrequencies and in mode shapes is considered. Mode shape uncertainty is recognized as more serious since it is the mode shapes which govern the location of plant zeros. In the common situation of lightly damped poles and zeros such mode shape uncertainty makes the location of the zeros highly uncertain, leading to the strong possibility of transfer function phase uncertainty of 180^0 or greater for dislocated sensor/actuator pairs.

This paper implicitly assumes that the poles of the plant transfer function are spaced much more widely than their bandwidth; $\omega_i - \omega_{i+1} >> \pi\zeta\omega_i$. In this case of low modal overlap, each pole can be considered practically in isolation, interacting at most with local plant zeros. The uncertainty in structural dynamic transfer function gain and phase as a function of modal overlap has been studied from a statistical perspective by [Lyon], and is inversely related to modal overlap.

GAIN STABILIZATION BEYOND THE BANDWIDTH

The result we report here is well known and has been reported elsewhere in many different forms [Gran, Spanos, Hughes, von Flotow]. The basic idea is that a poorly modeled or unmodeled flexible mode beyond the bandwidth must be gain stabilized. Since the gain of a flexible structure (from applied force or torque to displacement, rotation etc.) is maximized near each resonance at a value inversely proportional to damping ratio, the conclusion emerges that an undamped flexible mode can never be gain stabilized. How much damping ratio is required to ensure gain stabilization of modes beyond the control bandwidth depends then upon the gain roll–off of the loop, upon the spectral separation between the modal natural frequency and the control bandwidth and upon the modal participation or residue. The relationship is rather obvious and has been reported elsewhere [Gran, Spanos, Hughes, von Flotow]. It is this requirement that leads to one curve sketched in Figure 1b.

PHASE STABILIZATION WITHIN THE BANDWIDTH

If, for the purposes of disturbance rejection or command following, the control bandwidth must be broad and include one or several flexible modes, then each of these flexible modes must be robustly phase stabilized. In the absence of modeling error, this presents no particular difficulty; notch compensation or some other equivalent inversion of the structural dynamics is then an acceptable approach. Unfortunately, modeling errors are always present. In single–input, single–output LTI systems, the effect of these modeling errors upon control design can be summarized in terms of uncertainty in the location of the structural dynamic transfer function poles and zeros. Broadband control is then enabled by a sufficient level of passive damping, since approximate plant inversion is then feasible.

ROBUST POLE–ZERO CANCELLATION

If the closed loop bandwidth (bandwidth as defined in Figure 1a) is to extend past the eigenfrequency of a number of flexible modes, the only solution is pole–zero cancellation. In the absence of modeling errors, all flexible modes may be canceled and the closed loop bandwidth extended arbitrarily. When uncertainty regarding the eigenfrequencies exists, however, extra care needs to be taken in this strategy. A root locus departure angle argument serves well to explain the effect of uncertainty in eigenfrequency on the stability of the closed loop system where pole–zero cancellation is employed in compensation. Here, a single oscillatory mode system is considered and the damping is considered to be very small. Figure 2 assumes that the loop phase due to all other dynamics is -90^0 at the nominal value of the eigenfrequency in question.

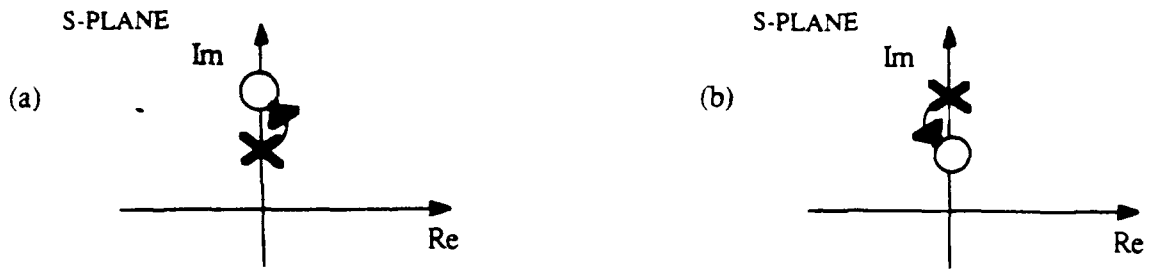

Figure 2. Departure angles due to pole–zero cancellation of single oscillatory mode.

Clearly, Figure 2b does not yield instability for small gains, as the departure angle is away from the imaginary axis. The phase lead added by the zero at frequency lower than the modal frequency ensures this. In Figure 2a, however, the departure angle is toward the imaginary axis, such that for sufficient uncertainty and sufficiently lightly damped poles, the closed loop system will be unstable.

CRITICAL DAMPING FOR ROBUST POLE–ZERO CANCELLATION

Considering the simple case of a single oscillatory mode, it is desirable to implement pole–zero cancellation as compensation in order to achieve a desired closed loop bandwidth. This, however, leads to possible instability if insufficient passive damping exists for a given level of uncertainty in modal frequency. This section serves to quantify ,to first order in relative uncertainty of the eigenfrequency, how much passive damping is necessary for stability (when employing this form of compensation) over the range of eigenfrequency uncertainty.

Phase Gradient with respect to Frequency

First, it is necessary to evaluate the "phase gradient" with respect to frequency, ω. Consider the single oscillatory mode represented by the transfer function

$$G(s) = \frac{1}{(s^2 + 2\xi\omega_n s + \omega_n^2)}$$

setting $s = j\omega$ and evaluating the phase at frequency ω

$$\phi(\omega) = -\tan^{-1}\left(\frac{2\xi\omega_n\omega}{\omega_n^2 - \omega^2}\right)$$

The gradient of this phase evaluated at $\omega = \omega_n$ can be shown to be

$$\frac{d\phi}{d\omega} = \frac{-1}{\xi\omega_n} \qquad (1)$$

representing the phase gradient with respect to frequency at the frequency of maximum amplification of the amplitude ratio (vis–a–vis the Bode magnitude plot) as illustrated in Figure 3. Now, if the eigenfrequency is unknown to an uncertainty $\delta\omega = \omega_n - \omega_{actual}$, then the phase at the nominal eigenfrequency, ω_n, will be uncertain by as much as

$$\delta\phi = \frac{-\delta\omega}{\xi\omega_n} \qquad (1a)$$

to first order in $\delta\omega/\omega_n$.

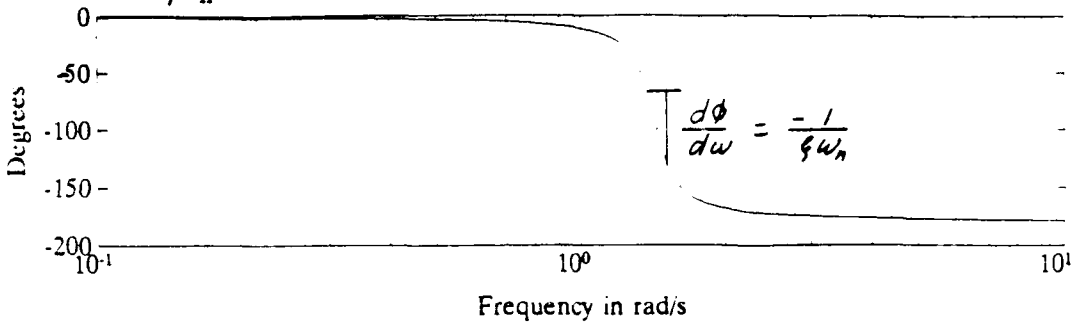

Figure 3. Bode plot illustrating the phase gradient wrt ω.

This allows estimates of local phase contributions due to oscillatory modes. Clearly, the phase gradient due to non–minimum phase oscillatory zeros of frequency ω_n and damping ζ (evaluated at ω_n), is also exactly (1), while that due to minimum phase zeros is the absolute value of (1).

Phase Excursions in Approximate Pole–Zero Cancellation

Using the relation (1a) it is now a simple matter to determine the relationship between the phase excursion due to inexact pole–zero cancellation. For the first uncertain mode in the system to be controlled, the Bode phase plot appears as in Figure 4, where the phase contribution due to the mode as well as the canceling zeros is depicted. Since $\delta\omega$ is assumed positive, the actual pole occurs at a frequency lower than that of the canceling zero and local phase lag is introduced.

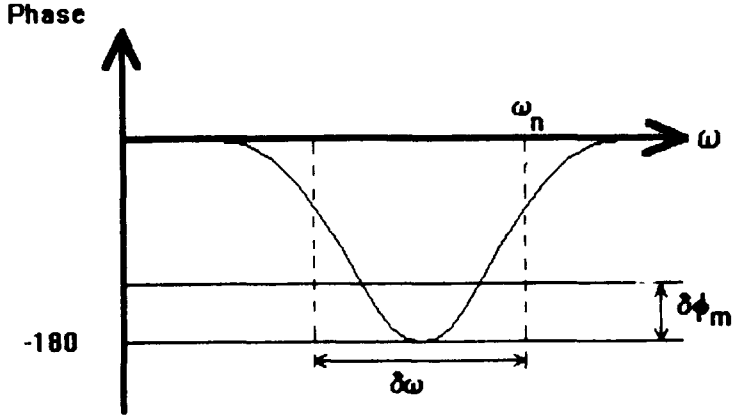

Figure 4. Bode phase plot of uncertain mode approximately canceled by compensator zeros in broadband structural control problem.

If $\delta\phi_m$ represents the "phase margin" at the canceled mode: i.e. the amount of unmodeled phase lag tolerable at this frequency, and if the linear approximation to the phase gradient (1) is assumed, a slightly pessimistic estimate of allowable $\delta\omega$ for a known level of passive damping, is given by this relation

$$\delta\omega \leq (\delta\phi_m)\zeta\omega_n$$

and if $\delta\phi_m = 1\text{rad}$

$$\delta\omega \leq \zeta\omega_n$$

This defines a first estimate of permissible modal eigenfrequency uncertainty in terms of

passive damping for any system with flexibility between the sensors and actuators and required bandwidth including flexible eigenfrequencies.

A more precise expression for the maximum phase excursion due to pole–zero cancellation can be verified to be [Garcia]

$$\delta\phi = 2\tan^{-1}\left(\frac{p_i - z_i}{2\zeta_i p_i}\right)$$

This expression is valid for large relative pole–zero spacing and correctly yields phase excursions limited to the range $\delta\phi \in (-180^0, 180^0)$. Since the zero frequency (z_i) is nominally chosen to cancel the pole, $z_i = \omega_n$ and the actual pole location is $p_i = \omega_{actual}$, then for small angles

$$\delta\phi = -\frac{z_i - p_i}{\zeta_i p_i}$$

$$\simeq \frac{-\delta\omega}{\zeta_i \omega_n}$$

which is the expression (1a).

HOW MUCH ζ IS SUFFICIENT IN THE BANDWIDTH?

For a system compensated by pole–zero cancellation, an estimate (to first order) of the passive damping ($\zeta_{required}$) necessary to maintain stability over $\delta\omega$ may be determined.

Assuming $\delta\omega << \omega_n$ and also $\delta\omega << (\omega_i - \omega_{i-1})$ ("i" indicates i'th mode) ,ensures that the phase plot is approximately linear over this range ($\delta\omega$) about ω_n. Assuming further that pole–zero cancellation is attempted and $\delta\omega$ is small enough that the effect of neighbouring poles and zeros may be ignored (if modal separation is too small, the effect of other contributing modes to the total phase gradient is easily accounted for by including these extra terms), then the local phase excursion due to the pole–zero pair under consideration is approximately (by equation 1a)

$$\delta\phi = \frac{\delta\omega}{\zeta\omega_n}$$

If the design provides a phase margin, $\delta\phi_m$, then for a pole–zero mismatch of $\delta\omega$ a damping ratio of

$$\zeta \geq \frac{1}{\delta\phi_m}\frac{\delta\omega}{\omega_n} \qquad (2)$$

will suffice.

An alternative viewpoint is available by considering the root locus in the vicinity of a nearly canceling pole–zero pair:

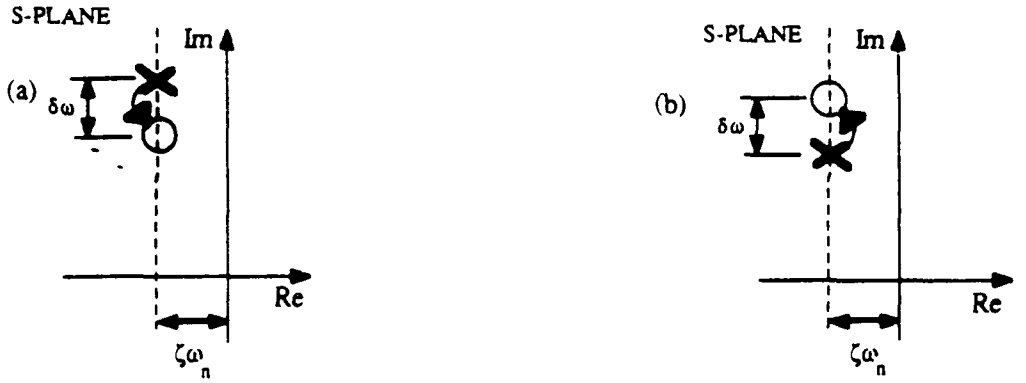

Figure 5. Root locus description of minimum damping ratio required to ensure stability of near pole–zero cancellation when assumed pole location is in error by $\delta\omega$.

PLANT ZERO UNCERTAINTY AND APPROXIMATE POLE–ZERO CANCELLATION

The preceding sections have implied that the plant contributes only poles which must be compensated with compensator zeros. Often the plant will contribute zeros, although their location, depending upon mode shapes, is typically more poorly known than the pole locations. Figure 6, from Rosenthal's PhD [Rosenthal], shows the possibility of a pole–zero "flip" when the inertia of one of the disks in this four degree of freedom system is changed by a factor of two. Near 20Hz, the plant phase is uncertain to ± 180°. In such a situation phase stabilization is impossible.

Although the precise sequence of poles and zeros in a transfer function through a flexible structure is very uncertain, their approximate location can be known with more certainty [Lyon]. The plant phase can thus be viewed as an average phase related to a pole/zero density (with respect to frequency) and local phase excursions from this average phase. These excursions must be either small or well modeled if the plant is to be phase stabilized. If a close pole/zero pair is identified, but the sequence is uncertain (as in the case of [Rosenthal]) then a sufficient level of passive damping is required.

In this section the arguments of the preceding section are directly applied to such pole–zero cancellation, suggesting that approximate plant pole–zero cancellation is effectively perfect cancellation if sufficient levels of passive damping are present.

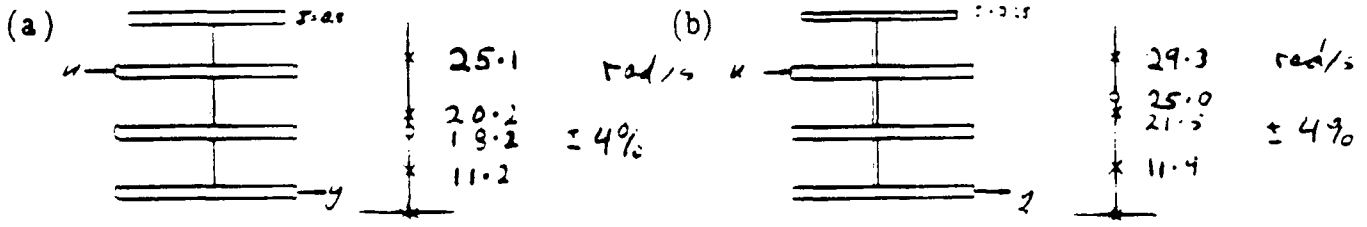

Figure 6. 4–Disk example by Rosenthal.

Poles and zeros in the loop transfer function are indistinguishable with respect to their origin; plant or compensator. We can thus apply the results of the preceding sections directly. If the plant pole–zero pair are known to be within $\delta\omega$ of one another, then a passive damping level of

$$\xi \simeq \frac{\delta\omega}{\omega_n}\frac{1}{\delta\Phi_m}$$

will suffice to ensure that their contribution will not destabilize the loop. For Rosenthal's system, the pole and zero frequencies were such that a passive damping ratio of 10 to 23 percent (for cases (a) and (b) of Figure 6, respectively) would have been sufficient. Such damping levels would then have permitted robust control of this plant with arbitrary bandwidth. For the intentionally low damping levels of Rosenthal's experiment ($\xi \simeq 0.004$), the closed loop bandwidth could never be made to approach this uncertain region near 20 Hz. Note that even for this laboratory system, the exact location of the plant poles and zeros was never known. For Rosenthal, this measurement uncertainty amounted to 1 to 4 percent. This implies that even for carefully identified lightly damped structures, a minimum passive damping level of 1 to 4 percent is needed to permit robust plant inversion in feedback control.

An Example. Bong Wie benchmark problem with pole–zero cancellation

The Bong Wie benchmark problem [ACC] has transfer function

$$G(s) = \frac{K(\xi\omega_n + \omega_n^2/2)}{s^2(s^2 + 2\xi\omega_n s + \omega_n^2)}$$

with uncertainty in modal eigenfrequency such that ω_{actual} may lie in the range $1.0 < \omega_{actual} < 2.0$ (ω in rad/s) and nominally $\omega_n = \sqrt{2}$ rad/s.

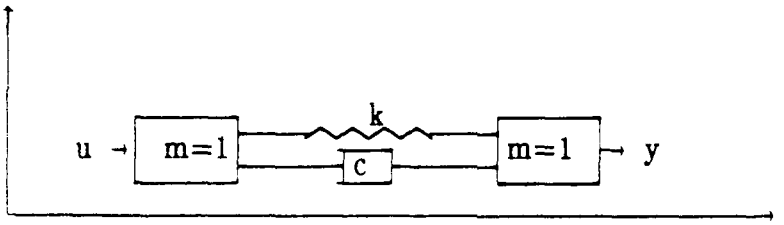

Figure 7. Bong Wie benchmark problem with dashpot providing passive damping.

For this eigenfrequency uncertainty, the estimate (1a) of necessary damping is evaluated as

$$\xi \geq (\sqrt{2} - 1)/\sqrt{2} \qquad = 0.29$$

Note that this assumes $\delta\phi_m = 1$ rad. The rigid body compensation, however, yields a phase margin of $\delta\phi \simeq 1.3$ rad at the nominal flexible mode eigenfrequency, yielding

$$\xi \geq 0.22.$$

The guidelines of the previous section, linear in $\delta\omega/\omega_n$, thus suggest that a passive damping level of 22 percent is needed for this huge uncertainty, if the nominal bandwidth is extended to beyond ω_n while maintaining stability.

It is necessary to verify if this estimate of the required level of passive damping is adequate. To this end, Figure 8 displays a root locus versus gain of the closed loop dynamics where broadband compensation using pole–zero cancellation is used. In the spirit of classical control design, the rigid body modes are first compensated by means of a low frequency zero. The flexible mode is then canceled by zeros at the nominal location of the flexible poles, with suitable high frequency poles yielding the desired roll–off, for a compensator transfer function

$$K(s) = \frac{(6.66s + 1)(s^2 + 2\xi_z\omega_n s + \omega_n^2)16}{(s^2 + 5.656s + 16)\omega_n^2}$$

where the damping ratio of the compensator zero is

$$\xi_z = 0.19$$

The loop gain is chosen to yield closed loop bandwidth of 4 rad/s, greater than the uncertain mode frequency. The system is evaluated for stability when the modal frequency is ω_{actual} = 1 rad/s (worst case, but including 22% passive damping ratio) and found to be stable (figures (8a and 8b)). Clearly the estimate yields a good first guess; the root locus of figure 8b doesn't quite cross into the right–half plane. Unfortunately, the lightly damped closed loop dynamics remaining due to imperfect pole–zero cancellation in Figure 8b limit the bandwidth to less than ω_n (bandwidth defined as in the introduction).

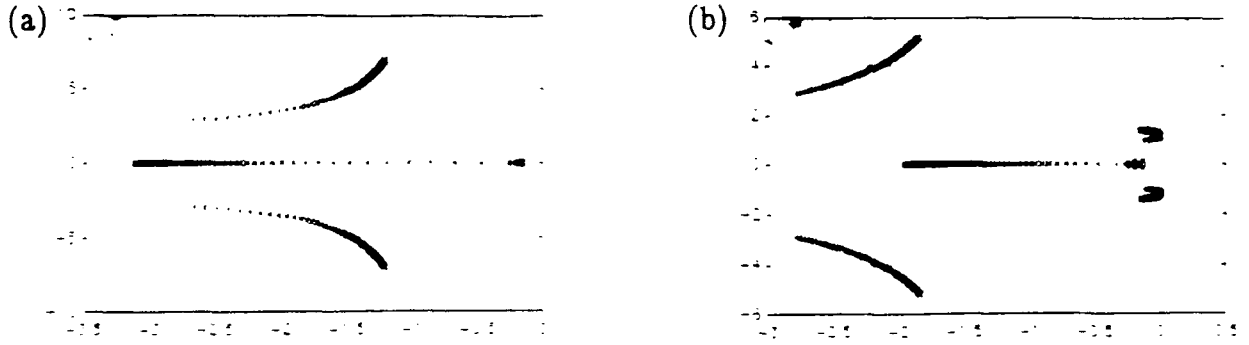

Figure 8. Root loci for Bong Wie problem. (a) shows the nominal case and (b) the nominal compensator implemented for the plant with eigenfrequency at the lower end of the uncertainty range.

Since it may not be practicable to implement the required amount of passive damping to achieve stability robustness for perfect cancellation of the nominal plant flexible modes, it is possible to exploit whatever passive damping is guaranteed by placing the compenastor zero somewhere inside the uncertainty bound for the achievable damping and ensuring stability over the entire uncertainty range as well as improving the nominal performance over conservative compensation with the zerc at the lower end of the uncertainty range.

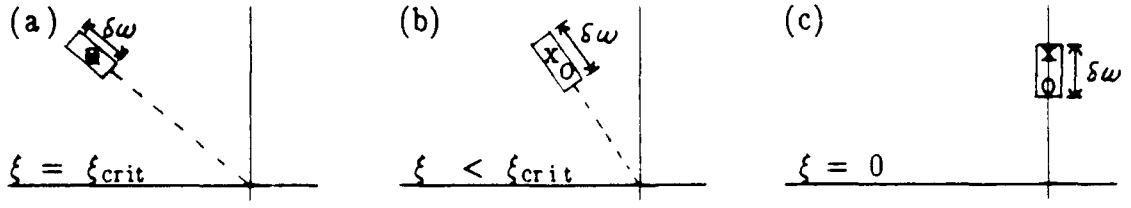

Figure 9. S–plane plots showing intermediate pole–zero cancellation achieving stability robustness and improved nominal performance over undamped uncertain design.

Figure 9 shows the transition in designs from exact pole–zero cancellation of the nominal flexible modes to approximate cancellation at the lower end of the eigenfrequency uncertainty range. For each case the uncertainty is the value $\delta\omega$ and the zero frequency for

cancellation may be estimated using equation 1a and the guaranteed level of passive damping ζ. Notice that in the case of this example, the rigid body compensation yields "phase margin" of approximately 75^0 ($\simeq$ 1.3 rad) in the frequency region near the uncertain poles. The frequency of the compensator zero should then be

$$\omega_z \quad \leq \omega_{lower} + \delta\phi\zeta \tag{3}$$

where ω_{lower} is the lower bound on the eigenfrequency range. A sequence of such designs for the Bong Wie benchmark problem yield Figure 10, showing the limiting value for the compensator zero as a function of plant damping ratio. This suggests that use of equation 3 is warranted for estimating the required zero frequency when a fixed level of passive damping is available and stability robustness with near pole–zero cancellation is desired.

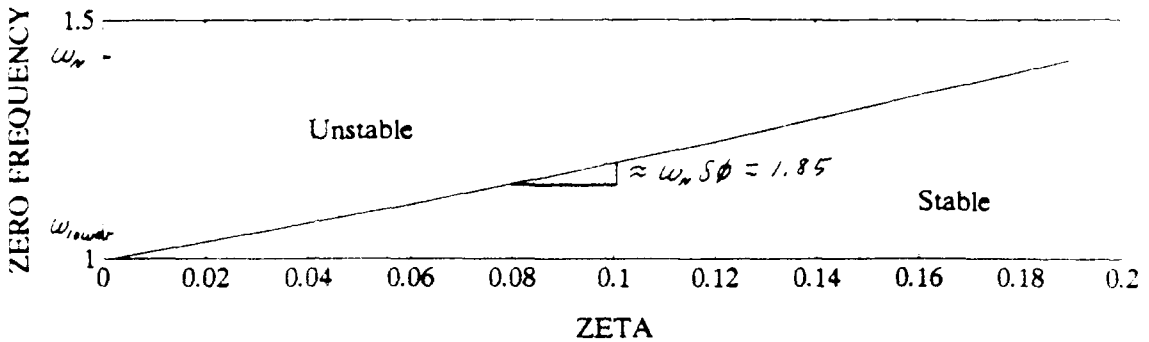

Figure 10. Stability boundary on ω_z vs ζ curve showing that equation 3 yields a good estimate of the zero frequency (ω_z) for near pole–zero cancellation of an uncertain mode where the minimum guaranteed level of passive damping is ζ.

INFERENCES FOR MIMO CONTROL

The preceding sections have presented simple arguments supporting the claim that broadband control of uncertain structural dynamics is impossible with LTI compensation unless a sufficient level of passive damping is present. Although it is not possible to extrapolate these arguments to MIMO systems with confidence, there appears to be little reason to believe that such systems are more benign. Each scalar transfer function of a MIMO system has pole–zero patterns like those described in the preceding sections. Worse, the mapping from actuators to sensors is a strong function of frequency, changing drastically in the near vicinity of each zero of any of the individual scalar transfer functions. The rate of change with frequency of these directions varies inversely with passive damping ratio.

Thus, in MIMO systems both the "directionality" and the phase behaviour of individual channels are comparably influenced by passive damping. Absent a better guideline, one might suggest that equation (2) yields a reasonable rule of thumb for the passive damping levels required for such systems. Here, relative uncertainty should perhaps be relative uncertainty in the zeros of the individual scalar transfer functions. This is not obviously correct and much remains to be understood about such MIMO situations.

SUMMARY

This paper has argued, simply but quantitatively, that a critical level of passive damping can be specified which will permit robust non–collocated LTI control of structural dynamics with the control bandwidth including many flexible eigenfrequencies. We have suggested that this level is as high as 1 to 4 percent, even for carefully identified laboratory

structures and much higher for uncertain structures. Figure 1 perhaps summarizes the thesis of this paper most succintly.

REFERENCES

ACC, "A Benchmark Problem for Robust Control Design," special session at American Control Conference, May 1990, San Diego, CA.

Balas,M.J., Quan, R. D. and Das, B., "Low–Order Control of Large Aerospace Structures Using Residual Mode Filters," CU–CSSC–88–05, College of Engineering, University of Colorado, April 1988.

Belvin, W. K. and Park, K. C., Structural Tailoring and Feedback Control Synthesis: An Interdisciplinary Approach," J. Guidance and Control, Vol. 13, No. 3, May–June 1990, pp. 424–429.

Bontsema, J., "Control of Flexible Structures: Robustness, Model Reduction and Spillover," ESTEC Workshop Proceedings, paper no. esa WPP–09, 15–16 June 1989, Noordwijk, The Netherlands.

Bryson, A.E., Jr., Hermelin, S. and Sun, J., "LQG Controller Design for Robustness," presented at ACC, Seattle, Washington, June 1986.

Garcia, J., "Broadband Positioning of Small Optical Components on a Resonant Substructure," Proceedings, ASME WAM, Dallas, TX, Nov 1990.

Gran, R., "Finite Dimensional Controllers for Hyperbolic Systems," Proceedings of 3rd VPI and SV/AIAA Symposium on Dynamics and Control of Large Flexible Spacecraft, June 15–17, 1981.

Hughes, P.C., "Stability of Proportional–PLus–Derivative–Plus–Integral Control of Flexible Spacecraft," J Guidance and Control, Vol. 2, No. 6, Nov–Dec 1979, pp. 499–503.

JPL Internal Report, Milman, M., Salama, M., Scheid, R., Bruno, R., Gibson, J.S., "Integrated Control–Structure Design: A Multiobjective Approach," JPL D–6767, Jan 1990.

Kopf, E.H., Brown, T.K., Marsh, E.L., "Flexible Stator Control on the Galileo Spacecraft," AAS Conf., Paper no. 79–161, Provincetown, MA, June 1979.

Lyon, R. H., "Statistics of Phase and Magnitude of Structural Transfer Functions," contribution to: Random Vibrations – Status and Recent Developments, Eds. I. Elishakoff and R.H. Lyon, Elsevier, Amsterdam, 1986, pp 201–209.

Rao. S.S., Venkayya, V. B. and Khot, N. S., "Game Theory Approach for the Integrated Design of Structures and Controls," AIAA Journal, Vol. 26, No. 4, April 1988, pp. 463–469.

Rosenthal, D. E., "Experiments in Control of Flexible Structures with Uncertain Parameters," PhD thesis, Stanford University, Dept of Aeronautics and Astronautics, March 8, 1984.

Rossi, J. A., "A Robust Compensator Design by Frequency–Shaped Estimation," J. Guidance and Control, Vol. 8, 1985, pp. 541–544.

Spanos, J. T., "Control–Structure Interaction in Precision Pointing Servo Loops," J. Guidance and Control, Vol. 12, No. 2, March–April 1989, pp. 256–263.

Venkayya, V. B. and Tischler, V. A., "Frequency Control and Its Effects on the Dynamic Response of Flexible Structures," AIAA Journal, Vol. 23, No. 11. Nov. 1985, pp. 1768–1774.

von Flotow, A.H., "Control–Motivated Dynamics Tailoring of Truss Work Structures," Proc. of AIAA Guidance and Control Conference, Williamsburg, V.A., Aug, 1986.

Wedell, E., Chuang, C.–H. and Wie, B., "Computational Analysis of a Stability Robustness Margin for Structured Real–Parameter Perturbations," AIAA paper no. 89–3505, AIAA GN&C Conference, August 1989.

Wie, B., Byun, K.–W., "New Generalized Structural Filtering Concept for Active Vibration Control Synthesis," J. Guidance and Control, Vol. 12, No. 2, March–April 1987, pp. 147–154.

Williams, T. and Juang, J.–N., "Pole/Zero Cancellations in Flexible Space Structures," J. Guidance and Control, Vol. 13, No. 4, July–August 1990, pp. 684–690.

PASSIVE CONTROL OF A FLEXIBLE PLANAR TRUSS USING A REACTION MASS ACTUATOR

David R. Lee
Lieutenant, USAF

Steven G. Webb*
Captain, USAF

Department of Engineering Mechanics
USAF Academy CO

ABSTRACT

Damping is an important aspect in controlling large flexible structures in space. This paper deals with the passive control of a flexible twenty–bay truss using a reaction mass actuator. The actuator was electronically tuned to the second mode of the truss and attached to the tip of the truss. The truss was then subjected to random vibrations. The results were impressive, with an 86 percent reduction in the peak amplitude of vibration of the second mode of the truss when compared to the structure's uncontrolled response. In addition, the peak amplitudes of vibrations of the higher modes of the truss were reduced with the actuator passively tuned to the second mode; there was a small change in the peak amplitude of vibration of the first mode. Further, the settling time for the structure with the passively tuned actuator was less when compared to that of the truss without the actuator attached. With no passive damping it took 19.5 seconds for the second mode of the truss to settle, while the addition of the passive actuator reduced the settling time to four seconds. The passively tuned reaction mass actuator is, therefore, an effective mechanism to reduce the vibrations of a flexible truss.

*Department of Engineering Mechanics (USAFA/DFEM)
United States Air Force Academy Colorado 80840–5000
(719) 472–2191

INTRODUCTION

It is envisioned that, in the near future, space structures will become larger and more complex. Due to the high cost of transporting materials into orbit, these future space structures will be made from lightweight and flexible components. While the components will reduce the number of launches required to place large space structures in orbit, their flexibility will become an important control issue.

A flexible structure's vibrations can be reduced, or eliminated, either by active control, passive damping, or a combination of both. Active control incorporates feedback control systems to sense the structure's vibrations and calculates control inputs to dampen unwanted oscillations. Passive damping deals with the structure damping its own oscillations as a result of its structural design, materials properties, or the addition of devices to the structure.[1] This paper deals only with examining the effects of passive damping on a structure.

Specifically, the purpose of this paper is to examine, both analytically and experimentally, the interactions between a passively tuned actuator and a flexible truss structure to which it is attached. A study similar to this has already been conducted,[2] but this work utilizes a truss structure with characteristics mirroring those anticipated on large flexible structures. In addition, while reference 2 dealt with reducing the magnitude of vibration of a structure's first resonant mode, this research effort has concentrated on reducing the vibrations of a structure's higher modes. A 20–bay planar truss has been built and a reaction mass actuator has been attached to its tip. In addition, a finite element model of the structure has been developed and validated. With these experimental and analytical tools, a study has been conducted to examine the interactions between the truss and the actuator. This paper summarizes the results of this study and addresses the experimental and analytical set–ups, as well as the results obtained when the actuator was used to passively dampen the vibrations on the truss.

PLANAR TRUSS SET -UP

This study was conducted using the 20–bay, 7.[illegible] g planar truss located in the Engineering Mechanics Laboratory at the US Air [illegible]demy (see Figure 1). The diagonal and side dimensions of each square bay w[illegible] and 0.354 m, respectively. The chordwise members were fastened to steel bar[illegible] provided extra mass to scale down the structure's natural frequencies. The chor[illegible] truss members were, then, effectively rigid when compared to the longeron and di[illegible]al members. The 239 pound truss was oriented in a horizontal plane and supported by 3/4 inch diameter steel balls on table tops. The steel balls rolled with very little friction on small steel plates which rested on the table surfaces. The root of the truss was attached to a heavy steel table that was bolted to a concrete floor, and the truss tip was free to move. Air jet thrusters were attached to the tip and mid–span of the truss. A complete description of the planar truss can be found in another study.[3]

Finite element models of the truss were generated using both MSC/NASTRAN and SDRC IDEAS, and these models were modified until they produced resonant frequencies close to those obtained from the experimental truss. These frequencies, shown in Table 1, validate the analytical models.

TABLE 1

Experimental and Analytical Natural Frequencies of the 20–Bay Truss

MODE	EXPERIMENTAL (Hz)	ANALYTICAL (Hz)	PERCENT ERROR FROM ANALYTICAL
1	1.837	1.585	–16.046
2	9.438	9.414	–0.255
3	24.250	24.850	2.415
4	42.297	44.042	3.985

Note the rather large discrepancy between the experimental and analytical frequencies for the first mode of the truss. The truss actually experiences Coulomb damping in the first mode, and this was not accounted for in the analytical model. Even so, it was determined that this discrepancy did not adversely affect the results of this study. Note also that Table 1 shows only the first four resonant frequencies of the truss. Higher modes are not shown since, for the purposes of determining the actuator's optimum tuning, only the first four modes were used and the analytical models were hence reduced to fourth–order systems.[2]

ANALYTICAL RESULTS

To conduct a study into the interactions between the truss and a passively tuned reaction mass actuator (RMA), the actuator's frequency and damping ratio had to be determined. Another paper[4] described a method to calculate the optimum tuning of an actuator attached to a multi–degree of freedom system. With the fourth–order mass and stiffness matrices from the finite element models, the RMA was optimally tuned to the analytical structure's second resonant frequency using the following equations:[4]

$$\bar{\omega}_{opt} = \mathbf{k}_{\omega} \left[\frac{\mu}{1 + \mu} \right] \tag{1}$$

$$\zeta_{opt} = \mathbf{k}_{\zeta} \left[\frac{3\mu}{8\ (1+\mu)^3} \right]^{1/2} \tag{2}$$

where μ is the ratio of the actuator mass to the modal mass of the second structural frequency, $\bar{\omega}_{opt} = \omega_{opt}/\omega_2$ is the optimum frequency ratio to tune the actuator (ω_{opt} is the optimum natural frequency and ω_2 is the frequency of the second structural mode), ζ_{opt} is the optimum damping ratio to tune the actuator, and $\mathbf{k}_{\omega}$ and $\mathbf{k}_{\zeta}$ are correction factors to obtain the optimum tuning.[2]

Figure 2 compares the frequency response functions of the baseline and optimally tuned structure from 6 to 12 Hertz, where baseline is defined to be the truss without the RMA. In this figure the effects of adding passive damping to the truss can readily be seen. The actuator, which is attached to the tip of the truss, introduces a new resonant mode to the structural characteristics in addition to altering the second mode of the truss. Specifically, the frequency of the second mode is shifted higher and the peak amplitude ratio is reduced. In fact, for the second mode, both peak amplitude ratios of the system response with passive damping are less than 1e percent of the structure's undamped peak amplitude ratio.

It is interesting to observe the actuator's effect on some of the other resonant modes of the 20–bay truss. Figure 3 compares the baseline and passively damped responses of the structure between 0 and 6 Hertz while Figure 4 shows the responses between 24 and 30 Hertz. Note that there are slight reductions in the peak amplitude ratios of the structure's first and third modes when the actuator, passively tuned to the structure's second resonant frequency, is attached to the 20–bay truss. In addition, with passive damping, the first resonant frequency is shifted lower while the third resonant frequency is shifted higher. Finally, for the structure's fourth resonant mode there is a slight reduction in the peak amplitude ratio and a shift to a slightly higher frequency with the passive actuator attached. However, the change in this mode's response is so small it can be neglected. Clearly, the analytical results show that attaching a RMA that is passively tuned to the second mode of the truss reduces not only the magnitude of vibration of the structure's second mode but also those of the first and third modes as well.

Figure 5 illustrates the sensitivity of the truss' structural characteristics if the RMA is not tuned to the optimum passive actuator parameters. Just a five percent mistuning of the actuator's optimum frequency causes noticeable shifts in the frequencies and peak amplitude ratios of the structure's second mode, as well as the new mode introduced by the actuator. However, the other resonant modes of the structure are not altered. Finally, it was observed that mis–tuning the actuator's optimum damping ratio by five percent produced almost no change in the structural characteristics of the 20–bay truss. Much larger errors in the tuning of the actuator's damping ratio introduce, of course, small differences in the peak amplitude ratios of the structure's resonant modes, but these differences are slight.

EXPERIMENTAL RESULTS

To verify the results obtained analytically, a reaction mass actuator assembly was attached to the tip of the 20–bay truss and the system was subjected to random vibrations from the air jet thrusters. The RMA assembly used for this study is shown in more detail in Figure 6. This assembly consisted of a moving mass core made up of a series of rare earth magnets encircling a stationary coil. A magnetic shaft, connected to this core, passed through the center of a stationary linear velocity transducer which sensed the velocity of the reaction mass relative to the truss. The RMA assembly also included a non–contacting transducer to sense the relative position of the reaction mass. Each of the resulting analog signals from the two transducers was multiplied by an appropriate gain constant and fed back to the RMA via a power amplifier to generate electromagnetic stiffness and damping on the RMA. In this manner the RMA's natural frequency and viscous damping factor could be varied by adjusting a pair of feedback gain potentiometers to their desired values. There was a small amount of uncontrollable rolling friction in the motion of the RMA shaft

through two sets of linear ball bearings; the total damping of the RMA was, therefore, a combination of this small, but uncontrollable, friction plus the controllable and much larger linear viscous damping.[2]

With the RMA attached to the truss and tuned to the optimum values of the frequency and damping ratio specified analytically, a transfer function of the structure's resonant frequencies was obtained with the aid of a Tektronix model 2630 Fourier Analyzer. Comparisons between the baseline and optimally tuned structural responses are shown in Figures 7–9. Figure 7 shows the structure's frequency responses from 0 to 50 Hertz; Figure 8 shows the responses from 0 to 10 Hertz; and Figure 9 shows the responses from 20 to 30 Hertz. Overall, it can be seen from the figures that the addition of the passive actuator to the truss does indeed reduce the magnitude of the structural vibrations.

In the optimally tuned response of Figure 8 there is a noticeable absence of the two peaks associated with the structure's second mode and the mode introduced by the actuator. Although these peaks are visible in the analytical response of Figure 2, they are significantly less than the baseline peak amplitude ratio. Experimentally, these peaks exist but are much less than the baseline response and, consequently, do not appear in Figure 8. Thus, the passively tuned actuator eliminates, for the most part, any vibrations associated with the second mode. The structural responses in Figure 8 mirror the analytical responses in Figure 3 in that the peak amplitude ratio of the first structural mode is slightly less when the passively tuned actuator is attached to the truss. However, experimentally the optimally tuned response shows the first frequency to be slightly higher than the baseline response. This is the opposite of the analytical result shown in Figure 3, but considering how close the baseline and passively damped frequencies are for the first mode the differences are not significant. Numerical and experimental inaccuracies can account for the difference in the results shown in Figures 3 and 8.

Figure 9 shows that the passively–tuned actuator does reduce the structure's vibrations at higher frequencies, as the peak amplitude ratio of the third mode is reduced by 59 percent. In addition, the resonant frequency is shifted higher, validating the analytical results of Figure 4. Finally, as shown in Figure 7, there is very little difference in the structural responses of the baseline and passively damped structures for the higher modes.

Based on the above observations, both the experimental and analytical results show that a RMA, passively tuned to the second resonant frequency of the 20–bay truss, reduces the flexible structure's vibrations. Specifically, adding a passive actuator to a flexible structure reduces the magnitude of the structure's vibrations, not only at the resonant mode to which the actuator is tuned, but at higher and lower modes as well. Selective tuning of the actuator produces the largest decreases in the magnitude of the structure's vibrations, but the beneficial effects of passive damping are not limited to the frequency of interest.

To experimentally observe the effects a mis–tuned actuator has on the structure's modal responses, the RMA was tuned to 95 percent and 105 percent of the optimal frequency. The results, shown in Figures 10 and 11, show that even a slight mis–tuning of the actuator's frequency causes noticeable shifts in the structure's first three resonant modes as well as the mode of the actuator. Notice, though, that higher resonant modes are not altered much. These results are similar to the analytical results summarized in Figure 5.

THE EFFECTS ON THE SETTLING TIME

One important aspect in reducing or eliminating a structure's vibrations is the time it takes to eliminate those vibrations due to an impulse disturbance. The settling time for the motion of the 20–bay truss can be determined experimentally by exciting the first three structural modes. A signal generator was used to produce a sine voltage to the air jet thrusters at one of the first three experimental natural frequencies shown in Table 1. The pair of thrusters located at the tip excited modal motion in the uncontrolled resonant mode of vibration corresponding to the desired excitation frequency. The signal amplitude was arbitrary, and when the motion reached a suitably high level the air jets were turned off, allowing the modal motion to gradually decay under the influence of inherent damping only.[3]

Time history decay traces for the first three modes of the truss in the uncontrolled configuration are displayed in the left–hand column of Figure 12. Decay traces of the truss with the RMA passively tuned to the structure's second resonant frequency are shown in the right–hand column of Figure 12, with the approximate time of when the thrusters are turned off marked by an arrow.

By comparing the baseline and passively damped decay times, it is readily apparent that the passively–tuned RMA does indeed reduce the settling time of the truss. There is a slight reduction in the settling time for the first mode; it takes about 19.5 seconds for the truss to settle without any passive damping while the addition of the RMA reduces this time to 14.5 seconds. The second mode shows a significant reduction in the settling time with the RMA attached to the truss. Without the passively tuned RMA the settling time for the second mode of the truss is again about 19.5 seconds. With the RMA attached to the truss this settling time is only 4 seconds. The settling time for the third mode is reduced from 9.5 seconds to 3.2 seconds when the RMA is added to the truss. Thus, the addition of the passively tuned RMA is quite effective in reducing the time it takes for the truss to settle after being excited in the first three resonant modes. It should be noted that the structure's higher resonant frequencies were not excited due to limitations in the electronics associated with the air jet thrusters.

CONCLUSIONS

It has been demonstrated that a passively tuned reaction mass actuator can be used to successfully reduce the vibrations of a flexible truss. The 20–bay truss was subjected to both random and sinusoidal excitations, and the RMA, when tuned to the structure's second resonant frequency and attached to the tip of the truss, reduced the magnitude of vibration and the settling time of the second resonant mode. In addition, the magnitudes of vibration and settling times of the first and third modes were also reduced when the actuator, still passively tuned to the structure's second resonant frequency, was attached to the tip of the truss. Selective tuning, then, produces the best results, yet the beneficial effects of passive damping is not limited to the frequency of interest. Finally, mis–tuning of the actuator's frequency does alter the structure's modal responses, particularly around the frequency to which the actuator is passively tuned.

The next step in this research effort is to utilize both active control and passive damping on the 20–bay truss. Since passive damping is an effective means of vibration suppression, it is hoped that a combination of active control and passive damping will produce a beneficial control system for flexible structures.

ACKNOWLEDGEMENTS

This work was sponsored by the US Air Force Academy and the US Office of Scientific Research. The authors are grateful for the contributions of Captain Jeff Turcotte and Mr Jim Smith.

REFERENCES

1. Lynch, P.J., and Banda, S.S., "Active Control for Vibration Damping," Large Space Structures: Dynamics and Control, Berlin: Spring–Verlag, 1988, p. 239.

2. Webb, Steven G., and Turcotte, Jeffrey S., "Analysis of a Passively tuned Actuator on a Low–Order Structure," 1990 AIAA Guidance, Navigation, and Control Conference, Portland OR, AIAA Paper 90–3500, 20–22 August 1990.

3. Hallauer, William L., Jr., and Lamberson, Steven E., "Experimental Active Vibration Damping of a Plane Truss Using Hybrid Actuation," 30th AIAA/ASME/ASCE/AHS/ASC Structures, Structural Dynamics and Materials Conference, Mobile AL, AIAA Paper 89–1169, 3–5 April 1989, pp. 80–90.

4. Duke, John P., Webb, Steven G., and Vu, Hung, "Optimal Passive Control of Multi–Degree of Freedom Systems Using a Vibration Absorber," 1990 AIAA Guidance, Navigation, and Control Conference, Portland OR, AIAA Paper 90–3499, 20–22 August 1990.

Figure 1. The Planar Truss

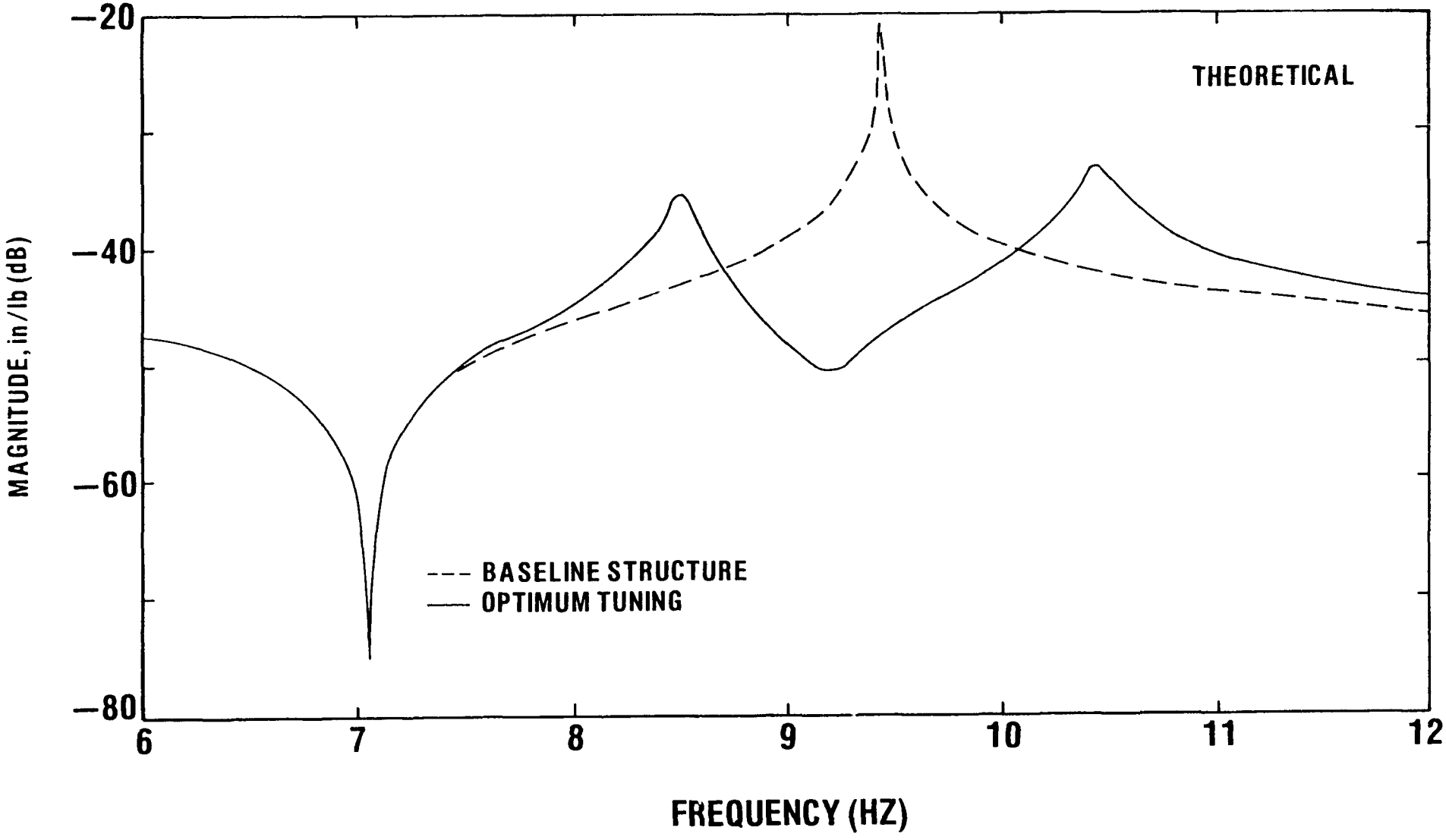

GBC-9

Figure 2. Analytical Baseline and Optimally Tuned Structural Responses from 6 to 12 Hertz

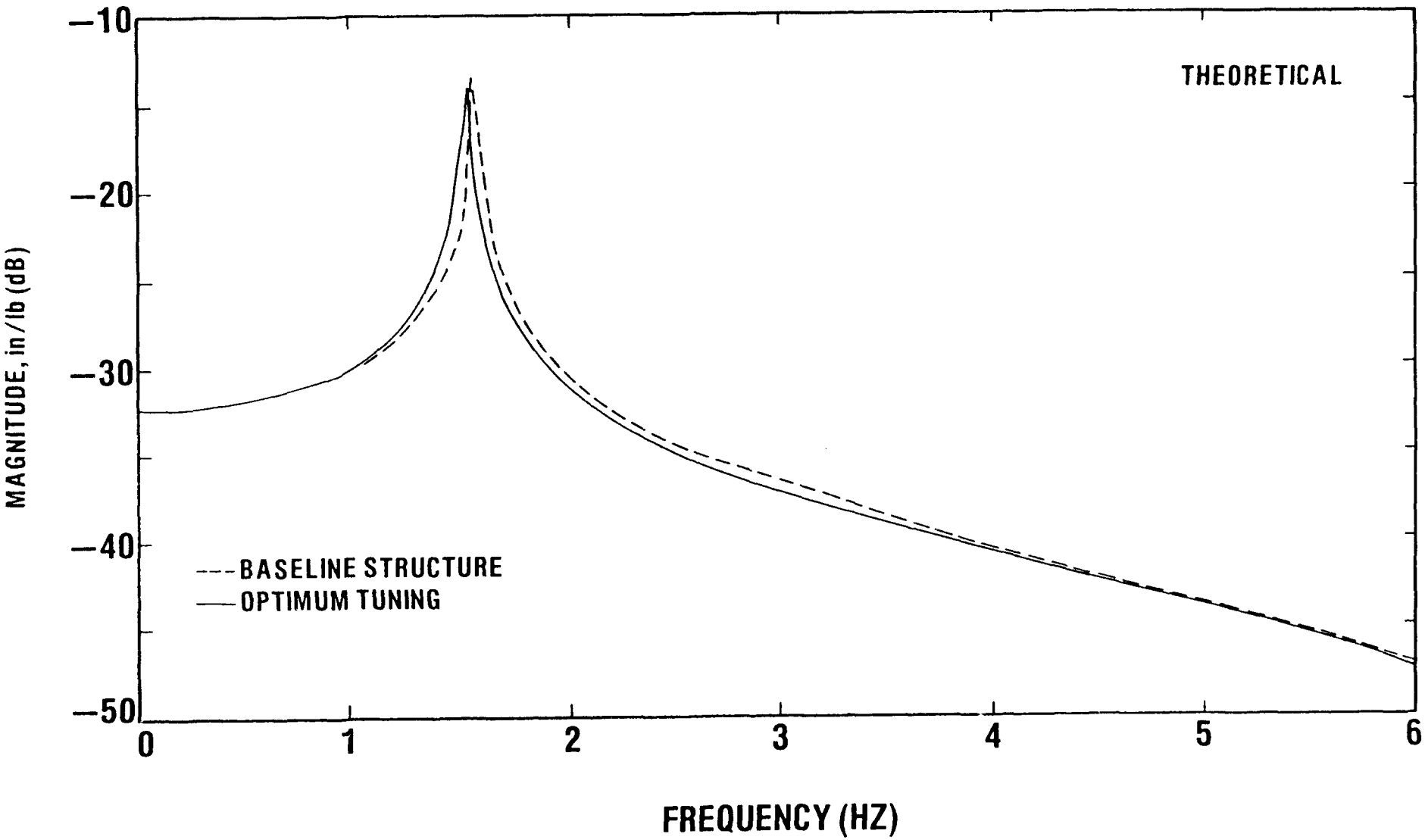

Figure 3. Analytical Baseline and Optimally Tuned Structural Responses from 0 to 6 Hertz

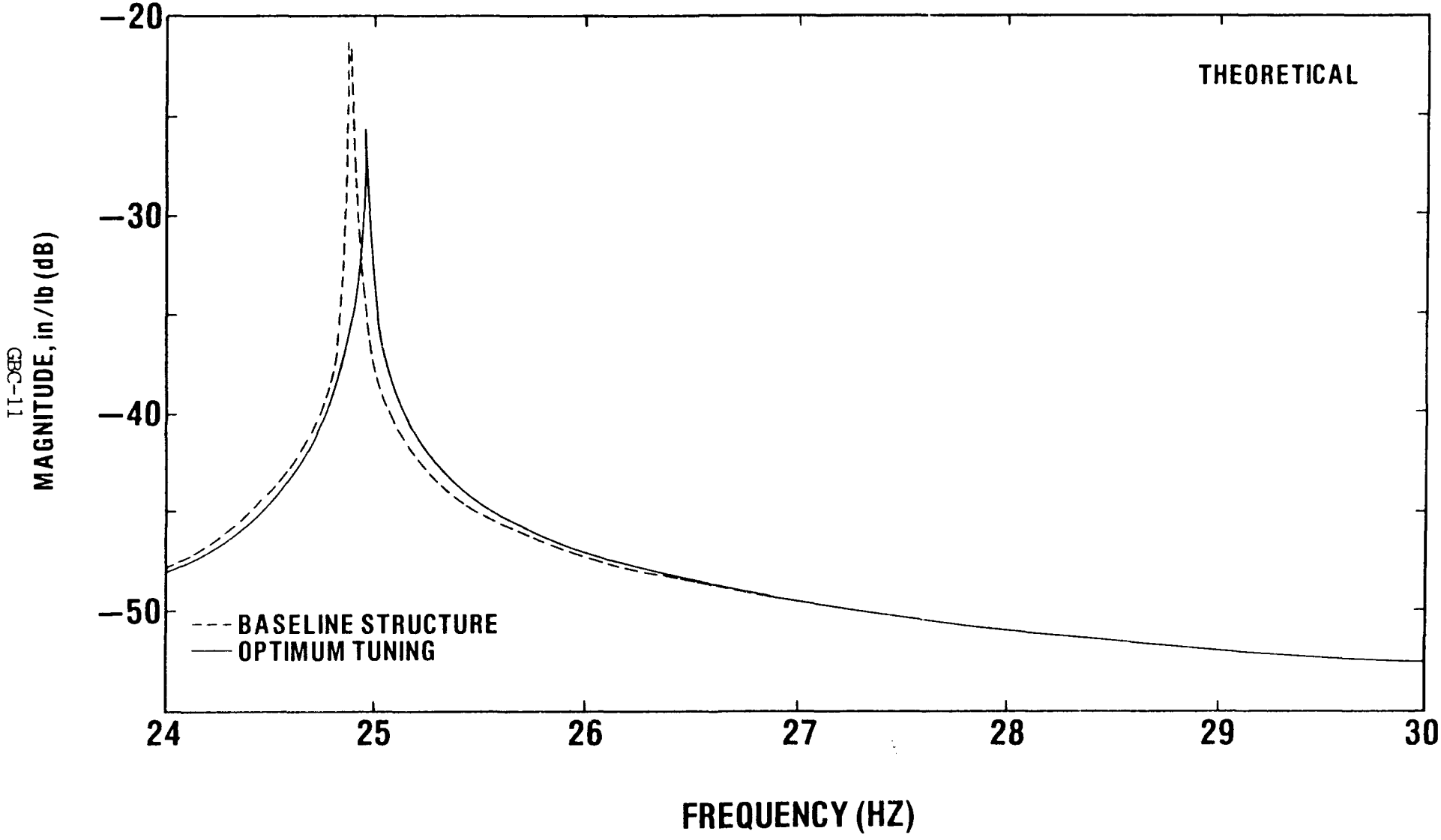

GEC-11

Figure 4. Analytical Baseline and Optimally Tuned Structural Responses from 24 to 30 Hertz

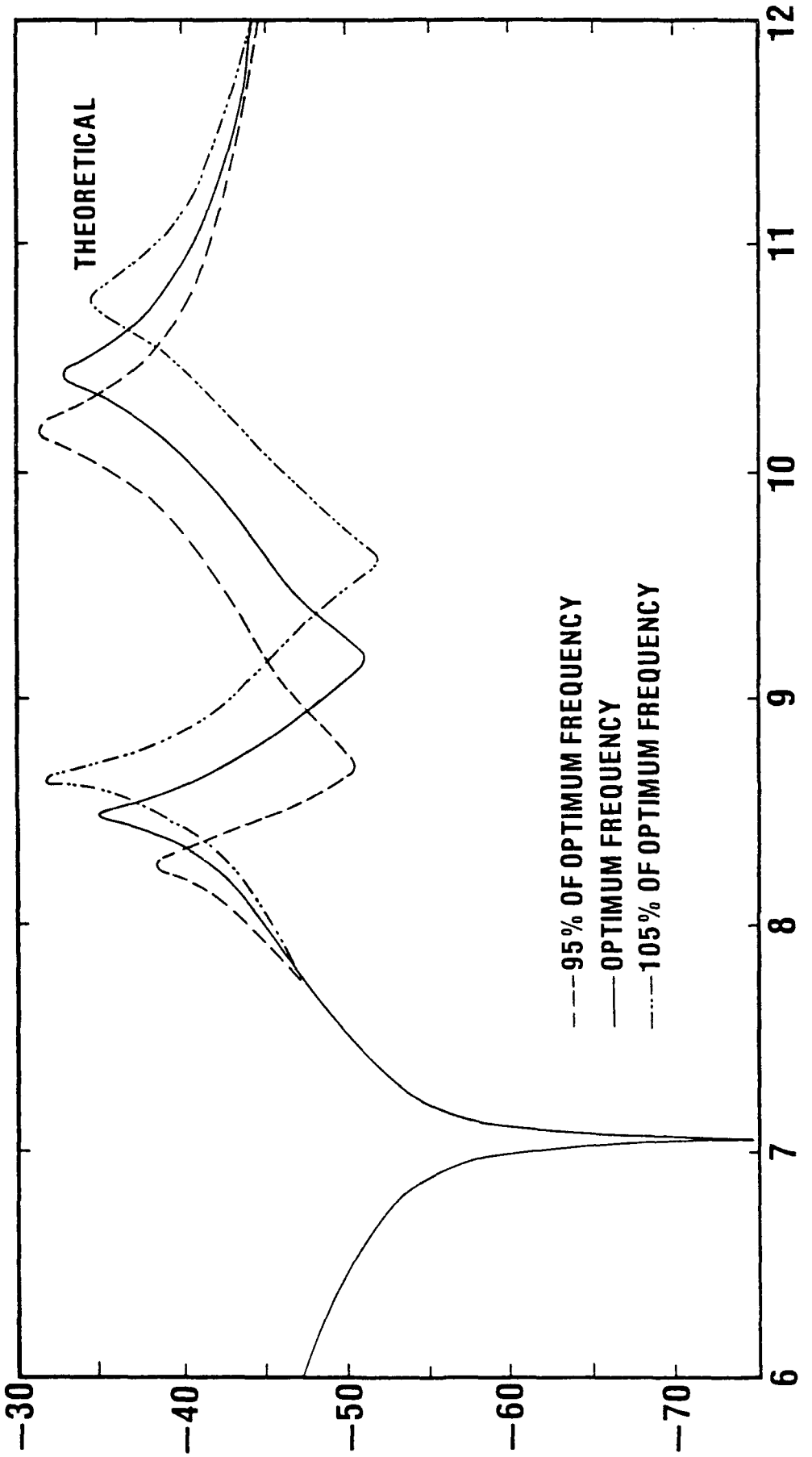

Figure 5. Analytical Optimally Tuned and Mis–Tuned Structural Responses

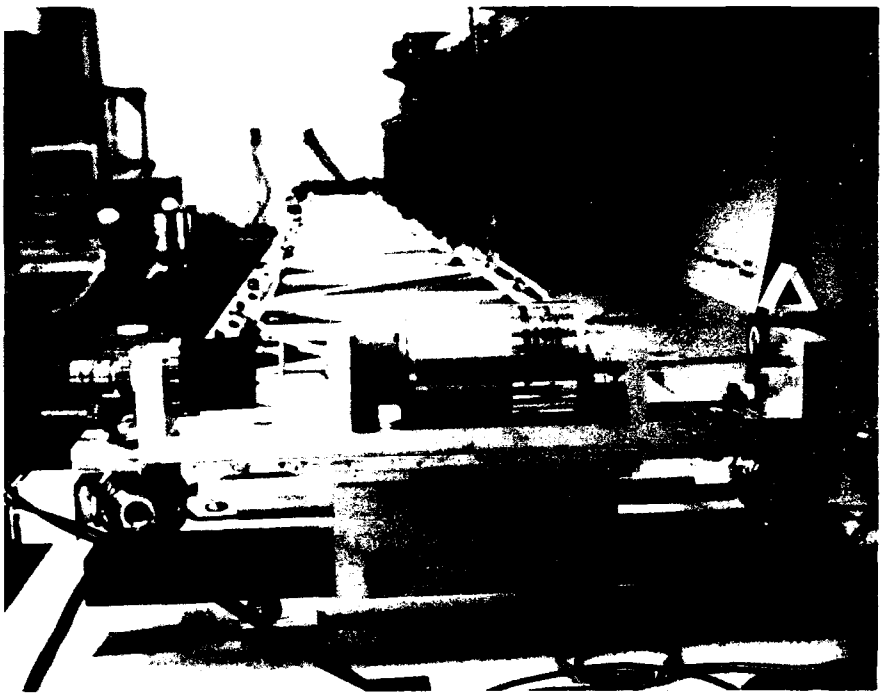

Figure 6. Reaction Mass Actuator Assembly

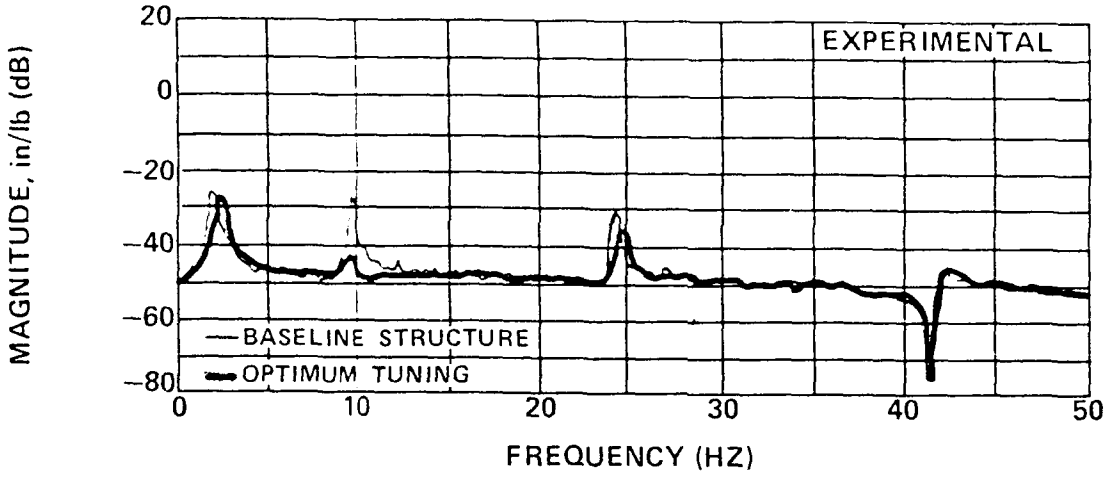

Figure 7. Experimental Baseline and Optimally Tuned Structural Responses from 0 to 50 Hertz

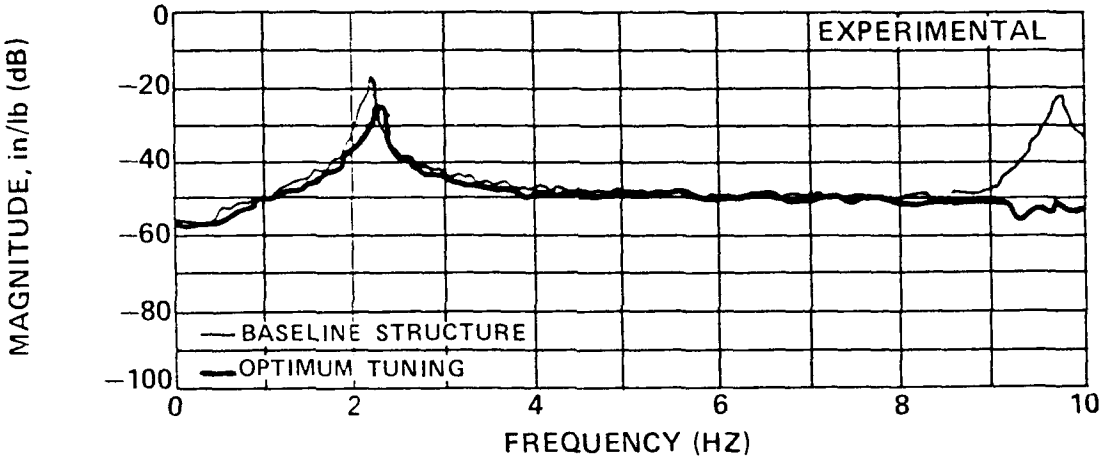

Figure 8. Experimental Baseline and Optimally Tuned Structural Responses from 0 to 10 Hertz

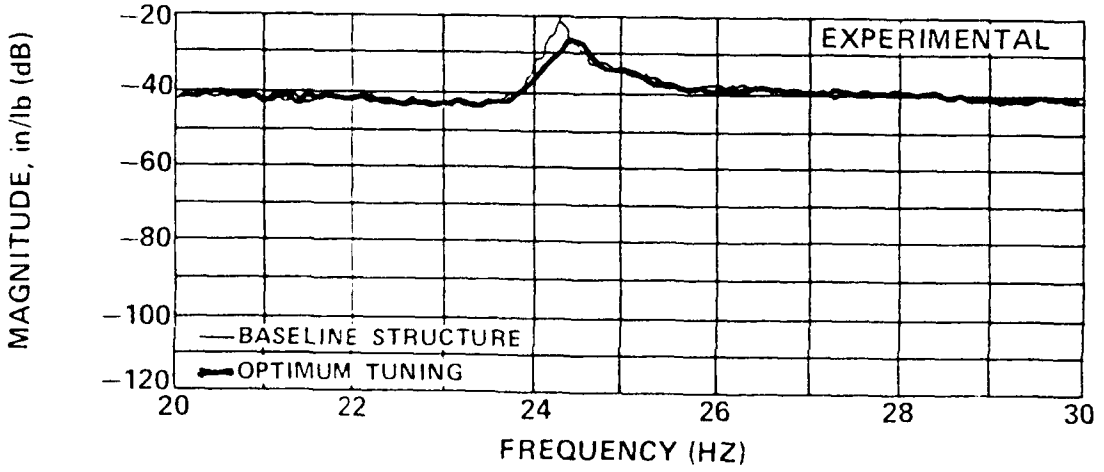

Figure 9. Experimental Baseline and Optimally Tuned Structural Responses from 20 to 30 Hertz

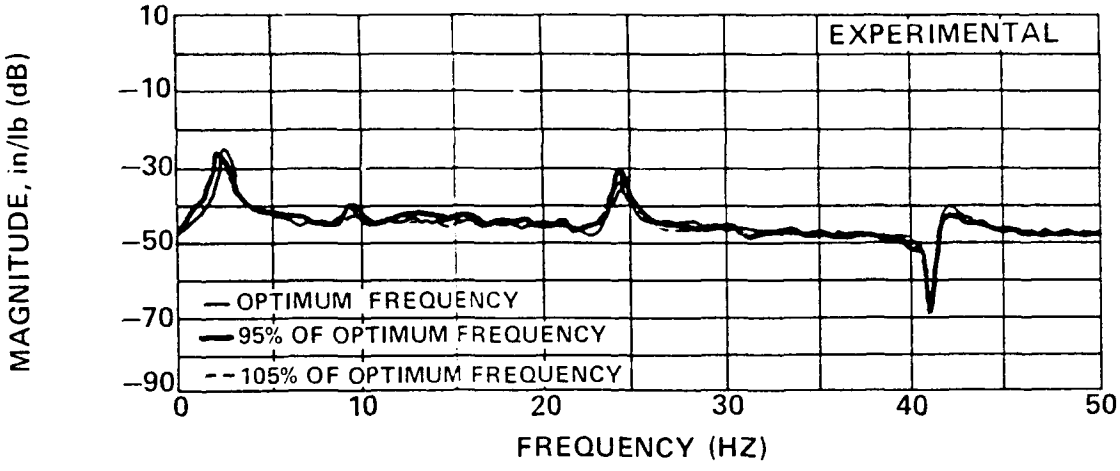

Figure 10. Experimental Optimally Tuned and Mis–Tuned Structural Responses from 0 to 50 Hertz

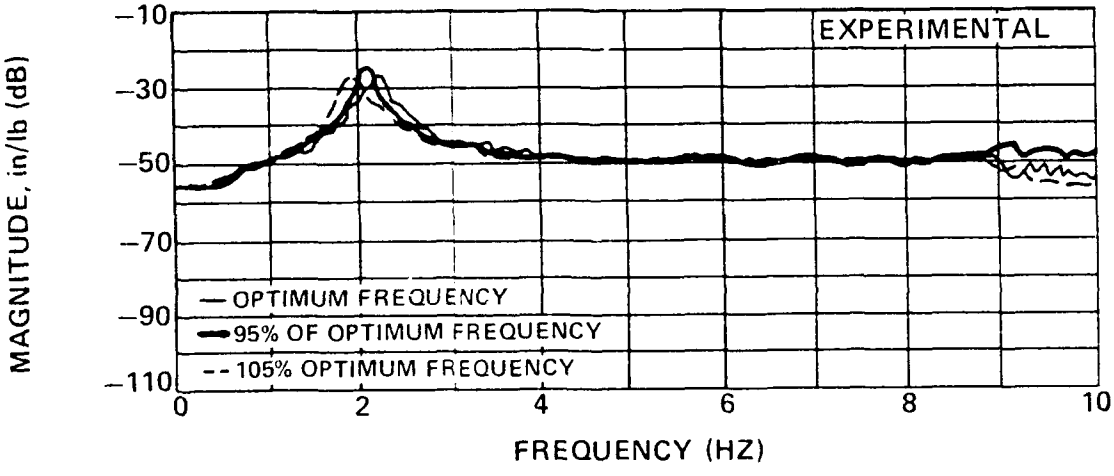

Figure 11. Experimental Optimally Tuned and Mis–Tuned Structural Response from 0 to 10 Hertz

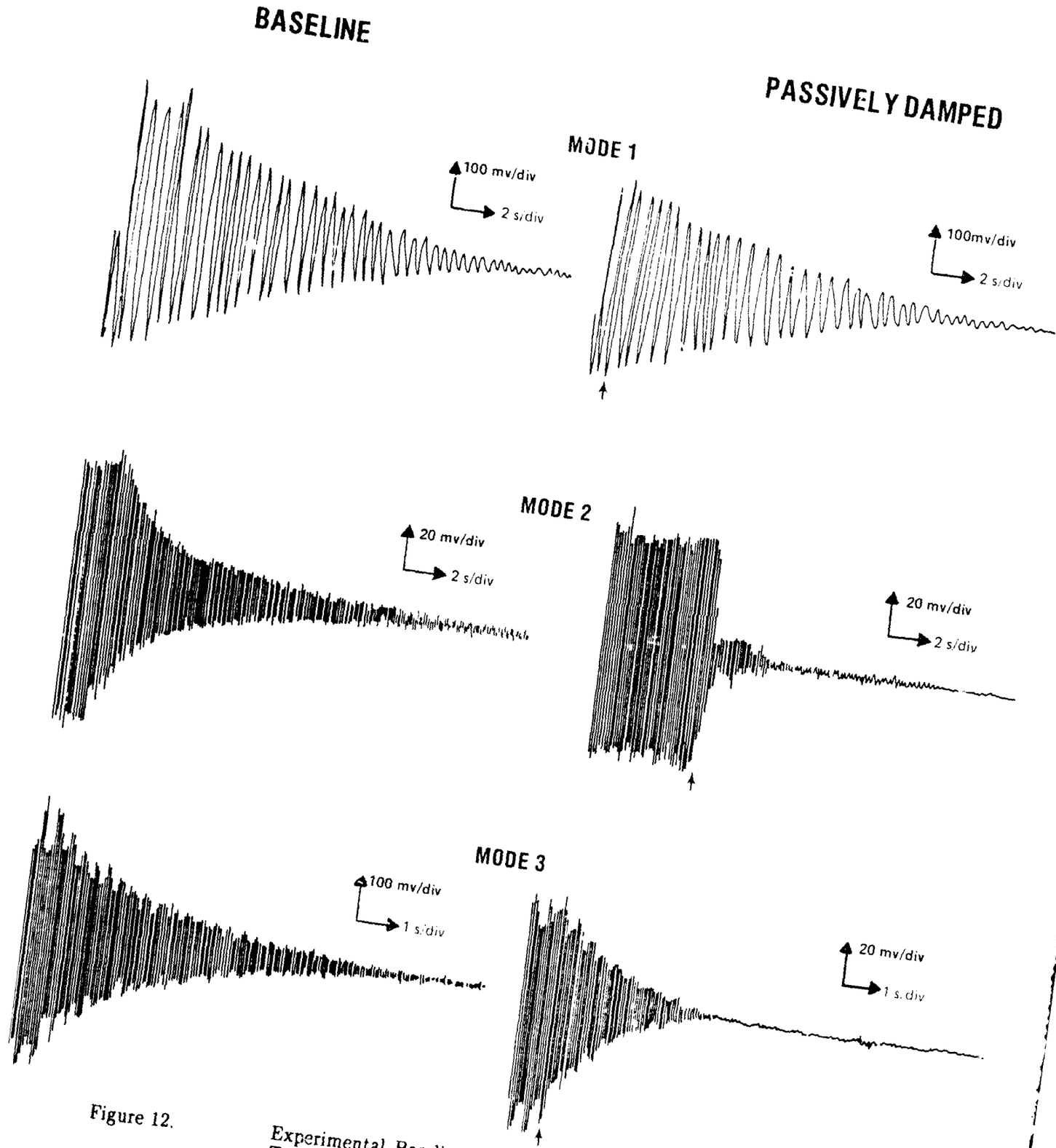

Figure 12. Experimental Baseline and Passively Damped Modal Decay Plots of Truss Tip Transverse Velocity